THE JOURNAL OF CHEMICAL PHYSICS

VOLUME 23 NUMBER 9

SEPTEMBER, 1955

1739 M60A

Published by the

AMERICAN INSTITUTE OF PHYSICS

Incorporated

Lancaster, Pa., and New York, N. Y.

THE
been su
to indu
under
chemica
fully in
lattice
presenc

A pu
When
Howeve
on "pro
and oth
have nu
enough
duce su
of adde

The

The
10^{-27} c
impurit
maximu

[1] H. S.
J. A. Wo

THE JOURNAL
OF
CHEMICAL PHYSICS

VOLUME 23, NUMBER 9 SEPTEMBER, 1955

Catalytic Activity Induced by Neutron Irradiation of Inert Silica

P. B. WEISZ AND E. W. SWEGLER
Socony-Vacuum Laboratories (A Division of Socony-Vacuum Oil Company, Inc.), Research and Development Department, Paulsboro, New Jersey
(Received December 14, 1954)

In pure silica gel, irradiation with 2 to 8×10^{18} fast neutrons/cm^2 produced a significant increase in catalytic activity for the double-bond isomerization in hexene. The effect is believed to be due to lattice dislocations.

INTRODUCTION

THE possibility of inducing changes of catalytic properties of solids by atomic radiations has been suggested.[1] We have attempted more specifically to induce catalytic properties by neutron irradiation under conditions where lattice defects alone and no chemical transmutations would be produced. Successfully induced activity would demonstrate the ability of lattice defects to participate in catalysis without the presence of chemical "promoter" impurities.

A pure SiO_2 gel was chosen for this investigation. When pure, SiO_2, is known to be catalytically inert. However, it will acquire considerable catalytic activity on "promotion" by other elements such as Al, Mg, Zr, and others. Yet both elemental constituents, Si and O have nuclei which for neutron irradiation present small enough cross sections for nuclear transmutations to produce substantially no *chemical* impurities, in the sense of added foreign elements.

The following transmutation schemes are known:

$$Si^{28}(n,2n)Si^{27}\xrightarrow{\beta^+}Al^{27}$$
$$Si^{30}(n,\gamma)Si^{31}\xrightarrow{\beta^-}P^{31}$$
$$O^{18}(n,\gamma)O^{19}\xrightarrow{\beta^-}F^{19}.$$

The cross section for all reactions is smaller than 10^{-27} cm^2. Therefore, the fraction of neutron induced impurities for the bombarded samples, which saw a maximum flux of 7.5×10^{18} neutrons/cm^2, will be

$$f<10^{-27}\times7.5\times10^{18}$$

or

$$f_{\text{transm}}<7.5\times10^{-9}.$$

For the number of lattice dislocations, previous work with germanium[2] has shown several hundred dislocations to result per scattered neutron so that with a scattering cross section of 1.7×10^{-24} cm^2, we obtain

$$f_{\text{disloc}}\approx1.7\times10^{-24}\times7.5\times10^{18}\times10^{2\cdots3}$$
$$f_{\text{disloc}}\approx10^{-2}\cdots10^{-3}.$$

The fraction of dislocated atoms, therefore, approaches a percent of the normal lattice sites.

PROCEDURE

A pure silica gel was produced from ethyl silicate by gelling an aqueous acid alcohol solution with NH_4OH at pH$\approx$7, washing, drying, and calcining the gel at 550°C for 16 hours.

One 20 gram sample was exposed (CA102M) in the Oak Ridge pile facilities to receive a total integrated (nvt) flux of 7.5×10^{18} cm^{-2} fast neutrons and an about equal magnitude of slow neutrons (<0.1 Mev). Another was exposed to one-fourth of this flux (C101W).

The irradiated samples, as well as control samples of unirradiated silica gel (CA100), were subjected to catalytic activity tests. Any radioactivity remaining in the bombarded samples was low enough not to be audibly discernable by gamma-ray sensitive Geiger tube equipment.

The activity for the cracking of isopropylbenzene

[1] H. S. Taylor (private communication, 1952); E. H. Taylor and J. A. Wethington, J. Am. Chem. Soc. **76**, 971 (1954).

[2] K. Lark-Horovitz, *Semiconducting Materials* (Buttersworth Scientific Publications, 1950), p. 47; Lark-Horovitz, Elec. Eng. **68**, 1047 (1949).

TABLE I. Percent conversion of hexene-1 to 2- and 3-hexenes (combined).

Thermal rate No. catalyst	CA100 No. irrad.	CA101W 1.8×10^{18} neutrons/cm²	CA102M 7.5×10^{18} neutrons/cm²
1.3 (M-83)	2.3 (M-81)	8.3 (M-86)	8.9 (M-82)
	5.3 (M-87)	5.3 (M-90)	10.2 (M-85)
	5.9 (M-87)	4.1 (HCW-3)	9.8 (M-91)
	0.9 (HCW-1)	0.7 (HCW-5)	11.9 (HCW-4)
	2.3 (HCW-6)		4.9 (HCW-2)
Average 1.3	3.3	4.6	9.4

was measured in a Schwab type[3] reactor at 420°C and atmospheric partial pressure of reactant.

Activity for catalyzing the isomerization of *n*-hexene-1 was studied in a conventional glass reactor tube, containing the sample of solids as 4.5 grams of 6–12 mesh particles. Hexane-1, Phillips Pure Grade, was charged at 0.75 LHSV at 350°C (by flowing 90 cc/min of helium through hexene-1 at 20°C) for 20 minutes. Essentially 100% of liquid was recovered and analyzed by mass spectrometer.

RESULTS

A. Specific Surface Areas of Samples

No significant changes of specific surface area were detected due to neutron irradiation. Surface areas measured by the BET method (nitrogen adsorption) gave

CA100 424 m²/g
CA101W 410 m²/g±10 m²/g.
CA101M 424 m²/g.

B. Isopropylbenzene Cracking Activity

No activity significantly above the thermal background, i.e., larger than 10^{-7} moles/g sec, could be detected. However, on removing the solid from the reactor, a brownish discoloration was observed on the irradiated sample, while the fresh silica had remained nearly white.

C. *n*-Hexene-1 Isomerization Activity

The liquid products from *n*-hexene-1 passed over the catalysts were examined by mass spectrometer analysis by comparing the resulting mass spectra with that of the charge liquid. Significant deviations were observed for the patterns of the liquids which had passed over bombarded silica. It was not feasible at this point to resolve the mass patterns in terms of the 16 possible olefin isomers as the unknown species.

In order to study the nature of the hexane isomerization products, part of the product liquids were subjected to hydrogenation at room temperature in acetic acid solution, using palladium supported on charcoal as a catalyst. The resulting mixtures of hexanes could then be analyzed by mass spectrometry for the four individual *skeletal* hexene isomers. No skeletal isomerization was found to have occurred.

The mass spectra of the product liquids were now analyzed in terms of the double bond isomers alone. The similar reference spectra of 2-hexene and 3-hexene were averaged to calculate the concentration of lumped 2- and 3-hexenes and of remaining 1-hexene. Table I shows the conversion to 2- and 3-hexenes obtained by this analysis.

A statistical examination of the data, using the *t*-test of significance, shows a 99.6 to 99.7% probability for the altered activity behavior of sample CA102M over the unbombarded material CA100. If we consider the information contained in the measurements on *both* samples, CA101W and CA102M, assuming the activity increase over the unbombarded sample to be proportional to the amount of bombardment, statistical analysis indicates a 99.9% probable significant change of catalytic activity in the samples subjected to bombardment.

CONCLUSIONS AND DISCUSSION

The irradiation of a silica gel by 7.5×10^{18} fast neutrons/cm² resulted in an increase in its catalytic activity for the double-bond isomerization of *n*-hexene-1.

No measurable change in macroscopic structural properties was induced by this magnitude of neutron flux as evidenced by observation of the specific surface area; this is in general agreement with observations on the density change of SiO_2 structures by irradiation.[4]

The induced activity is believed to be due to lattice dislocations produced by the nucleon bombardment, since the concentration of chemical impurities added by transmutation is several orders of magnitude below that of natural chemical impurities in the material.

[3] P. B. Weisz and C. D. Prater, *Advances in Catalysis* (Academic Press, Inc., New York, 1954), Vol. 6.

[4] M. Wittels and F. A. Sherrill, Phys. Rev. **93**, 1117 (1954).

Self-Diffusion in Lead

NORMAN H. NACHTRIEB AND GEORGE S. HANDLER
Institute for the Study of Metals, The University of Chicago, Chicago, Illinois
(Received November 18, 1954)

The rate of self-diffusion in single crystals of high purity lead has been measured over the temperature range 174° to 322°C by means of RaD. The data are fitted by the least squares equation $D=0.281 \times \exp[-24\,210/RT]$ cm² sec⁻¹.

INTRODUCTION

A CORRELATION between the activation energy for self-diffusion in cubic metals and their latent heats of fusion[1] has been reported recently and has been interpreted[2] in terms of lattice relaxation around vacancies. The relation

$$\Delta H = 16.5Lm \qquad (1)$$

predicts the activation energies for self-diffusion in gold, silver, copper, sodium, cobalt, α iron, and α-white phosphorus to within a few percent, well within experimental error in each instance. In the case of lead, however, it predicts an activation energy of 19 550 cal/g atom, in poor agreement with the experimental value of 27 900 cal/g atom reported by Hevesy, Seith, and Keil.[3] Although their study was carried out with great care and has been a standard of excellence for more than twenty years, it seemed worthwhile to repeat the work with the more precise radiochemical techniques and instruments now in common use. Diffusion in lead had been studied still earlier by Hevesy and Obrutschewa,[4] who concluded that diffusion in polycrystalline lead occurs chiefly along grain boundaries, and that atom movements in single crystal lead correspond to diffusion coefficients less than 10^{-13} cm² sec⁻¹ even very close to the melting point. Hevesy, Seith, and Keil demonstrated that there is no difference in the rate of self-diffusion in single crystal and polycrystalline lead at least down to 180°C, and that even work-hardened polycrystalline lead showed no differences within experimental error. Since the completion of the present work, the investigation of Okkerse on self-diffusion in polycrystalline lead has appeared,[5] with results essentially in agreement with ours, and differing from those of Hevesy, Seith, and Keil only in a lower activation energy (25 700 cal/g atom).

EXPERIMENTAL

Single crystal rods of lead 0.320 in. in diameter and several inches long were grown in Pyrex tubes by the Bridgman[6] method. The lead was obtained from the U. S. Smelting and Refining Co. and was reported to be 99.999 percent pure. Cylinders 0.300 in. in diameter and about $\frac{3}{8}$ in. long were carefully machined from the rods. Superficial recrystallization occurred when the depth of cut was only 0.001 in., and the disturbed layer was readily removed by an acetic acid-hydrogen peroxide etch solution. Metallic RaD, obtained by reduction of $Pb^{210}(NO_3)_2$ in aqueous solution with sodium borohydride, was evaporated on an end face of each lead cylinder in a vacuum of 10^{-5} mm or better. The cylinders were rotated during the tracer deposition to insure uniform distribution of the RaD. Deposit thickness varied from 100 A to 1000 A. Diffusion couples so prepared were sealed in glass ampoules at 10^{-6} mm pressure and placed in furnaces for the diffusion runs. Furnaces were controlled by Leeds and Northrup Micromax Potentiometer controllers with 4-junction chromel-alumel thermocouples for the sensing elements. Temperatures were measured and controlled to within 0.1°C with chromel-alumel thermocouples which were calibrated at the melting points of N.B.S. zinc, lead, and tin, and the steam point.

Following the diffusion period, which varied from several days to one month depending upon the temperature, the crystals were machined to a diameter of 0.260 in. to remove possible surface-diffused activity. They were then mounted in a sledge-base microtome and optically aligned with the plane of the blade's motion. To minimize crystal distortion, 2μ thick sections were cut and weighed in serial groups of ten slices. Weights amounted to about 8 mg and were made to the nearest 5 micrograms. The slices were then dissolved in nitric acid, and the aqueous solutions so obtained were evaporated in glass planchets to uniformly thin residues of lead nitrate suitable for β counting.

TABLE I. Self-diffusion in lead.

Temp. (°C)	D(cm² sec⁻¹).
173.8	4.81×10^{-13}
206.3	2.21×10^{-12}
225.9	6.41×10^{-12}
253.0	2.41×10^{-11}
285.1	8.79×10^{-11}
304.4	1.94×10^{-10}
322.4	4.09×10^{-10}

[1] Nachtrieb, Weil, Catalano, and Lawson, J. Chem. Phys. **20**, 1189 (1952).
[2] N. H. Nachtrieb and G. S. Handler, Acta Metallurgica (to be published).
[3] Hevesy, Seith, and Keil, Z. Physik, **79**, 197 (1932).
[4] G. Hevesy and A. Obrutschewa, Nature **115**, 674 (1925).
[5] B. Okkerse, Acta Metallurgica **2**, 551 (1954).
[6] P. W. Bridgman, Proc. Am. Acad. Arts Sci. **60**, 305 (1929).

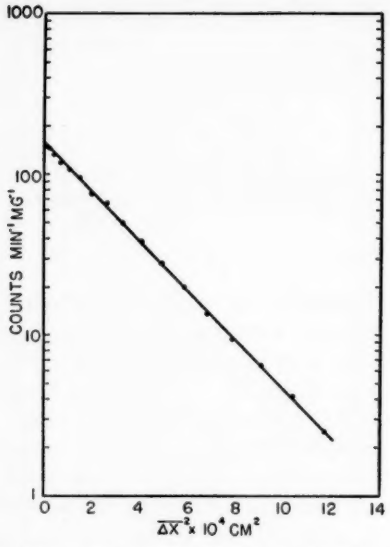

FIG. 1. Log D *versus* $1/T$ for lead self-diffusion.

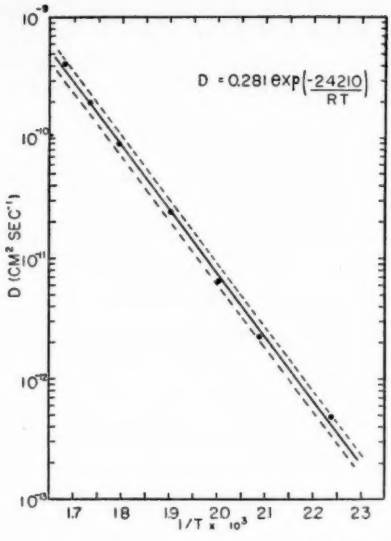

FIG. 2. Penetration profile for lead self-diffusion.

It was necessary to count the activity due to RaE, the bismuth daughter of RaD, because of the much more favorable energy of the beta particles of the former. This required the lapse of 30 days or so (6 half-lives of RaE) to establish secular equilibrium. The α activity from RaF (polonium) was excluded from the counter by a 10 mil aluminum absorber foil. Counting was done with a methane flow counter operated at 4500 volts in the proportional range. At least 10^4 counts above background were totaled for each slice group.

RESULTS

The solution to Ficks Law for the diffusion geometry employed is

$$C=\frac{C_0}{(\pi Dt)^{\frac{1}{2}}}\exp[-x^2/4Dt]. \quad (2)$$

[Figure (1) shows a typical penetration profile, a plot of log C *versus* x^2, from whose slope the diffusion coefficient is calculated.]

Table I summarizes the data obtained for seven temperatures from 174° to 322°C. Figure 2 shows a $1/T$ plot of these data with the solid line representing the least squares equation

$$D=0.281\exp[-24\,210/RT]. \quad (3)$$

The dotted lines are drawn for the 2σ limits. The probable error in ΔH is 770 cal/g atom.

A least squares analysis of the data reported by Hevesy, Seith, and Keil[3] gives

$$D=5.56\exp[-27\,680]/RT. \quad (4)$$

Only the α-counting measurements were included in Eq. (4), in accordance with the practice of the earlier workers.[7] The probable error in ΔH is 2500 cal/g atom for their results.

Okkerse[5] did not publish individual D values nor give the probable error in ΔH. Examination of his $1/T$ plot indicates that the present results are more precise, and that both sets agree within the limits of error.

CONCLUSIONS

The activation energy for self-diffusion in lead exceeds the value predicted from the correlation with the latent heat of fusion by about 4500 cal/g atom. This discrepancy is considerably larger than the experimental error, and may indicate an unusually large activation energy for diffusion in liquid lead.

ACKNOWLEDGMENTS

The research described was supported in part by the Aeronautical Research Laboratory, Wright Air Development Center, under United States Air Force Contract AF 33 (616)-2090. The single crystals were prepared by Mr. K. K. Ikeuye and Mr. F. D'Heurle, whose help is gratefully acknowledged.

[7] Professor Seith has kindly indicated in a private communication that the atom recoil measurements are less accurate than the α-particle ionization measurements because the range of the former in lead is less accurately known. Both are methods which depend upon the decrease in surface activity with time, and are inherently less accurate than the sectioning technique here employed.

Second Approximation to the Thermal Diffusion Factor on the Lennard-Jones 12:6 Model

S. C. SAXENA AND B. N. SRIVASTAVA
Indian Association for the Cultivation of Science, Calcutta 32, India
(Received December 13, 1954)

Several collision integrals useful for the calculation of the second approximation to the thermal diffusion factor have been evaluated for the Lennard-Jones 12:6 model and utilized to calculate $[R_T]_2$, the second approximation to the thermal separation ratio from the expressions developed by Mason for the exp-six model. It has been shown that the difference between $[R_T]_1$ and $[R_T]_2$ for the 12:6 model is very small and does not vitiate the method developed by us elsewhere for calculating the force constants from the thermal diffusion data. These considerations have been applied to argon and the results compared with the experimental data. A simple empirical relation connecting $[R_T]_1$ and $[R_T]_2$ has been derived for the Lennard-Jones 12:6 model.

I. INTRODUCTION

THE determination of the intermolecular force from various equilibrium and nonequilibrium properties of gases is essential for correlating and predicting the various properties of gases, liquids, and solids. Its evaluation from the temperature variation of gaseous transport properties is based on the theory of Chapman and Enskog which is, strictly speaking, applicable only to monatomic gases, at moderate pressures and sufficiently high temperatures so that quantum-mechanical effects are negligible. The Boltzmann integro-differential equation obtained under these conditions has been solved by Chapman and Enskog with the further restriction that the gradients of the physical quantities are small and therefore only the first approximation perturbation term need be considered. Under these conditions the transport properties have been expressed by them in terms of a set of collision integrals[1] which depend on the law of molecular interaction. These integrals have been evaluated for various molecular models of which the most appropriate appear to be the Lennard-Jones 12:6 and the modified Buckingham (exp-six) models. For the former model this evaluation has been done, among others, by Kihara and Kotani,[2] Hirschfelder, Bird, and Spotz,[3] and for the latter by Mason.[4]

The property most sensitive to the law of force and hence useful for its determination is the thermal diffusion of gases, though frequently viscosity is employed for this purpose, in view of the greater accuracy in its experimental determination. This is also partly due to the circumstance that the second approximation expression for the thermal diffusion factor had not been given by Chapman and Cowling and its magnitude has been vaguely estimated by a number of workers (Grew[5,6]) from the fact that in the case of rigid elastic spheres for the Lorentzian gas the error involved in neglecting the second-approximation term is 23%. Recently, however, Mason[4] has given the expression for the second approximation to thermal diffusion ratio $[K_T]_2$ and evaluated it for the exp-six model. It is the purpose of the present paper to evaluate $[K_T]_2$ for the 12:6 model and estimate its importance in the evaluation of the force parameters for this model.

II. THEORY AND FORMULAS

According to the Lennard-Jones 12:6 model, the potential energy function

$$E(r)=4\epsilon[(r_0/r)^{12}-(r_0/r)^6], \tag{1}$$

where ϵ is the minimum potential energy of attraction and r_0 the molecular separation for zero interaction energy. The first approximation to the thermal diffusion factor for a binary mixture of heavy isotopes is

$$[\alpha]_1=\frac{105}{118}[R_T]_1\left(\frac{M_1-M_2}{M_1+M_2}\right), \tag{2}$$

where

$$[R_T]_1=\frac{118}{7}\frac{(C-1)(1+A)}{A(11-4B+8A)}, \tag{3}$$

and A, B, C are defined by

$$A=\frac{W_2^2}{5W_1^1},\quad B=\frac{5W_2^1-W_3^1}{5W_1^1},\quad C=\frac{2W_2^1}{5W_1^1}. \tag{4}$$

The various W_n^l in (4) are the collision integrals for the interaction of dissimilar molecules and are functions of $kT/\epsilon=y$. These are related to the collision integrals Ω_n^l of Chapman and Cowling by

$$\Omega_n^l=2r_0^2(\pi kT/m)^{\frac{1}{2}}W_n^l. \tag{5}$$

It has now become more common to express the transport properties in terms of reduced collision inte-

[1] S. Chapman and T. G. Cowling, *The Mathematical Theory of Non-Uniform Gases* (Cambridge University Press, Teddington, England, 1952), second edition.
[2] T. Kihara and M. Kotani, Proc. Phys. Math. Soc., Japan, **25**, 602 (1943).
[3] Hirschfelder, Bird, and Spotz, J. Chem. Phys. **16**, 968 (1948).
[4] E. A. Mason, J. Chem. Phys. **22**, 169 (1954).
[5] K. E. Grew, Proc. Roy. Soc. (London) **A178**, 390 (1941).
[6] K. E. Grew, Proc. Roy. Soc. (London) **A189**, 402 (1947).

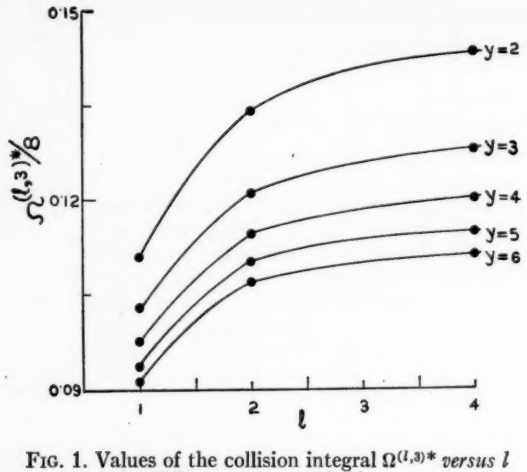

FIG. 1. Values of the collision integral $\Omega^{(l,3)*}$ *versus* l for different values of $kT/\epsilon \equiv y$.

grals $\Omega^{(l,n)*}$ which are just the collision integrals of Chapman and Cowling divided by their values for rigid elastic spheres of diameter r_0. Hence

$$\Omega^{(l,n)*}=8W_n{}^l/Z, \tag{6}$$

where

$$Z=\left[2-\frac{1}{l+1}\{1+(-1)^l\}\right](n+1)\,! \tag{7}$$

Mason's[4] formula for the second approximation $[\alpha]_2$ as applied to the case of heavy isotopes is

$$[\alpha]_2=\frac{105}{118}[R_T]_2\left(\frac{M_1-M_2}{M_1+M_2}\right), \tag{8}$$

where

$$[R_T]_2=(59/21)[X_1-X_2Y_1-X_3Y_2], \tag{9}$$

and X_1, X_2, X_3, Y_1, and Y_2 are defined by Mason.[4]

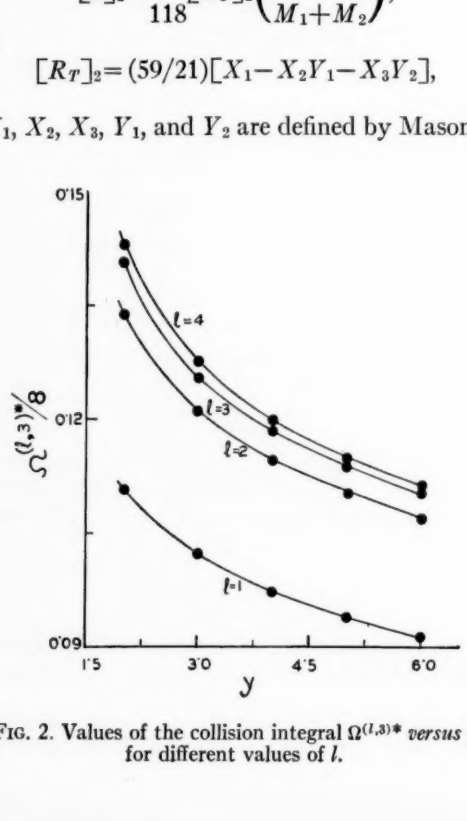

FIG. 2. Values of the collision integral $\Omega^{(l,3)*}$ *versus* y for different values of l.

III. EVALUATION OF COLLISION INTEGRALS

The foregoing formula for $[\alpha]_2$ contains several collision integrals, most of which have been tabulated by Hirschfelder, Bird, and Spotz[3] but some require evaluation. Of the latter $W_4{}^1$, $W_5{}^1$ can be easily evaluated with the help of the data given by them. For the collision integral $W_3{}^3$, however, no numerical computations have been carried out so far.

For evaluating $W_n{}^l$ Hirschfelder, Bird, and Spotz have given the formula

$$W^l(n,x)=\tfrac{1}{8}[2-\{(1+(-1)^l)/(l+1)\}]x^{n+2} \times\sum_i A_i{}^l\frac{\Gamma[n+n_i{}^l+2]}{[x+a_i{}^l]^{(n+n_i{}^l+2)}}, \tag{10}$$

where $x=\epsilon/kT=1/y$, and have tabulated the values of the constants $A_i{}^l$, $n_i{}^l$ and $a_i{}^l$ for $l=1$, 2, and 4. Utilizing these we obtained the values of $W^1(4,x)$ and $W^1(5,x)$ as:

$$\begin{aligned}W^1(4,x)=&\tfrac{1}{4}x^6[110.891x^{-5.845}+56.4362(x+0.439)^{-5.5}\\&+126766(x+3.675)^{-8.126}\\&-0.01122\exp(-0.8247x)\\&+8.914\times10^{-5}\exp(-0.3583x)\\&-4.868\times10^{-3}\exp(-0.6533x)],\\W^1(5,x)=&\tfrac{1}{4}x^7[654.001x^{-6.845}+310.399(x+0.439)^{-6.5}\\&+1030100(x+3.675)^{-9.126}\\&-9.251\times10^{-3}\exp(-0.8299x)\\&+3.500\times10^{-5}\exp(-0.3926x)\\&-3.181\times10^{-3}\exp(-0.6756x)].\end{aligned}$$

With these expressions the collision integrals $W^1(4,x)$ and $W^1(5,x)$ were evaluated for the required values of x. Values of these collision integrals are collected in Table I, columns 2 and 3, and their computational accuracy is of the order of 1 part in 300.

The evaluation of $W_3{}^3$ is a laborious task which could not be undertaken in the absence of computational assistance. Fortunately, we found that the formula for $[\alpha]_2$ was not very sensitive to the value of $W_3{}^3$ and in fact when, in place of $W_3{}^3$ the numerical values of $W_3{}^2$ and $W_3{}^4$ were alternately substituted, it was found that $[\alpha]_2$ changed only by 0.010%. This led us to adopt a simple interpolation method of evaluating $W_3{}^3$ as explained below. It further showed that for our present purpose it is useless to evaluate $W_3{}^3$ to a higher degree of accuracy.

By utilizing the constants given by Hirschfelder, Bird, and Spotz[3] and making use of Eq. (10), $W_3{}^4$ was found to be given by the expression

$$\begin{aligned}W^4(3,x)=&\tfrac{1}{5}x^5[27.1922x^{-4.86}+6.65570(x+0.1350)^{-4.5}\\&+38.2162(x+0.49593)^{-4.58915}\\&-5.99499\times10^{10}(x+7.5377)^{-12.3}\\&-0.08901\exp(-1.0280x)\\&-2.626\times10^{-3}\exp(-0.9121x)\\&-3.963\times10^{-3}\exp(-0.4182x)\\&-7.140\times10^{-3}\exp(-0.4538x)\\&-0.02538\exp(-0.6411x)\\&-0.01098\exp(-0.8059x)],\end{aligned}$$

which was evaluated for various values of x. These are also recorded in column 4 of Table I and their computational accuracy is 1 part in 300. These, along with the values of W_3^1 and W_3^2 as already tabulated by Hirschfelder, Bird, and Spotz were utilized for interpolating W_3^3. For the sake of interpolation it was found more convenient to plot $\Omega^{(l,3)*}$ rather than W_3^l against l in view of the large and irregular variation of the latter. The plot of $\Omega^{(l,3)*}$ *versus* l for different values of y is shown in Fig. 1, and in view of the slow change from $l=2$ to $l=4$ it is easy to estimate fairly accurately the value for $l=3$. These $\Omega^{(3,3)*}$ values for the corresponding values of y are plotted in Fig. 2, and a smooth curve is obtained. Curves for other values of l are also plotted to give an idea of the accuracy of this interpolation. From the graph in Fig. 2 values of the collision integrals $\Omega^{(3,3)*}$ could be read for the required values of y. These are recorded in column 5 of Table I and have the computational accuracy of the order of 1%.

We have stated above that the maximum error in $[\alpha]_2$ due to errors in estimating $\Omega^{(3,3)*}$ is 0.010%; actually it will be a small fraction of this. This is really due to a fortuitous circumstance that in Eq. (10) the leading term X_1 which contributes 98% of the value is independent of $\Omega^{(3,3)*}$, while the remaining two terms which contain $\Omega^{(3,3)*}$ have, respectively, negative and positive contributions.

TABLE I. Values of some collision integrals evaluated for the 12:6 model.

$y=kT/\epsilon$	$W^1(4)$	$W^1(5)$	$W^4(3)$	$W^3(3)$
2.53	24.37	142.0	5.122	6.33
3.23	23.39	136.4	4.817	5.93
3.80	22.78	130.0	4.651	5.73
4.43	22.23	129.8	4.512	5.57
5.00	21.61	127.4	4.413	5.46
6.00	21.20	123.9	4.276	5.29
7.00	20.51	120.9	4.170	5.17
8.00	20.09	118.5	4.083	5.06
9.00	19.72	116.3	4.012	4.95
10.00	19.40	114.4	3.950	4.88

IV. CALCULATION OF FORCE CONSTANTS FOR ARGON

In order to get an idea of the numerical magnitudes and in particular of the difference between $[R_T]_1$ and $[R_T]_2$, we shall apply the foregoing formulas to the particular case of argon. For this purpose the force parameter ϵ/k must be known or determined. For evaluating this parameter a slightly different procedure has been adopted here than that used earlier by Srivastava and Madan[7] as our present aim is to calculate the second approximation to the thermal diffusion factor, and consequently a high degree of accuracy is required for the value of ϵ. In the previous paper our calculations assumed that the first approximation formula for R_T gave the correct value of R_T and therefore the value of ϵ/k would be in error if $[R_T]_2$ differs appreciably from $[R_T]_1$. We want our present calculations to be independent of this assumption.

TABLE II. Force constant ϵ for argon.

Temp range (°K)	ϵ/k (First approx) °K (approx calculation)	ϵ/k (First approx) °K (refined calculation)
400–600	144.0	148.1
440–660	151.7	154.4
400–800	156.8	160.0
500–750	166.7	169.4
Mean	154.8	158.0

In Eq. (3) the variation of the term $(1+A)/A(11-4B+8A)=g$ with temperature is very small as shown later on. Hence following the procedure already adopted elsewhere (Srivastava and Madan),[8] we proceed to calculate ϵ from the variation of $[R_T]_1$ with temperature, assuming that this is only due to the term $(C-1)$. As is well known the R_T values refer to a wide temperature interval and the problem of assigning the proper temperature to a particular R_T value is a little complicated. This was done by Srivastava and Madan[7] for the experimental data of Stier[9] and for our present purpose we have simply utilized the values of R_T tabulated there. In this way the values of ϵ/k given in column (2) of Table II were obtained for different temperature intervals, giving an average value of $\epsilon/k=154.8$°K. For this value of ϵ/k, the quantity g was calculated at various temperatures and the values thus obtained are recorded in Table III. An inspection of these values shows clearly that the variation of g is less than 1%. Still, however, this variation was taken into account and following the method of successive approximations, a fresh graph was plotted for $[R_T]_1/g$ as a function of T and its variation with temperature was utilized to recalculate ϵ/k in the manner already mentioned. These first-approximation values thus obtained are recorded in column 3 of Table II and are seen to be higher than the values given in column 2 by about 2%, the mean of the first-approximation (refined calculation) values being 158°K.

This method of evaluating ϵ/k is better than the previous one as it does not assume the absolute value of R_T to be accurately given by the first-approximation value $[R_T]_1$. It merely assumes that the rate of variation of $[R_T]_1$ with temperature is the same as that of

TABLE III. Values of g.

Temp (°K)	400	500	600	700	800
g	4.685	4.671	4.661	4.654	4.645

[7] B. N. Srivastava and M. P. Madan, J. Chem. Phys. **21**, 807 (1953).

[8] B. N. Srivastava and M. P. Madan, Proc. Phys. Soc. (London) **A66**, 277 (1953).

[9] L. Stier, Phys. Rev. **62**, 548 (1942).

TABLE IV. Values of the first and second approximation to the thermal separation ratio.

Temp (°K)	Exp R_T	$[R_T]_1$	$[R_T]_2$	$[R_T]_2/[R_T]_1$
400	0.375	0.3751	0.3759	1.0022
510	0.442	0.4529	0.4599	1.0155
600	0.485	0.4940	0.5028	1.0179
700	0.525	0.5273	0.5406	1.0252

$[R_T]_{exp}$ and could be rigorously* accurate if the rate of variation of $[R_T]_1$ with temperature were the same as that of $[R_T]_2$ though the absolute values were different. It will be seen later that this expectation is not wholly fulfilled. The consequences of this are also investigated later on.

V. CALCULATION OF SECOND APPROXIMATION TO R_T

With these force constants the values of $[R_T]_2$ were calculated from Eq. (9) and are recorded in column 4 of Table IV along with the $[R_T]_1$ values and the experimental R_T values for a few moderately high temperatures. It will be seen that the second-approximation values are slightly higher than the first-approximation values, the difference being nowhere greater than 3% and decreasing with decrease of temperature. This completely falsifies the belief usually held because of some plausible arguments that the error involved in taking the first approximation to R_T may be quite appreciable. An indication of this was first given by Mason[4] for the exp-six model, and it is shown here that the same holds for the 12:6 model also.

Examination of column (5) further shows that the ratio $[R_T]_2/[R_T]_1$ increases very slowly by about 2% as the temperature is increased, whereas the $[R_T]_1$ values increase by about 40% in the same temperature range. This shows clearly that the error involved in calculating ϵ/k from the variation of $[R_T]_1$ will be extremely small. To confirm this $[R_T]_2$ was plotted as a function of y along with the plot of experimental R_T values *versus* temperature on the same graph paper and from a point-to-point correspondence for the same R_T values, the values of ϵ/k were calculated for different points on the graph and recorded in Table V, yielding a mean value of $\epsilon/k=164.8$, which is about 4% higher than the first-approximation value and 7% higher than the value obtained by us previously. Thus the usefulness of calculating ϵ/k from the variation of $[R_T]_1$ with the temperature is fully established and the value so obtained is not likely to be in error by more than 4%.

* This is based on the assumption that $[R_T]_2=[R_T]_{exp}$.

TABLE V. Values of ϵ/k (second approximation).

Temp (°K)	400	500	600	700
ϵ/k	157.1	163.9	169.9	168.3

It will be seen that the formulas for $[R_T]_1$ and $[R_T]_2$ are quite different algebraically and hence it is not possible to express $[R_T]_2$ in terms of $[R_T]_1$, though their numerical values differ by less than about 3%. It will therefore be interesting to examine this relationship empirically. For this purpose $\log\{[R_T]_2/[R_T]_1\}$ was plotted both *versus* log$y$ and *versus* log T. The plots were found to be straight lines indicating relations of the form

$$[R_T]_2=0.968[R_T]_1y^{0.039}, \tag{11}$$

or

$$[R_T]_2=0.795[R_T]_1T^{*0.039}. \tag{12}$$

Equation (11) should hold for any isotope for values of y lying between 2.5 and 4.5.

VI. DISCUSSION OF RESULTS

Table IV shows that the difference between $[R_T]_1$ and $[R_T]_2$ for the 12:6 model is very small and much less than the errors in the experimental determination of R_T. Hence the usefulness of the second approximation $[R_T]_2$ in the experimental determination of ϵ/k by the method outlined here is negligible and for all practical purposes, until the accuracy of the experiments is increased, it is useless to consider the second approximation term. Further the latter is of no use to us in deciding about the suitability of the model.

The values of $[R_T]_1$ and $[R_T]_2$ for the exp-six model have been extensively calculated by Madan[10] for a large number of values of y for $\alpha=14$ (case of argon). His results show a maximum difference of about 3% between the first- and the second-approximation values for the same range of y-values as employed here. The difference is thus of the same order as on the 12:6 model.

It may be mentioned that the third approximation term in the expression for self-diffusion can also be calculated with the help of the collision integrals evaluated in the present paper. This will be taken up later.

ACKNOWLEDGMENTS

We record our thanks to the Council of Scientific and Industrial Research, New Delhi, for sanctioning a research project under which the present investigation has been carried out and for the award of a research scholarship to one of us (S.C.S.)

[10] M. P. Madan, Indian J. Phys. **29**, 11 (1955).

Electronic States of the Naphthalene Crystal*

DONALD S. MCCLURE AND OTTO SCHNEPP†
Department of Chemistry and Chemical Engineering, University of California, Berkeley, California
(Received December 28, 1954)

The existing experimental data on the low-temperature fluorescence and absorption of naphthalene crystal is reviewed and correlated with our own data. Some preliminary work on crystals of $C_{10}D_8$ is included. A vibrational analysis of the first moderately strong absorption region, 31 476–33 700 cm^{-1} is made on the basis of the corresponding absorption of naphthalene in solid solution with durene. Some constants of the exciton theory of molecular crystals are obtained for the first and second excited singlet molecular states. Some discrepancies with the theory are pointed out; one of these is removed by calculating the crystal induced mixing of the two excited molecular states. Factor group splitting is found for certain vibronic levels of the ground and first excited state, but most vibronic levels of these states do not split appreciably.

I. INTRODUCTION

WE initially undertook to study the spectra of naphthalene crystal in the near ultraviolet in an effort to determine the symmetry properties of the first two excited singlet states. In order to do this it is essential to know the direction of light absorption with respect to molecular axes. This is by no means the simple matter of measuring polarized absorption in a few crystal directions and then utilizing the crystal geometry, as has almost universally been assumed heretofore. In our earlier report[1] we attempted to interpret the details of the polarized spectra as observed at 20°K on the *ab*-plane of single crystals. The symmetry assignment for the first excited singlet reached at that time differed from that of Craig and Lyons,[2] who studied the absorption of the *ab*-plane at room temperature, and in the light of subsequent work on mixed crystal spectra[3] has proved to be incorrect. If the symmetry assignments from the mixed crystal studies are accepted they can be used as a basis for interpreting the spectrum of the pure crystal. Furthermore, the vibrational analysis of the mixed crystal spectrum[3,4] makes possible a vibrational analysis of the crystal spectrum. We have therefore concentrated in this paper on elucidating the peculiarities of the pure crystal spectrum. We have tried to interpret the results in terms of the exciton theory of molecular crystals. It has become clear that this crystal is no "oriented gas." The intermolecular resonance is large, and there is good evidence that as a result, some molecular states are mixed in the crystal.

The absorption spectrum of naphthalene crystal has been the subject of a number of investigations.[1,2,5–8] Prikhotjko[8] has made a detailed analysis of the spectrum and has attempted to relate it to the spectrum of the vapor. The careful experimental work of this author was of considerable help to us in verifying the presence or absence of various spectral features. The fluorescence spectrum at 20°K has been published by Obreimov and Shabaldas.[9] We have very little of an experimental nature to add to their work, but have obtained the polarized fluorescence spectrum of octadeutero naphthalene, and will present the preliminary results on it here.

The recent experimental work of Broude, Medvedew, and Prikhotjko on benzene[10] and Davydov's paper on the interpretation of the results[11] is the most thorough study of a molecular crystal so far published. These authors demonstrated conclusively that an exciton band forms in the crystal.

The elementary theory of the excited states of a lattice of weakly interacting atoms has been reviewed by Seitz.[12] Peierls[13] extended the elementary theory to include the effect of lattice vibrations. Davydov[14] carried out a treatment of the excited states of naphthalene-like crystals, on the assumption that the molecules are fixed in equilibrium lattice positions.

There has been no explicit discussion in any of the literature, so far as we are aware, of the role of the higher frequency branches of the crystal vibrations, the essentially molecular vibrations. Winston[15] has recently shown in a general way, how to treat perturbations on exciton states in molecular crystals, which he suggests could be applied specifically to the vibration problem. The experimental work reported herein, gives qualitative and quantitative information about the influence of molecular vibrations on the spectrum.

The group theoretical methods that we will use have

* This work was supported by the Office of Naval Research under Contract N6-ori-211-T.O. III.
† Now at Israel Institute of Technology, Haifa, Israel.
[1] O. Schnepp and D. S. McClure, J. Chem. Phys. **21**, 959 (1953).
[2] D. P. Craig and L. E. Lyons, J. Chem. Phys. **20**, 1499 (1952).
[3] D. S. McClure, J. Chem. Phys. **22**, 1668 (1954).
[4] D. S. McClure, to be published.
[5] P. K. Seshan, Proc. Indian Acad. Sci. **A3**, 148, 172 (1936).
[6] A. Prikhotjko, J. Phys. U.S.S.R. **8**, 257 (1944).
[7] A. Prikhotjko, Akademia Nauk S.S.S.R., Ser. Fiz. **12**, 499 (1948).
[8] A. Prikhotjko, Zhur. Eksptl. i Teort. Fiz. **19**, 383 (1949).
[9] W. Obreimov and K. Shabaldas, J. Phys. U.S.S.R. **7**, 168 (1943).
[10] Broude, Medvedew, and Prikhotjko, Zhur. Eksp. i Teort. Fiz. **21**, 665 (1951).
[11] A. S. Davydov, Zhur. Eksptl. Teort. i Fiz. **21**, 673 (1951).
[12] F. Seitz, *Modern Theory of Solids* (McGraw-Hill Book Company, Inc., New York, 1940), pp. 414–419.
[13] Peierls, Ann. Physik **17**, 905 (1932).
[14] A. S. Davydov, Zhur. Eksptl. i Teort. Fiz. **18**, 210 (1948).
[15] H. Winston, J. Chem. Phys. **21**, 170 (1953).

been described by Winston,[16] and Davydov applied similar methods in his papers on naphthalene[14] and benzene.[11]

A theoretical study of the benzene crystal has recently been completed by Fox and Schnepp.[17]

The structure of the naphthalene crystal is accurately known from the work of Robertson and co-workers.[18] The crystal is monoclinic, C^5_{2h} with $a=8.29$ A, $b=5.95$, $c=8.68$, $\beta=122°55'$, and with two molecules per unit cell. The b-axis is a twofold screw axis, and the ac-plane, which contains the optic axes is a glide plane. The crystal has a center of symmetry which coincides with the molecular center of symmetry. The ab-plane is the cleavage plane, and therefore the one most used in the spectral studies. It is useful to describe the molecular orientations in a right-handed coordinate system consisting of the a-, b-, and c'-axes, where c' is perpendicular to the ab-plane. Let χ, ψ, and ω designate the angle from a given direction to a, b, and c', respectively, and let L, M, and N designate the long axis of the molecule, the short axis and the normal to the molecular plane, respectively. The molecular orientation is then given by the following table:

$\chi_L=115.8°$	$\chi_M=71.2°$	$\chi_N=32.8°$
$\psi_L=102.6$	$\psi_M=29.45$	$\psi_N=116.3$
$\omega_L=29.0$	$\omega_M=68.2$	$\omega_N=71.9$

The orientation of the other molecule is obtained by a reflection in the ac-plane, in other words, $\chi'=-\chi$, $\psi'=\pi-\psi$, $\omega'=-\omega$.

Experimental Methods

A three-meter quartz spectrograph was used for most of the spectral work. The dispersion was between 2 and 3 A/mm in the wavelength ranges used. A medium quartz spectrograph was used mostly for exploratory work. Crystals 0.1–10 mm thick were prepared by slowly growing from the melt. Crystals from about 3 to 30μ thick could be prepared by allowing the melt to cool between quartz plates pressed together. Mono-oriented regions could be found and masked off. The thinnest crystals were prepared by special methods of sublimation. All of the principal crystallographic planes were available by sectioning of the large crystals, but it was not feasible to polish sections below 100μ in thickness. All other methods of crystal growing furnished us with the ab-plane. Thickness of the crystals was estimated for the very thin ones by the order of the interference color. Thicknesses from 1 to 40μ were measured under the polarizing microscope by counting interference fringes between crossed polaroids in highly convergent light, or by use of the quartz wedge. Crystal orientation was determined by the interference figure and by measuring the birefringence of some of the samples. The crystal was mounted between quartz plates, inserted into a quartz Dewar in the optical train before the spectrograph slit, and rotated so that one of the dielectric axes was vertical, i.e., so that extinction would occur between a vertical and a horizontal polaroid. The crystal was used as its own polarizer. A Wollaston prism in back of the spectrograph slit separated the horizontally and vertically polarized beams. The oppositely polarized spectra appeared side by side on the plate. Separate iron arc calibration spectra were used for each polarized spectrum. The light of the arc traversed the same optical path within the spectrograph as the light from the crystal. In this way we feel we can be sure to determine frequency differences between oppositely polarized spectra of as little as 3 cm^{-1} for sharp absorption bands.

The b-axis is the symmetry axis of the naphthalene crystal, and therefore it is one of the principal dielectric axes. The other two are in the ac-plane, perpendicular to each other, but bearing no simple relation to the a- or c-directions. On account of this, the phenomenon of axial dispersion may arise, i.e., the dielectric axes may change direction with respect to the crystallographic axes when the wavelength used for observation changes. We therefore looked for axial dispersion on the ac-plane of naphthalene using wavelengths from 5790 A to 3341 A. As a result of this we can say that the axes remained fixed within 2°. In most of our work, where the ab-plane of naphthalene was used there is no question of axial dispersion. It was a possibility however, in the fluorescence and in the absorption of thick ac-cut crystals.

III. THE ABSORPTION SPECTRUM

We have obtained the polarized absorption spectrum of naphthalene crystal at 20°, 77°, and 298°K in crystals from 10 mm to 0.5 micron in thickness. Practically all of this work had been done before by Prikhotjko,[6,7] and our experimental work was done chiefly to provide more information on specific points. There are only a few areas of disagreement between our work and hers. The absorption region from 31 480 to 33 600 cm^{-1} is especially difficult to record because of the wealth of detail and the diffuseness of some bands. We therefore give our own measurements and a comparison with Prikhotjko's for this region. The entire absorption below 38 000 cm^{-1} can be divided into four distinct regions, as already shown by Prikhotjko, and as described in the following sections.

1. The absorption beginning at 29 945 cm^{-1} can be seen in crystals several millimeters thick as a group of very sharp lines, at 20°K. The absorption is about twice as strong along the b-axis as along the a-axis or the c-axis. In the ac-plane, this absorption appears unpolarized. We believe that the frequency is the same in each direction of the crystal, but Prikhotjko reports 29 944 in the b-axis and 29 931 in the a-axis. As already

[16] H. Winston, J. Chem. Phys. **19**, 156 (1951).
[17] D. Fox and O. Schnepp, J. Chem. Phys. **23**, 767 (1955).
[18] Abrahams, Robertson, and White, Acta Cryst. **2**, 233, 238 (1949).

mentioned, our experiments were designed to determine frequency differences in oppositely polarized spectra, and we believe that some systematic error is present in Prikhotjko's measurements. She used a Glan-Thompson prism which had to be rotated between exposures of oppositely polarized spectra, and some shift with respect to the calibration spectrum could possibly have resulted. In view of the thickness of the crystal, it is possible that some of the apparent vibrational additions to the 29 945 line are spurious, and caused by impurities. We agreed with Prikhotjko on the presence of the lines at 400 and 724 cm^{-1} from 29 945, but disagree on several more. We shall have to let a fuller report on this absorption system wait until a number of pure naphthalene samples from different sources have been studied.

The 29 945 band appears in the fluorescence spectrum. At 20°K it is no sharper than the lines of the main system which originate at 31 060 cm^{-1}. At 77°K, however, it appears much sharper than the other lines and stands out rather prominently; especially so in the fluorescence from the *ac*-plane. It is followed by bands at 512, 1380, and 1380+512. These are also sharp, and their relation to 29 945 is verified by their sharpness relative to the surrounding lines in the *ac*-plane emission at 77°K. This sharpness suggests that the upper level is a triplet, since it is expected that line broadening by energy transfer will be small for such states. The extreme weakness of the band is also evidence in favor of this interpretation.

A quite unexpected observation was made when we discovered that with certain (unknown) impurities present in the crystal, the 29 945 band and the other members of this system did not appear in fluorescence, although the main fluorescence progressions did appear. At the same time, the green emission characteristic of the lowest triplet state appeared. The triplet-singlet emission ("phosphorescence") does not appear when the crystal is pure. The impurity responsible for this effect was thought to be benzothiophene, but additions of benzothiophene in much larger amounts than could have been present in the impure crystals had only a small effect on reducing the 29 945 intensity. The 29 945 band system appears in absorption in crystals which do not show emission from this level.

The explanation of this effect may be that the impurity speeds up the internal conversion process to the lowest triplet state. Other evidence to be cited later shows that internal conversion in the crystal is slow in some processes. The impurity may break down translational selection rules, which are to some extent responsible for this slowness.

2. The second absorption region is represented by the single "line" at 31 062. This is the origin of the main fluorescence progressions. Our measurements show it to be polarized about 70% along the *b*-axis in the *ab*-plane and that it has the same frequency in both components. (Prikhotjko disagrees with the last point.) It is a weak line and cannot be observed in crystals less than 10–20 microns thick. The *ab*-plane fluorescence is polarized in the same sense as the absorption. We have not been able to find any absorption bands of comparable shape and intensity which reasonably could be expected to represent vibrational additions to 31 062. Prikhotjko has come to the same conclusion. It is remarkable that this line remains at almost the same apparent half-width in going from a 20μ to a 2000μ crystal, namely from3 cm^{-1} to 9 cm^{-1}. Other bands of the spectrum appear on a photographic plate to broaden almost in proportion to the crystal thickness. The discussion of the interpretation of this band will be deferred to the last section of this paper.

3. In the third region, from 31 480 to 33 600 cm^{-1}, the peaks of absorption are observed in crystals of about 0.5μ thickness, while details between the peaks are observable in one to two micron crystals. This part of the spectrum, illustrated in Figs. 1 and 2, corresponds to the first absorption region of the vapor spectrum. The bands are rather broad and have a complicated structure. In order to resolve all the structure, crystals of several thicknesses from 0.5 to 2μ would have to be used. We obtained spectra from only these two extremes, but were fortunate in being able to compare ours with Prikhotjko's[6] results. This worker reported many lines in crystals which must have been between 0.5 and 2μ thick. Our measurements on very sharp lines agreed with Prikhotjko's to within one or two cm^{-1}. For the broad or poorly resolved lines we were on the average less than 5 cm^{-1} from Prikhotjko's values. On some of the strongest peaks, our measurements are 15 cm^{-1} higher. We are not sure what the reason for this is, but it may be that Prikhotjko reports measurements made only on the *a*-axis of the crystal for these and that her plates show some splitting. We of course measured both *a*- and *b*-axis spectra, but are not sure if there is a difference in the frequency of the strong peaks of the two spectra. We do not believe that we could have missed a dichroic splitting of 15 cm^{-1}, however, even though the strong peaks were rather broad. The discrepancy may be connected with our disagreement with Prikhotjko on the splitting of the 29 945 and 31 062 lines. Prikhotjko found about 25 more lines between 31 476 and 33 542 than we did. The general agreement of the two sets of data gives one confidence that this complicated spectrum is correctly recorded except for the splitting discrepancies noted. Our data and a comparison with Prikhotjko's are given in Table I.

The key to the analysis of this spectrum is the spectrum of naphthalene in durene polarized along the *c'*-axis of the durene host crystal.[3] This is the short axis spectrum which has been interpreted as being induced by two b_{1g} vibrations of frequency 433 and 905 cm^{-1}. The 0—0 band of this spectrum is at 31 554 cm^{-1}. If the entire spectrum is shifted to the red by 10 cm^{-1}, it is found that almost every major peak of the mixed crystal spectrum coincides with a major peak of the pure crystal spectrum. There is only one major peak (except

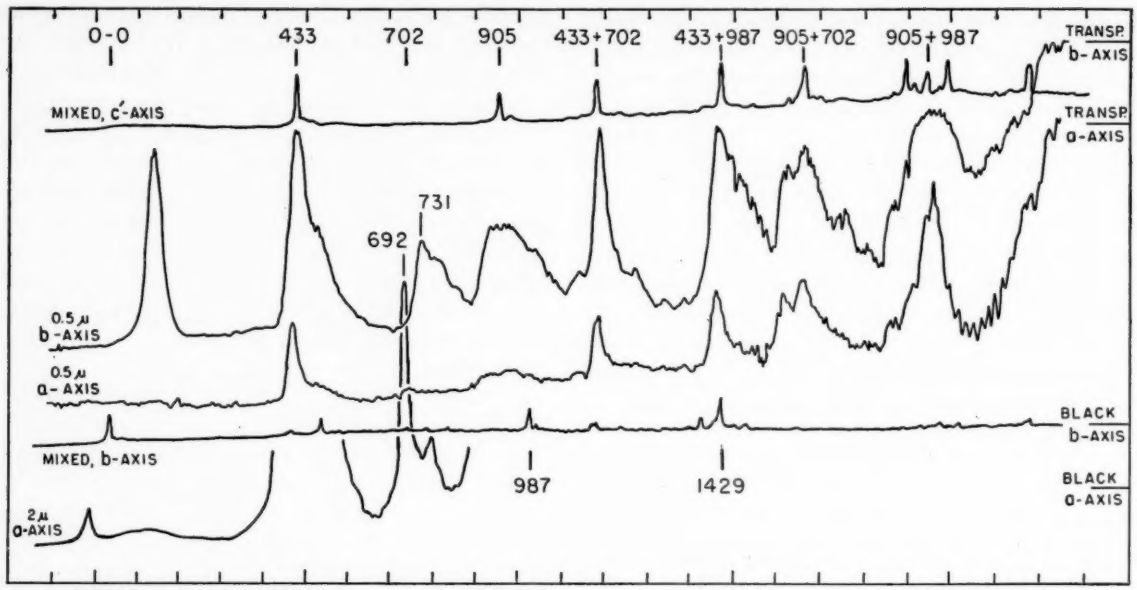

FIG. 1. Microphotometer tracings of the absorption spectra of naphthalene at 20°K. Reading from the top down, the various tracings are: (1) Mixed crystal spectrum of naphthalene in durene, c' axis (see reference 3), (2) b-axis of pure naphthalene crystal 0.5 micron thick, (3) a-axis of pure naphthalene crystal 0.5 micron thick, (4) mixed crystal spectrum along b-axis, (5) a-axis spectrum of pure naphthalene crytal 2 microns thick. The black and transparent refer to the 0.5 micron naphthalene crystal tracings. The first and fourth spectra demonstrate the similarity between the mixed crystal c' spectrum and the pure crystal spectrum, and the absence of much correlation with the mixed crystal b-spectrum. The mixed crystal spectra are shifted to the red by 10 cm^{-1}. The fifth spectrum is included to show the a-polarized component of the 0—0 band, which cannot be observed in 0.5 micron crystals, and to show the splitting of the 702 band.

for the 0—0 band components to be discussed presently) in the pure crystal spectrum not accounted for in this way, but this peak and its associated structure coincides approximately with the weak peaks at 702, 747, and 794 cm^{-1} in the b-spectrum of the mixed crystal. A shoulder in the pure crystal spectrum is also explained as the 987 peak in the b-mixed crystal spectrum. The agreement is not always exact, but is usually within 5 cm^{-1}. The two peaks in the pure crystal spectrum which are completely polarized are 31 476 (a-polarized) and 31 642 (b-polarized). We have already interpreted these as the two components of the 0—0 band, split apart by the intermolecular resonance in the crystal.[1] The 0—0 band for the vibrational analysis must be taken as 31 544, as we have just seen from the use of the mixed crystal spectrum. This is not far from the average value, 31 559 cm^{-1}, of the two 0—0 band components. The splitting of the 0—0 band into two components 166 cm^{-1} apart is caused by intermolecular resonance, and will be further discussed in Sec. V.

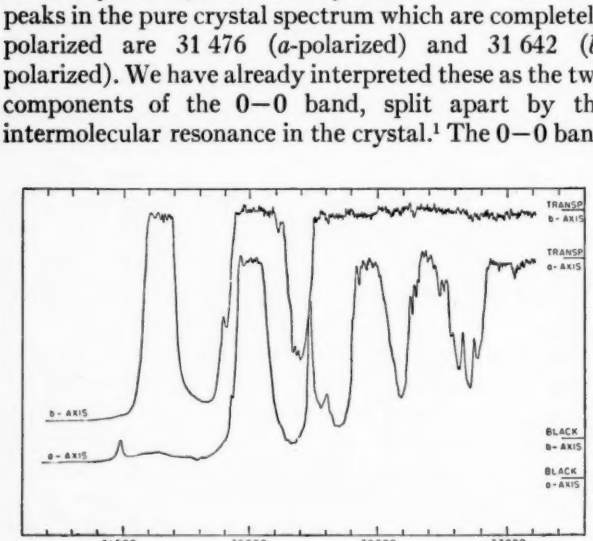

FIG. 2. Microphotometer tracing of the absorption spectrum at 20°K of a 2.0 micron naphthalene crystal. Part of the a-polarized spectrum of this crystal was also shown in Fig. 1.

The exact value to take for the 0—0 band for vibrational analysis is somewhat arbitrary, as perfect agreement with any choice is never obtained. The value 31 544 gives nearly exact agreement for the intervals 0–433; 0–433+987; 0–987; 0–905+987; and 433+502 +987. Except for 0–987, these are among the strongest peaks in the spectrum. The disagreements between observed peaks and peaks calculated from the analysis using 31 544 involve in three cases the 702 frequency. This recalls the fact that the worst disagreements in the mixed crystal spectrum always involved this frequency. Evidently it is strongly affected by perturbations of some kind. The peaks at 32 236 a-polarized and 32 275 b-polarized are the only moderately strong peaks except for the 0—0 band components which are definitely confined to one polarization. They are 692 and 731 cm^{-1} from the 0—0 band, 31 544 cm^{-1}. We believe they correspond to the 702 cm^{-1} frequency split by intermolecular resonance in the crystal. If our interpretation is correct, this is the only vibronic level of the third region which is appreciably split, and is further evidence that the 702 cm^{-1} mode is especially sensitive to

TABLE I. Column 1 gives the frequency in wave numbers of the absorption bands observed at 20°K in the polarized spectrum of the *ab* plane. The intensity column gives the intensity along each axis: note that the crystal thickness given in the next column must be taken into account in interpreting the intensity given. The frequencies reported by Prikhotjko (reference 6) are given for comparison with ours. The vibrational analysis is made on the basis of the c' spectrum of naphthalene in durene, and these frequencies with 10 cm^{-1} subtracted from them are listed for comparison with the pure crystal frequencies. A few of the frequencies listed here are for the *b*-axis of the mixed crystal.

Frequency cm^{-1}	Intensity *a*	Intensity *b*	Remarks	Frequency (Prikhotjko)[6]	Frequency in mixed crystal minus 10 cm^{-1}	Vibrational assignments
29 945			2 mm crystal	29 945		
31 062	w	m	23μ crystal	31 059		
31 476	w	o	1.9μ crystal	31 476	31 544	$a(0-0)$ $b(0-0)$ 0−0
31 642	o	vs	0.5μ crystal	31 636		
31 889	o	m	1.9μ Shoulder on strong band			
31 921	m	?	1.9μ Shoulder on strong band			
31 976	s	vs	0.5μ	31 960, 31 999, 32 026	31 977	433
32 122	w	s	1.9μ	32 118		
32 154	o	w	1.9μ	32 154		
32 170	o	w	1.9μ	32 174		
32 236	s	o	1.9μ	32 229, 32 255	32 244	$702\binom{692}{731}$
32 275	o	m	0.5μ	32 274		
32 298	w	m	1.9μ for *a*, 0.5μ for *b*	32 293, 32 303, 32 319, 32 333	32 291	747
32 353	o	w	0.5μ	32 346, 32 373	32 238, 32 258	794; 814
32 375	m	?	1.9μ Shoulder on strong band	32 385		
32 397	s	o	1.9μ	32 396		
32 420	s	m	1.9μ *a*, 0.5μ *b*. Step-out on strong band	32 412		
32 432	w	s	0.5μ } Peak not well resolved	32 430, 32 448	32 449	905
32 466	w	s	0.5μ }	32 462	32 476	433+502
32 495	w	s	0.5μ }	32 492		
32 535	w	m	0.5μ Shoulder on previous bands	32 537, 32 574, 32 595	32 531	987
32 621	m	?	1.9μ for *a*, 0.5μ for *b*	32 619		
32 640	m	w	1.9μ for *a*, 0.5μ for *b*	32 649		
32 690	m	vs	0.5μ	32 676	32 679, 32 689	433+702; 1145
32 710	?	m	0.5μ Poorly resolved shoulder	32 701, 32 718		
32 750	s	w	1.9μ for *a*, 0.5μ for *b*	32 747	32 745	502+702
32 772	s	w	1.9μ for *a*, 0.5μ for *b*	32 767		
32 794	w	?	1.9μ	32 786, 32 792, 32 807		502+747?
32 835	w	vw	1.9μ for *a*, 0.5μ for *b*	32 831, 32 862	32 840	502+794
32 880	w	vw	1.9μ for *a*, 0.5μ for *b*	32 876, 32 909		
32 962	m	vs	0.5μ	32 948, 32 958, 32 971	32 962, 32 973	433+987; 1429
32 990	w	vs	0.5μ }	32 983		
33 015	vs	s	0.5μ }	33 000, 33 013		
33 043	vw	s	0.5μ } Poorly resolved structure	33 029, 33 035	33 032	502+987?
33 060	vw	m	0.5μ }	33 055		
33 080	vw	w	0.5μ }	33 070, 33 089		
33 105	m	m	0.5μ } Step-outs on 33 127-not well resolved	33 103		
33 118	m	m	0.5μ }			
33 127	m	s	0.5μ	33 130	33 121	433+1145
33 149	m	s	0.5μ	33 151	33 156	905+702
33 163	m	s	0.5μ	33 167		
33 179	m	s	0.5μ	33 177		
33 204	w	w	0.5μ Poorly resolved shoulder	33 200		
33 220	w	w	0.5μ Poorly resolved shoulder	33 221		
33 243	vw	w	0.5μ	33 240		
33 257	vw	w	0.5μ	33 264, 33 289		
33 310	vvw	vw	0.5μ	33 301, 33 325, 33 337, 33 351		
33 366	w	m	0.5μ	33 369, 33 390	33 364, 33 387	433+1386; 433+2×702
33 412	m		0.5μ Broad peak in *b*. } Step-outs in *a*	33 413	33 406	433+1429
33 428	m		0.5μ }	33 428	33 430	502+1386?
33 441	s		0.5μ }	33 445	33 436	905+987
33 456	vs		0.5μ Max. in *b*. Max. in *a*		33 463	433+502+987
33 481	s		0.5μ } Shoulders in *a*	33 471, 33 500	33 482, 33 475	1938; 502+1429
33 518	w		0.5μ }		33 518	2×987
33 542	o	w	0.5μ	33 536		

perturbations from the crystal lattice. The one-quantum value of the 905 frequency in the pure crystal is 888 cm^{-1}. The two strong combinations involving this mode are best explained using the value 905 cm^{-1}. The weak line 32 948 reported by Prikhotjko could be 905+500. It is not observed in the mixed crystal spectrum but is calculated to lie at 32 949. The value of the 702 frequency to use in combinations cannot be determined with any accuracy. The 905+702 fits well, but 433+702 is 11 cm^{-1} below our measured peak. The 433+2×702 was a strong peak in the mixed crystal spectrum, but 6 cm^{-1} above the calculated position; in the pure crystal only a weak line reported by Prikhotjko appears near the calculated frequency 33 381, but a strong step-

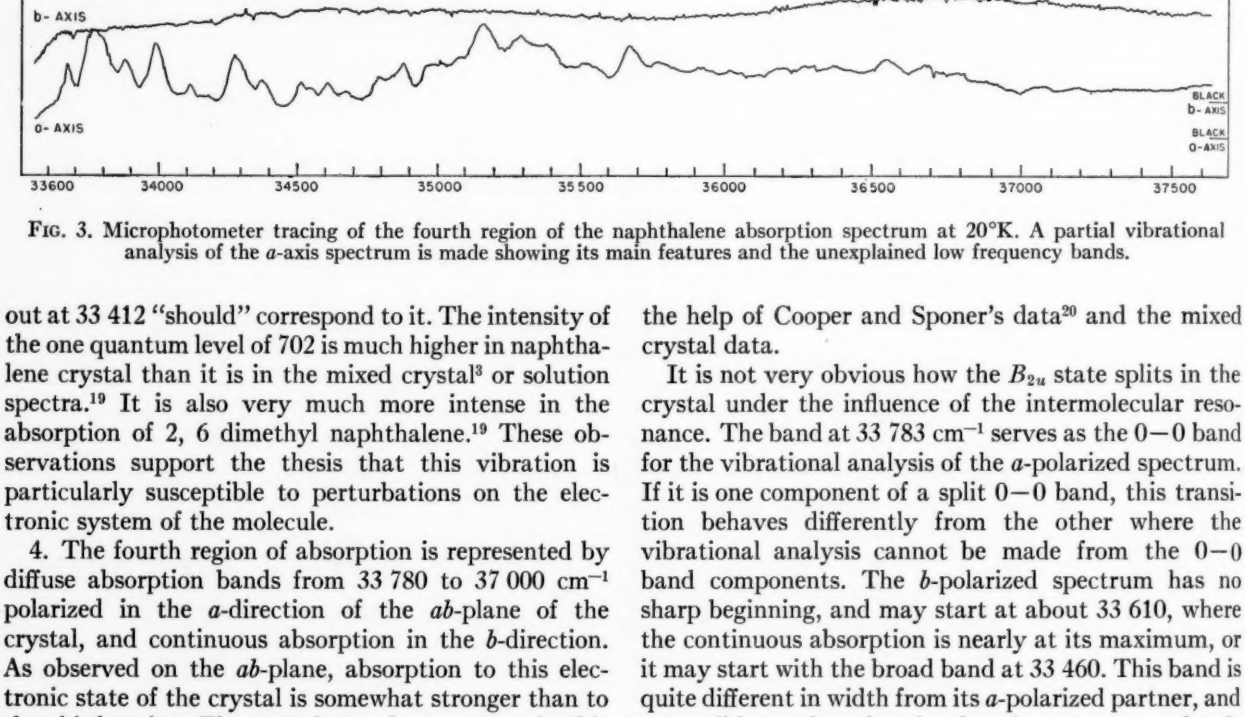

FIG. 3. Microphotometer tracing of the fourth region of the naphthalene absorption spectrum at 20°K. A partial vibrational analysis of the *a*-axis spectrum is made showing its main features and the unexplained low frequency bands.

out at 33 412 "should" correspond to it. The intensity of the one quantum level of 702 is much higher in naphthalene crystal than it is in the mixed crystal[3] or solution spectra.[19] It is also very much more intense in the absorption of 2, 6 dimethyl naphthalene.[19] These observations support the thesis that this vibration is particularly susceptible to perturbations on the electronic system of the molecule.

4. The fourth region of absorption is represented by diffuse absorption bands from 33 780 to 37 000 cm^{-1} polarized in the *a*-direction of the *ab*-plane of the crystal, and continuous absorption in the *b*-direction. As observed on the *ab*-plane, absorption to this electronic state of the crystal is somewhat stronger than to the third region. Figure 3 shows the spectrum in this region. If the strong band at 33 783 is taken as the *a*-polarized 0—0 band, the strongest bands of the spectrum can be explained as combinations of upper state frequencies 510 and 1400. If 510 is the analog of 512 in the ground state, then since it would be the lowest totally symmetric frequency of the upper state, there should be no bands between 0 and 0+510 since the spectrum is observed at 20°K. There are four bands of weak to medium intensity, however. They could correspond to nontotally symmetric vibrational modes of the $^1B_{2u}$ state caused to appear in the spectrum by environmental perturbations or by interaction with the higher vibrational bands of the B_{3u} state. It is also possible that they are vibrational levels of the B_{3u} state.

The spectrum of naphthalene in durene can be observed in this region for 1300 cm^{-1} before the durene absorption interferes. The spectra of pure and mixed crystal are not very much alike in this region. Most of the dissimilarity is in the position and relative intensity of the low-frequency bands. The mixed crystal, has 497 as one of the main repeating frequencies while the pure crystal has 510. These are close enough to be considered the same type of vibration. A detailed study of these bands can only be made with the help of the vapor spectrum. This will be carried out in another place with the help of Cooper and Sponer's data[20] and the mixed crystal data.

It is not very obvious how the B_{2u} state splits in the crystal under the influence of the intermolecular resonance. The band at 33 783 cm^{-1} serves as the 0—0 band for the vibrational analysis of the *a*-polarized spectrum. If it is one component of a split 0—0 band, this transition behaves differently from the other where the vibrational analysis cannot be made from the 0—0 band components. The *b*-polarized spectrum has no sharp beginning, and may start at about 33 610, where the continuous absorption is nearly at its maximum, or it may start with the broad band at 33 460. This band is quite different in width from its *a*-polarized partner, and a possible explanation is that it represents the *b*-component of the 0—0 band. The two possible splitting values are thus about 170 and 320 cm^{-1}.

IV. THE FLUORESCENCE SPECTRUM

The fluorescence spectrum of the crystal at 20°K has been reported in great detail by Obreimov and Shabaldas,[9] so that there is no need to report our measurements, which agreed in almost every detail with theirs. We do, however, present a tracing of the fluorescence in Fig. 4 in order to show its main features. Only one polarization is shown since the *a*- and *b*-polarized spectra are identical except for intensity at or below 31 062 cm^{-1}. The *b*-spectrum is about twice as intense as the *a*-spectrum. The 31 062 band coincides with the absorption band discussed in Sec. III-2, and is the origin upon which a vibrational analysis of the fluorescence can be based.

There are bands at higher frequencies, however, many of which were reported by Obreimov and Shabaldas. The 31 463 band is entirely *a*-polarized and nearly coincides with the *a*-component of the 0—0 band, 31 476. The frequency shift is probably caused by reabsorption, and we will assume that the upper state of the fluorescence and absorption band is the same.

In order to see if the interval 31 062–31 463, 401 cm^{-1},

[19] McConnell and McClure, J. Chem. Phys. **21**, 1296 (1953).

[20] C. D. Cooper and H. Sponer, J. Chem. Phys. **23**, 646 (1955).

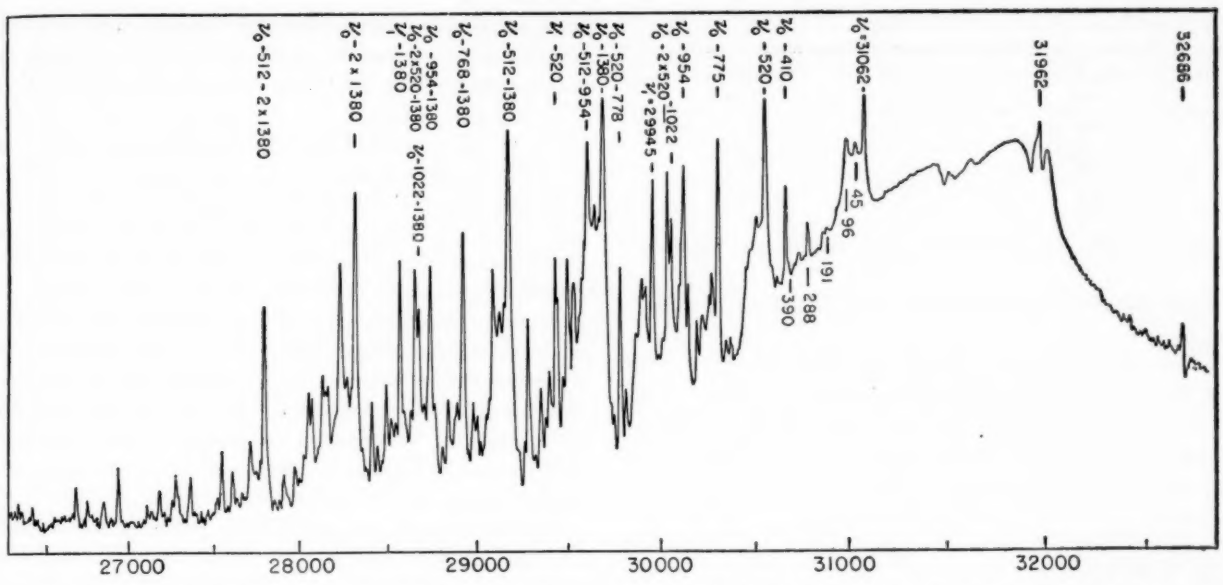

FIG. 4. The fluorescence from the *ab* plane of naphthalene at 20°K, polarized along the *b*-axis. The *a*-polarized spectrum is the same, but of lower intensity at and below 31062 cm^{-1}. The 31485 line appears only in the *a*-polarized spectrum. The exciting light was the 3125 A group from the high-pressure mercury arc, and a considerable amount of scattered light is evident in the high-frequency portion of the tracing. Some of the reflection lines can be seen on this scattered background, *viz.*, 31962 and 32686 cm^{-1}.

has its origin in vibrational or electronic effects, the fluorescence of a $C_{10}D_8$ crystal was photographed. This crystal had appreciable amounts of the two $C_{10}D_7H$ species; perhaps as much as 20%. The polarized band which appears to be the analog of 31 463 is at 31 582 cm^{-1}. The analog of 31 062 is either 31 154, a very strong band or 31 169, a much weaker band. The former could be the emission from the isotopic impurities, since internal conversion would tend to excite them rather than the host crystal whose transition energy is a little higher. The two possible frequency differences are therefore 428 and 413 cm^{-1}. In either case the deuteration shift is in the wrong direction for a vibrational interval, and we must conclude that the interval is electronic in origin.

The 31 463 band cannot be seen in Fig. 4 because of the background of exciting light near the beginning of the spectrum. The 3126–3131 A region of the high pressure mercury arc was used. If higher frequency excitation is used, this band is clearly seen polarized along the *a*-axis. We are using Fig. 4 to show some of the other high-frequency bands reported by Obreimov and Shabaldas, for which they had no interpretation. They reported a double line 31 960–31 965 cm^{-1} appearing between the 3126 and 3131 A mercury lines used for excitation. In Fig. 4 this "band" is seen as an emission line at the low-frequency edge of an absorption line. Several other features having this contour were found on the continuous scattered background of the mercury arc, but are not reported by Obreimov and Shabaldas. The prominent 32 686 band can be seen in Fig. 4. Others were 32 419 (vw); 32 951 (m); 33 104 (w); 33 153 (w). From the list of absorption frequencies in Table I, it can be seen that these bands fall at the red edge of each of the strongest absorption bands of the spectrum. Since there are no fluorescence bands which form progressions to the red of these, the crystal always returns to the ground state after excitation to the members of this system of levels. This probably means that the emitted light is coherent with the absorbed light: in other words, the emission is a resonance fluorescence or selective reflection process. Some qualitative observations on the angular dependence and polarization confirm this conclusion. This type of spectrum could be useful for studying absorption spectra of crystals too thick for an ordinary absorption study.

Our vibrational analysis of the fluorescence spectrum does not differ in any major respect from that of Obreimov and Shabaldas. It is of interest, however, to compare the fluorescence spectrum with the recent assignment of the Raman spectrum,[21] and to point out some effects of the crystal on the vibration frequencies.

The strongest lines in the spectrum are caused by the 1384 and 520 a_g frequencies, both of which form strong progressions based on 31 062. Also prominent are the a_g frequencies 775, 954, and 1022. Weak lines at 1240 and 1573 which appeared on one overexposed fluorescence plate may correspond to the 1240 and 1575 a_g frequencies. The first was not reported by Obreimov and Shabaldas, and the interpretation of the second as a fundamental was considered doubtful. The 3001 a_g C—H stretching frequency was extremely weak if present at all, but a frequency at 3058 (another C—H stretch) is present on our plates and is reported by Obreimov and Shabaldas. (An alternative assignment

[21] McClellan and Pimentel, J. Chem. Phys. **23**, 245 (1955).

TABLE II.

Pure crystal	Raman of liquid	Mixed crystal
520	512	509
775	762	760
954	943	938
1024	1024	1024
1384	1379	1378

given by them for this line, $2\times1382+294$, could be correct.)

The low-frequency bands 191 and 288 cm^{-1} from 31 062 are especially interesting from the point of view of the assignment of ground-state frequencies. It was not known whether the Raman lines corresponding to both of these frequencies were truly fundamentals or were caused by impurities, since not many investigators had reported them. An impurity, however, would not have the same fluorescence level as the naphthalene crystal, so that the appearance of these bands in the low-temperature fluorescence spectrum must be taken as evidence that they actually are naphthalene vibrations, and possibly fundamentals. Another possible explanation of them is that they are overtones of the lattice mode 96 cm^{-1}, but this does not seem tenable since 288 is stronger than 191. In the fluorescence of naphthalene *d*-8, the analogous bands are present at 170 and 264 cm^{-1}. These are close to the Raman lines 180 and 270 supposedly associated with 191 and 288.[21]

Other nontotally symmetric frequencies also appear in the fluorescence. A very weak line at 390 in ordinary and 340 in heavy naphthalene fluorescence also appears in the Raman spectrum and has been assigned to the b_{3g} class. A much stronger band in fluorescence, 406 (395 in *d*-8) is not assigned to a fundamental frequency. None of these lines appeared in the fluorescence spectrum of naphthalene in durene. There are several other lines in the fluorescence spectrum which can be interpreted as nontotally symmetric vibrations, but it is almost always possible, as Obreimov and Shabaldas have done, to interpret them as lattice additions to stronger lines. It is important, however, that no lines due to *u*-vibrations appear in the spectrum. The environment which causes the appearance of the nontotally symmetric *g*-modes is unable to induce the appearance of *u*-modes.

The effects of the crystal on the fluorescence spectrum are observably manifested in four ways: appearance of lattice vibrations; change in molecular vibration frequencies; factor group splitting of vibration frequencies; and introduction of vibronic transitions forbidden by the free molecule selection rules.

The lattice vibrations measured on our plates were strongest at the 31 062 line, but were identifiable after 520 and 1384 additions. We measured them to be 45 and 96 cm^{-1}, whereas Obreimov and Shabaldas report 15, 46, and 103. In the fluorescence of the mixed crystal 39 and 98 are found.[4] It is possible to interpret many lines as combinations with lattice modes, and a vibrational analysis is thereby made rather difficult. They are only surely present, however, in the strong combinations with 520 and 1384.

There are definite differences between the molecular vibration frequencies as determined from the low temperature crystal fluorescence and from the Raman spectrum of the liquid.[21] We agree with Obreimov and Shabaldas on the best average frequencies to use in the fluorescence analysis to within 1 cm^{-1}. The comparison, including the mixed crystal data is given in Table II. The 1384 is an average value for the two components of this vibration in the crystal. An interesting result of the shift in the 512 frequency to 520 cm^{-1} is that the first overtone can be observed separated from the 1024 frequency. The latter appears to remain the same within 1 cm^{-1} in the three media.

In the one and two quantum appearances of 1384 in the fluorescence, the line was doubled. At the three quantum level the line was broad and faint, and it could not be determined if the line doubling occurred. Some of the combination lines involving 1384 were doubled, but no other lines were. The measurements of the 1384 series made on an especially good fluorescence plate of pure naphthalene, and on a fluorescence plate of naphthalene in durene (*ab*-plane) are given in Table III.

Since the splitting is absent in the mixed crystal, we suppose that in the pure crystal it represents the factor group splitting of the vibrational level, i.e., mechanical coupling between molecular vibrations in different molecules. This would also explain the intensity difference between the two components in the one quantum level, since one component belongs to A_g, the other to B_g of the factor group. The largest dichroic splitting observed by Pimentel and McClellan[22] was about 8 cm^{-1}, for the 779 cm^{-1} band.

V. DISCUSSION

The gross features of the spectra are in accord with the predictions of the exciton theory of a molecular crystal, such as the treatment given by Davydov.[14] Both transitions are displaced and both are split into two. Some of the parameters of the exciton theory can be obtained from the spectra. But there are a number of

TABLE III.

v	ν cm^{-1}, pure crystal	ν cm^{-1}, mixed crystal	Interval Pure	Interval Mixed	Splitting
0	3 1060.8 (vs)	3 1551.6	0	0	
1	2 9681.2 (s) 2 9673.0 (vs)	3 0174.2	1379.6 1387.8	1377.4	8.2
2	2 8294.9 (s) 2 8288.7 (s)	2 8799.0	2765.9 2772.1	2752.6	6.2
3	2 6918.1 (m)	2 7427.1	4142.7	4124.5	

[22] Pimentel and McClellan, J. Chem. Phys. **20**, 276 (1952).

details not considered by present theory or actually at variance with it.

The factor group representations of the crystal can be used to classify the electronic states of the crystal for states in the neighborhood of $k=0$ where k is the wavenumber vector, and specifies the phase relations between unit cells. The character table for this group, isomorphous with C_{2h}, is shown in Table IV (see Davydov)[14]. The operations of this group interchange molecules in the unit cell and perform the corresponding point operations on the molecules as well. The crystal wave functions for $k=0$ can be written in terms of the sum (α states) or difference (β states) of the wave functions for the two molecules of a unit cell.[14] For a molecular wave function B_{2u}, the α state belongs to A_u of the factor group, and the β state to B_u. For a molecular B_{3u} state the α state belongs to B_u, the β to A_u.

The exciton theory gives the transition energies of the two component states as:

$$E_i^{\pm}=E_i^0+\Delta D_i\pm\epsilon,$$

where E_i^0 is the transition energy in the free molecule, ΔD_i is the shift of the center of gravity of the two states from the free molecule and 2ϵ is the factor group splitting, so called because the two states E_i^+ and E_i^- belong to different factor group representations. One is an α, the other a β state. The quantity ΔD_i includes band displacement terms arising both from excitation exchange and coulomb interaction between neighboring molecules.

Our original suggestion[1] that the bands at 31 476 cm^{-1} (a-polarized) and 31 642 cm^{-1} (b-polarized) are the components of the 0—0 band belonging to the first singlet state of the molecule still seems the best interpretation. We have abandoned the idea put forward earlier[1] that 31 062 is one component of the 0—0 band of the next higher molecular state. The splitting of this state in the crystal is not clearly observable, but seems to be one of the two possibilities mentioned in Sec. III, part 4. Table V gives the values of the parameters in the above equation for the two excited states, following the present interpretation.

The relative intensities of absorption in the two polarizations give important clues as to the transition mechanism. On the basis of the exciton theory, intensities are calculated to a first approximation by taking a certain vector sum of the transition moments of individual molecules and then squaring the result. The individual moment vectors are combined in a way determined by the representations of the factor group. For naphthalene crystal, this amounts simply to taking the sum and difference of the moments of the two molecules of the unit cell: $M=(M_1\pm M_2)$. The upper sign corresponds to the transition to an α state of the crystal, the lower to a β state. One of these crystal transitions is always b-polarized, and the other lies in the ac-plane. The actual results of this procedure are the same as for the "oriented gas" model, i.e., the theory of oriented but noninteracting molecules.

The intensity ratio was measured at room temperature by Craig and Lyons.[2] At this temperature, few details are resolved and the results refer to the average polarization throughout the region. For the 31 500 to 33 000 cm^{-1} region they found, on the ab-plane, $I_b/I_c=4.5-5:1$. This is somewhat below the exciton theory prediction for the $A_g\rightarrow B_{2u}$ transition. We do not think that this is evidence favoring this assignment, since B_{3u} seems to be well supported by the mixed crystal work.[3] Rather it seems to support the conclusion reached on the basis of the mixed crystal work that most of the $A_g\rightarrow B_{3u}$ transition intensity comes from the B_{2u} state via vibrational-electronic interaction.

When the intensity ratio is observed in the 20°K spectra, some important differences appear, though most of the vibronic levels still have the same polarization ratio as at the higher temperatures. The most striking of these differences is in the 0—0 band ratio, where the b-polarized 0—0 band is hundreds of times stronger than the a-polarized component. The b-polarized component has about the same intensity as the other strong bands in the b-spectrum, and it is the a-component which is abnormally weak. For a $A_g\rightarrow B_{3u}$ transition the a-component should be 4.2 times as strong as the b-component on the basis of exciton theory. The only way we have seen to explain this reversal and to retain the B_{3u} assignment for the upper state is to suppose that the crystal induces a mixing of B_{2u} and B_{3u} states. This may happen, of course, because each of these states splits in the crystal into a A_u and a B_u state of the factor group, and the components having the same symmetry may mix. The calculation shows that an amplitude coefficient of the B_{2u} state in the B_{3u} state equal to 0.07 is enough to cancel out the a-polarized component and to intensify the b-polarized component such that agreement with experiment is obtained. The

TABLE V. Effects of the crystal on the electronic transitions in the naphthalene molecule.

Electronic upper state	O—O band, cm^{-1} crystal a	crystal b	gas	F. G. splitting, cm^{-1}	Band shift, cm^{-1}
B_{3u}	31476	31642	32021	166	462
B_{2u}	33783	33610 or 33460	35910	170 or 320	2210 or 2290

TABLE IV. C_2^b=twofold screw axis about b crystal axis. σ^{ac}=glide plane, ac crystal plane. i=inversion. r_a, r_b, r_c=translation along a-, b-, or c-axis.

	I	C_2^b	σ^{ac}	i	
A_g	1	1	1	1	
A_u	1	1	−1	−1	r_b
B_g	1	−1	−1	1	
B_u	1	−1	1	−1	r_a, r_c

calculation is worked out in detail in Appendix 1. The matrix element of the mixing has also been estimated independently, and the value obtained is in good agreement with the one demanded by our calculation.[23] This mixing has practically no effect on the 0—0 band splitting or on the intensity of the vibrating levels of the excited state. It seems therefore, that in spite of appearances to the contrary, it is possible to retain the B_{3u} assignment. On this interpretation the spectral features in the pure crystal absorption are determined more by crystal perturbations and vibrational-electronic interaction than by the directly permitted electronic mechanism.

We observed the absorption spectrum of the third and fourth regions in crystals of the same thickness, viz. about 0.5μ. The fourth region appeared only slightly more intensely absorbing than the third. Yet in the mixed crystal spectra, it was necessary to dilute the crystals by a factor of ten to observe the peaks of the second transition (corresponding to the 4th absorption region of the crystal). This cannot be due to the orientation of the transition moment, since it is mainly along the short molecular axis in both transitions when the molecules are in the crystal. It may be therefore that the $A_g \rightarrow B_{2u}$ transition in the crystal is actually weaker than the free molecule transition by a factor of about five. The absolute intensity of the first transition seems to be the same as in solution. It would be interesting to have quantitative measurements of absorption intensity in a number of crystals. Craig[24] has discussed this phenomenon in some other molecular crystals.

The polarization ratio I_b/I_a in the fourth absorption region of the crystal is 2–3:1, according to Craig.[24] Our qualitative observations at 20°K are in agreement with this. This ratio does not agree with exciton theory predictions for either B_{2u} or B_{3u} excited states; probably the anomalously low intensity in this region is connected with this disagreement. There is also the fact that the *b*-spectrum is almost entirely structureless and the *a*-spectrum has very broad bands. All these facts suggest that the molecular interactions in the crystal are much stronger in the fourth than in the third regions, but as yet, no adequate explanation of them can be offered.

The vibrational levels of the excited electronic states of a molecule in the crystal are not subjected to the same perturbations as the vibrationless level. So far as we are aware, there has been no comprehensive theoretical study of this problem, but Winston[15] has suggested a method of attack on it. At any rate, it is clear from the structure of the spectra that there is almost no factor group splitting whatever among the vibronic levels of the $^1B_{3u}$ state. The only possible exception to this is the 702 cm^{-1} vibration, which, if our interpretation is correct is split by 42 cm^{-1}. This vibration behaved in an unusual way in the mixed crystal spectrum and some common explanation is suggested. The lack of splitting in the other vibrational levels of the B_{3u} state might be simply explained by saying that the vibration is essentially a localized molecular motion, and that energy transfer, and the consequent removal of the exchange degeneracy, cannot occur without at the same time transferring a vibrational quantum to a neighboring molecule. The Franck-Condon principle will permit this only for certain favorable positions and momenta of the nuclei, and therefore, since these configurations are relatively rare, the energy transfer probability is small. A suggestion as to how this may be worked out is given in Appendix 2. In the B_{2u} state, however, a vibrational progression is built on what we think is a component of the 0—0 band.

In their study of the spectrum of the benzene crystal Broude, Medvedew and Prikhotjko[10] observed a series of bands analogous to the ones we have observed in naphthalene, but in addition a weak polarized series of the 928 cm^{-1} progression built on each component of the 0—0 band. It is possible that such a weak series occurs in the third region naphthalene spectrum, but we did not observe it. These results for benzene show, however, that both kinds of vibrational additions occur, and the B_{2u} system of naphthalene (fourth region) is to be considered as an example of the second type, built on the 0—0 band components. We have suggested an explanation for progressions of the first type in Appendix 2. Perhaps the qualitative explanation of the progressions of the second type is that when the electronic state is characteristic of the crystal as a whole, the molecular vibrations are no longer strictly localized, but can more properly be described as branches of the lattice vibration distribution. They should no longer be sharp energy levels in this case. This may explain in part the breadth of the bands in the *a*-polarized B_{2u} absorption. Even in the vapor, however, these bands seem to be diffuse.

Some comment on the vibrational analysis of the third region is necessary. Several of the bands in the crystal spectrum are considered to correspond to bands found in the long axis spectrum of the mixed crystal. They are 702 (split), 987, and 1429, the last two being the strongest bands of the long axis spectrum. If the assignment is correct, these bands would be expected to have a polarization different from the others, unless there is some further effect of the crystal which we haven't considered. The assignments appear to be the only ones consistent with the band energy, but we cannot explain their polarization.

We have already noted that the fluorescence spectrum is not highly polarized except for the 31 463 *a*-polarized band. The ratio of *a*- to *b*-intensity is not in agreement with exciton theory predictions of the intensity ratio for any symmetry assignment of the excited state. The surprising fact is that the fluorescence origin 31 062 coincides with a very weak absorption band which apparently has no simple or obvious relation to the rest of

[23] O. Schnepp and D. Fox, unpublished work.
[24] D. P. Craig, Revs. Pure and Appl. Chem. (Australia) 3, 207 (1953).

the absorption spectrum. One might have expected that all the fluorescence at low temperatures would originate from 31 463, and that at higher temperatures the other 0−0 band component 31 642 would begin to emit. We might also have expected that the 31 463 band would serve as origin of progressions in ground-state vibrations, yet not only are there no other fluorescence lines having similar polarization, it also seems impossible to fit any bands into the expected progressions. This indicates that the *a*-polarized component of the 0−0 band (and by inference the other component) corresponds to a nonlocalized state of the crystal rather than a localized molecular level. This interpretation is also that of the exciton theory which we have already used to explain the existence of these levels.

Fluorescence originates from 31 062 because of internal conversion from 31 463 and higher levels. This is a slow process compared to most internal conversion processes. We might estimate the lifetime of the 31 463 level to lie in the vicinity of 0.1 to 1 μsec. The internal conversion to 31 062 must have a half time not much shorter than this, since otherwise no radiation would come from 31 463. In the vibrational cascade from one electronic state of a molecule to a lower one, the internal conversion rate must have a half time on the order of a $\mu\mu$sec. In the crystal, it is necessary for electronic energy to be transferred to the lattice, and this, apparently, is a much less efficient process than transfer of electronic energy to molecular vibrations.

We have no adequate interpretation of the 31 062 level. There are strong objections to considering it to be the lowest level of the exciton band in the crystal. In the first place, it would imply a band width of about 600 cm^{-1}, which seems much too high. And in the second place, a band occurring in violation of translational selection rules, as a "forbidden level" must, would not be expected to be sharper than the 31 463, 31 642 levels which presumably correspond to $k=0$. One argument favors the idea that it belongs to the band. We have already shown that the separation of 31 062 from 31 463 is essentially unchanged by deuteration, so that there seems to be some relationship between them which is electronic in nature.

Another possibility is the defect or impurity level. The distinct presence of factor group splitting in the 1384 vibration suggests some measure of crystal perfection in the vicinity of an emitter, however. The absence of *u*-vibrations suggests that C_i selection rules (site group rules) are strictly obeyed; they would be violated to some degree in the presence of a defect or impurity. We used crystals of very high chemical purity and found the same absorption and emission bands as have been reported by others, so a chemical impurity seems out of the question.

Conclusions

We think we have demonstrated several important facts about the naphthalene crystal, which are probably true in some measure for a large number of organic crystals. In the first place, the "oriented gas" model does not give a good account of the polarizations, and the exciton theory of a stationary lattice yields the same result. In the case of the ${}^1A_{1g}-{}^1B_{3u}$ transition, it is hard to separate the effects of the site perturbation upon the peculiar upper state from the effects of intermolecular energy transfer. Naphthalene is probably atypical in this respect. In the next transition, molecular and lattice motion is so important that exciton theory in its present form cannot be expected to give a very good account of the phenomena observed. Interaction between the two upper states seems certainly to occur, and its magnitude has been estimated. The evidence for factor group splitting of the ${}^1B_{3u}$ state seems quite clear, yet the exciton band structure cannot be considered as understood until the 31 062 band is explained.

APPENDIX 1

Calculation of the interaction between B_{3u} and B_{2u} states in the naphthalene crystal.

a. The Wave Functions

Table VI gives the starting wave functions (for $k=0$) and the exciton theory intensity for transitions from the ground state in terms of free molecule intensity. In this table, n is a three index symbol and designates the translationally equivalent molecules of, say set 1, and i represents the translationally equivalent molecules of set 2, there being two molecules per unit cell.

$$\phi_n{}^2=\prod_a{}^{2N}{}'\psi_a{}^1\cdot\psi_n{}^2 \quad \text{and} \quad \phi_n{}^3=\prod_a{}^{2N}{}'\psi_a{}^2\psi_n{}^3,$$

where the continued product is taken over all molecules of the crystal, and all but the nth is in its ground state. The ground state is indicated by the superscript 1, the B_{2u} state by 2 and the B_{3u} state by 3. The ϕ_n should be antisymmetrized, but we shall assume for simplicity that no electron exchange occurs.

TABLE VI.

Symmetry Molecular	Symmetry Factor group	Intensity a-axis	Intensity b-axis	
B_{3u}	$A_u(\beta)$	0	0.045	$\frac{1}{\sqrt{2N}}[\sum_n \phi_n{}^3-\sum_i \phi_i{}^3]=\psi_A{}^{03}$
B_{3u}	$B_u(\alpha)$	0.19	0	$\frac{1}{\sqrt{2N}}[\sum_n \phi_n{}^3+\sum_i \phi_i{}^3]=\psi_B{}^{03}$
B_{2u}	$A_u(\alpha)$	0	0.76	$\frac{1}{\sqrt{2N}}[\sum_n \phi_n{}^2+\sum_i \phi_i{}^2]=\psi_A{}^{02}$
B_{2u}	$B_u(\beta)$	0.1025	0	$\frac{1}{\sqrt{2N}}[\sum_n \phi_n{}^2-\sum_i \phi_i{}^2]=\psi_B{}^{02}$

To use second-order perturbation theory, the wave functions corrected to the first order are needed:

$$\psi_A{}^3=\psi_A{}^{03}+\frac{\int\psi_A{}^{03}H'\psi_A{}^{02}}{E_3{}^0-E_2{}^0}\psi_A{}^{02}\text{ etc.}$$

The integral representing the energy of interaction $H_{32}{}^A$ can be written out in terms of the wave functions given, and neglecting all interactions except nearest neighbor interactions one finds,

$$H_{32}{}^A=\sum_n\sum_i(\phi_n{}^3|H'|\phi_i{}^2)-\sum_n\sum_i(\phi_i{}^3|H'|\phi_n{}^2)=-X.$$

Similarly it can be seen that $H_{32}{}^B=X$. Now we abbreviate by letting $y=-X/(E_3{}^0-E_2{}^0)$ and write down the perturbed wave functions to first order:

$$\psi_A{}^3=\psi_A{}^{03}+y\psi_A{}^{02},$$
$$\psi_B{}^3=\psi_B{}^{03}-y\psi_B{}^{02},$$
$$\psi_A{}^2=\psi_A{}^{03}-y\psi_A{}^{03},$$
$$\psi_B{}^2=\psi_B{}^{02}+y\psi_B{}^{03}.$$

b. The Intensities

The electric moments for transitions from the ground state are:

$$M_A{}^{(3)}=M_A{}^{03}+yM_A{}^{02},\quad M_A{}^{(2)}=M_A{}^{02}-yM_A{}^{03},$$
$$M_B{}^{(3)}=M_B{}^{03}-yM_B{}^{02},\quad M_B{}^{(2)}=M_B{}^{02}+yM_B{}^{03}.$$

The $(M_A{}^{03})^2$ etc. are proportional to the entries in the table of part a. In the free molecule, the B_{2u} transition is 90 times as intense as the B_{3u} transition.[25] But according to an estimate made elsewhere,[3] this ratio for the purely electronic portions of the intensity must be about four times as great. We therefore take $M^{02}/M^{03}=20$. From this and the data in the table:

$$\frac{M_A{}^{(3)}}{M_B{}^{(3)}}=\frac{0.183+17.5y}{0.436-\ 6.4y};\quad\frac{M_A{}^{(2)}}{M_B{}^{(2)}}=\frac{17.5-0.183y}{6.4+0.436y}.$$

Although the f-numbers for the entire electronic components of the free-molecule transitions have been used, this calculation applies only to the components of the 0—0 band of the crystal spectrum. The form of the first of these expressions shows that for positive values of y on the order of 0.05, the intensity of the b-polarized component of the B_{3u} transition, proportional to $(M_A{}^{(3)})^2$, will be much greater than that of the a-polarized component. The value 0.068 which makes the a-polarized component vanish, is close to the best value which could be used (in the absence of accurate intensity measurements). A direct theoretical estimate of y shows that this value is reasonable. If we use 0.0005 and 0.18 as the correct absolute f-numbers for the purely electronic parts of the B_{3u} and B_{2u} transitions, respectively, then the f-number for the purely electronic transition polarized in the b-direction of the naphthalene crystal can be calculated from the equation for $M_A{}^{(3)}$, and is 0.0008. This seems to be a reasonable value, and is high enough to account for the strong b-polarized component of the 0—0 band.

The intensity ratio for the B_{2u} transition even by this calculation should be only slightly below the value based on the oriented gas model. This is in the right direction, but experimentally the ratio is well below the oriented gas value. The weakly absorbing B_{3u} state would not be expected greatly to influence the absorption to B_{2u}. It may well be that other electronic states must be considered to mix appreciably with B_{2u}.

c. Factor Group Splitting

The factor group splitting is not greatly affected by the $B_{3u}-B_{2u}$ interaction. The distortion of the splitting is given by:

$$\Delta E^{(3)}=\Delta E_0{}^{(3)}+y^2\langle\Delta E\rangle_{Av},$$
$$\Delta E^{(2)}=\Delta E_0{}^{(2)}-y^2\langle\Delta E\rangle_{Av},$$

where $\langle\Delta E\rangle_{Av}$ is the average of the two splitting energies and $\Delta E_0{}^{(3)}$, $\Delta E_0{}^{(2)}$ are the values of the splitting in the absence of the interaction. Since $y^2\cong0.005$, the splitting is almost unaffected.

APPENDIX 2

Factor group splitting of vibrational levels of the B_{3u} state. If we assume that the A_u and B_u component wave functions of the B_{3u} state are the same as those in Appendix 1, except that the ϕ_n etc. apply to a vibronic state, then the factor group splitting is simply given by:

$$\Delta E=\frac{1}{N}\int(\sum_n\phi_n)V(\sum_i\phi_i)d\tau_e d\tau_n,$$

where V is the perturbing intermolecular potential, and the integration is over both electronic and nuclear coordinates. The sum over n is for molecules of set 1, and the one over i for molecules of set 2. Since for a given molecule there are four translationally nonequivalent molecules nearby (in the ab-plane), the above reduces approximately to

$$\Delta E=4\int\psi_1'\psi_2V\psi_2'\psi_1d\tau_e d\tau_n$$

(where the prime indicates an excited state). If V is independent of nuclear coordinates, as in a first approximation it must be, the integral over the vibronic wave functions $\chi_i{}^{(1)}$, etc., can be written, assuming

[25] Klevens and Platt, J. Chem. Phys. 17, 470 (1949).

product type functions:

$$\Delta E=\left\{4\int \Phi_{B_{3u}}{}^{(1)}\Phi_{A_g}{}^{(2)}V\Phi_{B_{3u}}{}^{(2)}\Phi_{A_g}{}^{(1)}d\tau_e\right\}$$
$$\times\int \chi_i{}^{(1)}\chi_0{}^{(1)}d\tau_n{}^{(1)}\int \chi_i{}^{(2)}\chi_0{}^{(2)}d\tau_n{}^{(2)}.$$

The first factor is the electronic factor group splitting of the 0−0 band. The two integrals over nuclear coordinates are, together, the square of the vibrational overlap between ground and excited molecular states. This is likely to be a very small quantity, and thus the factor group splitting of the vibronic level must be small.

THE JOURNAL OF CHEMICAL PHYSICS VOLUME 23, NUMBER 9 SEPTEMBER, 1955

Thermal Conductivities of Organic Vapor Mixtures

L. A. Bennett and R. G. Vines
C.S.I.R.O., Division of Tribophysics, University of Melbourne, Carlton, Australia
(Received December 28, 1954)

The thermal conductivities of binary mixtures of organic vapors have been investigated in the temperature range 60–125°C. When nonpolar vapors of similar viscosity and molecular weight are used, the variation of conductivity with composition of the mixture is roughly linear. Mixtures of nonpolar and strongly polar vapors, on the other hand, exhibit pronounced maxima in the conductivity *vs* composition curves. The difference in behavior is due to the strong interaction between polar molecules on collision.

I. INTRODUCTION

In a recent paper[1] measurements of the thermal conductivities of a large number of organic vapors were reported. It was shown that the results for both polar and nonpolar vapors can be interpreted in terms of an expression first proposed by Eucken[2]:

$$K^0=\frac{\eta}{M}[f_{\text{trans}}Cv_{\text{trans}}+f_{\text{int}}Cv_{\text{int}}], \qquad (1)$$

where K^0 is the thermal conductivity at zero pressure, η the viscosity, and M the molecular weight of the vapor. Cv_{trans} and Cv_{int} are the translational and "internal" (vibrational and rotational) components of the total molar heat-capacity at constant volume Cv_0, and f_{trans} and f_{int} are the corresponding transport factors for translational and internal energies.

For nonpolar substances values of f_{int} were calculated from the experimental results assuming[3] that $f_{\text{trans}}=2.5$, the value of the classical Chapman/Enskog transport factor. With both simple molecules[4] and organic vapors,[1] f_{int} increases with temperature towards a limiting value of ~1.3 at about 100–150°C. For polar vapors, on the other hand, the value of f_{trans} appears to be less than 2.5, the decrease corresponding roughly to the polarity of the molecule as given by its "reduced dipole energy."[5]

The present paper reports measurements of the conductivities of binary mixtures of organic vapors, and it will be shown that, with polar/nonpolar mixtures, the results obtained may also be explained in terms of the above observations.

Previous investigations of thermal conduction in gas mixtures have shown that a linear relationship between the conductivity and composition of a mixture is rarely observed; in fact the variation of conductivity with composition may be extremely complicated and difficult to predict. Deviations from a linear relationship are due to three principal factors. If the components of the mixture differ substantially in mass, conductivities are usually less than those expected from such a relation; negative deviations have been found, for example, with helium/argon mixtures.[6] Similar effects occur if the components have different collision diameters. On the other hand, if the intermolecular forces of the components are very different, marked positive deviations occur; these are sometimes so pronounced that maxima are observed in the conductivity *vs* composition curves, as in case of air and ammonia mixtures.[7]

Lindsay and Bromley[8] have developed an empirical formula for the conductivity of mixtures of simple gases, which is reasonably satisfactory even when the masses and collision diameters of the components are dissimilar. The formula is based on an expression

[1] R. G. Vines and L. A. Bennett, J. Chem. Phys. **22**, 360 (1954).
[2] A. Eucken, Physik. Z. **14**, 324 (1913).
[3] The validity of this assumption has been demonstrated by the work of Keyes (reference 13). In a study of the conductivity of hydrogen he showed that, as the rotational energy becomes progressively less at low temperatures, the value of f (as defined by the relation $K^0M/\eta Cv_0=f=[f_{\text{trans}}Cv_{\text{trans}}+f_{\text{int}}Cv_{\text{int}}]/Cv_0$) approaches the limiting value of 2.5. This is characteristic of a gas possessing translational energy only, and implies $f_{\text{trans}}=2.5$. [See W. G. Kannuluik and E. H. Carman, Proc. Phys. Soc. (London) **B65**, 701 (1952); R. G. Vines, Revs. Pure Appl. Chem. (Australia) **4**, 207 (1954)].
[4] E. R. Grilly, Am. J. Phys. **20**, 447 (1952).
[5] J. S. Rowlinson, Trans. Faraday Soc. **45**, 974 (1949).
[6] J. Wachsmuth, Physik. Z. **7**, 235 (1908).
[7] H. Gruss and H. Schmick, Wiss. Veroffentl. Siemens-Konzern **7**, 202 (1928).
[8] A. L. Lindsay and L. A. Bromley, Ind. Eng. Chem. **42**, 1508 (1950).

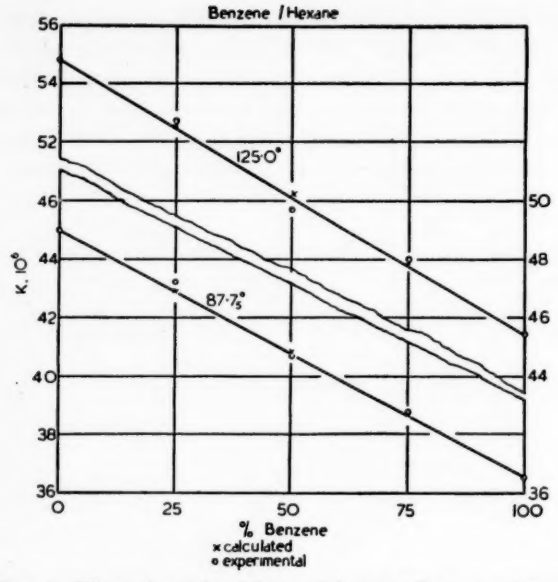

FIG. 1. Thermal conductivities of benzene/hexane mixtures. In Figs. 1–8 compositions are expressed as mole percentages. Units of K-cal cm^{-1} sec^{-1} deg^{-1}.

originally suggested by Wassiljewa[9]:

$$K_{\text{mixture}}=\frac{K_1}{1+A_{12}\frac{x_2}{x_1}}+\frac{K_2}{1+A_{21}\frac{x_1}{x_2}}, \qquad (2)$$

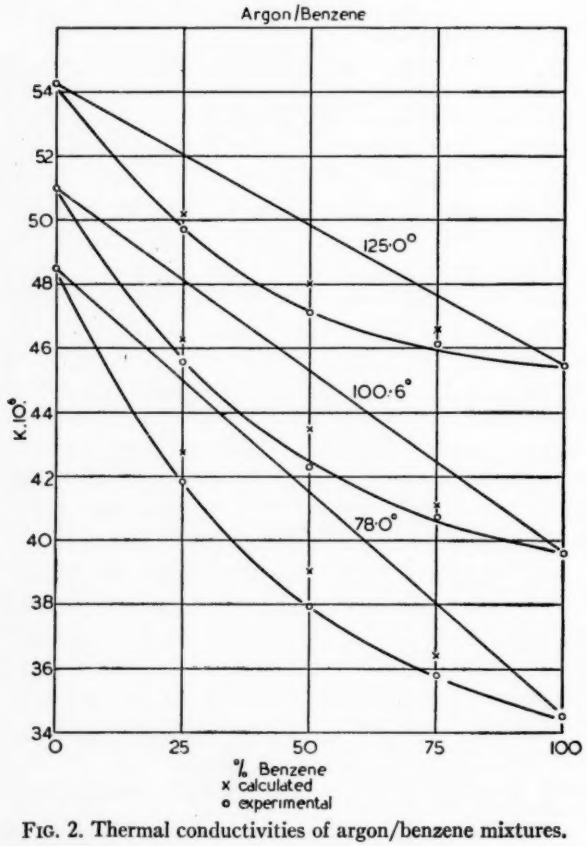

FIG. 2. Thermal conductivities of argon/benzene mixtures.

[9] A. Wassiljewa, Physik. Z. 5, 737 (1904).

K_1, K_2 being the conductivities of the pure components, and x_1, x_2 their corresponding mole fractions. According to Lindsay and Bromley, A_{12} is given by

$$A_{12}=\frac{1}{4}\left\{1+\left[\frac{\eta_1}{\eta_2}\left(\frac{M_2}{M_1}\right)^{\frac{3}{4}}\frac{(1+S_1/T)}{(1+S_2/T)}\right]^{\frac{1}{2}}\right\}^2\cdot\frac{(1+S_{12}/T)}{(1+S_1/T)}, \qquad (3)$$

where T is the temperature and η_1, η_2, M_1, M_2, and S_1, S_2 are the viscosities, molecular weights, and Sutherland constants of the components. (To obtain A_{21} the subscripts are interchanged.) Sufficiently accurate values for Sutherland's constant may be obtained from the approximate relation $S=1.5T_B$, T_B being the boiling point of the substance at atmospheric pressure. For mixtures of nonpolar vapors or weakly polar vapors, S_{12} is assumed to be the geometric mean of S_1 and S_2.

Lindsay and Bromley's equation is not satisfactory for polar/nonpolar mixtures because of attractive forces between the polar molecules. Agreement with experiment is improved by the substitution

$$S_{12}=\text{const}(S_1S_2)^{\frac{1}{2}}, \qquad (4)$$

where, according to calculations by Gruss and Schmick,[7] the constant has the value of 0.733. However this procedure is somewhat arbitrary; moreover Gruss and Schmick's calculations are of doubtful validity.

Further experimental study of mixtures, especially of polar/nonpolar mixtures, is desirable if their behavior is to be properly understood. In the present work organic vapors of roughly similar masses and viscosities (and thus collision diameters) have been used. With mixtures of appropriate polar and nonpolar compounds it was possible to observe effects resulting almost entirely from differences in the attractive forces of the molecules.

II. EXPERIMENTAL

The apparatus was of the hot wire type, and was the same as that used in earlier measurements.[1,10] The mixtures were prepared by admitting the components, at suitable pressures, to a heated vessel attached to the apparatus. A magnetically operated stirrer was moved to and fro within the vessel to ensure uniformity of composition,[11] and the mixture was then introduced directly into the conductivity cell. Subsequent experimental procedure was identical with that previously described.[10] Measurements were made at several pressures from 10–65 cm Hg, and the results extrapolated to zero pressure.

The method is relative, and the conductivity of each mixture was compared with that of air at the same temperature. Absolute values were calculated using results for the conductivity of air recently obtained by Kannuluik and Carman.[12]

[10] R. G. Vines, Australian J. Chem. 6, 1 (1953).

[11] Adsorption effects were apparently unimportant since the results were independent of the order of admission of the vapors.

[12] W. G. Kannuluick and E. H. Carman, Australian J. Sci. Research A4, 305 (1951).

III. RESULTS

Nonpolar and Weakly Polar Vapors

The validity of the Lindsay/Bromley equation for nonpolar vapors was tested initially by measuring the conductivities of benzene/hexane mixtures. The results are given in Fig. 1. Within the limits of experimental error there is a linear variation of conductivity with composition, which might be expected since the molecular weights and viscosities of the vapors are not very different. Values calculated from the equation of Lindsay and Bromley (also shown in the figure) agree well with the measurements.

Figure 2 shows results for mixtures of argon and benzene. The viscosity of argon[13] is considerably larger than that of most organic vapors, and it is not surprising that this affects the shape of the conductivity *vs* composition curves. The Lindsay/Bromley formula does not reproduce the experimental values exactly, but it does predict negative deviations of the type obtained.

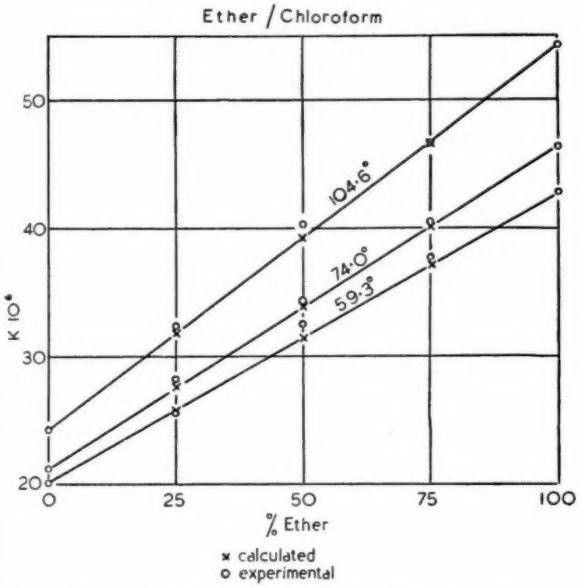

FIG. 3. Thermal conductivities of ether/chloroform mixtures.

Ether and chloroform (and probably diethylamine) are weakly polar substances if their "reduced dipole energy" is taken as a criterion of dipole character (see reference 1). Results for weakly polar mixtures of this type (ether/chloroform, and diethylamine/ether) are given in Figs. 3 and 4. The conductivity *vs* composition curves are again approximately linear, and in good agreement with values calculated from Lindsay and Bromley's equation.

Mixtures of Polar and Nonpolar Vapors

If polar and nonpolar vapors are mixed, deviations from a linear conductivity-composition relationship are to be expected. This is verified by experiment, as may be seen from Figs. 5, 6, 7 where results for acetone/benzene, methyl alcohol/hexane, and methyl alcohol/argon mixtures are given (the significance of the broken lines will be explained later). The measurements may be compared with those of Vargaftig and Timroth[14] for water vapor/nitrogen and water vapor/carbon dioxide mixtures, which are also shown in Fig. 8. In every case the curves exhibit well-defined maxima, and Lindsay and Bromley's formula was found to reproduce the experi-

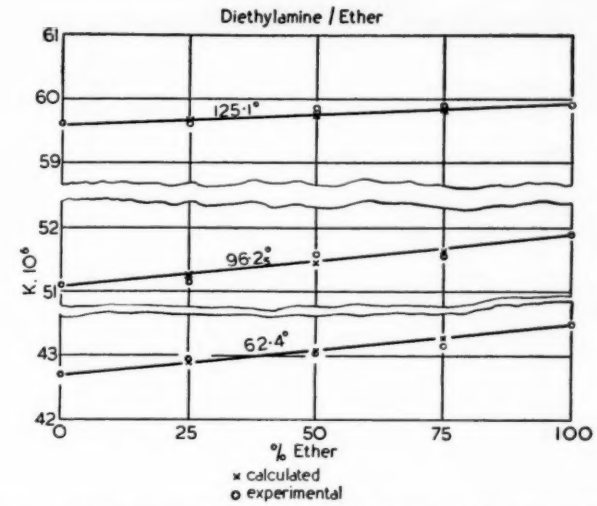

FIG. 4. Thermal conductivities of diethylamine/ether mixtures.

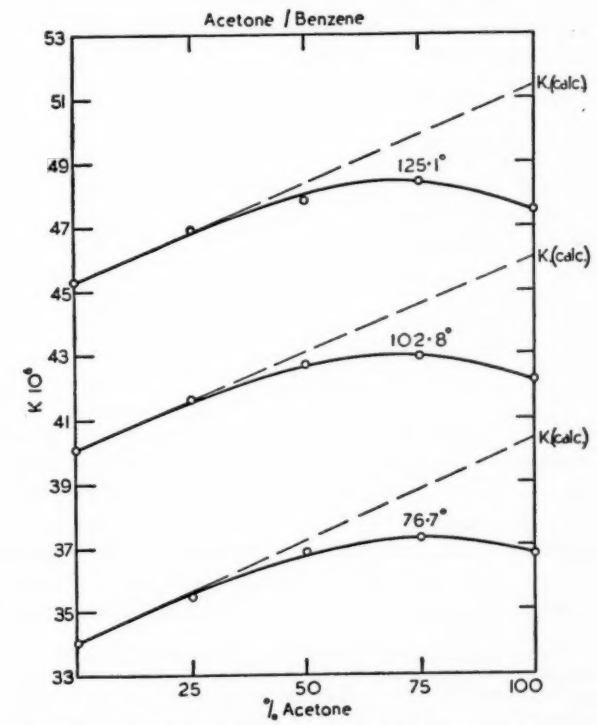

FIG. 5. Thermal conductivities of acetone/benzene mixtures.

[13] F. G. Keyes, Tech. Report, 37. Project Squid MIT April (1952).

[14] N. B. Vargaftig and D. L. Timroth, *Trans. Fourth World Power Conference III* (Lund-Humphries, London, 1952), p. 1642.

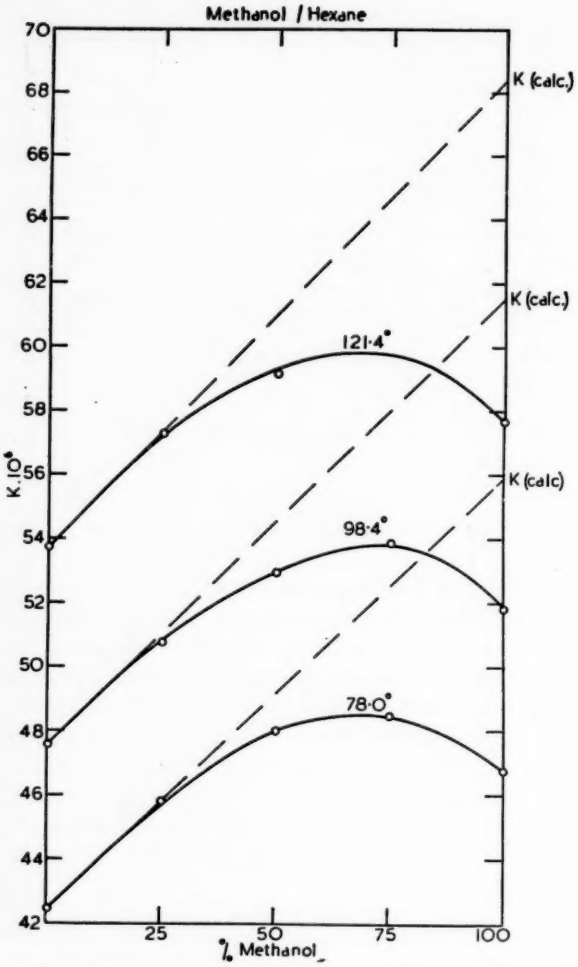

FIG. 6. Thermal conductivities of methanol/hexane mixtures.

mental results only if the constant in Eq. (4) was adjusted for each mixture separately.[15] Even then, agreement was poor for the steam mixtures.

A few measurements were also carried out with mixtures of triethylamine and ethyl chloride. Positive deviations were again observed, but these were very much less than for the other mixtures.

IV. DISCUSSION

It is clear that the conductivity *vs* composition curves for nonpolar or weakly polar organic vapors are roughly linear, provided that the molecular weights, viscosities, etc. of the vapors are not substantially different. On the other hand, marked positive deviations (which cannot be predicted accurately on the basis of the Lindsay/Bromley equation) are observed with polar/nonpolar mixtures. The cause of such behavior is to be found in the decrease[1] in the Chapman/Enskog factor, f_{trans}, for polar vapors, as a consequence of the orientation effects involved in collisions between polar molecules.[16,17] The resultant interaction reduces the rate of transfer of translational energy, and the thermal conductivities of polar vapors are therefore less than those of corresponding vapors with nonpolar characteristics.

With a mixture containing only a small proportion of polar vapor, this interaction is greatly reduced, since the polar molecules collide mainly with nonpolar molecules. In the absence of orientation effects on collision, the polar vapor will possess an increased "nonpolar" conductivity, which may be calculated from Eq. (1) by substituting for f_{trans} the value of 2.5, and assuming a temperature dependence of f_{int} identical with that observed for nonpolar vapors (see reference 1). The results of such calculations for methyl alcohol, acetone, and water vapor at several temperatures are summarized in Table I.

Mixtures containing a small proportion of polar vapor should exhibit essentially nonpolar behavior with a linear relationship between conductivity and composition. Thus the conductivity *vs* composition curves should be directed initially towards the point $K_{(calc)}$, which represents the theoretical "nonpolar" conductivity of the undiluted (polar) component. This expectation is verified by experiment, for in Figs. 5, 6, and 8 the experimental curves follow the straight lines shown, until the proportion of polar vapor is 15% or more. The conductivity "falls off" only at higher concentrations of the

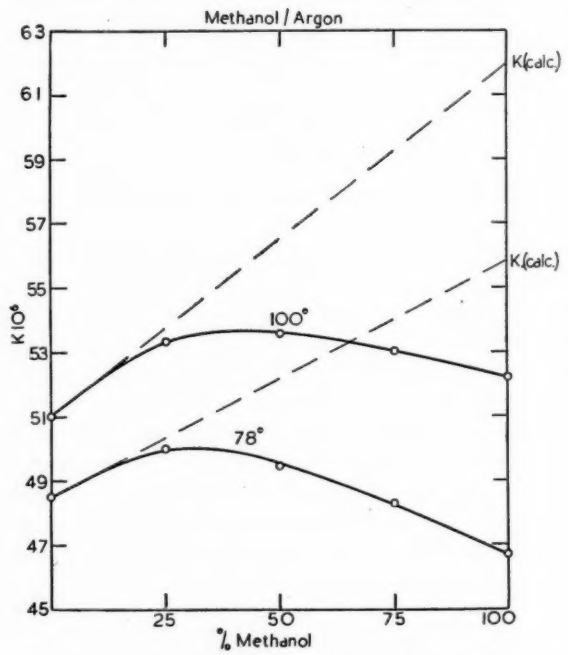

FIG. 7. Thermal conductivities of methanol/argon mixtures.

[15] This is unsatisfactory, particularly since the calculation is very sensitive to the value employed; furthermore, there does not appear to be any systematic variation in the constant which can be correlated with the properties of the individual mixtures. The selected constants are as follows: acetone/benzene 0.85, methanol/argon 0.93, methanol/hexane 0.60, water vapor/nitrogen 0.7, water vapor/carbon dioxide 0.7. Thus, deviations from the recommended value of 0.733 are sometimes considerable.

[16] K. Schäfer, Z. Physik. Chem. **B53**, 149 (1943).

[17] P. M. Craven and J. D. Lambert, Proc. Roy. Soc. (London) **A205**, 439 (1951).

polar vapor, when the polar/polar collisions are more frequent. Mixtures of methanol and argon (Fig. 7) behave similarly, in spite of the fact that the viscosity of argon is considerably greater than that of methyl alcohol (see the results for benzene/argon in Fig. 2).

Triethylamine/ethyl chloride mixtures also exhibit positive deviations. However the "reduced dipole energy" of ethyl chloride is less than that of methanol, acetone, or water vapor, and the diminution in f_{trans} is correspondingly reduced.[1] This explains why the deviations observed with triethylamine/ethyl chloride mixtures are less pronounced.

When two polar organic vapors are mixed together, all collisions involve polar molecules and the resulting interaction should not be dependent on composition in the manner described above. Provided that the polar character of the vapors is not very different, linear conductivity *vs* composition curves should again be observed. This is the case for ether/chloroform where the reduced dipole energy of both vapors is small, and also for the weakly polar diethylamine/ether mixtures (Figs. 3, 4).

It is apparent that the results for both polar and nonpolar mixtures can be interpreted qualitatively in this way. In previous investigations the maxima so frequently observed in the conductivity *vs* composition curves were not explained satisfactorily: the value of the present work is that it relates these unambiguously to differences in the polar character of the mixture components.

TABLE I. Theoretical "nonpolar" conductivities of polar vapors.

Substance	Temp. °C	f_{trans}	f_{int}	C_{v_0} cal mole^{-1}	$\eta \cdot 10^7$ g cm^{-1} sec^{-1}	$K_{(calc)} \cdot 10^6$ cal cm^{-1} sec^{-1} deg^{-1}
Methyl alcohol	78	2.5	1.23[a]	9.49[b]	1160[e]	55.9
	98.4	2.5	1.25	9.91	1225	61.5_5
($M=32.0_5$)	100	2.5	1.25	9.94	1230	62.0_5
	121.4	2.5	1.27	10.37	1300	68.3_5
Acetone	76.7	2.5	1.22	18.5[c]	890[e]	40.4
($M=58.0_5$)	102.8	2.5	1.25	19.4	955	45.9_5
	125.1	2.5	1.27	20.3	1010	51.4
Water vapor ($M=18.0$)	65	2.5	1.22	6.07[d]	1185[f]	75.0

[a] See reference 1.
[b] J. S. Rowlinson, Nature **162**, 820 (1948).
[c] Collins, Coleman, and De Vries, J. Am. Chem. Soc. **71**, 2929 (1949). Results corrected for gas imperfection (Bennett to be published).
[d] McCullough, Pennington, and Waddington, J. Am. Chem. Soc. **74**, 4439 (1952).
[e] T. Titani, Bull Chem. Soc. Japan **4**, 277 (1929); **5**, 98 (1930); **8**, 255 (1933). (See also reference 17.)
[f] See reference 13.

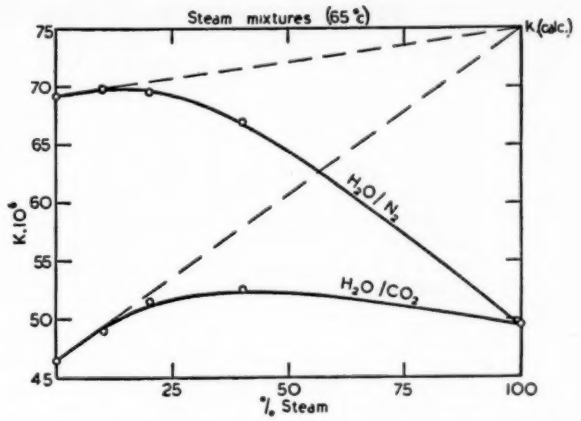

FIG. 8. Thermal conductivities[14] of steam mixtures at 65°C.

APPENDIX. VARIATION OF THE THERMAL CONDUCTIVITY OF MIXTURES WITH PRESSURE

Molecular interaction is also responsible for the variation of thermal conductivity with pressure. It was shown previously[10] that, for pure nonpolar vapors, the pressure dependence of conductivity is small at pressures up to a few atmospheres. In the present work it was noticed that mixtures of nonpolar vapors likewise exhibit only slight conductivity changes as the pressure is varied; as might be expected the pressure coefficients are of the same order as those found for the pure components.

Pure polar vapors, on the other hand, exhibit a very large increase in conductivity with pressure.[10] However with mixtures of polar and nonpolar vapors the pressure coefficients were relatively small except when the proportion of polar component was greater than about 75%. Only in the case of the (polar/polar) ether-chloroform mixtures did the conductivity of the mixture increase with pressure more rapidly than that of the pure components. Here, of course, molecular interaction is so pronounced as to lead to hydrogen bonding. Specific results for ether/chloroform mixtures have been given in detail elsewhere (see reference 10, Appendix III).

Infrared Spectrum of Two-Stage Cool Flame of Diethyl Ether

RUSSELL E. DONOVAN AND WILLIAM G. AGNEW
Research Laboratories Division, General Motors Corporation, Detroit, Michigan
(Received December 1, 1954)

An optical system has been made so that absorption and emission spectra from stages of a combustion process can be observed. Spectra from the two-stage cool flame of diethyl ether indicate that carbonyl compounds are formed as intermediates and final products are HCHO, CO_2, H_2O, CO, and C_2H_4. Also identified are CH_3OH and CH_4. Temperature calculations indicate that the infrared emission from this reaction is of thermal origin in contrast to the visible emission which is undoubtedly chemiluminescence. Calculated temperatures range from 700°K in the first cool flame to ~1000° in the second-stage flame.

INTRODUCTION

ONE of the more intriguing combustion reactions is that of the "cool" flame. This reaction occurs for a wide variety of fuels and results in the formation of excited formaldehyde whose characteristic blue fluorescence often is used to identify this reaction. Several types of study have been made of this reaction and considerable information has been obtained, but the basic mechanism is as yet not known. One method of study which appears to have received little attention is that of infrared absorption and emission. Since cool-flame reactions have been demonstrated to be closely related to self-ignition in an internal-combustion engine, our laboratory is interested in any information concerning this reaction and means of studying it. For this reason we have investigated the application of infrared spectroscopy to the study of this reaction. This paper describes the way in which the spectra were obtained and gives some preliminary interpretations.

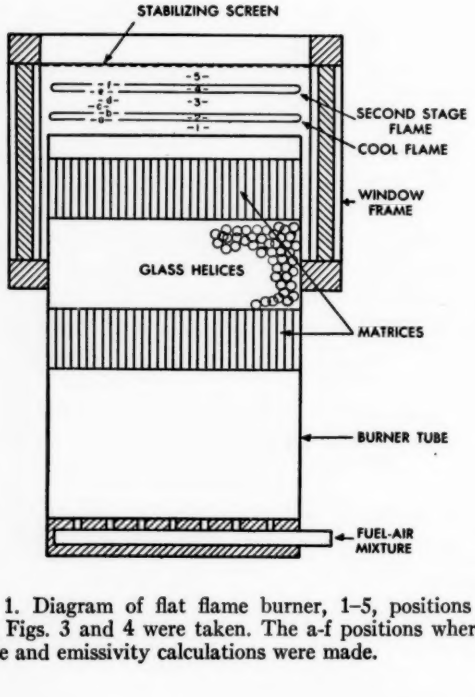

FIG. 1. Diagram of flat flame burner, 1–5, positions where spectra Figs. 3 and 4 were taken. The a-f positions where temperature and emissivity calculations were made.

EXPERIMENTAL

A fundamental difficulty in this type of investigation is that of getting sufficient volume of reactants at any stage of the reaction in a position to permit a spectrum to be taken. This difficulty has been overcome in the present work by examining the reaction *in situ* in a flat flame burner of the type described by Powling[1] and Egerton and Thabet.[2]

The burner used in the present experiments is shown in cross section in Fig. 1. The combustible mixture flows upward through the matrices and glass helices, which render the velocity distribution uniform, into the upper tube which supports a stabilizing screen. When the mixture is ignited a flame or flames are formed in the upper tube with an equilibrium between the mixture flow and the flame speed. In our application with a rich diethyl ether-air mixture (about three times stoichiometric) and a mixture flow of about 300 cm^3 per second, two flames are produced in positions 2 and 4 separated by about 1 cm. These flames apparently are similar to those described by Maccormac and Townend[3] and Topps and Townend.[4] The visible emission spectrum of each under these conditions is principally the formaldehyde fluorescence.

The burner is rectangular, the lower tube having a cross section 2.5×4 in. The upper tube has a composite structure with end windows of rock salt and sides of glass. The matrices were constructed from alternate flat and corrugated metal strips; the triangular holes formed have an area of about 1 mm^2.

The optical system which permits viewing stages of this reaction is shown schematically in Fig. 2. The source, a Nernst glower, is mounted horizontally and focused at the midpoint of the burner. The emerging beam is refocused upright on the spectrometer slit by the series of mirrors. The spectrometer "sees" a wedge of gas in the burner whose extreme height at the ends of the burner is about 5 mm and which narrows to the

[1] J. Powling, Fuel, **28**, 25 (1949).
[2] A. C. G. Egerton and S. K. Thabet, Proc. Roy. Soc. (London) **A211**, 445 (1951).
[3] M. Maccormac and D. T. A. Townend, J. Chem. Soc. **142**, 143 (1940); **142**, 151 (1940).
[4] J. E. C. Topps and D. T. A. Townend, Trans. Faraday Soc. **42**, 345 (1946).

slit width at the center. The burner position can be vertically adjusted to permit different stages in the reaction to be viewed.

Emission spectra can be taken by blocking off the source, or absorption spectra can be taken by viewing the source through the gas.

The spectra were observed with the 6-in. vacuum spectrograph built in this laboratory.[5,6] The remainder of the optical path outside of the burner was evacuated to eliminate atmospheric absorption.

INFRARED SPECTRA

Figures 3 and 4 show the emission and absorption spectra at the five positions in the burner numbered in Fig. 1. The emission spectra, Fig. 3, are discontinuous at positions where the slits were changed to accommodate the energy available. The successive intensity scales are displaced twenty divisions. The absorption spectra are presented as ratios of the signals

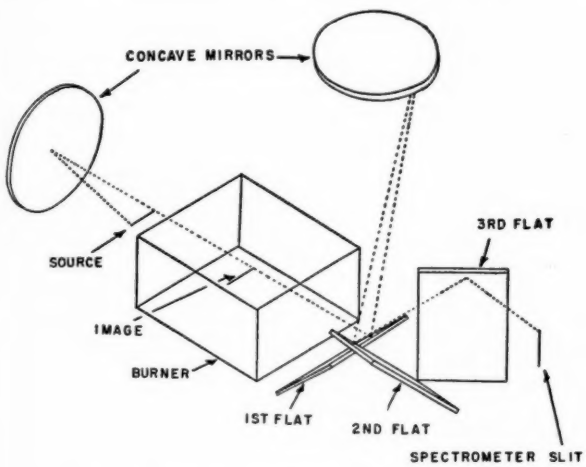

FIG. 2. System for projecting horizontal reaction zones on vertical slit.

received when viewing the source through the gas to the signals when viewing the source alone. These spectra were obtained with a memory-type ratio-recording circuit which will be described elsewhere.

In Fig. 4, spectrum 1 taken 3 mm below the first flame is apparently that of the fuel mixture. All bands are attributable to diethyl ether, CO_2 or H_2O. In the plane of the first flame, spectrum 2, some pronounced changes may be noted. The bands of diethyl ether at 10.6, 7.6, and 5.0μ have all disappeared or become very weak, indicating that a substantial portion of the fuel has been changed. The bands at 3.4, 7.3, and 9μ which persist are the strongest of the fuel spectrum but are also characteristic of the C—H and C—O group frequencies and could be due to either residulas

[5] Martin, Fisher, Mandel, and Nusbaum, J. Opt. Soc. Am. **37**, 923 (1947).

[6] Rassweiler, Liston, Lash, and Fry, J. Opt. Soc. Am. **37**, 963 (1947).

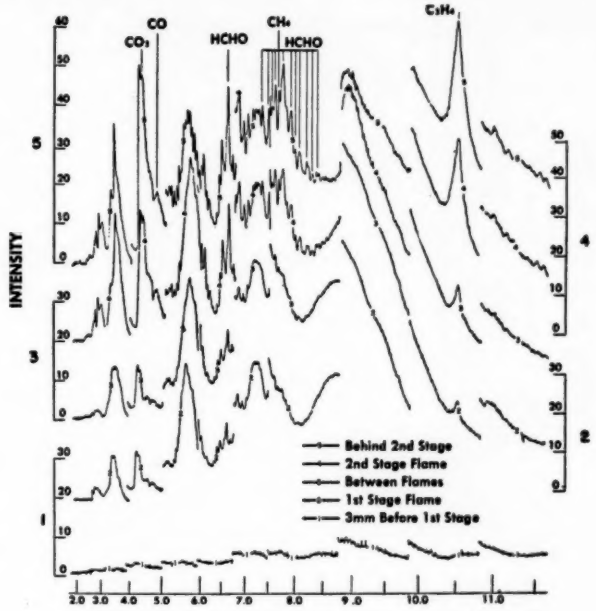

FIG. 3. Emission from reacting gases at numbered positions in Fig. 1.

of the fuel or new molecules containing these basic structures. There is an increase in the CO_2 absorption. New molecules identified are C_2H_4 absorbing at 10.5μ, CH_4 at 7.6μ, and possibly CH_3OH at 9.7μ. The most pronounced change is the appearance of the strong band at 5.65μ characteristic of the C=O group.

The spectra at the positions higher in the burner are similar to the spectrum of the first-stage flame, except that they are less intense due to the temperature increase. The CO can be identified at 4.7μ in spectra 4 and 5, and water-vapor absorption at 2.8μ and in the 6μ region increases notably from spectrum 3 to spectrum 4. Formaldehyde can be identified by the ν_3Q branch at 6.7μ and by the irregular structure of ν_5 extending from 7.5μ to 8.0μ.

The emission spectra, in Fig. 3, are very similar to the absorption spectra, except that the intensities progress from a very small amount in the fuel-air mixture below the first flame to rather large values in the products above the second-stage flame. No new products can be assigned which were not observed in the absorption spectra. One item of interest, however, is that the C=O band at 5.65μ decreases in intensity with the change of position from the second-stage flame to the region above the second-stage flame, yet the HCHO intensity increases. Thus, there must be molecules other than HCHO formed in the region of the first flame which contain C=O structure and these molecules undergo further reaction in the second flame.

If one compares these identifications with the chemical analyses of Maccormac and Townend[3] on quenched products of similar flames one finds essential agreement. However, it appears from our spectra that probably more fuel is consumed in our cool flame than

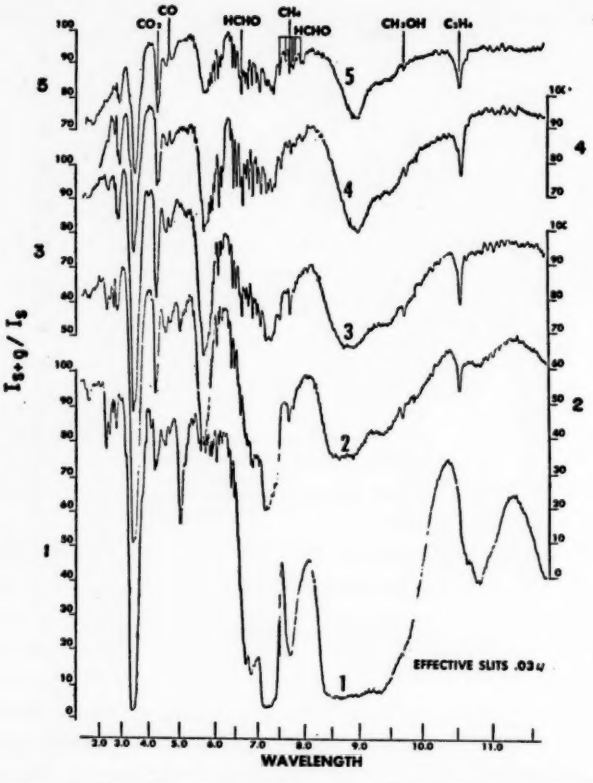

FIG. 4. Absorption by reacting gases. Numbering on curves indicate the following positions; 1, 3 mm below cool flame; 2, in the plane of the cool flame; 3, between the flames; 4, in the plane of the second flame; 5, 3 mm above the second flame.

is indicated in their chemical analysis. We have not yet identified some of the lesser products which they identified, notably peroxides and acids. We have identified CH_3OH which they did not. It also appears that the C=O structure referred to earlier is probably acetaldehyde. We cannot conclusively identify this compound with the resolution we have here, since all bands of acetaldehyde are coincident with the strong group frequencies.

VIBRATIONAL "TEMPERATURES"

One of the major objectives of this investigation is that of determining the feasibility of using radiation measurements for temperature determinations in dynamic reactions of this type, e.g. precombustion reactions in an internal combustion engine. This would be possible only if the radiation is of thermal origin. This is, of course, not true for the visible radiation from cool flame which is definitely chemiluminescence. It is still possible that the molecules giving rise to the visible radiation are a relatively small portion of the total and that the remaining molecules are in reasonable thermal equilibrium. To check this possibility, some temperature calculations were made by a method similar to that proposed by Silverman.[7]

The signal from the spectrometer at any wavelength may be written:

$$D_g = K\epsilon_g C_1/\lambda^5[\exp(C_2/\lambda T_g)-1]^{-1}, \quad (1)$$

$$D_s = K(1-\alpha_w)\epsilon_s C_1/\lambda^5[\exp(C_2/\lambda T_s)-1]^{-1}, \quad (2)$$

$$D_{s+g} = D_s(1-\alpha_g)+D_g. \quad (3)$$

Where D_g, D_s, D_{s+g} are the signals with the gas, source, and source plus gas in the optical path respectively, K is an instrumental constant, ϵ_g, ϵ_s the gas and source emissivities, T_g, T_s the gas and source temperatures, α_w the fraction of source intensity lost at the optical components between the source and the gas, and α_g the gas absorption. The third equation is different from Silverman's since our optical system did not allow the use of a chopper between the source and the burner so that we could not measure $D_s(1-\alpha_g)$ directly as Silverman did. The equations are solvable for emissivity and gas temperature provided Kirchoff's law holds and the source temperature and emissivity are known. The source was a Nernst glower operating at 0.6 amp. At this current we determined that it approximates a black body at 1700°K in energy distribution from 2 to 10μ. We have not attempted emissivity calibration but, since we were at first more interested in the validity of the thermodynamic equilibrium than in precise temperature measurements, we considered an assumed emissivity and window transmission product of 0.75 sufficiently accurate.

Temperature and emissivity calculations were made for the six positions, 3 mm apart, indicated by letters in Fig. 1 at each wavelength listed in Table I. The individual temperatures calculated for each position and wavelength are tabulated in Table I as well as the average at each position for all wavelengths. With the

TABLE I.

Wavelength assignment position	3.38μ C−H Stretch	4.33μ CO_2	5.65μ C=O	7.3μ C−H Bend	8.85μ C−O−C	10.5μ C_2H_4	Average
	Temperature °K						
a	810	605	645	684	795	682	704
b	890	738	775	705	833	785	788
c	890	794	820	756	812	832	817
d	900	816	860	822	894	874	861
e	1030	912	980	972	960	960	969
f	1055	1070	1100	1060	1005	1035	1055

[7] S. Silverman, J. Opt. Soc. Am. 39, 275 (1949).

exception of the two lowest positions in the burner where the emission intensity was very low due to the low temperature the values for all wavelengths at any position do not differ greatly. The average temperatures are shown plotted *vs* distance through the burner in Fig. 5. The shaded areas represent the regions of visible flame luminosity. These average temperatures agree within $\pm 5\%$ with thermocouple measurements made by Foresti[8] in a similar flat flame burner. Since there is reasonable agreement in temperatures calculated at various wavelengths corresponding to the principal emitters in the infrared, and since the temperatures are in agreement with thermoelectric measurements, it appears that the infrared radiation is of thermal origin.

EMISSIVITIES

If enough high-temperature data were available, the emissivities could be used to calculate the changes in composition of the mixture through the reaction zone. We do not as yet have sufficient information to do this, so the concentration changes can only be qualitatively inferred from the emissivities. From the emissivities plotted in Fig. 6, which are those calculated in making the temperature calculations, several points can be deduced. First, since at some wavelengths the emissivities are nearly one, little loss in signal would result at those wavelengths from decreasing the burner size and thus improving the spatial resolution for more accurately pin pointing temperature changes. Second,

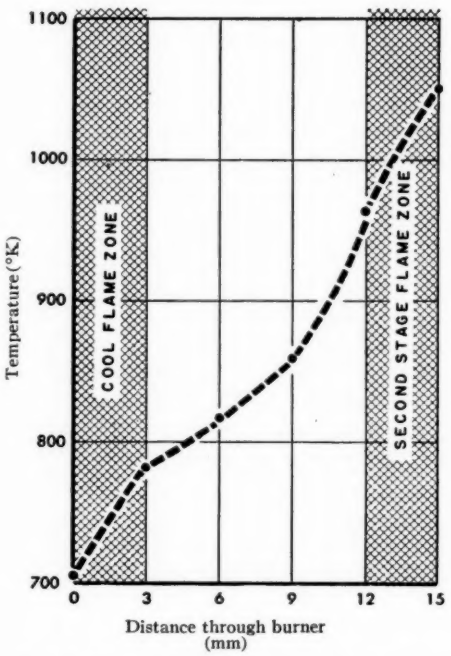

FIG. 5. Temperatures through reaction zone.

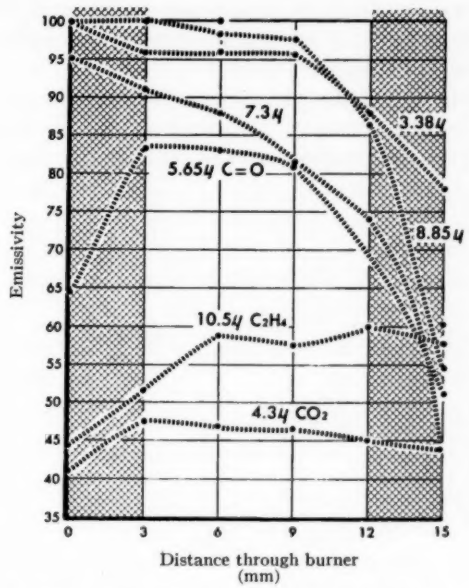

FIG. 6. Monochromatic emissivity at major band maxima through reaction zone. The shaded areas indicate the regions of visible luminosity as labeled in Fig. 5.

the validity of the argument made earlier concerning the formation of C=O compounds as intermediates is more definitely demonstrated, since the emissivity at 5.65μ increases markedly in the first flame and decreases sharply through the second flame.

It must be pointed out that good temperature measurements are required and the effects of temperature on the emissivities must be known before the emissivities can be reduced to concentrations. Temperatures at various levels in the burner are doubly important, since the entire reaction occurs at atmospheric pressure and with a decrease in molecular density resulting from the temperature increase as the reaction proceeds. It will be of interest to determine whether the decrease in CO_2 emissivity in the second-stage flame, Fig. 6, is caused by decreased molecular density or whether it actually corresponds to a decrease in CO_2 concentration. The present burner appears well-suited to such a study.

SUMMARY

The flat flame burner has some desirable properties for the study of combustion reactions, particularly low speed multiple stage reactions. The burner allows space resolution, and this coupled with the controlled flame depth makes possible measurements of the course of the reaction not possible by other methods.

In essence, our spectra agree with the results of chemical studies of Maccormac and Townend on a similar reaction but under different conditions. Our results differ from theirs in that: (1) we have not yet identified some of the lesser components (peroxides

[8] R. J. Foresti, Paper No. 4 Fifth Symposium on Combustion, Pittsburgh, Pennsylvania, August 30, 1954.

and acids) which they found and (2) it appears that considerably more fuel is consumed in our first-stage flame than in their cool flame.

Radiation temperature measurements indicate that there is approximate thermodynamic equilibrium throughout the reaction zone except for the molecules that give rise to visible luminosity. Thus spectroscopic temperature measurements based on infrared emission should be valid.

Application of the infrared method to the study of various fuels, mixtures, and flame conditions should contribute important information about these reactions.

THE JOURNAL OF CHEMICAL PHYSICS VOLUME 23, NUMBER 9 SEPTEMBER, 1955

Oxidation States of Phosphorus-32 Produced by Neutron Irradiation of Potassium Chloride*

T. A. CARLSON AND W. S. KOSKI
Department of Chemistry, The Johns Hopkins University, Baltimore 18, Maryland
(Received December 20, 1954)

An investigation of the oxidation states of P^{32} formed by neutron irradiation of KCl shows that like the simultaneously formed S^{35} the ratio of the different oxidation states depends on the preirradiation treatment. Through outgassing of the crystals results in the production of lower oxidation states. On the other hand, the oxidation states of P^{32}, unlike S^{35}, are strongly affected by the presence of x- or γ radiation. The recoil energy of the newly formed P^{32} fragment seems to have little effect on its final oxidation state.

INTRODUCTION

WHEN potassium chloride is irradiated with neutrons, two of the reactions that take place are $Cl^{35}(n,p)S^{35}$ and $Cl^{35}(n,\alpha)P^{32}$. From simple considerations of conservation of energy and momentum, one can estimate the energies of the recoiling S^{35} and P^{32}. Since[1,2] it is believed that self-ionization by a rapidly moving particle is probable only at velocities comparable to the effective velocities of free electrons, the recoiling S^{35} will undergo no appreciable ionization by the process of electron ejection and capture. In P^{32} the recoil energy is appreciably higher but it still appears to be too low to produce ionization by this mechanism, except under high-energy neutron bombardment. An approximate neutron energy of 5 Mev would be required to give the P^{32} sufficient recoil to strip the first electron.

The proton or alpha particle on leaving the irradiated chloride will reduce the nuclear charge by $+1$ in the case of sulfur or $+2$ in the case of phosphorus, leaving the residual sulfur with a -2 charge and the phosphorus with a -3 charge. The charge may be reduced by electron capture by the proton or alpha as they move through the electronic field of the sulfur or phosphorus fragment, respectively. Such considerations would lead one to believe that the sulfur or phosphorus activity should be present in low-oxidation states. In sulfur, this has been found to be the case[3] if the material was subjected to proper preirradiation treatment which removes possible oxidants.

Some work has been done on the oxidation states of P^{32} produced from neutron bombardment of KCl. Aten[4] found that irradiation of NaCl with neutrons from a Ra-Be source gave P^{32}; 65% of the P^{32} was carried by $PO_3^=$ and HPO_2^-. Süe and Caillat[5] found that P^{32} formed in the chlorides of Li, Na, and K by pile irradiation is divided almost equally between the valence states $+5$ and less than $+5$. Furthermore, heating the NaCl crystals to 350°C after irradiation decreased the amount of $+5$ phosphorus. Unpublished work at this laboratory indicated that pile irradiation of KCl produced all of the resulting P^{32} in the $+5$ state. In order to resolve these discrepancies and extend the work specifically to the -3 state, we have made a careful investigation of some of the factors that affect the oxidation state of P^{32} formed from neutron irradiation of KCl.

EXPERIMENTAL

Preirradiation Treatment of KCl

Approximately $\frac{1}{2}$ to 1 gram of analytical grade KCl was placed in a quartz tube. The tube was attached to a vacuum system and heated by an oven to about 800°C while under vacuum. The pressure in the system ranged from 3×10^{-6} to 4×10^{-7} as measured by an ionization gauge. This treatment caused the KCl to sublime to a cooler part of the quartz tube. The treatment was continued from 12 to 24 hours and then the portion of the tube into which the KCl sublimed was sealed off and irradiated with neutrons. The efficiency of purification was checked by examining the oxidation

* This work was performed under the auspices of the U. S. Atomic Energy Commission.
[1] H. A. Bethe, Revs. Modern Phys. **9**, 262–265 (1937).
[2] J. Knipp and E. Teller, Phys. Rev. **59**, 659 (1941).
[3] W. S. Koski, J. Am. Chem. Soc. **71**, 4042 (1949).
[4] A. Aten, Phys. Rev. **71**, 641–2 (1947).
[5] P. Süe and Caillat, Comp. rend. **230**, 1666–1667, 1864–1865 (1950).

states of sulfur after irradiation. This was found to be a sensitive test for presence of oxidizing impurities.

Separation of Carriers

To analyze for the various oxidation states, a solution containing carriers of phosphate, phosphite, hypophosphite, and sulfate ions is saturated with H_2S. In a dry box flushed with oxygen free nitrogen, PH_3 is also added to this solution in which the irradiated KCl is then dissolved. The PH_3 is generated by adding PH_4I to an alkaline solution and is passed through a soda lime trap to insure absorption of HI. The H_2S and PH_3 are then swept out with nitrogen into a bromine water trap where they are oxidized to $SO_4^=$ and $PO_4^{\equiv}$ which in turn are precipitated as $BaSO_4$ and $MgNH_4PO_4$, respectively. The remaining oxidation states are treated in the following manner: $PO_4^{\equiv}$ is precipitated as $MgNH_4PO_4$. The filtrate is then oxidized with nitric acid converting the phosphite and hypophosphite ions to phosphate which in turn is precipitated as $MgNH_4PO_4$. The filtrate from this precipitate contains $SO_4^=$ which is precipitated as $BaSO_4$. The initial P^{32} states are now in the same chemical form and the amounts of carriers used have been adjusted so all precipitates are of the same weight. A similar situation exists with the various $BaSO_4$ precipitates. The activities of all of these samples are then measured under reproducible geometry with an end-window counter using appropriate electronic equipment.

The analysis for neutral phosphorus was carried out separately by making a water-alcohol solution capable of dissolving elementary phosphorus, and +5, +3, and +1 phosphorus carriers. In this solution some irradiated KCl was dissolved. The neutral phosphorus was extracted with carbon disulfide. In case appreciable amounts of S^{35} were present, appropriate absorbers of aluminum were used to screen out this radiation. The half-life of the activity was measured to verify that only P^{32} was being measured.

DISCUSSION OF RESULTS

Effect of Preirradiation Treatment

In view of our experience with the effect of the preirradiation treatment on oxidation states of S^{35} formed from neutron irradiation of KCl, it was decided to examine the influence of this factor on the oxidation state of P^{32}. The presence of the S^{35} in the irradiated KCl served as a convenient check on the thoroughness of preirradiation elimination of oxidants from the KCl crystals. These results are summarized in Table I. It is clear that in the sample which had no preirradiation treatment the S^{35} and P^{32} occur in their highest oxidation states. As the crystals are outgassed more and more thoroughly the sulfur activity tends to concentrate in the lowest oxidation state. The figure of 88% is a typical one and in some samples as much as 98% of the sulfur has been found in the lowest oxidation state. In the case of phosphorus, the effect is not as pronounced but the lowering of the +5 state from essentially 100% to 88% indicates that the preirradiation treatment also plays some role, in the oxidation of the P^{32}. As will be shown below, the effect of the irradiation level is also extremely important. The comparative results for a treated and untreated sample formed from a much lower neutron dose than the samples subjected to pile irradiations are shown at the end of Table I. It should be noted that most, but not all of the unpurified sample goes to +5P whereas in the case of sulfur all of it is in the +6 state.

Effect of Irradiation Conditions on the Oxidation State

The second factor which was found to influence the oxidation state of P^{32} was the irradiation conditions. The results of these experiments are summarized in Table II. Sample 3a was subjected to pile neutron irradiation, sample 4 to neutrons produced by bombardment of beryllium with 20-Mev alpha particles, and sample 3b was irradiated by 14-Mev neutrons from the $T(d,n)He^4$ reaction. Furthermore, 3a and 3b were portions of the same purified sample. It is clear that as the neutron dosage decreases the P^{32} tends to lower oxidation states. It will be recalled that as the neutron level decreases the γ level also decreases tremendously. To test if γ rays have any influence on the oxidation state of P^{32}, portions of sample 4 were taken after neutron irradiation and subjected to bombardment with 100-kev x-rays and Co^{60} γ rays, respectively. In each case, it is evident that the amount of +5 state has increased considerably. It may therefore be concluded that x-rays and gamma rays can have a profound influence on the oxidation state. Since we were not able to vary the neutron level to the exclusion of the γ's one is not certain of the effect of neutron level alone, but it is likely that in pile irradiations the γ's associated with the neutrons are responsible for the oxidation of the phosphorus to the pentavalent state. It is of some interest to speculate on the mode of oxidation of the phosphorus. It is reasonable to expect

TABLE I. The effect of preirradiation treatment of KCl on the oxidation states of P^{32} and S^{35} produced by pile neutron bombardment ($\sim 10^{18} n$, cm^{-2}).

Sample	Percent of oxidation state: Phosphorus +5	Phosphorus +1, +3	Sulfur −2	Sulfur +6	Preirradiation treatment
2	88	12	88	12	outgassed
3a	96	4	46	54	outgassed
1	99	1	3	97	outgassed but then exposed to air
3	99.2	0.8	0.2	99.8	none
4[a]	40	60			outgassed
4[a]	89	11			none

[a] These samples were irradiated with 10^{14} neutrons, cm^{-2} using the D−T reaction as a source.

TABLE II. Effect of irradiation conditions on the oxidation states of P^{32} produced by neutron bombardment of KCl.

Sample	Percent oxidation state −3	+1, +3	+5	Irradiation conditions
3a	1.9	2.8	95.3	10^{18} total neutrons, cm^{-2}
4	32	32	36	$\sim 10^{14}$ total neutrons, cm^{-2}
3b	39	43	18	5×10^{10} total neutrons, cm^{-2}
4	31[a]		69	$\sim 10^{6}$ roentgens of 100 kev x-rays, after neutron irradiation
4	38[a]		62	2.5×10^{6} roentgens of Co^{60} γ's after neutron irradiation

[a] In these experiments, only the sum of the oxidation states below +5 was measured.

that when KCl is put into a pile some free chlorine is formed and this could oxidize the P^{32}. Attempts were made to distill from the crystal any PCl_5 that might be formed, but heating to 850°C failed to separate the phosphorus activity from the KCl. This treatment, furthermore, did not influence the amount of the +5 state which is an observation which appears to conflict with the work of Süe, referred to earlier. Under these conditions, it might be expected that if the phosphorus was present as PCl_5, it would dissociate to PCl_3.

On heating the KCl crystals to 800°C in an atmosphere of PCl_3, it was found that most of the P^{32} could be extracted into the gas phase. This observation has no significance as far as the identity of the radioactive compound in the crystal is concerned since under the same conditions one has exchange of activity between $Na_3P^{32}O_4$ and PCl_3. It is, however, a convenient way of extracting the P^{32} from the crystals. The failure to observe volatile phosphorus activity would seem to eliminate the possibility that the phosphorus activity is in the form of PCl_3 or PCl_5, however, it may be possible that the oxidation is still being produced by the chlorine but the resulting compound may be an ionic complex involving the potassium ions in the lattice and hence would be difficult to separate from the KCl crystals. The presence of traces of water as an impurity in the crystals might also be expected to produce oxidation of the phosphorus either by direct reaction or reaction with hydroxyl radicals, peroxides, etc. produced from the water. The latter species would produce oxidation which would be dosage dependent since the amounts of such oxidants present would depend on the number of gamma rays passing through the sample. In view of the careful preirradiation efforts to remove such impurities and whenever such efforts were made the sulfur activity was found in a low oxidation state, we believe that this mode of oxidation of the phosphorus is not a very likely one.

Attempts have been made especially with sample 4 to detect the presence of elementary phosphorus in the irradiated crystal, but in all cases negative results were obtained. This is not too surprising since, if elementary phosphorus occurs in the crystal it would very probably be in an atomic form and not in the form of the carrier phosphorus, therefore, exchange may be slower than possible reaction with the much more abundant water molecules. As a matter of fact, the ratio of the activity in the −3 state to the activity in the +1, +3 state was approximately constant for all experiments as indicated in Table II. This might suggest that if atomic phosphorus was formed, it disproportionated on contact with the water into two oxidation states which were carried by phosphine and hypophosphite-phosphite carriers. Such disproportionation has been reported for phosphorus heated with water.

It has also been suggested to us that it might be possible for trapped electrons, trapped holes and atoms, produced in the crystal by gamma rays, to react with water on dissolving to form H, OH, H_2O_2, etc. which could bring about oxidation and reduction since the phosphorus may be in close proximity to such defects. However, heating experiments of the type cited above essentially rule out such a possibility.

In conclusion, it may be pointed out that sample 4 was irradiated with 14-Mev neutrons and under such conditions one might expect to strip three electrons off the recoiling phosphorus fragment. This sample, however, had the least amount of + 5 state phosphorus, indicating that the recoil energy has little to do with the final oxidation state. If a positively charged phosphorus fragment is formed, since its ionization potential is higher than that of the other ions in the crystal it apparently quickly picks up electrons from its neighbors and becomes neutral phosphorus. If this phosphorus comes in contact with atomic or molecular chlorine it may form radicals such as PCl, etc., which on contact with water would undergo oxidation and reduction reactions. As the gamma-ray dosage is increased the concentration of free chlorine increases and then the radicals would convert to materials like PCl_3, PCl_5 and even ionic complexes involving potassium ions in the lattice.

ACKNOWLEDGMENTS

One of the authors (TAC) wishes to acknowledge a grant-in-aid from the Hynson, Wescott, and Dunning Research Fund. We are also indebted to Dr. B. L. Cohen of Oak Ridge National Laboratory, to Dr. Louis Rosen of Los Alamos, and to Dr. A. O. Allen of the Brookhaven National Laboratory for some irradiations of our samples.

Calculation of the Correction to be Applied to Gas Isotherms Measured in the Presence of Mercury

W. B. JEPSON AND J. S. ROWLINSON
Department of Chemistry, The University of Manchester, England

(Received December 16, 1954)

A calculation is made of the correction for the volatility of mercury which should be applied to observed pressures of compressed gases, when mercury is used as the confining fluid. The usual correction is simply the subtraction of the normal vapor pressure of mercury corrected for the effect of hydrostatic pressure (the Poynting effect). Here we show that this is an inadequate treatment of the problem, as the mixture of mercury atoms and compressed gas cannot behave as an ideal mixture. An estimation of the intermolecular forces between mercury atoms and the added gas leads to values of the virial coefficients from which a revised correction can be computed, assuming that the system is at equilibrium. This revised correction can be considerably larger than the usual correction and is often of opposite sign.

ACCURATE measurements of the pressures of compressed gases are usually made by transmitting this pressure to a suitable gauge by means of a column of mercury. Such measurements have been made, for example, by Michels and his colleagues at temperatures up to 150°C and pressures up to 3000 atmos, and by Beattie and his colleagues up to 300°C and about 500 atmos. Mercury is appreciably volatile at these temperatures, having a vapor pressure of 2.81 mm at 150°C and 246.8 mm at 300°C. It is the purpose of this note to calculate the correction which should be applied to the observed gas pressure to compensate for the presence of mercury in the gas phase. The usual procedure is simple —the normal vapor pressure of mercury is subtracted from the observed pressure. A more refined treatment[1] allows for the enhancement of the vapor pressure caused by the hydrostatic pressure of the gas. This effect (usually called after Poynting) increases the vapor pressure by a factor of $\exp[pV_2^l/RT]$, where p is the applied pressure and V_2^l is the molar volume of liquid mercury. This factor differs appreciably from unity only at the highest pressures, owing to the unusually small molar volume of liquid mercury. However, we wish to draw attention to two other effects, closely related to each other, which in our opinion can cause the correction for the presence of mercury to differ considerably from that calculated in this way. First, the enhancement of the vapor pressure by the compressed gas is given by Poynting's correction only if there is no interaction in the gas phase between molecules of the gas and the atoms of mercury. It has been established in systems such as solid carbon dioxide in the presence of compressed air,[2] or solid naphthalene in the presence of compressed ethylene[3] that such interaction can increase the concentration in the gas phase of the volatile solid or liquid component by factors of up to 10^4 times that calculated from Poynting's correction. This effect can be satisfactorily calculated from a knowledge of the intermolecular forces between the two components, by using the virial equation of state of the gas mixture.[4,5] Secondly, the correction to be applied to the observed gas pressure for the presence of this increased concentration of mercury atoms cannot be calculated on the assumption that the gas is perfect, but must be calculated by using again the virial equation of state of the mixture. A calculation of the total correction due to these two effects may be made as follows.

Let x_2^0 be the mole fraction of mercury in the gas phase, calculated on the assumption that the concentration is that of the pure saturated vapor at the same temperature. Then x_2, the actual mole fraction, is given by an expansion of which the first two terms are,[5]

$$\ln\frac{x_2}{x_2^0}=\frac{V_2^l-2B_{12}}{V}+\frac{V_2^lB_{11}-\frac{3}{2}C_{112}}{V^2}+, \qquad (1)$$

where V is the molar volume of the gas mixture, B_{11} is the second virial coefficient of the pure gas, and B_{12} and C_{112} the second and third virial coefficients for the interaction of, respectively, one and two molecules of the gas with one atom of mercury. The terms with V_2^l are the Poynting terms. Any solubility of the gas in the mercury has been neglected in deriving this equation. The effect of the concentration represented by x_2 on the observed gas pressure may be calculated by comparing the virial expansions for the pressure p_1 of n_1 moles of gas in a volume v in the absence of mercury, with the pressure p of n_1 moles of gas and n_2 moles of mercury $(n_2/(n_1+n_2)=x_2)$ in the same volume v at the same temperature T. Neglecting powers of n_2 higher than the first, these pressures are given by

$$p_1=\frac{n_1RT}{v}+\frac{n_1^2B_{11}RT}{v^2}+\frac{n_1^3C_{111}RT}{v^3}+\cdots, \qquad (2)$$

[1] J. A. Beattie, Proc. Am. Acad. Arts Sci. **69**, 389 (1934).
[2] T. J. Webster, Proc. Roy. Soc. (London) **A214**, 61 (1952).
[3] G. A. M. Diepen and F. E. C. Scheffer, J. Am. Chem. Soc. **70**, 4085 (1948).
[4] S. Robin and B. Vodar, Discussions Faraday Soc. **15**, 233 (1953).
[5] Ewald, Jepson, and Rowlinson, Discussions Faraday Soc. **15**, 238 (1953).

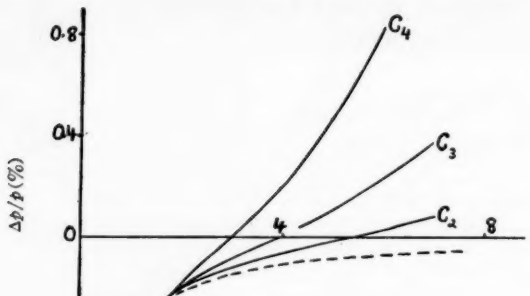

FIG. 1. The calculated correction for ethane, propane, and butane at 275°C. The dashed curve shows the calculated correction including only Poynting's term.

$$p=\frac{(n_1+n_2)RT}{v}+\frac{(n_1^2B_{11}+2n_1n_2B_{12})RT}{v^2}+\frac{(n_1^3C_{111}+3n_1^2n_2C_{112})RT}{v^3}+\cdots. \quad (3)$$

The correction Δp, which must be applied to compensate for the presence of mercury, is given by the difference of these pressures. Hence,

$$\frac{\Delta p}{p}=-x_2\left\{1+\frac{2B_{12}-B_{11}}{V_1}+\frac{3C_{112}-C_{111}+B_{11}^2-2B_{11}B_{12}}{V_1^2}+\cdots\right\}, \quad (4)$$

where $V_1=v/n_1$, and so is the experimentally observed molar volume of the gas. The first term of this series $-x_2$ is the correction for an ideal gas mixture of this composition, but even this differs from the correction usually applied which is $-x_2^0$.

The right-hand sides of Eqs. (1) and (4) can be calculated if an estimate can be made of B_{12} and C_{112}. (The coefficients B_{11} and C_{111} can be derived from the observed isotherms.) Here we estimate B_{12} and C_{112} from what knowledge we have of the intermolecular forces between mercury atoms and valence-saturated molecules. The interaction of two mercury atoms in their ground states (^1S) can be described by a potential of the usual 12:6 inverse-power kind with the collision diameter and energy of[6]

$$\sigma_{22}=2.898\text{A}, \quad \epsilon_{22}/k=851\pm32°\text{K}.$$

This potential is based on the viscosity of mercury vapor and agrees reasonably well both with Kuhn's estimate[7] of ϵ_{22}/k from the band-spectrum of mercury vapor (750–1050°K), and with Heller's estimate[8] of 2.77A and 998°K, based on a quantal calculation of the strength of the London dispersion forces. The values of σ_{12} and ϵ_{12} for the interaction of a mercury atom with a molecule of known σ_{11} and ϵ_{11} may then be found from the usual combining rules for such interactions[9] that σ_{12} is the arithmetic mean of σ_{11} and σ_{22} and that ϵ_{12} is the geometric mean of ϵ_{11} and ϵ_{22}. In the case of xenon, this leads to $\sigma_{12}=3.36$A and $\epsilon_{12}=464$°K which compare well with the values of $\sigma_{12}=3.26$A and $\epsilon_{12}=486$°K found by Heller for this interaction. Values of B_{12} may be obtained directly from such parameters, and values of C_{112} by an approximate method which has been discussed and justified elsewhere.[5,10]

Figures 1 and 2 compare values of $\Delta p/p$ calculated in this way with those calculated by allowing only for the Poynting term. All the calculations are for systems which have been studied experimentally. The most striking feature of the calculated corrections is that they can become large and positive at high temperatures and densities. Their size is due mainly to the enhancement of the mercury atom concentration calculated from Eq. (1). At 275°C and a density of 6 moles/l the calculated values of (x_2/x_2^0) are 3.30, 4.87, and 7.59 in ethane, propane, and butane, respectively. The positive sign of the calculated correction means that the addition of mercury atoms at constant volume to the pure compressed gas results in a diminution of the pressure, that is, the partial molar volume of mercury in this region is negative. Similar, but even more extreme behavior has been found experimentally[11] for the solution of NaCl in steam above its critical point. Here the observed partial molar volume of the salt was as low as −5 l/mole. The observed pressure[12] and the calculated correction (in

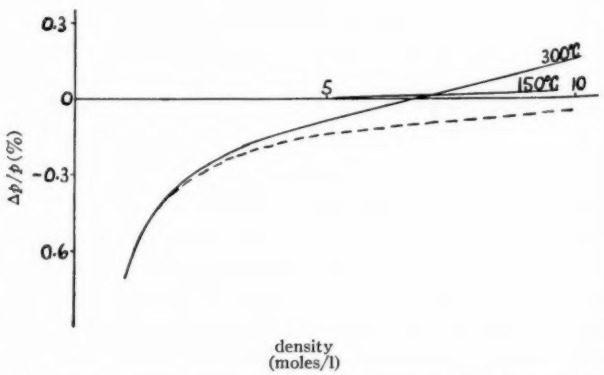

FIG. 2. The calculated corrections for xenon at 150°C and 300°C. The dashed curve shows the calculated correction at 300°C, including only Poynting's term.

[6] L. F. Epstein and M. D. Powers, J. Phys. Chem. **57**, 336 (1953).
[7] H. Kuhn, Proc. Roy. Soc. (London) **A158**, 212, 230 (1937).
[8] R. Heller, J. Chem. Phys. **9**, 154 (1941).
[9] Hirschfelder, Curtiss, and Bird, *Molecular Theory of Gases and Liquids* (John Wiley and Sons, Inc., New York, 1954).
[10] Rowlinson, Sumner, and Sutton, Trans. Faraday Soc. **50**, 1 (1954).
[11] Benson, Copeland, and Pearson, J. Chem. Phys. **21**, 2208 (1953).
[12] Beattie, Kay, and Kaminsky, J. Am. Chem. Soc. **59**, 1589 (1937); Beattie, Simard, and Su, J. Am. Chem. Soc. **61**, 26, 926 (1939).

atmos) for ethane, propane, and butane at 275°C and 6 moles/l are, respectively, 258.87 and +0.19, 234.26 and +0.55, 217.68 and +1.80. The usual correction, including only the Poynting term, is −0.18 atmos in each case. The observed pressure[13] and the calculated correction for xenon at 150°C and 10 moles/l are 270.92 and +0.09 atmos. The usual correction, including only the Poynting term, is here less than 0.01 atmos. At 300°C and 8 moles/l, the observed pressure[13] and calculated correction are 377.41 and +0.20 atmos, while the correction, including only the Poynting term, would be −0.33 atmos. It is clear that above 200°C the calculated correction becomes much larger than the usual estimates of the experimental error which vary from 1 part in 500 to 1 part in 3000. Even at 150°C, the correction may become large at 3000 atmos, the pressure to which Michels' measurements usually extend.[13]

There is some uncertainty in the estimation of the intermolecular forces on which these calculations are based, and at high densities a further source of error is our ignorance of the virial coefficients above the third. Nevertheless, we believe that the order of magnitude of the calculated correction cannot be in error. We conclude that the absolute accuracy of gas-isotherms measured in the presence of mercury at high temperatures and densities is very much less than the apparent experimental error, and will remain so, in view of the uncertainty of these calculations, until direct measurements of the effects discussed in this note have been made.

These calculations have been made on the assumption that the gas phase is of uniform composition. Such equilibrium will be established at different rates in different types of apparatus. It will probably be slow, for example, in an apparatus such as that of Michels, Michels, and Wouters[14] in which the mercury surface is small. It will probably be quite rapid in the apparatus of Beattie[1] in which the mercury surface is large and the temperature high, and must be very rapid in an apparatus such as that of Kay[15] in which the gas phase is stirred.

Calculations of a kind similar to these were first made by Lurie and Gillespie[16] for the effect of added nitrogen on the concentration of ammonia in equilibrium with a solid ammine. This system showed experimentally an enhancement of the concentration of ammonia in the gas phase, similar to that postulated here for mercury, which they discussed in terms of the Keyes equation of state—an approach which is unfortunately of little help in calculating the concentration in this problem.

[13] Beattie, Barriault, and Brierley, J. Chem. Phys. **19**, 1219 (1951); Michels, Wassenaar, and Louwerse, Physica **20**, 99 (1954).

[14] Michels, Michels, and Wouters, Proc. Roy. Soc. (London) **A163**, 201, 214 (1935).

[15] W. B. Kay, Ind. Eng. Chem. **28**, 1014 (1936).

[16] E. Lurie and L. J. Gillespie, J. Am. Chem. Soc. **49**, 1146 (1927).

THE JOURNAL OF CHEMICAL PHYSICS VOLUME 23, NUMBER 9 SEPTEMBER, 1955

Low-Frequency Rotational Spectrum of HDO†

SAMUEL WEISBAUM,* YARDLEY BEERS, AND GABRIEL HERRMANN
Physics Department, College of Engineering, New York University, University Heights, New York 53, New York

(Received July 16, 1954)

In the region between 475 and 3500 Mc/sec one *P*-branch and five *Q*-branch lines in the spectrum of HDO have been completely measured and identified. These data have contributed materially to an evaluation of the structural constants of the molecule. From the data obtained by this and other microwave spectroscopy projects we have computed the principal moments of inertia, respectively, as having the values of 1.1982, 3.0862, and 4.3887 in units of gm cm^2×10^{-40}. In addition, the shape of the $3_2 \rightarrow 3_3$ line at 824.64 Mc/sec has been extensively studied. At low pressure the wings of the line have been shown to be wider than is consistent with the Lorentz line shape probably due to the presence of sattelite lines arising from the hyperfine splitting of the energy levels by the quadrupole moment of the deuteron. The observed effects are consistent with a quadrupole coupling constant of 272±90 kc/sec with respect to an axis along the O−D bond.

I. INTRODUCTION

A STARK-MODULATED microwave spectrometer has been constructed for operation at frequencies less than 6000 Mc/sec. This system has been used to investigate the asymmetric rotor HDO. This molecule is of considerable interest from the theoretical point of view since with it centrifugal distortion effects are large, and thus the study of it leads to the opportunity to check the validity of theories of centrifugal distortion. It should be pointed out that the HDO species of water has a spectrum which qualitatively differs from the spectra of the single isotope species, H_2O and D_2O. Because with HDO the dipole moment is oblique to both the axes of least *a*- and intermediate *b*-moment of inertia instead of coinciding with the *b*-axis, the selection rules are

† Supported by the Office of Naval Research and by the U. S. Air Force, through the Office of Scientific Research of the Air Development Command.

* Present address: Bell Telephone Laboratories, Inc., Murray Hill, New Jersey.

considerably less restrictive. These rules permit the observation of Q-branch ($\Delta J=0$) lines as well as P- and R-branch ($\Delta J=\pm 1$) lines, which are observable with H_2O and D_2O. Thus there is considerably greater possibility with HDO of observing in the microwave region an adequate number of lines. In fact all but one of the lines discovered in this work are of the Q-branch type. At the same time, data obtained with HDO may be employed to evaluate the structure of H_2O and D_2O.

At the time this investigation was started only four HDO lines had been found previously by microwave methods,[1,2] and this number was completely inadequate for evaluating the constants of the molecule. At the same time the published calculations of King, Hainer, and Cross[3] clearly indicated the possibility of observing several lines in the frequency region below 3000 Mc/sec.

II. EXPERIMENTAL TECHNIQUES

The spectrometer employed Stark modulation and, except for the features due directly to its comparatively low operating frequency, was conventional in design. The absorption cell consisted of a 3 in. $\times 1\frac{1}{2}$ in. wave guide and was 20 ft long. With 707, 726A, 2K29 and 2K56 klystrons, the range from 2150 to 4400 Mc/sec could be covered. The square wave Stark voltage generator operated at 5 kc and the voltage was variable from zero to 1000 volts. The detecting system was the usual crystal detector, amplifier, phase detector, and recording milliammeter.

Special techniques were necessary for the observation of the $3_2 \rightarrow 3_3$ and $5_2 \rightarrow 5_3$ transitions. Since the predicted frequency lay below the cutoff of the TE_{10} mode of the wave guide, it was necessary to devise a technique whereby the cell could operate in its TEM mode. The rf power, supplied by a 6AF4 triode in a Mallory TV-101 television converter, and the 5-kc square wave generator were both connected to the Stark septum through a matching and decoupling network near one end of the cell. At the other end was connected a crystal detector with a special adapter which effected capacitative coupling to the Stark septum through the mica window. The crystal detector was connected to a tuned amplifier and phase sensitive detector in the conventional manner. With this equipment these lines were found.

III. OBSERVATIONS

The lines which have been discovered in this work are given in Table I along with their calculated absorption coefficients. These coefficients were modified from those obtained by King, Hainer, and Cross[3] by the use of the line width parameter 0.38 cm^{-1} due to Strandberg[2] and in some cases by the use of revised values of the frequency. The observed intensities were roughly consistent with the calculated ones. Some of these data have been published in preliminary form.[4,5]

Four of the lines could be positively identified by their well resolved Stark patterns. Stark information gave circumstantial evidence for the identification of a fifth line, the $4_0 \rightarrow 5_{-5}$, since the calculated coefficient for it was very small, and no resolved splitting was observed with this line. This tentative identification was confirmed by Benedict[6] on the basis of his work in the infrared. The identification of the $12_{-1} \rightarrow 12_0$ line is not completely definite since a line of comparable intensity was observed at 2991 Mc/sec, and neither it nor the one at 2961 Mc/sec had splittings which could be resolved. However, because of the almost perfect agreement of 2961 Mc/sec with the calculated value of the frequency of the $12_{-1} \rightarrow 12_0$ line, it appears that the present assignment is correct. Apparently the line at 2991 Mc/sec is due to some contaminating vapor.

IV. ANALYSIS OF DATA

We have made a detailed analysis of Q-branch, transitions for which $\Delta J=0$ and $\Delta K_{-1}=0$. The principal parameters involved are

$$\frac{a-c}{2} \quad \text{and} \quad \kappa=\frac{2b-a-c}{a-c},$$

where a, b, and c are the rotational constants respectively relative to the principal axes of least, intermediate, and greatest moments of inertia. The rigid rotor frequencies have been calculated by the methods of King, Hainer, and Cross.[7] However, with such a light molecule, centrifugal distortion effects are large, and the rigid rotor approximation is very inadequate. Recently Kivelson and Wilson,[8] using first-order perturbation theory, have derived a formula for correction of rigid rotor frequencies which may be applied to Q-branch transitions. For purposes of analysis, it is convenient to write this formula as follows:

$$f=f_0\{1+J(J+1)(Kx+y)+K(K^2+2)B +K(K-1)(2K-1)C+K(K^2-1)D\}, \quad (1)$$

TABLE I. Measured lines of HDO.

Transition ($J_\tau \rightarrow J_{\tau'}$)	Measured frequency (Mc/sec)	Absorption coefficient (cm^{-1})
$5_2 \rightarrow 5_3$	486.50±0.15	1.5×10^{-8}
$3_2 \rightarrow 3_3$	824.64±0.05	1.5×10^{-7}
$6_1 \rightarrow 6_2$	2394.56±0.05	2.9×10^{-7}
$4_0 \rightarrow 5_{-5}$	2887.4 ±0.1	1.5×10^{-8}
$12_{-1} \rightarrow 12_0$	2961 ±1	1.6×10^{-9}
$9_0 \rightarrow 9_1$	3044.71±0.10	3.4×10^{-8}

[1] C. H. Townes and F. R. Merritt, Phys. Rev. **70**, 558 (1946).
[2] W. M. P. Strandberg, J. Chem. Phys. **17**, 901 (1949).
[3] King, Hainer, and Cross, Phys. Rev. **71**, 433 (1947).
[4] Weisbaum, Beers, and Herrmann, Phys. Rev. **90**, 338 (1953).
[5] Y. Beers and S. Weisbaum, Phys. Rev. **91**, 1014 (1953).
[6] W. S. Benedict (private communication).
[7] King, Hainer, and Cross, J. Chem. Phys. **11**, 27 (1943).
[8] D. Kivelson and E. B. Wilson, J. Chem. Phys. **20**, 1575 (1952).

where K is the K_{-1} index of the two levels which combine to give the transition, J is the quantum number of total angular momentum, f_0 is the rigid rotor frequency, and f is the corrected frequency. The quantities x, y, B, C, and D are closely related to the centrifugal distortion parameters δ_J, D_{JK}, R_5, D_K, and R_6. Since f_0 depends upon κ and $(a-c)/2$, there are seven adjustable parameters. These are selected to obtain the best possible fit with observed frequencies. In our work, constants were adjusted to fit nine lines. Since this calculation was performed four additional lines have been found. These results are shown in Table II. The four lines denoted by asterisks in the first column are the ones which were not employed in the evaluation of the constants. It may be seen that the agreement is very good except in the case of the $11_{-2} \rightarrow 11_{-1}$ line, which, however, has a very large distortion correction. The values of the constants which were employed are shown in Table III.

From the analysis of P- and R-branch transitions, two additional constants are evaluated. These are another distortion constant D_J and $(a+c)/2$, where a and c have their previous definition. For this purpose it is convenient to write the total rotational energy as follows:

$$W=\frac{a+c}{2}J(J+1)-D_JJ^2(J+1)^2+E, \qquad (2)$$

where E is the so-called "reduced energy." E is evaluated from the reduced energy matrices (including centrifugal distortion).[9] The elements of these matrices are evaluated in terms of the constants determined from the analysis of Q-branch transitions.

Using the values $(a+c)/2=4.456524\times10^5$ Mc/sec and $D_J=6.71064$ Mc/sec a "best fit" was obtained with the three observed transitions of this type. Data on these transitions are shown in Table IV.

Since there was some doubt as to whether the 4_0 is higher or lower than the 5_{-5} level and whether the 6_{-2} level is lower or higher than the 7_{-6} level, calculations were made with all four of the possible combinations. Meaningless results were obtained except with the assignment indicated in Table IV, that is, with the 4_0 and 6_{-2} being the respective lower levels.

TABLE II. Q-branch transitions of HDO.

Transition ($J_\tau \rightarrow J_{\tau'}$)	Distortion correction (Mc/sec)	Measured frequency (Mc/sec)	Measured-calculated frequency	Reference
$2_1 \rightarrow 2_2$	−79.44	10 278.99	−0.01	2
$3_0 \rightarrow 3_1$	−469.87	50 236.90	+0.02	2
$3_2 \rightarrow 3_3$*	−14.95	824.64	+0.03	This work
$4_1 \rightarrow 4_2$	−118.87	5702.78	+0.01	9
$5_0 \rightarrow 5_1$	−540.98	22 307.67	−0.02	2
		22 309		1
$5_2 \rightarrow 5_3$*	−17.52	486.50	+0.03	This work
$6_1 \rightarrow 6_2$	−98.20	2394.56	+0.07	This work
$7_0 \rightarrow 7_1$	−402.24	8577.7	−0.20	9
$8_{-1} \rightarrow 8_0$	−1336.12	24 884.77	+1.53	9
		24 884.85		10
$9_0 \rightarrow 9_1$	−238.78	3044.71	+1.24	This work
$10_{-1} \rightarrow 10_0$*	−785.13	8836.95	+6.42	9
$11_{-2} \rightarrow 11_{-1}$*	−2269.64	22 581.1	+30.2	9
$12_{-1} \rightarrow 12_0$	−403.82	2961	−2	This work

[9] R. E. Hillger and M. W. P. Strandberg, Phys. Rev. **83**, 575 (1951).

TABLE III. Constants evaluated from Q-branch transitions.

Constant	Value
κ	−0.6830
$(a-c)/2$	2.54495×10^5 Mc/sec
x	-0.59612×10^{-4}
y	-1.47052×10^{-4}
B	-3.3569×10^{-4}
C	8.9140×10^{-4}
D	-12.3185×10^{-4}

With reference to the paper of Kivelson and Wilson[8] distortion constants in conventional form may be computed from the constants given in Table III. Posener and Strandberg[10] have calculated values of the constants from essentially the same data but using reduced energy matrices in the analysis of Q-branch transitions as well as with P- and R-branch ones. They have also computed "theoretical" values of these constants from infrared data.

Posener and Strandberg[10] have maintained that the use of approximation methods (e.g., the Kivelson-Wilson formula) must be checked by "exact" (matrix) calculations otherwise the constants obtained cannot be "true" molecular parameters but only constants in a semiempirical formula. This contention would seem to be supported by the fact that our values of the distortion constants are generally in poor agreement with their theoretical ones. However, it should be pointed out that the complete significance of these theoretical constants is not clear since Posener and Strandberg have not assigned errors to them nor have they discussed how these errors depend upon the errors in the infrared data from which they are computed. In fact, since their calculations were made, the results of Benedict, Gailer, and Plyler[11] on D_2O have yielded for the symmetrical stretching vibration $\nu_1=2671.79$ cm^{-1}, which is appreciably different from the value 2666 cm^{-1} upon which the calculations were based. Because of the complicated functional relationship between the distortion constants and the vibrational frequencies, without a great deal of computation it cannot be said whether the effect of this error would be large or small. However, until the errors in these theoretical constants are evaluated, a completely significant comparison between the theoretical and the experimental constants cannot be made.

Another possible explanation for the discrepancy between our distortion constants and the theoretical ones of Posener and Strandberg has been offered by

[10] D. W. Posener and W. M. P. Strandberg, J. Chem. Phys. **21**, 1401 (1953); Phys. Rev. **95**, 374 (1954).

[11] Benedict, Gailar, and Plyler, J. Chem. Phys. **21**, 1301 (1953).

TABLE IV. *P*- and *R*-branch transitions.

Transition ($J_\tau \rightarrow J'_{\tau'}$)	Measured frequency (Mc/sec)	Measured-calculated frequency	Reference
$4_{-3} \rightarrow 3_1$	20 460.4	−184.8	a
$4_0 \rightarrow 5_{-5}$	2887.4	−230.7	b
$6_{-2} \rightarrow 7_{-6}$	26 880.38	+323.4	c
	26 880.47		d

[a] See reference 2.
[b] This work.
[c] See reference 10.
[d] Jen, Bianco, and Massey, J. Chem. Phys. **21**, 520 (1953).

E. B. Wilson (private communication). Since effective moments of inertia are used in our calculations they implicitly take into account the effect of cubic terms in the potential energy. However, if the cubic terms are very small we may have, in effect, an overdetermined system, since only four potential constants, two equilibrium moments of inertia, and an inertial defect would be available as independent constants. Hence we could expect to determine only seven independent quantities from our equations rather than the nine we have obtained. Calculations of the effect of the cubic terms on the effective moments of inertia would be necessary to settle this point.

We should like to point out that since the Kivelson-Wilson treatment is a first-order perturbation method, it should give reliable results when the percentage correction is small. Since the two levels which combine to give a *Q*-branch transition are very closely related, a small percentage correction in frequency inevitably results in a small percentage correction in term value as well. When the correction is larger, higher order perturbations may have to be considered. Table II has shown that for distortion corrections up to about 8% of the observed frequency excellent agreement is obtained between calculated and experimental results (first 10 lines). It is only for the higher *J*-lines (10–12) that serious disagreement occurs. It is probable that the inclusion of higher order terms might be necessary when the distortion correction is of the order of 10%.

Although we have been able to fit a very wide range of data and to predict accurately the frequencies of four lines which were found later, our constants cannot be considered to give reliable predictions in all cases since their physical significance has not been established.

Nevertheless, while our distortion constants are in poor agreement with those of Posener and Strandberg, our rotational constants are in excellent agreement with both their "theoretical" and "experimental" ones. Furthermore, principal moments of inertia calculated from our rotational constants are in excellent agreement with those obtained by Benedict, Gailar, and Plyler[12] from infrared data, as shown in Table V. Also shown in Table V are values of the inertial defect $\Delta = I_a - I_b - I_c$. Classically Δ would be equal to zero, and its finite value is to be attributed to zero-point energy.

[12] Benedict, Gailar, and Plyler, J. Chem. Phys. **21**, 1302 (1953).

Therefore it would appear that in cases where only the rotational constants and moments of inertia are of interest, the Kivelson-Wilson formula may be employed with a considerable saving of effort in comparison with the exact method.

V. QUADRUPOLE SPLITTING OF THE $3_2 \rightarrow 3_3$ LINE

The observation of the $3_2 \rightarrow 3_3$ line offers a favorable opportunity for detecting hyperfine splitting arising from the interaction of the nuclear quadrupole moment of the deuteron with the electric field of the molecule. This opportunity is favorable because with such a low value of J the splittings are comparatively large. At the low frequency at which this line occurs excellent absolute resolution is obtainable as a result of the high degree of frequency stability easily obtainable and as a result of the small line width possible with the use of a large absorption cell. Earlier[5] we reported the presence of satellite lines 30 kc/sec on either side of the main line which we attributed to this splitting, but later experiments have shown that this effect was spurious. While no complete resolution has been obtained, these later experiments have exhibited changes of line shape with pressure which seem explicable only in terms of this hyperfine splitting, and which, in fact, yield an estimate of the quadrupole coupling constant. These observations will be described after a brief discussion of the theory of the splitting.

With a nuclear spin of $I=1$ for the deuteron, each of the two original $J=3$ levels is split into three levels having respectively total angular momenta of $F=2$, 3, and 4. From the first-order theory of Bragg,[13] which appears to be adequate for the present purpose, the splittings for the 3_3 and the 3_2 levels may be calculated to be given by

$$E_3 = eQ(1.4936q_a + 0.2960q_b + 0.2104q_c)Y(F,I,J) \quad (2)$$

and

$$E_2 = eQ(1.4958q_a + 0.2832q_b + 0.2210q_c)Y(F,I,J), \quad (3)$$

where eQ is the quadrupole moment of the deuteron, q_a, q_b, and q_c are, respectively, the second spatial partial derivatives along the axes of least, intermediate, and greatest moments of inertia, and $Y(F,I,J)$ is a function of the quantum numbers generally known as Casimir's function.

TABLE V. Principal moments of inertia of HDO.

Quantity	(Units are g cm^2 × 10^{-40}) This work	Benedict *et al.*[a]
I_a	1.1982	1.196
I_b	3.0862	3.076
I_c	4.3887	4.360
Δ	0.1043	0.088

[a] See reference 12.

[13] J. K. Bragg, Phys. Rev. **74**, 533 (1948).

For $I=1$ and $J=3$, $Y(F,I,J)$ has the values of 0.200, -0.250, and 0.083 respectively for $F=2$, 3, and 4. Transitions take place between these sets of hyperfine levels subject to the selection rule $\Delta F=0, \pm 1$. Since the numerical coefficients in Eqs. (2) and (3) are, respectively, very nearly equal, it may be inferred that the splittings of 3_3 and 3_2 levels are, respectively, very nearly equal. Therefore the three $\Delta F=0$ transitions occur at essentially the same frequency. The four $\Delta F=\pm 1$ lines form an approximately symmetrical pattern about this frequency, each of these having a theoretical intensity of about three percent of the combined intensity of the three $\Delta F=0$ transitions. However, under experimental conditions their relative intensities are exaggerated. With the low gas pressure required for high resolution a condition of partial power saturation is inevitable, and since the satellites have smaller transition matrix elements, their intensities are not diminished as much by the partial power saturation. A similar effect in the microwave spectrum of ammonia is well known.[14]

The average separation of these four satellite $\Delta F=\pm 1$ lines from the central $\Delta F=0$ line may be computed approximately in terms of eQq where q is the second spatial partial derivative with respect to the direction of the OD-bond by use of Eqs. (2) and (3). To evaluate q_a, q_b, and q_c in terms of q, three mathematical expressions are required. One of these is obtained from geometrical considerations involving transformation of axes. A second is immediately available since by Laplace's equation $q_a+q_b+q_c=0$. A third is obtained by assuming that the field has azimuthal symmetry about the bond. Although the validity of this assumption is somewhat dubious from many points of view, in the present calculation it can be considered a reliable approximation because of a very fortunate chance combination of the numerical values of the parameters. The bond is nearly parallel to the "a"-axis, the angle of inclination being about 17 degrees, and thus q_a is roughly equal to q. Any deviation from axial symmetry then affects mainly the values of q_b and q_c. On the other hand, it may be seen that in Eqs. (2) and (3) the coefficients of q_a are very much larger than the others, and therefore the results are not seriously affected by errors in the values of q_b and q_c. The result of these calculations is that

$$\Delta f=0.426eQq, \tag{4}$$

where Δf is the average magnitude of the spacing of the four satellites from the central $\Delta F=0$ line and where Δf and eQq are expressed in the same units.

In the experiment, the wings of the line appeared abnormally intense at low pressures. At high pressures, corresponding to half-power line widths of 100 kc/sec and greater, the one-tenth-power and one-fifth-power line widths were in the proportions expected from the Lorentz theory of line shapes. As the pressure was decreased the one-tenth-power line width increased steadily in proportion to the one-half-power line, while the one-fifth-power line width increased only slightly. The smallest observed half-power line width observed was about 30 kc/sec.

By comparing these observations with a series of calculated line shapes, a value of $\Delta f=93$ kc/sec was estimated. Another value was obtained by measuring the centers of the wings of the line in a number of recordings of the line made at high resolution. A value of 141 kc/sec was obtained. If the average value 117 kc/sec is substituted into Eq. (4), the value 272 ± 90 kc/sec is obtained for eQq. This value is in reasonable agreement with those obtained by White,[15] who has measured values of -175 ± 20 kc/sec for DCCCl and 300 ± 150 kc/sec for DCN.

The line shape should not have had significant distortion due to superposition of Stark components during the "on" portion of the cycle. On the "off" portion, imperfect zero basing may have made a very slight contribution to the minimum line width. Also the response time of the recording equipment was not quite negligible and made a slight contribution to the minimum line width. Most recordings appeared somewhat asymmetrical, the sign of the asymmetry depending upon the tuning of the rf system, which had a band width of 4 Mc/sec. Calculations in regard to the effect of this finite band width indicated that it could not explain the major observations which have been reported but residual effects of this type might tend to make the value of eQq of 272 kc/sec a few percent too large rather than too small.

V. ACKNOWLEDGMENTS

We wish to thank Professor M. W. P. Strandberg and Dr. D. W. Posener of MIT for helpful discussions and for access to their results prior to publication. Also we wish to thank Professor C. H. Townes and Dr. R. L. White of Columbia University for helpful discussions concerning quadrupole splittings.

Several important pieces of equipment were obtained from the Western Electric Company through its College Gift Program.

We wish to thank Fred Sterzer for performing measurements on the $5_2 \rightarrow 5_3$ line; Leon Arnell, Leonard Yarmus, and Sol Krongelb for building some of the equipment; and Howard Greenberg for performing some of the calculations.

[14] R. L. Carter and W. V. Smith, Phys. **73**, 1053 (1948).

[15] R. L. White, Phys. Rev. **91**, 1014 (1953).

Infrared Spectra of Intermediate Species in the Formation of Ammonium Azide from Hydrazoic Acid*†

DAVID A. DOWS,‡ GEORGE C. PIMENTEL, AND ERIC WHITTLE§
Department of Chemistry and Chemical Engineering, University of California, Berkeley 4, California
(Received December 20, 1954)

Infrared spectroscopic studies have been made of the solid formed when the products of the glow-discharge decomposition of hydrazoic acid are condensed on a surface cooled to 90°K. Spectra were obtained at several temperatures as the solid was allowed to warm to 230°K. The solid shows absorptions attributed to HN_3, NH_4N_3, and NH_3, and to two intermediate species in the reaction. These intermediates are interpreted to be N_2H_2 and $(NH)_x$, where x may be equal to 4. The presence of the imine radical, NH, in the solid at 90°K is inferred.

RICE and Freamo[1] have shown that when gaseous hydrazoic acid at low pressures is passed through a furnace or electric discharge, and the resulting gases are condensed on a surface cooled with liquid nitrogen, a blue, paramagnetic solid is formed. Upon warming to 148°K there is a sudden transition to a white solid, found to be ammonium azide. These authors propose that hydrazoic acid is decomposed according to the reaction

$$HN_3 \rightarrow NH + N_2$$

and that the imine radicals thus formed condense on the cold surface either as NH or as some polymer thereof. At 148°K the condensed radicals become capable of further reaction to form ammonium azide. The blue color and paramagnetic properties are attributed to the presence of the unpaired electrons of the imine radical, of diimide, N_2H_2, or of higher polymers, $(NH)_x$.

In a similar experiment, Mador and Williams[2] condensed the gases resulting from the decomposition of HN_3 and studied the solid so obtained spectroscopically. In the infrared region all spectral features could be attributed either to the undecomposed reactant, hydrazoic acid, or to the final product, ammonium azide. In the visible and ultraviolet region, absorption bands were observed at 3500 and 6500 A which disappeared when the solid was warmed above 148°K. These bands were ascribed to small amounts of NH and NH_2, respectively, present in the blue solid.

This paper presents the results of independent investigations of the infrared spectrum of the blue solid.[3] The infrared spectra contrast with those described by Mador and Williams in that unidentified infrared spectral features were observed which display the temperature behavior appropriate to unstable intermediate species. The temperature dependences of these features were studied carefully to aid in the identification of the intermediates.

EXPERIMENTAL

In the experiments to be described, the solid film was prepared by passing hydrazoic acid through a glow discharge at a pressure of about 0.1 mm of mercury and condensing the resulting gases on the cold window of a low-temperature optical cell. The cell was continuously evacuated to remove any noncondensable gases (e.g. nitrogen) produced in the reaction. The hydrazoic acid was prepared as described earlier.[4] The low-temperature cell was similar to others described in the literature[5] except for details of sample inlet and window mounting. The temperature of the sample was measured with a copper-constantan thermocouple, which was protected by a thin gold tube and imbedded in the center of the silver chloride window. (A sodium chloride window was used in several experiments without any effect on the results.)

The glow discharge tube and the sample inlet tube were combined, as shown in Fig. 1. This device was connected to the body of the cold cell near the window assembly by a taper joint, and extended into the cell, terminating in a glass spray-on tube which directed

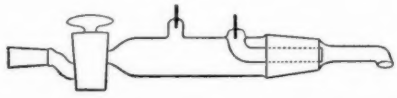

FIG. 1. Glow discharge and sample inlet tube. The electrodes are tungsten rods sealed directly into the Pyrex tube. The tube is joined to the cold cell by the large taper joint.

* Taken from a dissertation presented to the Faculty of the Graduate School of the University of California by David A. Dows in partial fulfillment of the requirements for the Ph.D. degree.

† This work was supported by the Office of Naval Research under contract number N-222(16).

‡ Present address: Department of Chemistry, Cornell University, Ithaca, New York.

§ Present address: Department of Chemistry, University College, Cardiff, Great Britain.

[1] F. O. Rice and M. Freamo, J. Am. Chem. Soc. **73**, 5529 (1951); **75**, 548 (1953).

[2] I. L. Mador and M. C. Williams, J. Chem. Phys. **22**, 1627 (1954).

[3] Henceforth the condensed hydrazoic acid decomposition products will be called the "blue solid" although the blue color described by Rice and Freamo could not be observed under conditions suitable for infrared studies.

[4] D. A. Dows and G. C. Pimentel, J. Chem. Phys. **23**, 1258 (1955).

[5] See, for example, E. L. Wagner and D. F. Hornig, J. Chem. Phys. **18**, 296 (1954).

the gases onto the window. The tube was curved in such a way that it could be turned out of the optical path without breaking the vacuum after the sample was prepared. The design of this tube brought the end of the glow discharge region to within 3 cm of the cold window. This reduced the loss of reaction intermediates in the time between their production and their condensation on the cold window. Other experiments using glow discharge tubes and pyrolysis ovens at approximately 15 cm from the cold window failed to give distinct evidence of reaction intermediates in the solid.

The spectra were obtained using a Perkin Elmer Model 21 Spectrophotometer with sodium chloride optics. Frequency accuracy is about 30, 15, and 5 cm^{-1} at 3000, 2000, and 1000 cm^{-1}, respectively. Spectral slit widths are shown on the spectra.

RESULTS

Reaction Products

Experiments were performed to determine whether there were any other products of the reaction beside ammonium azide, which was found by Rice and Freamo[1] and confirmed by this work as the only solid product. It was found that no noncondensable gas was given off when the blue solid warmed to room temperature. Condensable gaseous products were observed, in one experiment ammonia and in all others undecomposed hydrazoic acid. There is eivdence that both ammonia and hydrazoic acid are present in the solid, and it appears that ammonia is formed in the reaction but is removed by reaction with HN_3.

Spectroscopic Observations

During the deposition of the solid films studied spectroscopically, the window of the cold cell was kept at 85 to 90°K. The infrared spectrum of the solid was obtained with the sample at 90°K, and then the liquid nitrogen coolant was allowed to evaporate so that the sample warmed, first to 120°K and then in steps of approximately 10°K to 230°K. The spectrum was recorded at each step. Figure 2 shows several of the spectra obtained in a typical experiment. Other spectra obtained at intermediate temperatures showed no significant changes, and are omitted.

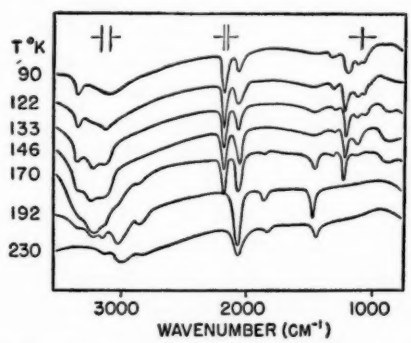

FIG. 2. Infrared spectra of the blue solid as a function of temperature. Percentage transmission at each temperature is plotted on the ordinate.

TABLE I. The effect of increasing temperature on intensities of the infrared absorption bands of the blue solid.

T°K	HN_3	NH_4N_3	A 3320 cm^{-1} 1090 cm^{-1}	B 3230 cm^{-1} 860 cm^{-1}	NH_3 1060 cm^{-1}
90	present	present	present	···	present
120–124	transition[a]	no change	no change	present	no change
120–124	no change	no change	no change	increase	no change
130–135	no change	no change	no change	increase	no change
144–148	decrease	increase	no change	increase	absent
145–151	no change	increase	no change	increase	···
152–160	no change	increase	decrease	no change	···
168–172	no change	increase, transition[b]	decrease	no change	···
178–182	no change	increase	absent	decrease	···
190–194	absent	increase	···	decrease	···
208–213	···	no change	···	no change	···
230	···	decrease	···	absent	···

[a] See reference 3.
[b] See reference 5.

The spectrum obtained with the solid at 90°K shows bands due to[4] HN_3 (at 3100, 2160, 1300, and 1180 cm^{-1}) and to[6] NH_4N_3 (at 2050 and 1440 cm^{-1}). Also present are three other bands, at 3320, 1090, and 1060 cm^{-1}. At 120°K two new bands have appeared, at 3230 and 860 cm^{-1}, and the changes in the spectrum of HN_3 which accompany its transition[4] have occurred.

The changes in intensity of the five unassigned bands (at 3320, 3230, 1090, 1060, and 860 cm^{-1}) indicate that these bands can be assigned to three compounds. The first, compound *A*, gives rise to the two bands at 3320 and 1090 cm^{-1}, which are present in the spectrum obtained at 90°K and disappear at about 175°K. The second, compound *B*, gives rise to the bands at 3230 and 860 cm^{-1}, which appear between 90 and 120°K and disappear above 190°K. The band at 1060 cm^{-1} is ascribed with confidence to ammonia, for two reasons. First, the strongest band in the spectrum of solid ammonia[7] is known to be at 1060 cm^{-1}. Second, the disappearance of the band at 1060 cm^{-1} is accompanied by a decrease in the intensity of the HN_3 absorption and an increase in the intensity of NH_4N_3 absorption. It seems clear that ammonia reacts with undecomposed hydrazoic acid to form ammonium azide.

The changes in intensity of the various bands as the temperature is increased are summarized in Table I. The entries in the table indicate the changes in the intensities of absorption by the substances listed at the top when the temperature is raised to the value given in the first column.

DISCUSSION

Since the absorptions of compounds *A* and *B* are not due to the reactant or to the final product of the reaction, these compounds must be intermediate species in the reaction. In addition, since the bands at 3230 and 860 cm^{-1} (and therefore the intermediate *B*)

[6] Dows, Whittle, and Pimentel, J. Chem. Phys. **23**, 1475 (1955).
[7] F. P. Reding and D. F. Hornig, J. Chem. Phys. **19**, 594 (1951).

appear without the decrease of any other bands, there is probably a third intermediate present, C, which is not observed spectroscopically.

The evidence available indicates that all the intermediates are eventually converted into ammonium azide. From the fact that the two clearly observed intermediates, A and B, disappear at different temperatures, each forming some ammonium azide, each of these intermediates is assumed to have the chemical constitution $(NH)_x$. In this case, the third intermediate, C, whose presence was inferred from the growth of B, may also be a species with formula $(NH)_x$. Since considerable amounts of C must be present to account for the high intensity of B, the most likely identity of C is NH. This molecule has only one absorption frequency, which could easily be obscured by the strong absorptions of HN_3 and NH_4N_3 near 3000 cm^{-1}. Any more complicated molecule which might be postulated for C should have been observed spectroscopically.

This interpretation does not utilize the species NH_2, proposed by Mador and Williams[2] to account for the absorption near 6500 A. The lack of any evidence of the most intense infrared features of solid hydrazine[8] tends to corroborate the absence of NH_2. The possibility that species A could be NH_2 does not seem large in view of the absence of spectral evidence of any final product except NH_4N_3. Hence no interpretation of the detailed observations on that premise is presented. On the other hand, the inference that species A, B, and C, all have the stoichiometry of N_xH_x seems to be sufficiently likely to search for a self-consistent explanation of all of the observations. The following interpretation is based upon this inference.

Interpretation of Observations

The material condensed on the window at 90°K consists of a mixture of NH_4N_3, HN_3, a small amount of NH_3, and two reaction intermediates, A and C. The reaction intermediate C is presumed to be NH, and the blue color and paramagnetism observed by Rice and Freamo are attributed to this species. The species A is presumed to have the formula $(NH)_x$, with x greater than 2.

As the temperature is raised the smallest molecular species present will begin to diffuse through the solid. The smallest molecules present are the NH radicals, and these will diffuse until collision between two NH radicals permits formation of N_2H_2, diimide. It seems reasonable to assume that the NH radicals cannot react with either HN_3 or NH_4N_3 or they would not have survived the preparation process. In addition, it seems unlikely that the reaction $NH+(NH)_x \rightarrow (NH)_{x+1}$ has occurred, since the spectrum of $A=(NH)_x$ has not been altered. The diffusion of NH to form N_2H_2 accounts for the gradual appearance of compound B over a range of temperature. In this same temperature range the transition of solid HN_3 is observed, and the ammonia molecules disappear, presumably by diffusion and then reaction with HN_3 to form NH_4N_3.

At still higher temperatures, diffusion of the larger molecules begins. In sequence, the transition of NH_4N_3 is observed, then the rearrangement of $A=(NH)_x$ to ammonium azide, and finally the diffusion and combination of diimide molecules to give ammonium azide. When the temperature reaches 190°K, HN_3 sublimes out of the solid. This leaves only solid ammonium azide, which itself sublimes away above 230°K. The interdependent interpretations involved in this explanation are summarized below.

1. The spectral features at 3320 and 1090 cm^{-1} are due to the same compound, A, and those at 3230 and 860 cm^{-1} are due to another single compound, B.
2. Since the spectrum of B appears without decrease of the spectrum of any other compound, B is produced from a third, unobserved compound, C.
3. Each of the substances A and B produce ammonium azide without evidence of other products, hence each is assumed to have the same stoichiometry as ammonium azide, $(NH)_x$.
4. The substance C is assumed to be the radical NH. This identification explains the paramagnetism, the blue color, the absence of infrared spectral evidence of C, the formation of B at a low temperature, and the stoichiometry of B.
5. If C is NH, then B is N_2H_2, diimide.
6. If C is NH and B is N_2H_2, then $A=(NH)_x$ must correspond to x above 2.

The Structure of Diimide

Presuming the correct identification of species B as diimide, the spectral features contain information concerning the structure of this species. Three possible structures are: (1) linear, $D_{\infty h}$, as in acetylene, (2) planar, zig-zag, C_{2h}, and (3) nonplanar, C_2, as in hydrogen peroxide. These structures imply, respectively, two, three, and six infrared-active fundamental frequencies. On the basis of the observation of only two features assignable to B, structure (3) is least likely. There seems to be no basis for choice between structure (1) and structure (2).

All structures which could be proposed for $A=(NH)_x$ should have more than two infrared-active vibrations. If $-NH_2$ groups are involved, absorptions near 1600 cm^{-1} and 800 cm^{-1} should be observed. The absence of such absorptions implies a molecule of the type $(\cdots NH-NH-NH\cdots)$. Such a structure might have unpaired electrons on the terminal nitrogen atoms. Therefore this intermediate might contribute to the color and magnetic properties of the blue solid.

[8] Strong infrared absorption bands of solid hydrazine were observed at 1061 and 881 cm^{-1} by W. Haunschild, Ph.D. thesis, University of California, 1954.

CONCLUSIONS

The infrared spectral evidence clearly indicates the presence in the blue solid of molecular species which are intermediate in the decomposition of hydrazoic acid to form ammonium azide. The behavior of these species on warming suggests that they have the stoichiometry of NH, and a self-consistent interpretation of all of the observations can be based upon this premise. The value of the experimental technique as a means of identifying reactive or unstable molecules is established. When the identity of such a molecule has been determined, the spectrum contains valuable information concerning bond strengths and molecular structure.

ACKNOWLEDGMENTS

The authors are grateful for the valuable aid and guidance of Professor Richard E. Powell.

THE JOURNAL OF CHEMICAL PHYSICS VOLUME 23, NUMBER 9 SEPTEMBER, 1955

Adsorption of Strontium and of Barium on Tungsten

GEORGE E. MOORE AND H. W. ALLISON
Bell Telephone Laboratories, Inc., Murray Hill, New Jersey
(Received December 6, 1954)

Sr or Ba was deposited on W ribbon receivers by evaporation from source filaments in which a chemical reaction produced the metal at least 99.7% pure. The receiving surfaces could be cleaned at will by heating to high temperatures; repeated tests were thus possible. By thermionic measurements, adsorption and desorption were observed independently under nonequilibrium conditions. By using radioactive Sr isotopes, the deposit corresponding to any thermionic activation was measured. For each ribbon, thermionic activation was apparently a reversible function of the amount adsorbed.

Our experimental methods give information on kinetics, rather than equilibria. The adsorption mechanism more nearly resembles that proposed in Langmuir's later papers rather than that of his earlier theories but treatment of desorption by the theory of absolute reaction rates is considerably more satisfactory. This accounts for desorption kinetics over the experimental temperature range by only two disposable constants, the activation energy for desorption, (a.e.d.), and a repulsive energy of interaction between adatoms.

The work function φ for a monolayer of Sr is $\sim$2.2 v and for Ba is $\sim$1.9 v. The thermionic activation is explained in terms of polarized adatoms, rather than by the usual assumption of partial ionization, which has no experimental justification for Ba or Sr films. The theory proposed gives a reasonable value for the polarizability of Sr and of Ba, which when substituted into the theory of Prosen, Sachs, and Teller predicts a heat of physical desorption agreeing well with the observed a.e.d. This also agrees with the heat of desorption (h.d.) determined by the usual method of applying the Clapeyron equation to kinetics of this kind. We therefore believe that this adsorption should be called "physical," rather than "chemical," although the mean a.e.d.'s are, for Sr 77.4, and for Ba 80.7 kcal/mole, considerably larger than for most examples of chemisorption.

INTRODUCTION

FOR fundamental measurements in adsorption, electropositive metals on tungsten surfaces have major experimental advantages. Of adsorbing surfaces, only W, Mo, and Ta can be cleaned conveniently to yield reproducible and definable surfaces. Among adsorbates, the electropositive metals form relatively stable films which modify surface properties so profoundly that effects are readily measured; their tendency to form diatomic molecules is so slight that dissociation phenomena do not complicate interpretation.

Martin[1] and Nichols[2] showed important differences between the crystal faces of tungsten adsorbents. Ideally, one should, therefore, study adsorption on a definite face of a clean tungsten crystal, but crystals sufficiently large are scarce. Therefore, tungsten ribbons were used. The process of rolling tungsten often[3–5] orients the flat surface[6] in the (100) direction within 10°, thus giving a more homogenous surface than wires. Even when the ribbons were good approximations to the 100 face, there were definite differences from ribbon to ribbon that we attribute to variations in the distribution of crystal faces.

EXPERIMENTAL

Tube Design

Several methods are available for supplying Ba (or Sr) for adsorption experiments. Anderson[7] used a reservoir of bulk Ba and transferred it to the adsorbent surface by repeated fractional distillation. Others have used commercial getters. For our work, production of Sr or Ba metal by chemical reaction in the experimental

[1] S. T. Martin, Phys. Rev. **56**, 947 (1939).
[2] M. Nichols, Phys. Rev. **57**, 297 (1940).
[3] W. G. Burgers and J. J. A. Van Amstel, Physica **3**, 1064 (1936).
[4] J. F. H. Custer and J. C. Riemersma, Physica **12**, 195 (1946).
[5] Apker, Taft, and Dickey, Phys. Rev. **73**, 46 (1948).

[6] Tests made with the guidance of Mrs. E. A. Wood showed this same trend in our ribbons, during approximately the first half of this work; the crystals of W were small, usually about 0.01 cm in diameter. Examination of the later ribbons shows that the crystals became much larger with a mean orientation about 17° to 25° off the 100 direction. This trend was not detected by any of the measurements of adsorption, probably because faces near the 100 are most strongly affected by adsorption.
[7] P. A. Anderson, Phys. Rev. **47**, 958 (1935); and later papers.

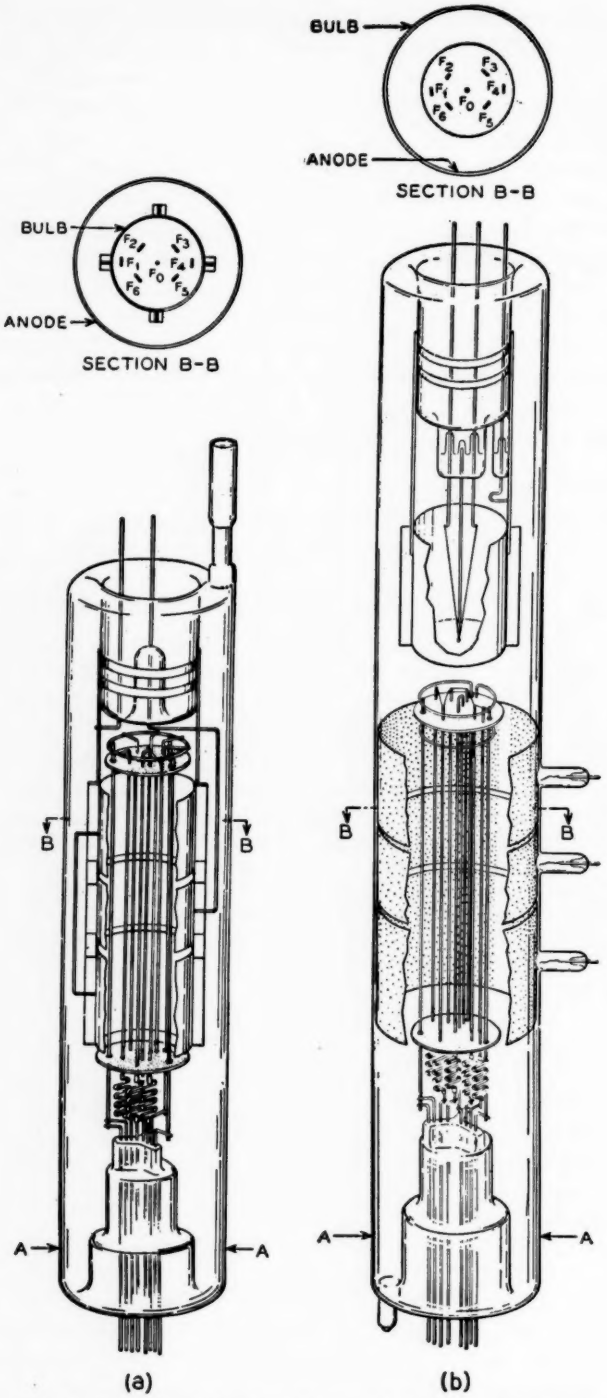

FIG. 1. Experimental tubes. On completing thermionic tests, tubes opened along AA to remove bulb and anode from filament structure. Filaments then demounted without contamination, for radioactive counting. (a) Design used for most work; θ for Sr must be less than 2.0. (b) Design used for preparing multilayer films. Upper anode is Mo coated with Zr. To improve vacuum, this can be heated by electron bombardment.

tube was more convenient; this permitted a design similar to those used in measurements[8] with SrO and BaO.

[8] G. E. Moore and H. W. Allison, Phys. Rev. **77**, 246 (1950).

Adsorption was examined by a combination of thermionic and radioactive techniques. Thermionic measurements were made during repeated adsorption and desorption of Sr and/or Ba on each ribbon. Then the tube was opened and the ribbon receivers removed. The deposit was determined radiochemically and correlated with thermionic activity. Because of the short half-life (12 days) of Ba, radioactive tests were made only with Sr;* the behavior of Ba was assumed analogous.

Figures 1(a) and 1(b) show the experimental tubes. Filament F_0 served as a source of Sr or Ba metal and filaments F_1–F_6 were clean W ribbons. One side of these intercepted atoms of Sr or Ba produced in F_0. Alternatively, F_0 was a clean tungsten ribbon and four outer filaments were sources, two for Ba atoms and two for Sr. In this way, Ba and Sr were compared by applying either metal to both sides of a given receiver surface. The construction gives a long insulation path between filaments and anode, making for accurate measurement of small emission currents.

Because coatings in excess of the monolayer evaporate comparatively readily, the receiver temperatures must be low to observe multilayer adsorption. To produce Sr sufficiently rapidly for convenient experiment, the source filament must operate at 1200°K or higher, which requires about 12 watts. Reflection of this energy from the bright Mo anode surfaces causes the receivers to operate to 500° to 600°K during Sr deposit, as determined from resistivity measurements. A receiver temperature, during deposit, of not over 450°K is achieved in the design of Fig. 1(b) because the anodes consist of aquadag rings on the glass bulb. Double layer deposits of Ba are obtained, in either design. Sixteen tubes of the two designs were used in various experiments.

Vacuum

In common with earlier work,[8] the pressure in tubes as in Fig. 1(a) was less than 10^{-14} mm for any gas which could affect the work function by 0.1 volt or more. These high vacua result[8] from a rigorous exhaust schedule and the use of Zr getters. In the design of Fig. 1(b), results indicate a poorer vacuum, of the order of 10^{-13} to 10^{-12} mm, probably because of the aquadag anodes and the smaller Zr surface available.

Sources of Sr and of Ba

The material leaving a hot tungsten filament coated with bulk SrO consists[9] of 99.7% Sr atoms, and about 0.3% SrO molecules. Such filaments, usually with added W powder, were the sources of Sr metal. The Ba source was a commercially available mixture[10–12]

* Supplied by Oak Ridge National Laboratory, Oak Ridge, Tennessee.

[9] Moore, Allison, and Morrison, J. Chem. Phys. **18**, 1579 (1950).

[10] E. A. Lederer and D. H. Wamsley, RCA Rev. **1**, 117 (1937).

[11] E. A. Lederer, RCA Rev. **4**, 310 (1940).

[12] RCA Bulletin TPM 1500, "Batalum Getters for Electron Tubes."

of $BaBeO_2$ and Ti powder applied to Mo ribbons 0.040 in.×0.0005 in. or Mo wires 0.010 in. diameter. Presumably, substantially all BaO is in the form of $BaBeO_2$ which has a vapor pressure much lower than that of BaO. These sources supplied Ba at experimentally practical rates at such a low temperature that not over 1 part in 430 could be BaO even after producing 100 monolayers of Ba on the receivers. The sources of Ba are less convenient than the Sr sources and produce Ba at a rate which declines with age. Either source required considerable aging before results were reproducible.

Measurements

Adsorption of electropositive elements to tungsten decreases the work function from that of clean tungsten to that characteristic of the adsorbed monolayer; additional deposit causes no further decrease, and may cause an increase.

To avoid evaporation, thermionic activity was usually measured by determining the temperature, T, required for a fixed emission density, usually 5.1×10^{-8} amps/cm², rather than by Richardson plots. As the clean receivers were coated with Sr, T decreased from about 1460°K, appropriate for clean tungsten, to 795°K±5°. T can be used for approximate determination of φ in Richardson's equation,

$$I=AT^2\exp(-\varphi e/kT).$$

Measurements illustrated in Appendix I suggest that A is ~60 at all coverings for all receiver filaments, although precision is inherently low. Assuming that $A=60$ for every observation, and neglecting variation in the T^2 term, φ can be calculated directly from a measurement of temperature for fixed emission density from

$$\varphi=\varphi_0 T/T_0. \qquad (1)$$

φ and T apply to the coated tungsten for the fixed emission density, and φ_0 and T_0 apply to the clean tungsten ribbon. φ determined from Eq. (1) agrees approximately with determinations from Richardson lines.

Radioactive measurements were made by comparing the count from the experimental ribbons with the count from calibration samples, each consisting of a known amount of the mixture used to coat the source. Calibration samples were deposited on tungsten or tantalum sheet, to avoid background error in comparison with counts from experimental tungsten ribbons. The 25-year isotope, Sr^{90}, was used in all experiments.

RESULTS

1. Amount of Sr in a Monolayer

Two methods were used to prepare monolayers; the activation curves of Fig. 2 illustrate the first. Abscissas show the hours during which Sr metal was deposited. The ordinates are temperatures required for the fixed emission of 5.1×10^{-8} amp/cm². Because φ is usually[13,14] considered a minimum for a monatomic film, one would expect a monolayer at the 11 hour point of Fig. 2(a). Because of gradual approach to horizontal, accurate detection of this point is difficult until it has been passed. Table I gives the density on the three sections of the ribbon, each corresponding to the adjacent section of the anode. The 12% rms spread between sections is typical. The central section supplies the measured emission, so that the monolayer is taken as 0.0708 μg/cm², or 4.91×10^{14} atoms/cm².

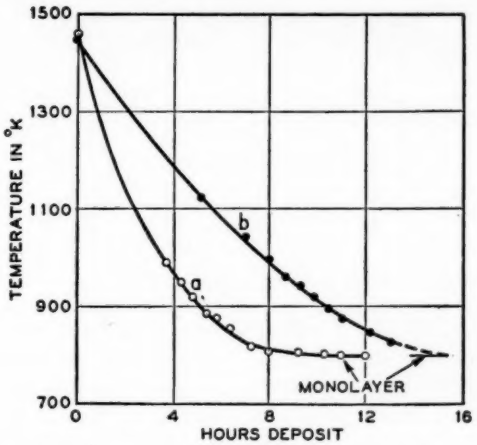

FIG. 2. Activation curves illustrating first method for preparing monolayers. (a) Receiver 2 tube 50–2 run 19A, coated to the monolayer. (b) Receiver 2 tube 19–3 run 6A, not coated quite to monolayer; curve extrapolated on dotted line by comparison with past runs on same receiver. Difference in shape of curves illustrates individuality of different receiver ribbons.

Figure 2(b) shows a modification. The receiver was not coated quite to the horizontal portion of the activation curve, which was therefore extrapolated to 800°K, by comparison with past runs on this same receiver. The comparison indicated that 0.90 layer had been applied, so that the amount found, 4.48×10^{14} atoms/cm², was divided by 0.90 to give 4.99×10^{14} atoms/cm² for the monolayer.

In the second method, several layers of Sr were applied, as judged by the deposit time required for a monolayer. Because the first layer is generally believed much more stable than the second and higher layers, the receiver was then heated for 1 hour at 800°K. At this temperature, vaporization of bulk Sr is very rapid,

TABLE I. Sr on receiver 2, tube 50–2.

Center	0.0708 micrograms/cm²
Top	0.0867
Bottom	0.0665
Mean	0.0747±12% rms

[13] Langmuir [Phys. Rev. 44, 423 (1933)] believed that the minimum work function occurs at less than a monolayer, about 0.67 for Cs-on-W and 0.70 for Th-on-W, but most authors accept the monolayer condition.

[14] J. H. DeBoer, *Electron Emission and Adsorption Phenomena* (Cambridge University Press, Cambridge, England, 1936).

TABLE II. Amount of Sr in a monolayer.

Tube	Fil. #	Method	Density of Sr (atoms/cm² ×10⁻¹⁴)
50–2	2	1	4.91
359	2	2	5.01
19–3	2	1	4.99
437	2	1	4.86
437	3	2	4.66
			Mean 4.89±0.132 rms

but the thermionic emission of a monolayer, and hence presumably its physical state, remains unaffected. The Sr residue after such treatment agreed with that found by the first method. Measurements of a monolayer by the two methods are summarized in Table II. The probable error in each determination is not over 2% and the probable graphical error in preparing a monolayer is of this same order. The tungsten surface was considered smooth.

The amount found is comparable with that expected as shown in Fig. 3. Only alternate adsorption sites could be occupied on a surface with sites spaced at 3.15 A. Thus, 5.03×10^{14} atoms of Sr could be adsorbed per cm²; the observed amount $4.89(\pm0.13)\times10^{14}$, agrees reasonably well. The amounts to be expected on some other crystal faces would be about the same.

2. Amounts Less Than a Monolayer

By the surface phase postulate,[13] behavior of an adsorption system is completely determined by temperature and amount adsorbed. The preceding experiments indicate that this postulate applies at the monolayer condition, because the thermionic emission of the monolayer is independent of the direction from which the monolayer was approached. The next experiments examine behavior for amounts less than a monolayer.

Ideally, one would make detailed measurements, on each of several receivers, of thermionic activity and corresponding amounts of Sr for several different coatings. Each value of θ (the fraction of the surface coated) would be approached from both directions. But radioactive counting requires dismounting the ribbon which thus can yield only a single point.

The experiments are divided into two groups. In the first, eight receivers from four tubes were coated with less than a monolayer, and then counted. Each ribbon was cut into three sections, and the amount found on the central section plotted against the observed emission level, in Fig. 4, as open circles. In the second group, five filaments in three tubes were each coated with from two to six layers and then heated until their thermionic activity indicated less than a monolayer; they were then counted. Their data are shown as solid circles.

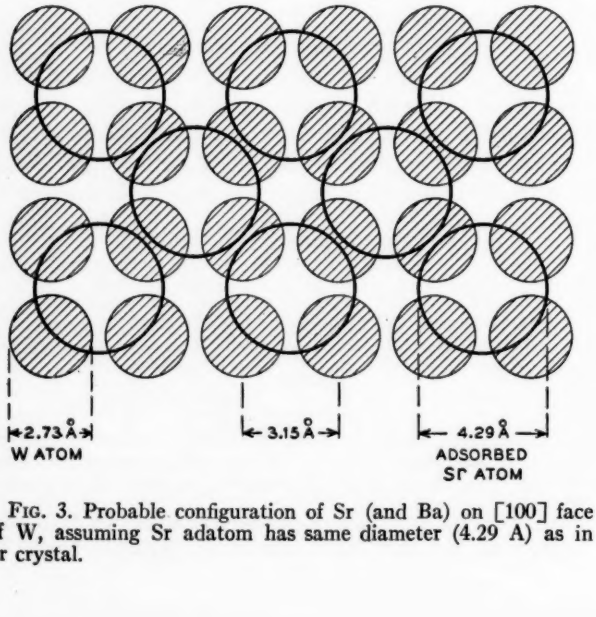

FIG. 3. Probable configuration of Sr (and Ba) on [100] face of W, assuming Sr adatom has same diameter (4.29 A) as in Sr crystal.

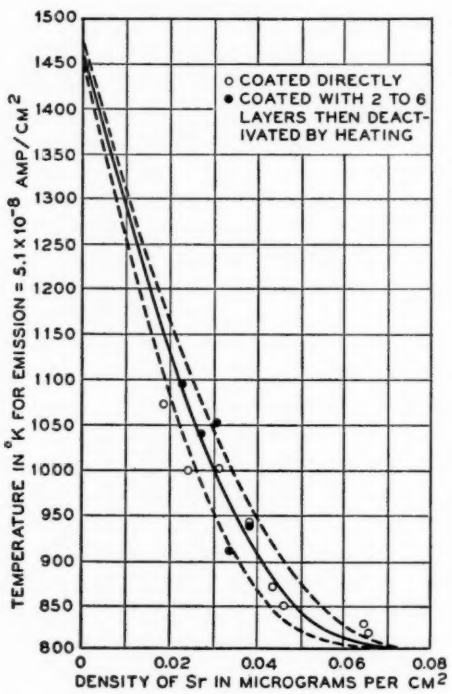

FIG. 4. Test of Surface Phase Postulate. Because solid points, obtained by approaching indicated density from right, agree with central curve as well as open points, obtained by approaching from left, the postulate is believed confirmed. Scatter is result of individuality of receivers, rather than error in measurement. Monolayer of 4.89×10^{14} atoms or 0.0705 μg per cm².

Densities in column 4 apply to the central section. Column 5 gives the rms spread over the three sections, as in Table I, and indicates the nonuniformity of Sr deposit along the length of the receiver. This variation probably results principally from variations in chemical activity along the source filaments, and seems random; density on the central sections, with minimum end-cooling, was not significantly different from the density on the end sections. The final column is discussed in Sec. 3.

The solid curve of Fig. 4 was constructed by averag-

ing activation data for all eight filaments. Curves on any one filament were reproducible. One therefore constructs an "experimental" curve of "density of deposit" *vs* "test temperature," as in Fig. 4, down to 825°K for each filament by using the measured amount of Sr and the preceding complete run for that filament. The mean abscissae of the eight samples were computed at each 50° ordinate. This gave the solid curve; the dotted curves show the rms spread about this mean. The open circles show the experimental points of Table III. Their rms deviation from the solid curve is 0.0056 $\mu g/cm^2$. The spread at 800°K is that for the monolayer from Table II.

The second set of measurements is given in Table IV and in Fig. 4 by solid circles. The rms deviation of Table IV is 0.0037 $\mu g/cm^2$, (about $\frac{2}{3}$ as great as for the points in Table III which determine the curve) suggesting that a nonuniform density of deposit tends to equalize when multilayer coatings are heated to 1000°K or above. The available data are, therefore, consistent with the Surface Phase Postulate; thermionic activity is probably determined reversibly to a first approximation on any *one* receiver by density of deposit, whether that density is fresh deposit or the residue after heating a larger deposit. One can therefore investigate desorption by studying deactivation.

TABLE III. Coating tests for amounts less than a monolayer (method I).

Tube#	Fil.#	Coated to	Sr in atoms/cm²	R.M.S.%	Atoms/cm² indicated in a monolayer
19–3	2	826°K	4.48×10^{14}	37.8	4.98×10^{14}
37–1	2	817	4.52	24.4	5.34
37–1	5	942	2.63	13.7	5.12
37–1	6	1000	1.66	20.7	4.98
69–1	3	1073	1.27	33.2	4.36
70–1	2	1002	2.14	16.3	5.05
70–1	6	848	3.18	14.8	4.44
70–1	7	870	3.01	18.1	5.20
				Mean 22.4	4.94 ±7% rms

We believe the scatter in Fig. 4 depicts an "individuality" in the receiver filaments, originating in such factors as variations in distribution of exposed crystal faces, cracks, or variations in surface roughness, all of which are observable. Desorption experiments give further evidence of individuality.

3. Uniform Time Rate of Deposit up to the Monolayer

In combination, the data for each filament of Table III and its activation curve suggest that during any coating run, Sr is adsorbed at a uniform rate. Thus the density of Sr on filament 5 of tube 37–1 was 2.63×10^{14} atoms per cm^2 after operation of the source for 315 min. In the preceding run, the monolayer was achieved in 615 min, judged by thermionic activity. Then, with uniform adsorption rate for $0<\theta<1$, the monolayer will contain

$$615/315\times2.63\times10^{14}=5.12\times10^{14}\ \text{atoms/cm}^2.$$

Similarly calculated values are entered in the final column of Table III. The mean of all eight tests, 4.94×10^{14} atoms per cm^2, agrees (fortuitously well) with the more directly measured amount, 4.89×10^{14} atoms per cm^2, of Table II. Precision in Table III is poorer, but the results strongly suggest that the probability of adsorption is unity for $\theta\leq1.0$.

TABLE IV. Receivers coated with 2 to 6 layers and deactivated by heating, to less than a monolayer (method II).

Tube#	Fil.#	Preparation	Density atoms/cm²	rms%
37–1	4	Apply 2 layers; heat at 1000°K; deactivate to 936°K.	2.63×10^{14}	28.6
37–1	6	Apply 2 layers; heat at 1000°K; deactivate to 912°K.	2.30	3.3
469–1	2	Apply 3 layers; heat at 1000°K; deactivate to 1040°K.	1.87	23.2
469–1	4	Apply 6 layers; heat at 1050°K; deactivate to 1052°K.	2.12	10.9
70–1	3	Apply 3 layers; heat at 1100°K; deactivate to 1096°K.	1.56	12.1
				Mean 15.6%

This uniform deposition rate contradicts the assumption in Langmuir's original derivation[15] of the adsorption isotherm, that incoming atoms which strike a site already covered, evaporate immediately. The probability that an incoming Sr atom first strikes an occupied adsorption site increases rapidly with θ. If such atoms re-evaporate almost immediately, or re-evaporate during subsequent thermionic test, the second half layer would form much more slowly than the first. The observed uniform rate indicates that Sr atoms deposited initially in a partial second layer probably migrate to vacant lattice sites.

4. Deposits Thicker Than Monatomic

One might predict[16–18] that films thicker than one or two atomic layers would vaporize very much like bulk metal. At 600°K, a layer of bulk Sr evaporates[16] in 4 or 5 sec. At 550°K this requires about 55 sec and at 450°K, about 31 hr.

Several filaments in tubes made according to Fig. 1

[15] I. Langmuir, J. Am. Chem. Soc. **38**, 2221 (1916).
[16] Computed from constants given by S. Dushman *Scientific Foundations of Vacuum Technique* (John Wiley and Sons, Inc., New York, 1949).
[17] L. N. Dobretzov and G. A. Morozov, Physik. Z. Sowjet union **9**, 352 (1936).
[18] I. Langmuir, J. Franklin Inst. **217**, 543 (1934).

TABLE V(a).

Tube#	Fil.#	Treatment	Density Sr atoms/cm²	Layers
19–3	4	Deposit 2½ layers. Heat for thermionic test only.	8.74×10^{14}	1.79
359	3	Deposit 16 layers. Heat 1 hour at 700°K.	9.85×10^{14}	2.02
469	5	Deposit 6 layers. Heat at 650°K for 4 hours.	4.74×10^{14}	0.97
469	6	Deposit 6 layers, Heat at 700°K for 3 hours.	5.33×10^{14}	1.09
469	7	Deposit 6 layers. Heat at 700°K for 3 hours.	4.35×10^{14}	0.89
470	4	Deposit 6 layers. Heat at 600°K for 50 minutes.	6.30×10^{14}	1.29
470	5	Deposit 6 layers. Heat at 550°K for 70 minutes.	5.96×10^{14}	1.22

or 2 received Sr sufficient for several layers, if all adhered. No thermionic tests were made after the monolayer; the receivers were then heated to temperatures given in Table V(a) and prepared for radioactive count.

Note that in only one of the seven tests is the deposit as much as 2 atoms thick, although in five cases the deposit is appreciably greater than monatomic. This suggests that the second layer is more tenacious than the third and higher layers but not nearly so tenacious as the first.

Table V(b) shows attempts to produce coatings more than two layers thick, utilizing the aquadag-on-glass anode system.

Each receiver retained more than two layers but less than the amount deposited. These filaments all operated at 450° to 500°K during coating as a result of radiation from the source filament. Deposit was continued for 13.3 hours after attaining a monolayer. Comparison of columns 2 and 4 shows the evaporation of between 0.5 and 8.6 layers during the 13.3 hours, implying that the coating evaporates at approximately the bulk rate, above the third layer.

For Ba films, work function is optimum at a monolayer. Additional deposit decreases the activity, but double layer films are stable at temperatures of 800°K

TABLE V(b). Multilayer films attained in design of Fig. 1(b).

Fil.#	Treatment	Observed density (atoms/cm²)	Observed layers
2	Deposit 7.5 layers	20.5×10^{14}	4.20
3	Deposit 3.4 layers	13.5×10^{14}	2.76
5	Deposit 13.5 layers	24.0×10^{14}	4.91
7	Deposit 4.2 layers	17.9×10^{14}	3.66

and can, therefore, be tested readily. Furthermore, the activity level at the optimum can be recovered readily by heating the thick film to 1000°K for 1 to 3 minutes. Multilayer films of Ba might be more stable than corresponding films of Sr because:

(1) The vapor pressure of bulk Ba is[16] about an order of magnitude lower than that of bulk Sr.

(2) Monatomic or thinner films of Ba in the present work are nearly two orders of magnitude more stable than corresponding films of Sr. Some of this greater stability probably extends to the second layer.

5. Desorption

For Sr the systems lose thermionic activity at a convenient rate between 900°K and 1100°K. Preceding

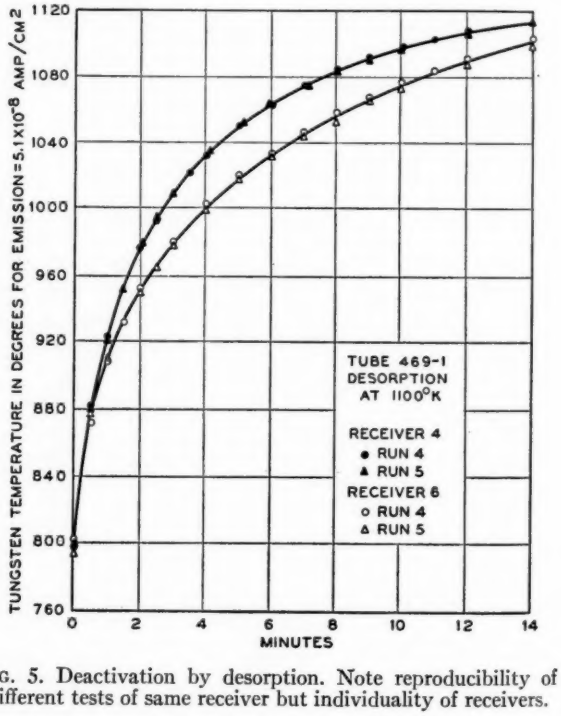

FIG. 5. Deactivation by desorption. Note reproducibility of different tests of same receiver but individuality of receivers.

evidence suggests that deactivation results primarily from evaporation of adatoms. If we can exclude other deactivating mechanisms, such as migration or agglomeration into multilayer patches, the decrease of thermionic activity can then measure re-evaporation.

Figure 5, representing two typical deactivation runs for each of two filaments, shows that the decay rate for each filament is reproducible but the two filaments do not behave identically. This illustrates the necessity for comparing successive tests on a given filament, rather than comparing the deactivation of two different receivers.

Figure 6 illustrates measurements of the temperature coefficient of the rate of deactivation in 4 runs on one filament. Two were made at 1100°K and two at 1000°K. The time scale for the former was multiplied by 32.8, to

give the best "fit" of the 1100°K data to the 1000°K curve. Such data are sometimes[17–20] employed, usually in conjunction with the Clapeyron[17,20] equation, to compute a *heat* of desorption. In these measurements (as well as our own) desorption alone occurred, without adsorption. Equilibrium, therefore, did not prevail and one is not justified in designating the result "a *heat* of desorption" or in applying the Clapeyron equation to the measurements. One actually measures only the temperature coefficient of emission decay; *assuming* this decay to be caused by desorption alone, application of the Arrhenius equation to the relative rates gives an

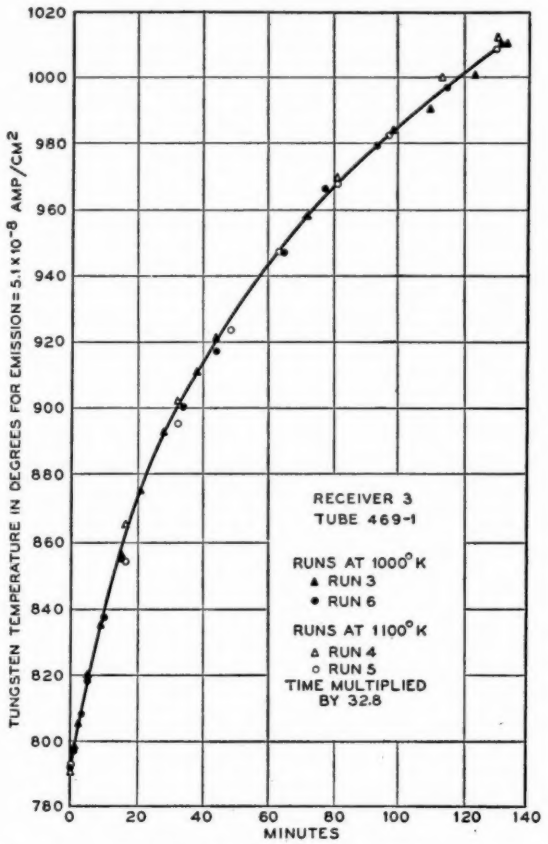

FIG. 6. Measurement of Temperature Coefficient of Deactivation; filament deactivates 32.8 times as rapidly at 1100°K as at 1000°K.

activation energy for desorption. Thus, taking 32.8 as the ratio of the desorption rate of Sr at 1000°K to that at 1100°K, the activation energy for desorption, L, was 76.6 kcal. L so measured was usually constant with θ, although for a few receivers, it increased by about 10% over the experimental range $\theta = 1.0$ to 0.3. Because available data† suggest that the sticking coefficient of Sr to W is unity, the activation energy so derived probably applies to *adsorption* as well as to desorption.

[19] S. Dushman, Revs. Modern Phys. **2**, 400 (1930).
[20] I. Langmuir and D. S. Villars, J. Am. Chem. Soc. **53**, 486 (1931).
† See Table III of this paper, also reference 16, and Moore, Allison, and Wolfstirn, J. Chem. Phys. **22**, 726 (1954).

TABLE VI. Heats of adsorption—tube 469.

Fil. No.	L (kcal)	rms spread of L in deactivation curve (kcal)
2	74.8	1.9
3	77.2	2.1
4	76.6	1.7
5	79.7	2.8
6	76.8	1.3
7	81.0	2.0
	Mean 77.6	

Table VI summarizes L for six receivers in tube 469. None exhibited any variation with θ. Approximately 50 other pairs of runs in 20 other filaments were studied without significant difference. Each rms deviation was obtained by computing 10 or more "pressure" ratios for each filament. Curves similar to Fig. 6 were also obtained at 900°, 950°, 1050°, and 1150°K.

Various authors[17–20] have used this method of measuring a heat of adsorption without establishing that thermionic deactivation is caused primarily by desorption, rather than by other processes such as agglomeration etc. Such questions can be explored more readily by using radioactive tracers than by other methods. Unpublished tests by the writers show that deactivation on heating SrO films on W filaments *cannot* be used to determine their heat of adsorption because their deactivation results primarily from processes other than evaporation of SrO molecules. Use of the Clapeyron equation is really justified only under equilibrium conditions, which certainly do not exist

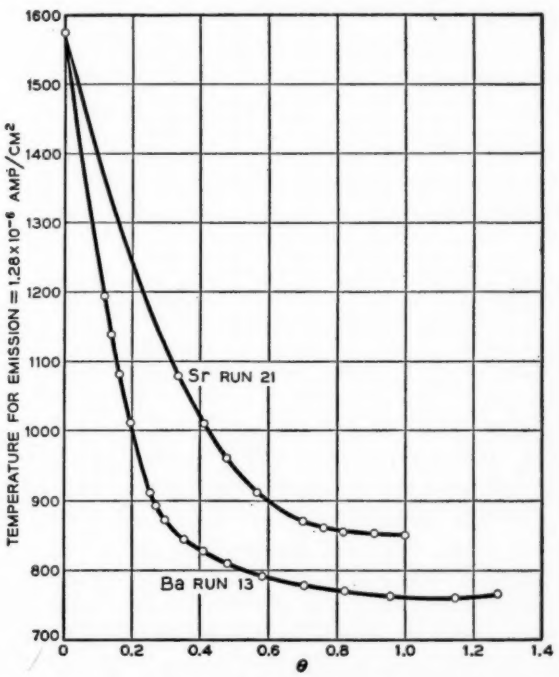

FIG. 7. Comparison of activation by Sr and by Ba. Central receiver coated on both sides, tube 613. Test emission higher than in previous tests because of electrical leakage; tube design as in Fig. 1, reference 14. Note greater activation by Ba.

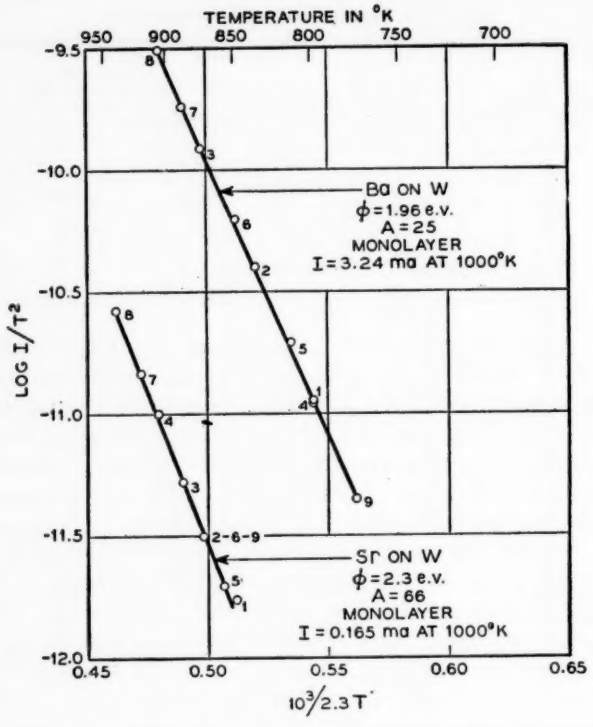

FIG. 8. Richardson lines. Tungsten receiver coated to monolayer on both sides; tube 613. Numbers on Richardson lines indicate order of measurement and show stability of monolayer films.

here. The results therefore do not necessarily give a true heat of adsorption.

6. Comparison between Ba and Sr

The two metals were compared by depositing one or the other on both sides of the same centrally located receiver. Two results were invariably duplicated:

1. The optimum thermionic activation with Ba was much greater than with Sr.
2. The Ba films were much more stable than the Sr films.

Figure 7 shows the first effect by the temperature of a given W receiver required for the emission of 1.28×10^{-6} amps/cm². Abscissae are plotted in terms of θ, the fraction of the ribbon covered. This was determined from previous results for Sr: (1) a monolayer corresponds to the horizontal tangent of the activation curve, and (2) every incoming Sr (or Ba) atom is adsorbed until the monolayer is complete. At $\theta=1$ the temperature required for emission of the standard current is about 100° less for Ba than for Sr. Figure 8 compares Richardson lines for the monolayer condition.

Figure 9 compares the stability of Ba and Sr films on the same receiver in terms of θ against time of heating at both 1000° and 1100°K, for 4 runs with Sr and 3 runs with Ba. The fit to the curve is adequate at any temperature with Sr and the ratio of times for the two runs is 40.0, in satisfactory agreement with ratios previously stated. Reproducibility with Ba is somewhat less; the runs shown are more reproducible than usual. The ratio of the time at 1000 to the time at 1100°K for equivalent deactivation is 49.0 as shown. The initial rate of deactivation of the Ba film is about an order of magnitude slower than for Sr, and the shapes of the curves differ.

DISCUSSION

Polarization *vs* Ionization

Thermionic activation by thin films of electropositive metals on tungsten, etc., is usually attributed to ionization of some of the adatoms. Ions are evaporated[21,22] on heating adatoms whose ionization potential (in free space) is less than the work function of the absorbent (such as Cs on W), leading[21,23] to the assumption that some of the adsorbed Cs was present as ions which were primarily responsible for low work function. This assumption has been extended to systems such as Ba-on-W[14,23,24] or Th-on-W[14,24] where the ionization potential of the adatom is greater than the work function of the adsorbent. Plausible theoretical arguments have been advanced[14] for the existence of *doubly* charged ions in such systems, but experimentally there is not even the indirect evidence of ions in the evaporated product.

Adions, if they occurred, would be most dense on tungsten surfaces of highest work function, such as the 110. The work function of these surfaces would be decreased more than those adjacent; this effect seemed present in Martin's tests[1] of Cs on W but absent in his work with Ba-on-W. It was also not observed in our own tests of Sr-on-W in projection tubes.

On the other hand, intense short-range electric fields certainly exist at clean metal surfaces and all atoms are polarizable. Adatoms are therefore polarized

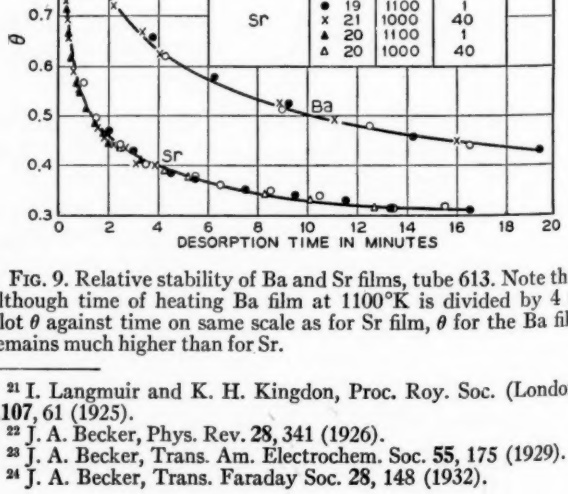

FIG. 9. Relative stability of Ba and Sr films, tube 613. Note that although time of heating Ba film at 1100°K is divided by 4 to plot θ against time on same scale as for Sr film, θ for the Ba film remains much higher than for Sr.

[21] I. Langmuir and K. H. Kingdon, Proc. Roy. Soc. (London) **A107**, 61 (1925).
[22] J. A. Becker, Phys. Rev. **28**, 341 (1926).
[23] J. A. Becker, Trans. Am. Electrochem. Soc. **55**, 175 (1929).
[24] J. A. Becker, Trans. Faraday Soc. **28**, 148 (1932).

and experimental activation curves can be understood in terms of this dipole layer alone without invoking ionization. Sharp distinction between polarization and partial ionization may be difficult, but because of greater simplicity and utility, we assume the former. Effects of heterogeneity in the adsorbent surface are most pronounced, and ionization is most probable, for low values of θ; to avoid these, desorption was studied only in the range $\theta=1.0$ to 0.30.

Shape of the Activation Curves

Explanation in terms of dipoles permits evaluation of the electric field polarizing the adatoms. This field has two components: (a) E_0 exerted by the tungsten site, assumed the same at every site, polarizing the Sr with the positive charge outward and (b) the field exerted by other adatoms causing mutual depolarization; its magnitude depends on θ. These fields are perpendicular to the surface; the dipoles also repel each other across the surface. This repulsion presumably keeps the adatoms approximately equidistant. Two adatoms, of separation b, exert a depolarizing field on each other of μ/b^3 where μ is the dipole moment per atom. The net polarizing field on each adatom is thus

$$E_0-\mu\sum\frac{1}{b^3},$$

where the summation is over all neighboring sites; b is here a variable. μ is found from the measured decrease in work function,

$$\Delta\varphi=4\pi\sigma\mu,\ddagger \qquad (2)$$

where $\sigma=$ the number of dipoles per cm^2. The value of $\Sigma(1/b^3)$ is unique only if the adatoms are equally spaced, a condition assumed for the symmetric cases $\theta=1$, 0.50 and 0.25 of spacings $\sqrt{2}a$, $2a$, $2\sqrt{2}a$, "a" being 3.15 A, the spacing between adjacent tungsten atoms. For these conditions, Fig. 7 gives for Ba adsorption the constants shown in Table VII. It has been shown[25] that

$$\sum(\mu/b^3)=9.00\mu/b_0^3, \text{ where at } \theta=1,\ b_0 \text{ is } \sqrt{2}\ a$$

TABLE VII. Constants derived from shape of activation curves.

θ	$\Delta\varphi$	μ	$b_0=$Mean spacing between adatoms
1.0	2.34 volts	1.27×10^{-18} esu	4.46×10^{-8} cm
0.50	1.665 volts	1.81×10^{-18} esu	6.3×10^{-8} cm
0.25	1.04 volts	2.26×10^{-18} esu	8.9×10^{-8} cm

‡ For derivation, see e.g. Abraham and Becker, *The Classical Theory of Electricity and Magnetism* (Blackie and Sons Limited, London, England, 1937), p. 29. Some authors use 2 as a coefficient instead of 4—for example R. Gomer, J. Chem. Phys. **21**, 1869 (1953) or W. D. Harkins and E. K. Fischer, J. Chem. Phys. **1**, 860 (1933). The coefficient 4 is correct if the adatom is metallic and the dipole is caused entirely by polarization of the adatom. Our treatment here neglects the depolarizing effect based on Gomer's Eq. (7).

[25] J. Topping, Proc. Roy. Soc. (London) **A114**, 67 (1927).

TABLE VIII. Constants for adatoms.

E_0(stat v/cm)	α_0(cm^3)	k(cm^3/stat v/cm)	μ(esu cm) at $\theta=0.25$
Ba 1.29×10^5	38.0×10^{-24}	1.6×10^{-28}	2.26×10^{-18}
Sr 1.10×10^5	42.0×10^{-24}	2.4×10^{-28}	1.87×10^{-18}
Cs 1.96×10^5	43.1×10^{-24}	0.66×10^{-28}	5.49×10^{-18}

so the polarizing field acting on any dipole is

$$E=E_0-\frac{9.00\mu}{b_0^3},$$

and the polarizability $\alpha=\alpha_0-kE$. The dipole moment per atom will then be $\mu=\alpha E=\alpha_0E-kE^2$

$$=\alpha_0E_0-\frac{9.00\mu\alpha_0}{b^3}-kE_0^2+\frac{18kE_0\mu}{b^3}+\frac{81k\mu^2}{b^6}, \qquad (3)$$

where E_0, α_0 and k are computed from (3) for $\theta=1.0$, 0.5 and 0.25.

The only solution corresponding to physical reality is $E_0=1.29\times10^5$ esu/cm or 3.88×10^7 v/cm. This gives $\alpha_0=38.4\times10^{-24}$ cm^3, and $k=1.59\times10^{-28}$ cc per stat volt.

This method, applied to Sr on W and to the Langmuir-Taylor data[13] for Cs on W, gives the constants shown in Table VIII.

The dipole moments μ are equivalnet to the displacement of one of the two valence electrons in the alkaline earth atoms by about 0.4 A and by slightly more than 1 A for the valence electron of Cs. For Cs, the deflection of an atomic beam gave[26] $\alpha_0=42\times10^{-24}$ cm^3; the Stark effect gave[27] 60×10^{-24} cm. For Ba, the point electron microscope gave[28] $62\pm6\times10^{-24}$ cm^3.

Desorption

Several quantitative treatments of desorption have been published. Langmuir[15,29] first considered that the adatoms did not interact, and proposed the equations

$$-(d\theta/dt)=q\theta;\quad \theta=e^{-qt}, \qquad (4)$$

where q is the evaporation rate from a filled layer. To compare with present experiments, q was evaluated at the final point of the experimental curve. The resulting curve (that for $p=1$) is compared in Fig. 10 with experimental data, shown by the open points. The disagreement suggests that interaction occurs. More recently Langmuir[13,30] considered statistical cooperation, without forces between adatoms, and derived the equations:

$$d\theta/dt=q\theta^p \text{ or } \theta^{p-1}=1/1-(p-1)qt, \qquad (5)$$

where p is the number of adatoms cooperating in a single desorption. He concluded that p must be 4 or 5.

[26] H. Scheffers and J. Stark, Physik. Z. **35**, 625 (1934).
[27] E. Fues, Z. Physik **82**, 536 (1933).
[28] M. Drechsler and E. W. Müller, Z. Physik **132**, 195 (1952).
[29] I. Langmuir, J. Am. Chem. Soc. **40**, 1361 (1918).
[30] I. Langmuir, Chem. Revs. **13**, 147 (1933).

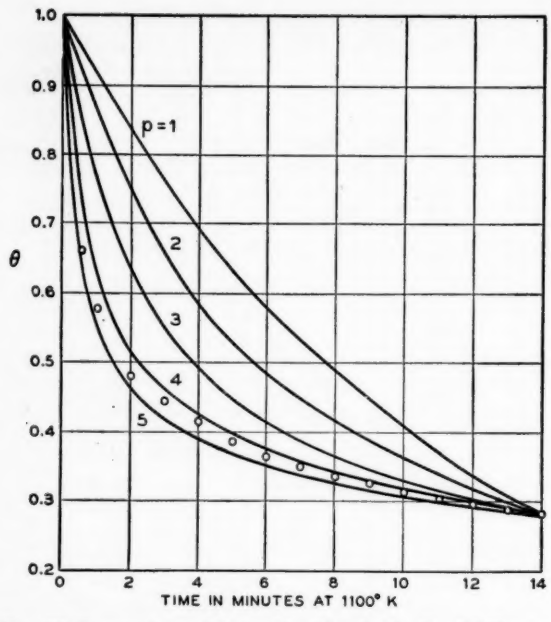

FIG. 10. Comparison of desorption kinetics for Sr with Langmuir Theories. Receiver 4, tube 469. Curves all begin at $\theta=1$ and are normalized at the 14 minute abscissa by choice of q in Eqs. (4) and (5). p is the number of adatoms cooperating for desorption of a single adatom.

To compare with experiment in Fig. 10, the curves were normalized to agree at the final experimental point. The fit is adequate for p between 4 and 5, suggesting cooperation, but adequate fit requires two adjustable constants, p and q, and the theory does not predict the effect of temperature.

Depolarizing effects computed in the preceding section indicate that interaction energy between dipoles cannot be neglected. Incorporation of this energy into a general statistical desorption equation leads to unwieldy expressions, but H. Reiss suggested an equation from the Theory of Absolute Reaction Rates, which considers in an approximate way the interaction energy between adatoms but assumes low probability for migration from one site to another, implying a binding energy to the site much larger than kT. The equation[31] is

$$-\frac{d\theta}{dt}=\frac{kT}{h}\theta\exp\left(\frac{\Delta S}{R}\right)\exp\left(\frac{-\epsilon+4\theta V}{kT}\right). \qquad (6)$$

Here k, T, and h have their usual meanings: ΔS is the entropy of activation for desorption and is assumed zero for our case, ϵ is the activation energy for desorption from a clean surface, and V is the repulsive energy per pair of adatoms and is assumed independent of θ. The factor 4 enters because each site has 4 nearest neighbors and interaction is considered only with adatoms on adjacent sites. Occupancy of adjacent sites is thus considered proportional to θ; this is higher than for the theory used to compute α, E_0, and k. Integration[32] gives

$$t\frac{kT}{h}e^{-\epsilon/kT}=Ei\left(\frac{-4V\theta}{kT}\right)-Ei\left(\frac{-4V}{kT}\right). \qquad (7)$$

The constants ϵ and V were evaluated by fitting the desorption curve for a given temperature at two arbitrary points and the entire curve was then plotted using these values of V and ϵ. Using these constants, the theory predicts almost within experimental precision all desorption data from $\theta=1.0$ to 0.3 at *any* temperature in the experimental range.

For example, Fig. 11(a) shows for Sr the decay of θ with time at 1000°K and 1100°K in tube 613. The curve at 1000°K was computed from Eq. (7) by fitting θ and t at 10 and 80 minutes giving the interaction energy 0.22 eV per pair of adatoms on adjacent sites, and the activation energy $\epsilon=3.56$ eV per atom. A more significant test is application to the 1100°K desorption from the same filament, shown in curve B. Here there is no disposable constant but the experimental desorption data fit the computed curve almost within experimental precision.

Figure 11(b) shows desorption of Ba from this *same* receiver. Curve A for 1100°K was fitted at $\theta=0.65$ and $\theta=0.325$, giving

$$\epsilon=3.68\ eV$$
$$V=0.13\ eV.$$

The experimental data scatter more than for Sr but the fit is adequate to $\theta=0.30$. The same values of ϵ and V were used to compute curve B, for Ba desorption at 1000°K. The absolute magnitudes at 1000°K are accurately predicted from the constants of the 1100° curve, although the rates differ by a factor of 48.2. The fit is poor from $\theta=0.3$ to $\theta=0.2$ (not shown) probably because of heterogeneity of the tungsten surface and lower probability than θ for occupancy of adjacent sites. More retentive surfaces hold a larger fraction of the adsorbed Ba at low θ.

Figure 11(c) shows Sr desorption at temperatures of 1100, 1000 and 950°K from filament 4 of tube 469–1. Values of ϵ and V were determined from the curve at 1000°K and applied to the other temperatures with adequate fit.

Three features are surprising. First, the interaction energy V of Sr in Tube 613 was 0.222 eV and only 0.133 eV on Fil. 469–1. This quantity should be very sensitive to the spacing of adatoms and a small difference in crystal orientation in the tungsten ribbons might explain this. Second, the value of V for Ba (0.129 eV) on the Fil. of Tube 613 is less than the value for Sr

[31] Glasstone, Laidler, and Eyring, *The Theory of Rate Processes* (McGraw-Hill Book Company, Inc., New York, 1941). See particularly Eq. (53), p. 365. We have assumed their $\alpha=0$, and have separated their free energy term into terms involving energy, ϵ, and entropy, ΔS.

[32] The Ei functions are listed by Jahnke and Emde, *Tables of Functions* (Dover Publications, New York, 1943). L. A. MacColl suggested their use in the present work.

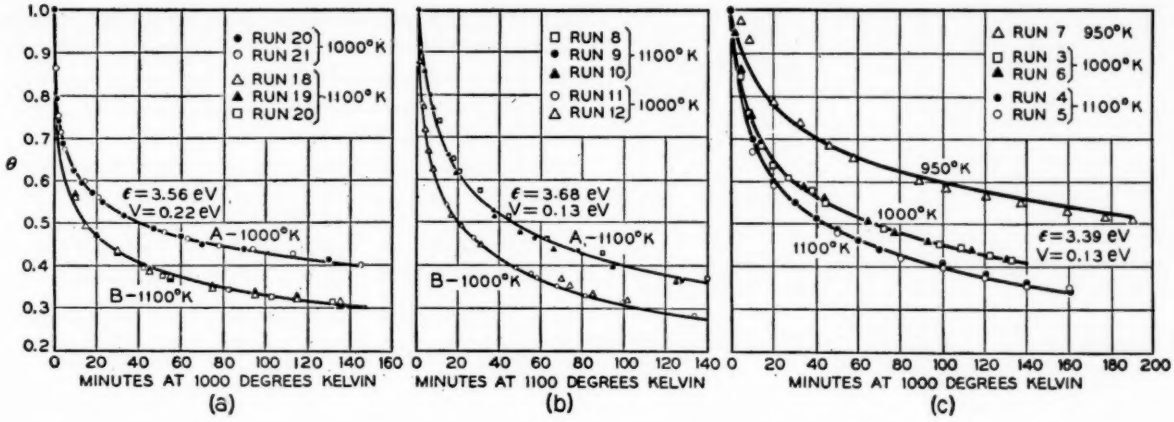

FIG. 11. Comparison of experimental desorption kinetics with theory of absolute reaction rates. In each section two experimental values of t and θ at one value of T, were inserted in Eq. 7 to determine ϵ and V. The curve shown for that temperature is computed. The same values of ϵ and V were then used to compute the curves shown at other temperatures. The agreement exhibited probably indicates inadequacy of experiment to give critical test of theories, which are oversimplified.

on the same filament. This was unexpected because the Ba atom is larger than the Sr atom in the bulk metal state. However, Ba adatoms are polarized more than Sr (Table VIII), which may make their size less in the adsorbed state than for Sr. In all cases the activation energy for desorption is over 30 fold greater than kT so that the criterion for an immobile film is satisfied. Third, the interaction energy V should actually depend on θ as indicated from the variability of μ computed in Table VII. For Sr, because of mutual depolarization, μ varies from 1.1×10^{-18} esu at $\theta=1$ to 2.18×10^{-18} at $\theta=0$.

The energy V involves at least three components:

(a) The repulsive electrostatic interaction[33] of dipoles which is $\mu^2/4b_0^3$ ergs per atom, at $\theta=1$. For Sr, this is 1.9×10^{-3} eV per atom, more than an order of magnitude less than values of V computed from desorption kinetics.

(b) The van der Waals attractive energy, which can be computed approximately from the theory[34] of Slater and Kirkwood. This gives 0.128 eV per atom at $\theta=1$ to 0.0521 at $\theta=0$.

(c) The exponential repulsive energy of contact. This might be relatively very large at $\theta=1$ and would disappear at $\theta=0$; this could cause the occupancy of adjacent sites to be far less probable than θ. The repulsive energy V may depend almost entirely on this factor.

From these considerations, the agreements between experiment and (a) a theory neglecting *any interaction energy* between adatoms shown in Fig. 10 for $p=4$ to 5, or (b) a theory neglecting *any variation* of specific interaction energy with θ, shown in Fig. 11 are surprising. Existing experimental technique appears adequate to test only gross differences between theories, yet much of the recent work on adsorption consists of elaborate and refined theories pertaining to systems not now experimentally realizable.

The Heat of Adsorption

Several theories have been proposed[35] for calculating the heat of *physical adsorption*, a rather loosely defined term in which polarization forces between adsorbent and adsorbate are usually thought predominant.[35] Heats of adsorption from 75 to 85 kcal/mole, as in the present experiments, are usually associated with "chemisorption," another loosely defined term. We calculate the heat of adsorption caused by polarization forces, using the theory[36,37] of Prosen, Sachs, and Teller:

$$\lambda=\frac{\alpha e^2}{8\pi^2}(3\pi^2\rho)^{\frac{1}{3}}\frac{\ln 2r(3\pi^2\rho)^{\frac{1}{3}}}{r^2},$$

λ = the heat of adsorption per atom in ergs, α = the polarizability of the adatom, for $\theta=0$, e = electronic charge, r = radius of adatom, assumed 2.175 A for Ba; 2.145 A for Sr; 2.63 A for Cs, and ρ = number of conduction electrons per cc of W, assumed one per atom, so $\rho=0.617\times10^{23}$.

This gives heats of adsorption shown in the second column of Table IX. Agreement is sufficiently good that the major component of the heat of adsorption is probably the sort of polarization force considered in the P.S.T. theory.

It is a pleasure to acknowledge the value of discussions, especially with Howard Reiss, Conyers Herring and A. H. White, and the skill of V. L. Lundahl and V. J. DeLucca in assembly and H. C. Geissler in processing the tubes.

[33] See e.g. A. R. Miller, *The Adsorption of Gases on Solids* (Cambridge University Press, Cambridge, England, 1949), p. 107.
[34] J. C. Slater and J. G. Kirkwood, Phys. Rev. **37**, 682 (1931).
[35] S. Brunauer, *The Adsorption of Gases and Vapors* (Princeton University Press, Princeton, New Jersey, 1943).
[36] Prosen, Sachs, and Teller, Phys. Rev. **57**, 1066 (1940).
[37] E. J. R. Prosen and R. G. Sachs, Phys. Rev. **61**, 65 (1941).

TABLE IX. Comparison of theoretical and experimental heats of adsorption.

	Calculated λ	Measured activation energy ϵ or heat of desorption λ
Ba on W	85.4 kcal/mole	ϵ^a=80–86 kcal/mole
Sr on W	75.6	ϵ^a=75–82
Cs on W	73.0	λ^b=65.1 for θ=0 λ^b=45.0 for θ=0.67

[a] Activation energy for desorption—present experiments.
[b] Heat of desorption—Langmuir and Taylor experiments.[13]

APPENDIX I. CONSTANCY OF A DURING ACTIVATION

The most fundamental parameter for evaluating the activation of a tungsten surface is the change of work function. The work function determined thermionically involves the treatment of Richardson lines and the difficulty[38] in distinguishing between the value of φ and its change with temperature. Also the temperature range over which a Richardson line can be studied on such a composite surface is limited by instability of the film; precision in determining the Richardson constants is limited by the available temperature. Thus, a 10° error at one extremity of a 100° temperature range would lead to error in A by a factor of 10 or more. With the proviso that the precision within which A can be determined is poor, one can show experimentally that A remains approximately constant during activation and deactivation. This is illustrated for deactivation of a typical receiver in Table X. The first two columns give A and φ determined from Richardson lines, the third column gives the temperature required for the fixed emission and the following column gives the value of φ determined by Eq. (1) while the last column gives the temperature range over which Richardson lines were taken. Those entries in which the two values of φ are in widest disagreement are those in which the value of A is in greatest disagreement with the mean, suggesting error in these values of A and Richardson φ. The work function determined from 1 is generally about 0.2 volt greater than that determined by Richardson lines, probably because of neglecting the change in T^2 during activation. Such data are believed to justify the conclusions that A remains approximately constant during activation and that φ is approximated reasonably well by (1).

TABLE X. Deactivation of receiver #2—tube 50-2.

Richardson A	φ(v)	T°K	Using (1) φ	$\Delta\varphi$	Temp. range
79.5	2.40	805	2.45	+0.05	100°
16.6	2.31	813	2.48	+0.17	100°
0.8	2.13	825	2.51	+0.38	100°
11.5	2.36	840	2.56	+0.20	100°
14.8	2.43	857	2.61	+0.18	100°
330	2.79	892	2.72	−0.07	60°
79.5	2.69	900	2.74	+0.05	100°
8.9	2.61	930	2.83	+0.22	123°
4.0	2.63	960	2.92	+0.19	113°
3.2	2.73	995	3.03	+0.30	81°
7.1	2.87	1022	3.11	+0.24	53°
0.5	2.70	1041	3.17	+0.47	53°
144	3.25	1058	3.22	−0.03	53°
Mean 53.8				+0.18	

[38] C. Herring and M. H. Nichols, Revs. Modern Phys. **21**, 185 (1949).

APPENDIX II. EXCLUSION OF DEACTIVATION PROCESSES OTHER THAN EVAPORATION

1. Essentially No Migration around Receivers

Thorium[39] can migrate around a tungsten ribbon at 1260–1380°K. The writers have observed, using projection tubes, that Sr as well as SrO can migrate around tungsten wires 0.005″ to 0.010″ diameter. Similar data are available for mixtures[40] of Ba and BaO, as well as for[41] relatively pure Ba. However, such qualitative tests do not tell how much material migrated in a given time.

After depositing radioactive Sr on one side of a ribbon, migration to the reverse side could be investigated quantitatively by counting each side. Even with no migration, counts from the uncoated side of 0.0005″ W are 68% of the count from the coated side, because this fraction of the β's have energy sufficient to pass completely through the W; this limits precision. The ratio was measured by placing W sheet between the GM tube and Sr deposit, or by preparing calibration deposits on only one side of W sheet. Migration around the ribbon would cause the ratio of the counts from the two sides to be higher than 0.68. Because of variations in thickness, etc., such ratios could be determined no closer than 5%. Ratios were measured on ribbons which had been heated with their deposits at 1100°K up to an hour, or at 1000°K up to 40 hours or at 900° or 800°K up to 500 hours. The ratio of counts on deposits which had been heated was never (in 24 ribbons so examined) significantly higher than for those which had not been heated.

Migration was investigated by another method. The dismounted receiver was cut into several sections. Alternate sections were imbedded with the coated side up and with the coated side down, in an asphalt varnish impervious to water and counts then taken on all samples. Each mounted sample was then washed§ to remove Sr from the exposed surface, and recounted. If the coated side were exposed, treatment always reduced the count nearly to background; but if the uncoated side were exposed, treatment had essentially no effect. Precision in the second method suffered from difficulty in making a water-tight seal to one surface without

[39] J. A. Becker and W. H. Brattain, Phys. Rev. **43**, 428 (1933).
[40] J. A. Becker and G. E. Moore, Phil. Mag. **29**, 129 (1940).
[41] M. Drechsler, Z. Elektrochem. **58**, 340 (1954).
§ Reagents included HCl, HNO_3, and superoxol, which partially dissolves the W itself. Washing unmounted ribbons in any of these reagents reduced the count to background. This also shows that the Sr is not dissolved in the W.

partially covering the other, and because some of the radioactive material was smeared into the varnish. As a result of the two types of test we believe that not over 1% of the deposit remaining on any ribbon had migrated to the uncoated side. Ribbons coated on both sides behaved on desorption just like ribbons coated on only one side, which also suggests that migration was negligible.

2. No Re-Evaporation from the Anode Surfaces

Relatively large quantities of Sr were deposited on the anodes during exhaust and subsequent tests; the volatility of Sr suggests that appreciable quantities might re-evaporate from the anode as a result of incidental heating, and deposit on the receivers. This possibility was examined by flashing all the receivers and then operating one sufficiently hot to raise the anode temperature above the value attained by heat from the source filament. No activation of the other receivers was ever observed, so that Sr deposited by evaporation from the anode seems negligible.

In summary, tests described justify treatment of the deposits as forming monolayers by migrating over previously adsorbed atoms to vacant sites. Measurements are substantially unaffected by solution in the W, migration around to the reverse side, or by re-evaporation from the anode.

APPENDIX III. RATE OF CHEMICAL REACTION IN THE SOURCE

The rate of Sr production by chemical reaction was measured previously[9] in a tube consisting of essentially only the source filament and glass bulb, so that pyrometer readings could be corrected by reflectometer. Total bulb deposit was divided by the total time that the source had operated at a controlled temperature, to give the mean rate of Sr production. Each tube therefore gave only one rate measurement which was assumed uniform. The mean rate so determined appeared unaffected by addition, to the coat, of tungsten powder which increased the interfacial area threefold.

The present work permits more detailed analyses of reaction rate because many experiments can be performed with each tube and because the rate for different azimuths is measurable. However, counteracting these advantages, anodes decrease precision in temperature measurement because the reflectometer cannot be used to determine spectral emissivity.

The mean rate of reaction, as determined by the time required to deposit monolayers of Sr on receivers, agrees with the preceding work. Figure 12, showing typical data for two source filaments, illustrates the greater

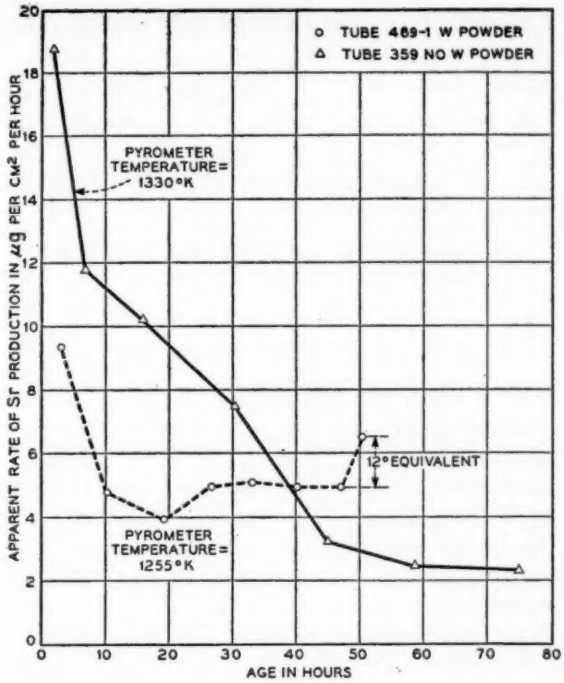

FIG. 12. Effect of W powder on constancy of reaction rate in source filament. Powder increases interfacial area by factor greater than 20. Note effect of hypothetical 12° increase of temperature.

uniformity in rate of Sr production always achieved by addition of W powder, which in the present experiments, increased the interfacial area by a factor greater than 20. (Note that the pyrometer temperatures of the two filaments were unequal.) Observation of this effect was impossible in the former work in which the measurement corresponded to the mean ordinate under such a curve, for the first 10 to 15 hours. The decreased rate of reaction with time in the one filament is believed to be the result of a $SrWO_3$ interface between the SrO and W, diffusion through this layer gradually becoming a rate limiting process. The effect corresponding to a (hypothetical) 12° error of temperature shows the need for careful control of source temperature. Throughout both curves, pyrometer temperature was held constant and all rate variations were for unknown reasons.

Rate differences in azimuth were occasionally observed amounting to as much as 50% in an angle of 90° around the source. This distance is of the order 0.02 cm; sometimes this difference in azimuthal rate could be correlated with azimuthal differences in pyrometer temperatures, probably caused in turn by nonuniform coating thickness.

Kinetics of the Isotope Exchange Reaction of Fluorine with Hydrogen Fluoride*†

RICHARD M. ADAMS, RICHARD B. BERNSTEIN,‡ AND JOSEPH J. KATZ
Chemistry Division, Argonne National Laboratory, Lemont, Illinois
(Received December 7, 1954)

The exchange of radioactive F^{18} between hydrogen fluoride and fluorine has been studied over a wide range of concentrations at three temperatures in the range 194° to 257°C. The exchange may be accounted for entirely by a heterogeneous catalysis mechanism involving competitive adsorption of the Langmuir-Hinshelwood type. Experiments have been performed indicating the important role of surface treatment on the kinetics of the exchange.

I. INTRODUCTION

IN a previous publication[1] on the kinetics of the fluorine-halogen fluoride exchanges, it was postulated that exchange takes place either through a heterogeneous catalysis by the metal fluoride coating on the walls of the reaction vessel, or by a combination of the heterogeneous mechanism plus a homogeneous gas phase exchange in those cases where a measurable amount of dissociation of the halogen fluoride occurs at the temperature of exchange. If this mechanism may be extended to cover the fluorine-hydrogen fluoride exchange then the latter would be expected to take place entirely by means of heterogeneous catalysis since HF is undissociated at the temperatures at which these exchanges are carried out. Reasoning by analogy it would seem that the heterogeneous catalysis might involve competitive adsorption of the Langmuir-Hinshelwood type as in the case of the fluorine-halogen fluoride exchanges.

A qualitative investigation of the fluorine-hydrogen fluoride gas-phase exchange has been carried out by Dodgen and Libby[2] who suggested that the exchange observed at about 200°C occurred primarily through heterogeneous catalysis. However, it seemed worthwhile reinvestigating this exchange with the methods and apparatus used in the study of the fluoride-halogen fluoride exchanges in order to obtain comparable quantitative data.

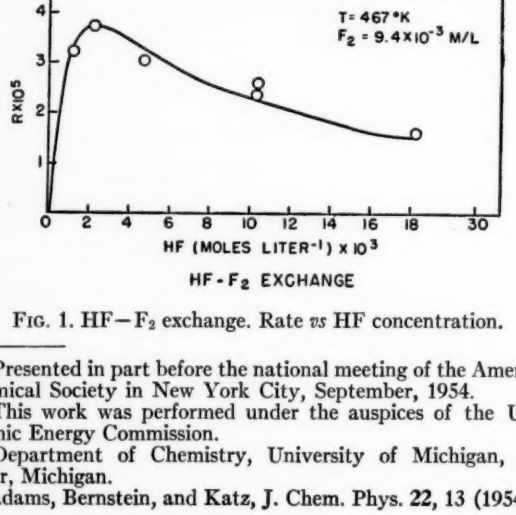

FIG. 1. HF—F_2 exchange. Rate *vs* HF concentration.

II. MATERIALS, APPARATUS, AND PROCEDURE

High-purity tank hydrogen fluoride (>99%, Pennsylvania Salt Company) was further purified on the

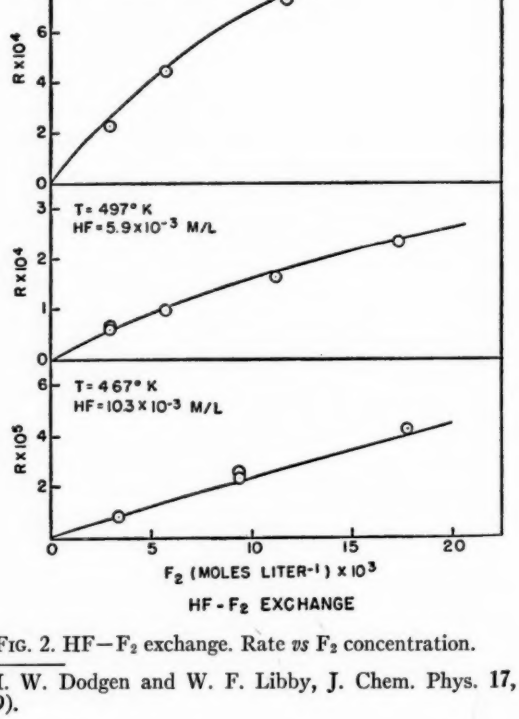

FIG. 2. HF—F_2 exchange. Rate *vs* F_2 concentration.

* Presented in part before the national meeting of the American Chemical Society in New York City, September, 1954.

† This work was performed under the auspices of the U. S. Atomic Energy Commission.

‡ Department of Chemistry, University of Michigan, Ann Arbor, Michigan.

[1] Adams, Bernstein, and Katz, J. Chem. Phys. **22**, 13 (1954).

[2] H. W. Dodgen and W. F. Libby, J. Chem. Phys. **17**, 951 (1949).

TABLE I. Values of the constants in the rate equation.

T°K	k_2(mole liter^{-1} min^{-1})	x(liter mole^{-1})	y(liter mole^{-1})
467	1.8×10^{-3}	9.5	4.7
498	2.5×10^{-3}	3.8×10^{1}	3.8×10^{2}
530	6.9×10^{-3}	6.6×10^{1}	3.3×10^{2}

vacuum line by absorbing the gas on sodium fluoride and pumping away all the unabsorbed gaseous impurities. The $NaHF_2$ was then used as a reservoir from which HF could be obtained by heating to 350°C.

Fluorine (Pennsylvania Salt Company) was used directly from the tank. Analysis showed a fluorine content[3] of 96.0±1.0%. Mass spectrometric analysis indicated that the inert residual 4% impurity was essentially air.

The 112-minute nuclide F^{18} was prepared according to the method given previously,[1] by utilizing the nuclear reaction $O^{16}(t,n)F^{18}$.

The apparatus and exchange procedure were identical to those described in the previous publication.[1] Essentially the exchange procedure consists of incorporating F^{18} into a sample of hydrogen fluoride, mixing in the gas phase a known quantity of the radioactive hydrogen fluoride with a known quantity of inactive fluorine, separating the two components after a certain period of exchange at a constant temperature, and determining the amount of activity in each of the gases after exchange.

The exchange was studied at the three temperatures 194°C, 224°C, and 257°C, at which the contact times were generally about 60 minutes, 30 minutes, and 10 minutes, respectively. Concentrations of HF ranged from about 1×10^{-3} to 30×10^{-3} mole liter^{-1}, and of F_2 from about 3×10^{-3} to 20×10^{-3} mole liter^{-1}. In order to avoid making corrections for association, the pressure of HF in the counting vessel (at room temperature) was always kept below 100 mm. Under these conditions association is expected to be less[4] than 2%.

No correction for association was necessary for the calculation of the concentration of HF in the reaction vessel since pressures were always measured at the reaction temperature (194°C or above). From an estimate of determinate errors and from the results of duplicate experiments, it is felt that the rate results are reliable to ±10%.

III. RESULTS

The results are given in Figs. 1 and 2 which show the variation of the rate with the HF concentration and the F_2 concentration respectively at the three temperatures studied. (It should be noted that all these results were obtained on the same surface. The reaction vessel was kept evacuated between experiments and never exposed to any substances other than HF and F_2.) The points represent the experimental data while the solid lines represent calculated curves based on the following analysis. The assumption that exchange takes place by heterogeneous catalysis involving the Langmuir-Hinshelwood type of competitive adsorption on the fluoride coating on the walls of the reaction vessel leads to the rate equation

$$R=\frac{k_2x[F_2]y[HF]}{\{1+x[F_2]+y[HF]\}^2} \tag{1}$$

where R is the observed rate, k_2 is the rate constant, and x and y are the adsorption coefficients of F_2 and HF, respectively. The three unknowns k_2, x, and y may be estimated by a method of successive approximations. Thus, if the $x[F_2]$ term in the denominator of Eq. (1) were negligible, then at the maximum in the R *vs* [HF] curve

$$y=\frac{1}{[HF]_{max}}. \tag{2}$$

However, if the $x[F_2]$ term is not negligible then at the maximum

$$y=\frac{1+x[F_2]}{[HF]_{max}}. \tag{3}$$

The fact that the R *vs* (F_2) curves depart only slightly from linearity suggests that the $x[F_2]$ term is small but not negligible. Therefore, by first obtaining y from

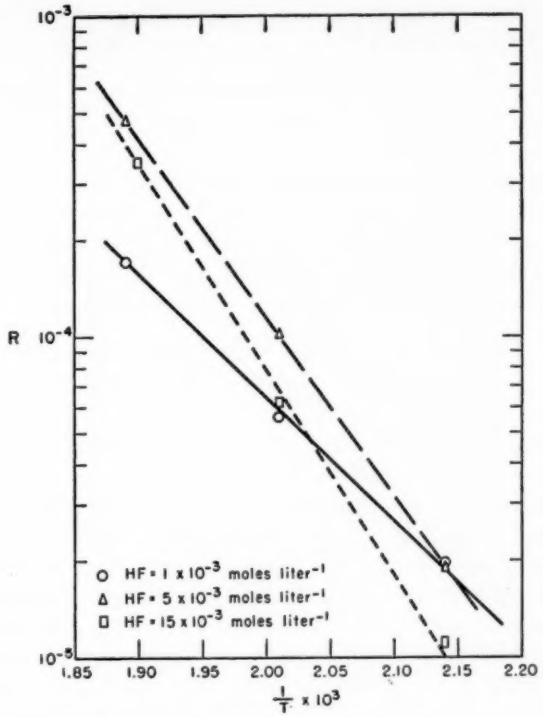

FIG. 3. HF−F_2 exchange. Experimental apparent activation energy plot.

[3] This value supersedes the value 93.5±1.0% given in the previous publication[1] for the identical tank of fluorine.

[4] W. Strohmeier and A. Briegleb, Z. Electrochem. **57**, 662 (1953).

TABLE II. Apparent activation energies

[HF](mole liter^{-1})	E_a(kcal mole^{-1})
1×10^{-3}	18
5×10^{-3}	25
15×10^{-3}	29

Eq. (2) and taking x to be some small fraction of y it is possible to fit the equation to the observed data as shown, obtaining k_2 from the relationship,

$$k_2=\frac{4R_{\max}(1+x[F_2])}{x[F_2]}. \quad (4)$$

The values of k_2, x, and y used to obtain the calculated curves in Figs. 1 and 2 are given in Table I.

An apparent activation energy E_a may be obtained from a semilog plot of experimental values[5] of R against $1/T$ (Fig. 3).[6] However, E_a should increase with increasing concentration of the more strongly adsorbed substance, in this case HF, as has been pointed out by Laidler,[7] owing to the fact that the heat of adsorption is positive. Table II shows that E_a does in fact increase with increasing HF concentration.[8]

If this exchange takes place by a heterogeneous mechanism then the rate should be dependent on the amount and kind of surface. Accordingly, a number of experiments designed to test this dependence were carried out. An attempt was made to vary the kind of surface by hydrogenating and/or fluorinating the surface of the reaction vessel at high and low temperatures, and by exposing the surface to dry air and moist air. The amount of surface was varied by adding powdered nickel fluoride to the reaction vessel. The results are shown in Table III. All the experiments listed in Table III were run at the same temperature, with the same HF (5.9×10^{-3} mole liter^{-1}) and F_2 (7.5×10^{-3} mole liter^{-1}) concentrations. Before each experiment the reaction vessel was heated at the reaction temperature (225°C) and evacuated to an ultimate pressure of less than 2 microns for about 3 hours.

It is clear from the results given in Table III that,

TABLE III. Surface effects on HF$-F_2$ exchange.

Exp.	Surface	Rate (moles liter^{-1} min^{-1})
A	Fluorinated 16 hours at 250°C	1.84×10^{-4}
B	Hydrogenated 60 hours, fluorinated 16 hours at 280°C	1.86×10^{-4}
C	Hydrogenated 16 hours, fluorinated 24 hours at 350°C	0.65×10^{-4}
D	Exposed to dry air 16 hours at 225°C	1.71×10^{-4}
E	Exposed to moist air 16 hours at 25°C	2.82×10^{-4}
F	11.0 g NiF_2 added, fluorinated 16 hours at 350°C	2.05×10^{-3}

while the surface effects are not necessarily simple, the rate of exchange does indeed depend on the kind and amount of surface. It seems possible that the effect of exposure to moist air to increase the rate of exchange, and the effect of high-temperature hydrogenation and fluorination to reduce the rate are related. Thus, it may be that exposure to moist air produces a chemical species which is a more active catalyst than the nickel fluoride itself, and that high temperature hydrogenation and fluorination gives a more complete reduction to nickel fluoride, although it should be noted that there is no direct evidence to support this particular interpretation of the observed results. In regard to the amount of surface (Exp. F, Table III) the interpretation is somewhat clearer. Microscopic examination of the particles of added nickel fluoride powder showed an average diameter of about 1.3 microns, and on the assumption that the particles are spherical, the apparent surface area is calculated to be 11×10^4 cm^2. Since the surface area of the reaction vessel was about 11×10^2 cm^2 it appears that the increase in rate of about 30, (given by the ratio of Exps. F to C, Table III) is similar to the increase in surface area. That the agreement is not more exact is not surprising, especially in view of the fact that Beeck[9] has found the internal surface of an evaporated nickel film to be as much as 300 times the apparent surface area. It would thus appear to be reasonable to conclude that the exchange is dependent on the amount of nickel fluoride present.

A number of alternative homogeneous reaction mechanisms have been considered but with no success. A simple atomic mechanism is improbable since it leads to a rate expression involving the square root of the fluorine concentration (see footnote 18 in reference 1). It thus appears that the HF$-F_2$ isotope exchange may be accounted for entirely by a heterogeneous catalysis mechanism involving competitive adsorption of the Langmuir-Hinshelwood type.

[5] The values of R are used rather than calculated k_2 values because the latter are dependent upon the values chosen for x. However a difference of a factor of 2 in x does not shift the placement of the R *vs* $[F_2]$ curves significantly.

[6] All the values of R plotted in Fig. 3 have been normalized to $[F_2]=5.8\times10^{-3}$ mole liter^{-1}.

[7] K. J. Laidler, Discussions Faraday Soc. **8**, 51 (1950).

[8] It is interesting to note that the measurements made by Dodgen and Libby[2] correspond to an apparent activation energy of 27 kcal mole^{-1} at HF$=19\times10^{-3}$ mole liter^{-1}, $F_2=20\times10^{-3}$ mole liter^{-1}.

[9] O. Beeck, Revs. Modern Phys. **17**, 61 (1945).

Absorption Cross Sections of Carbon Dioxide and Carbon Monoxide in the Vacuum Ultraviolet

H. SUN AND G. L. WEISSLER
Department of Physics, University of Southern California, Los Angeles 7, California
(Received November 23, 1954)

Absorption cross sections of CO_2 and CO in the region from 1306 A to 374 A have been measured. The absorption spectrum of CO_2 consists of strong resonance bands between 1306 A and 700 A, with one of them at 923 A showing an unusually large cross section of 117×10^{-18} cm². A continuum with bands superimposed on it was observed to start at about 860 A or 14.4 ev which corresponded to the first ionization potential of CO_2. From 700 A toward shorter wavelengths, the contour of the continuum was better defined and smooth with a broad maximum of 36×10^{-18} cm² at 550 A and a total f-value of 4.4. The CO absorption between 1306 A and 955 A was less than 10^{-18} cm². Prominent resonance bands appeared at 924 A and extended to 600 A. An absorption continuum could be identified between 876 A and 374 A showing maximum values of $\sigma\simeq19\times10^{-18}$ cm² between 750 A and 550 A with perhaps a small dip of 15×10^{-18} cm² at 644 A. The f-value of this continuum was 2.8.

INTRODUCTION

THE structure and systematics of the resonance absorption bands of CO_2 and CO in the vacuum ultraviolet have been studied by several investigators with, however, very few measurements of the absolute absorption cross sections for these two gases. The CO_2 bands were studied by Lyman,[1] Leifson,[2] Henning,[3] Rathenau,[4] and Price and Simpson,[5] while Wilkinson and Johnston[6] measured its absorption cross sections between 1670 A to 1440 A and, separately, Inn *et al.*[7] in the same region down to 1060 A. Vacuum ultraviolet absorption bands of CO were investigated by Hopfield and Birge,[8] Henning,[3] and Tanaka.[9] Watanabe *et al.*[10] measured its absorption cross sections between 1650 A and 1050 A. In the present work cross sections of these two gases are reported for the region from 1306 A to 374 A with an attempt to delineate absorption continua as differentiated from resonance bands.

The absorption cross section is calculated from the well-known relation

$$I=I_0\exp\{-(n_0\sigma T_0pL)/(p_0T)\},$$

where I_0 and I are the intensities of the incident and transmitted light, L the length of the absorption path, σ the absorption cross section at standard conditions p_0T_0, n_0 the number of molecules per cm³, and p and T the pressure and temperature of the absorbing gas. Experimental details were the same as previously reported.[11] The absorption coefficient was defined by $k=n_0\sigma$. The pressure range of CO_2 or CO in the tank of the vacuum spectrograph, namely between 10 and 40 microns, was suitable only for measurements of σ larger than 10^{-18} cm². With air pressures of 20 to 80 microns in the light source, the interdiffusion of the two gases (CO or CO_2 in the tank and air in the source) through the primary slit of the spectrograph did not effect adversely accurate measurements of larger cross sections. Both the absorbing gas and the air flowed in a continuous stream into their respective chambers which in turn were pumped separately.

CARBON DIOXIDE

Tank CO_2, obtained from the Matheson Company and purified by repeated condensation and fractional distillation, was used in this work. Its resultant purity was higher than the 99.0% stated by the manufacturer. The absorption cross sections, with σ in mb,[12] of 94 source emission lines ranging from 1306 A to 374 A, were calculated from four plates, and are listed in Table I and Fig. 1. The first column of Table I contains the wavelengths listed by Boyce and Robinson.[13] The symbol $2x$ indicated that the corresponding line was observed in the second order. The middle columns contain the absorption cross sections, σ, for individual plates, and the last columns give the average values of σ and k with their probable errors.

As shown in Fig. 1, the absorption spectrum of CO_2 may be divided into several parts. In the range from 1306 A to 860 A, extremely strong resonance bands were present with a σ value as high as 117 mb at 923 A. A very dense band system between 1175 A and 912 A was found and measured by Rathenau.[4] The head of each band is shown in the upper-left portion of Fig.1. Continuous absorption seemed to start at about 860 A

[1] T. Lyman, Astrophys J. **27**, 87 (1908).
[2] S. W. Leifson, Astrophys J. **63**, 73 (1926).
[3] H. J. Henning, Ann. Physik **13**, 599 (1932).
[4] G. Rathenau, Z. Physik **87**, 32 (1934).
[5] W. C. Price and D. M. Simpson, Proc. Roy. Soc. (London) **A169**, 501 (1938).
[6] P. G. Wilkinson and H. L. Johnston, J. Chem. Phys. **18**, 190 (1950).
[7] Inn, Watanabe, and Zelikoff, J. Chem. Phys. **21**, 1048 (1953).
[8] J. J. Hopfield and R. T. Birge, Phys. Rev. **29**, 922 (1947).
[9] Y. Tanaka, Sci. Papers Inst. Phys. Chem. Research (Tokyo) **40**, 371 (1943); **39**, 447 (1942).
[10] Watanabe, Zelikoff, and Inn, AFCRC Technical Report No. 52—23; Geophysical Research Paper No. 21 (June, 1953).
[11] H. Sun and G. L. Weissler, J. Chem. Phys. **23**, 1160 (1955) (CH_4 and NH_3).
[12] 1 mb (megabarn) $=10^{-18}$ cm².
[13] J. C. Boyce and H. A. Robinson, J. Opt. Soc. Am. **26**, 133 (1936).

TABLE I. Absorption cross sections of carbon dioxide (0 means <1 mb).

Wavelength	σ(mb) from 4 individual plates 1	2	3	4	Average σ(mb)	Average k (cm^{-1})
1306.0 OI		1.7		1.5	1.6± 0.1	43± 3
1304.9 OI		2.4		2.1	2.3± 0.1	61± 3
1302.2 OI		5.6		6.7	6.1± 0.5	160± 13
1243.3 NII		0		0		
1200.7 NI		0		0		
1200.2 NI		0		0		
1199.5 NI		0		0		
1184.5 NIII		0		0		
1183.0 NIII		0		0		
1135.0 NI		18		23	20 ± 3	530± 80
1134.4 NI		19		23	21 ± 2	560± 53
1127.8 SiIV				96	96	2580
1122.3 Cl				25	25	670
1084.0 NII	7.5			10	8.8± 1.1	240± 30
991.5 NIII	42	47		52	47 ± 3	1260± 80
989.8 NIII	13	7.3			10 ± 3	270± 80
979.9 NIII	28				28	750
977.0 CIII	24	28			26 ± 2	700± 53
955.5 NIV			66	82	74 ± 7	1980±190
924.3 NIV		49		63	56 ± 6	1500±160
923.7 NIV		41		61	51 ± 9	1370±240
923.2 NIV		104		130	117 ±12	3140±320
923.0 NIV		34		45	40 ± 5	1070±130
922.5 NIV		106		119	113 ± 6	3030±160
916.7 NII		35			35	940
916.0 NII		53		52	52	1390
915.9 NII		67		85	76 ± 8	2040±210
904.5 CIII		26		40	33 ± 6	880±160
903.6 CIII		28		37	33 ± 4	880±110
835.3 OIII		3.5			3.5	94
835.1 OII		4.8			4.8	130
833.7 OIII		8.9			8.9	240
833.3 OIII		12			12	320
832.8 OIII		7.0			7.0	190
799.9 CII		25	32	26	28 ± 3	750± 80
799.7 CII		38	32	27	32 ± 4	860±110
796.7 OII		18	15	22	18 ± 2	480± 53
790.1 OIV		13	13	14	13 ± 0	350± 0
787.7 OIV		23	27	30	27 ± 2	720± 53
776.0 OII		23	20	26	23 ± 2	620± 53
773.0 NIII		29	25	32	29 ± 2	780± 53
772.4 NIII		20		28	24 ± 4	640±110
771.9 NIII		26		28	27 ± 1	720± 27
771.5 NIII		34	37	45	39 ± 4	1040±110
765.1 NIV		74	81	68	75 ± 4	2010±110
764.4 NIII		49	56	65	57 ± 5	1530±130
764.3 NIII		36	29	38	34 ± 3	910± 80
747.0 NII		16	16	19	17 ± 1	460± 27
745.8 NII		29	33	32	31 ± 1	830± 27
718.6 OII		15		22	19 ± 3	510± 80
703.9 OIII		17		23	20 ± 3	530± 80
702.9 OIII		21		26	23 ± 2	620± 53
702.3 OIII		40	38	46	41 ± 3	1100± 80
686.3 NIII		21	19	31	24 ± 4	640±110
685.8 NIII				26	26	700
685.5 NIII				29	29	780
685.0 NIII		20	16	25	20 ± 3	530± 80
673.8 OII		21	33	33	29 ± 5	780±130
672.9 OII		25	35	33	31 ± 4	830±110
672.0 NII			34	39	36 ± 3	960± 80
671.8 NII		26		38	32 ± 5	860±130
671.4 NII		28	39	37	34 ± 4	910±110
660.3 NII		25	29	33	29 ± 3	780± 80
645.2 NII		30		39	36 ± 3	960± 80
2×645.2		36	33	40		
644.8 NII			33	40	36 ± 3	960± 80
2×644.8		31		40		
644.6 NII		26		37	33 ± 3	890± 80
2×644.6		29	34	38		
644.1 NII		30	30	40	34 ± 3	910± 80
2×644.1		35	33	40		
635.2 NII		24	35		30 ± 4	800±110
2×617.1 OII		31	38		35 ± 3	940± 80
2×616.3 OII		30	38		34 ± 3	910± 80
2×599.6 OIII		33	28	32	31 ± 2	830± 53
2×597.8 OIII		32		41	36 ± 4	960±110
2×582.2 NII		25	31		28 ± 3	750± 80
2×581.0 NII		24	38		31 ± 6	830±160
2×580.4 OII		25	35		30 ± 5	800±130
2×555.3 OIV			38	38	38 ± 0	1020± 0
2×555.1 OII			30	40	35 ± 5	940±130
2×555.0 OII			34	38	36 ± 2	970± 53
2×554.5 OIV			37	34	35 ± 2	940± 53
2×553.3 OV				40	40	1070
2×539.9 OII		27	33	32	31 ± 2	830± 53
2×539.5 OII		27		36	31 ± 4	830±110
2×539.1 OII		25		35	30 ± 5	800±130
2×538.4 OII		31		35	33 ± 2	880± 53
2×537.8 OII		28		38	33 ± 5	880±130
2×525.8 OIII		28		31	30 ± 1	800± 27
2×509.9 NIII				31	31	830
2×508.2 OIII				30	30	800
2×507.7 OII				31	31	830
2×507.4 OIII				33	33	880
2×434.3 NII		20	30	30	26 ± 4	700±110
2×434.0 NII		21	29	29	26 ± 3	700± 80
2×374.3 OIII		22	26	33	27 ± 4	720±110
2×373.8 OIII		24	33	35	31 ± 4	830±110

with Henning's[3] bands superimposed. The absorption cross sections of this continuum were tentatively determined by connecting the ordinates of the source lines of lowest absorption in the various groups. In this way, it may be inferred that the σ values of the continuous absorption in this part were lower than 30 mb while the highest one of the superimposed bands was 75 mb. From 700 A toward shorter wavelengths the continuum was found to be quite smooth, with the values of σ increasing gradually to a broad maximum of 36 mb at 550 A and decreasing slowly towards shorter wavelengths reaching 29 mb at 374 A.

The results obtained here in the region from 1306 A to 1084 A overlapping with Inn *et al.*[7] were compared, and both sets of data showed bands in the vicinity of 1300 A, low absorption of less than 1 mb between 1243 A and 1183 A, and again band absorption towards shorter wavelengths. Since band absorption is characterized by large fluctuations in σ, no detailed comparisons were possible for lines of exactly equal wavelengths since Inn *et al.*[7] employed the *unresolved* many-lined spectrum of H_2 as a light source. However, the over-all aspects seemed to indicate commensurate results in the wavelength region shorter than 1243 A. In the neighborhood of 1300 A their absorption seemed to be somewhat smaller than that reported here.

The first ionization potential of CO_2 has been determined both spectroscopically[5] and from electron impact work.[14] The former gave a Rydberg series limit of 903 A or 13.73 ev, also shown in Fig. 1, while the result given by the latter was 860 A or 14.4 ev. By extrapolating the dashed curve in Fig. 1 towards longer wavelengths it seems more probable that the continuous absorption of CO_2 begins in the neighborhood of 860 A corresponding to 14.4 ev. This value is also in

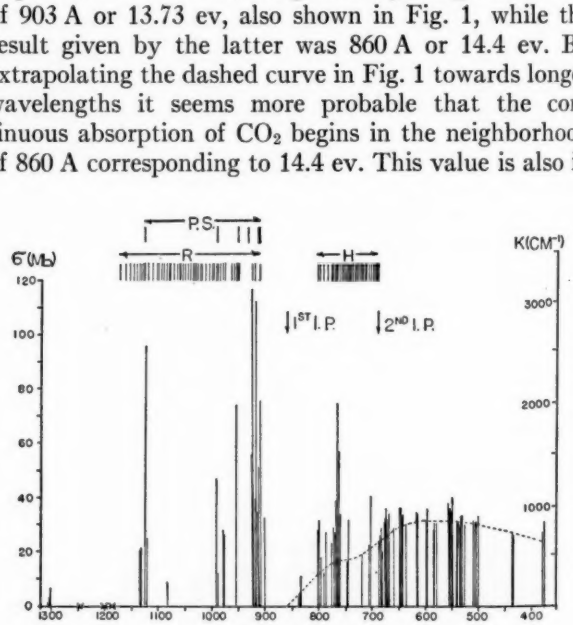

FIG. 1. Absorption cross sections of carbon dioxide. The height of each line represents the absorption cross section σ (left ordinate), or the absorption coefficient k (right ordinate), at the corresponding wavelength. The short lines in the upper portion represent the band heads measured by Rathenau (R), Henning (H), and Price and Simpson (PS). The crosses on the abscissa indicate measurements of σ<1 mb.

[14] H. D. Smyth and C. G. Stueckelberg, Phys. Rev. **36**, 472 (1932).

TABLE II. Absorption cross sections of carbon monoxide (0 means <1 mb).

Wavelength	σ(mb) from 3 individual plates 1	2	3	Average σ(mb)	Average (cm^{-1})
1306.0 OI		0	0		
1276.7 NII		0	0		
1184.5 NIII	0	0	0		
1175.5 CIII	0	0	0		
1152.2 OI	0	0	0		
1135.0 NI	0		0		
1006.0 NII		0	0		
979.9 OI			0		
955.3 NV			0		
924.3 NIV	11	11		11	300
923.7 NIV	11	12	9.7	11 ±1	300± 27
923.2 NIV	17	31	21	23 ±5	620±130
923.0 NIV	41	36	27	35 ±5	940±130
922.5 NIV	0	0	0		
916.7 NII		7	10	8.5±1.4	230± 38
916.0 NII	43	60	41	48 ±7	1290±190
915.9 NII	18	32	19	23 ±5	620±130
904.5 CIII	16	20		18 ±2	480± 53
903.6 CIII	18	21		19 ±2	510± 53
835.1 OIII	12		15	14 ±2	380± 53
834.5 OIII	15	21		18 ±3	480± 80
833.3 OII	16	19		18 ±1	480± 27
832.8 OII	16	22	20	19 ±2	510± 53
799.9 CII			17	17	460
799.7 CII			19	19	510
796.7 OII	56	42	41	46 ±6	1230±160
790.1 OIV	14	19	16	16 ±2	430± 53
787.7 OIV	19	24	24	22 ±2	590± 53
776.0 OII	24	27	23	25 ±2	670± 53
773.0 NIII	23	24	23	23	620
772.4 NIII	21	24	22	22 ±1	590± 27
771.5 NIII	14	18	18	17 ±1	460± 27
765.1 NIV	17	23	22	21 ±2	560± 53
764.4 NIII	24	32	30	29 ±3	780± 80
763.3 NIII	18	19	23	20 ±2	530± 53
747.0 NII	16	21	18	18 ±2	480± 53
745.8 NII	17	22	21	20 ±2	530± 53
718.6 OII	15	19	24	19 ±3	510± 80
703.9 OIII	15	18	18	17 ±1	460± 27
702.9 OIII	17		19	18 ±1	480± 27
702.3 OIII	18		15	17 ±1	460± 27
686.3 NIII	15	17	16	16 ±1	430± 27
685.0 NIII	17	13	17	16 ±1	430± 27
672.9 OII	24	19	18	20 ±2	530± 53
672.0 NII	15	20	16	17 ±2	460± 53
671.8 NII	18	18	18	18	480
671.6 NII	17	21	19	19 ±1	510± 27
671.4 NII	26	28	20	25 ±3	670± 80
660.3 NII	18	19	15	17 ±1	460± 27
2×660.3 NII			17		
645.2 NII	16	17	15	17 ±1	460± 27
2×645.2 NII		15	17		
644.8 NII	16	17	17	16 ±1	430± 27
2×644.8 NII		15	16		
644.6 NII	16	17	17	16 ±1	430± 27
2×644.6 NII		16	15		
644.1 NII	18	18	13	16 ±1	430± 27
2×644.1 NII		15			
635.2 NII	24	22		22 ±1	590± 27
2×635.2 NII		21	22		
629.4 NII	21			21 ±1	560± —
2×617.1 OII	20		20	20	530
2×616.3 OII	19		20	20	530
2×599.6 OIII		19	17	18 ±1	480± 27
2×597.8 OIII		19	20	19	510
2×582.2 NII	21	17	16	18 ±2	480± 53
2×581.0 OII	20	18	16	18 ±2	480± 53
2×580.4 OII	20	15	19	18 ±2	480± 53
2×574.7 NII		19	18	18 ±1	480± 27
2×555.3 OIV	18	18		18	480
2×554.5 OIV	18	21	19	19 ±1	510± 27
2×553.3 OIV	20		23	21 ±1	560± 27
2×539.9 OII		19	20	20	530
2×539.5 OII		20	19	19 ±1	510± 27
2×539.1 OII		19	19	19	510
2×538.3 OII			19	19	510
2×537.8 OII		19	18	19 ±1	510± 27
2×529.9 NII	18	20	19	19	510
2×529.7 NII	19	22	18	20 ±1	530± 27
2×529.5 NII	18	20	17	18 ±1	480± 27
2×525.8 OIII	18	22	17	19 ±2	510± 53
2×509.6 NIII		18	21	19 ±1	510± 27
2×508.2 OIII	17	16	17	17	460
2×507.7 OIII	18	16	18	17 ±1	460± 27
2×507.4 OIII	21	14	21	19 ±3	510± 80
2×434.3 NIII	16		17	17 ±1	460± 27
2×434.0 NIII	18		16	17 ±1	460± 27
2×374.3 NIII	13	13	14	13	350
2×373.8 OIII	15	16	16	16	430

agreement with recent data on direct photoionization measurements by Wainfan, Walker, and Weissler.[15] The second ionization potential suggested by Henning[3] and Price and Simpson[5] was at 690 A or 18 ev, the limit of the second series of bands. Smyth and Stueckelberg[13] also found dissociative ionization processes for CO_2 in the wavelength region studied here:

$CO_2 \rightarrow CO + O^+$ (19.6 ev or 632 A),
$CO_2 \rightarrow (CO_2^+ + CO_2) \rightarrow 2CO + O_2^+$ (20.0 ev or 620 A),
$CO_2 \rightarrow CO^+ + O$ (20.4 ev or 607 A),
$CO_2 \rightarrow C^+ + 2O$ (28.3 ev or 438 A).

These four processes together with the second ionization continuum and a portion of the first ionization continuum might make their appearance in the region between 690 A and 374 A. The results obtained here should be a combination of all of these reactions. Since no conspicious bands due to the dissociative ionization reactions listed were observed, the contributions due to these processes might be small in comparison with that of the ionization continua. According to Mulliken,[16] the two outermost orbits of a CO_2 molecule contain four π^*2p-nonbonding and four $\pi 2p$-bonding electrons. The first continuum beginning at 860 A should be due to the removal of a nonbonding π^*2p-electron while a large portion of the continuum below 690 A might correspond to the ionization of $\pi 2p$-electrons. Indication of a small discontinuity in the absorption contour in the neighborhood of 690 A possibly might suggest the starting point of the second ionization continuum. By integrating the area under a curve obtained by plotting the absorption coefficients *versus* wave number, the f-value of CO_2 due to continuous absorption in the region from 860 A to 374 A was found to be 4.4. Extrapolation of the dashed curve in Fig. 1 from 374 A towards shorter wavelengths increased this value to

[15] Wainfan, Walker, and Weissler, Phys. Rev. **99**, 542 (1955).
[16] R. S. Mulliken, Phys. Rev. **40**, 55 (1932).

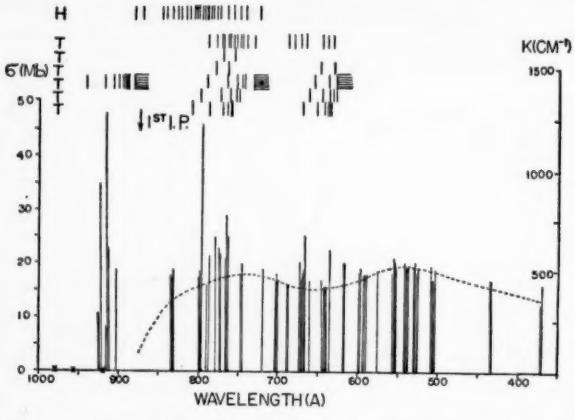

FIG. 2. Absorption cross sections of carbon monoxide. The height of each line represents the absorption cross section σ (left ordinate) or the absorption coefficient k (right ordinate) at the corresponding wavelength. The short lines in the upper left portion show the band heads as measured by Henning (H), and Tanaka (T). The crosses on the abscissa indicate measurements of $\sigma<1$ mb.

about 5.5 or 6. This may be compared to the dispersion data of Fuchs[17] who used a four-term equation to represent the indices of refraction of CO_2 between 1800 A and 13 microns. His first term contained a characteristic wavelength $\lambda_1=720.41$ A with an oscillator strength $f_1=6.716$. If one were to ascribe to the dense band system[4] between 1175 A and 912 A an f-value of about 0.5 to 1.0, then the total oscillator strength determined from absorption data would agree well with that obtained from the dispersion equation. A separation of the observed absorption continuum into the two ionization continua associated with the first and second ionization limits, respectively, does not seem possible from the available data.

CARBON MONOXIDE

Tank CO was purified by the same method as described for CO_2. The absorption cross sections of 83 source lines from three plates in the range from 1306 A to 374 A are presented in Table II and Fig. 2. At long wavelengths all σ values were less than 1 mb until prominent band absorption appeared at 924 A and extended to 600 A. The most conspicuous resonance bands yielded cross sections of 48 mb and 46 mb at 916.0 A and 796.7 A, respectively. Tanaka[9] measured three Rydberg series and five progressions of CO between 938 A and 638 A while Henning[3] found 26 members of bands between 881 A and 726 A. The position of these band heads are also shown in the upper-left portion of Fig. 2. Below 600 A no bands have been observed. The continuum reported here began somewhere between 900 A and 835 A; however, since there were no convenient source lines in this region, its exact starting point could not be determined. The entire continuous spectrum is rather flat with a maximum value of 19 mb between 750 A and 500 A and probably a small dip of about 15 mb at 644 A. All absorption cross sections of CO between 1306 A and 1050 A are less than 1 mb, and therefore a detailed comparison with Watanabe's[10] results in this region is not possible.

The first ionization potential of CO, 14.1 ev or 880 A, was determined from electron impact work by Hagstrum[18] who also found three dissociative ionization processes which might fall into the region measured here:

$$CO \rightarrow C^+ + O^{-*} \text{ (20.9 ev or 594 A)},$$
$$CO \rightarrow C^+ + O^* \text{ (22.8 ev or 544 A)},$$
$$CO \rightarrow C + O^+ \text{ (23.2 ev or 534 A)}.$$

Tanaka[9] identified three Rydberg series limits at 13.94 ev (884 A), 16.45 ev (751 A), and 19.58 ev (632 A). Since there is no indication of band absorption due to the above three dissociative ionization reactions, the continuum reported here might be mainly due to pure electronic ionization. Using Hagstrum's value of 14.1 ev or 880 A as the starting point of this continuum and integrating its area, it was found that the f-value of CO, between 880 A to 374 A, is 2.8. As shown in Fig. 2 the strong bands were located in the regions of Tanaka's three Rydberg series, while between these series limits, the absorption seems to be continuous and flat. From its appearance it seemed evident that no differentiation into several distinct ionization continua was possible.

ACKNOWLEDGMENTS

The continued support of the Office of Naval Research is gratefully acknowledged.

[17] O. Fuchs, Z. Physik **46**, 519 (1927).

[18] H. D. Hagstrum, Revs. Modern Phys. **23**, 185 (1951).

Rate of Convergence of Madelung Series by the Method of Bertaut*

DAVID H. TEMPLETON
Department of Chemistry and Radiation Laboratory, University of California, Berkeley, California
(Received December 8, 1954)

A calculation is made of the correction to be applied to the Madelung constant when computed by a method given by Bertaut with a finite number of terms.

THERE are many problems in crystal chemistry in which it is of interest to consider the electrostatic energy of a crystal resulting from the interaction of the ions considered as point charges. This energy is given by the sum of an infinite series which converges slowly and conditionally.

Bertaut[1] noticed the connection between the terms of this series and the Patterson function of the charge distribution. He showed how the calculation could be carried out if the point charges are replaced by spherically symmetrical charges of various shapes. If the charge of each ion is spread uniformly over the volume of a sphere of radius R, with R no greater than the shortest interionic distance, an expression results which has several advantages for numerical work:

$$A=-\frac{WL}{\epsilon^2}=\frac{3L}{5RZ}\sum_j z_j^2 - \frac{18\pi R^2L}{ZV}\sum_h |F|^2\frac{(\sin\alpha-\alpha\cos\alpha)^2}{\alpha^8} \quad (1)$$

where

$$\alpha=2\pi hR \quad (2)$$

and

$$F=\sum_j z_j e^{2\pi i(h_1x_{1j}+h_2x_{2j}+h_3x_{3j})}. \quad (3)$$

Equation (1) is Bertaut's Eq. (41) with slight changes of notation. Here A is the Madelung constant based on L as unit distance, W is the electrostatic energy per molecule, ϵ is the electronic charge, Z is the number of molecules in the unit cell, z_j is the charge number of atom j, V is the volume of the unit cell, and h is the magnitude of the vector $(h_1h_2h_3)$ in reciprocal space or the reciprocal of the spacing d of the planes $(h_1h_2h_3)$. The coordinates of atom j are x_{1j}, x_{2j}, x_{3j}. The sum over h in Eq. (1) includes the infinite number of reciprocal vectors corresponding to all combinations of integral values of h_1, h_2, and h_3, positive, zero, and negative. It is convenient to insert a factor p, the multiplicity of the form $(h_1h_2h_3)$ for the crystal under consideration, and to include in the sum only one term for each group of equivalent terms. The sums over j in Eqs. (1) and (3) include the atoms of one unit cell.

In the application of Eq. (1) it is advantageous to know the error introduced if the sum over h includes only those values of h not greater than some quantity m. This becomes especially of interest when the number of terms in a small interval of h becomes large. Under this condition $|F|^2$ may be replaced by its average value[2] $\Sigma_j z_j^2$. The density of terms in reciprocal space is V. Therefore the error, ΔA,

$$\Delta A=\frac{18\pi R^2L}{ZV}\sum_{h>m}|F|^2\frac{(\sin\alpha-\alpha\cos\alpha)^2}{\alpha^8} \quad (4)$$

is approximated by an integral

$$\Delta A=\frac{18\pi R^2L}{ZV}\int_m^\infty\sum_j z_j^2\frac{(\sin\alpha-\alpha\cos\alpha)^2}{\alpha^8}4\pi h^2V\,dh \quad (5)$$

$$=\frac{9L\Sigma z^2}{\pi RZ}\int_\beta^\infty\frac{(\sin\alpha-\alpha\cos\alpha)^2}{\alpha^6}d\alpha \quad (6)$$

where

$$\beta=2\pi Rm. \quad (7)$$

The integral in Eq. (6) can be reduced by five successive integrations by parts to the form

$$\Delta A=\frac{3L\Sigma z^2}{5\pi RZ}\left\{\frac{3\sin^2\beta}{\beta^5}-\frac{6\sin\beta\cos\beta}{\beta^4}+\frac{2+\cos^2\beta}{\beta^3}-\frac{\sin\beta\cos\beta}{\beta^2}-\frac{1-2\sin^2\beta}{\beta}+\pi-2Si(2\beta)\right\} \quad (8)$$

where

$$Si(2\beta)=\int_0^{2\beta}\frac{\sin t}{t}dt. \quad (9)$$

TABLE I. Corrections for termination of the series.

β/π	Q	$100\Delta A/A$
0.5	0.172664	43
1.0	0.015992	4
1.5	0.004715	1
2.0	0.001950	0.5
2.5	0.000996	0.2
3.0	0.000574	0.1
3.5	0.000362	0.09
4.0	0.000242	0.06
4.5	0.000170	0.04
5.0	0.000123	0.03

* This research was supported by the U. S. Atomic Energy Commission.

[1] F. Bertaut J. phys. radium **13**, 499 (1952).

[2] The derivation given by H. Lipson and W. Cochran [*The Determination of Crystal Structures* (G. Bell and Sons, Ltd., London, 1953), p. 134] applies equally well when some of the z's are negative.

The function $Si(x)$ can be found in tables.[3] The error may be written as

$$Q=\frac{\Delta ARZ}{L\Sigma z^2}=\frac{-\Delta WRZ}{\epsilon^2\Sigma z^2}. \quad (10)$$

Selected values of Q are tabulated in Table I. It so happens[4] that the value of $ARZ/L\Sigma z^2$ is always of the order of 0.4 if R is half the shortest interionic distance. Therefore we can also list in Table I approximately the percentage error in A if the series is terminated at $\alpha=\beta$.

If the calculated errors listed in Table I are applied as corrections to the computed series, then the accuracy of the result is an order of magnitude better than without the correction. This table is also very useful for planning the work so that enough but only enough terms are included to obtain the desired accuracy.

One should not interpolate in Table I, because the function $Q(\beta)$, though monotonic, has zero slope at certain points near those where β is a half-integral multiple of π.

I thank Mrs. Carol Dauben for aid with the calculations.

[3] U. S. Bureau of Standards, *Tables of Sine, Cosine, and Exponential Integrals* (Work Projects Administration, New York, 1940), two volumes.

[4] This can be shown by a simple extension (unpublished) of the generalizations of A. Kapustinsky [Z. physik. Chem. **B22**, 257 (1933)] and D. H. Templeton [J. Chem. Phys. **21**, 2097 (1953)].

THE JOURNAL OF CHEMICAL PHYSICS VOLUME 23, NUMBER 9 SEPTEMBER, 1955

Screw Dislocations in Growth from the Melt

G. W. SEARS
General Electric Research Laboratory, Schenectady, New York

(Received December 13, 1954)

The screw dislocation growth mechanism is shown to be operative for the growth from the melt of certain faces of PbI_2 at small supercoolings.

FRANK[1] first recognized that perfect crystals should not grow from the vapor phase below a critical supersaturation necessary to two-dimensionally nucleate new layers. He proposed that only imperfect crystals should grow. In particular, he pointed out that a screw dislocation terminating at the crystal surface would provide a permanent growth step, making two-dimensional nucleation unnecessary. The comprehensive treatment of the growth of crystals has been presented by Burton, Cabrera, and Frank.[2]

The faces of crystals which have been grown by the screw mechanism should present spiral growth marking when one or a few screw dislocations have dominated the growth in a region. The first evidence was reported by Griffin[3] who found growth markings on a natural beryl crystal. Since then spiral growth patterns have been reported for a large variety of crystals which have been grown from the vapor. The evidence has been summarized by Verma.[4]

In addition, it has been established that at low supersaturations in solution the screw growth mechanism

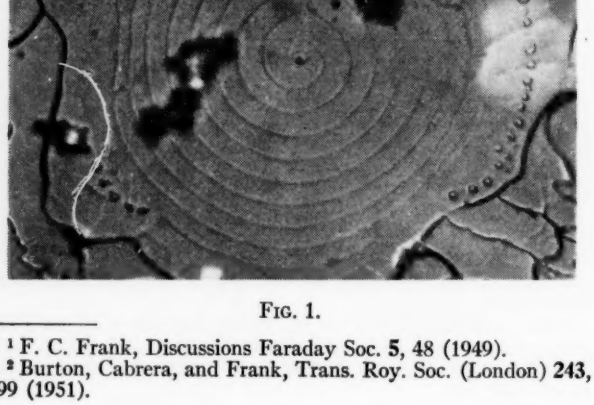

FIG. 1.

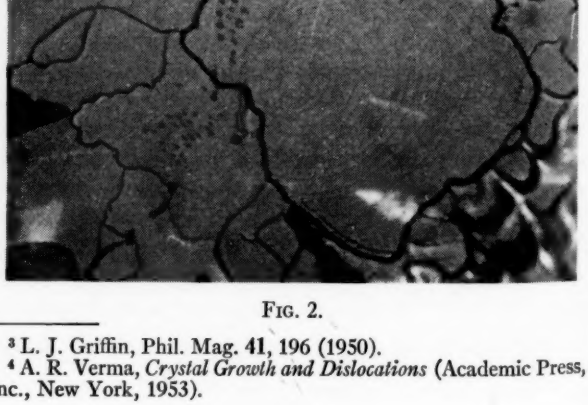

FIG. 2.

[1] F. C. Frank, Discussions Faraday Soc. **5**, 48 (1949).
[2] Burton, Cabrera, and Frank, Trans. Roy. Soc. (London) **243**, 299 (1951).
[3] L. J. Griffin, Phil. Mag. **41**, 196 (1950).
[4] A. R. Verma, *Crystal Growth and Dislocations* (Academic Press, Inc., New York, 1953).

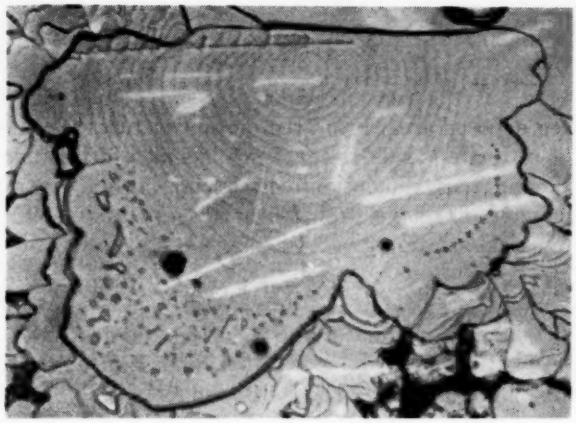

FIG. 3.

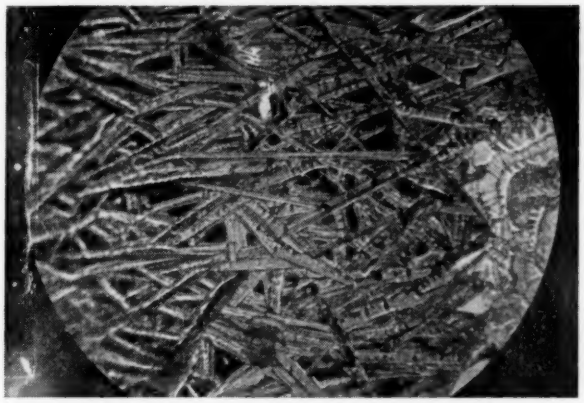

FIG. 4.

is operative. Motion pictures[5,6] of moving spirals on the faces of thin hexagonal crystals of CdI_2 growing from solution are perhaps the most striking evidence for the reality of the Frank growth mechanism.

Sears[7,8] has investigated the growth behavior of very thin crystalline whiskers of mercury from the vapor. It has been proposed that a nucleus containing a single screw dislocation should grow as a whisker at constant radius. It has been proposed and experimentally supported[9] that the critical condition for whisker growth should be that the supersaturation be maintained below the critical value for two-dimensional nucleation. Newkirk and Sears[10] have shown that the same considerations may be used to rationalize the growth of thin rods of potassium halide from aqueous solution.

Amelinckx and co-workers[11,12] have observed spiral growth patterns on crystals of salol and thymol grown from the melt. No spirally terraced growth hills were observed. It was not established that the observed screw dislocations were operative in the growth of a crystal surrounded by its own melt.

The present paper presents evidence which indicates that for low degrees of supercooling the screw mechanism is operative in growth of PbI_2 crystals from their own melt.

EXPERIMENTAL

A few grams of CP PbI_2 crystals were heated to melting in a test tube. When the mass was entirely molten the liquid was poured quickly out of the test tube. Almost instantaneously to the eye, the liquid stream in the test tube froze into a thin bar of PbI_2 crystals. The surface of this bar was examined for spiral growth patterns. Photomicrographs of representative growth patterns are shown in Figs. 1–4. The magnifications are 1000× for Fig. 1 and 500× for Figs. 2–4. A photomicrograph of the surrounding surface is shown at 500× in Fig. 4.

A motion picture was taken of the freezing process at 80 frames/sec. A telephoto lens with extension tube was used to obtain about 3-fold magnification. The melting and pouring was carried out in a test tube whose top quarter had been removed with a glass saw. The tube was rotated on a fixed axis against a stop so that the stream flowed and froze in the focal plane of the camera. It was found that the time interval between the first appearance of crystals and complete freezing was 0.3 sec. A line of crystals first appeared at the edges of the stream and advanced to the center of the stream. At no time was a single crystal isolated from neighboring crystals.

A freezing point curve was measured for a sample of the same size as used in the preceding experiments. No supercooling was detected within experimental error in temperature measurement for a cooling rate of 35°C per minute. The maximum error was estimated at 2°C and this was taken as the maximum supercooling in PbI_2. The frozen PbI_2 was always composed of a large number of crystals.

The spiral-bearing crystals were scattered randomly over the length and breadth of the PbI_2 polycrystalline bar. Since the freezing process proceeded from the outside edges, it is implied that the concentration of soluble impurities in the melt during the freezing process had no significant effect on the existence and operation of growth spirals.

DISCUSSION

There are three conceivable transport processes by which crystals bearing spiral growth markings might have grown from the melt. At low supercoolings the screw dislocation might be operative for growth of solid completely immersed in its own melt. Since the

[5] A. J. Forty, Phil. Mag. **43**, 377 (1952).
[6] J. B. Newkirk, to be published in *Acta Metallurgica*.
[7] G. W. Sears, Acta Metallurgica **1**, 457 (1953).
[8] G. W. Sears, "Growth mechanism of mercury whiskers" (to be published).
[9] G. W. Sears, "Whisker growth mechanism. II" (to be published).
[10] J. B. Newkirk and G. W. Sears, *Growth of Potassium Halide Crystals From Aqueous Solution* (to be published).
[11] S. Amelinckx, Naturwiss. **39**, 547 (1952).
[12] Votava, Amelinckx, and Dekeyser, Naturwiss. **40**, 143 (1953).

spirals were finally exposed, it is also possible that they might have grown by vapor transport or by surface diffusion.

The possibility of spiral growth by surface diffusion is eliminated when Fig. 1 is examined, for example. The operating screw dislocation is located at the dot at the center of the crystal. The equally spaced turns of spiral show that the supersaturation was uniform over the surface of the crystal during growth. Such a condition could not obtain by surface diffusion since each turn of the spiral represents a growth step. Either vapor-solid or liquid-solid transfer would provide uniform supersaturation over the crystal surface.

Since the liquid PbI_2 is poured into a vapor-free space to freeze, the vapor transport must involve evaporation and diffusion from the supercooled liquid and diffusion to and condensation on a solid surface. It is only necessary to establish an upper limit for the amount of material carried by vapor transport, not the least upper limit, so the evaporation process is ignored.

The actual transport process is replaced by a model in which the crystal surface is taken as a single diffusion sink surrounded by air having a partial pressure of PbI_2 vapor in equilibrium with supercooled liquid PbI_2. The sink is taken as a rectangle 50μ in width and of infinite length.

For a small amount of supercooling, δT, it can be written that the vapor pressure difference, δp, between crystal and supercooled liquid is

$$\delta p=\frac{\Delta H_f\cdot\delta T\cdot p_s}{RT^2} \tag{1}$$

where p_s is the vapor pressure of solid PbI_2, ΔH_f is the heat of fusion, and δT is the supercooling. The heat of fusion[13] of PbI_2 is 5300 cal/mole and the vapor pressure of PbI_2 at the melting point[14] is approximately 0.1 mm Hg. The maximum supercooling was measured as ≤ 2°C. Solving Eq. (1) numerically, it is found that

$$\delta p\leq 10^{-3}\text{ mm Hg}. \tag{2}$$

The diffusion constant for PbI_2 vapor through air is unknown, so the measured value[15] of mercury vapor in air at 760 mm pressure is used as an approximation, $D_s=0.14$ cm^2/sec. The mean diffusion path, λ, is calculated from

$$\lambda=(2Dt)^{\frac{1}{2}} \tag{3}$$

where t is the time in which the sink remains at its fixed exposed area. From the motion pictures the time, t, is estimated as 0.01 sec when the sink width is taken as 50μ. This dimension corresponds to an average diameter for the spiral-bearing crystallites. The numerical solution gives

$$\lambda=5.2\times10^{-2}\text{ cm}. \tag{4}$$

The amount of material which could be deposited on a crystal of $50\mu\times50\mu$ surface by vapor diffusion is the PbI_2 vapor contained in a half-cylinder of 5.2×10^{-2} cm radius and 5×10^{-3} cm length. The mass, w_{calc}, is given by

$$w_{\text{calc}}=\frac{\delta pM\pi\lambda^2L}{2RT} \tag{5}$$

where $\delta p\leq10^{-3}$ mm Hg, $M=465$ g, $\lambda=5.2\times10^{-2}$ cm, $L=5\times10^{-3}$ cm, $R=8.31\times10^7$ erg/deg, and $T=680$°C.

$$w_{\text{calc}}\leq4.5\times10^{-13}\text{ g}. \tag{6}$$

The amount of material which has been deposited on the crystal by the screw mechanism can be estimated. In Fig. 1, for example, there are twelve terraces visible. A good estimate for step height is 1000 A. The height of the screw pyramid, h, is then about 12 000 A. The estimation of the pyramid height is confirmed by the observation that the top and bottom terraces of the large spirals in Fig. 2 and 3 cannot be brought into focus simultaneously with a 40× objective. The mass of deposited material, w_{obs}, is

$$w_{\text{obs}}=\frac{\pi r^2h\rho}{3} \tag{7}$$

where r is the base radius (25μ) and $\rho=6.2$ g/cm^3. The deposited mass is calculated numerically to be

$$w_{\text{obs}}=5.0\times10^{-9}\text{ g}. \tag{8}$$

Comparing Eqs. (6) and (8) it can be seen that the rate of transport by vapor diffusion is at least 10 000 times too slow to account for the spiral growth patterns. By elimination the growth spirals would seem to have grown by direct liquid-solid transfer.

CONCLUSIONS

It is concluded that certain faces of PbI_2 crystals grow from the melt at small supercoolings by the screw dislocation mechanism.

[13] *Handbook of Chemistry and Physics* (Chemical Rubber Publishing Company, Cleveland, Ohio, 1950), thirty-second edition, p. 1914.
[14] D. Stull, Ind. Eng. Chem. **39**, 540 (1947).
[15] J. L. Spier, Physica **6**, 453 (1939).

Adsorption of Helium on Titanium Dioxide*

J. G. Aston, S. V. R. Mastrangelo,† and R. J. Tykodi‡
Cryogenic Laboratory of the College of Chemistry and Physics, The Pennsylvania State University, University Park, Pennsylvania
(Received November 15, 1954)

The absorption characteristics of helium adsorbed on TiO_2 (anatase) have been studied in the temperature range 2°–20°K. Isotherms are reported at 2.60°, 4.17°, 13.96°, and 20.28°K. Isosteric heats of adsorption at low coverage have been measured at 17.1°K. The data are interpreted in terms of a previously discussed model.

UNDER the title "The Anomalous First Layer of Adsorbed Helium and a Modified B.E.T. Theory" Aston and Mastrangelo[1] have discussed the rather unusual adsorption characteristics of helium and have suggested some simple modifications of the ordinary B.E.T. formalism in order to account for their data pertaining to the adsorption of helium on TiO_2. They have briefly discussed their isotherm data in the region 1.9° to 4.2°K and have suggested that a transition analogous to melting in the first or second layer may be expected to occur in the range 2.6° to 3.4°K.

The experimental work of Aston and Mastrangelo for the adsorption of helium on TiO_2 (230 m^2/g) was continued, using the same apparatus and technique.

EXPERIMENTAL

Apparatus

The apparatus used was essentially that described by Mastrangelo and Aston[2] with the following modifications: the helium bomb and adsorption calorimeter were replaced by new units. The new bomb had a capacity of 370 cc. The adsorption calorimeter contained 39.5 g of TiO_2 in an available space of 43.1 cc. The TiO_2 used was part of a sample, C–198, of acid precipitated anatase.[3] As determined by the B.E.T. nitrogen adsorption method the surface area of the sample was 230 m^2/g. Prior to beginning the adsorption measurements the adsorbent was outgassed at 100°C for several days until the residual pressure in the calorimeter was less than 1×10^{-5} mm Hg.

Method

Pressures were measured in the 12.5 mm diameter mercury manometer; temperatures, by means of the constantan resistance thermometer; and corrections applied, according to the techniques of Mastrangelo and Aston.[2] Isosteric heats of adsorption were calculated from the 13.96°K and the 20.28°K isotherms and were also measured calorimetrically at the lowest coverages. The calorimetric measurements were planned merely to establish the existence of the high heats of adsorption apparent from the isotherms; an over-all accuracy of 5 percent was all that was sought. A complete measurement consisted of heat capacity determinations for the total system both before and after a small increment of gas (approximately 100 cc S.T.P.) was admitted to the system and the determination of the rise in temperature of the system as a result of the increment of gas. The calorimeter was cooled after each complete measurement so that the initial temperature was in each case approximately 13.5°K. The two sets of heat capacity data (heat capacities of the calorimeter plus adsorbed gas before and after each increment of gas) were reduced to convenient temperatures (13.51° and 16.54°K) by small linear extrapolations, thus yielding plots of heat capacity *versus* coverage for two different temperatures. The heat capacity of the system calorimeter-plus-adsorbed-gas corresponding to the mean temperature and mean amount adsorbed for a given heat of adsorption measurement was determined by linear interpolation between the aforementioned reduced heat capacity plots. In expressing the heat of adsorption results at the common temperature 17.1°K it was assumed that $q_{st}(T_2)=q_{st}(T_1)+\Delta(RT)$. The remaining calculations were carried through in a straightforward manner.[4–7] The desorption correction to the heat capacity measurements was, in the worst case, 5.3 percent of the heat capacity of the total system; the compression correction to the heat of adsorption measurements, under similar conditions, was 40 cal/mole.

Results

Figures 1 and 2 show a representative selection of the isotherm data and the heat of adsorption data, respectively. The adsorption data below 4.2°K were plotted

* Contribution No. 77 from the Cryogenic Laboratory of the College of Chemistry and Physics. This work carried out under contract number N6 ONR-269 T.O.X. of the Office of Naval Research.
† Present address: The Barrett Division, Allied Chemical and Dye Corporation, Philadelphia, Pennsylvania.
‡ American Cyanamid Fellow 1951–1952.
[1] J. G. Aston and S. V. R. Mastrangelo, J. Chem. Phys. **19**, 1067 (1951).
[2] S. V. R. Mastrangelo and J. G. Aston, J. Chem. Phys. **19**, 1370 (1951).
[3] Obtained from the New Jersey Zinc Company, Palmerton, Pennsylvania, through the courtesy of C. W. Siller.
[4] G. L. Kington and J. G. Aston, J. Am. Chem. Soc. **73**, 1929 (1951).
[5] Morrison, Los, and Drain, Trans. Faraday Soc. **47**, 1023 (1951).
[6] L. E. Drain and J. A. Morrison, Trans. Faraday Soc. **48**, 840 (1952).
[7] E. L. Pace and S. A. Greene, J. Am. Chem. Soc. **76**, 3286 (1954).

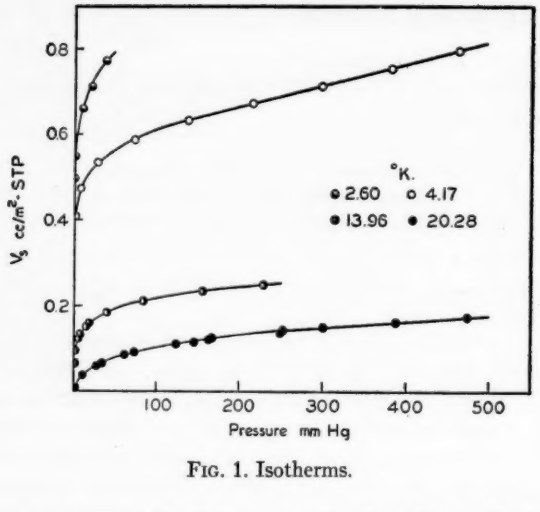

FIG. 1. Isotherms.

at approximately 0.2° intervals; both ordinary B.E.T.[8] and modified B.E.T.[1] plots were constructed from the isotherms. It was found that while the ordinary B.E.T. Eq. (1) fit the data only up to $P/P_0 \sim 0.3$

$$\frac{P/P_0}{(1-P/P_0)V_s}=\frac{1}{CV_m}+\frac{C-1}{CV_m}\frac{P}{P_0} \tag{1}$$

the modified B.E.T. Eq. (2) fit the data up to $P/P_0 \sim 0.5$

$$\frac{P/P_0(1-P/2P_0)}{(1-P/P_0)V_s}=\frac{1}{CV_m}+\frac{C-1}{CV_m}\frac{P}{P_0}. \tag{2}$$

Figure 3 consists of modified B.E.T. plots of representative adsorption data. The solid lines represent the best lines through the 4.2°, 3.4°, 2.6°, and 2.0°K data, respectively (reading from top to bottom). The plotted points represent only a part of the data taken. The

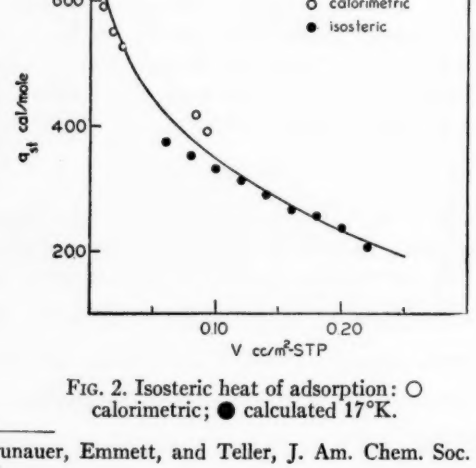

FIG. 2. Isosteric heat of adsorption: ○ calorimetric; ● calculated 17°K.

[8] Brunauer, Emmett, and Teller, J. Am. Chem. Soc. **60**, 309 (1938).

slope of the plots changes but slowly below 2.6°K; similarly above 3.4°K. The rapidly changing slope in the region 2.6°–2.4°K indicates a major change in V_m, probably due to a change in the density of the adsorbed phase. The value of V_m calculated from the slope of the 2.6°K plot is 0.66 cc/m²–S.T.P.; this corresponds to two layers of solid helium[1,2] under a pressure slightly larger than the melting pressure (approximately 56 atmospheres at 2.6°K).[9] It therefore seems likely that the behavior of the adsorbed phase between 2.6° and 3.4°K is analogous to the melting of solid helium under high pressure. Of course, to establish the nature of the phenomenon unequivocally, heat capacity measurements at various coverages are needed; a new simplified apparatus has been constructed to investigate this and other problems. It may be mentioned that Frederikse[10] found for helium adsorbed on jeweler's rouge that at the lowest coverages no lambda point was observed for

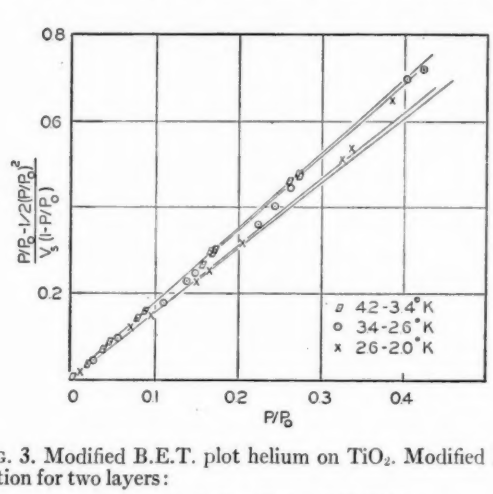

FIG. 3. Modified B.E.T. plot helium on TiO_2. Modified B.E.T. equation for two layers:

$$\frac{1}{CV_m}+\frac{C-1}{CV_m}\frac{P}{P_0}=\frac{P/P_0-\frac{1}{2}(P/P_0)^2}{V_s(1-P/P_0)}.$$

the adsorbed film; the low heat capacity of the film indicated solid-like behavior.

In a recent publication Atkins,[11] by considering a model based on the Polanyi theory of adsorption, reached much the same conclusions as Aston and Mastrangelo, i.e., two solid-like layers of adsorbed helium, a change in V_m with temperature due to melting in the second layer, and a general correlation of the properties of adsorbed helium with those of bulk helium under pressure. Strauss, as reported by Long and Meyer,[12] found for helium adsorbed on jeweler's rouge a rather uniform change in V_m with temperature, V_m being determined from ordinary B.E.T. plots. Since the modified B.E.T. equation yield plots that are linear over a greater range of P/P_0 values than the ordinary

[9] W. H. Keesom, *Helium* (Elsevier Publishing Co., Inc., Houston, Texas, 1942), p. 202.
[10] H. P. R. Frederikse, Physica **15**, 860 (1949).
[11] K. R. Atkins, Can. J. Phys. **32**, 347 (1954).
[12] E. Long and L. Meyer, Advances in Physics **2**, 1 (1953).

B.E.T. equation, slopes derived from the former are better defined than those derived from the latter. It is possible that variations in the rate of change of slope, if they exist, may be obscured by uncertainties in plotting when ordinary B.E.T. coordinates are used.

The extremely high heats of adsorption (Fig. 2) at low coverage indicate that, at temperatures below the critical, the energy of interaction of helium atoms with the TiO_2 surface will be considerably in excess of the bulk energy of vaporization per molecule for the first two adsorbed layers, thus serving to substantiate the considerations of Aston and Mastrangelo[1,2] and Atkins.[11] The high heats of adsorption found in the present study may be compared to those obtained by other investigators. Van Itterbeek and Van Dingenen[13] found for helium on charcoal at 17.6°K and low coverage heats of adsorption in the range 400–450 cal/mole. Keesom and Schweers[14] found for helium on glass at 3.7°K, *in what appears to be the second adsorbed layer*, heats of adsorption of 60–100 cal/mole. Steele and Halsey[15] obtained for the energy of interaction of a helium atom with a carbon black surface a value of 600 cal/mole.

Finally, in the course of the heat of adsorption measurements, it was found that at 13.51° and 16.54°K the partial molar heat capacity of the adsorbed helium was essentially constant in the range 0.0–0.1 cc/m²–S.T.P., having the values 6.1 and 4.8 cal/mole deg, respectively; the estimated accuracy, however, is only 5 to 10 percent. For comparison it may be mentioned that according to the data of Zelmanov[16] the heat capacity (C_p) of gaseous helium under 60 atmospheres pressure at 13.5° and 16.5°K is 5.40 and 5.60 cal/deg mole, respectively. Also, assuming the classical law of the equipartition of energy, an assembly of systems with (a) 3 vibrational degrees of freedom (b) 1 vibrational and 2 translational degrees of freedom has a heat capacity (C_v) of (a) $3R$ (b) $2R$ cal/deg mole. The uncertainty in the measured heat capacity values (assuming that the constant partial molar values are equivalent to molar values) is such that almost any model of the adsorbed phase will yield heat capacity values of about the right order.

APPENDIX

The role of the pressure variable in the work of Aston and Mastrangelo[1,2,17] has been rather generally misunderstood. In this appendix we review the concept briefly. The functional or operational content of the theory of Aston and Mastrangelo may be summarized by the following assertion: *the properties of adsorbed helium are analogous to those of bulk helium under pressure.* The manner in which the assertion is used for treating experimental data is clear from the two preceding papers. The physically real thing is assumed to be the interatomic spacing in the adsorbed layer. In bulk helium equivalent interatomic spacings are obtained by placing the bulk material under pressure. In its bleakest form, then, the pressure used by Aston and Mastrangelo may be defined as that pressure which, when applied to bulk helium, yields the same interatomic spacing for the bulk as is observed in a layer of adsorbed helium. The fundamental assertion implies further that the local thermodynamic environment in an adsorbed layer with an interatomic spacing corresponding to that of bulk helium under a certain pressure is quite equivalent to the local environment in a sample of the bulk under the given pressure. The strangest thing about the whole procedure is that it is astonishingly successful.

Now it should be clear that any theory which passes back and forth between adsorbed helium and bulk helium by means of some correlative parameter (pressure, density, interatomic spacing, etc.) must be equivalent, in the operational sense, to the theory of Aston and Mastrangelo.

The treatment of Aston and Mastrangelo was purely thermodynamic. No explicit speculation was offered as to the origin of the forces packing the helium atoms so closely together; there was, of course, the implication that the forces emanated from the adsorbent. Atkins[11] has now shown that the appropriate pressures are derivable from the assumption that the adsorbent is the source of a potential field which is independent of the presence of adsorbed material (the field of the London or dispersion forces treated like a gravitational field).

Finally, according to the treatment of Fowler and Guggenheim[18] the fundamental equation for a single phase of a one component system in mechanical equilibrium with its surroundings is given by [Eq. (222,16)]

$$dE = TdS - \Sigma X dx + \mu dN,$$

where the x's are geometric parameters and the X's are generalized mechanical forces exerted by the phase tending to increase the appropriate x's. Aston and Mastrangelo have, in effect, dealt with the combined terms ($\Sigma X dx$); they did not attempt to interpret the individual terms or even assert that ($\Sigma X dx$) could be treated, approximately, as a single term; Atkins has gone somewhat further.

[13] A. Van Itterbeek and W. Van Dingenen, Physica **5**, 529 (1938).
[14] W. H. Keesom and J. Schweers, Physica **8**, 1020 (1941).
[15] W. Steele and G. D. Halsey, Jr., J. Chem. Phys. **22**, 979 (1954).
[16] J. Zelmanov, J. Physics U.S.S.R. **8**, 135 (1944).
[17] Aston, Mastrangelo, and Tykodi, Proceedings of the International Conference on Low Temperature Physics, Oxford, August, 1951, p. 73.
[18] R. Fowler and E. A. Guggenheim, *Statistical Thermodynamics* (Cambridge University Press, Cambridge, England, 1952), p. 59.

Vibrational Spectra and Structure of Cyclopropane and Cyclopropane-d_6*

A. W. BAKER† AND R. C. LORD
Spectroscopy Laboratory and Department of Chemistry, Massachusetts Institute of Technology, Cambridge 39, Massachusetts

(Received December 28, 1954)

Cyclopropane-d_6 has been synthesized from deuterium oxide and magnesium tricarbide in steps giving successively methyl acetylene-d_4, propylene-d_6, allyl chloride-d_5, 3-bromo-1-chloropropane-d_6, and cyclopropane-d_6. Infrared spectra of cyclopropane and cyclopropane-d_6 have been obtained in the spectral region 350 to 3700 cm^{-1} for the vapor and 650 to 3700 cm^{-1} for the liquid. Raman spectra, including semi-quantitative depolarization factors, have been determined for the liquid state. The spectroscopic results satisfy the Teller-Redlich product rule for a molecule of D_{3h} symmetry. All active fundamentals in cyclopropane-d_6 but one have been directly observed. The inactive fundamentals in both molecules have been located provisionally from overtone assignments. An attempt to determine the molecular geometry from rotational contours of the infrared bands was not successful, but high-resolution work on cyclopropane-d_6 shows that the C−C distance is 1.524±0.014 A.

INTRODUCTION

THE interatomic distances and bond angles in cyclopropane are of considerable interest from the standpoint of valence theory, and there have been numerous structural studies of the molecule. The early work by means of infrared and Raman spectra has been summarized by Herzberg[1] and more recent investigations are discussed below. Since the molecule appears to have no dipole moment, it is presumably not directly accessible to study by microwave spectroscopy. There have been recent electron-diffraction studies[2] which support the D_{3h} structure generally accepted by chemists and give the C−C distance as 1.52±0.02 A, the C−H distance as 1.08 A, and the HCH angle as 118°. Since interatomic distances involving hydrogen are more difficult to measure than those of heavier atoms, the latter two figures are somewhat more uncertain than the C−C distance.

The present work was undertaken in the hope that the additional information to be obtained from the deuterium derivative would not only enable a more complete and reliable vibrational analysis to be made, but might also provide further data from which to obtain the interatomic distances and angles.

EXPERIMENTAL DETAILS

Preparation of Cyclopropane-d_6

The six steps involved were:

1. Preparation of magnesium tricarbide, Mg_2C_3.
2. Reaction of Mg_2C_3 with D_2O to give methyl acetylene-d_4.
3. Reduction of methylacetylene-d_4 to propylene-d_6 with D_2 gas.
4. High-temperature chlorination of propylene-d_6 to allyl chloride-d_5.
5. Addition of DBr to the double bond of allyl chloride-d_5 under proper conditions to obtain 3-bromo-1-chloropropane-d_6.
6. Ring closure with zinc dust.

By means of these reactions, most of which gave relatively high yields, about 6 g (0.125 mole) of cyclopropane-d_6 were prepared. Physical properties and infrared spectra indicated that chemical and isotopic purity were high, the latter about 99 atom-percent.[3]

The individual steps were carried out as follows:

1. Magnesium forms two carbides, either of which can be prepared pure by proper choice of conditions.[4] If a suitable hydrocarbon such as *n*-pentane is passed over magnesium powder at 700°C, Mg_2C_3 is formed with little or no MgC_2. The reaction was carried out in an asbestos-covered iron pipe wound with chromel heating coils. Vycor was used for one or two runs but disintegrated because of reaction with magnesium. Iron boats were used to contain the magnesium powder. Dry hydrogen was passed over the magnesium to displace the air in the system and subsequently to carry the *n*-pentane through the reaction chamber at the proper space velocity. Reaction was confined largely to the surface of the magnesium, necessitating broad, shallow boats. The estimated yield of Mg_2C_3 was 70 to 75%.[5]

2. The Mg_2C_3 was transferred rapidly after preparation to an all-Pyrex apparatus consisting of a 30-cm horizontal tube (about 40 mm diam) as reaction chamber, with a container for admitting D_2O at one end and a trap for collection of methyl acetylene-d_4 at the other. The reaction chamber was wound with heating coils and contained two thermocouple ports for following the reaction temperature. After Mg_2C_3 had been placed in the chamber, with glass wool plugs at each end to keep it from blowing around, the chamber was heated at 400°C for 8 to 10 hours under diffusion-pump vacuum to decompose any $Mg(OH)_2$ which might have been formed by atmospheric or other water vapor. The chamber was

* This paper is based on a thesis submitted by A. W. Baker to the Graduate School of Massachusetts Institute of Technology in partial fulfillment of the requirements for the Ph.D. degree, September, 1950. A detailed account of the chemical procedures for preparation of cyclopropane-d_6 is given in the thesis.

† Present address: Spectroscopy Laboratory, Dow Chemical Company, Midland, Michigan.

[1] G. Herzberg, *Infrared and Raman Spectra* (D. Van Nostrand Company, Inc., New York, 1945), pp. 351–353, 437.

[2] O. Bastiansen and O. Hassel, Tidsskr. Kjemi, Bergvesen Met. **6**, 71 (1946); J. D. Dunitz and V. Schomaker, J. Chem. Phys. **20**, 1703 (1952) (reference 19, p. 1705).

[3] Analyses were made by infrared absorption and mass spectrometry. We are indebted to Dr. F. L. Mohler, National Bureau of Standards, for the mass-spectrometric analysis.

[4] J. Novak, Z. physik. Chem. **A73**, 513 (1910).

[5] Further details are given in the Ph.D. thesis of A. W. Baker. L. C. Leitch and R. Renaud [Can. J. Chem. **30**, 79 (1952)] have also published detailed directions for preparation of Mg_2C_3 and methyl acetylene-d_4.

allowed to cool to 140° and D_2O was admitted to the side tube. No free space was allowed above the magnesium carbide so that the D_2O was forced to diffuse through the carbide, reacting completely as the reaction progressed down the tube. Only a slight excess of D_2O was necessary for almost quantitative conversion of the carbide. The evaporation of the D_2O, which governed the rate of the reaction, was controlled by the pressure maintained in the reaction chamber and by the temperature of the side tube. Because of the liberation of large amounts of heat, with subsequent danger of fires and explosions, the passage of D_2O over Mg_2C_3 must be carefully regulated.

In addition to methyl acetylene-d_4, small amounts of allene-d_4 were generated. The yield of allene-d_4 could be increased by raising the reaction temperature.[6]

3. A catalyst of activated cocoanut charcoal containing 0.5% palladium was used for the reduction of methyl acetylene-d_4 to propylene-d_6. The catalyst was placed in an eight-foot Pyrex tube (12 mm i.d.) wound with a heating element and was outgassed at high vacuum and 400°C for five days. Deuterium gas was then admitted at room temperature and atmospheric pressure, and the catalyst again baked out under vacuum. This precaution was necessary to minimize the effect of any hydrogen-containing substances initially present on the catalyst. A mixture of methyl acetylene-d_4 and deuterium, the latter in slight excess, was passed very slowly over the catalyst at 150°C. The infrared spectrum of the product[7] showed that the conversion to propylene-d_6 was complete.

4. Allyl chloride-d_5 was prepared by high-temperature chlorination[8] of propylene-d_6. The latter was mixed at 550°C with chlorine (from a cylinder) in a Vycor oven which provided for pre-heating of the reactants. The ratio of propylene-d_6 to chlorine was followed by means of flow meters, the rate of flow being controlled by pressure regulation at the condensing trap on the output side. Space velocity of the gases was critically important. If the gases passed too slowly through the oven, excessive pyrolysis occurred, and if too rapidly, the reaction occurred partly outside the oven, with the production of undesired products such as 1,2 dichloropropane. Optimum total pressure for the reaction with propylene-d_6 was about 50 mm. The allyl chloride-d_5 was purified by a trap-to-trap distillation to remove DCl, followed by distillation through an efficient column of low hold-up to separate the organic chlorides.

5. The addition of DBr to allyl chloride-d_5 to form 3-bromo-1-chloropropane-d_6 was carried out in a thick-walled Pyrex tube of 15-ml capacity and capable of withstanding pressures in excess of 30 atmospheres. The tube was fitted with a standard-taper stopper sealed in with a high-melting wax. Anhydrous DBr, prepared by suitable modification of the method of Ruhoff *et al.*[9] was distilled into the tube to 30% excess, after which benzoyl peroxide and oxygen were admitted.[10] After the tube was sealed, it was slowly allowed to warm to room temperature and to stand for 15 hours. It was then chilled to liquid nitrogen temperature and opened. The 3-bromo-1-chloropropane-d_6 (80% yield) was fractionated with great care to obtain a clean-cut separation from any 2-bromo-1-chloropropane-d_6 formed, since the latter would cause contamination of the cyclopropane-d_6 with propylene-d_6.

6. The conversion of 3-bromo-1-cyclopropane-d_6 to cyclopropane-d_6 was effected by the procedure of Ort.[11] The 3-bromo-1-chloropropane-d_6 (24.5 g) was added dropwise to a mixture of 59 ml absolute alcohol, 8.7 ml of water, 1.2 ml of 5% aqueous $FeCl_3$, 20 g of zinc dust, 5.5 g MgO and 2.7 g KBr. The mixture was refluxed at 85°C until evolution of gas ceased (10 to 15 hours), After separating water and alcohol from the condensed product. 7 ml of pure liquid cyclopropane-d_6 were obtained. The infrared spectrum of the product gave no evidence of impurities such as propylene-d_6[7] and the spectroscopically estimated isotopic purity was in excess of 99 atom-percent deuterium.

Prior to the synthesis described above, other routes to cyclopropane-d_6 were investigated. Although they were not successful, they are listed here for completeness.

TABLE I. Infrared bands of cyclopropane.

Wave number (cm^{-1}) and intensity Vapor	Liquid	Assignment	Wave number (cm^{-1}) and intensity Vapor	Liquid	Assignment
720 Q vw		$\nu_9-\nu_{14}$?	2070.4 P		
740 R vw			2095.7 Q m	2083 s	$\nu_4+\nu_5$
	745 vw	ν_{14}	2112.0 R		$2\nu_{13}$
836.7 P			2160 P		
854 Q' vvs		ν_7	2188.8 Q w	2172 m	$\nu_9+\nu_{14}$
868.5 Q vvs	866 vs	ν_{11}	? R		
898.0 R			Region of poorly defined band minima	2211 w	$\nu_3+\nu_{10}$
1007.5 P				2303 w	$\nu_9+\nu_{11}$
1028.7 Q vs	1024 vs	ν_{10}		2458 w	$\nu_9+\nu_{10}$
1051.6 R				2500 w	$\nu_2+\nu_{10}$
	1188 w	ν_3	2621 vw	2621 w	$\nu_3+\nu_9$
1422.0 P			2640 vw		?
1441.8 Q m	1434 vs	ν_9	2850 P		
1455.7 R			2873 Q w	2863 m	$2\nu_9$
1480 sh vw		$2\nu_{14}$	$-$ R		
1505 sh vw	1510 vw	?		2881 w	$\nu_2+\nu_9$
1739.9 w	1727 m	$2\nu_{11}$	2937 vw	2933 ms	$2\nu_{14}+\nu_9$
	1765 m	$\nu_{10}+\nu_{14}$	3009.4 P		
		$\nu_5+\nu_{11}$	3028.1 Q vs	3019 vs	ν_8
1779 w		$\nu_{13}+\nu_{14}$	3050.6 R		
1865 vw		$\nu_4+\nu_{14}$	~3075 P		
1894 ms	1887 s	$\nu_{10}+\nu_{11}$	3102.9 Q s	3090 vs	ν_6
1935.8 vw	1940 (sh)	$\nu_5+\nu_{10}$?	3129 R		
		$\nu_3+\nu_7$	3229 vw		Ternary
2044 vw	2048 m	$\nu_3+\nu_{11}$	3241 vw		overtones
		$2\nu_{10}$			

[6] R. C. Lord and J. Ocampo, J. Chem. Phys. **19**, 260 (1951); R. C. Lord and P. Venkateswarlu, J. Chem. Phys. **20**, 1237 (1952).
[7] Cf. R. C. Lord and P. Venkateswarlu, J. Opt. Soc. Am. **43**, 1079 (1953).
[8] H. P. A. Groll and G. Hearn, Ind. Eng. Chem. **31**, 1239, 1530 (1939).
[9] Ruhoff, Burnett, and Reid, Org. Syntheses **2**, 338 (1943).
[10] M. S. Kharasch and F. R. Mayo, J. Am. Chem. Soc. **55**, 2468 (1933).
[11] J. N. Ort, U. S. Patent 2,240,513.

TABLE II. Infrared bands of cyclopropane-d_6

Wave number (cm^{-1}) and intensity Vapor	Liquid	Assignment	Wave number (cm^{-1}) and intensity Vapor	Liquid	Assignment
614 w	(beyond range)	ν_7	— P 1670 Q vw 1692 R	1667 w	$\nu_3+\nu_{11}$ $2\nu_{13}$
694.4 P 720.1 Q vs 745.5 R	720 vs	ν_{11}			
	750 sh?	?	1765.4 ms	1760 s	$2\nu_{10}$
838 vvw	832 vw	ν_{13}?	1773.7 m	1783 w	$\nu_9+\nu_{11}$
864.7 P 886.9 Q ms 907.9 R	883 s	ν_{10}	1941.7 vw 1965 sh	1935 vw 1951 w	? $\nu_9+\nu_{10}$
				2028 w	$\nu_3+\nu_9$
	956 w	ν_3	2141.4 w	2132 m	$2\nu_9$
	1002 vvw	?	2194 P		
	1019 vvw	?	2211.4 Q vs 2231.3 R	2204 vs	ν_8
1055.3 P			2316 P		
1074.3 Q s 1090.0 R	1068 s	ν_9	2336 Q vs 2360 R	2330 vs	ν_6
1148 vw	1141 vw	$\nu_7+\nu_{14}$	2860 vw	2854 vw	$\nu_1+\nu_7$ $\nu_{12}+\nu_{14}$ $\nu_6+\nu_{14}$
1240 vw 1247 vw	1244 w	$\nu_{11}+\nu_{14}$			
	1279 vw	ν_2	2943 vw	2937 w	$\nu_7+\nu_{12}$
1329.6 vw	1330 vw	$\nu_4+\nu_{14}$	3039 P		
1404 vw	1402 vw	$\nu_{10}+\nu_{14}$	3059 Q w 3073 R	3050 w	C_3D_5H $\nu_{11}+\nu_{12}$
1435.6 w	1434 w	$2\nu_{11}$		3087 w	$\nu_8+\nu_{10}$
	1535? sh	?		3162	$\nu_3+\nu_8$ $\nu_{12}+\nu_{13}$
1571.4 P					
1586.5 Q ms 1602.3 R	1584 ms	$\nu_4+\nu_5$	3294 w	3291	$\nu_3+\nu_6$
			3379 P		
			3400 Q w 3420 R	3391 m	$\nu_9+\nu_{12}$
			3485 vw	3470 vw	$\nu_2+\nu_8$
			3614 vw	3614 vw	$\nu_2+\nu_6$

1. Exchange between D_2O and cyclopropane. No exchange could be effected using D_2O and a variety of catalysts such as platinum-on-asbestos, palladium-on-charcoal, nickel-on-kieselguhr, PtO_2, and slightly poisoned nickel-on-kieselguhr. The temperatures ranged from 25°C up to the decomposition temperature of cyclopropane (about 280°C for the conditions used). In some instances contact of D_2O and cyclopropane with the catalyst was maintained for 3 to 4 days.

2. Exchange between D_2 and cyclopropane. Under any conditions of catalysts and temperature that seemed likely to promote exchange, deuterium opened the ring to give propane-d_2. There was a slight indication of exchange when a very low D_2/cyclopropane ratio was used but complete deuteration was impractical by this method.

3. Synthesis from malonic ester. An attempt was made to reduce malonic ester-d_2 to 1,3-dihydroxy propane-d_8 with lithium aluminum deuteride. None of the desired compound could be obtained.

4. Synthesis from malononitrile. This procedure is a modification of No. 3. Malononitrile-d_2 is synthesized and then reduced to the completely deuterated diamine with lithium aluminum deuteride. Benzoyl chloride is added to the diamine to form dibenzoyl propylene diamine, and addition of phosphorus pentabromide will give 1,3-dibromopropane-d_6. It was found that malononitrile could not be reduced by lithium aluminum deuteride.

5. Synthesis from malononitrile. An electrolytic method is said to reduce malononitrile to the diamine in 50% yield.[12] Although this method would open the way for the application of the remaining steps of procedure No. 4, no work was attempted along these lines.

[12] Ohta, J. Chem. Soc. Japan **63**, 1762–5 (1942).

Infrared Spectra

The infrared absorption spectra were obtained over the spectral range 350 to 3700 cm^{-1} for the vapor and 650 to 3700 cm^{-1} for the liquid with a Perkin-Elmer 12B single-beam spectrometer modified as previously described.[13] Prisms of CaF_2, NaCl, and KBr were used in their respective regions of best resolution, which seldom was much worse than 3 cm^{-1} except in the 3000 cm^{-1} region. Two absorption cells for the vapor were respectively 6 cm and 4 m in path length, while the liquid was measured in the low-temperature cell of Lord, McDonald, and Miller.[13] The wave numbers (vac) of sharp bands are probably accurate to ± 2 cm^{-1} except above 2500 cm^{-1}, where the accuracy may change to as much as ± 5 cm^{-1}. Reproducibility is somewhat better than this, being 1 cm^{-1} or less below 2000 cm^{-1}.[13] The results of the infrared studies are given numerically in Tables I and II and graphically in Figs. 1 and 2. Qualitative intensities are denoted by symbols whose meanings are: s = strong, m = medium, w = weak, v = very, sh = shoulder. When two or three adjacent peaks are believed to be rotational maxima for the same vibration they are labeled P, Q, R.

It is believed that the infrared results for cyclopropane vapor are a considerable improvment in completeness, resolution and accuracy over those hitherto

[13] Lord, McDonald, and Miller, J. Opt. Soc. Am. **42**, 149 (1952).

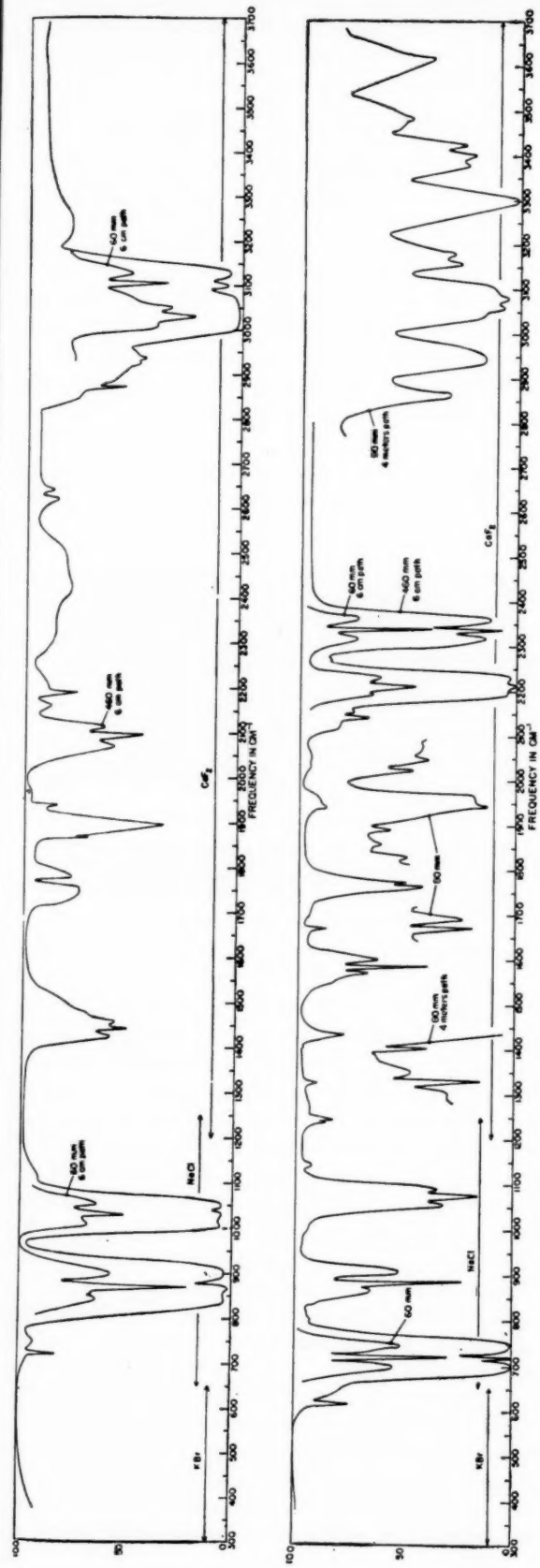

FIG. 1. Infrared absorption spectra of gaseous cyclopropane (top) and cyclopropane-d_6 (bottom).

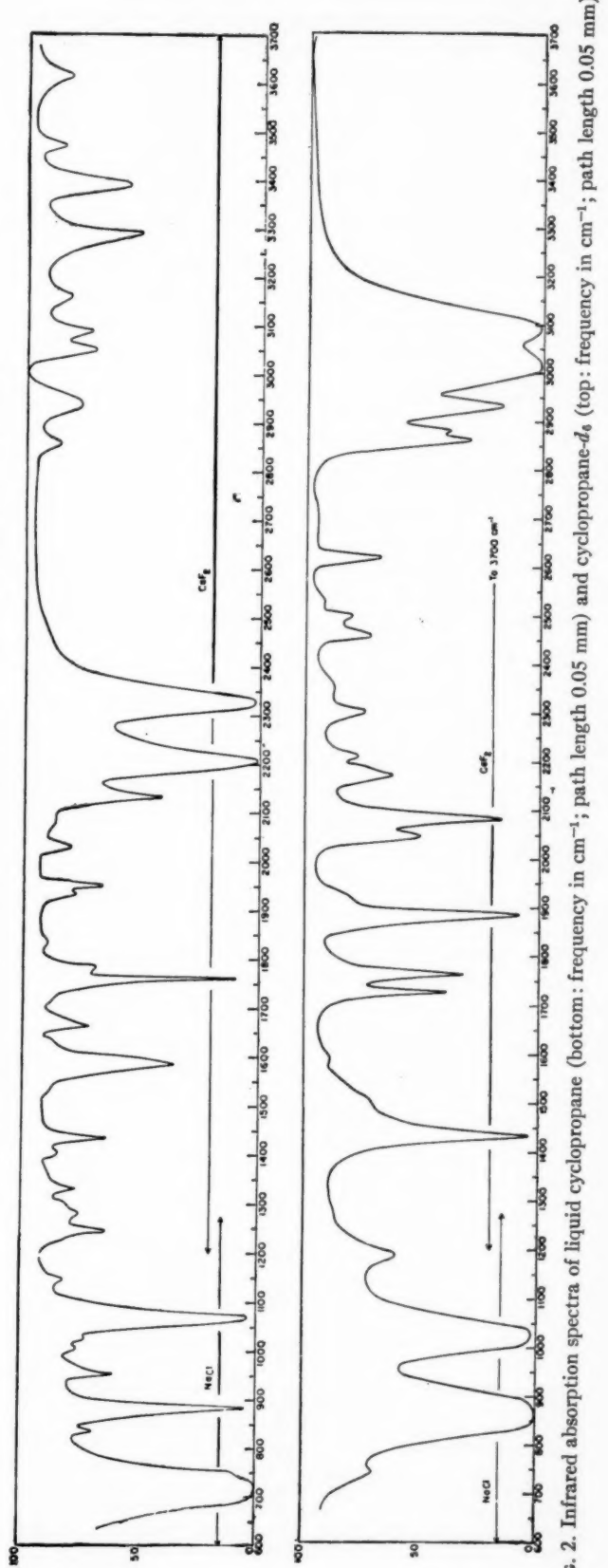

FIG. 2. Infrared absorption spectra of liquid cyclopropane (bottom: frequency in cm^{-1}; path length 0.05 mm) and cyclopropane-d_6 (top: frequency in cm^{-1}; path length 0.05 mm).

TABLE III. Raman spectrum of liquid cyclopropane.

Wave number (cm^{-1})	Int. and Pol.	Assignment	Wave number (cm^{-1})	Int. and Pol.	Assignment
741	(1) dep	ν_{14}	1504.2	(1) pol	$2\nu_{14}$
866	(8) dep	ν_{11}	2859	(2) pol	$2\nu_9$
1023	(0) ···	ν_{10}	2954	(6) pol	$2\nu_2$
1188.2	(9) pol	ν_3	3009	(10) pol	ν_1
1433.6	(5) dep	ν_9	3027	(9) pol	ν_3
1453.3	(3) pol	ν_2	3075	(9) dep	ν_{12}

published for the region up to 3500 cm^{-1}. This is due partly to the improved performance of the Model 12B spectrometer equipped with a CaF_2 prism, and partly due to the removal of absorption by atmospheric water and carbon dioxide.[14]

The infrared spectrum of liquid cyclopropane and the vapor and liquid spectra of cyclopropane-d_6 have not been reported previously.

Raman Spectra

The Raman spectra of liquid cyclopropane and cyclopropane-d_6 were obtained at about $-90°C$ with a Zeiss three-prism spectrograph. The techniques employed have been described in some detail by Lord and Nielsen.[15] Depolarization measurements were made only on cyclopropane-d_6. They were semiquantitative, but were adequate to distinguish polarized lines with $\rho<0.75$ from depolarized lines. Wave number accuracy is ± 2 cm^{-1} except for weak or fuzzy lines, for which it may be ± 5 cm^{-1}. Measured wave numbers (vac), visually estimated intensities on an arbitrary scale of 10, and state of polarization (for cyclopropane-d_6 only) are listed in Tables III and IV, and the spectra are shown photographically in Fig. 3.

The spectrum of cyclopropane agrees with the one summarized in Herzberg,[1] except that the lines at 382 and 1873 could not be found. The former is difficult to explain reasonably, and the latter, if real, must surely be an overtone, and hence is not likely to be of significance in the assignment of fundamentals. The remarkable intensity changes caused by deuterium substitution will be discussed later.

TABLE IV. Raman spectrum of liquid cyclopropane-d_6.

Wave number (cm^{-1})	Int. and Pol.	Assignment	Wave number (cm^{-1})	Int. and Pol.	Assignment
528	(1) dep	ν_{14}	1338	(0) ···	$\nu_7+\nu_{11}$
721	(4) dep	ν_{11}	1587	(0) ···	$\nu_9+\nu_{14}$
884	(6) dep	ν_{10}	2131	(3) pol	$2\nu_9$
956	(7) pol	ν_3	2204	(3) dep	ν_8
1068	(1) dep	ν_9	2236	(10) pol	ν_1
1229	(2) pol	$2\nu_7$	2329	(7) pol	ν_{12}
1274	(8) pol	ν_2			

[14] The authors have had the opportunity of seeing unpublished spectra of the strong bands of cyclopropane measured by Dr. L. G. Smith with a grating instrument. They have also had the privilege of examining the 1953 thesis of Dr. H. W. Neill, describing work carried out under the direction of Professor G. B. B. M. Sutherland at the University of Michigan. This thesis reports a very complete study of the infrared spectrum of cyclopropane vapor at both grating and prism resolution. The present results are in good agreement with the prism spectra of Neill and Sutherland.

[15] R. C. Lord and E. Nielsen, J. Opt. Soc. Am. **40**, 655 (1950); J. Chem. Phys. **19**, 1 (1951).

INTERPRETATION OF THE SEPCTRA

Discussion of the vibrational spectra of cyclopropane by all previous investigators, including Herzberg,[1] has been based on the D_{3h} structure. This basis will be used here, since it will be shown that there is a considerable amount of spectroscopic evidence in favor of it and none to the contrary. The distribution of the modes of vibration of cyclopropane among the various D_{3h} symmetry species and their spectroscopic activities are shown in Table V. The qualitative descriptions[16] of the modes of vibration are those in rather general use, but it is perhaps worthwhile to say that CH_2 deformation refers to the symmetrical scissors-like bending of the CH_2 bonds, CH_2 wagging to the "fanning" motion of the CH_2 group perpendicular to its own plane, CH_2 twisting to a torsion of the CH_2 group about the bisector of the HCH angle, and CH_2 rocking to the rotary motion of the CH_2 group as a unit about an axis perpendicular to its own plane. Since there are three CH_2 groups, the symmetry species of a given type of motion is determined not only by the nature of the motion of the individual groups but also by their mutual phase relationships.

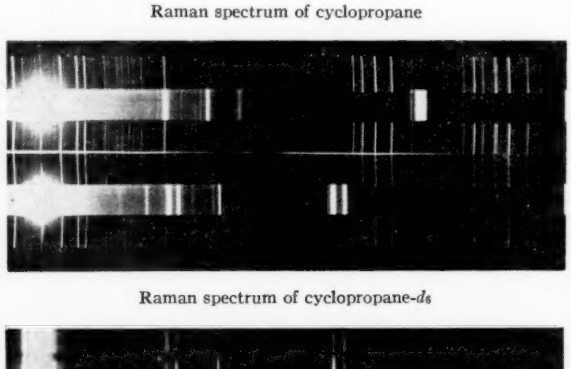

FIG. 3. Raman spectra of cyclopropane and cyclopropane-d_6.

From Table V the assignment of the observed infrared and Raman frequencies is straightforward in principle. Polarized Raman lines must belong to A_1', depolarized Raman lines not coincident with infrared bands should belong to E'', infrared bands not coincident with Raman lines to A_2'' (these bands should also have "parallel" structure, if this can be determined), and Raman lines coincident with infrared bands (of perpendicular structure) to E'. The two vibrations of species A_2' and A_1'' are inactive in both spectra. These characteristics are satisfactory for the assignment of

[16] See reference 1, Table 108, p. 351.

TABLE V. Symmetry species, selection rules, and frequency assignments (D_{3h} structure).

Species	Vib'n. no.	Approximate form of vibration	Selection rules		Assignment		Product rule	
			Raman	Infrared	C_3H_6	C_3D_6	τ_{obs}	τ_{calc}
A_1'	1	CH stretching	pol	f	3009	2236	1.94	2.000
	2	CH_2 deformation			1475[a]	1270[a]		
	3	Ring breathing			1188	956		
A_1''	4	CH_2 twisting	f	f	(1125)[b]	(800)	(1.40)	1.414
A_2'	5	CH_2 wagging	f	f	(975)	(790)	(1.23)	1.235
A_2''	6	CC stretching	f	Parallel	3102.9	2338	(1.85)	1.871
	7	CH_2 rocking	f	bands	(854)	614		
E'	8	CH stretching	depol	Perpen-	3028.1	2211.4	2.57	2.646
	9	CH_2 deformation		dicular	1441.8	1074.3		
	10	Ring deformation		bands	1028.7	886.9		
	11	CH_2 wagging			868.5	720.1		
E''	12	CH stretching	depol	f	3075	2329	(2.30)	2.351
	13	CH_2 twisting			(1050)	(835)		
	14	CH_2 rocking			741	528		

[a] Corrected approximately for Fermi resonance.
[b] Parentheses indicate estimated values.

all observed infrared bands and Raman lines, and the ease with which the assignment can be made is adequate confirmation of the D_{3h} structure.

Species A_1'

The totally symmetrical frequencies are easily located in both cyclopropane and cyclopropane-d_6, although the frequency changes observed in the latter are rather surprising. There are two weak polarized Raman lines at 1453 and 1504 cm^{-1} in cyclopropane. On the basis of the D_{3h} structure, they are best explained as a Fermi-resonance doublet resulting from interaction between a fundamental expected at about 1475 cm^{-1} and the first overtone of the Raman-active fundamental at 741 cm^{-1}. The intensity ratio of the two lines indicates that the lower component lies nearer to the "unperturbed" fundamental, which must be very close to 1475. The other two A_1' frequencies are readily placed at 1188 and 3009 cm^{-1}, though the exact position of the latter is undoubtedly influenced by Fermi resonance also, in view of the polarized companion of lesser intensity at 3027.

In cyclopropane-d_6 the frequencies and intensities of the A_1' lines change remarkably. No Raman lines occur between 1068 and 1229, whereas one might expect both the 1188 ring frequency and the 1475 CH_2 deformation frequency of cyclopropane to be displaced to this range. Instead the 1188 line shifts 24% to 956 and the 1475 frequency moves by 16% to 1274. The intensity change in the latter is even more remarkable, from a weak line (estimate 3) to the second strongest line (8) in the spectrum. However, the product rule for species A_1' is well satisfied with the expected small deviation (3%).

The explanation of these changes is straightforward. There is strong (first-order) coupling between the CD_2 deformation and the ring breathing vibrations in cyclopropane-d_6 because of the close proximity of their frequencies. This coupling causes a mixing of the two modes to such an extent that it is no longer accurate to describe one of them as the "CD_2 deformation vibration" and the other as the "ring breathing vibration." The mixing also results in a transfer of Raman intensity from the latter to the former and accounts for the increased intensity of the former. The phenomenon is observed in many deuterium compounds, an exactly analogous effect having been found, for instance, in the A_1 frequencies of allene and allene-d_4.[6] Other examples have been reported in the spectra of deuterated propanes by McMurry and Thornton,[17] who give the same explanation. Since the observed mixing is the direct result of coupling between deuterium deformation and heavy-atom vibrations when their frequencies are nearly equal, one concludes that such coupling should also exist under comparable circumstances between any hydrogen bending vibrations and skeletal vibrations. A contrary view has been put forward recently by I. Nakagawa.[18]

Species A_2''

The parallel rotational structure expected for infrared bands of this species enables the CH and CD stretching fundamentals to be located at 3102.9 and 2336 cm^{-1} respectively. The other frequency (CH_2 rocking) was placed by Smith[19] at 872 cm^{-1}, where it was said to be observed underlying the fine structure of the very strong perpendicular band at 868. Since there is considerable doubt about this, it is helpful that a weak infrared band, apparently of parallel structure, is observed at 614 cm^{-1} in cyclopropane-d_6. This band has no counterpart in the Raman effect, and hence should be assigned to A_2''. If the assignment is correct, the product rule indicates that Smith's estimate of 872 is somewhat high. A more compatible value is 854 cm^{-1}, at which point a weak maximum is observed between the P and Q branches of the 868 band (see Fig. 1). This maximum may be the sharp Q-branch of the A_2''

[17] H. L. McMurry and V. Thornton, J. Chem. Phys. **19**, 1014 (1951).
[18] I. Nakagawa, J. Chem. Soc. Japan **75**, 178 (1954); Chem. Abst. **48**, 4975b (1954).
[19] L. G. Smith, Phys. Rev. **59**, 924 (1941).

fundamental or perhaps part of the structure of the 866 band. In any event, if the cyclopropane-d_6 band is correctly assigned, the A_2'' band in the light compound must be very close to 854.

Species E'

This species is easily assigned because its fundamentals are both Raman and infrared active. All are observed in both spectra for both compounds. In Table V the vapor-phase infrared frequencies are used to calculate the product rule, but the liquid-phase Raman frequencies are all within 10 cm^{-1} (usually much less) of the vapor frequencies. The product rule is well satisfied. The assignment agrees with that of Herzberg[1] and various earlier investigators, but the additional evidence furnished by the spectrum of cyclopropane-d_6 is considerable. It enables a clear-cut rejection of the suggestion of Scott *et al.*,[20] based on normal-coordinate calculations for cyclopropane and spiropentane, that 868 be assigned to E'' and the Raman-active frequency at 741 be put in E' in its place. The analog of 741 in cyclopropane-d_6 is clearly the line at 528, which is also Raman-active and silent in the infrared. If these two frequencies be substituted for 868 and 720 respectively, the observed E' frequency-product ratio deviates from the theoretical product rule by 17% in a direction opposite to that expected from anharmonicity. To be sure, the infrared band at 614 can be paired with the 741 Raman line to preserve the product-rule value, but this would be objectionable on the ground that 741 is Raman-active but infrared-forbidden while 614 is just the reverse.

Finally it may be commented that species E', which contains both CH_2 deformation and wagging modes, as well as a ring vibration, also exhibits unusual frequency shifts. Here, however, the CH_2 deformation shows a "normal" shift (34%), while the ring and CH_2 wagging vibrations couple strongly and shift about 16% and 20% respectively. Moreover, it appears that considerable coupling prevails in both cyclopropane and cyclopropane-d_6.

Species E''

There are only hydrogen degrees of freedom in E'', which is Raman-active and infrared-forbidden. Depolarized Raman lines without counterparts in the infrared spectrum of the vapor are found at 3075 and 741 cm^{-1} in cyclopropane and at 2329 and 528 cm^{-1} in cyclopropane-d_6, and may be assigned to this species. The higher frequencies belong to CH and CD stretching modes and the lower to CH_2 and CD_2 rocking. The rocking assignment is different from that of Herzberg,[1] but is indicated by a considerable amount of evidence of various sorts. The A_2'' rocking frequency at 614 in cyclopropane-d_6 is not far removed from 528. In ethylene oxide, cyclobutene, and cyclobutane, and their deuterium derivatives,[21] the band types of certain infrared bands of comparable frequency (in the range 630–850 for the H-compound), indicate clearly their species, from which it may be concluded that the vibration in question is either a twisting or a rocking. In cyclobutane, however, for symmetry reasons, the band must be due to a rocking mode (A_{2u} of D_{4h}). This is true even though the symmetry of cyclobutane may actually be D_{2d}, for the selection rules obeyed by the infrared and Raman spectra are closely those of D_{4h}, and the band is quite strong in both light and heavy cyclobutane.

No twisting frequency is directly observed in cyclopropane, but by analogy with the corresponding observed twisting frequencies in ethylene oxide and cyclobutene, these should lie near 1100 in the light compound and 830 in the heavy. With the help of the product rule for the A_1'' and E'' species and the overtone band assignments (see below), the estimates given in Table V were made.

Species A_1'' and A_2'

Each of these contains one spectroscopically inactive frequency. The twising frequency (A_1'') was located from overtones 1125 and 800 cm^{-1} (see below) and the A_2' wagging at 975 and 790 cm^{-1} in cyclopropane and cyclopropane-d_6. While these values are uncertain, they are about what one expects and fit the product rules satisfactorily.

COMBINATION TONE ASSIGNMENTS

The high symmetry of cyclopropane imposes considerable restriction on the infrared activity of combination tones. The inactive fundamentals, however, may combine with others to give rise to allowed overtones and it might reasonably be expected that such overtones could be used to locate the inactive fundamentals. This turns out to be the case, but the evidence is not very extensive, and confirmation of these values from other sources (infrared spectra of single crystals, higher overtones, normal coordinate calculations) is needed.

There are about sixty allowed binary summation tones. In cyclopropane half of these lie above 3700 cm^{-1} and half below 3000 cm^{-1}, none being calculated for the intermediate region. The present investigation did not extend above 3700 cm^{-1}.[22] Below 3000 cm^{-1}, bands have been found at spectral locations where 21 of the 31 binary summation tones were expected. In cyclopropane-d_6 the corresponding bands lie below 2200 cm^{-1}, and 13 of the expected 30 are observed. Of these 13, 11 correspond to the same combinations observed

[20] Scott, Finke, Hubbard, McCullough, Gross, Williamson, Waddington, and Huffman, J. Am. Chem. Soc. **72**, 4664 (1950).

[21] R. C. Lord and B. Nolin, succeeding paper on ethylene oxide; D. G. Rea, thesis, MIT, 1954, for cyclobutene and cyclobutane.

[22] S. P. Sinha [J. Chem. Phys. **18**, 217 (1950)] investigated the region above 4100 cm^{-1} in a long-path cell, but came to no conclusions about the positions of the inactive fundamentals.

for cyclopropane. There are nine overtones found in cyclopropane-d_6 in the range 2700–3700 cm^{-1} and all of these can be explained readily as binary summation tones.

The values of inactive frequencies in cyclopropane and cyclopropane-d_6 obtained from the interpretation of combination tones are: ν_4, 1125 and 800, and ν_5, 975 and 790. However, the value for ν_5 in cyclopropane is based mainly on a band (2095.7, $\nu_4+\nu_5$) for which there is an alternate explanation ($2\nu_{13}$). In the event that the latter is correct, the value for ν_5 becomes very doubtful, but ν_{13} is evaluated as 1050 or thereabouts. A similar ambiguity about ν_{13} exists in cyclopropane-d_6.

Assignments of the overtone bands have been given in Tables I and II. Ternary combinations have not been considered (with one exception) because few will fall below 3000 cm^{-1} in cyclopropane and 2000 cm^{-1} in cyclopropane-d_6, and because they are expected to be less intense than the binary summation tones. Similarly binary difference tones have been omitted because the Boltzmann factors are expected to be small. The interpretation has not apparently suffered thereby with one exception.

The exception is the very weak and sharp band at 720 cm^{-1} in cyclopropane. This band, of which a broader companion at 740 cm^{-1} may be the *R*-branch, has not been reported previously. This is understandable, even if the band is genuine, because it coincides with a carbon dioxide band of moderate intensity. However, all trace of atmospheric carbon dioxide absorption was removed from our instrument by flushing with dry nitrogen, as was indicated by the complete absence of the powerful 667 cm^{-1} band, and contamination of the sample itself by carbon dioxide is ruled out by the same evidence.

The only infrared-active binary difference frequency near 720 cm^{-1} and with a reasonably large Boltzmann factor is $\nu_9-\nu_{14}$, for which the frequency calculated from the gas-phase value of ν_9 and liquid-phase value of ν_{14} is 701 cm^{-1}. The difference is well beyond experimental error. Unless it be assumed that the gas-phase value of ν_{14} is 15–20 cm^{-1} *smaller* than the liquid-phase value (there is some evidence to the contrary), that the value of ν_9 is in error, or that the very intense band at 866 cm^{-1} (ν_{11}) causes a displacement in the position of the *Q*-branch of the overtone, this explanation must be rejected. In view of the absence of any corresponding band in the spectrum of cyclopropane-d_6 which is in accord with the product rule, the band is left without definite assignment. Possibly it should be rejected as not belonging to cyclopropane.

Geometrical Configuration of Cyclopropane

It was hoped at the outset of this work that the rotational contour of a parallel band in cyclopropane-d_6 might be used in the evaluation of the double moment of inertia for that molecule with the help of the treatment of Gerhard and Dennison.[23] The expression for the double moment I_{xy} of cyclopropane is:

$$I_{xy}=m_C r^2_{CC}/2+m_H[(r_{CC}+\sqrt{3}r_{CH}\cos\phi)^2+6r_{CH}^2\sin^2\phi]$$

where m_C and m_H are the carbon and hydrogen masses, r_{CC} and r_{CH} the carbon-carbon and carbon-hydrogen internuclear distances, and 2ϕ, the HCH bond angle. Since the first term and the quantity in square brackets are the same for both cyclopropane and cyclopropane-d_6, measurements of I_{xy} for both molecules enables evaluation of the quantity in square brackets without detailed determination of r_{CC}, r_{CH}, and ϕ. Hence r_{CC} can be obtained directly once the two values of I_{xy} are known.

Unfortunately the $P-R$ separation in the only parallel band which could be accurately measured in the spectrum of cyclopropane-d_6 ($\Delta\nu_{P-R}=43.1$ cm^{-1} for the band at 2336 cm^{-1}) gives a highly implausible value for I_{xy} and hence for r_{CC}. The correct values of I_{xy} as determined from high-resolution studies[24] are 41.82 and 60.48, $\times10^{-40}$ g-cm^2, from which it follows that $r_{CC}=1.524$ A.

Thermodynamic Functions

The fundamental frequencies of Table V and the moments of inertia implied by the foregoing values of I_{xy} coupled with a reasonable assumption about r_{CH} are closely similar to those used by Ruhrwein and Powell[25] in the calculation of the entropy of cyclopropane vapor, as indicated by their *Note added in proof*. The difference in the entropy which would result from use of the present values would be about -0.05 eu at the boiling point, 240.3°K. Recalculation of the thermodynamic functions scarcely seems worthwhile.

ACKNOWLEDGMENTS

The authors wish to acknowledge financial assistance from the Office of Naval Research under Contract N5ori–07810. One of us (AWB) thanks E. I. duPont deNemours and Company for grant of a fellowship during 1949–1950. Dr. T. L. Cairns of the duPont Company proposed the use of Mg_2C_3 for preparation of methyl acetylene-d_4 and gave other helpful suggestions. Deuterium oxide was obtained on allocation from the U. S. Atomic Energy Commission, to whom we are grateful for cooperation.

We should also like to thank Professor G. B. B. M. Sutherland for opportunity to examine the thesis of H. W. Neill, and Dr. L. G. Smith for photostats of his unpublished high-resolution spectra.

[23] S. L. Gerhard and D. M. Dennison, Phys. Rev. **43**, 197 (1933).
[24] Günthard, Lord, and McCubbin (unpublished).
[25] R. A. Ruhrwein and T. M. Powell, J. Am. Chem. Soc. **68**, 1063 (1946).

Intermolecular Potentials of Argon, Krypton, and Xenon*

E. WHALLEY AND W. G. SCHNEIDER
National Research Council, Ottawa, Canada
(Received October 27, 1954)

The intermolecular potentials of argon, krypton, and xenon are investigated using the recently measured second virial coefficients and the crystal properties at 0°K. The potential functions considered are the 9:6, 12:6, and exp:6. The methods of determination of parameters are reviewed and the method of least squares used in this paper described. All the potentials fitted the second virial coefficient very well, but with the same parameters fitted the crystal properties only moderately well.

I. INTRODUCTION

ACCURATE information about the forces between molecules can be obtained from physical properties only if the theory of the physical property is sufficiently well known that comparison of experimental and theoretical values serve to test the force law rather than the theory. Such properties are few in number. They are (a) the second and third virial coefficients and related properties; (b) transport properties of the dilute gas; (c) crystal properties at 0°K.

The third virial coefficient measurements are not accurate enough for more than a rough comparison with theory. It is well known that the agreement is not very good[1,2] and little more information is obtainable with present measurements. They are therefore not discussed in this paper.

Measurements of the viscosity of the dilute gas are accurate and are available over a wide temperature range. The property is well suited to an investigation of intermolecular potentials; detailed discussions of the data have been given in previous papers.[3,4] Good fits were not obtained over a wide temperature range using any of the potentials considered below.

In this paper we discuss the second virial coefficient of the gas and the crystal properties at 0°K. This has been done recently for the gases we are considering by Corner[5] for argon and by Mason and Rice[6] for argon, krypton, and xenon. Recently experimental values of the second virial coefficients of these gases have been measured in this laboratory over a wider temperature range than hitherto available. We have consequently re-examined the intermolecular potentials using the new data.

All the potentials used in this study, and in fact all potentials which are at present seriously considered as applicable to more than one gas, are of the form

$$u=\epsilon f(r_0/r), \tag{1}$$

where u is the potential energy of two molecules separated by a distance r, ϵ is an energy which will usually be the depth of the potential energy minimum, and r_0 a length which will usually be either the value of r for which $u=0$ or the value of r for which u is a minimum; in the latter case it will be called r_m. The more important of the potentials which have been considered are

1. 12:6 potential: $f=4\{(r_0/r)^{12}-(r_0/r)^6\}$, (2)

2. 9:6 potential: $f=2(r_m/r)^9-3(r_m/r)^6$, (3)

3. exp:6 potential:

$$f=\frac{1}{1-6/\alpha}\left\{\frac{6}{\alpha}\exp\left(1-\frac{r}{r_m}\right)-\left(\frac{r_m}{r}\right)^6\right\}. \tag{4}$$

It is well known[1,2] that the second virial coefficient can be quite well fitted by any of these potentials. Therefore in order to obtain the maximum useful information from the data it is necessary to use a more critical method of fitting than employed in discussing the viscosity. Graphical comparison of reduced viscosity = reduced temperature curves were found to be adequate to show clearly the relative degrees of fit.

The object of this investigation was to determine whether any of the foregoing potentials is a significantly better fit to the experimental second virial coefficient than the others. The best fit to available data may give some information about the force law and would provide probably the best available method of extrapolating the measured virial coefficients to higher temperatures.

The procedure used in fitting the potentials differs from that used by Corner[5] and Mason and Rice.[6] These authors used the zero degree crystal properties to determine the potential parameters and calculated second virial coefficients and other properties from this. We have preferred to start with the virial coefficients and have used these to determine the potential parameters. The zero degree crystal properties were then calculated from the parameters obtained. The reasons for adopting this procedure are: (i) Crystal data depend

* Contribution No. 3720 from the Divisions of Applied and Pure Chemistry, National Research Council, Ottawa, Canada.

[1] Hirschfelder, Curtiss, and Bird, *Molecular Theory of Gases and Liquids* (John Wiley and Sons, Inc., New York, 1954).

[2] E. A. Guggenheim, Australian Revs. Pure Appl. Chem. **3**, 1 (1953).

[3] E. Whalley, Can. J. Chem. **32**, 485 (1954).

[4] E. Whalley and W. G. Schneider, J. Chem. Phys. **20**, 657 (1952).

[5] J. Corner, Trans. Faraday Soc. **35**, 711 (1939); **44**, 914 (1948).

[6] E. A. Mason and W. E. Rice, J. Chem. Phys. **22**, 843 (1954).

only on that part of the potential from near the minimum of the potential energy curve to large values of r, whereas the virial coefficients also reflect the potential energy curve at much smaller values of r. (ii) Virial coefficient data have now been extended to cover a wide temperature range. (iii) The theory of the crystal properties involves the principle of superposition of potentials, an assumption which may not be strictly valid.[7]

II. DETERMINATION OF PARAMETERS

1. The Virial Coefficients and Transport Properties

An excellent review of the theory of the compressibility and the transport properties of dilute gases is given by Hirschfelder, Curtiss, and Bird.[1] For potentials of type (1) the second and third virial coefficients and the coefficients of viscosity, thermal conductivity, and concentration diffusion, are given by equations of the kind

$$\xi=\rho\varphi(\tau),$$

where ξ is the coefficient concerned perhaps multiplied by some power of the temperature, ρ is dependent on r_0 or r_m, the mass of the molecules etc., but not on ϵ or the temperature T, and $\varphi(\tau)$ is a function of $\tau=kT/\epsilon$ only and not of r_0 or r_m. Values of ξ, ρ, and φ are given in reference 1. In principal only two values of ξ are necessary to determine ϵ and r_0 or r_m. In practice one usually has more than two values of ξ available, usually over a fairly wide temperature range and the problem arises of finding the parameters which give the best fit over a part or the whole of the temperature range. Several methods are available and are discussed below.

(a) *Lennard-Jones Method*[8]

Log ξ *vs* log T is plotted on transparent paper and superposed on a plot of $\log\varphi(\tau)$ *vs* $\log\tau$ on the same scale by shifting parallel to both axes. The shift along the $\log\varphi(\tau)$ axis gives $\log\rho$ and that along the $\log\tau$ axis gives $\log\epsilon/k$. This method is rather rapid and permits quick comparison of several potentials if they are plotted on the same graph. It is, however, not sufficiently sensitive for a detailed comparison of several potentials which agree approximately with the data.

(b) *Buckingham Method*[9]

The quantities

$$\log X=\log\xi-\log\varphi,$$
$$\log Y=\log T-\log\tau,$$

are calculated at each temperature for several values of τ around that expected. The intersection of two curves for two values of ξ gives values of ϵ/k and ρ

$$\log X=\log\rho,$$
$$\log Y=\log\epsilon/k,$$

which satisfy the two values of ξ. The mean of all the intersections will give a "best" value of ρ and ϵ/k. However, when this method was tried for the second virial coefficients for the gases and potentials considered here it was possible readily to adjust the "best" values so obtained to reduce the deviations of the experimental from the calculated values of the second virial coefficient. It was concluded that a "best" fit in no accepted sense is given by this method and it has no advantage over method (*a*). A modification of the Buckingham method which is sometimes used involves adjusting ϵ/k until the ratio of two experimental values of ξ at two temperatures is equal to the ratio of the corresponding φ values.

(c) *Least Squares Method*

As pointed out above the Lennard-Jones method is adequate for a quick comparison of various potentials; if two or more potentials agree quite well with the experimental data a more critical comparison is necessary. For this the method of least mean squares was chosen. The method of fitting is that described by Deming.[10]

Approximate values of ρ and ϵ/k, say ρ_0 and $(\epsilon/k)_0$, are chosen, usually by method (*a*) above. Then if

$$\epsilon/k=(\epsilon/k)_0-K,$$
$$\rho=\rho_0-L,$$

the normal equations for computing the small correction terms K and L are, written with detached coefficients,

$$\begin{array}{ccc} K & L & = \quad 1 \\ \sum F_{\epsilon/k}^2 & \sum F_{\epsilon/k}F_\rho & \sum F_{\epsilon/k}F_0 \\ & \sum F_\rho^2 & \sum F_\rho F_0, \end{array}$$

where

$$F_0=\xi-\rho\varphi(kT/\epsilon),$$

$$F_{\epsilon/k}=-\frac{\rho}{\epsilon/k}\tau\frac{\partial\varphi}{\partial\tau},$$

$$F_\rho=\varphi(kT/\epsilon).$$

F_0, $F_{\epsilon/k}$, and F_ρ, are to be calculated using the approximate values of ϵ/k and ρ. The standard deviation from the measurements and the standard error of the parameters are readily obtained. If the approximate values of ϵ/k and ρ were more than a few percent different from the final values the fitting was done using the better approximations.

[7] B. M. Axilrod and E. Teller, J. Chem. Phys. **11**, 299 (1943); **19**, 719, 724 (1951).

[8] J. E. Lennard-Jones, Proc. Roy. Soc. (London) **A106**, 463 (1924).

[9] R. A. Buckingham, Proc. Roy. Soc. (London) **A168**, 264 (1938).

[10] W. E. Deming, *Statistical Adjustment of Data* (John Wiley and Sons, Inc., New York, 1943).

TABLE I. Potential parameters and crystal data for argon from second virial coefficients.

	ϵ/k°K	b_0 ml mole^{-1}	r_m angstroms	σ ml mole^{-1}	a_0 angstroms	$\Delta H_v(0)$ cal mole^{-1}
9:6	89.64±0.24	85.77±0.56	4.082±0.009	0.39	3.929±0.009	1718±5
12:6	119.49±0.33	49.92±0.35	3.826±0.007	0.42	3.764±0.007	2033±6
exp:6, $\alpha=15$	131.49±0.45	68.37±0.61	3.784±0.010	0.53	3.742±0.010	2128±7
Exptl.					3.81 ±0.02	1998±40

2. Crystal Data

The heats of sublimation and the lattice spacing at 0°K are simply related to the intermolecular potential. The heat of sublimation is dependent mainly on that part of the potential from the minimum outwards to larger values of r. The equations for the lattice spacing, including the effect of the zero point energy have been given by Corner[5] for an n:6 and exp:6 potential and for the potentials here considered reduce to

$$9{:}6 \quad C_9\left(\frac{r_m}{a_0}\right)^3+\left\{\frac{h^2}{3\pi^2 m\epsilon r_m^2}\right\}^{\frac{1}{2}}\frac{11C_{11}(r_m/a_0)^3-5C_8}{\{4C_{11}(r_m/a_0)^7-(5/2)C_8(r_m/a_0)^4\}^{\frac{1}{2}}}=C_6, \tag{5}$$

$$12{:}6 \quad 2C_{12}\left(\frac{r_0}{a_0}\right)^6+\left\{\frac{h^2}{8\pi^2 m\epsilon r_0^2}\right\}^{\frac{1}{2}}\frac{77C_{14}(r_0/a_0)^6-10C_8}{\{22C_{14}(r_0/a_0)^{10}-5C_8(r_0/a_0)^4\}^{\frac{1}{2}}}=C_6, \tag{6}$$

$$\text{exp:}6 \quad 12(\theta'-0)\exp\alpha\left(1-\frac{a_0}{r_m}\right)+C_6\left(\frac{r_m}{a_0}\right)^7 + \left\{\frac{h^2(1-6/\alpha)}{2\pi^2 m r_m^2\epsilon}\right\}^{\frac{1}{2}}\frac{\left\{3[-\alpha^2+2\alpha r_m/a_0+2(r_m/a_0)^2]\exp\alpha\left(1-\frac{a_0}{r_m}\right)+10C_8\left(\frac{r_m}{a_0}\right)^9\right\}}{\left\{12\left(\alpha-2\frac{r_m}{a_0}\right)\exp\alpha\left(1-\frac{a_0}{r_m}\right)-5C_8\left(\frac{r_m}{a_0}\right)^8\right\}^{\frac{1}{2}}}=0, \tag{7}$$

where C_6, C_8, C_9, C_{11}, C_{12}, and C_{14} are numerical constants calculated by Lennard-Jones and Ingham,[11] involved in summing inverse power interactions over an infinite crystal lattice; θ is a function of $\alpha a_0/r_m$ tabulated by Corner similarly concerned in summing an exponential interaction and θ' is $\partial\theta/\partial(\alpha a_0/r_m)$. Equations (5), (6), and (7) are readily solved for a_0 either graphically or by successive approximations.

TABLE II. Comparison of experimental and calculated second virial coefficients of argon.

T°K	B_v(expt.) ml mole^{-1}	B_v(expt.) $-B_v$(calc) 9:6	12:6	Exp 6, $\alpha=15$
173.16	−63.82	+0.12	+0.40	+0.74
223.16	−36.79	+0.52	+0.36	+0.32
273.16	−22.10	−0.61	−0.73	−0.84
298.16	−16.06	−0.24	−0.33	−0.48
323.16	−11.17	−0.02	−0.09	−0.24
348.16	− 7.37	−0.17	−0.20	−0.32
373.16	− 4.14	−0.24	−0.27	−0.38
398.16	− 0.96	+0.07	+0.09	−0.01
423.16	+ 1.46	+0.04	+0.06	−0.02
447.16	3.72	+0.25	+0.26	+0.18
473.16	4.99	−0.48	−0.44	−0.48
573.16	10.77	−0.41	−0.33	−0.30
673.16	15.74	+0.82	+0.88	+1.05
773.16	17.76	+0.21	+0.27	+0.49
873.16	19.48	+0.05	+0.07	+0.35
Standard deviation, σ(ml mole^{-1})		0.39	0.42	0.53

The heats of sublimation including the zero point energy $\Delta H_v(0)$ are calculated from the equations

$$9{:}6 \quad \Delta H_v(0)=\frac{N\epsilon}{2}\left\{2C_9\left(\frac{r_m}{a_0}\right)^9-3C_6\left(\frac{r_m}{a_0}\right)^6\right\}, \tag{8}$$

$$12{:}6 \quad \Delta H_v(0)=2N\epsilon\left\{C_{12}\left(\frac{r_0}{a_0}\right)^{12}-C_6\left(\frac{r_0}{a_0}\right)^6\right\}, \tag{9}$$

$$\text{exp:}6 \quad \Delta H_v(0)=\frac{N\epsilon}{2(1-6/\alpha)} \times\left\{\frac{72\theta}{\alpha}\exp\alpha(1-a_0/r_m)-C_6\left(\frac{r_m}{a_0}\right)^6\right\}. \tag{10}$$

The standard errors were calculated by the usual methods of statistics.

The kind of packing in the crystal should be determined by the intermolecular force law. Recently T.

[11] J. E. Lennard-Jones and A. E. Ingham, Proc. Roy. Soc. (London) **A107**, 636 (1925).

TABLE III. Parameters and crystal data for krypton from second virial coefficients.

Potential	ϵ/k°K	b_0 ml mole^{-1}	r_m angstroms	σ ml mole^{-1}	a_0 angstroms	$\Delta H_v(0)$ cal mole^{-1}
9:6	125.07±0.33	107.76±0.75	3.943±0.009	0.35	3.776±0.009	2400±6
12:6	166.67±0.47	62.92±0.44	4.130±0.009	0.36	4.041±0.009	2848±8
exp:6 $\alpha=12$	144.87±0.56	103.65±1.08	4.348±0.006	0.46	4.214±0.006	2536±10
$\alpha=15$	183.64±0.56	86.01±0.70	3.962±0.011	0.42	3.904±0.011	2574±8
Exptl.					3.93 ±0.03	2733

Kihara and S. Koba[12] have investigated the relative energies of hexagonal and cubic close packing and find that for the 12:6 and exp:6 potentials the hexagonal close packed structure is more stable by about 0.01%. Apart from helium the inert gases all crystallize in cubic close packing. They conclude from this that the energy well must be wider than given by the 12:6 potential to explain the stability of the cubic structure. The difference is so small, however, that little weight should be placed on this conclusion.

(c) *Procedure in Fitting Potentials*

The procedure followed in fitting the potentials was in all cases the same.

The fit of the various potentials to the second virial data was examined by least mean squares and the parameters obtained were used to calculate the lattice spacing and the heat of sublimation at 0°K. These were compared with experimental values. The experimental values were recalculated from all the available experimental data and are given in the appendix.

III. RESULTS

1. Argon

The data for the virial coefficients were taken from a previous paper.[13] They were converted to values of B_v in ml mole^{-1} by the relation

$$B_v = V_N B_p,$$

where V_N is the volume occupied by one mole of gas at NTP. The B_v values were fitted to 9:6, 12:6, and exp:6 potentials by the method of least mean squares. The "best" parameters are given in Table I together with their standard error and the standard deviation of the calculated from the experimental virial coefficients. For the exp:6 potential graphical comparison by method (a) above showed that only $\alpha=15$ agreed with all the points moderately well and only this potential was used. In Table II the experimental and calculated values of B_v are compared. The calculated values of the heat of sublimation at 0°K and the lattice spacings are given in Table I and compared with the experimental values. The calculation of the experimental value of $\Delta H_v(0)$ is given in the appendix. The experimental value of a_0 is extrapolated from the value at 40°K of 3.83±0.02 A[14] and at 20°K of 3.82 A.[15]

The integrals $\varphi(\tau)$ for the viscosity are calculated only for the 12:6 and exp:6 potentials. The 12:6 potential is a better fit to the experimental viscosity data over a wide temperature range but a close fit is not obtained[3,4] and above about 850°K no real solution for ϵ/k and r_0 for argon is possible from the viscosity data.[14,16]

2. Krypton

The second virial coefficient data were obtained from a recent paper[17] and were treated in the same way as argon. The exp:6 potentials with $\alpha=12$, 13, 14, and 15, appeared equally good by graphical comparison and least squares were used for each potential. The parameters and crystal data are given in Table III and the virial coefficient and their deviations in Table IV. The lattice spacing has been measured by Nasini and Natta[18] as 4.09 A at 77°K, by Keesom and Mooy[19] as 3.95 at 20°K and by Ruhemann and Simon[20] as 4.03 at 88°K. The best value of a_0 is probably 3.93±0.03 A. The calculation of the experimental value of $\Delta H_v(0)$ is given in the appendix.

TABLE IV. Comparison of experimental and calculated second virial coefficients of krypton.

		B_v(expt.) − B_v(calc)					
				Exp:6			
T°K	B_v ml mole^{-1}	9:6	12:6	$\alpha=12$	$\alpha=13$	$\alpha=14$	$\alpha=15$
273.16	−62.70	+0.03	+0.20	−0.05	+0.33	+0.35	+0.43
323.16	−42.78	+0.02	−0.05	−0.27	−0.03	−0.06	−0.11
373.16	−29.28	−0.45	−0.54	−0.77	−0.59	−0.58	−0.61
423.16	−18.13	+0.46	+0.37	+0.14	+0.26	+0.27	+0.25
473.16	−10.75	0.00	−0.05	−0.24	−0.19	−0.14	−0.16
573.16	+ 0.42	0.10	+0.11	−0.02	−0.01	+0.05	+0.07
673.16	+ 7.24	−0.45	−0.42	−0.45	−0.50	−0.43	−0.40
773.16	+12.70	−0.22	−0.17	+0.20	−0.18	−0.16	−0.09
873.16	+17.19	+0.42	+0.48	+0.70	+0.83	+0.67	+0.61
Standard deviation σ, ml mole^{-1}		0.35	0.36	0.46	0.47	0.41	0.42

[12] T. Kihara and S. Koba, J. Phys. Soc. Japan **7**, 348 (1952); Revs. Modern Phys. **25**, 831 (1953).
[13] Whalley, Lupien, and Schneider, Can. J. Chem. **31**, 722 (1953).
[14] J. de Smedt and W. H. Keesom, Comm. Phys. Lab. Univ. Leiden, 178*b*; Physica **5**, 344 (1925).
[15] F. Simon and C. V. Simson, Z. Physik **25**, 160 (1924).
[16] E. Whalley, in discussion. Trans. Am. Soc. Mining Met. Engrs. **76**, 983 (1954).
[17] E. Whalley and W. G. Schneider. Trans. Am. Soc. Mining Met. Engrs. **76**, 1001 (1954).
[18] A. G. Nasini and G. Natta, Rend. Accad. Lincei **12**, 141 (1930); Nature **125**, 889 (1930).
[19] W. H. Keesom and H. H. Mooy, Nature **125**, 889 (1930); Proc. Acad. Sci. Amsterdam **33**, 447 (1930).
[20] B. Ruhemann and F. Simon, Z. Physik. Chem. **B15**, 389 (1932).

TABLE V. Parameters and crystal data for xenon from second virial coefficients.

Potential	ϵ/k°K	b_0 ml mole^{-1}	r_m angstroms	σ ml mole^{-1}	a_0 angstroms	$\Delta H_v(0)$ cal mole^{-1}
9:6	168.4±1.2	147.8 ±2.2	4.894±0.024	1.20	4.681±0.024	3236±23
12:6	225.3±1.1	84.96±0.84	4.568±0.013	0.82	4.454±0.013	3850±10
exp:6 $\alpha=12$	196.1±1.1	140.3 ±1.6	4.795±0.018	0.88	4.636±0.018	3397±18
$\alpha=14$	233.3±1.0	121.1 ±1.0	4.579±0.013	0.70	4.476±0.013	3861±16
$\alpha=15$	248.9±1.0	114.7 ±1.0	4.497±0.013	0.62	4.410±0.013	4043±16
Exptl.					4.33	3936

3. Xenon

The second virial coefficient data were obtained from a recent paper.[21] The parameters and the crystal data are given in Table V and the second virial coefficients and their deviations in Table VI. The lattice spacing has been measured by Natta and Nasini[22] as 4.37±0.02 A at 77°K and by Ruhemann and Simon[20] as 4.41 A at 88°K. The best value of a_0 will be about 4.30±0.04. More accurate crystal data on argon, krypton, and xenon would be very useful. The calculation of the experimental value of $\Delta H_v(0)$ is given in the appendix.

IV. DISCUSSION

From an examination of Tables I–VI the following facts are evident.

1. The standard deviation of the experimental from the calculated values of the second virial coefficient using the various potentials is always less than three times, and mostly less than twice the standard error of the experimental data. Thus all the potentials tried fit quite well and none of the potentials is a very much better fit than the rest.

2. The several potentials obtained from the same measurements can be very different; for example, for argon there is a spread of 42° in ϵ/k, for krypton 58°, and for xenon 81°. This is rather surprising in view of the close similarities in the curves of f of Eq. (1). This is readily seen in Fig. 1 where $f=u/\epsilon$ is plotted against r/r_0 for the 9:6 and exp:6, $\alpha=15$ potentials. The 12:6 and other exp:6 potentials fall between these two lines.

3. In spite of the large variation in ϵ/k the calculated values of $\Delta H_v(0)$ are not very dissimilar. The crystal properties are moderately well predicted using any of the potentials obtained from second virial data and one can usually be chosen which will fit either a_0 or $\Delta H_v(0)$ very well, but not both together; the potentials are too simple to fit all three properties exactly.

It has been shown previously[3,4] that good fits to the viscosity data were not obtained by any potential which is a reasonable approximation to the true potential. The comparison of viscosity data, therefore, is a more critical evaluation of potential curves than the second virial coefficient.

One concludes from all this that a potential whihc best fits even several gas properties is not necessarily closely related to the true potential. The depth of the actual potential minimum could differ by more than 20% from the values derived in this paper. However,

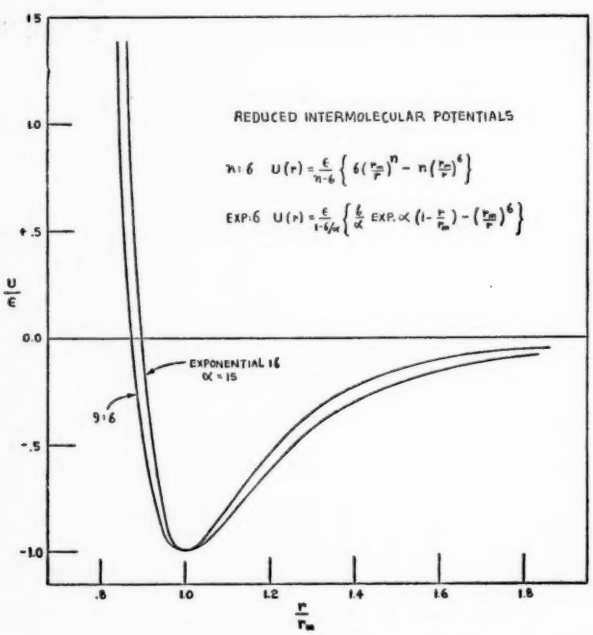

FIG. 1.

TABLE VI. Comparison of experimental and calculated second virial coefficients of xenon.

		B_v(expt.) − B_v(calc)				
				exp:6		
T°K	B_v ml mole^{-1}	9:6	12:6	$\alpha=12$	$\alpha=14$	$\alpha=15$
273.16	−154.74	−2.77	−1.79	−1.84	−1.39	−1.01
298.16	−130.21	−0.26	−0.18	+0.03	0.00	+0.01
323.16	−110.62	+0.99	+0.78	+0.90	+0.78	+0.78
348.16	− 95.04	+1.42	+1.04	+1.15	+0.82	+0.67
373.16	− 82.13	+1.25	+0.94	+0.94	+0.67	+0.56
423.16	− 62.10	+0.80	+0.31	−0.37	+0.06	−0.12
473.16	− 46.74	+0.46	+0.03	0.00	−0.20	−0.36
573.16	− 25.06	−0.15	−0.28	−0.39	−0.42	−0.47
673.16	− 10.77	−0.72	−0.65	−0.77	−0.71	−0.69
773.16	− 0.13	−0.68	−0.41	−0.51	−0.34	−0.29
873.16	+ 7.95	−0.45	−0.05	−0.08	+0.13	+0.21
973.16	+ 14.22	−0.16	+0.31	+0.36	+0.59	+0.69
Standard deviation σ ml mole^{-1}		1.20	0.82	0.88	0.70	0.62

[21] Whalley, Lupien, and Schneider, Can. J. Chem. **33**, 633 (1955).

[22] G. Natta and A. G. Nasini, Rend. Accad. Lincei **11**, 1009 (1930); Nature **125**, 457 (1930).

potentials derived using the same model for several gases will be approximately relatively correct.

For extrapolating experimental second virial coefficients to high and low temperatures either the 12:6 or the exp:6 potential appears to be equally good. One would perhaps prefer the 12:6 because it is rather simpler to use. Some caution in extrapolation is, however, necessary, particularly when the potential parameters have been derived from experimental data extending only over a very limited temperature range.

ACKNOWLEDGMENTS

We wish to thank Mr. G. David and Mr. G. Kell for help with the computations.

APPENDIX. HEATS OF SUBLIMATION AT 0°K

The heat of sublimation at 0°K $\Delta H_v(0)$ can be calculated from the equation

$$\Delta H_v(0)=\Delta H_v(T)+\int_0^T C_p dT-\int_0^T C_p^0(g)dT+\Delta H_{JT}, \tag{11}$$

where $\Delta H_v(T)$ is the heat of sublimation at temperature T, C_p is the heat capacity at constant pressure of the solid or liquid, $C_p^0(g)$ is the heat capacity of the ideal gas and ΔH_{JT} is the isothermal heat of expansion of the gas (Joule-Thomson effect) from the vapor pressure at temperature T to zero pressure. The change in heat content on expansion is small and can be calculated from the equation of state. This we write in the form

$$PV=RT+BP.$$

Then

$$\Delta H_{JT}=H(P,T)-H(O,T)=\left(B-\frac{TdB}{dT}\right)P. \tag{12}$$

It has been shown[23] that the value of B for vapors is calculated with fair accuracy from the equation

$$B=\frac{9}{128}\frac{RT_c}{P_c}\left(1-6\frac{T_c^2}{T^2}\right).$$

This formula agrees well with a 12:6 formula over the temperature range $T/T_c=0.25$ to 1.6[23] and is quite adequate for calculating the relatively small term ΔH_{JT}. Insertion of this into (12) gives

$$\Delta H_{JT}=\frac{9}{128}\frac{RT_c}{P_c}\left(1-18\frac{T_c^2}{T^2}\right)P. \tag{13}$$

Critical data for the gases were taken from the compilation of Kobe and Lynn.[24]

[23] Lambert, Roberts, Rowlinson, and Wilkinson. Proc. Roy. Soc. (London) **A196**, 113 (1949).

[24] K. A. Kobe and R. E. Lynn, Chem. Revs. **52**, 117 (1953).

1. Argon

Several measurements have been reported which can be used to derive $\Delta H_v(0)$ for argon. It is most convenient to choose the temperature T as the melting point. For $\Delta H_v(T)$ for solid argon the following direct values have been obtained:

Calorimetric, Eucken[25]	1739 cal mole^{-1}
Vapor pressure of solid argon, Crommelin[26] calculated by Nernst[27]	1819 cal mole^{-1}
Vapor pressure of solid argon, Born[28]	1830 cal mole^{-1}

$\Delta H_v(T)$ can also be obtained from the heat of vaporization of the liquid and the heat of melting. The following values for the heat of melting are given:

Eucken[27]	267.9 cal mole^{-1}
Eucken and Hanck[29]	265.2 cal mole^{-1}
Clusius[30]	280.8 cal mole^{-1}
Mean	271.3 cal mole^{-1}

Using the mean value and the heats of vaporization of the liquid obtained by various workers we find the following values for the heat of vaporization of solid argon at the melting point:

V.P. of liquid argon, Crommelin[26] calculated by Nernst[27]	1830 cal mole^{-1}
V.P. of liquid argon Born[28]	1842 cal mole^{-1}

The mean of all values of $\Delta H_v(T)$ for solid argon is 1823 ± 18 cal mole^{-1}.

The heat capacity of solid argon has been measured by Eucken[25] and by Clusius.[30] From Eucken's results Born[30] found $\int_0^{\text{m.p.}} C_p dT=406$ cal mole^{-1}. From Clusius' results by graphical interpolation we find $\int_0^{\text{m.p.}} C_p dT=395$ cal mole^{-1}. The data of Clusius are the more extensive so this value will be used. The heat of expansion ΔH_{JT} is from Eq. (13) 17 cal mole^{-1}. For the heat of sublimation at 0°K we obtain therefore $\Delta H_v(0)=1818$ cal mole^{-1}. As a rough estimate of the standard error 40 cal mole^{-1} seems reasonable. For calculations of $\Delta H_v(0)$ from the intermolecular potential we need to allow for the zero point energy. This is $9/8R\theta$ where θ is the Debye characteristic temperature. The Clusius value of θ gives 178 cal mole^{-1}, is probably the most accurate, and will be used. The heat of vaporization including the zero point energy is therefore 1998 ± 40 cal mole^{-1}.

[25] A. Eucken, Verh. deutsch. physik. Ges. **18**, 4 (1916).

[26] C. A. Crommelin, Comm. Univ. Leiden 138a and 140a.

[27] W. Nernst, Z. Electrochem. **22**, 185 (1916).

[28] F. Born, Ann. Physik **69**, 473 (1922).

[29] A. Eucken and F. Hanck, Z. Physik. Chem. **134**, 161 (1928).

[30] K. Clusius, Z. Physik. Chem. **31**, 459 (1936).

2. Krypton

The only data for obtaining the heat of vaporization are the density and vapor pressure measurements of Mathias, Crommelin, and Meihuizen.[31] The empirical equation proposed to represent the results is

$$\Delta H_v(T) = 0.01896T(209.39-T)^{\frac{1}{2}} + 0.3837T - 0.004346T^2 + 1.212\,10^{-5}T^3, \quad (14)$$

based on measurements down to 126°K. The specific heat measurements[30,32] extend only to 123°K so Eq. (13) was extrapolated to this value giving

$$\Delta H_v(123°) = 2052 \text{ cal mole}^{-1}.$$

The value of $\int_0^{123} C_p dT$ is[30,32] 1118 cal mole^{-1}. The heat of expansion to zero pressure from Eq. (13) at 123°K is 28 cal mole^{-1}, the $\int_0^{123} C_p^0(g)dT$ is 611 cal mole^{-1}, and the zero point energy, using Clusius value of the Debye θ is 140 cal mole^{-1}. The heat of vaporization at 0°K is therefore 2589 cal mole^{-1}, and adding the zero point energy this becomes 2729 cal mole^{-1}. A standard error of about 50 cal mole^{-1} is probably a reasonably good rough estimate.

3. Xenon

The heat of vaporization at the normal boiling point 165.1°K has been measured by Clusius and Riccoboni[33] as 3020±3 cal mole^{-1}. The $\int_0^{165.1} C_p dT$ is from the data of Clusius and Riccoboni[33] 1566 cal mole^{-1}. The heat of expansion at 165.1° from 760 mm to zero pressure is calculated from Eq. (13) as 38 cal mole^{-1}. The $\int_0^{165.1} C_p^0(g)dT$ is 801 cal mole^{-1}. The heat of sublimation at 0°K is therefore 3828 cal mole^{-1}. The zero point energy using the Clusius value of θ is 123 cal mole^{-1}, so the heat of sublimation at 0°K, including the zero point energy, is 3946 cal mole^{-1}.

[31] Mathias, Crommelin, and Meihuizen, Ann. Physik **8**, 467 (1937).
[32] Clusius, Kruis, and Konnertz, Ann. Physik **33**, 642 (1938).
[33] K. Clusius and L. Riccoboni, Z. Physik. Chem. **B38**, 81 (1937).

THE JOURNAL OF CHEMICAL PHYSICS VOLUME 23, NUMBER 9 SEPTEMBER, 1955

Magnetic Susceptibilities of Some Uranium (IV) Compounds*

CLYDE A. HUTCHISON, JR., AND CHARLES M. HERZFELD†
Institute for Nuclear Studies and Department of Chemistry, University of Chicago, Chicago, Illinois
(Received December 10, 1954)

The magnetic susceptibilities of $U(SO_4)_2 \cdot 4.22H_2O$, $U(C_2O_4)_2 \cdot 6H_2O$, $UF_4 \cdot NaF$, $(\gamma)UF_4 \cdot 2NaF$, and $UF_4 \cdot 3NaF$ have been measured in the temperature range from 14°K to 300°K. The results are presented in graphical form and their general form is discussed. The susceptibilities of all five compounds appear to approachfinite values at 0°K.

INTRODUCTION

In a previous paper from this laboratory Hutchison and Elliott[1] have reported measurements of the magnetic susceptibilities of some uranium (IV) compounds from 60°C down to the boiling point of liquid N_2. In the work described in the present paper the measurements on the hydrated sulfate and oxalate have been extended down to the triple point of H_2 and the susceptibilities of three other compounds have been measured over this extended temperature range. References to earlier work on the susceptibilities of uranium (IV) compounds were given in the previous paper.[1] Since that time a number of measurements on various uranium (IV) compounds have been reported.[2] None of these was made at temperatures lower than the triple point of N_2 and most of them only down to the boiling point of N_2 or air. The extension of measurements to much lower temperatures is of great importance for theoretical interpretation of the results in terms of the nature of the electronic states of the ions.

PREPARATION AND ANALYSIS OF COMPOUNDS

$U(SO_4)_2 \cdot 4.22H_2O$ (Designated by US)

This compound was prepared by essentially the same method as previously described.[1] It was analyzed for U by ignition to U_3O_8. The average of two analyses was 47.31±0.02% U. After two years four more analyses were made, the average being 47.03±0.03%. The calculated value for $U(SO_4)_2 \cdot 4H_2O$ is 47.40% U.

* This work was supported by the Office of Naval Research.
† Now at the Naval Research Laboratory, Washington, D. C.
[1] C. A. Hutchison, Jr., and Norman Elliott, J. Chem. Phys. **16**, 920 (1948).
[2] Organic complexes of U(IV): L. Saccioni, R. C. Lincei, 6 Sem 1 (5), 639 (1949); UF_4: N. Elliott, Phys. Rev. **76**, 431 (1949); J. K. Dawson, J. Chem. Soc. 429 (1951); UO_2: W. Trzebiatowski and P. W. Selwood, J. Am. Chem. Soc. **72**, 4504 (1950); J. K. Dawson and M. W. Lister, J. Chem. Soc. 2181 (1950); 2889 (1951); 1185 (1952); E. Slowinski and N. Elliott, Acta Cryst. **5**, 768 (1952); UCl_4: J. K. Dawson, J. Chem. Soc. 429 (1951); R. Stoenner and N. Elliott, J. Chem. Phys. **19**, 950 (1951); UBr_4: see, UCl_4, Dawson; $UF_4 \cdot 2KF$, $UF_4 \cdot KF$, $UF_4 \cdot CaF_2$, and $UF_4 \cdot 3NaF$; see, UF_4, Elliott.

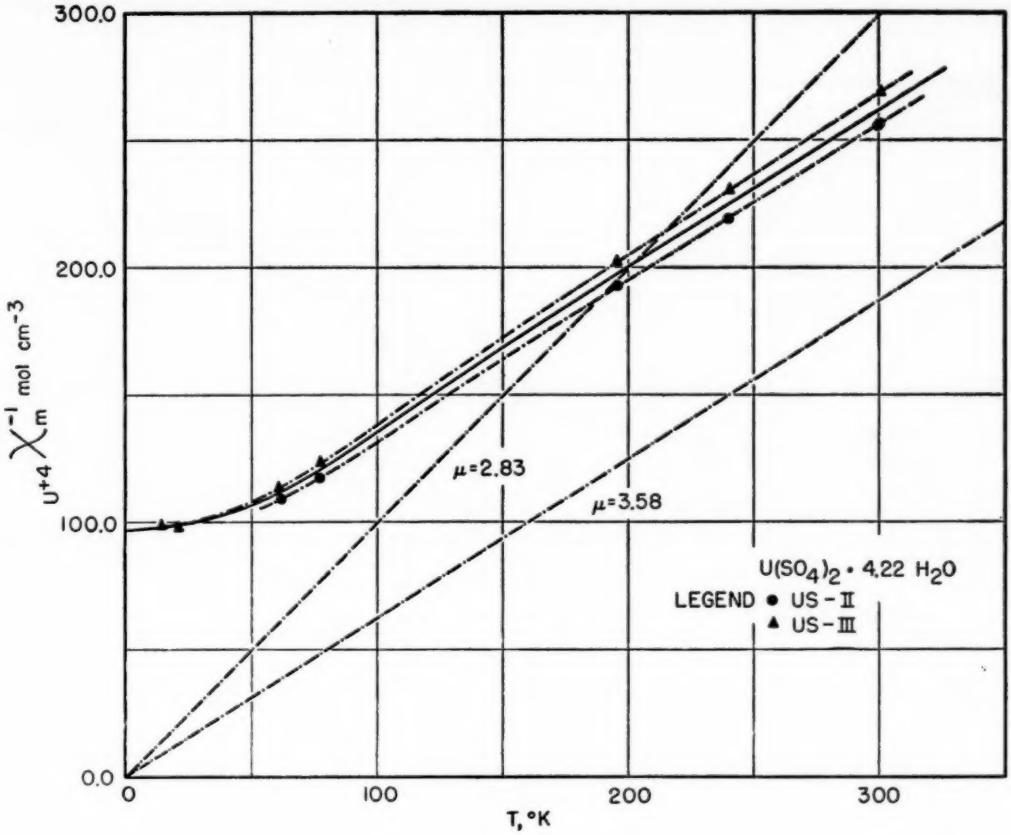

FIG. 1.

The compound was analyzed for SO_4 by precipitation of $BaSO_4$. The analysis showed 37.84±0.35% SO_4 as the average of four analyses. The mol ratio SO_4/U is 1.994±0.010. Assuming the value of SO_4/U to be 2 and using the measured percent of U given previously, we find 4.22 molecules of H_2O of hydration.

$U(C_2O_4)_2 \cdot 6H_2O$ (Designated by UO)

This compound was prepared by essentially the same method as previously described.[1] Analysis for U by ignition to U_3O_8 showed 45.65±0.15% U as an average of four analyses; two years later 45.67±0.03% U as an average of four analyses. The calculated value is 45.60% U.

It should be noted that in the previous studies by Hutchison and Elliott[1] the analysis for U indicated the presence of about five molecules of H_2O per U atom in the oxalate. The compound investigated here is seen to be the hexahydrate described by Gmelin.[3]

$UF_4 \cdot NaF$ (Designated by UD)

This compound was kindly prepared for us by Professor W. H. Zachariasen by fusing stoichiometric quantities of UF_4 and NaF in a Pt dish in an atmosphere of HF. The compound was analyzed for U by removal of F during heating with HNO_3 and H_2SO_4, precipitation with NH_3, and ignition to U_3O_8. The average of three analyses was 66.97±0.05% U. The calculated value is 66.86%.

(γ)$UF_4 \cdot 2NaF$ (Designated by UE)

This compound was also prepared by Professor Zachariasen by the same method and analyzed by the method just described. The average of three analyses was 59.97±0.26% U. The calculated value is 59.81%.

$UF_4 \cdot 3NaF$ (Designated by UF)

This compound was prepared by Professor Zachariasen by the same method and analyzed in the same manner. The average of three analyses was 54.18% U. The calculated value is 54.10%.

MAGNETIC MEASUREMENTS

The Gouy method was employed for making the measurements of the magnetic susceptibility. The apparatus was essentially the same as that described in the previous paper[1] with such modifications as were necessary to extend the range of measurement down to 14°K. The susceptibilities were calculated from the data and various values from the literature by methods

[3] Gmelin, Handbuch der Anorganischen Chemie, System Number 55 (1936).

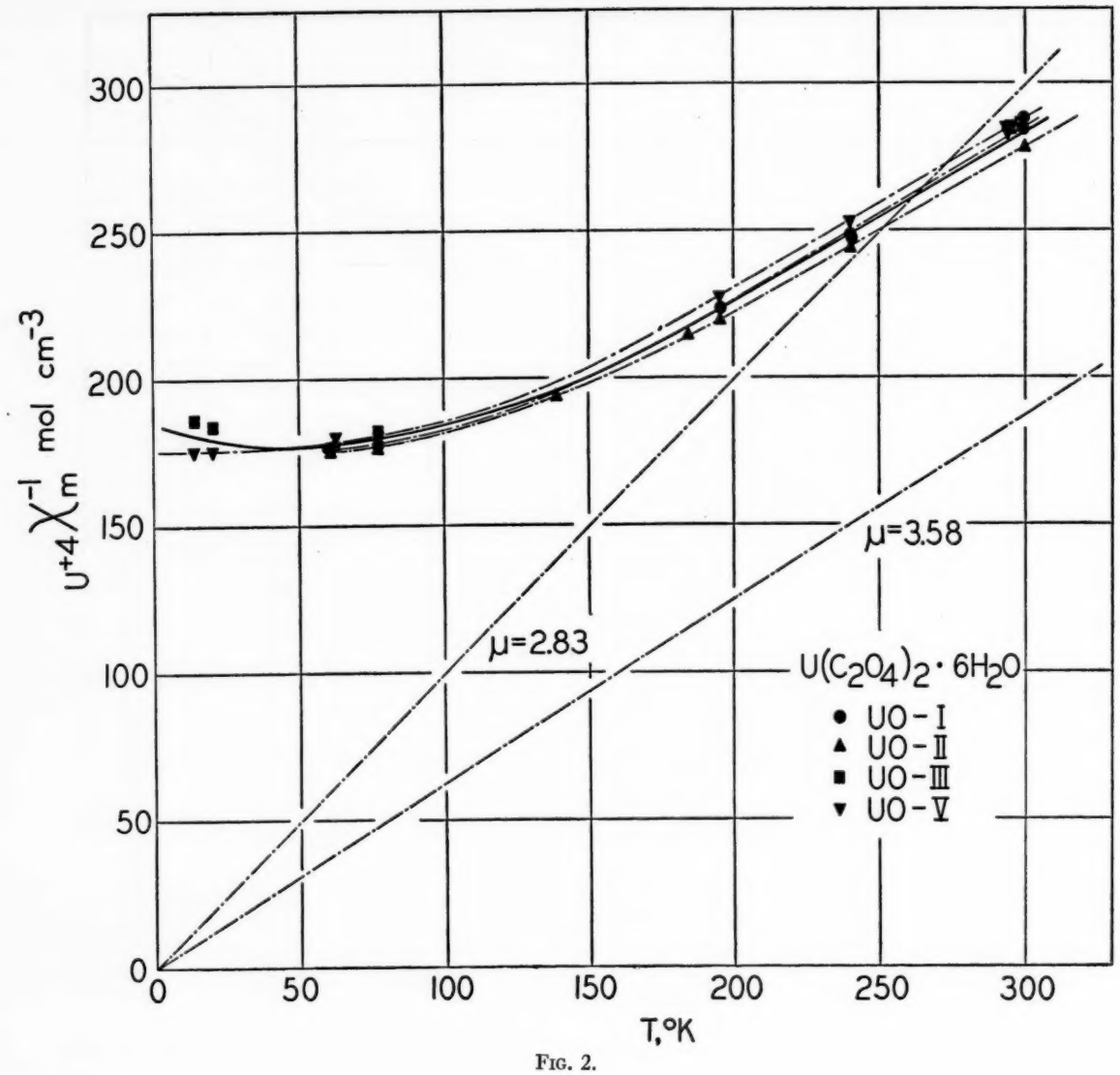

FIG. 2.

essentially the same as described previously.[1,4] The temperatures at which measurements were made and the method of temperature measurement are those described by Gruen and Hutchison.[5] In a dummy run the readings of the thermocouples with H_2 at its bp in the apparatus were checked against that of a similar couple embedded in the U salt in the Gouy tube and with long helical leads. The normal thermocouples agreed within 0.1 degree or better with the couple in the sample and with the temperatures of the H_2 as determined by vapor pressure measurements. The sample followed temperature changes in its surroundings to within 0.1 degree or better with a time lag of at most 5 minutes.

The magnetic force (weight with current on minus weight with current off) varied from ~0.14 g to ~0.04 g for US; from ~0.02 g to ~0.09 g for UO; from ~0.17 g to ~0.07 g for UD; from ~0.06 g to ~0.19 g for UE; and from ~0.04 g to ~0.18 g for UF over the ranges of magnet currents and temperatures used in the experiments. The reproducibility of the measurements is indicated by the fact that the forces at given magnet current on the standard substance, Mohr's salt, corrected for variations in the average density, varied by 1.5% from the average for six different fillings of the sample tube. No variation in calculated susceptibility with magnet current at fixed temperatures was observed. No force on the empty container was observable. The calculated demagnetization corrections were negligible at all temperatures.

EXPERIMENTAL RESULTS

A total of 667 measurements of magnetic forces on samples of the five compounds was made at various temperatures and magnet currents. Two different tube

[4] A precise statement of the calculations is given in the material of reference 6.

[5] D. M. Gruen and C. A. Hutchison, Jr., J. Chem. Phys. **22**, 386 (1954).

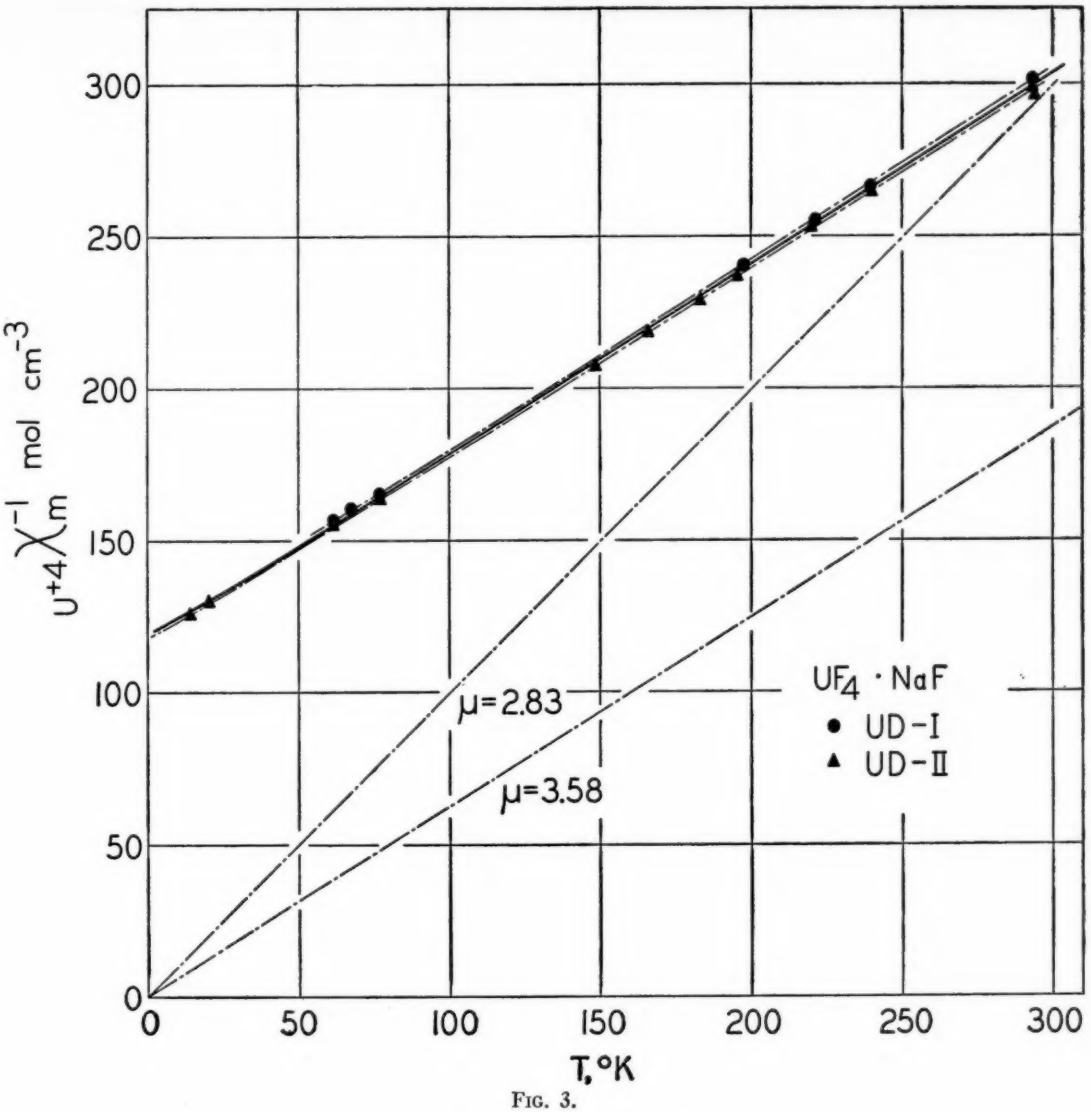

FIG. 3.

fillings were employed in the cases of US, UD, UE, and UF and four for UO. The results were tabulated for reference[6] but the detailed tables containing magnet current readings, thermocouple readings, temperatures, forces, readings from the curve of force *vs* magnet current for the standard substance, densities, diamagnetic corrections, susceptibilities of U^{+4} ion, and reciprocals of the susceptibilities of U^{+4} ion are too extensive to reproduce here.

The results are summarized in this paper in the form of five graphs (Figs. 1, 2, 3, 4, and 5), one for each compound investigated. In these graphs $_{U^{+4}}\chi_m^{-1}$, the reciprocal of the molar susceptibility in the unrationalized system using units mol cm^{-3}, is plotted against T, the temperature in degrees K. The $_{U^{+4}}\chi_m^{-1}$'s calculated from the measurements of a given series at a given temperature for a given tube filling were averaged. (The average number of measurements in a series was eight.) These averages were plotted for each of the compounds. Least-squares straight lines were drawn through all points above 190°K for each filling of the sample tube for which more than two points above 190°K were plotted. Smooth curves through all points below 190°K obtained for a given filling of the sample tube were visually fitted to these straight lines. The resulting curves are shown as broken lines in the figures. For each compound a curve was drawn which was the average of the broken lines (at lower temperatures points not on broken lines were included in the averaging). Two other broken lines (straight lines) are shown in each figure. They are plots of the function $\chi^{-1}=3kT/Ng^2\beta^2\lambda(\lambda+1)$ where N is Avogadro's con-

[6] For detailed paper, extended version, or supplementary material, order Document 4680 from American Documentation Institute, 1719 N Street N.W., Washington 6, D. C., remitting $2.00 for microfilm (images one inch high on standard 35-mm motion-picture film readable in microfilm reader or under low-power microscope) or $3.75 for photocopies (6×8 inches readable without optical aid).

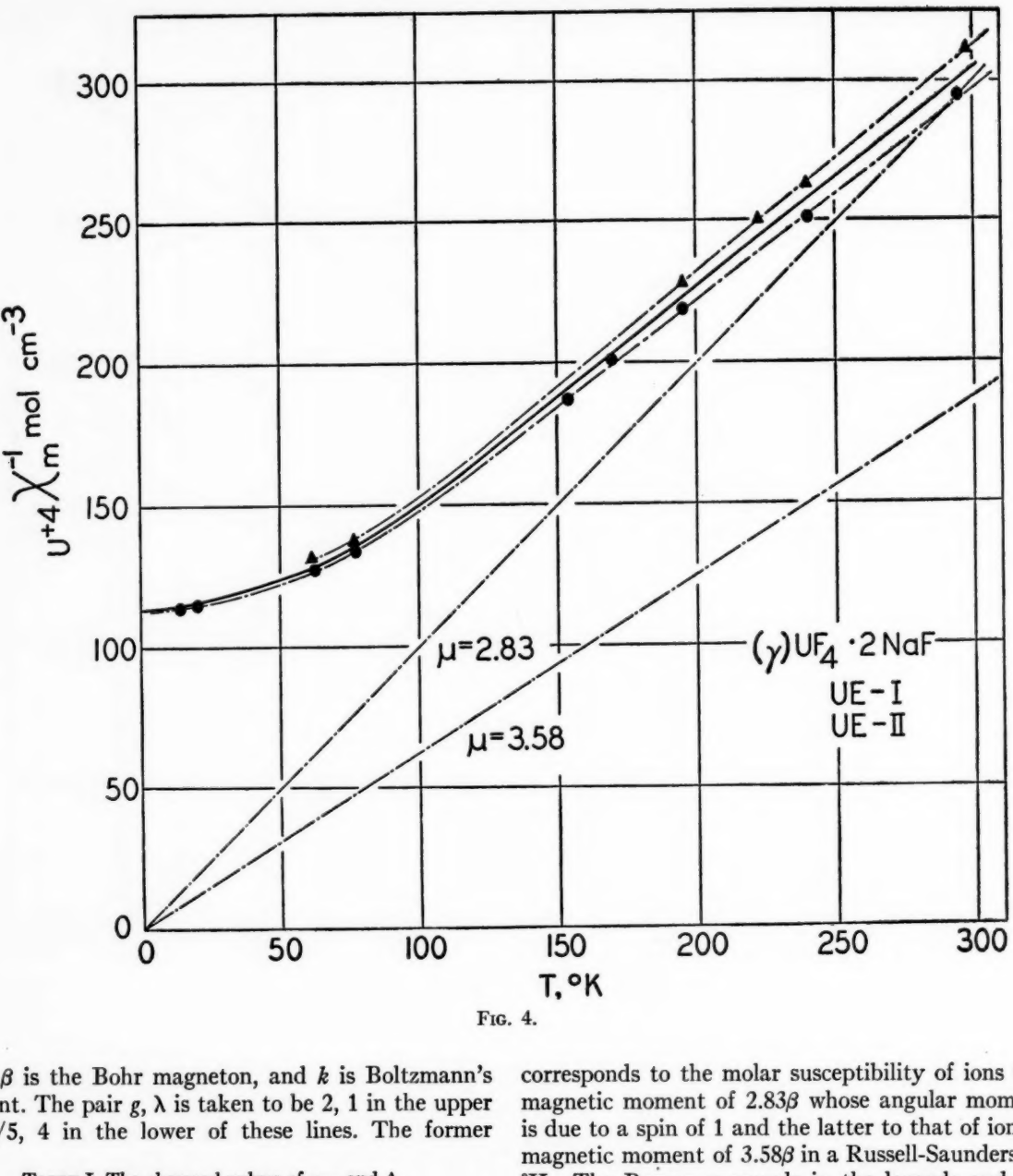

FIG. 4.

stant, β is the Bohr magneton, and k is Boltzmann's constant. The pair g, λ is taken to be 2, 1 in the upper and 4/5, 4 in the lower of these lines. The former corresponds to the molar susceptibility of ions with a magnetic moment of 2.83β whose angular momentum is due to a spin of 1 and the latter to that of ions with magnetic moment of 3.58β in a Russell-Saunders state, $^3H_4$. The Roman numerals in the legends and in the table denote different sample tube fillings.

TABLE I. The observed values of μ_{exp} and Δ.

Compound	μ_{exp} Bohr magneton	Average μ_{exp}	Δ °K	Average Δ
$U(SO_4)\cdot 4.22H_2O$		3.60±0.04		125±1
US–II	3.64		124	
US–III	3.56		125	
$U(C_2O_4)_2\cdot 6H_2O$		3.70±0.06		188±12
UO–I	3.63		171	
UO–II	3.76		192	
UO–V	3.74		202	
$UF_4\cdot NaF$		3.57±0.03		184±6
UD–I	3.54		178	
UD–II	3.61		190	
(γ)$UF_4\cdot 2NaF$		3.18±0.05		86±2
UE–I	3.23		89	
UE–II	3.13		84	
$UF_4\cdot 3NaF$				
UF–I	3.30		81	

DISCUSSION OF RESULTS

For each compound values of $\mu_{exp}=[(3k/\beta^2N)\sigma^{-1}]^{\frac{1}{2}}=(7.997\sigma^{-1})^{\frac{1}{2}}$ were computed for each broken curve where σ is the slope of the straight line portion of the broken curve. Also values of $\Delta=(\chi/\sigma)^{-1}-300$ at $T=300°K$ were calculated. These quantities together with their average values and the average deviations from these average values are listed in Table I.

The magnetic susceptibilities of US and UO have been measured previously by Hutchison and Elliott[1] over a more limited temperature range. The present results agree with these earlier ones within the expected

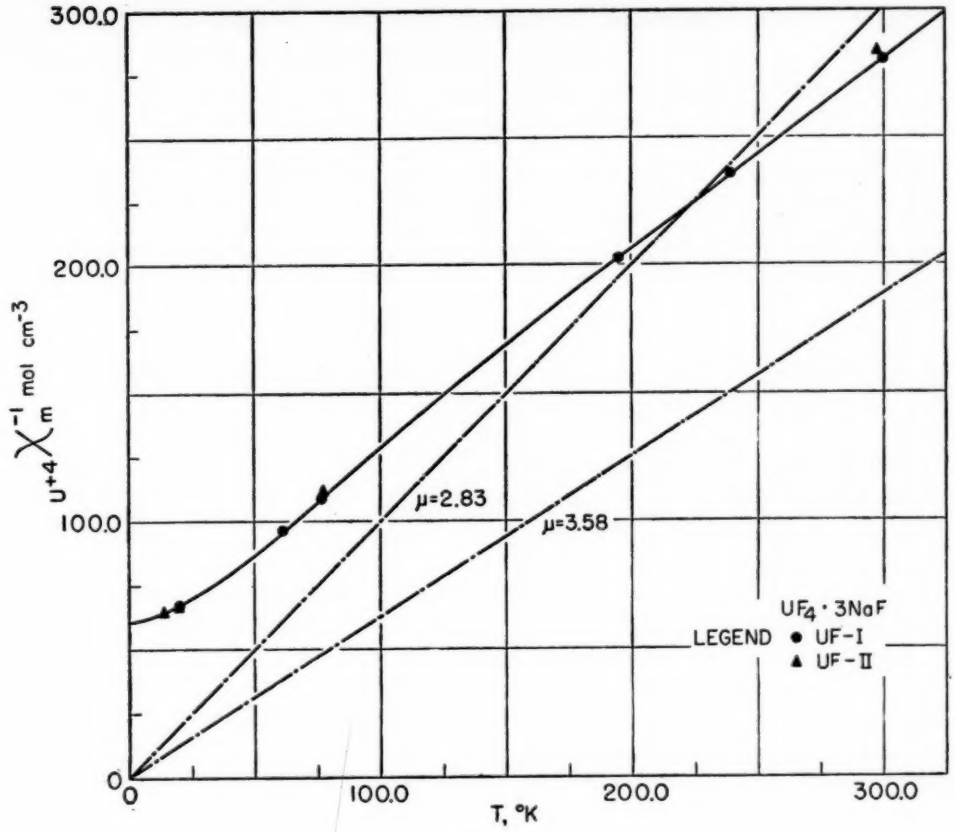

FIG. 5.

experimental errors. It should also be noted in this connection that there are some differences in composition between the samples employed in the two studies.

The interpretation of these results in terms of possible crystalline field perturbations of electronic states of the ions is a very complicated question and is not undertaken here. For most of the cases there are not sufficient structural data. In the case of UE the structure is known[7] and a calculation along the lines described by Gruen and Hutchison[5] could be made. The Δ's are large and deviations from straight-line behavior occur at relatively high temperatures and are very large which would be expected on the basis of many models involving large perturbations by the fields arising from the crystalline environment. There is one common characteristic of all the curves, namely that the susceptibilities appear to approach finite values at 0°K. From the previous paper[1] this did not appear to be the case for US since the points at liquid N_2 temperatures lie below the extrapolated high-temperature straight line. The behavior indicates that the ground state is not degenerate and that the lowest excited states lie a considerable distance above it. This behavior is in marked contrast to that of Np (V)[4] or of Pu (VI)[8] which also contain two unpaired electrons. At the lowest temperatures the susceptibilities of compounds containing these ions are still increasing rapidly.

ACKNOWLEDGMENTS

The kindnesses of Professor W. H. Zachariasen in supplying compounds, of the Institute for the Study of Metals in supplying liquid H_2, and of Professor J. W. Stout and Professor L. Meyer in advising concerning the low-temperature measurements are gratefully acknowledged.

[7] W. H. Zachariasen, Acta Cryst. **1**, 265 (1948).

[8] J. K. Dawson, J. Chem. Soc. 2705 (1952).

Excluded Volume in Polymer Chains*

MARSHALL FIXMAN
Department of Chemistry, Massachusetts Institute of Technology, Cambridge, Massachusetts
(Received December 13, 1954)

A perturbation theory of the excluded volume effect in chain polymers is developed. The theory is applied to the mean square end-to-end distance, $\langle L^2\rangle$, of a linear chain (second-order perturbation), and to the mean square radius of a linear and a branched chain (first-order perturbation). Flory's approximate theory is found to be in fair agreement with the second-order perturbation theory. Integro-differential equations are developed to discuss the behavior of $\langle L^2\rangle/nb^2$ as $n\to\infty$, for a chain composed of n segments of length b.

I. INTRODUCTION

THE net effect of the Van der Waals interactions between nonadjacent segments of a polymer chain will usually be an effect of repulsion, and will lead to an expansion of the chain. This expansion can be detected directly by a diffraction experiment, and indirectly by its influence on intrinsic viscosity, osmotic second virial coefficient, friction constant, etc. Flory's[1] approximate treatment of the excluded volume effect has frequently been applied to the interpretation of intrinsic viscosity measurements,[2] while exact calculations have been confined to a first-order perturbation theory[3–7] of $\langle L^2\rangle$, the mean square end-to-end distance of the coil. Here we will extend the latter calculation to a second-order perturbation, and carry through the first-order perturbation theory of $\langle R^2\rangle$, the mean square radius of gyration, for a linear and a branched molecule.[8]

Note that it is $\langle R^2\rangle$, given by the equivalent formulas

$$\langle R^2\rangle=\frac{1}{n}\sum\langle R_i^2\rangle,$$
$$\langle R^2\rangle=\frac{1}{2n^2}\sum\sum\langle L_{ij}^2\rangle, \tag{1}$$

that is obtained from light scattering measurements.[9] In Eq. (1), n is the number of segments in the chain, R_i is the distance of the ith segment from the center of mass, and L_{ij} is the distance between segments i and j.

We first present our perturbation calculation, and then compare our results with Flory's theory.

II. FORMULATION OF EQUATIONS

We represent the ith segment or link by a vector $\mathbf{r}_i$ of mean value $\langle r_i^2\rangle=b^2$, and assume that the probability that the n vectors $\mathbf{r}_i$ lie between $\mathbf{r}_i+d\mathbf{r}_i$ is

$$\frac{\exp(-\sum\sum_{i>j}V(L_{ij})/kT)\prod_i^n(\frac{3}{2}\pi L^2)^{-\frac{3}{2}}\exp(-3r_i^2/2b^2)d\mathbf{r}_i}{\int\cdots\int\exp(-\sum\sum_{i>j}V(L_{ij})/kT)\prod_i^n(\frac{3}{2}\pi b^2)^{-\frac{3}{2}}\exp(-3r_i^2/2b^2)d\mathbf{r}_i}. \tag{2}$$

The assumptions involved in (2), that the distribution of $\mathbf{r}_i$ is Gaussian and that the interaction potential is additive over segment pairs, are sufficiently standard that we will not comment on them. Now, following Zimm[10] (the development is analogous to the Ursell-Mayer theory of imperfect gases), we write

$$\exp(-V(L_{ij})/kT)=1-\chi(L_{ij}), \tag{3}$$

and assume that $\chi(L_{ij})$ approaches zero so rapidly as L_{ij} increases from zero that we may substitute for $\chi(L_{ij})$ as follows:

$$\chi(L_{ij})=\delta(\mathbf{L}_{ij})\int[1-\exp(-V(L_{ij})/kT)]d\mathbf{L}_{ij}$$
$$=\delta(\mathbf{L}_{ij})X \tag{4}$$

where $\delta(\mathbf{L}_{ij})$ is a normalized function of $\mathbf{L}_{ij}$, sharply peaked at $L_{ij}=0$ (e.g., a three-dimensional Dirac delta function). Then

$$\exp(-\sum\sum_{i>j}V(L_{ij})/kT)=\prod\prod_{i>j}[1-\chi(L_{ij})]$$
$$=1-X\sum\sum_{i>j}\delta(\mathbf{L}_{ij})+\cdots.$$

We note for future reference (Sec. V) that since the effect of repulsion between two particular segments on,

* Work supported by the Office of Ordnance Research.

[1] P. J. Flory, J. Chem. Phys. **17**, 303 (1949).
[2] P. J. Flory, *Principles of Polymer Chemistry* (Cornell University Press, Ithaca, New York, 1953), Chap. XIV.
[3] E. Teramoto, Busseiron Kenkyu **39**, 1 (1951); and succeeding papers by Teramoto, Yamamoto, and Matsuda. A brief English summary of the Japanese work is given by P. J. Flory, J. Polymer Sci. **14**, 1 (1954).
[4] T. B. Grimley, J. Chem. Phys. **21**, 185 (1953).
[5] F. Bueche, J. Chem. Phys. **21**, 205 (1953).
[6] H. M. James, J. Chem. Phys. **21**, 1628 (1953).
[7] Zimm, Stockmayer, and Fixman, J. Chem. Phys. **21**, 1716 (1953).
[8] W. H. Stockmayer and M. Fixman, Ann. N. Y. Acad. Sci. **57**, 334 (1953).
[9] B. H. Zimm and W. H. Stockmayer, J. Chem. Phys. **17**, 1301 (1949).
[10] B. H. Zimm, J. Chem. Phys. **14**, 164 (1946).

say, $\langle L^2\rangle$, is infinitesimal we have

$$1-\chi(L_{ij})=\exp[-X\,\delta(\mathbf{L}_{ij})]$$

$$\exp[-\textstyle\sum\sum_{i>j} V(L_{ij})/kT]=\exp[-X\sum\sum_{i>j}\delta(\mathbf{L}_{ij})].$$

We now multiply (2) by L^2 and integrate over all $\mathbf{L}$, where $\mathbf{L}=\sum_i \mathbf{r}_i$. The application of Eqs. (3) and (4) results in

$$\langle L^2\rangle=\frac{\langle L^2\rangle_0-X\sum\sum_{i>j}\int L^2P(\mathbf{L},O_{ij})d\mathbf{L}+\cdots}{1-X\sum\sum_{i>j}P(O_{ij})+\cdots},$$
$$\langle L^2\rangle_0=nb^2 \text{ (random flight)}. \tag{5}$$

We have used P's to denote probability densities computed using random flight statistics. For example, the probability density $P(\mathbf{L},O_{ij})$ is defined by

$$P(\mathbf{L},O_{ij})=\left(\frac{3}{2\pi b^2}\right)^{3n/2}\int\cdots\int\delta(\mathbf{L}_{ij})\times\exp(-3\textstyle\sum_i \mathbf{r}_i^2/2b^2)d\mathbf{r}_1\cdots d\mathbf{r}_n/d\mathbf{L}$$

and $P(O_{ij})=\int P(\mathbf{L},O_{ij})d\mathbf{L}$. Verbally, $P(\mathbf{L},\mathbf{L}_{ij})$ is the bivariate probability distribution of $\mathbf{L}$ and $\mathbf{L}_{ij}$ (a bivariate Gaussian function), and $P(\mathbf{L},O_{ij})=P(\mathbf{L},\mathbf{L}_{ij})_{\mathbf{L}_{ij}=0}$ Now expand the denominator of the r.h.s. of Eq. (5) in a geometric series[11] and collect powers of X. Thus,[12]

$$\begin{aligned}\langle L^2\rangle=\langle L^2\rangle_0&-X\sum\sum_{i>j}\int L^2[P(\mathbf{L},O_{ij})-P(\mathbf{L})P(O_{ij})]d\mathbf{L}\\&+X^2\sum\sum_{\substack{i>j,\\k>i}}\sum\sum_{k>l}\int L^2[P(\mathbf{L},O_{ij},O_{kl})\\&-P(\mathbf{L})P(O_{ij},O_{kl})+2P(O_{ij})P(O_{kl})P(\mathbf{L})\\&-P(\mathbf{L},O_{ij})P(O_{kl})-P(\mathbf{L},O_{kl})P(O_{ij})]d\mathbf{L}+\cdots.\end{aligned} \tag{6}$$

In Eq. (6) we have used, and will use again, the fact that i, j, k, l are dummy variables of summation.

Similarly,

$$\langle L_{ij}^2\rangle=\langle L_{ij}^2\rangle_0-X\sum\sum_{k>l}\int L_{ij}^2[P(\mathbf{L}_{ij},O_{kl})-P(\mathbf{L}_{ij})P(O_{kl})]d\mathbf{L}_{ij}+\cdots. \tag{7}$$

We turn first to the computation of $\langle L^2\rangle$.

III. END-TO-END DISTANCE

The probabilities required in Eq. (6) are given in the Appendix. We find, after some combination of terms, that $\langle L^2\rangle=nb^2+C_1X+C_2X^2+\cdots$, where

$$C_1=(\tfrac{3}{2}\pi b^2)^{\frac{3}{2}}b^2\textstyle\sum\sum_{i>j}(i-j)^{-\frac{1}{2}}$$

$$C_2=(\tfrac{3}{2}\pi b^2)^3b^2\sum\sum_{\substack{i>j,\\k>i}}\sum\sum_{k>l}\times\left\{\frac{(i-j)(k-l)[2S-(i-j)-(k-l)]}{[(i-j)(k-l)-S^2]^{5/2}}+(i-j)^{-\frac{1}{2}}(k-l)^{-\frac{1}{2}}+(i-j)^{-\frac{1}{2}}(k-l)^{-\frac{1}{2}}\right\},$$

$$S=\begin{cases}0 & \text{if } l>i\\ (i-j) & \text{if } j>l\\ (i-l) & \text{if } j<l<i\end{cases}.$$

The sums may be converted to integrals, and the integrations proceed in terms of elementary functions. The results are (for $n^{\frac{1}{2}}\gg 1$),

$$C_1=(4/3)b^2(\tfrac{3}{2}\pi b^2)^{\frac{3}{2}}n^{\frac{1}{2}}$$

$$C_2=-\left(\frac{16}{3}-\frac{28\pi}{27}\right)b^2(\tfrac{3}{2}\pi b^2)^3n^2.$$

Although we have not evaluated any higher order terms, a simple consideration of the expressions for the P's shows that the coefficient of X^i in the series for $\langle L^2\rangle/\langle L^2\rangle_0$ is proportional to $[(\frac{3}{2}\pi b^2)^{\frac{3}{2}}n^{\frac{1}{2}}]^i$. Hence $\langle L^2\rangle/\langle L^2\rangle_0$ is a universal function of the variable z, where

$$z=X(\tfrac{3}{2}\pi b^2)^{\frac{3}{2}}n^{\frac{1}{2}}$$
$$\langle L^2\rangle/\langle L^2\rangle_0=1+(4/3)z-\left(\frac{16}{3}-\frac{28\pi}{27}\right)z^2+\cdots. \tag{8}$$

We note that James[6] has formally retained terms of order greater than z in his series for $\langle L^2\rangle/\langle L^2\rangle_0$. They are without significance, however; the coefficient of z^2 in the James series, for example, is incorrect in sign as well as magnitude.

IV. RADIUS OF GYRATION

A. Linear Chain

According to Eq. (1) we are required to compute $\langle L_{ij}^2\rangle$. We take $i>j$ since, for a linear chain, $\langle R^2\rangle=n^{-2}\sum\sum_{i>j}\langle L_{ij}^2\rangle$; then, from Eq. (7) and the Appendix,

$$\langle L_{ij}^2\rangle=b^2(i-j)+Xb^2(\tfrac{3}{2}\pi b^2)^{\frac{3}{2}}\sum\sum_{k>l}f_{kl}^2(k-l)^{-5/2}+\cdots, \tag{9}$$

where

$$f_{kl}=\begin{cases}k-j & \text{if } 0<l<j;\ j<k<i\\ i-j & \text{if } 0<l<j;\ i<k<n\\ k-l & \text{if } j<l<k<i\\ i-l & \text{if } j<l<i;\ i<k<n\\ 0 & \text{if } 0<l<k<j \text{ or } i<l.\end{cases}$$

[11] The denominator certainly lies between 1 and 0 if $X>0$, and so the expansion is justified. If X is much less than zero the polymer will not dissolve.

[12] The possibility of the cluster development of Eq. (6) has been mentioned by R. J. Rubin [J. Chem. Phys. **20**, 1940 (1952)]. The coefficient of X is the basis of the work of Teramoto and Yamamoto[3] on $\langle L^2\rangle$.

The tedious but straightforward integrations over $k>l$ to yield $\langle L_{ij}^2\rangle$, and over $i>j$ to yield $\langle R^2\rangle$, finally give

$$\langle R^2\rangle/\langle R^2\rangle_0=6\langle R^2\rangle/nb^2=1+134z/105+\cdots. \quad (10)$$

B. Cruciform Molecule

The cruciform molecule has one branch point from which lead four branches each having $n/4$ segments. Instead of Eq. (1) for $\langle R^2\rangle$ we use the equivalent expression[9]

$$\langle R^2\rangle=-\frac{4}{n}\sum_{s=0}^{n/4}\langle L_s^2\rangle-\langle B^2\rangle,$$

where L_s is the distance between the branch point and the sth segment of a particular branch, and B is the distance from the branch point to the center of mass. The vector $\mathbf{B}$ may be obtained in terms of the segment vectors from[9]

$$\mathbf{B}=\sum_{v=1}^{4}\sum_{s=1}^{n/4}\mathbf{L}_{sv}$$

where L_{sv} is the vector from the branch point to the sth segment of the vth branch. The lengthy calculation of $\langle R^2\rangle$ introduces nothing new. One has equations similar to Eq. (7) and Eq. (9) for $\langle L_s^2\rangle$ and $\langle B^2\rangle$. The various types of single contacts may be distinguished and the probabilities computed. The result is

$$\langle R^2\rangle=\langle R^2\rangle_0+(\tfrac{3}{2}\pi b^2)^{\frac{1}{2}}n^{\frac{1}{2}}b^2X[(601\sqrt{2}/480)-1667/1008]+\cdots;$$
$$\langle R^2\rangle_0=5nb^2/48$$

or

$$\langle R^2\rangle/\langle R^2\rangle_0=1+1.12z+\cdots. \quad (11)$$

The particularly interesting feature of Eqs. (10) and (11) is the implication that a branched chain has a slightly smaller $\langle R^2\rangle/\langle R^2\rangle_0$ than an unbranched chain of the same molecular weight. Although branching increases the probability of segment-segment contacts, the shorter chains in the branched molecule are less susceptible to the effect of interactions since the excluded volume effect arises from the interactions of segments which are far removed from each other along the backbone of the chain.

V. APPROXIMATE THEORIES

A. Flory's Theory

As we noted in Sec. II,

$$\exp-\textstyle\sum\sum_{i>j}V(L_{ij})/kT=\exp-X\sum\sum_{i>j}\delta(\mathbf{L}_{ij}).$$

Now the instantaneous density $\rho(\mathbf{r})$ (in number of segments per unit volume) at any point $\mathbf{r}$ is given by $\rho(\mathbf{r})=\sum_i\delta(\mathbf{r}-\mathbf{R}_i)$, if the center of mass is taken as the origin. Also

$$\int\rho^2(\mathbf{r})d\mathbf{r}=2\sum\sum_{i>j}\delta(\mathbf{R}_i-\mathbf{R}_j)+\sum\delta(\mathbf{R}_i-\mathbf{R}_i).$$

While the $\delta(\mathbf{R}_i-\mathbf{R}_i)$ may be very large (infinite if we use infinitely peaked δ functions), they will be completely independent of configuration, and because of the normalization (2) may be freely added to the interaction energy. Then

$$\exp-\sum\sum_{i>j}V(L_{ij})/kT=\exp-\frac{X}{2}\int\rho^2(\mathbf{r})d\mathbf{r}$$

which is essentially the interaction energy used by Flory.[1] Flory then assumed that $\rho(\mathbf{r})$ in a particular configuration could be approximated by a Gaussian function chosen to yield the proper value of R^2, where

$$R^2=n^{-1}\sum R_i^2=n^{-1}\int r^2\rho(\mathbf{r})d\mathbf{r}.$$

It will suffice, however, merely to assume that $\rho(\mathbf{r})$ is a function only of n, r, and R; since $\rho(r)$ is the number of segments per unit volume $\rho(r)$ must be of the form

$$\rho(r)=nR^{-3}\nu(r/R)$$

where ν is some unknown function of r/R. Then

$$\int\rho^2(r)d\mathbf{r}=4\pi n^2R^{-3}\int\left(\frac{r}{R}\right)^2\nu^2(r/R)d(r/R)$$
$$=\text{constant}\times n^2R^{-3}. \quad (12)$$

The R^{-3} dependence of the interaction energy characterizes Flory's theory. He assumes that the probability distribution of R is Gaussian and finds that α, the ratio of the most probable R in the actual chain to the most probable R in a random flight chain is given by

$$\alpha^5-\alpha^3=\text{constant}\times z. \quad (13)$$

In applying Flory's theory one assumes that $\alpha^2=\langle R^2\rangle/\langle R^2\rangle_0$. The constant in Eq. (13) can then be found from Eq. (8) or Eq. (10). (Of course this procedure was not followed in Flory's theory; there the choice of a Gaussian $\rho(r)$ fixed the constant.) If one wishes to know the expansion of the end-end distance, for example,

$$\alpha^5-\alpha^3=(4/3)z. \quad (14)$$

(Flory's assumption of a Gaussian $\rho(r)$ leads to a far too large constant in $\alpha^5-\alpha^3=\text{constant}\times z$. However, as we have just seen, the main features of Flory's theory, and the main result, that $\alpha^5-\alpha^3$ is proportional to the square root of the molecular weight, do not require the specific choice of a Gaussian $\rho(r)$.) In order to compare Flory's result with our perturbation theory we expand α^2 as given by Eq. (14) in a power series in z:

$$\alpha^2=1+(4/3)z-(8/3)z^2+\cdots$$

while Eq. (8) states that $\alpha^2=1+(4/3)z-(6.23/3)z^2+\cdots$. We see that Flory's equation is in fair agreement with the second-order perturbation theory (when forced to fit the first-order theory).

B. Asymptotic Behavior of α^2

Let us abbreviate the set of segment coordinates by $\{Q\}$ and the random flight probability density by $P\{Q\}$. Then

$$\langle L^2\rangle=\frac{\int L^2\exp[-X\sum\sum_{i>j}\delta(\mathbf{L}_{ij})]P\{Q\}d\{Q\}}{\int\exp[-X\sum\sum_{i>j}\delta(\mathbf{L}_{ij})]P\{Q\}d\{Q\}}. \quad (15)$$

Differentiation of Eq. (15) with respect to X yields

$$\frac{\partial\langle L^2\rangle}{\partial X}=\sum\sum_{i>j}\int L^2[F(\mathbf{L})F(O_{ij})-F(\mathbf{L},O_{ij})]d\mathbf{L}, \quad (16)$$

where the probability densities, the F's, have the same significance as the P's previously defined, but the F's are to be computed taking into account the segment-segment repulsions.

From a consideration of the increase in $L^2\rangle$ brought about by adding one segment to a chain of n segments we find an equation similar to the one derived by James[6]:

$$\frac{\partial\langle L^2\rangle}{\partial n}=b^2+X\sum_{j=1}^{n}\int L^2[F(\mathbf{L})F(O_{nj})-F(\mathbf{L},O_{nj})]d\mathbf{L}. \quad (17)$$

Now it has sometimes been conjectured that the effect of segment-segment repulsions at very large molecular weights can be accounted for in the same manner as hindered rotation, that is, by using Gaussian forms for the F's with b replaced by αb, where α is supposed to be independent of molecular weight. If we make this substitution in Eqs. (16) and (17) we find

$$\frac{\partial\langle L^2\rangle}{\partial X}=(4/3)n^{\frac{1}{2}}(\tfrac{3}{2}\pi b^2)^{\frac{1}{2}}b^2/\alpha=nb^2\frac{\partial\alpha^2}{\partial X}, \quad (16a)$$

$$\frac{\partial\langle L^2\rangle}{\partial n}=b^2+2Xn^{\frac{1}{2}}(\tfrac{3}{2}\pi b^2)^{\frac{1}{2}}b^2/\alpha=b^2\alpha^2+nb^2\frac{\partial\alpha^2}{\partial n}. \quad (17a)$$

(The b^2 in the r.h.s. of Eq. (17) is a random flight b^2, hence not to be replaced by $b^2\alpha^2$.) Equations (16a) and (17a) show one thing clearly, namely that the assumption of an α independent of n or X is an inconsistent assumption at all molecular weights. Both equations yield $\alpha^3/z\to$constant as $z\to\infty$. The actual expressions for α^2 obtainable from Eqs. (16a) and (17a) are in severe disagreement with our second-order perturbation theory, so we shall not pursue them further.

VI. SUMMARY

We have found that

(1) $\langle L^2\rangle/\langle L^2\rangle_0$ is a universal function of $(\frac{3}{2}\pi b^2)^{\frac{1}{2}}Xn^{\frac{1}{2}}$ for sufficiently large n.

(2) $\langle L^2\rangle/\langle L^2\rangle_0$ and $\langle R^2\rangle/\langle R^2\rangle_0$ are approximately equal.

(3) branching has little effect on $\langle R^2\rangle/\langle R^2\rangle_0$.

(4) Flory's expression for α^2, as given in Eq. (14), is in fair agreement with the second-order perturbation theory of α^2.

(5) $F(\mathbf{L})$, $F(\mathbf{L},O_{ij})$, etc., the probability distribution functions pertaining to the actual molecule, cannot be given by Gaussian forms at any molecular weight.

VII. ACKNOWLEDGMENTS

Advice and ideas received from Professor W. H. Stockmayer have been abundant and indispensable during the course of this research.

VIII. APPENDIX

Let $\mathbf{V}_p$ be one of s vectors constructed from the segment vectors $\mathbf{r}_t$ by the equation

$$\mathbf{V}_p=\sum_{t=1}^{n}\psi_{pt}\mathbf{r}_t,$$

where the ψ_{pt} are constants. By a simple generalization of a derivation given by Wang and Uhlenbeck[13] one finds that the simultaneous probability distribution of $\mathbf{V}_1, \mathbf{V}_2, \cdots, \mathbf{V}_s$ is given by

$$P(\mathbf{V}_1,\cdots,\mathbf{V}_s)=(\tfrac{3}{2}\pi b^2)^{3s/2}C^{-\frac{1}{2}}\times\exp[(-\tfrac{3}{2}b^2c)\sum_{i=1}^{s}\sum_{j=1}^{s}C^{ij}\mathbf{V}_i\cdot\mathbf{V}_j],$$

where C^{ij} is the cofactor of the element C_{ij} in the s^2 matrix $[C_{ij}]$, with

$$C_{ij}=\sum_{t=1}^{n}\psi_{it}\psi_{jt},$$

and C is the determinant of $[C_{ij}]$.

[13] Ming Chen Wang and G. E. Uhlenbeck, Revs. Modern Phys. **17**, 323 (1945).

Analysis of the 6140 cm^{-1} Band of HDS*

GLENN A. CROSBY,† EDWARD J. BAIR,‡ AND PAUL C. CROSS
Department of Chemistry, University of Washington, Seattle, Washington

(Received November 19, 1954)

Absorption observed in the region 6140 cm^{-1} was analyzed to yield the following constants: $\nu_0=6140.0$ cm^{-1}, $A''=9.743$, $B''=4.922$, $C''=3.232$, $A'=9.411$, $B'=5.019$, $C'=3.137$ cm^{-1}. The inertial defect of the ground state, $\Delta''=I_C''-I_A''-I_B''=0.101\times10^{-40}$ g cm^2, is approximately half that estimated for use in the interpretation of the microwave spectrum. This accounts for the major part of the discrepancy between the sets of moments of inertia of the molecule obtained by the two methods.

INTRODUCTION

SINCE the moments of inertia of HDS in the ground state as determined by microwave spectroscopy[1] differ from what one would predict from the accurately known H_2S geometry, an independent check of these parameters was undertaken in the hope of resolving this inconsistency. Results of this work should be useful for the more accurate prediction of expected microwave absorption frequencies and, in addition, yield information pertinent to the complete theoretical interpretation of H_2S spectra.

EXPERIMENTAL

D_2S was prepared by distilling 98.2% D_2O into a system containing granulated Al_2S_3 with the Al_2S_3 spread out in 50 mm Pyrex tubing (total length 12 ft) to increase the surface area. The tubes were baked out at 300°C to recover the D_2S adsorbed on the Al_2O_3 by-product. The generated D_2S was collected in dry ice-acetone traps and fractionated twice over liquid nitrogen before a final distillation into the absorption cell to a total pressure of 35 cm Hg. Dry H_2S was then passed into the cell increasing the pressure to 65 cm Hg. An approximate 1–2–1 mole mixture of H_2S–HDS–D_2S was obtained by the exchange reaction to give an estimated HDS pressure of 30 cm Hg.

The absorption cell is of a type previously described by White.[2] It is constructed of a 10 in. copper pipe (17.5 ft in length, 10 in. in diameter) equipped with evaporated gold mirrors.

The HDS was investigated spectroscopically over the region of $1.0-1.9\mu$ using a 21 ft kinematically focused concave grating spectrometer[3] with a lead sulfide detector and a low-intensity carbon arc light source. For wavelength calibration, the spectrum of a Pfund iron arc was simultaneously taken by a dual pen Speedomax recorder, using a photomultiplier tube for detector.

A thorough search of the region covered, employing path lengths of up to 280 feet, revealed one relatively intense HDS band which was partly overlapped by the (111) H_2S band previously analyzed.[4] The band was recorded employing a path length of 70 feet and resolution of ~0.5 cm^{-1}. Over one hundred well-resolved peaks were measured and calibrated against third- and fourth-order iron lines. No other HDS absorption sufficient for a rotational analysis was observed.

ANALYSIS

Since in HDS there is no symmetry axis with which a principal inertial axis may coincide, one would expect an absorption band governed by both A-type and B-type selection rules,[5] the actual appearance depending on the relative magnitude of the components of the dipole moment vector derivative parallel (A-type) or perpendicular (B-type) to the least inertial axis.

A glance at this HDS band (Fig. 1) shows a prominent collected Q-branch immediately establishing the band as predominantly A-type. Throughout the subsequent analysis, only A-type selection rules were assumed—an assumption that is adequately justified by the results.

The band was analyzed in detail to determine seven parameters: the effective ground (A'', B'', C'') and excited (A', B', C') state inertial constants and the band center (ν_0), where $A''=h/8\pi^2cI_A''$ cm^{-1}, etc. The procedure used was the stochastic method previously described.[6] Essentially, the method consists of making an enlightened guess at the inertial parameters of the molecule and calculating the energy level pattern for both the excited and ground states using published asymmetric rotor tables.[7] A centrifugal distortion correction is also applied to each energy level (see following). A trial spectrum is then drawn up employing these energy levels and appropriate selection rules.

* From a thesis submitted by Glenn A. Crosby in partial fulfilment of the requirements of the degree of Doctor of Philosophy. Partially supported by the Office of Naval Research.

† National Science Foundation Pre-doctoral Fellow, 1953–1954. Present address: Department of Chemistry, Florida State University, Tallahassee, Florida.

‡ Present address: Department of Chemistry, Indiana University, Bloomington, Indiana.

[1] R. E. Hillger and M. W. P. Strandberg, Phys. Rev. **83**, 575 (1951).

[2] J. U. White, J. Opt. Soc. Am. **32**, 285 (1942).

[3] Bair, Cross, Dawson, Wilson, and Wise, J. Opt. Soc. Am. **43**, 681 (1953).

[4] Allen, Cross, and Wilson, J. Chem. Phys. **18**, 691 (1950); H. C. Allen, Jr., and E. K. Plyler, J. Research Natl. Bur. Standards **52**, 205 (1954).

[5] G. Herzberg, *Infrared and Raman Spectra of Polyatomic Molecules* (D. Van Nostrand Company, Inc., New York, 1945).

[6] P. C. Cross, Phys. Rev. **47**, 7 (1935).

[7] King, Hainer, and Cross, J. Chem. Phys. **11**, 27 (1943).

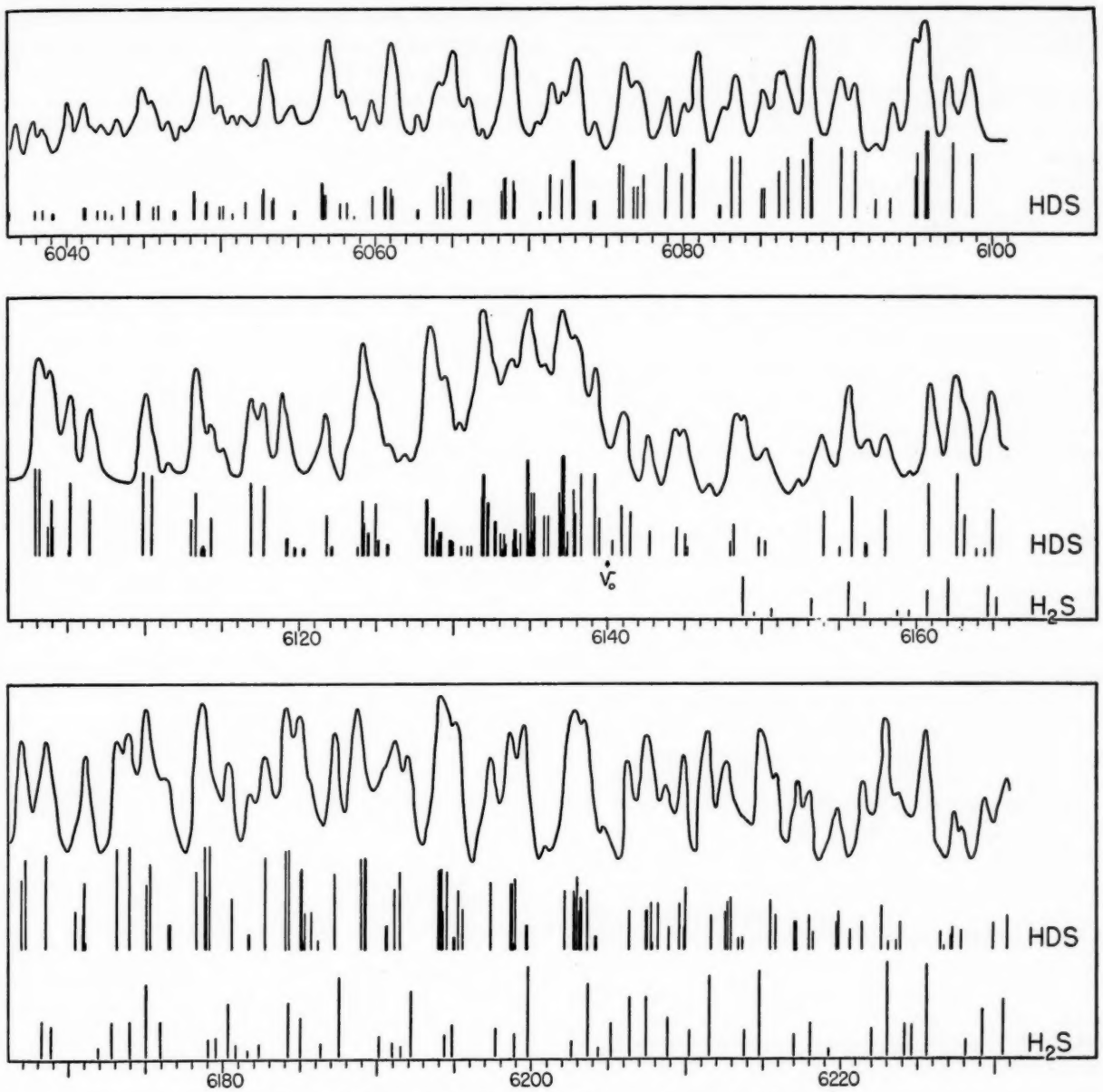

FIG. 1. Absorption (maximum 90%) *versus* frequency in cm^{-1}.

The trial spectrum is completed by computing relative line intensities, again with the aid of published tables.[8]

By comparison of HDS spectra calculated in the above manner with the experimentally observed spectrum, the various inertial parameters were adjusted until a sufficiently good fit of the spectrum was obtained to allow all calculated transitions to be correlated with the experimental absorption maxima. The labor of this procedure was considerably reduced by the preparation of tables of derivatives of energy levels with respect to the inertial parameters for both the excited and the ground states. Finally a "best set" of moments of inertia and band center was calculated by using the method of least squares on 51 lines.

[8] Cross, Hainer, and King, J. Chem. Phys. **12**, 210 (1944).

These adjusted parameters completely account for all observed peaks and demonstrate that the band is essentially *A*-type, *B* transitions being too weak to observe. The final calculated spectrum is reproduced in Fig. 1 under the experimental envelope. The interfering H_2S lines are also represented.[9]

Table I summarizes the results for the band center and inertial constants of the HDS band observed in this work together with values obtained from an analysis of microwave data for the ground state. The agreement is not satisfactory, but it can be resolved in the following

[9] Energies, intensities, centrifugal corrections, and derivatives are tabulated in: Glenn A. Crosby, thesis, University of Washington, 1954 (available from University Micro-films, Ann Arbor, Michigan).

TABLE I. Rotational parameters of HDS.

	Present work	Hillger and Strandberg	
A''	9.743	9.682	cm^{-1}
B''	4.922	4.844	cm^{-1}
C''	3.232	3.140	cm^{-1}
$A''-C''$	6.511	6.542	cm^{-1}
$B''-C''$	1.690	1.704	cm^{-1}
Δ''	0.101	0.244	$\times 10^{-40}$ g cm^2
A'	9.411		cm^{-1}
B'	5.019		cm^{-1}
C'	3.137		cm^{-1}
Δ'	0.371		$\times 10^{-40}$ g cm^2
ν_0	6140.0		cm^{-1}

manner: The microwave data were used directly to determine only two relations involving the three moments of inertia of the ground state. For a third relation a theoretical value of Δ'', the inertial defect

$$\Delta''=I''_C-I''_A-I''_B$$

was used involving the frequencies of the vibrational fundamentals. This value differs considerably from that obtained experimentally in this work (Table I) and can account for the major part of the discrepancy existing between the two sets of effective moments of inertia. However, the difference $(B''-C'')$ and $(A''-C'')$ which are observed directly in the microwave region can properly be compared with the same quantities in the present work. The agreement is still not completely satisfactory, but part of the difference possibly can be explained. In the microwave determination $(B''-C'')$ is observed directly and involves energy levels which have very small centrifugal distortion corrections. In the infrared analysis, however, B'' and C'' are both determined independently using all lines and then the difference computed, thus making the combined uncertainty in $B''-C''$ larger. Therefore, it is not too unreasonable to attribute the difference in $(B''-C'')$ between the two sets of measurements as essentially due to experimental error. The value of $(A''-C'')$ as determined in the infrared work is again subject to the uncertainty of both A'' and C'', but this discrepancy seems rather large for explanation as just experimental error. However, part of the disagreement could arise from the different centrifugal distortion corrections applied in the two cases. Since both corrections were approximate, it is probable that an accurate determination of $(A''-C'')$ can best be obtained by using more exact distortion corrections on a microwave spectrum.

TABLE II. Centrifugal distortion constants of HDS.

	Present investigation		Hillger and Strandberg		
	Ground state	Excited state	Ground state (calc)	Ground state (obs)	
A_1	−0.201	−0.192			$\times 10^{-4}$ cm
A_2	+0.964	+0.882			$\times 10^{-4}$
A_3	−1.324	−1.148			$\times 10^{-4}$ cm^{-1}
A_4	+29.724	+25.119			$\times 10^{-4}$ cm^{-1}
A_5	+59.813	+50.229			$\times 10^{-4}$ cm^{-1}
A_6	−8.633	−7.454			$\times 10^{-4}$
σ	+6.724	+5.730			
D_J	+8.017	+8.269	+8.28		$\times 10^{-5}$ cm^{-1}
D_K	−4.359	−4.670	−1.64		$\times 10^{-4}$ cm^{-1}
D_{JK}	+9.115	+8.728	+9.16	+9.133	$\times 10^{-4}$ cm^{-1}
R_5	−2.299	−2.225	−2.21	−2.808	$\times 10^{-4}$ cm^{-1}
R_6	−0.357	−0.420	−1.90	+0.695	$\times 10^{-5}$ cm^{-1}
δ_J	+2.834	+3.193	+2.69	+2.531	$\times 10^{-5}$ cm^{-1}

VIBRATIONAL ASSIGNMENT

As shown by Hillger and Strandberg the normal modes of HDS can be described approximately as a D−S stretch (ν_1), an H−S stretch (ν_3), and a bending mode (ν_2). It is also demonstrated that the A (least) and B (intermediate) inertial axes lie very closely along the D−S and H−S bonds, respectively. Since the 6140 cm^{-1} band is nearly pure A-type, the dipole moment vector derivative is essentially oriented along the D−S bond.

The magnitude of the value of Δ' for the excited state of HDS argues strongly for the inclusion of a bending mode (ν_2) in the assignment. Frequency considerations[5] then indicate the assignment $\nu_2+2\nu_3$.

TABLE III. Force constants of HDS.

	Present investigation[a]	Hillger and Strandberg	
f_{r_1}	4.28	4.25	$\times 10^5$ dyne/cm
f_{r_2}	4.28	4.33	$\times 10^5$ dyne/cm
f_θ	0.783	0.866	$\times 10^{-11}$ dyne-cm
f_{rr}	0.0035	0.04	$\times 10^5$ dyne/cm
$f_{r\theta}$	0.148	0.067	$\times 10^{-3}$ dyne

[a] Constants derived from those given in H. C. Allen's thesis, University of Washington, 1951.

The large hydrogen amplitude (ν_3) and hence the importance of anharmonicities would also account for the fairly high intensity of the band relative to other combinations falling in the same frequency range.

CENTRIFUGAL DISTORTION

According to Kivelson and Wilson[10] the energy of a rotational state (with distortion) is expressed by the formula $W=W_0+A_1W_0^2+A_2W_0J(J+1)+A_3J^2(J+1)^2+A_4J(J+1)\langle P_z^2\rangle+A_5\langle P_z^4\rangle+A_6W_0\langle P_z^2\rangle$. In the computation for HDS the approximation $(\partial W_0/\partial A)^2=\langle P_z^2\rangle^2=\langle P_z^4\rangle$ was made. Although this approximation is quite good for high τ levels, it gets progressively worse as one goes toward lower τ energy levels. But since the magnitude of the correction also decreases rapidly toward lower τ levels it becomes relatively unimportant.

Table II summarizes the geometry dependent constants used to calculate the centrifugal distortion corrections for HDS. The last six constants[10] are given for comparison with values calculated by Hillger and

[10] D. Kivelson and E. B. Wilson, Jr., J. Chem. Phys. **20**, 1575 (1952).

Strandberg[1] although only the A's were used for all distortion corrections in this work. The A's were derived from an assumed HDS geometry H−S =1.349 A, D−S=1.345 A <HSD=92°18′ based on previously determined geometries of H_2S[6] and D_2S[11] and employing the procedure of Kivelson and Wilson.[12] The excited state A's were calculated from experimental values of effective moments of inertia in the excited state while assuming the same bond angles and distances as for the ground state. Since centrifugal distortion is of such small consequence, the ground-state corrections could have been used for the excited state also without any significant effect on the final results for the moments of inertia.

Table III lists the force constants assumed for HDS and used for computing the constants given in Table II together with a set used by Hillger and Strandberg. Since the force constants employed in this work were derived from extrapolation to a nonvibrating H_2S molecule, the two sets are not equivalent.

ACKNOWLEDGMENTS

The authors are greatful to George E. Blomgren and to John T. Lund, Jr., for valuable assistance during the course of this work.

[11] Allen, Naylor, and Plyler (to be published).
[12] D. Kivelson and E. B. Wilson, Jr., J. Chem. Phys. 21, 1229 (1953).

THE JOURNAL OF CHEMICAL PHYSICS VOLUME 23, NUMBER 9 SEPTEMBER, 1955

Contributions of Fluctuations and Anisotropy to Dielectric Polarization in Polar Substances

FRANK E. HARRIS
Department of Chemistry, Harvard University, Cambridge, Massachusetts

(Received December 20, 1954)

The theory of dielectric polarization in polar substances is extended to include the effect of fluctuations in the dipole moments of the individual molecules. The effect of optical anisotropy is also taken into account. The resulting expression for the dielectric constant is identical in its leading terms to an earlier result of Harris and Alder, in which fluctuations are neglected, but differs significantly from an equation derived by Frohlich, which is here explicitly shown to involve an additional approximation. Application of the theory to gases is discussed briefly. It is pointed out that Onsager's formula for relating the permanent dipole moment of a molecule to its average moment in the dielectric involves an approximation which produces an incorrect limiting behavior at large volumes, so that it should not be applied to polar gases at normal pressures. Calculations are presented showing the various contributions to the dielectric polarization of gaseous ammonia. The fluctuation term contributes of the order of 20% of the term expressing the correlation in orientation of the average dipole moments. The theory is also applied to liquid water, using Pople's bendable hydrogen bonded model for that substance. In water the fluctuation term is but 6% of the direct correlation term, and opposite in sign. The results are discussed briefly.

I. INTRODUCTION

THE theory of dielectric polarization in polar substances was originally formulated in classical statistical mechanics by Kirkwood,[1] with remarkably few approximations for the limiting case where the dipolar molecules are assumed to be completely unpolarizable. Since the work of Kirkwood, there have been several attempts to describe consistently the effect of the distortion polarization upon the total polarization of the dielectric. The most complete such description is that of Harris and Alder,[2] who showed that the average polarization of a sample of dielectric could be written as a sum, one term of which represented the distortion polarization by the applied field, and the other term of which depended upon the average of the square of the instantaneous total electric moment of the sample, where the average is to be computed using distribution functions appropriate to the system in the absence of an external field. However, Harris and Alder made the approximation, common to all the existing treatments of polarization in polar dielectrics, that the fluctuations in the dipole moments of the individual molecules could be neglected, and that the dipole moment of each molecule could be approximated as the sum of its permanent moment and the average additional moment induced by its surroundings. Since there is a correlation between the instantaneous induced moment of a molecule and the positions of its neighbors, the fluctuations in the dipole moment of a molecule will be inter-related with fluctuations in its environment, and neglect of this relation must to some extent alter the calculated dielectric polarization. The result obtained by Harris and Alder differs from that obtained by Frohlich,[3] and, in the appropriate limit,

[1] J. G. Kirkwood, J. Chem. Phys. 7, 911 (1939).
[2] F. E. Harris and B. J. Alder, J. Chem. Phys. 21, 1031 (1953). This paper will be referred to as HA I.
[3] H. Frohlich, *Theory of Dielectrics* (Oxford University Press, London, 1949).

also differs from the equation of Onsager,[4] which is an approximation for systems possessing no short-range forces between neighboring molecules, so that the environment of a molecule can be represented as a continuous dielectric characterized only by macroscopic parameters.

Frohlich[5] has examined the theory as presented by Harris and Alder. He concludes that the entire difference between their result and his own is due to the omission of the aforementioned fluctuations, and he further states that his methods for calculating dielectric polarization do not involve either the omission of the fluctuations or any other equally serious approximation. Simultaneously, Harris and Alder[6] discussed the approximations necessary to obtain the Onsager equation, to which Frohlich's formula reduces in the absence of short-range forces between the dipoles, and pointed out that the additional approximations which were necessary should make the Onsager equation a less accurate approximation than the equation derived by Harris and Alder. This conclusion was reached, not because it was believed that Onsager committed an error in the derivation of his equation, but because his model is not as general as the statistical mechanical treatment. At that time, no explicit discussion was made of the exact location of the approximations made in the derivation of Frohlich's equation.

The present paper is primarily devoted to further development of the theory of dielectric polarization in polar substances, so as to include the effect of the fluctuations. It is found that the now more complete theory, which does not contain the approximation to which Frohlich attributed the difference between his result and that of Harris and Alder, agrees with the theory of Harris and Alder in its leading terms, and that the higher terms, which depend upon microscopic properties of the molecular systems, are small relative to the difference between Harris and Alder's and Frohlich's formulas. In addition, for the sake of completeness, a further discussion is included explicitly setting forth the reasons why Frohlich obtains a less accurate result. It is therefore shown that not only is the difference between the formulas of Frohlich and of Harris and Alder due to an approximation in the derivation of Frohlich's equation, but that when the main approximation made in the derivation of the equation of Harris and Alder is removed, their equation is identical to the limiting form of the more precise equation, whereas that of Frohlich is not.

In addition to the inclusion of the effect of fluctuations, it also proved to be convenient to treat the additional contributions arising from optical anisotropy of the molecules. Since molecules possessing permanent electric moments may also possess polarizabilities along the direction of the moment which differ considerably from the polarizability in the perpendicular directions, the anisotropy may result in significantly different values of the induced moment relative to that calculated assuming the polarizability to be isotropic. Both the fluctuations and the anisotropy may be taken into account by combining, with the previous theory,[2] features of Kirkwood's procedure[7] for the discussion of fluctuations in nonpolar dielectrics arising from translational and rotational motion of the molecules. The expression for the field at a molecule of the dielectric is written in terms of the applied field and the positions and orientations of the other molecules. By suitable manipulation of this equation, it is possible to obtain a series expansion for the instantaneous moment of a given molecule in terms of the coordinates of all the other molecules, but independent of their instantaneous induced dipole moments. The leading terms, as mentioned above, account for the contributions to the dielectric polarization as previously developed,[2] while subsequent terms, dependent upon increasing powers of the molecular polarizability, represent the effects of fluctuation and anisotropy terms of corresponding orders.

In view of the close degree of approximation reached for gases when the fluctuation and anisotropy terms are included, it seemed also desirable to consider the extent of the approximations made in using the Onsager reaction field[4] to calculate the average dipole moment of a molecule in the system. While the Onsager calculation might be quite adequate for polar liquids where the intermolecular forces are not too strong, it is shown here that such a calculation cannot properly describe the limiting dipole moment for a polar gas at high dilution. In fact, the Onsager formula predicts that the reaction field, and hence the average induced moment, will approach zero at high dilution as the inverse second power of the volume, whereas a more exact treatment which considers the interaction between an isolated pair of molecules indicates a linear limiting dependence of the induced moment upon the inverse volume. It is further pointed out that the failure of Onsager's formula is a consequence of the *ad hoc* assumption that the cavity around a dipole, introduced in the derivation of that formula, is in volume equal to the volume available per molecule in the system. While such an assumption may be adequate in liquids, where the molecules are indeed packed together in a volume not much larger than that of the molecules themselves, in a gas neighboring molecules have an appreciable opportunity to approach to distances considerably closer than their average separation, and these closer encounters contribute to alter the limiting dependence of the induced moment upon volume.

II. BASIC DERIVATION

Consider a macroscopic spherical sample of the dielectric, in a vacuum, containing N molecules numbered

[4] L. Onsager, J. Am. Chem. Soc. **58**, 1486 (1936).
[5] H. Frohlich, J. Chem. Phys. **22**, 1804 (1954).
[6] F. E. Harris and B. J. Alder, J. Chem. Phys. **22**, 1806 (1954).
[7] J. G. Kirkwood, J. Chem. Phys. **4**, 592 (1936).

serially and in a volume V. Let the permanent electric dipole moment of the ith molecule be $\boldsymbol{\mu}_i$, and let its polarizability, which will not be assumed to be isotropic, be described by the symmetric dyadic $\boldsymbol{\alpha}^{(i)}$. Let $\mathbf{p}_i$ be the total dipole moment of the ith molecule, so that $\mathbf{p}_i$ is the vector sum of $\boldsymbol{\mu}_i$ and the induced moment created by the electric field at the ith molecule. It should be noticed that due to the varying environments of the various molecules of the sample, although $\boldsymbol{\mu}_i$ will differ only in direction from one molecule to another, $\mathbf{p}_i$ will differ both in direction and magnitude. The electric field, $\mathbf{F}_{ik}$, at the center of the ith molecule due to the dipole $\mathbf{p}_k$ of the kth molecule, is

$$\mathbf{F}_{ik}=-\mathbf{T}_{ik}\cdot\mathbf{p}_k \tag{1}$$

where $\mathbf{T}_{ik}$ is a symmetric dyadic defined as

$$\mathbf{T}_{ik}=\frac{1}{r_{ik}^3}\left[\mathbf{1}-\frac{3\mathbf{r}_{ik}\mathbf{r}_{ik}}{r_{ik}^2}\right],\quad i\neq k,\quad \mathbf{T}_{ii}=0, \tag{2}$$

where $\mathbf{1}$ is the unit dyadic, and $\mathbf{r}_{ik}$ is the vector distance from the center of molecule i to that of molecule k. Let a uniform external electric field be applied by a fixed charge distribution such that, in the absence of the sample, the field strength would be $\mathbf{E}_0$. Then, at each molecule i of the sample, the total electric field may be regarded as the sum of $\mathbf{E}_0$ and the dipole fields $\mathbf{F}_{ik}$, $(k=1,\cdots,N)$, if the field strength associated with the higher multipole moments of the molecules is neglected. If it is further assumed that the induced moment of each molecule can be calculated from the field at its center, the moment $\mathbf{p}_i$ may be expressed in the form

$$\mathbf{p}_i=\boldsymbol{\mu}_i+\boldsymbol{\alpha}^{(i)}\cdot\mathbf{E}_0-\boldsymbol{\alpha}^{(i)}\cdot\sum_k\mathbf{T}_{ik}\cdot\mathbf{p}_k.\quad i=1,\cdots,N. \tag{3}$$

The problem under consideration is the evaluation, in terms of quantities not *a priori* unknown, of the statistical mechanical average of the quantities $\mathbf{p}_i$, whose instantaneous values are related as in Eq. (3).

Following Kirkwood's procedure for nonpolar dielectrics,[7] one may recognize that Eqs. (3) may be written as a single operator equation in Hilbert space,

$$[\mathbf{I}+(\boldsymbol{\alpha}\cdot\mathbf{T})]\cdot(\mathbf{p})=(\boldsymbol{\mu}+\boldsymbol{\alpha}\cdot\mathbf{E}_0) \tag{3'}$$

where $\mathbf{I}$ is the identity operator, whose diagonal elements are all equal to the unit dyadic $\mathbf{1}$, and $(\boldsymbol{\alpha}\cdot\mathbf{T})$ is an operator with elements $\boldsymbol{\alpha}^{(i)}\cdot\mathbf{T}_{ik}$, and $(\mathbf{p})$ and $(\boldsymbol{\mu}+\boldsymbol{\alpha}\cdot\mathbf{E}_0)$ are vectors with components $\mathbf{p}_i$ and $\boldsymbol{\mu}_i+\boldsymbol{\alpha}^{(i)}\cdot\mathbf{E}_0$, respectively. Multiplying both sides of Eq. (3′) on the left by $[\mathbf{I}+(\boldsymbol{\alpha}\cdot\mathbf{T})]^{-1}$, one may obtain

$$(\mathbf{p})=[\mathbf{I}+(\boldsymbol{\alpha}\cdot\mathbf{T})]^{-1}(\boldsymbol{\mu}+\boldsymbol{\alpha}\cdot\mathbf{E}_0). \tag{4}$$

Introducing the expansion for $[\mathbf{I}+(\boldsymbol{\alpha}\cdot\mathbf{T})]^{-1}$ in powers of $(\boldsymbol{\alpha}\cdot\mathbf{T})$,

$$[\mathbf{I}+(\boldsymbol{\alpha}\cdot\mathbf{T})]^{-1}=\sum_{n=0}^{\infty}(-\boldsymbol{\alpha}\cdot\mathbf{T})^n, \tag{5}$$

one may write a component of (4) in the form

$$\mathbf{p}_i=\sum_{n=0}^{\infty}\sum_{k=1}^{N}[(-\boldsymbol{\alpha}\cdot\mathbf{T})^n]_{ik}\cdot\boldsymbol{\mu}_k+\sum_{n=0}^{\infty}\sum_{k=1}^{N}[(-\boldsymbol{\alpha}\cdot\mathbf{T})^n]_{ik}\cdot\boldsymbol{\alpha}^{(k)}\cdot\mathbf{E}_0. \tag{6}$$

The total instantaneous moment of the sample, $\mathbf{M}$, is simply the sum over all molecules i of $\mathbf{p}_i$. If the discussion be restricted to isotropic media, so that it is only necessary to consider the average component of $\mathbf{M}$ in the direction $\mathbf{e}$ of the applied field, it is possible to use the formalism already developed for dielectric polarization in systems where the fluctuations were neglected. Using the development of HA I, note that $\mathbf{M}$ as given by Eq. (6) is a sum of two terms, the first of which depends only on the coordinates of all the molecules, and the second of which depends also upon the applied field. Accordingly, it is possible to identify the first term as $\mathbf{M}_0$ of HA I, and the second term as $\mathbf{M}_d$,

$$\mathbf{M}_0=\sum_{n=0}^{\infty}\sum_{i,k=1}^{N}[(-\boldsymbol{\alpha}\cdot\mathbf{T})^n]_{ik}\cdot\boldsymbol{\mu}_k\equiv\sum_{i=1}^{N}\mathbf{p}_i^0 \tag{7}$$

$$\mathbf{M}_d=E_0\sum_{n=0}^{\infty}\sum_{i,k=1}^{N}[(-\boldsymbol{\alpha}\cdot\mathbf{T})^n]_{ik}\cdot\boldsymbol{\alpha}^{(k)}\cdot\mathbf{e} \tag{8}$$

where $\mathbf{p}_i^0$ is the total moment of the ith molecule excluding that part explicitly dependent upon $\mathbf{E}_0$. In HA I it was demonstrated, in a manner not involving approximate treatment of the fluctuation terms, that through terms linear in the applied field, the average component of $\mathbf{M}$ in the direction $\mathbf{e}$, for applied field $\mathbf{E}_0$, is [see Eq. (8) of HA I]

$$\langle\mathbf{M}\cdot\mathbf{e}\rangle_{E_0}=\frac{E_0}{kT}\langle(\mathbf{M}_0\cdot\mathbf{e})^2\rangle_s+\langle\mathbf{M}_d(\mathbf{E}_0)\cdot\mathbf{e}\rangle_s \tag{9}$$

where the quantities in angular brackets with the subscripts s on the right-hand side of the equation represent statistical mechanical averages to be calculated for the spherical sample using potentials valid in the absence of an applied field.

The argument for the treatment of the distortion polarization term of (9) follows exactly that valid when the fluctuations are neglected, so that [see HA I, Eq. (11)]

$$\langle\mathbf{M}_d(\mathbf{E}_0)\cdot\mathbf{e}\rangle_s=\frac{3V}{4\pi}\left(\frac{\epsilon_\infty-1}{\epsilon_\infty+2}\right)E_0 \tag{10}$$

where ϵ_∞ represents the dielectric constant at frequencies high compared to those such that orientation has time to take place. The quantities ϵ_∞ and n^2 differ in that the atomic polarization, which is not included in n^2 as measured at optical frequencies, is to be included at its full value in ϵ_∞. It should be pointed out, however, that although Eq. (10) is exactly what one would pre-

dict using the Clausius-Mossotti equation, the assumptions necessary to use that equation have not been made, and therefore ϵ_∞ is not to be related to the molecular polarizability by the Clausius-Mossotti formula, but rather by direct evaluation of the average on the left side of Eq. (10). Since $\mathbf{M}_d$ as given in Eq. (8) is similar to the form obtained originally by Kirkwood in his treatment of nonpolar dielectrics, the present development shows that his result describes the behavior of the distortion polarization of a polar substance. In comparing Eqs. (8) and (10) with Kirkwood's results, it must be remembered that the averages given here are to be computed for a spherical sample, whereas Kirkwood's are for a disk-shaped sample, and the difference in surface shape accounts for the apparent difference in the formulas.

Returning to the orientation polarization term, observe, that since the probability of a configuration is totally independent of $\mathbf{e}$, $\langle(\mathbf{M}_0\cdot\mathbf{e})^2\rangle_s$ may be replaced by $\langle\frac{1}{3}M_0^2\rangle_s$. In addition, introduce the defining equation

$$\frac{\epsilon-1}{4\pi}E=\frac{\langle\mathbf{M}\cdot\mathbf{e}\rangle_{E_0}}{V}$$

where E is the macroscopically calculated field in the sample and is related to E_0 by $E=[3/(\epsilon+2)]E_0$. Then, one may obtain

$$\frac{\epsilon-1}{\epsilon+2}=\left(\frac{4\pi}{9VkT}\right)\langle M_0^2\rangle_s+\frac{\epsilon_\infty-1}{\epsilon_\infty+2}. \tag{11}$$

Further attention must now be given to $\langle M_0^2\rangle_s$. Using the definition of $\mathbf{p}_i^0$, one may write, remembering that all the molecules i are *a priori* equivalent

$$\langle M_0^2\rangle_s=N\langle\mathbf{p}_i^0\cdot\langle\mathbf{M}_i\rangle_s\rangle, \tag{12}$$

where $\langle\mathbf{M}_i\rangle_s$ is the average total moment of the sample for the given value of $\mathbf{p}_i^0$, the average to be computed for the spherical specimen. Notice that the final averaging, over $\mathbf{p}_i^0\cdot\langle\mathbf{M}_i\rangle_s$, is independent of the presence of a spherical surface of the sample, since the local environment, which determines $\mathbf{p}_i^0$, is, except for the negligible proportion of the molecules near the surface, independent of its presence. However, $\langle\mathbf{M}_i\rangle_s$ does differ from the average moment of the entire sample in the absence of the spherical surface, because the spherical sample possesses a small uniform polarization which becomes independent of the size of the sphere when its radius becomes large. If the average moment of the entire sample when immersed in an infinite and boundless dielectric be represented by $\langle\mathbf{M}_i\rangle$, it has been shown that [see HA I, Eq. (9), and HA I, Appendix I]

$$\langle\mathbf{M}_i\rangle_s=\left(\frac{2}{\epsilon+2}\right)\left(\frac{3\epsilon}{2\epsilon+1}\right)\langle\mathbf{M}_i\rangle. \tag{13}$$

Returning now to the definition of $\mathbf{M}_i$, and using Eqs. (12) and (13), it may be seen that the argument leading to Eq. (12) may be reversed, leading to an equation analogous to Eq. (11), but in which the average is to be computed for a sample of infinite extent.

$$\frac{\epsilon-1}{\epsilon+2}=\left(\frac{4\pi}{9VkT}\right)\left(\frac{3}{\epsilon+2}\right)\left(\frac{3\epsilon}{2\epsilon+1}\right)\langle M_0^2\rangle+\frac{\epsilon_\infty-1}{\epsilon_\infty+2}. \tag{14}$$

Substitution into Eq. (14) from Eq. (7) leads to a more explicit expression

$$\frac{\epsilon-1}{\epsilon+2}-\frac{\epsilon_\infty-1}{\epsilon_\infty+2}=\left(\frac{3}{\epsilon+2}\right)\left(\frac{3\epsilon}{2\epsilon+1}\right)\left(\frac{4\pi N\mu^2 g_0}{9VkT}\right) \tag{14'}$$

where

$$N\mu^2 g_0=\sum_{n,n'=0}^{\infty}\sum_{i,k,i',k'=1}^{N}$$

$$\times\langle\mathfrak{y}_{k'}\cdot[(-\mathbf{T}\cdot\boldsymbol{\alpha})^{n'}]_{k'i'}\cdot[(-\boldsymbol{\alpha}\cdot\mathbf{T})^{n}]_{ik}\cdot\mathfrak{y}_k\rangle. \tag{14''}$$

The dielectric correlation parameter g_0 defined in Eq. (14'') is not an exact generalization of the quantity g introduced in the previous theory,[1,2] as g_0 is to be used with the permanent moment μ, rather than the average total moment. This fact is signified by the subscript 0.

III. GENERAL DISCUSSION

The dielectric polarization has been related in the preceding section to a sum of averages of the kind appearing in Eq. (14''). Each term of that sum can be regarded as the average component of a dipole moment at molecule i' along the direction of a dipole moment at molecule i. The terms for $n=n'=0$ represent the average correlation of the permanent moments at i and i', while nonzero values of n or n' characterize terms involving induced dipole moments of order n or n' at molecules i or i' respectively. An induced dipole moment of order n here refers to that dipole moment induced at a molecule by a dipole moment of order $n-1$ on some other molecule. It is readily seen that the summands of Eq. (14'') may be divided among two types, the first of which includes only terms for which $i'=i$, the remaining terms, for which $i\neq i'$, being of the second type. In many instances it might be expected that the terms of the first type would be larger than otherwise corresponding terms of the second type, since there would be expected to be, on the average, a correlation between quantities at the same molecule even under conditions such that the correlation between quantities at different molecules is small. In fact, the terms of the first type are responsible for the increase with concentration of the average total dipole moment over the permanent moment, whereas frequently even the leading term of the second type, $\mathfrak{y}_{i'}\cdot\mathfrak{y}_i$, representing the correlation between the permanent moments of a pair of distinct molecules, contributes negligibly relative to μ_i^2.

In general, it will not be possible to evaluate Eq. (14″) in closed form even for relatively simple models of polar systems, and use must be made of the existing series form. Expanding g_0, keeping all terms through order α, and rearranging dummy indices whenever this permits consolidation of similar terms,

$$\mu^2 g_0=\mu^2+(N-1)\langle\mathfrak{y}_1\cdot\mathfrak{y}_2\rangle -2(N-1)\{\langle\mathfrak{y}_1\cdot\mathbf{T}_{12}\cdot\boldsymbol{\alpha}^{(2)}\cdot\mathfrak{y}_1\rangle+\langle\mathfrak{y}_1\cdot\mathbf{T}_{12}\cdot\boldsymbol{\alpha}^{(2)}\cdot\mathfrak{y}_2\rangle +(N-2)\langle\mathfrak{y}_1\cdot\mathbf{T}_{12}\cdot\boldsymbol{\alpha}^{(2)}\cdot\mathfrak{y}_3\rangle\}+\cdots. \quad (15)$$

When Eq. (15) is to be used for a system where the individual molecules are assumed to be localized, as in a crystalline solid, the averages on the right-hand side must include the average over all choices of the molecules indicated by subscripts. The terms of the first type are μ^2 and $\langle\mathfrak{y}_1\cdot\mathbf{T}_{12}\cdot\boldsymbol{\alpha}^{(2)}\cdot\mathfrak{y}_2\rangle$, while the remaining terms shown are of the second type.

Under certain conditions, the polarizability tensor can be removed from some of the averages. For example, consider the situation when the dipole axis coincides with one of the principal axes of $\boldsymbol{\alpha}$, for which $\alpha=\alpha_{\parallel}$, and the polarizability in the other two characteristic directions is equal to $\alpha_\perp$, so that there is cylindrical symmetry. Then, letting $\mathbf{s}_1^{(i)}$ and $\mathbf{s}_2^{(i)}$ be unit vectors perpendicular both to each other and to $\mathfrak{y}_i$,

$$\boldsymbol{\alpha}^{(i)}=\alpha_{\parallel}\frac{\mathfrak{y}_i\mathfrak{y}_i}{\mu^2}+\alpha_\perp(\mathbf{s}_1^{(i)}\mathbf{s}_1^{(i)}+\mathbf{s}_2^{(i)}\mathbf{s}_2^{(i)}).$$

Then,

$$\langle\mathfrak{y}_1\cdot\mathbf{T}_{12}\cdot\boldsymbol{\alpha}^{(2)}\cdot\mathfrak{y}_2\rangle=\alpha_{\parallel}\langle\mathfrak{y}_1\cdot\mathbf{T}_{12}\cdot\mathfrak{y}_2\rangle \quad (16)$$

and

$$\begin{aligned}\langle\mathfrak{y}_1\cdot\mathbf{T}_{12}\cdot\boldsymbol{\alpha}^{(2)}\cdot\mathfrak{y}_1\rangle&=(\alpha_{\parallel}-\alpha_\perp)\left\langle\frac{(\mathfrak{y}_1\cdot\mathfrak{y}_2)}{\mu^2}(\mathfrak{y}_2\cdot\mathbf{T}_{21}\cdot\mathfrak{y}_1)\right\rangle\\&\quad+\alpha_\perp\Big\langle\frac{(\mathfrak{y}_1\cdot\mathfrak{y}_2)}{\mu^2}(\mathfrak{y}_2\cdot\mathbf{T}_{21}\cdot\mathfrak{y}_1)\\&\quad+(\mathfrak{y}_1\cdot\mathbf{s}_1^{(2)})(\mathbf{s}_1^{(2)}\cdot\mathbf{T}_{21}\cdot\mathfrak{y}_1)\\&\quad+(\mathfrak{y}_1\cdot\mathbf{s}_2^{(2)})(\mathbf{s}_2^{(2)}\cdot\mathbf{T}_{21}\cdot\mathfrak{y}_1)\Big\rangle\\&=(\alpha_{\parallel}-\alpha_\perp)\left\langle\frac{(\mathfrak{y}_1\cdot\mathfrak{y}_2)}{\mu^2}(\mathfrak{y}_2\cdot\mathbf{T}_{21}\cdot\mathfrak{y}_1)\right\rangle\\&\quad+\alpha_\perp\langle\mathfrak{y}_1\cdot\mathbf{T}_{21}\cdot\mathfrak{y}_1\rangle\end{aligned} \quad (17)$$

where the last step follows because

$$\frac{\mathfrak{y}_2\mathfrak{y}_2}{\mu^2}+\mathbf{s}_1^{(2)}\mathbf{s}_1^{(2)}+\mathbf{s}_2^{(2)}\mathbf{s}_2^{(2)}=\mathbf{1}.$$

Equation (14) gives an expression for the dielectric polarization in terms of the vacuum dipole moment and the polarizability tensor. However, for comparison with previous work, it is desirable to recast Eq. (14) into a form where the vacuum moment μ is replaced by m, the average total moment of a molecule in the dielectric. This restatement would be expected to remove the terms of the first type appearing in Eq. (14′) concomitantly with the change from μ to m. Let $\mathbf{m}_i$ be defined as

$$\mathbf{m}_i=\langle\mathbf{p}_i^0\rangle=\frac{\mathfrak{y}_i}{\mu^2}\langle\mathfrak{y}_i\cdot\mathbf{p}_i^0\rangle \quad (18)$$

since $\langle\mathbf{p}_i^0\rangle$ must, even for anisotropic molecules, be in the direction of $\mathfrak{y}_i$. Notice that since both $\mathfrak{y}_i$ and $\mathbf{p}_i^0$ are composed only of contributions of molecule i, it is immaterial whether the average is taken for a spherical or a boundless specimen. From the definition of $\mathbf{p}_i^0$, Eq. (18) is equivalent to

$$\mathbf{m}_i=\sum_{n=0}^{\infty}\sum_{j=1}^{N}\frac{\mathfrak{y}_i}{\mu^2}\langle\mathfrak{y}_i\cdot[(-\boldsymbol{\alpha}\cdot T)^n]_{ij}\cdot\mathfrak{y}_j\rangle. \quad (18')$$

It is then evident that

$$\begin{aligned}\langle M'^2\rangle&\equiv\sum_{ij}\langle\mathbf{m}_i\cdot\mathbf{m}_j\rangle\\&=\sum_{n,n'=0}^{\infty}\sum_{i,j,k,k'=1}^{N}\frac{\langle\mathfrak{y}_i\cdot\mathfrak{y}_j\rangle}{\mu^4}\langle\mathfrak{y}_i\cdot[(-\boldsymbol{\alpha}\cdot\mathbf{T})^n]_{ik}\cdot\mathfrak{y}_k\rangle\\&\quad\times\langle\mathfrak{y}_j\cdot[(-\boldsymbol{\alpha}\cdot\mathbf{T})^{n'}]_{jk'}\cdot\mathfrak{y}_{k'}\rangle\end{aligned} \quad (19)$$

where $\langle M'^2\rangle$ is defined by Eq. (19) so as to include the correlation in orientation of the average total moments, but not fluctuation contributions. With the aid of Eq. (19), Eq. (14) may be expressed in the form

$$\frac{\epsilon-1}{\epsilon+2}-\frac{\epsilon_\infty-1}{\epsilon_\infty+2}=\left(\frac{3}{\epsilon+2}\right)\left(\frac{3\epsilon}{2\epsilon+1}\right)\left(\frac{4\pi Nm^2g}{9VkT}\right), \quad (20)$$

$$\begin{aligned}Nm^2g&=\langle M'^2\rangle+\sum_{n,n'=0}^{\infty}\sum_{i,j,k,k'=1}^{N}\\&\quad\times\Big\{\langle\mathfrak{y}_i\cdot[(-\mathbf{T}\cdot\boldsymbol{\alpha})^n]_{ik}\cdot[(-\boldsymbol{\alpha}\cdot\mathbf{T})^{n'}]_{k'j}\cdot\mathfrak{y}_j\rangle\\&\quad-\frac{1}{\mu^4}\langle\mathfrak{y}_i\cdot[(-\mathbf{T}\cdot\boldsymbol{\alpha})^n]_{ik}\cdot\mathfrak{y}_k\rangle\langle\mathfrak{y}_k\cdot\mathfrak{y}_{k'}\rangle\\&\quad\times\langle\mathfrak{y}_{k'}\cdot[(-\boldsymbol{\alpha}\cdot\mathbf{T})^{n'}]_{k'j}\cdot\mathfrak{y}_j\rangle\Big\}\end{aligned} \quad (20')$$

where g is the correlation parameter as defined in previous work.[1,2] In obtaining Eq. (20′) the dummy indices have been arranged so as to emphasize that the quantities in curly brackets are fluctuation terms. By direct expansion it may be verified that the term $n=n'=0$ vanishes so that the leading term of the sum in Eq. (20′) is of order α. The expansion of (20) com-

parable to (15) is

$$m^2g=m^2+(N-1)\langle\mathbf{m}_1\cdot\mathbf{m}_2\rangle-2(N-1)$$
$$\times\Big\{\langle\boldsymbol{\mu}_1\cdot\mathbf{T}_{12}\cdot\boldsymbol{\alpha}^{(2)}\cdot\boldsymbol{\mu}_1\rangle+(N-2)\langle\boldsymbol{\mu}_1\cdot\mathbf{T}_{12}\cdot\boldsymbol{\alpha}^{(2)}\cdot\boldsymbol{\mu}_3\rangle$$
$$-\frac{(N-1)}{\mu^4}\langle\boldsymbol{\mu}_1\cdot\mathbf{T}_{12}\cdot\boldsymbol{\alpha}^{(2)}\cdot\boldsymbol{\mu}_2\rangle\langle\boldsymbol{\mu}_2\cdot\boldsymbol{\mu}_3\rangle\Big\}+\cdots. \quad (21)$$

While Eqs. (14) and (20) must given identical results if evaluated precisely, Eq. (20) provides the additional possibility of combining a value of m obtained on the basis of an approximate treatment with a calculation of $\langle\mathbf{m}_1\cdot\mathbf{m}_2\rangle$ to yield a result, neglecting fluctuations, much more easily than by solution of the entire problem. Since the Onsager formula,[4]

$$m=\mu\left(\frac{\epsilon_\infty+2}{3}\right)\left(\frac{2\epsilon+1}{2\epsilon+\epsilon_\infty}\right) \quad (22)$$

yields a satisfactory approximate relation between m and μ in many liquids where the short-range forces are not too strong, Eq. (20) is likely to be useful even when Eq. (14) is not.

One may now see that the expression in terms of m, Eq. (20), is identical to the expression given by Harris and Alder[2] if, in Eq. (20′), the fluctuation terms are suppressed. In subsequent sections calculations will be presented which verify that in the systems considered the fluctuation terms are indeed small relative to the leading terms of Eq. (20′), so that their suppression is a legitimate initial approximation. Note also that the fluctuation terms involve averages which are not simple expressions in terms of macroscopic quantities, but are only conveniently evaluated on a microscopic basis, so that the difference between the result of Harris and Alder and that of Frohlich[3,5] cannot be explained in terms of the fluctuation contributions to the dielectric polarization.

It is therefore of interest to examine more closely the derivation[5] of Frohlich's formula to determine what approximations were introduced to cause that formula to differ from Eq. (20). First, a particular molecular model was used consisting of a rigid dipole embedded in a continuous sphere of dielectric, rather than characterizing the molecules only in terms of μ and α. The adoption of this model requires the assumption of spherical symmetry for α, but otherwise should not affect the dielectric behavior to a first approximation. A more important approximation in Frohlich's formula actually lies in the conversion of $\langle M_0^2\rangle_s$ to another, more tractable expression. As was shown in HA I, and also in the present paper in the argument leading from Eq. (11) to Eq. (14),

$$\langle M_0^2\rangle_s=\left(\frac{3}{\epsilon+2}\right)\left(\frac{3\epsilon}{2\epsilon+1}\right)\langle M_0^2\rangle \quad (23)$$

where the derivation of Eq. (23) depends upon arguments involving macroscopic quantities only, and in no way involves imprecise treatment of fluctuations. In obtaining Eq. (23), one of the factors $\mathbf{M}_0$ was decomposed into contributions of single molecules, $\mathbf{p}_i^0$, as in Eq. (12), following which the average $\langle\mathbf{M}_i\rangle_s$ appearing in Eq. (12) was evaluated [cf. Eq. (13)] by methods first used by Kirkwood[1] and discussed further in HA I. Examination of the derivation of Eq. (13) (see HA I, Appendix I) shows that that equation can only be obtained when the entire dipole moment which is fixed in position (i.e. $\mathbf{p}_i^0$) is contained in a region at the center of the spherical sample which is small relative to the radius of the sample. This condition is necessary because in the derivation of Eq. (13) it is assumed that the probability of any value of $\mathbf{p}_i^0$ is the same in both the spherical and the boundless specimens considered. These probabilities will be equal if and only if the local field at $\mathbf{p}_i^0$ is independent of a surface at large distances. It is pointed out in HA I that the local field is independent of the presence of a surface if the aforementioned spatial restrictions are satisfied.

On the other hand, now consider what happens if a different decomposition of $\mathbf{M}_0$ than that used in Eq. (12) is employed. If, following Frohlich, $\mathbf{M}_0$ is expressed as a sum of moments $\mathbf{m}_i'$ each of which is the sum of the permanent moment of molecule i and the moment induced by it in each molecule of the spherical sample, one may write analogous to Eq. (12)

$$\langle M_0^2\rangle_s=N\langle\mathbf{m}_i'\cdot\langle\mathbf{M}_i\rangle_s'\rangle \quad (12')$$

where $\langle\mathbf{M}_i\rangle_s'$ is different from $\langle\mathbf{M}_i\rangle_s$ in that the former average is to be computed with $\mathbf{m}_i'$ fixed, in contrast to the latter average, which is to be computed with $\mathbf{p}_i^0$ fixed. If now one considers use of a formula for $\langle\mathbf{M}_i\rangle_s'$ corresponding to Eq. (13), it is clear that since an appreciable fraction of the charge distribution implied by $\mathbf{m}_i'$ is not in a portion of the spherical sample which is small relative to its over-all dimensions, Eq. (13) does not apply, and one may not conclude that $\langle\mathbf{M}_i\rangle_s'$ is the quantity calculated by Kirkwood. Frohlich's formula[3,5] is the result of approximating Eq. (23) by use of Eqs. (12′) and (13) with $\langle\mathbf{M}_i\rangle_s'$ in place of $\langle\mathbf{M}_i\rangle_s$, and thereby differs substantially from the expression to be obtained without making such an approximation.

It is of course possible to use Frohlich's molecular model in conjunction with the accurate expression (23) to obtain an equation describing the dielectric polarization, and if this is done, one obtains the equation previously derived by Harris and Alder.[2] The fluctuation terms do not appear, because in the use of Frohlich's model it is assumed that a system containing a number of dipolar molecules can be represented as a continuum of dielectric constant ϵ_∞ in which is embedded the requisite number of unpolarizable dipoles. In that model, the interactions between molecules, which in real

systems will cause inhomogeneous distribution of the polarizable matter, will have no such effect, and therefore the existence of fluctuations is not recognized by the model.

It is therefore clear that the difference between the formulas of Frohlich[3,5] and Harris and Alder[2] is not based upon different treatment of fluctuations, since both formulas neglect fluctuations, but is due to an approximation for $\langle Mo^2\rangle_s$ which is made by Frolich[3,5] but not by Harris and Alder.[2]

IV. APPLICATION TO GASEOUS SYSTEMS

Equation (14″) may be readily applied to gaseous systems by expanding each of the averages on the right-hand side of that equation in powers of $1/V$. Although the interaction potential between molecules cannot be separated into pair potentials, due to the presence of the polarizability terms, it is nevertheless possible to make an expansion by the methods developed originally for the equation of state.[8] It is not necessary, however, to discuss the general method in order to obtain the term corresponding to the second virial coefficient, i.e. the contribution dependent upon the interaction between an isolated pair of molecules. Therefore, rather than attempting to write down a more general expression, the present discussion will be limited to pairwise interactions, leading to a contribution to g_0 proportional to $1/V$. Analogously to the corresponding contribution to the equation of state, the coefficient of $1/V$ has been called the second dielectric correlation coefficient.[9] Since the primary objective at this time is to obtain an indication of the size of the fluctuation effect, it will be assumed that the polarizability is spherically symmetric, and that the intermolecular potential V_{12} for an isolated pair of molecules can be written in the form

$$V_{12}=V_{12}{}^0+V_{12}{}'=\lambda r_{12}{}^{-s}-cr_{12}{}^{-6}+V_{12}{}', \quad s>6 \tag{24}$$

where $V_{12}{}'$ is the part of the potential arising from the interaction of the dipoles on molecules 1 and 2, both permanent and induced. The first term of V_{12} is an empirical repulsion term, while the second term is the well-known Van der Waals attraction. The potential (24) is the same as that used in earlier work on the equation of state of polar gases by Lennard-Jones[10] and Stockmayer,[11] and was used by Harris and Alder[9] in their calculations, neglecting fluctuations, of the dielectric polarization. The term $V_{12}{}'$ may be expressed

$$\begin{aligned}V_{12}{}'&=\sum_{n,n'=0}^{\infty}(-\alpha)^{n+n'}\sum_{k,j=1,2}(\boldsymbol{\mu}_j\cdot(\mathbf{T}^n)_{jj'}\cdot T_{12}\cdot(\mathbf{T}^{n'})_{2k}\cdot\boldsymbol{\mu}_k)\\&=\sum_{n=0}^{\infty}(2n+1)(-\alpha)^{2n}(\boldsymbol{\mu}_1\cdot(\mathbf{T}_{12})^{2n+1}\cdot\boldsymbol{\mu}_2)\\&\quad+(n+1)(-\alpha)^{2n+1}\{(\boldsymbol{\mu}_1\cdot(\mathbf{T}_{12})^{2n+2}\cdot\boldsymbol{\mu}_1)\\&\qquad+(\boldsymbol{\mu}_2\cdot(\mathbf{T}_{12})^{2n+2}\cdot\boldsymbol{\mu}_2)\}\end{aligned} \tag{25}$$

where use has been made of the fact that $\mathbf{T}_{12}=\mathbf{T}_{21}$, and all terms involving molecules other than 1 and 2 have been suppressed.

The portion of Eq. (14″) containing terms through order $1/V$ may be written down in a simple form for optically isotropic molecules. Performing the summations over i, k, i', k', neglecting all terms involving more than a pair of molecules, it is possible to see that

$$\begin{aligned}\mu^2g_0=\mu^2+(N-1)\langle\boldsymbol{\mu}_1\cdot\boldsymbol{\mu}_2\rangle+\sum_{n=1}^{\infty}(N-1)(n+1)(-\alpha)^n\\\times\{\langle\boldsymbol{\mu}_i(\mathbf{T}_{12})^n\cdot\boldsymbol{\mu}_1\rangle+\langle\boldsymbol{\mu}_1\cdot(\mathbf{T}_{12})^n\cdot\boldsymbol{\mu}_2\rangle\}.\end{aligned} \tag{26}$$

The average values appearing in Eq. (26) may be written as power series in the polarizability by expansion of the factor $\exp(-V_{12}{}'/kT)$ in the formula for the average,

$$\begin{aligned}\langle f^{(1,2)}\rangle=\frac{1}{\Omega V}\int f^{(1,2)}\\\times\exp(-V_{12}{}^0/kT)\sum_{t=0}^{\infty}\frac{1}{t!}\left(-\frac{V_{12}{}'}{kT}\right)^t d\tau_{12}\end{aligned} \tag{27}$$

where the integration is to be extended over all relative positions $\mathbf{r}_{12}$ and all orientations. The quantity $V_{12}{}^0$ is defined in Eq. (24) and Ω is the normalizing factor for the integration over orientations. If the averages are all regarded as expanded in this way, Eq. (26) provides an expression for the second dielectric correlation coefficient in increasing powers of α. Calculations will only be made here including terms linear in α, so that but a small amount of numerical work need be carried out. Since it will be found that the fluctuation term of order α is less than 25% of the total dielectric correlation coefficient, it is to be presumed that higher order fluctuations amount to but a few percent of the total.

From Ha II, one may find that to order α,

$$\begin{aligned}\langle\boldsymbol{\mu}_1\cdot\boldsymbol{\mu}_2\rangle=\frac{\delta_1{}'\mu^2}{V}=\frac{\mu^2}{V}\cdot 2^6\pi\sigma^3y^{6/s}\\\times[\sum_{n=1}^{\infty}\sum_{t=0}^{\leq(n-1)/2}y^{(ns-6n+6t)/s}p^{2t+1}J_{n(2t+1)\,t}\\+p^2q\sum_{n=1}^{\infty}\sum_{t=0}^{\leq(n-2)/2}y^{(ns-6n+6t)/s}p^{2t}J_{n(2t+2)\,t}]\end{aligned} \tag{28}$$

[8] For example, see J. E. Mayer and M. G. Mayer, *Statistical Mechanics* (John Wiley and Sons, Inc., New York, 1940), or D. ter Haar, *Elements of Statistical Mechanics* (Rinehart and Company, Inc., New York, 1954).

[9] F. E. Harris and B. J. Alder, J. Chem. Phys. **21**, 1351 (1953). This paper will be referred to as HA II.

[10] J. E. Lennard-Jones, Proc. Roy. Soc. (London) **A106**, 463 (1924).

[11] W. H. Stockmayer, J. Chem. Phys. **9**, 398 (1941).

where the new quantities appearing in Eq. (28) are defined as follows:

$$\sigma^{s-6}=\frac{\lambda}{c},\quad y=\frac{c}{kT\sigma^6},\quad p=\frac{\mu^2\sigma^3}{c},\quad q=\frac{\alpha}{\sigma^3}.$$

The coefficients J_{nkl} are defined in HA II. By methods similar to those used to obtain Eq. (28), one may also find that to first order in α,

$$-\alpha\langle\mathfrak{y}_1\cdot\mathbf{T}_{12}\cdot\mathfrak{y}_1\rangle=\frac{\delta_1''\mu^2}{V}=\frac{\mu^2}{V}\cdot 2^5\pi\sigma^3 q \times\sum_{n=0}^{\infty}\sum_{k=0}^{\leq n/2} y^{(ns-6n+6k)/s}p^{2k}C_{nk}, \quad (29)$$

$$-\alpha\langle\mathfrak{y}_1\cdot\mathbf{T}_{12}\cdot\mathfrak{y}_2\rangle=\frac{\delta_1'''\mu^2}{V}=\frac{\mu^2}{V}\cdot 2^5\pi\sigma^3 q y^{3/s} \times\sum_{n=1}^{\infty}\sum_{k=0}^{\leq (n-1)/2} y^{(ns-6n+6k)/s}p^{2k+1}D_{nk} \quad (30)$$

where

$$C_{nk}=\frac{1}{s}\Gamma\left(\frac{6n-6k}{s}\right)\frac{2^{2k}(k+1)\,!^2}{(n-2k)\,!(2k+2)\,!(2k+3)\,!}\times\sum_{t=0}^{k}\frac{(2t)\,!}{t\,!^2}(3t-k), \quad (31)$$

$$D_{nk}=\frac{1}{s}\Gamma\left(\frac{6n-6k-3}{s}\right)\frac{2^{2k}(k+1)(k+1)\,!^2}{(n-2k-1)\,!(2k+3)\,!^2}\times\sum_{t=0}^{k+1}\frac{(2t)\,!}{t\,!^2}. \quad (32)$$

Observe that Eqs. (28), (29), and (30) define quantities δ_1', δ_1'', and δ_1''', such that, to order α,

$$g_0=1+\frac{(N-1)}{V}(\delta_1'+2\delta_1''+2\delta_1''')=1+\frac{N\delta_1}{V} \quad (33)$$

where the difference between N and $N-1$ is neglected, and the quantity δ_1 is defined as the second dielectric correlation coefficient. Note that δ_1 is referred to the expression in terms of g_0 and μ, rather than to that in terms of g and m, so that its value is independent of any assumed relation between μ and m.

The computations performed in HA II, in which fluctuations were neglected, were made using the leading term of Eq. (20′), with m related to μ by the Onsager formula (22). To first order in N/V and α,

$$g=1+\frac{(N-1)}{V}(\delta_1'+2\delta_1'') \quad (34)$$

using the fact that $\mathbf{m}_i$ and $\mathfrak{y}_i$ are parallel and equal in magnitude except for terms of order $1/V$. Since $\mu^2 g_0$ and $m^2 g$ are equivalent expressions of the same quantity, Eqs. (33) and (34) can be seen to be consistent to order $1/V$ when the expression (18) is used to relate m and μ. To order $1/V$, Eq. (18) indicates for spherically symmetric α,

$$\frac{m}{\mu}-1=\left(\frac{N-1}{V}\right)\delta_1'''. \quad (35)$$

Equation (35) is to be contrasted with the Onsager formula (22). Equation (22) may also be expanded in powers of $1/V$, using the fact that the Clausius-Mossotti equation is valid in the limit of large V, giving to order $(1/V)^2$

$$\frac{m}{\mu}-1=\left(\frac{N}{V}\right)^2\left(\frac{32\pi^2\alpha}{9}\right)\left(\frac{\mu^2}{3kT}+\alpha\right). \quad (36)$$

The fact that Eq. (36) predicts a dependence of $(m/\mu)-1$ as $(1/V)^2$ as opposed to the limiting $1/V$ dependence of Eq. (35) means that the Onsager formula becomes increasingly inaccurate at large volumes. The reason for this incorrect limiting behavior lies in the *ad hoc* assumption of the Onsager formulation that the effect of the neighbors on a molecule may be calculated by considering the given molecule to be in a cavity of the volume per molecule, cut in material of the macroscopic dielectric constant. Since at large volumes the cavity becomes large relative to the volume of the molecule itself, the probability of finding neighboring molecules entering the cavity increases with dilution, and the effect of these close neighbors is not included in the Onsager model. But the major contribution to the induced moment arises from just these interactions at short distances, whose effect only diminishes as V is increased due to a decreasing number of molecular pairs at short distances, therefore being proportional to N/V. However, the Onsager formulation in addition effectively increases the molecular diameter as the volume increases, so that the over-all effect decreases as V^{-2}. The arguments of this paragraph indicate on the other hand that in denser systems, particularly liquids, where the molecular volume and the volume per molecule are not seriously disparate, the Onsager formula should remain as a good approximation whenever the intermolecular forces are not too strong.

TABLE I. The contributions to the second dielectric correlation coefficient of ammonia. The three terms represent, respectively, the effects of direct correlation of orientation of a pair of permanent moments, first-order fluctuations in the induced moment, and average induced moment.

Temp. °K	δ_1'	$2\delta_1''$ liters/mole	$2\delta_1'''$	δ
323	0.0190	0.0037	0.0236	0.0463
373	0.0103	0.0022	0.0171	0.0296
423	0.0063	0.0015	0.0131	0.0209
473	0.0042	0.0010	0.0107	0.0159

TABLE II. Relation between average total moment m and permanent moment μ for ammonia at various volumes according to (a) the Onsager formula and (b) actual calculation. Tabulated quantity is $(m/\mu)-1$.

Temp. °K	10 liters/mole (a)	10 liters/mole (b)	0.1 liter/mole (a)	0.1 liter/mole (b)
323	1.18×10^{-3}	1.10×10^{-6}	1.18×10^{-1}	1.10×10^{-2}
373	0.86	1.04	0.86	1.04
423	0.66	0.98	0.66	0.98
473	0.53	0.95	0.53	0.95

To obtain an estimate of the relative importance of the fluctuation term δ_1, and to see how much difference exists between the Onsager moment and that given by (35), calculations were performed for ammonia using the experimental values of μ and α, and the values of σ and c found in HA II to best represent the second pressure virial coefficient. The calculation was only made for $s=\infty$, representing a rigid sphere core potential. As may be seen by inspection of Table I, the fluctuation term $2\delta_1''$ is of the order of 20% of the term δ_1' calculable independently of consideration of the fluctuations. The contribution from the fluctuation remains a constant fraction of the total correlation in orientation at large volumes.

The remaining term, $2\delta_1'''$, is related to the difference between the vacuum moment and the average moment of an ammonia molecule in the gas. Table I shows that the contribution from this source is more important than either of the terms arising from the correlation in orientations. If the average moment m in the gas is computed from the given values of δ_1''' and μ, a comparison may be made with values of m as calculated from the Onsager equation. Because of the incorrect limiting behavior of the Onsager formula, it is necessary to make comparison at definite volumes, as has been done in Table II. In that table, values of $(m/\mu)-1$ are tabulated at volumes of 10 and 0.1 liters per mole, showing that until quite high pressures are reached, the Onsager formula grossly underestimates the increase in m due to interaction between a molecule and its neighbors.

V. APPLICATION TO LIQUID WATER

To obtain an indication of the relative importance of the fluctuation terms in a polar liquid where there is considerable correlation between the orientations of neighboring dipoles, consider the dielectric polarization of liquid water. As in HA I, calculations will be made using a bendable hydrogen bonded model discussed by Pople.[12] It is definitely more convenient to use Eq. (20′) here rather than its counterpart Eq. (14″). The average moment m has been calculated by Pople, including the effects of nearest neighbors, and the correlation parameter, neglecting fluctuations,

$$g'm^2=m^2+(N-1)\langle\mathbf{m}_1\cdot\mathbf{m}_2\rangle$$

has been evaluated through the third shell of neighbors, at which point the additional contribution from further outlying shells not included appears to be of the order of 1% of the total. In both calculations optical isotropy is assumed.

The fluctuation term of order α, the leading term omitted in g', expresses the difference between (i),

$$\langle-\alpha\sum_{\substack{j,k\\ j\neq1}}(\boldsymbol{\mu}_k\cdot\mathbf{T}_{kj}\cdot\boldsymbol{\mu}_1)\rangle,$$

μ times the average component in the direction of the permanent dipole of molecule 1, of the moment induced at a molecule j by all the permanent dipoles, summed over all molecules $j\neq1$, and (ii)

$$\sum_{\substack{j,k\\ j\neq1}}\langle-\alpha(\boldsymbol{\mu}_k\cdot\mathbf{T}_{kj}\cdot\boldsymbol{\mu}_j)\rangle\left\langle\frac{\boldsymbol{\mu}_j\cdot\boldsymbol{\mu}_1}{\mu^2}\right\rangle,$$

μ times the component, in the direction of the permanent dipole of molecule 1, of the average moment induced at molecule j by all the permanent dipoles, also summed over $j\neq1$, where the average in (ii) is to be taken without specifying the orientation of molecule 1. The quantities described by (i) and (ii) may be calculated on Pople's model, as far as the contributions of molecules which are nearest neighbors of j simply by successive resolution of dipole moment components and averaging the effects of the rotation about the hydrogen bonds, which in Pople's model are assumed to rotate freely. The effect of the bending of the hydrogen bonds is allowed for by assuming each bond to be permanently bent to an angle θ, where $\cos\theta\sim1-kT/g_b$ is the average value of the cosine of the deformation angle when the bending force constant is g_b.[12] Pople's value of g_b is 3.78×10^{-13} erg. The effect of the bending is computed by averaging orientations of the permanently bent bond about the normal bond position.

The major contribution to (i) will arise when molecules j and 1 are nearest neighbors. It is found that all possible relative positions of 1 and j give the same result. To see how the calculation works out, suppose that molecule 1 is bonded to j through one of the hydrogens of j. There will be one other molecule, 2, also bonded through a hydrogen, with an angle $1-j-2$ between the two bonds equal to $\beta=105°$, the normal H−O−H angle in water. Two other molecules, 3 and 4, are bonded to j through its lone pair, and the angles $1-j-3$ and $1-j-4$ will have the value $\gamma=\cos^{-1}(-\cos^2\beta/2)$. Remembering that the dipole axis of each molecule makes an angle $\beta/2$ with the normal direction of each bond terminating on that molecule, it is possible by straightforward means to show that the average component in the direction of the dipole on 1 of the induced moment at j, arising from molecule 2, is

$$\frac{2\mu\alpha}{d^3}\cos^2\beta/2\,\cos\beta\,\cos^4\theta$$

[12] J. A. Pople, Proc. Roy. Soc. (London) **A205**, 163 (1951).

TABLE III. Correlation parameter and dielectric constant of liquid water.

Temp. °C	g'[a]	g''[b]	ϵ no fluctuations	ϵ complete calculation	ϵ experiment[c]
0	2.60	−0.15	90.7	83.7	88.2
25	2.55	−0.14	79.9	74.0	78.5
62	2.49	−0.14	65.7	60.2	66.4
83	2.46	−0.14	59.6	54.8	60.4

[a] Total correlation excluding fluctuations.
[b] Correlation effect of fluctuations.
[c] J. Wyman, Jr. and E. N. Ingalls, J. Am. Chem. Soc. **60**, 1182 (1938)

where d is the average distance between the centers of adjacent molecules. The corresponding average dipole moment component induced by molecule 3 is

$$-\frac{2\mu\alpha}{d^3}\cos^2\beta/2\cos\gamma\cos^4\theta$$

with an identical expression for the effect of molecule 4. Finally consider the moment induced at j by molecule 1 itself. Since the moment induced by 1 is correlated with the position of 1, more care is needed in averaging out the effects of the free rotations. One may show that the average dipole moment component induced by molecule 1 is

$$\frac{3\alpha\mu}{2d^3}(3\cos^2\beta/2\cos^2\theta-\cos^2\beta/2-\cos^2\theta+\tfrac{1}{3}).$$

Combining the above, and multiplying by μ, one may obtain the result of considering nearest neighbors to j,

$$-\alpha\sum_{j,k}\langle\mathfrak{y}_k\cdot\mathbf{T}_{kj}\cdot\mathfrak{y}_1\rangle=4\left(\frac{8\alpha\mu^2}{d^3}\right)\cos^4\beta/2\left[1-\frac{kT}{g_b}\right]^4$$
$$+4\left(\frac{\alpha\mu^2}{2d^3}\right)\left\{-4\cos^2\beta/2\left[1-\frac{kT}{g_b}\right]^4\right.$$
$$\left.+(9\cos^2\beta/2-3)\left[1-\frac{kT}{g_b}\right]^2-3\cos^2\beta/2+1\right\}. \quad (37)$$

The initial factor 4 appearing in Eq. (37) arises because there are 4 molecules j adjacent to 1.

The quantities necessary to evaluate (ii) to the same approximation to which (i) was evaluated have already been calculated by Pople. Including nearest neighbors of j, and assuming j and 1 are nearest neighbors,

$$-\frac{\alpha}{\mu^2}\sum_{j,k}\langle\mathfrak{y}_k\cdot\mathbf{T}_{kj}\cdot\mathfrak{y}_j\rangle\langle\mathfrak{y}_j\cdot\mathfrak{y}_1\rangle$$
$$=\frac{32\alpha\mu^2}{d^3}\cos^4\beta/2\left[1-\frac{kT}{g_b}\right]^4. \quad (38)$$

Although Pople has worked out the contributions to $\langle\mathfrak{y}_j\cdot\mathfrak{y}_1\rangle$ from shells beyond the first, it is more consistent not to include them here because similar contributions were not included in Eq. (37).

By insertion of Eqs. (37) and (38) into Eq. (20′), the correlation parameter g may be calculated. Calculations were made at 4 temperatures ranging from 0° to 83°C, as shown in Table III. In that table, g'' represents the difference between g as here calculated and g', the value of g neglecting fluctuations. As is apparent from the table, the fluctuation terms result in a decrease of approximately 6% in the dielectric constant, causing the calculated values to lie somewhat below the experimental results. As has been pointed out previously by Pople, and in HA I, omitted factors which may be responsible for the small deviation between the theoretical and experimental values include lack of treatment of effects arising from larger scale distortion of the water structure, and the approximation that the polarizability could be treated assuming spherically symmetric point molecules. The first of these effects would slightly decrease the calculated dielectric constant, while the second could account for an increase. The higher order fluctuation terms which have not thus far been included would be expected to be too small to materially affect the results now obtained.

It is of interest to observe that in the relatively rigid structure exhibited by liquid water as contrasted to a polar gas, the fluctuation effects are relatively a smaller part of the total dielectric polarization, and that, moreover, the fluctuations contribute to decrease the dielectric constant in water, whereas their effect is to increase it in the gas. The increase observed for the gas is the result to be expected in the absence of a rigid structure since the relative configurations of lowest interaction energy are also configurations where the dipoles are pointed in the same direction. In the liquid, then, the more rigid structure restricting the choice of configurations around any molecule would tend to decrease the size of the fluctuation effect, and it must be surmised that the specific structure will determine the sign of the effect.

Nuclear Magnetic Resonance: Structure of the Amino Group I*

R. A. KROMHOUT AND W. G. MOULTON
Departments of Physics and Pharmacology, University of Illinois, Chicago, Illinois
(Received November 27, 1954)

Line widths and second moments of the proton magnetic resonance absorption line of ten amines, amides, and amino acids have been measured. It is shown that hydrogen bonds in the amides and amino acids strongly affect the structure. New evidence for the existence of glycine in the dipolar form in the solid state is presented. The N—H bond distances in urea and glycine are calculated from observed second moments and are found to be 1.077±0.007 A and 1.074±0.014 A, respectively. The bond angles of the amino group are assumed tetrahedral in both cases in making the calculation.

ALTHOUGH there have been several investigations of ammonium halides by the method of nuclear magnetism,[1–3] there has been relatively little work on the amino group. Shaw[4] has concluded that glycine has the zwitterion structure in the solid. Andrew[5] has demonstrated the planarity of the urea molecule from second moment studies on a single crystal of urea. Gutowsky and Pake[6] studied the effect of temperature on the second moment and line width of methylamine.

We are, however, aware of no nuclear resonance work on the bond distances, nor of direct evidence for the effect of hydrogen bonds on the structure of the amino group. This paper is a report on nuclear resonance studies of a series of amines, amides, and amino acids. In the case of urea and of glycine, we have derived some detailed information about the structure from the second moments.

I. APPARATUS

The instrumentation was similar in design to that described by Gutowsky *et al.*[7] A feedback oscillator was used as a plate detector, and a 2.5-cc sample was placed in the tank coil. The tank coil and its surrounding shield were silver plated. A permanent magnet with a field strength of 5255 gauss was used for these experiments, the inhomogeneity over the sample being less than 0.1 gauss. The static magnetic field was modulated sinusoidally at 33 cycles per second by means of coils wound on the pole caps. The signal from the plate detector was fed to a synchronous detector[8] after narrow band amplification, and the derivative of the proton magnetic resonance plotted on a recording galvanometer. Slow scanning of the resonance over a 30-gauss range was supplied by an electronic triangular-wave current generator with a 25-minute period. The time constant of the recording galvanometer circuit was usually 18 seconds, although a four-second time constant was sometimes employed. The cryostat was similar in design to that described by Gutowsky.[7]

Second moments were obtained by numerical integration of the first and third moments of the derivative curves. The modulation correction in all cases was negligible.[2] Error in the second moment due to calibration of the scanning circuit is estimated to be 3% or less. The errors stated with the second moments are standard deviations of several measurements or 3%, whichever is larger.

II. IMPURITIES

The nuclear resonance absorption derivatives showed the presence, in most of the samples, of a narrow absorption line (<0.1 gauss) at the center of the resonance. From the amplitude of this line it was estimated that the line could be due to an impurity, either liquid or gaseous, of about 0.1%. Inquiry revealed that the firms supplying the samples could not suggest the origin of this line.

In an attempt to remove the impurity, samples were kept under vacuum in a molten state for sixteen hours. In no case was there a significant change in the narrow line upon observation of the resonance immediately after removing the sample from the vacuum. The line persisted at temperatures down to about −80°C, suggesting the possibility that ammonia might be present in small quantities in the crystals. Moist litmus paper, placed in a trap between the sample and a vacuum pump, indicated the presence of a base in those samples exhibiting the narrow absorption line. It is believed, therefore, that there is a trace of ammonia in most of our samples. It is very unlikely that these small amounts of impurity vitiate our results.

The source and grade of each compound are stated with the results for that compound.

III. BENZIDINE

The second moment of benzidine at −196°C is 14.2±0.7 gauss.[2] If one assumes that the diphenyl second moment is approximately that of naphthalene

* This work is supported by Department of Health, Education, and Welfare grant PHS 3722R. The equipment was provided through a grant-in-aid from the Research Corporation.

[1] Gutowsky, Kistiakowsky, Pake, and Purcell, J. Chem. Phys. **17**, 972 (1949).
[2] Gutowsky, Pake, and Bersohn, J. Chem. Phys. **22**, 643 (1954).
[3] R. Bersohn and H. S. Gutowsky, J. Chem. Phys. **22**, 651 (1954).
[4] T. M. Shaw, Phys. Rev. **85**, 762 (1952).
[5] E. R. Andrew, Proc. Phys. Soc. (London) **A66**, 1187 (1953).
[6] H. S. Gutowsky and G. E. Pake, J. Chem. Phys. **18**, 162 (1950).
[7] Gutowsky, Meyer, and McClure, Rev. Sci. Instr. **24**, 644 (1953).
[8] N. A. Schuster, Rev. Sci. Instr. **22**, 254 (1951).

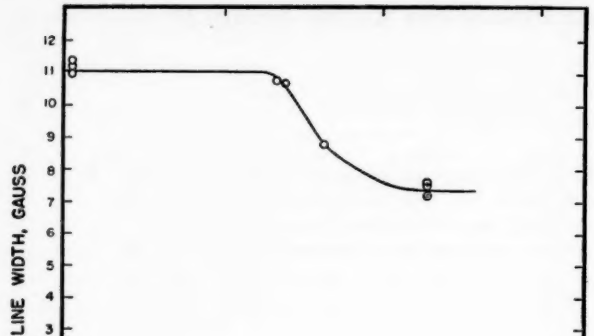

FIG. 1. The width of the proton magnetic resonance absorption line of a powder sample of benzidine as a function of temperature.

and benzene[9] (10 gauss^2), and the N−H bond distance is 1.014 A as in ammonia,[10] the calculated rigid lattice second moment is 13 gauss^2. This estimate includes 6-gauss^2 broadening, as in benzene. The line shape shows no fine structure.

The line width as a function of temperature, Fig. 1, shows a line width transition centering near −40°C. There is a corresponding change in second moment to 10.9±0.2 gauss^2. The rigid lattice second moment of the isolated NH_2 group is 14.1 gauss^2 for the 1.014 A N−H bond distance assumed in the aforementioned. If this group rotated about an axis perpendicular to the interproton line, the change would be $\frac{3}{4}(14.1)=10.5$ gauss^2. Since the NH_2 groups include $\frac{1}{3}$ of the protons of the molecule, the calculated change in second moment of the molecule for this motion is 3.5 gauss^2. The observed change in second moment is 3.3 gauss^2, and we therefore assign the transition at −40°C to the onset of rotation of the NH_2 groups.

The benzidine sample was Baker Analyzed Reagent grade, M.P. 127.5°C.

IV. ISOBUTYLAMINE

The second moment of isobutylamine is 23.3±1.1 gauss^2 at −196°C. Assuming 6.0 gauss^2 for the intermolecular broadening and 1.014 A as the N−H bond length, one estimates 22 gauss^2 for the rigid lattice second moment. It is interesting to note that Gutowsky and Pake[6] obtained a value of 20 gauss^2 for methylamine, which is close to what one would expect using an N−H bond distance of 1.014 A.[11]

No temperature data were taken on this compound. The isobutylamine was obtained from the Eastman Kodak Company.

[9] E. R. Andrew, J. Chem. Phys. **18**, 607 (1950).

[10] G. Herzberg, *Infra-red and Raman Spectra of Polyatomic Molecules* (D. Van Nostrand Company, Inc., New York, 1935), p. 439.

[11] As pointed out by Gutowsky (private communication), the 40 gauss^2 estimated in reference 6 is incorrect.

V. TRICHLOROACETAMIDE

Data and Discussion

Trichloroacetamide undergoes a small line width and second-moment transition centering at about −60°C. The line width above the transition is 10 gauss, and below the transition it is 11.8 gauss. The second moment changes correspondingly from 12.5±0.7 gauss^2 above the transition to 17.7±1.0 gauss^2 below the transition.

If one assumes an N−H bond distance of 1.014 A, the calculated rigid lattice intramolecular second moment is 14.2 gauss^2, which requires an intermolecular broadening of 3.5 gauss^2 to give agreement with the 17.7 gauss^2 found experimentally. On the other hand, the assumption of a bond distance of 1.07 A (as found for urea and glycine in Secs. VIII and IX) leads to an intermolecular broadening of 7.4 gauss^2. The latter broadening is larger than expected in view of the large size of the trichlor group and its small contribution to the second moment (0.1 gauss^2). It seems likely, therefore, that the N−H bond distance is smaller in trichloroacetamide than in urea or glycine. A line shape analysis of trichloroacetamide is planned at a later date.[12] We have found no crystal structure data on this compound.

The decrease in second moment near −60°C is too small to be accounted for by a rotation of the NH_2 group about any axis,[13] and is too large to be attributed to rotation of the CCl_3 group, but is consistent with an amino-group rotational oscillation with amplitude of 35° about an axis perpendicular to the interproton line.[14]

Preparation of Trichloroacetamide

The trichloroacetamide was prepared in this laboratory by Mr. Arthur Rosen by the method of McBee, Pierce, and Bolt.[15] Forty-five grams of trichloroacetic acid and 64 grams of absolute ethanol were refluxed with 0.2 ml of HCl for six hours yielding the ethyl ester on distillation. The ester was dissolved in 40 ml of anhydrous di-ethyl ether and cooled to ice temperature. Anhydrous ammonia was bubbled in for 20 hours. The trichloroacetamide separated from the solution and was recrystallized from anhydrous ether. The melting point of the product was 140.5°C.

VI. FORMAMIDE

The second moment of formamide at −196°C is 12.4±1.2 gauss^2. The assumption of 1.014 A for the N−H bond distance leads to a broadening of 2.9 gauss^2 (if the lattice is rigid at −196°C), while a bond distance of 1.07 A (as found in glycine and urea, Secs.

[12] We have calculated the rigid lattice spectrum for the NH_2 group, but have not completed the necessary averaging over the powder sample. The spectrum contains eight lines in addition to the two expected for an isolated proton pair.

[13] J. G. Powles and H. S. Gutowsky, J. Chem. Phys. **21**, 1702 (1953).

[14] E. R. Andrew, J. Chem. Phys. **18**, 1702 (1953).

[15] McBee, Pierce, and Bolt, Ind. Eng. Chem. **39**, 391 (1947).

VIII and IX) requires a broadening of 5.5 gauss² to account for the observed second moment. The latter value of the broadening seems to us to be the more reasonable. We therefore believe 1.07 A to be a reasonable estimate for the N−H bond distance in formamide in the absence of crystal data permitting a more accurate estimate. We intend to analyze the detailed line shape for formamide when our calculation is complete.

A transition centering about −62°C results in a reduction of the second moment to 9.4 gauss². As in trichloroacetamide, the change in second moment is too small to be accounted for by rotation of the NH_2 group,[13] but is consistent with a rotational oscillation with an amplitude of 29° about an axis perpendicular to the interproton line.[14]

Associated with the reduction of the second moment is a line-width transition from 10.5 gauss at −196°C to 9.3 gauss at −15°C.

The formamide, 99.9%, was obtained from Matheson, Coleman, and Bell.

VII. ACETAMIDE

Neither the second moment nor the line shape for acetamide changes in the temperature range studied by us, −196°C to 64°C. The average value of the second moment over this temperature range was 11.5±0.5 gauss². This value is less than the weighted sum of the second moments of the isolated NH_2 and methyl groups (17.3 gauss², rigid lattice), or for a rigid methyl group and rotating NH_2 group (14.6 gauss²), if the amino group is assumed to rotate about an axis perpendicular to the interproton line. These calculations are based on an N−H bond distance of 1.07 A (see Secs. VIII and IX); the assumption of 1.014 A for this bond would lead to larger discrepancies. A rotation of the methyl group about the C−C axis would account for the observed second moment, if a rigid amino group and an intermolecular broadening of 4.1 gauss² were assumed.

The acetamide was a Merck Reagent.

VIII. UREA

The second moment of urea at 0°C, where the lattice is assumed to be rigid, is 20.8±0.6 gauss². Difficulty was encountered in obtaining reliable second moment data at −196°C because of sample saturation.

The N−H bond distance was obtained by calculating the second moment according to the method of Van Vleck,[16] utilizing the N−H bond distance as a parameter to obtain agreement with the observed second moment. The second moment averaged over a powder sample is:

$$H_2=\frac{3}{5}\frac{I(I+1)g^2\beta^2}{N}\Sigma_j'\Sigma_k r_{jk}^{-6}+\frac{4}{15}\frac{\beta^2}{N}\Sigma_j\Sigma_m I_m(I_m+1)g_m^2 r_{jm}^{-6}.$$

[16] J. H. Van Vleck, Phys. Rev. 74, 1168 (1948).

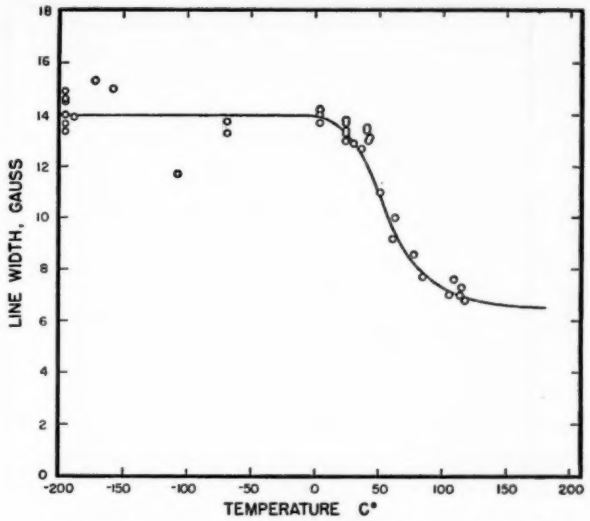

FIG. 2. The proton magnetic resonance line width of urea as a function of temperature.

Where, for urea, I is the proton spin, g the proton g factor, I_m and g_m are the corresponding quantities for the nitrogen nucleus, and β is the nuclear magneton. The internuclear distances are r_{jk} and r_{jm}, where j and k refer to the N protons in the sample, and m refers to the nitrogen nuclei. The prime indicates the summation is not to be taken over $j=k$. The crystal structure used was that given by Bunn.[17] The molecule was assumed entirely planar, as shown by Waldron and Badger[18] from the infrared spectrum and by Andrew from nuclear resonance studies of a single crystal,[5] and the two protons of the amino group were taken to be symmetric about the C−N axis with an H−N−H bond angle of 109°28′. A total of 28 neighboring molecules were taken into account, and the contribution of the remainder (0.05 gauss²) was estimated by a spherical approximation. This calculation yields 1.077±0.007 A for the N−H bond distance in urea. The calculated intermolecular contribution to the second moment for this bond distance is 14.70 gauss² and the intermolecular contribution is 6.10 gauss².

Since two of the strong hydrogen bonds in urea form an angle of 150°, it is possible that the H−N−H bond angle is somewhat greater than the tetrahedral angle. If an H−N−H bond angle of 120° is assumed, the N−H bond distance is 1.010±0.007 A. Since this bond angle is at present unknown, we are unable to determine a unique value of the N−H bond distance. We are planning experiments on a single urea crystal which will give a unique value for both the bond angle and bond distance in this compound.

There is a transition in urea, as shown in Fig. 2. The line width below the transition is 14.1 gauss and drops to a value of about 7.2 gauss above the transition.

[17] C. W. Bunn, *Chemical Crystallography* (Oxford University Press, London, 1946), p. 299.

[18] R. D. Waldron and R. M. Badger, J. Chem. Phys. 18, 566 (1950).

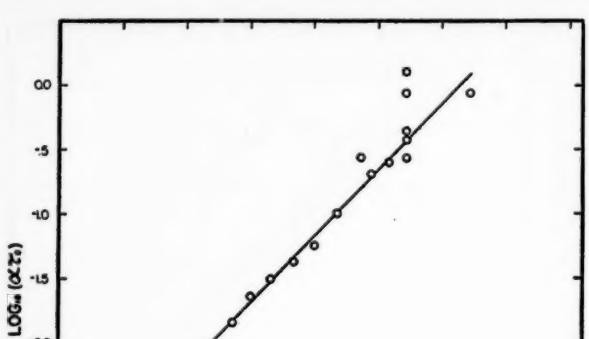

FIG. 3. Logarithm of $\alpha\tau_c$ *versus* the reciprocal of the absolute temperature according to the one-parameter theory [Eq. (2)] for urea.

The second moment correspondingly drops from 20.8 gauss^2 to 6.9 gauss^2. These are the expected changes in line width and second moment if the transition is attributed to onset of rotation of the NH_2 groups about the C−N bond.

An obvious extension of the one-parameter theory of Bloembergen, Purcell, and Pound[19] leads to the following relations between the line width (or root second moment) and the absolute temperature:

$$(\delta H)^2=\frac{2}{\pi}\Sigma n C_n^2 \tan^{-1}[\alpha\tau_n\delta H], \tag{1}$$

$$\tau_n=\tau_{no}\, e^{V_n/RT}, \tag{2}$$

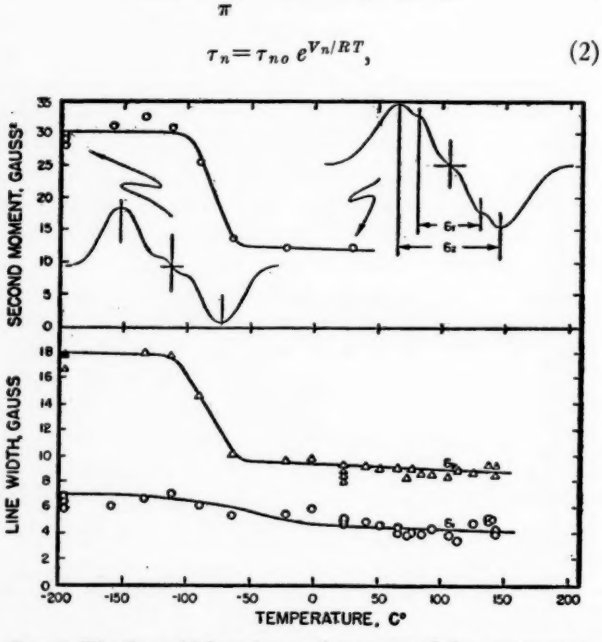

FIG. 4. The line width and second moment of the proton magnetic resonance of glycine as a function of temperature. The shapes of the derivatives of the line above and below the transition temperature are indicated on the second-moment curve.

[19] Bloembergen, Purcell, and Pound, Phys. Rev. **73**, 679 (1948).

where δH is the line width, or root second moment, C_n is a constant, τ_n is the correlation time for the nth molecular motion, τ_{no} is a constant, V_n is the excitation energy for the nth motion, α is a constant depending on line shape, but of the order of magnitude of the gyromagnetic ratio divided by 2π, k is Boltzmann's constant, and T is the absolute temperature. If the thermal transitions are clearly separated, Eq. (1) can be simplified to[20]

$$(\delta H)^2=B^2+\frac{2C^2}{\pi}\tan^{-1}(\alpha\tau_c\delta H) \tag{3}$$

where B is the line width above the transition and $(B^2+C^2)^{\frac{1}{2}}$ is the line width below the transition.

The solid curve in Fig. 2 represents Eq. (3) for urea, while Fig. 3 is the corresponding plot of Eq. (2). The excitation energy, V_n, and correlation constant, τ_{no}, corresponding to Fig. 3 are 9.4 kcal per mole and 5×10^{-11} sec. While the detailed line shape given by Eq. (3) is probably not significant, Fig. 2 does support our assumption that the lattice is essentially rigid at 0°C. It is interesting to note that saturation measurements of T_1 at room temperature agree with the one-parameter theory. If one assumes that bond resonance in urea results in a positive charge on each amino group of about 20% of the electronic charge and a corresponding negative charge on the oxygen,[21] one can calculate the electrostatic excitation energy for rotation of the amino group. The result is approximately the same as Vn from Eq. (2).

No difference was observed between the two samples of urea used, a Baker Analyzed Reagent and a Merck Reagent.

IX. GLYCINE

Line width, second moment, and line shape of glycine as a function of temperature are given in Fig. 4.[22] The rigid lattice second moment is 30.3±1.3 gauss^2. Table I and Fig. 5 show the results of the calculation of the second moment by the method of Van Vleck[16] for several positions of the protons on the glycine molecule. The crystal structure data were taken from the work of Albrecht and Corey.[23]

As may be seen from Table I, several reasonable molecular configurations can be assumed which have the observed second moment: No. 1; No. 5; a configuration intermediate between No. 6 and No. 7; No. 8; and possibly No. 9. Except for No. 1 and No. 9, however, the existing infrared data[24,25] and the large

[20] Equation (3) has been used by Pake and Gutowsky.[6]

[21] W. D. Kumler and M. Fohlen, J. Am. Chem. Soc. **64**, 1944 (1942).

[22] We are in essential agreement with the line width reported by Shaw.[3]

[23] G. Albrecht and R. B. Corey, J. Am. Chem. Soc. **61**, 1087 (1939).

[24] J. Klotz and D. Gruen, J. Phys. Colloid Chem. **52**, 961 (1948).

[25] L. J. Bellamy, *The Infra-red Spectra of Complex Molecules* (John Wiley and Sons, Inc., New York, 1954), p. 200.

TABLE I. Theoretical second moments for the different molecular models of glycine shown in Fig. 5.

Model	r Angstroms	Intra H_2 gauss^2	Inter H_2 gauss^2	Total gauss^2
1. $-NH_3^+$, regular tetrahedron; protons approximately along hydrogen bonds [Fig. 5(b)].	$r_{NH}=1.074$	24.1	6.2	30.3
2. Unionized form, NH_2 and OH protons along the short hydrogen bonds[a] [Fig. 5(c)]. OH proton on O_{II}.	$r_{NH}=1.00$ $r_{OH}=1.03$	15.8	$\simeq$ 11	$\simeq$ 26.8
3. Unionized form $\phi=120°$, OH as in 2, $C_\alpha-NH_2$ form a plane parallel to plane of the short hydrogen bonds [Fig. 5(c)].	$r_{NH}=1.00$ $r_{OH}=1.03$	13.1	$\simeq$ 11	$\simeq$ 24.1
4. Unionized, NH_2 as in 3, $\phi=120°$, O−C−OH form a plane [Fig. 5(a)].	$r_{OH}=1.03$ $r_{NH}=1.07$	12.6	>1000	>1000
5. Unionized, NH_2 as in 3, $\theta=180°$ [Fig. 5(a)].	$r_{OH}=1.045$ $r_{NH}=1.07$	19.1[b]	11.2[b]	30.3
6. Unionized, NH_2 as in 3, $r_{NH}=1.07$, O−C−OH form a plane, $\theta=233°18'$ [Fig. 5(a)].	$r_{OH}=1.03$ $r_{OH}=1.06$	24.4 25.1	$\geqslant$ 6 $\geqslant$ 6	$\geqslant$ 30.4 $\geqslant$ 31.1
7. Unionized, NH_2 as in 3, $r_{NH}=1.07$, $\theta=210°$ [Fig. 5(a)].	$r_{OH}=1.10$ $r_{OH}=1.03$	16.3 16.0	11.9 11.5	28.2 27.5
8. $-NH_3^+$, two protons as in the NH_2 group of No. 3, $r_{NH}=1.07$, r_{NH}' along hydrogen bond approximately parallel to c-axis of crystal [Fig. 5(b)].	$r_{NH}'=1.50$ $r_{NH}'=1.70$ $r_{NH}'=1.90$	87.3 33.0 23.1	$\geqslant$ 6	$>$ 30.3 $>$ 30.3 $\geqslant$ 29.1
9. $-NH_3^+$, protons along hydrogen bonds[a] [Fig. 5(b)].	$r_{NH}=r_{NH}'=1.10$	25.7	$\geq$ 6	$\geq$ 31.7

[a] As suggested by Albrecht and Corey.[23]
[b] In calculation of the intra-molecular second moment, the OH proton was assumed to be attached to the nearest neighbor along the crystalline c-axis.

change in the second moment near −85°C would be very difficult to explain. Since the more symmetrical model No. 1 yields a smaller, and, to us, a more reasonable value for the N−H bond distance, we do not assume, as did Albrecht and Corey, that the protons lie exactly along the hydrogen bonds. For the configuration of model No. 1, the N−H bond distance is 1.074±0.014 A.[26]

There is a transition in glycine centering at about −85°C where the line width changes from 18 gauss to 7.5 gauss, and the second moment changes from 30.3 gauss^2 to 12.7 gauss^2. The unbroadened NH_3^+ group second moment is calculated to be 13.6 gauss^2. Since there will be some decrease in the external broadening, and it is likely the motion will not take place exactly about the C−N bond due to the asymmetry of the molecule, this motion is a reasonable explanation of the observed 17.6 gauss^2 decrease in second moment. The dielectric constant shows a corresponding change from 2.70 to 2.80 centering at about −85°C (Fig. 6).[27]

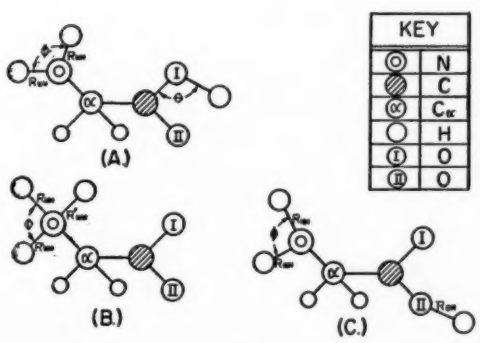

FIG. 5. Models of the glycine molecule for which the second moment was calculated. The results are tabulated in Table I. The only differences among the models is that the hydrogen normally assigned to the oxygen is moved to the various positions shown in the sketches.

[26] It has been suggested by Gutowsky (personal communication) that the NH_3^+ group may be undergoing sufficient zero-point torsional oscillation to cause the second moment at −196°C to differ slightly from the rigid lattice value. Lack of infrared data on the frequency of the zero-point torsional oscillation of the NH_3^+ group precludes the possibility of a careful correction for this motion. However, we have calculated the barrier height against rotation from the temperature data to be about 4 kcal/mole, and from this estimated the correction to the second moment to be about 10%. A sinusoidal potential barrier was assumed in making this estimate. This would decrease the bond distance for models 1 and 9 by about the stated error.

[27] S. T. Bayley, Trans. Faraday Soc. 47, 509 (1950).

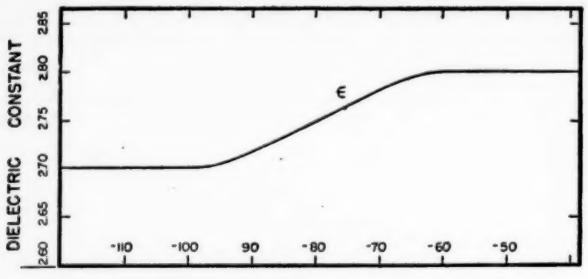

FIG. 6. Dielectric constant, ϵ, of glycine as a function of temperature.[27]

X. α ALANINE

Both *dl*- and *l*-α-alanine were studied. There was no significant difference in the line width, second moment, or line shape between these compounds. The line shape as a function of temperature is shown in Fig. 7, while the line widths and second moments are shown in Fig. 8.

The transition centering near −130°C results in a change in second moment of 4.6 gauss², while that near −50°C results in a change of 18.0 gauss². These second-moment changes cannot be simply assigned to the onset of rotation of single groups about a symmetry axis. The second moment at −196°C is 31.8±2.3 gauss², while the room temperature second moment is 9.2±0.4 gauss². The methyl groups on neighboring molecules in α alanine have been shown by Levy and Corey[28] to be exceptionally close together.

The alanines were obtained from Nutritional Biochemicals Corporation and were stated to be 99.5% pure.

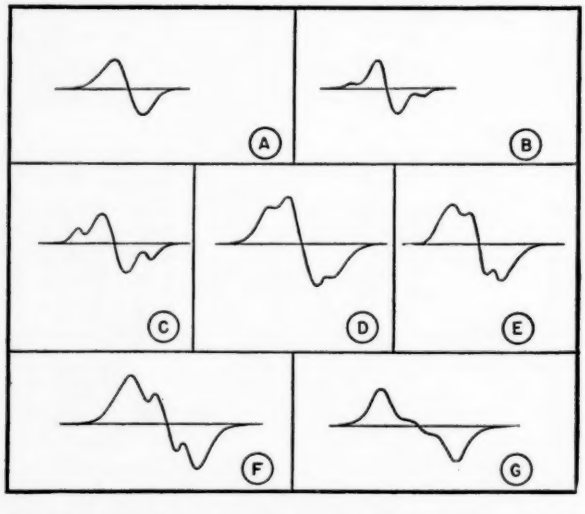

FIG. 7. Derivatives of the proton magnetic resonance line for α alanine at the temperatures indicated by the corresponding letters on Fig. 8.

[28] H. A. Levy and R. B. Corey, J. Am. Chem. Soc. **63**, 2095 (1941).

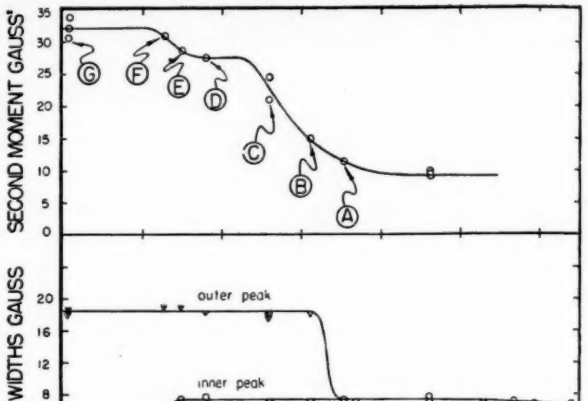

FIG. 8. The width and second moment of the proton magnetic resonance line in α alanine as a function of temperature.

XI. β ALANINE

The second moment of β alanine at −196°C is 34.9±1.8 gauss², while at 28°C it is 15.0±0.4 gauss². There is a transition centering near −25°C shown by the line-width data (Fig. 9). This is probably due to the onset of rotation of the NH_3^+ group. No detailed crystal structure data are available.

The β alanine was obtained from Nutritional Biochemicals Corporation and was stated to be 99% pure.

XII. ATROLACTAMIDE

Samples of *d*-atrolactamide and *dl*-atrolactamide were investigated at room temperature. Insufficient *d*-atrolactamide was available to permit further study. The second moments obtained were 7.5±0.3 gauss² for *dl*-atrolactamide and 10.8±0.8 gauss² for *d*-atrolactamide.

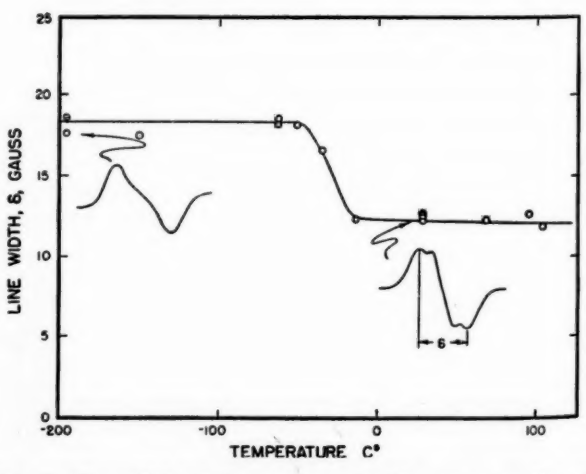

FIG. 9. The width of the proton magnetic resonance line of β alanine as a function of temperature.

XIII. SUMMARY AND DISCUSSION

The study of this group of amines, amides, and amino-acids indicates that N—H . . . O hydrogen bonds exert a strong influence on molecular structure, partly through the electrostatic field of the "hydrogen bond," but probably largely through the electronic structure that results in this field. In urea and glycine, in which strong hydrogen bonds exist, it was shown that the amino hydrogens have the relatively large N—H bond distance of about 1.075 A. Also it appears that in the case of urea, the hydrogen bonds produce a strong hindering against the rotation of the amino groups. Further evidence for the existence of the dipolar form of glycine in the solid state has been presented.

Lack of crystal structure data prevents accurate calculation of the N—H bond distance in the amines. However, these data are consistent with an N—H bond distance of 1.014 A.

XIV. ACKNOWLEDGMENTS

We wish to thank Mr. Arthur Rosen for the synthesis of the trichloroacetamide and for his work on the purification and analysis of the other samples, and Mr. Robert Polk, who constructed the electronic scanning circuit. We also wish to express our gratitude to the Graduate Research Board of the University of Illinois for their support during the early stages of this research.

Note added in proof.—The N—H bond distance in urea given in the above paper has been revised in light of more recent crystal data [P. A. Vaughan and J. Donahue, Acta Cryst. **5**, 530 (1952)], and the results of Andrew and Hyndman [E. R. Andrew and D. Hyndman, Trans. Farraday Soc. (to be published)] showing from nuclear magnetic resonance experiments that the H—N—H bond angle is nearly 120°.

The revised value is 1.036±0.009 A. This value is in agreement with the value obtained by Andrew and Hyndman from single crystal data.

We would like to thank Professor E. R. Andrew for permission to use his results in advance of final publication.

THE JOURNAL OF CHEMICAL PHYSICS VOLUME 23, NUMBER 9 SEPTEMBER, 1955

Binary Diffusion of Similar or Isotopic Molecules in Three Component Systems*

WILLIAM P. SENETT, FRED GOLLOB, AND T. I. TAYLOR
Department of Chemistry, Columbia University, New York, New York

(Received July 19, 1954)

The application of Maxwell's equations to obtain the diffusion coefficient for the mixing of two gases in the presence of a fixed concentration of a third leads to an inconsistency so that only an approximate solution may be obtained. Since the approximation becomes better as the diffusing species become similar, isotopic species are a favorable case. The two bulb mixing problem for isotopic gradients in each of two molecular species but no molecular gradient as a whole is now solved as two independent three component systems leading to relatively simple equations. The validity of the treatment is confirmed by a series of experiments in which agreement between the calculated relaxation time and observed one is well within the estimated error of about 5%.

INTRODUCTION

ONE of the problems in understanding the mechanism of operation of thermal diffusion columns with chemical exchange[1] is the evaluation of the relative half-lives of diffusive mixing due to isotopic gradients in two molecular species. Experimental confirmation has been obtained for certain relations derived as an approximation from more general theoretical equations.

As a concrete illustration, consider two bulbs connected by a capillary tube of dimensions large compared to the mean free path of the gas. Each bulb contains a mixture of carbon monoxide and carbon dioxide at the same pressure, temperature, and molecular composition. The carbon monoxide in one bulb is enriched in $C^{13}O$ and is of normal isotopic abundance in the other. The carbon dioxide in one of the bulbs is enriched in $C^{13}O_2$ and is normal in the other. Under these conditions, we wish to know the half-lives for isotopic mixing for the carbon monoxide system and for the carbon dioxide system.

THEORETICAL

General transport equations for multi-component gas mixtures may be found in the literature[2] but for more than two components, the exact treatment leads to very unwieldy expressions. From a physical point of view, it is apparent that the four component system $C^{12}O$, $C^{13}O$, $C^{12}O_2$, $C^{13}O_2$ described above (see Fig. 1) behaves, as far as the isotopic mixing by diffusion of CO is concerned, very much like the three component system $C^{12}O$, $C^{13}O$, $C^{12}O_2$. Similarly, the $C^{12}O_2$ and $C^{13}O_2$ will mix to a first approximation as if the system were $C^{12}O_2$, $C^{13}O_2$, and $C^{12}O$. Thus we see that we may reduce our 4 component problem to two independent

* This work was supported by contract AT (30-1) 755 with the U. S. Atomic Energy Commission. Publication assisted by the Ernest Kempton Adams Fund for Physical Research of Columbia University.

[1] R. B. Bernstein and T. I. Taylor, J. Chem. Phys. **16**, 903 (1948).

[2] See for example C. F. Curtiss and J. O. Hirschfelder, J. Chem. Phys. **17**, 550 (1949); E. J. Hellund, Phys. Rev. **57**, 319 (1940).

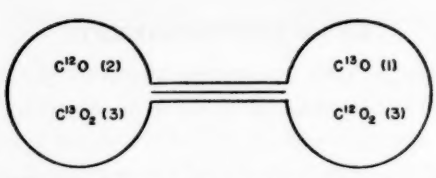

FIG. 1. Representation of a four component system. All gases at same partial pressure for which the mean free path is small compared to the diameter of the capillary.

three component systems. In each three component system we have only two components diffusing, the mole fraction of the third component being considered the same everywhere.

Maxwell's equations[3] may be written in terms of the mole fractions c_i and convection velocities $\mathbf{V}_i$ of the individual components[4] at constant T and P as follows:

$$-\text{grad } c_1=\frac{c_1c_2}{D_{12}}(\mathbf{V}_1-\mathbf{V}_2)+\frac{c_1c_3}{D_{13}}(\mathbf{V}_1-\mathbf{V}_3)$$
$$-\text{grad } c_2=\frac{c_2c_1}{D_{21}}(\mathbf{V}_2-\mathbf{V}_1)+\frac{c_2c_3}{D_{23}}(\mathbf{V}_2-\mathbf{V}_3). \quad (1)$$

The D_{ij} here are the ordinary binary diffusion coefficients, so that $D_{12}=D_{21}$. Now assume that the convection velocity for the third component is zero, $\mathbf{V}_3=0$, so that c_3 will remain constant. Then since

$$\sum \text{grad } c_i=0, \quad \text{grad } c_2=-\text{grad } c_1$$

from which follows

$$\frac{c_1c_3\mathbf{V}_1}{D_{13}}=-\frac{c_2c_3\mathbf{V}_2}{D_{23}}. \quad (2)$$

But $\sum c_i\mathbf{V}_i=\mathbf{V}$ by definition of the convection velocity and $\mathbf{V}=0$ for this case. Hence $c_1\mathbf{V}_1=-c_2\mathbf{V}_2$, and Eq. (2) leads to

$$D_{13}=D_{23}. \quad (3)$$

As a general statement Eq. (3) is not true and the assumption that $\mathbf{V}_3=0$ is not correct. However, in searching for an approximate solution, we may say that the approximation $\mathbf{V}_3=0$ becomes better as D_{13} approaches D_{23}. For the case described, where components one and two are isotopic molecules, we should have a good approximation. Therefore, to get a consistent set of equations from Eq. (1) with $V_3=0$, we replace D_{13} and D_{23} by $\bar{D}$, for simplicity assuming $\bar{D}$ is their arithmetic mean

$$\bar{D}=\tfrac{1}{2}(D_{13}+D_{23}). \quad (4)$$

Then from (1) we find using the relations given that

$$-\text{grad } c_1=c_1\mathbf{V}_1\left[\frac{(c_1+c_2)}{D_{12}}+\frac{c_3}{\bar{D}}\right] \quad (5)$$

so that the binary diffusion coefficient D of components one and two in solvent gas three is found from

$$\frac{1}{D}=\left[\frac{(c_1+c_2)}{D_{12}}+\frac{c_3}{\bar{D}}\right]. \quad (6)$$

In a two bulb diffusion experiment, it is sufficient to determine the concentration of one of the diffusing components as a function of time. Consider two bulbs A and B of volume V_A and V_B connected by a capillary tube of cross section A and length L. Let the concentrations in moles per cc of the component of interest be C_A and C_B. Then the flux density is given by

$$-D \text{ grad } C$$

where D is given by Eq. 6. If the total number of moles is $N=C_AV_A+C_BV_B$, it can be shown that

$$\frac{dC_A}{dt}=-\frac{DA}{V_AV_BL}[C_A(V_A+V_B)-N]. \quad (7)$$

Integrating and setting $C_A=C_A^0$ for $t=0$, it follows that

$$\frac{C_A(V_A+V_B)-N}{C_A^0(V_A+V_B)-N}=\exp\left[-\frac{DA}{L}\frac{(V_A+V_B)}{V_AV_B}\right]t. \quad (8)$$

Let $C_A=C_A^\infty$ as $t\to\infty$, then, since $C_A^\infty=C_B^\infty$, it follows that $(V_A+V_B)C_A^\infty=N$. Hence (8) may be written

$$\frac{C_A-C_A^\infty}{C_A^0-C_A^\infty}=e^{-t/\tau} \quad (9)$$

where τ is the relaxation time given by

$$\tau=\frac{L}{A}\frac{V_AV_B}{(V_A+V_B)}\left[\frac{(c_1+c_2)}{D_{12}}+\frac{c_3}{\bar{D}}\right]. \quad (10)$$

EXPERIMENTAL

As a test of the equations derived, two three component systems were studied in a two bulb apparatus described (see Fig. 2). Let us call the "nondiffusing" component the "solvent gas." The diffusive mixing of nitrogen and argon was studied in the presence of two different solvent gases, namely helium and krypton. In this way, the effect of a varying molecular weight of the solvent gas could be investigated.

A second set of runs, the diffusing components being isotopic molecules, was carried out with a solvent gas which itself had an isotopic gradient. For example, both bulbs are filled to the same partial pressure of CO_2 and Ne. However, in the first bulb the CO_2 is isotopically enriched in C^{13} and the Ne is of normal isotopic composition; the second bulb contains CO_2 of normal abundance and Ne enriched in Ne^{22}. This mixture is approximately two independent three component systems as previously described.

[3] T. K. Sherwood, *Absorption and Extraction* (McGraw-Hill Book Company, Inc., New York, 1937), Chap. 1.
[4] See, e.g., R. C. Jones and W. H. Furry, Revs. Modern Phys. **18**, 154 (1947).

Apparatus

The all Pyrex diffusion apparatus consists of two bulbs connected by a capillary tube. See Fig. 2 for details. Stopcocks are provided to permit filling each bulb separately. A 12/5 female ball joint is provided as an inlet for a stainless steel capillary tube. This tube is the leak of a Nier type 60° mass spectrometer. In this way, the gas sample may be analyzed continuously.

Materials

The argon, helium, krypton, nitrogen, normal carbon dioxide, and normal neon of high purity commercial grade were in tanks. The enriched Ne was produced in a one meter thermal diffusion column.[1] It contained 17.5% Ne^{22} compared to 8.8% Ne^{22}, in normal Ne. The enriched CO_2 (33% C^{13}) was produced by heating a mixture of $BaCO_3$ enriched in C^{13}† and $PbCl_2$ in a previously evacuated system at 500°C.[5] This method was the most convenient of several tried. All gases were analyzed for possible interfering impurities on the mass spectrometer before they were used.

Procedure

Mixtures of gases were prepared in a separate system (not shown) and stored until used. The diffusion apparatus was connected to the mass spectrometer at both ball joints. The background of the mass spectrometer was read for the masses of all gases of interest, and later subtracted from all subsequent readings of these masses. Mass 32 (oxygen) was monitored for air leaks. The gas mixture used in bulb B was then introduced into bulbs A and B at the desired pressure through the sample system. The peak heights of the various gases were read, choosing the ions of appropriate mass number, and stopcock B was closed. Bulb A was then evacuated. The gas mixture used in bulb A was then introduced and adjusted to the same pressure as that in bulb B. Stopcock A was then closed and stopcock B opened for thirty seconds to equilibrate minor pressure differences. The diffusion apparatus was then disconnected from the sample system at joint A and clamped in a water bath so that the capillary tube was horizontal and below the level of both bulbs. The flexibility of the capillary leak to the mass spectrometer permitted the apparatus to be moved about relatively freely. The bath was neither temperature controlled nor stirred since preliminary experiments had shown that no significant error was introduced in this way. (The maximum temperature drift was 1.5°C in one run. For most runs it was considerably less.) The peak heights of the gas mixture were then read and taken as the zero time readings. Stopcock B was then opened and

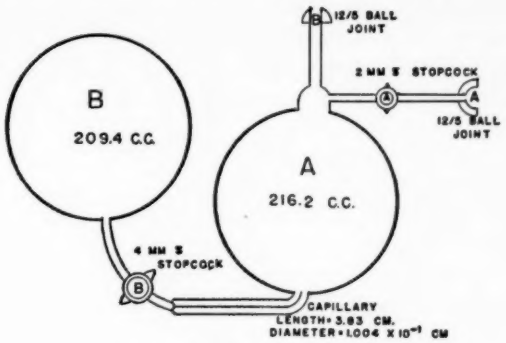

FIG. 2. Diffusion apparatus.

readings of the various peak heights were made at regular time intervals. The equilibrium point was determined in different runs in one of two different ways. In some cases, the apparatus was left in the bath until equilibrium was established. In other cases, the apparatus was removed from the bath and rejoined to the sample system at joint A. The Toepler pump in the sample system was then used to establish equilibrium rapidly by alternately expanding and compressing the gas. The readings obtained during the filling of bulb B, for bulb A at zero time, and at equilibrium, were used to check the stoichiometry.

In one case, the doubly-charged ion of carbon dioxide produced a mass 22 peak superimposed on the neon 22 peak. The filament to case voltage in the mass spectrometer was then reduced from 75 to 40 volts. This reduced the production of doubly-charged carbon dioxide ion by a factor of ten, and allowed higher precision in reading peak height.

Data

Experimental results for six runs at the indicated temperatures and pressures are given in Table I. The rate of mixing may be measured by calculating the fractional approach to equilibrium F as a function of time. The quantity F is given by $(h_\infty - h_t)/(h_\infty - h_0)$ where h_∞ is the peak height at equilibrium, h_0 the peak height at the time zero and h_t the peak height at any time t. The half-life for mixing corresponds to the time, $t_{\frac{1}{2}}$, when $F = \frac{1}{2}$. In Fig. 3 and Fig. 4 $\log F$ is plotted *vs* t for all runs. Corrections to h for small fluctuations in the sensitivity of the mass spectrometer were made by normalizing to a constant sum for the 20 plus 22 peak heights.

Precision

The precision attained varied with the experiment. The peak heights on the mass spectrometer could be read with a precision of ±1%. The error introduced in F by this factor increases with the approach to equilibrium. In all cases except the neon runs, the maximum error from this source was ±3%; the precision of the half-lives was also ±3%. Due to the relatively small

† Obtainable from The Eastman Kodak Company, Rochester, New York.

[5] Zweibel, Turkevich, and Miller, J. Am. Chem. Soc. **71**, 376 (1949).

total change in the neon ratio, an error of $\pm 1\%$ in h produced an error of from $\pm 5\%$ to 20% in F. The method of least squares was used to find the best line for the neon plots; the precision of these half-lives was found to be $\pm 5\%$.

In comparing the experimental results with the predicted values, two other sources of errors are introduced. The first of these inaccuracies is the proportions of the gas mixtures. As seen in Eq. (6), D is a function of the mole fractions of the gases in the mixture. The error in composition is $\pm 1\%$. This error is reflected into D as a $\pm 2\%$ error. The other source of error is the precision of measurement of the physical dimensions of the diffusion apparatus. The volumes of the bulbs were measured by expansion of gas from a known volume with a precision of $\pm 0.5\%$. The length and diameter of the capillary were measured with a traveling microscope; the precision of these measurements was $\pm 1\%$. The over-all error introduced by the measurements of these dimensions is $\pm 2\%$. As a result of these additional sources of error the probable over-all precision of the calculated half-lives is $\pm 7\%$ for Ne and $\pm 5\%$ for the others.

DISCUSSION OF RESULTS

The half-lives were calculated from Eq. (10) and the expression $t_{\frac{1}{2}}=0.69\tau$. The values for D, the diffusion coefficient of the ternary system, were calculated from Eq. (6). The first approximations to the binary diffusion coefficients were used and calculated from viscosity data and equations given in the literature.[6,7]

A comparison of the experimental half-lives with the theoretical calculations in Table I shows agreement within the precision of the experiment in every case. This substantiates the general treatment used and shows that the approximation in Eq. (6) is valid. This is unexpected for such dissimilar molecules as argon and nitrogen (see Table I).

If the peak heights are assumed proportional to the concentrations, then the left-hand side of Eq. (9) becomes equal to F. Therefore, F should vary exponentially with time; it may be observed in Figs. 3 and 4 that the plot of "F" on a logarithmic scale *vs* time produces a straight line, verifying the equation. For the isotopic mixtures we may replace c_1+c_2 by x_1, and c_3 by x_2, where x_1 and x_2 are the mole fractions of molecular composition. It follows that $t_{\frac{1}{2}}$ is a linear function of x_1. In Fig. 5 the lines are calculated values of $t_{\frac{1}{2}}$ as a function of x_1 for the systems indicated. The

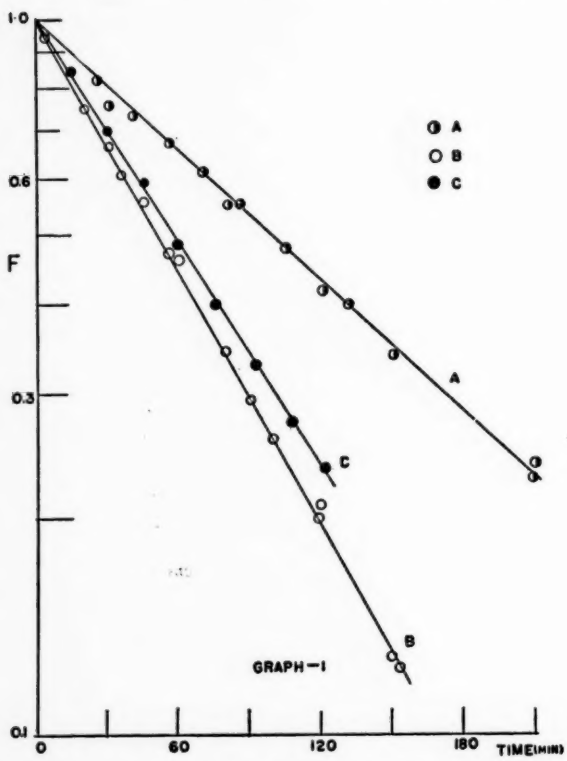

FIG. 3. Diffusive mixing of argon and nitrogen in the presence of helium or krypton. Log F *vs* time. $F=(x_t-x_\infty)/(x_0-x_\infty)$ where x_t is the mass spectrometric peak height of either argon (mass 40+) or nitrogen (mass 28+) at time t. Plot A was used to calculate $t_{\frac{1}{2}}$ No. 1. Plots B and C were used to calculate $t_{\frac{1}{2}}$ No. 2. For further details see Table I.

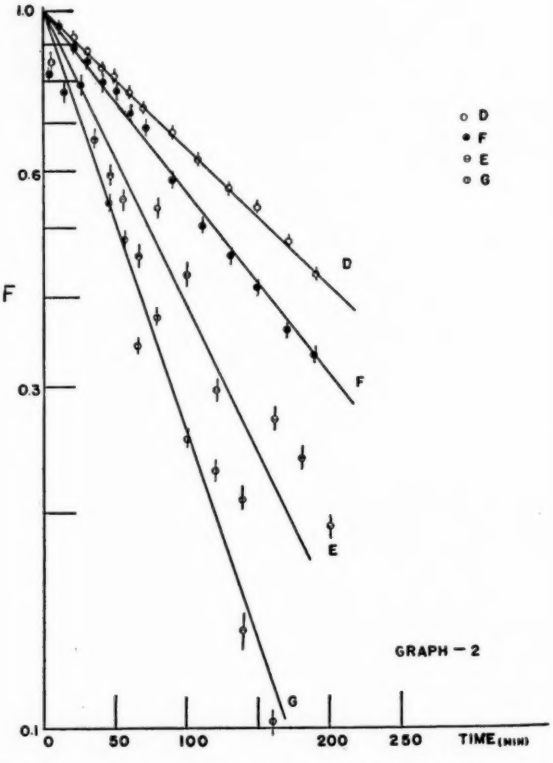

FIG. 4. Simultaneous diffusive mixing of carbon dioxide isotopes and neon isotopes. Log F *vs* time. $F=(x_t-x_\infty)/(x_0-x_0)$ where x_t is the fraction at time t of either carbon dioxide or neon which is rare, e.g., $x_t=C^{13}O_2/(C^{12}O_2+C^{13}O_2)$ where the symbols refer to the mass spectrometric peak heights for the corresponding molecular masses. Plots D, E, F, and G were used to calculate $t_{\frac{1}{2}}$ No. 3, 4, 5, and 6, respectively. For further details see Table I.

[6] Hirschfelder, Bird, and Spotz, J. Chem. Phys. **16**, 968 (1948).
[7] Hirschfelder, Bird, and Spotz, Chem. Revs. **44**, 205 (1949).

TABLE I. Half-lives for diffusive mixing.

Mixture no.	Curve no.	Half-life (min) Av exp	Calc	Gas mixture Bulb A	Bulb B
1	*A*	98	94	argon, 50% krypton, 50% $P=2$ cm,	nitrogen, 50% krypton, 50% $T=26.8°C$
2	*B,C*	53	51	argon, 50% helium, 50% $P=2$ cm,	nitrogen, 50% helium, 50% $T=27.1°C$
3	*D*	160	156	carbon dioxide, 50%, (C^{13}, 32.8%, C^{12}, 67.2%)	carbon dioxide, 50%, (C^{13}, 1.13%, C^{12}, 98.87%)
4	*E*	74	72	neon, 50% (Ne^{22}, 8.99%, Ne^{20}, 91.01% $P=3$ cm,	neon, 50% (Ne^{22}, 18.3%, Ne^{20}, 81.7%) $T=26.5°C$.
5	*F*	123	120	carbon dioxide, 19%, (C^{13}, 32.7%, C^{12}, 67.3%)	carbon dioxide, 19%, (C^{13}, 1.17%, C^{12}, 98.83%)
6	*G*	55	57	neon, 81% (Ne^{22}, 9.05%, Ne^{20}, 90.95%) $P=3$ cm,	neon, 81% (Ne^{22}, 18.4%, Ne^{20}, 81.6%) $T=27.7°C$

Ratios of half-lives					
Ratio of no.	Exp	Calc	Ratio of no.	Exp	Calc
1/2	1.85	1.84	2/6	0.964	0.895
1/3	0.611	0.602	3/4	2.16	2.17
1/4	1.33	1.31	3/5	1.30	1.30
1/5	0.798	0.782	3/6	2.91	2.74
1/6	1.78	1.65	4/5	0.602	0.600
2/3	3.31	3.27	4/6	1.34	1.26
2/4	0.716	0.708	5/6	2.23	2.10
2/5	0.431	0.425			

experimental points fall on these lines within the experimental precision.

A better indication of the validity of Eq. (6) is obtained by comparing the theoretical ratio of half-lives in any two systems to the observed ratio. This ratio, as will be evident from Eq. (10), is independent of all dimensional errors. The comparison, given in Table I, shows agreement within experimental error. The worst error is found always in ratios involving the $t_{\frac{1}{2}}$ of least precision, number 6.

Having thus established the validity of the derivation used within the limits given for the isotopic systems described previously, it is now possible to apply this treatment to more general situations. We conclude with a numerical example for a system of interest to us. In the system specified by Fig. 1, for each gas shows that at a partial pressure of 0.5 atmos in the diffusion apparatus of Fig. 2, the half-lives for the CO and CO_2 systems may now be calculated with some confidence as 15.7 hr, and 22.7 hr, respectively.

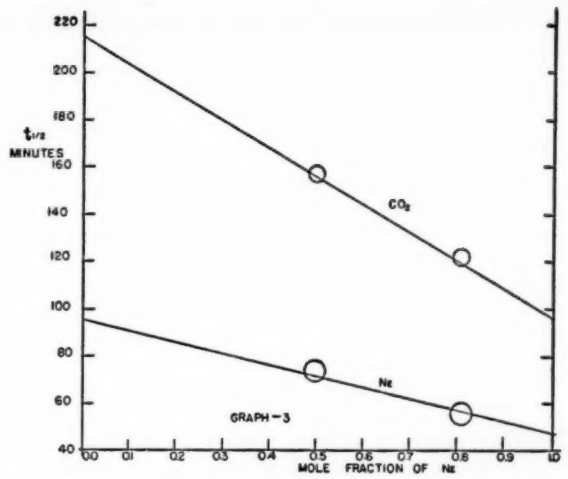

FIG. 5. Half-life ($t_{\frac{1}{2}}$) *vs* Mole Fraction Ne. The full lines were calculated; the circles show experimental values. The gas mixture was Ne^{20}, Ne^{22}, $C^{12}O_2$, $C^{13}O_2$. The system is similar to that of Fig. 1. For further details see Table I and the text.

APPENDIX‡

Equation (1) is identical with equation 8: 1–3 of the book by Hirschfelder, Curtiss and Bird, except that the temperature gradient has been put equal to zero (i.e., any temperature differences set up by the inverse thermal diffusion effect has been neglected).

There is the further formal difference that in Hirschfelder's equation $\bar{v}$ is the *difference* between v and the mass average velocity; however this drops out from $v_i - v_j$.

Approximately, one sets

$$\sum_{cj} v_j = 0 \quad v_3 = 0.$$

This seems a good approximation for isotopes, since, if

$$c_1 v_1 + c_2 v_2 = 0,$$

very closely also

$$c_1 m_1 v + c_2 m_2 v_2 = 0.$$

One other approximation is made in writing Eq. (7). It is assumed that the adjustment of concentration in the capillary to the changing concentrations in the bulbs is fast compared to the change of concentration in the bulbs.

‡ This critical survey of the equations of this paper is the work of Professor Karl F. Herzfeld.

Raman and Infrared Spectra and Structure of 2,6-Dioxaspiro(3,3)heptane

S. C. SIRKAR,* FRED L. VOELZ,† AND FORREST F. CLEVELAND
Spectroscopy Laboratory,‡ Department of Physics, Illinois Institute of Technology, Chicago 16, Illinois
(Received December 14, 1954)

The Raman spectrum of 2,6-dioxaspiro(3,3)heptane in the molten state and infrared spectra of CS_2 and CCl_4 solutions have been investigated. The polarization of the Raman lines of the liquid also has been studied. The results indicate a symmetry D_{2d} for the molecule. The appearance of two extra strongly polarized Raman lines near the 2874K (kayser, cm^{-1}) line, which corresponds to the totally symmetric C—H stretching oscillation, has been accounted for by assuming Fermi resonance between overtones of C—H bending vibrations and the symmetric C—H stretching mode.

INTRODUCTION

FROM a study of the polarization of the Raman lines Cleveland, Murray, and Gallaway[1] concluded that spiropentane has the symmetry D_{2d}, since seven of the observed lines can be assigned to the skeleton C_2CC_2 and since three of them are polarized. A structure of symmetry D_{3h} would yield only five Raman lines for the skeleton.

A new molecule has been prepared by the Hercules Powder Company by (in effect) opening up the C—C bond in each of the two C_2 groups of the spiropentane molecule and introducing an oxygen atom so as to form the molecule (Fig. 1) called 2,6-dioxaspiro (3,3)heptane. The object of the present investigation was to study the Raman and infrared spectra of the substance and also the polarization character of the Raman lines in order to come to a definite conclusion regarding the structure of the molecule.

EXPERIMENTAL

The compound is a colorless crystalline substance melting at 88.4 to 89.8°C. It sublimes rapidly under reduced pressure even at room temperature. Preliminary investigations of the Raman spectrum in CS_2 solution showed that the Raman lines of the substance are very weak in comparison with those of CS_2. An attempt was therefore made instead to study the Raman spectrum in the molten state at a temperature a few degrees above its melting point. The substance was distilled under low pressure into a narrow Raman tube joined to a distilling flask of Pyrex glass and the tube was sealed off at its tail-end under reduced pressure. The Raman tube was then put coaxially in a jacket of Pyrex glass through which hot air was blown continuously to keep the temperature inside the jacket at *ca* 110°C. To avoid fluorescence of the liquid and also to facilitate unequivocal assignment of the Raman lines to the respective exciting lines, the 4046 A group of Hg lines was cut off by using as a light filter a 2% alcoholic solution of *p*-nitrotoluene plus one part in 50 000 of rhodamine 5 GDN extra. Two glass tubes of *ca* 2.5 cm o.d. filled with this solution focused 2 Hg arcs on the axis of the Raman tube. The Raman spectra were photographed with a Hilger E-612 spectrograph using both high-speed and high-dispersion cameras.

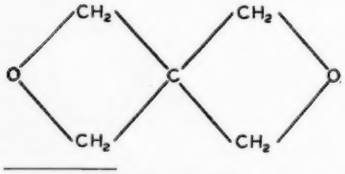

FIG. 1. The molecule 2,6-dioxaspiro(3,3)heptane.

The polarization of the Raman lines of the liquid was studied by photographing simultaneously the horizontal and vertical components, using a split-field Polaroid disk in front of the plane window of the Raman tube, as previously described.[2] The channels used in the previous investigation to get an almost parallel beam of incident light could not be used in the present investigation because of the presence of the wide jacket around the Raman tube, but reliable information regarding the depolarization factors of the Raman lines could be obtained by studying the polarization of the Raman lines of $CHCl_3$ and CCl_4 under an identical arrangement and measuring the densities of the vertical and horizontal components of each of the Raman lines with a Gaertner microdensitometer.

The infrared spectra of the solutions in CS_2 and CCl_4 were studied with a Beckman IR-2 spectrophotometer (KBr optics). The wave numbers above 1200K (kayser, cm^{-1})[3] are only approximate since the dispersion of KBr in this region is small and the errors are therefore rather large.

* On leave from the Indian Association for the Cultivation of Science, Calcutta 32, India.

† Present address: Sinclair Research Laboratories, Harvey, Illinois.

‡ Publication No. 112.

[1] Cleveland, Murray, and Gallaway, J. Chem. Phys. **15**, 747 (1947).

[2] F. F. Cleveland, J. Chem. Phys. **13**, 101 (1945).

[3] In accord with the recommendation of the Joint Commission for Spectroscopy (created under the auspices of the International Council of Scientific Unions by the International Union for Pure and Applied Physics and the International Astronomical Union), σ is used as the symbol for wave number and K (kayser) is used for the wave-number unit [see J. Opt. Soc. Am. **43**, 410 (1953) and Spectroscopia Molecular **3**, 67 (1954)]. The use of σ for wave number was also recommended by the Committee on Letter Symbols and Abbreviations of the American Association of Physics Teachers, and this was approved by the American Standards Association [see Am. J. Phys. **16**, 164 (1948)].

RESULTS

The Raman shifts and wave numbers of the bands observed in the infrared spectra are given in Table I. The approximate intensities of the lines as estimated visually are also indicated. The polarization character of the Raman lines is indicated by using the letter *P* to indicate a value of the depolarization factor less than 6/7 and the letter *D* to indicate a value equal to 6/7. The intensities of the infrared bands are indicated as strong and weak by using the letters s and w, respectively. The approximate absorption curves deduced from the traces obtained with the spectrophotometer are reproduced in Fig. 2.

DISCUSSION

It can be seen from Table I that of the 14 observed Raman lines 6 are polarized and 8 are depolarized.

TABLE I. Raman and infrared spectra of 2,6-dioxaspiro(3,3)heptane.[a]

Raman			Infrared	
$\Delta\sigma$ (K)	Approximate intensity	Polarization state	σ (K)	Relative intensity
275	1*b*	*D*	...	...
365	1*b*	*D*	...	...
491	3*b*	*P*	...	...
880	1*b*	*D*	814[b]	s
969	6	*P*	933	s
...	...	...	981	s
1134	4	*P*	...	...
1278	2	*D*	1222	w
1336	0	*D*	...	...
1360	1	*D*	...	...
1478	5*b*	*D*	...	...
...	...	...	2820	s
2874	10	*P*	...	...
2944	5*b*	*P*	...	...
2953	2	*D*	...	...
2982	2	*P*	...	...

[a] $\Delta\sigma$ = Raman displacement; σ = wave number, K = kayser = cm^{-1}, *b* = broad, *D* = depolarized, *P* = polarized, s = stong, and w = weak.
[b] CS_2 solution; in CCl_4 solution the observed value was 794. All other wave numbers were unaltered.

If we assume the structure of the molecule to have a symmetry D_{2d} (as for spiropentane), we expect 6 a_1, 4b_1, 6b_2, and 10*e* Raman lines. Three a_2's are forbidden both in the Raman and the infrared spectrum. Considering the skeleton alone, we expect for the same symmetry 3a_1, 1b_1, 3b_2, and 4*e* Raman lines. Of these the first three should have Raman shifts less than 1200K. The lines 491, 969, and 1134K can be identified with these. The line 969K is probably due to a C—C stretching mode, the line 1134K to a C—O stretching mode, and the line 491K may be due to a simultaneous bending of both the C—C and C—O bonds. Of the three polarized lines at 2874, 2944, and 2982K, the first is obviously due to the totally symmetric, C—H stretching mode, but it is difficult to visualize any other symmetric mode which would involve C—H stretching; the two lines at 2944 and 2982K must thus be assigned

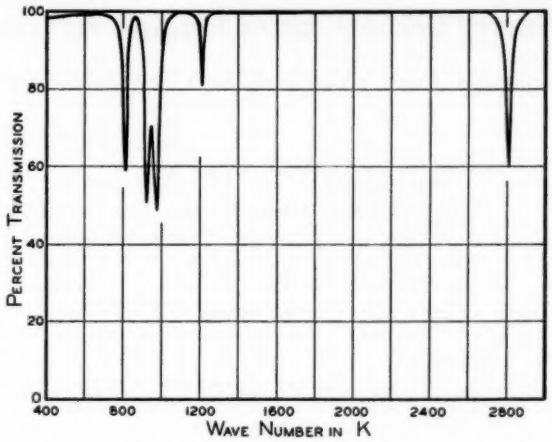

FIG. 2. Infrared absorption bands of 2,6-dioxaspiro(3,3)heptane.

to some other modes of vibration. The totally depolarized line at 1478K is due to a C—H bending mode. Its first overtone has a wave number near enough to that of the strong 2874K line to produce Fermi resonance, so that the overtone becomes intense and produces the 2944K line of intensity smaller than that of the 2874 line. The 2982 line is weaker than the 2944 line and is also probably due to such a resonance with an overtone of some other fundamental near 1400K, the fundamental itself being too weak to be observed in the Raman spectrum.

It is thus evident from the foregoing discussion that only four of the six strongly polarized Raman lines expected for the molecule of symmetry D_{2d} have actually been observed. Any other symmetry of the molecule would yield a larger number of strongly polarized Raman lines. The number of bands observed in the infrared spectrum of the molecule is also very small. Of course, wave numbers below 400K could not be observed with the instrument used in the present investigation, and the molecule is expected to produce a few infrared bands in that region, but the number should be very small. The vibrations of type a_1 are forbidden in the infrared for the symmetry D_{2d} and since none of the strongly polarized Raman lines coincides exactly with any wave number in the infrared, the assignment of symmetry D_{2d} to the molecule seems to be correct.

ACKNOWLEDGMENTS

This investigation was part of a research program which has been aided by grants from the Research Corporation and from the American Academy of Arts and Sciences. The sample was kindly furnished by the Hercules Powder Company through the courtesy of Dr. Robert H. Saunders. One of the authors (SCS) is indebted to the Government of India for a grant towards his traveling expenses which enabled him to join this laboratory for a short period.

Energy Calculations of Multiple Hydrogen-Atom Systems by VB and MO Methods*

ROLAND S. BARKER, RICHARD L. SNOW, AND HENRY EYRING
Department of Chemistry University of Utah, Salt Lake City, Utah

(Received December 28, 1954)

The equivalence of complete valence bond (VB) and of total configuration interaction molecular orbital (CIMO) methods has often been discussed. The two methods give identical expressions for H_2. Treatment of H_2 by the method of Coulson and Fischer also gives the same result. An extension of this method of semi-localized orbitals to the H_3^+ and H_3 systems is attempted and found to be unsatisfactory. This indicates that a single configuration treatment, however general the molecular orbitals may be, is a poorer approximation than either the extended VB or CIMO treatments.

R. Taylor's exact integral (LCI) molecular orbital treatment for linear H_4 is compared with the exact integral covalent bond (HL) method. A single structure of the latter method gave a ground-state energy of -57.02 ev while the two covalent structure treatment gave -58.59 ev. An energy of -55.64 ev is reported by Taylor using the best single MO configuration while he found an energy of only -56.40 ev using six of twelve possible MO ground-state configurations. It appears in view of the equivalence of the refined forms of the two treatments that the omitted higher energy configurations contribute more strongly to the ground-state energy than the lower energy ones. This indicates that low energy is not a good criterion for inclusion of configurations in a limited configuration interaction treatment. Recent work by A. Pullman on butadiene supports this conclusion.

1. INTRODUCTION

RECENT developments in molecular quantum mechanics have been confined in the main to refinement and use of the valence bond, VB, and molecular orbital, MO, approximations. Each of these methods has its own limitations and the particular problem under consideration seems to determine which method should be applied. Comparison of exact calculations by the two methods has been a stimulus to theoretical development, but until recently precise calculations for molecules of greater complexity than H_2 have usually necessitated mathematical approximations of uncertain magnitude.

Exact evaluation of some difficult multicenter integrals[1–3] in these complex problems has now allowed a careful consideration of a few multiparticle systems.[4–6] In this paper VB and MO wave functions for multi-hydrogenic systems are compared. Numerical results for the ground-state energy of the linear H_4 system are also discussed.

2. EQUIVALENCE OF VB AND MO TREATMENTS IN POLYATOMIC SYSTEMS

The equivalence of the VB treatment to the complete MO treatment has been discussed before.[7,8] Equivalence of these formulations has been specifically examined for the H_3^+ and H_3 systems.[4,6] The possible equivalence of the extended VB method to refinements of the Coulson and Fischer[9] treatment of H_2 has not received the same consideration. Some attempts[4,5] have been made in this direction, but these have not proved completely satisfactory. The semilocalized orbital theory of Mueller and Eyring[10] may be considered from this point of view. Consideration of electron repulsion has been included in their single configuration treatment with improved results. However the decomposition of their semilocalized orbitals into the proper atomic orbitals at infinite separation only partially duplicates Coulson's result with H_2. Even for H_3^+ and H_3 calculations have not met with equivalent success. In view of such work we have analyzed the wave functions of H_3^+ and H_3 by decomposing the most general unsymmetrical molecular orbital wave functions for these systems into the constituent atomic orbitals. The possible equivalence of this MO treatment to the VB treatment for these simple systems is thus tested. The wave function for the linear H_3^+ system may be formulated as

$$\Psi=\begin{pmatrix}A & A'\\ \alpha & \beta\end{pmatrix}-\begin{pmatrix}A & A'\\ \beta & \alpha\end{pmatrix} \tag{2.1}$$

where,

$$A=\lambda_1 a+\lambda_2 b+\lambda_3 c$$
$$A'=\mu_1 a+\mu_2 b+\mu_3 c.$$

Upon simplification of expression (2.1) and equating like terms to those obtained in the extended VB treatment (covalent plus ionic terms) one has the inconsistent equations,

$$\begin{aligned}C_1&=\lambda_1\mu_2+\lambda_2\mu_3=\lambda_2\mu_3+\lambda_1\mu_2\\&=\lambda_2\mu_1+\lambda_3\mu_2=\lambda_3\mu_2+\lambda_2\mu_1\\C_2&=\lambda_1\mu_1+\lambda_3\mu_3=\lambda_3\mu_3+\lambda_1\mu_1\\C_3&=2\lambda_1\mu_3=2\lambda_3\mu_1\\C_4&=2\lambda_2\mu_2.\end{aligned} \tag{2.2}$$

* This work was assisted in part by a grant from the National Science Foundation.

[1] Hirschfelder, Eyring, and Rosen, J. Chem. Phys. **4**, 121 (1936).
[2] M. P. Barnett and C. A. Coulson, Trans. Roy. Soc. (London) **A243**, 221 (1951).
[3] R. S. Barker and H. Eyring, J. Chem. Phys. **21**, 912 (1953).
[4] Walsh, Moore, and Matsen, J. Chem. Phys. **18**, 1070 (1950).
[5] J. M. Walsh and F. A. Matsen, J. Chem. Phys. **19**, 526 (1951).
[6] R. G. Pearson, J. Chem. Phys. **16**, 502 (1948).
[7] A. Meckler, J. Chem. Phys. **21**, 1750 (1953).
[8] P. O. Löwdin, Quarterly Progress Report of the Massachusetts Institute of Technology Solid-State and Molecular Theory Group (January, 1952).
[9] C. A. Coulson and I. Fischer, Phil. Mag. **40**, 386 (1949); C. A. Coulson, Trans. Faraday Soc. **33**, 1479 (1937).
[10] C. R. Mueller and H. Eyring, J. Chem. Phys. **19**, 1495 (1951).

Numerical values of the C's were obtained by Hirschfelder[11] using the complete VB wave function,

$$\psi=C_1\left\{\begin{pmatrix}a&b\\ \alpha&\beta\end{pmatrix}-\begin{pmatrix}a&b\\ \beta&\alpha\end{pmatrix}+\begin{pmatrix}b&c\\ \alpha&\beta\end{pmatrix}-\begin{pmatrix}b&c\\ \beta&\alpha\end{pmatrix}\right\}$$
$$+C_2\left\{\begin{pmatrix}a&c\\ \alpha&\beta\end{pmatrix}-\begin{pmatrix}a&c\\ \beta&\alpha\end{pmatrix}\right\} \tag{2.3}$$
$$+C_3\left\{\begin{pmatrix}a&a\\ \alpha&\beta\end{pmatrix}+\begin{pmatrix}c&c\\ \beta&\alpha\end{pmatrix}\right\}+C_4\begin{pmatrix}b&b\\ \alpha&\beta\end{pmatrix}.$$

No consistent values of λ_1, λ_2, λ_3, μ_1, μ_2, and μ_3 could be found. A similar analysis was made for the H_3 molecule and again inconsistent parametric equations were obtained. Thus it has been concluded that no single configuration treatment for even these simple molecules will give results equivalent to the complete VB treatment or the complete MO treatment.

3. ENERGY CALCULATIONS FOR THE LINEAR H_4 SYSTEM

a. Valence Bond Calculation

The wave functions for the covalent structures of the ground-state H_4 linear symmetrical system may be represented by

$$\psi_1=\psi_{ab,\,cd}=\begin{pmatrix}a&b&c&d\\ \alpha&\beta&\alpha&\beta\end{pmatrix}-\begin{pmatrix}a&b&c&d\\ \beta&\alpha&\alpha&\beta\end{pmatrix}$$
$$-\begin{pmatrix}a&b&c&d\\ \alpha&\beta&\beta&\alpha\end{pmatrix}+\begin{pmatrix}a&b&c&d\\ \beta&\alpha&\beta&\alpha\end{pmatrix} \tag{3.1}$$

$$\psi_2=\psi_{ad,\,bc}=\begin{pmatrix}a&b&c&d\\ \alpha&\alpha&\beta&\beta\end{pmatrix}-\begin{pmatrix}a&b&c&d\\ \beta&\alpha&\alpha&\beta\end{pmatrix}$$
$$-\begin{pmatrix}a&b&c&d\\ \alpha&\beta&\beta&\alpha\end{pmatrix}+\begin{pmatrix}a&b&c&d\\ \beta&\beta&\alpha&\alpha\end{pmatrix}. \tag{3.2}$$

The function for $\psi_{ac,\,bd}$ need not be considered as it is easily shown to be a combination of (3.1) and (3.2).

The notation and symbols are those used previously. The wave function for the VB covalent structural approximation is then, $\psi=k_1\psi_1+k_2\psi_2$. The complete Hamiltonian operator for the system is,

$$\mathcal{H}=-\tfrac{1}{2}\sum_{n=1}^{4}\nabla_n^2+\sum_{b>p=a}^{d}R_{1p}^{-1}-\sum_{l=a,\,n=1}^{d,\,4}r_{1n}^{-1}+\sum_{n>m=1}^{4}r_{mn}^{-1}. \tag{3.3}$$

The ground-state energy may be computed by solution of the usual second-order secular determinant. Reduction of the matrix elements to atomic orbital integrals is made in the usual way.[12] Thus one obtains,

$$H_{11}=\int\psi_1\mathcal{H}\psi_1 d\tau=8a^2b^2abab+4a^2b^2c^2d^2+8adbcacac$$
$$-8a^2abacbc-8adb^2acab-4a^2c^2acac$$
$$-2a^2a^2bcbc-2adadb^2b^2+4acacacac$$
$$+4adadbcbc-8acacabab+4abababab. \tag{3.4}$$

$$H_{12}=H_{21}=8a^2bdc^2db+8a^2bdcbdc-4a^2b^2cddc$$
$$-4a^2bccddb-2a^2b^2c^2d^2+8acb^2cdda$$
$$-2a^2bccbd^2+8abbccdda-2adb^2c^2da$$
$$-4adbccadb-2abbdcadc-2acbdcadb$$
$$-2abbacddc-2adbccbda-2acbacddb$$
$$-4adb^2cadc. \tag{3.5}$$

$$H_{22}=\int\psi_2\mathcal{H}\psi_2 d\tau=4a^2b^2c^2d^2-4a^2b^2cddc+4abbacddc$$
$$+4adb^2c^2da+4a^2bccbd^2-4a^2bdc^2db$$
$$-4a^2bccddb-4a^2bdcbdc+4acbacddb$$
$$+4abbdcadc+4acbdcadb-4adb^2cadc$$
$$-4acb^2cdda+4adbccbda-4acbdcbda$$
$$-4adbacbda. \tag{3.6}$$

The atomic orbital integrals are written symbolically,

$$\int a(1)a(2)b(3)b(4)\,|\mathcal{H}|\,d(1)d(2)c(3)c(4)d\tau$$
$$=(aabb\,|\mathcal{H}|\,ddcc)=adadbcbc.$$

They may then be easily expressed[11] in terms of composite integrals of the types $I_{ac}=\int a(n)c(n)d\tau_n$ (overlap), $K_{a,\,bc}=\int(1/r_{an})b(n)c(n)d\tau_n$ (nuclear attraction), $L_{ad,\,bc}=\int(1/r_{nm})a(n)d(n)b(m)c(m)d\tau_n d\tau_m$ (electron repulsion), and $T_{ab}=\int a(n)\,|-\tfrac{1}{2}\nabla^2|\,b(n)d\tau_n$ (kinetic energy). This kinetic energy integral may be further simplified to an expression in terms of the elemental overlap, attraction, and repulsion types listed.

The needed numerical evaluations of the elemental integrals for the internuclear distance selected for the H_4 system are all tabulated by Taylor.[13] This selected internuclear distance is $R=R_{ab}=R_{bc}=R_{cd}=1.4$ a.u. The values, given in electron volts, were obtained by series methods[1,2] and are believed to be accurate to the given four significant figures.

Results obtained for the linear symmetrical H_4 system give a ground-state energy of -57.02 ev for the single covalent structure represented by the VB wave function ψ_1(3.1) and an energy of -58.59 ev for the complete covalent-bond representation, $\psi=k_1\psi_1+k_2\psi_2$.

b. Molecular Orbital Calculation

The MO treatment of the linear symmetrical H_4 system is given explicitly by Taylor.[13] The separate phases of the theory are therefore not examined in detail. In the examination of the configuration interaction MO approach however consideration might well be given to the specific MO's used.

The four molecular orbitals (MO's) for the H_4 system are constructed from linear combinations of 1s atomic orbitals (LCAO) considered to be associated

[11] J. O. Hirschfelder, dissertation, Princeton University (1935).

[12] R. S. Barker and H. Eyring, J. Chem. Phys. **22**, 1182 (1954).

[13] R. Taylor, Proc. Phys. Soc. (London) **64**, 249 (1951).

with the four nuclei $\mathfrak{A}$, $\mathfrak{B}$, $\mathfrak{C}$, and $\mathfrak{D}$. These orbitals may be designated, as $a(n)$, $b(n)$, $c(n)$, and $d(n)$. The orbital d when occupied by electron n is thus $d(n)=(Z_d^3/\pi)^{\frac{1}{2}}e^{-Z_d r_{dn}}$. The molecular orbitals may then be formulated as,

$$\begin{aligned}A(n)&=k_{aA}a(n)+k_{bA}b(n)+k_{cA}c(n)+k_{dA}d(n)\\B(n)&=k_{aB}a(n)+k_{bB}b(n)+k_{cB}c(n)+k_{dB}d(n)\\C(n)&=k_{aC}a(n)+k_{bC}b(n)+k_{cC}c(n)+k_{dC}d(n)\\D(n)&=k_{aD}a(n)+k_{bD}b(n)+k_{cD}c(n)+k_{dD}d(n).\end{aligned}\tag{3.7}$$

The capital letters $L(A, B, C,$ or $D)$ represent the different molecular orbitals, the small letters $(a, b, c,$ or $d)$ the atomic orbitals and the k_{1L}'s the appropriate coefficients. Various techniques for obtaining numerical values for these molecular orbital coefficients, k_{1L}, have been used. One frequently favored, the Roothaan technique,[14] proceeds by way of an iterative self-consistent field (SCF) method employing a matrix procedure. Other simpler "inconsistent" coefficients are used by Taylor.[13] The question of comparative worth of such techniques will be commented upon later.

Compounding the MO's of the system into "spin-orbital composition functions" parallels development with the valence-bond method.[15,16] Definition of a particular so-called spin-orbital composition function, "antisymmetrized product (A.P.)" or "Slater determinant" follows. The various notational forms are,

$$\psi=\sum P_\nu(-1)^\nu(A\alpha)_1(A\beta)_2(B\alpha)_3(B\beta)_4 \tag{3.8}$$

$$=(4!)^{-\frac{1}{2}}\begin{vmatrix}(A\alpha)_1 & (A\beta)_1 & (B\alpha)_1 & (B\beta)_1\\(A\alpha)_2 & (A\beta)_2 & (B\alpha)_2 & (B\beta)_2\\(A\alpha)_3 & (A\beta)_3 & (B\alpha)_3 & (B\beta)_3\\(A\alpha)_4 & (A\beta)_4 & (B\alpha)_4 & (B\beta)_4\end{vmatrix} \tag{3.9}$$

$$=\begin{pmatrix}A & A & B & B\\ a & \beta & \alpha & \beta\end{pmatrix}. \tag{3.10}$$

The foregoing notations (3.8), (3.9), and (3.10) explain in part the profusion of names used in the literature. From the first representation as "a linear combination of products" the antisymmetric nature of the function with electron exchange is apparent. The "expanded Slater determinant notation" (3.9) makes satisfaction of the Pauli principle obvious from the laws of determinants. The third notation (3.10) stresses the particular spin-orbital assignment. Each such "spin-orbital composition function" is associated with a definite assignment of the spins to each component molecular orbital. These functions singly or linearly combined give the so-called molecular-orbital configurations.

For the linear symmetrical H_4 system allowed allocation of the electrons to the molecular orbitals of the system define the following spin-orbital composition functions Φ_n.

These spin-orbital composition functions, Φ_n, of Table I may be compounded into configurations by the usual considerations. Thus the $^1\Sigma_g$ configurations are,

$$\Psi_{\rm I}=\Phi_1=\begin{pmatrix}A & A & B & B\\ \alpha & \beta & \alpha & \beta\end{pmatrix},\quad \Psi_{\rm II}=\Phi_2,\quad \Psi_{\rm III}=\Phi_3,$$

$$\Psi_{\rm IV}=\Phi_4,\quad \Psi_{\rm V}=\Phi_5,\quad \Psi_{\rm VI}=\Phi_6,$$

$$\Psi_{\rm VII}=\Phi_7-\Phi_6=\begin{pmatrix}A & A & B & D\\ \alpha & \beta & \alpha & \beta\end{pmatrix}-\begin{pmatrix}A & A & B & D\\ \alpha & \beta & \beta & \alpha\end{pmatrix}$$

$$\Psi_{\rm VIII}=\Phi_9-\Phi_{10},\quad \Psi_{\rm IX}=\Phi_{11}-\Phi_{12},\quad \Psi_{\rm X}=\Phi_{13}-\Phi_{14},$$

$$\Psi_{\rm XI}=\Phi_{15}-\Phi_{16}-\Phi_{17}+\Phi_{18}$$

$$\Psi_{\rm XII}=\Phi_{15}+\Phi_{18}-\Phi_{19}-\Phi_{20}.$$

Six of the foregoing $^1\Sigma_g$ configurations were used by Taylor[13] in a limited configuration interaction (LCI) treatment. Increasing order of orbital energies is indicated by the MO series A, B, C, and D (Taylor's i, j, k, and l). Orbitals A and C (i,k) are symmetrical (σ_g) while B and D (j,l) are antisymmetric (σ_u) with respect to reflection in the plane normal to the line of protons at the geometrical midpoint. Numerical values for the MO coefficients, k_{1L}, obtained by usual techniques are given in the appendix of Taylor's article.

The wave function for configuration interaction may be written,

$$\Psi=\sum_{N=1} K_N\Psi_N. \tag{3.11}$$

The coefficients, K_N, and the ground-state energy may be found in the usual way from the Nth-order secular

TABLE I. Spin-orbital (σ_g) composition functions for H_4.

Φ_n	Occupied Cap. letter notation	Orbitals Taylor's notation	$A(g)$ or i	$B(u)$ or j	$C(g)$ or k	$D(u)$ or l
Φ_1	(A^2B^2)	(i^2j^2)	$\alpha\beta$	$\alpha\beta$		
Φ_2	(A^2C^2)	(i^2k^2)	$\alpha\beta$		$\alpha\beta$	
Φ_3	(A^2D^2)	(i^2l^2)	$\alpha\beta$			$\alpha\beta$
Φ_4	(B^2C^2)	(j^2k^2)		$\alpha\beta$	$\alpha\beta$	
Φ_5	(B^2D^2)	(j^2l^2)		$\alpha\beta$		$\alpha\beta$
Φ_6	(C^2D^2)	(k^2l^2)			$\alpha\beta$	$\alpha\beta$
Φ_7	(A^2BD)	(i^2jl)	$\alpha\beta$	α		β
Φ_8			$\alpha\beta$	β		α
Φ_9	(AB^2C)	(ij^2k)	α	$\alpha\beta$	β	
Φ_{10}			β	$\alpha\beta$	α	
Φ_{11}	(BC^2D)	(jk^2l)		α	$\alpha\beta$	β
Φ_{12}				β	$\alpha\beta$	α
Φ_{13}	(ACD^2)	(ikl^2)	α		β	$\alpha\beta$
Φ_{14}			β		α	$\alpha\beta$
Φ_{15}			α	β	α	β
Φ_{16}			α	β	β	α
Φ_{17}	$(ABCD)$	$(ijkl)$	β	α	α	β
Φ_{18}			β	α	β	α
Φ_{19}			α	α	β	β
Φ_{20}			β	β	α	α

[14] C. C. J. Roothaan, Revs. Modern Phys. **23**, 69 (1951).
[15] J. C. Slater, Phys. Rev. **38**, 1109 (1931).
[16] Eyring, Walter, and Kimball, *Quantum Chemistry* (John Wiley and Sons, Inc., New York, 1944), p. 190 ff.

determinant, the secular equations, and the trial function normalization condition. Taylor's LCI treatment $N=6$, used the six lowest energy configurations. With such treatment using simple inconsistent MO's he obtained a ground-state energy of $E=-56.40$ ev. The lowest single configurational energy of this set was $E=-54.11$ ev. A better single configuration energy was obtained using the single determinant (SCF) MO's. Such treatment gave $E=-55.64$ ev. The results of both MO and VB approximations are given in Table II. The usual abbreviations, (SC-MO) single-configuration molecular orbital, (TCI) total configuration interaction, and (LCI) limited-configuration interaction are used in the table.

Comparison of the results for the H_4 system given in Table II disclose that the best single-configurational MO treatment is 2 ev poorer than the best single-covalent structural VB result. Further the LCI-MO treatment using the six lowest energy configurations is 3 ev poorer than the LCI-VB treatment using just the two covalent structures. As the TCI treatments of both VB and MO approximations are equivalent, one is led to conclude that for this system a simple VB treatment is preferable to the simple MO treatment. The poor LCI-MO results may be due to the inclusion of too much "ionicity" in the low-energy MO configurations. The substitution of neglected higher energy MO configurations for the low-energy ones in the LCI treatment might give a better result. Recent work by Pullman[17] on butadiene indicates that such may be the case. A full configuration interaction treatment of the nine $^1\Sigma_g$ functions of butadiene show the ground-state energy to consist of 87% of the lowest energy configuration, and of 5.5% and 1% of the highest and next highest energy configurations respectively. Calculations of the dipole and other properties are even more affected by the high energy configurations.

The results of our work and of Pullman's paper lend emphasis to the recent melancholy conclusion of Coulson, Craig, and Jacobs[18] that "It appears beyond any doubt, that configuration interaction plays a significant role" and that "there appear to be no simple rules for determining in advance which (MO) configurations will interact most strongly with one another." The poor energy comparison of the "best" single MO configuration of the H_4 system with the simple Heitler-London type VB calculation supports the further conclusion that control of "the extent of interaction by such means as a better choice of basic MO's is not really satisfactory." Such conclusions, however, do not alter the present position with respect to a choice of VB or MO approximation. The paramagnetism of the ground state of O_2 is still best accounted for by the MO treatment while some individual energy calculations of the VB treatment are best. The choice must still be made for the particular problem under consideration.

[17] A. Pullman, J. chim. phys. **51**, 188 (1954).
[18] Coulson, Craig, and Jacobs, Proc. Roy. Soc. (London) **A206**, 308 (1951).

TABLE II.

System and type treatment	Energy of system (ev)
Single H atom	−13.537
Molecular H_2	
Experimental ($R=1.4$ au)	−31.95
SC-VB (Covalent structure) $R=1.66$	−30.35
SC-VB Wang refinement ($R=1.45$)	−30.96
SC-MO ($R=1.6$ au)	−29.89
TCI ($R=1.6$ au)	−30.43
TCI ($R=1.4$ au)	−30.03
Four free H atoms	−54.148
Two H_2 molecules TCI ($R=1.4$ au)	−60.06
Linear symmetrical H_4 ($R=1.4$ au)	
SC-MO	−54.11
SC-MO (SCF)	−55.64
LCI-MO (6 of 12)	−56.40
SC-VB (Single covalent structure)	−57.02
SC-VB (SCF Wang-like refinement)	−57.03
LCI-VB (2) Both covalent structures	−58.59

5. OTHER POSSIBLE REFINEMENTS

A common type refinement for simple hydrogen-atom-containing systems of both VB and MO type treatments is inclusion of a so-called "effective charge" parameter Z. Taylor rightly decided on the basis of previous calculations by Coulson and on the basis of the unequal placement of the nuclei, a and d at the end and b and c in between, that such a Wang-like refinement would alter the energy of the H_4 system very little. Similar reasoning would apply to the VB treatment.

Another possible refinement of the treatments might include a more realistic internuclear distance parameter. The experimental internuclear H_2 distance $R=1.4$ au is smaller than the best distance minimization values of comparable H_2 calculations. For the loosely bound H_4 system the internuclear distance R would certainly be greater. However, in view of the difficulty in re-evaluating the difficult multicenter integrals and in view of the fact that this linear H_4 system's greatest importance would seem to be in testing various types of computations such a refinement has not been attempted.

ACKNOWLEDGMENTS

We should like to thank M. Krauss and A. L. Wahrhaftig, Chemistry Department, University of Utah for helpful discussions of phases of this problem.

Complete π-Electron Treatment of Allyl Radical and Allyl Ion*

H. C. LEFKOVITS,† JANICE FAIN, AND F. A. MATSEN
Department of Chemistry and Department of Physics, The University of Texas, Austin, Texas
(Received December 16, 1954)

The wave functions for the allyl radical and ion are linear combinations of all independent antisymmetrized products of π-electron wave functions. The ground-state energy of the radical is $3W_{2p}-28.963$ ev and of the ion $2W_{2p}-30.471$ ev. Setting $-W_{2p}$ equal to the ionization energy of methyl, the ionization energy of allyl is calculated to be 8.44 ev, compared to an experimental value of 8.16 ev. The resonance energy of the ion is calculated to be $\sim$1.50 ev greater than that of the radical. An experimental comparison based on methyl and neglecting some compression energy is $\sim$1.70 ev.

INTRODUCTION

THE allyl radical and allyl ion are of considerable interest to organic chemists as potential intermediates in a number of chemical reactions. There is additional interest because experimental values for the ionization energy of the allyl radical have appeared in the literature and because of discussions on the presence or absence of resonance energy in the allyl ion. The π-electron treatment of these systems is simple enough to be done completely, yet complicated enough to reflect many of the difficulties which arise in more complex systems.

A molecular orbital treatment with complete configuration interaction has been carried out for the radical[1a,1b,2] and for the ion.[1b] The radical and the ion have also been treated by a simplified self-consistent field molecular orbital scheme.[3] In the present paper there is employed the valence bond approach, using all covalent and ionic structures. The results should be identical with those of references 1a, 1b, 2.

THE ALLYL RADICAL, C_3

Formally the theory for the ground states of C_3 and C_3^+ is identical to that of H_3 and H_3^+ treated by Hirschfelder *et al.*[4] The present paper will consider, in addition, the excited states of both species.

There are for C_3 nine independent Slater determinants which can be constructed from π orbitals with a spin assignment of two α's and one β:

$$\phi_1=\begin{pmatrix} a & b & c \\ \alpha & \beta & \alpha \end{pmatrix},[5] \quad \phi_2=\begin{pmatrix} a & b & c \\ \alpha & \alpha & \beta \end{pmatrix}, \quad \phi_3=\begin{pmatrix} a & b & c \\ \beta & \alpha & \alpha \end{pmatrix}, \quad \phi_4=\begin{pmatrix} a & a & c \\ \alpha & \beta & \alpha \end{pmatrix}, \quad \phi_5=\begin{pmatrix} c & c & a \\ \alpha & \beta & \alpha \end{pmatrix},$$

$$\phi_6=\begin{pmatrix} a & b & b \\ \alpha & \beta & \alpha \end{pmatrix}, \quad \phi_7=\begin{pmatrix} b & b & c \\ \alpha & \beta & \alpha \end{pmatrix}, \quad \phi_8=\begin{pmatrix} a & a & b \\ \alpha & \beta & \alpha \end{pmatrix}, \text{ and } \quad \phi_9=\begin{pmatrix} b & c & c \\ \alpha & \beta & \alpha \end{pmatrix}.$$

The ionic terms, ϕ_4 to ϕ_9 are all eigenfunctions of S^2 with $S=\frac{1}{2}$. The nonionic terms ϕ_1, ϕ_2, and ϕ_3 are not, but linear combinations of them are eigenfunctions of S^2. Thus,

$$\phi_1+\phi_2+\phi_3(S=\tfrac{3}{2}), \quad \phi_2-\phi_3(S=\tfrac{1}{2}),$$

and

$$2\phi_1-\phi_2-\phi_3(S=\tfrac{1}{2}).$$

The problem is further simplified when advantage is taken of the twofold axis of symmetry. The proper orbitals for point group C_{2v} are the following:

$^2B_1$, $\psi_1=\phi_2-\phi_3$, $\psi_2=\phi_4+\phi_5$, $\psi_3=\phi_6-\phi_7$ and $\psi_4=\phi_8-\phi_9$

$^2A_2$, $\psi_1=2\phi_1-\phi_2-\phi_3$, $\psi_2=\phi_4-\phi_5$, $\psi_3=\phi_6+\phi_7$ and $\psi_4=\phi_8+\phi_9$

$^4A_2$, $\psi_1=\phi_1+\phi_2+\phi_3$.

The familiar variation theory yields two fourth-order and one first-order determinants.

The values of the integrals were taken from Parr, Craig, and Ross.[6] The values of (ab,bc) and (ac,bb) were obtained by the approximation method of Craig.[7] The determinantal equations then become

* This work was supported by Contract DA-23-072-ORD-774 of the U. S. Office of Ordnance Research. A portion of this work appeared in the Annual Report 1951–52 of Project N8 onr-70 800 of the Office of Naval Research.

† Present address: Exploration and Products Research Division, Shell Oil Company, Inc., Houston, Texas.

[1a] O. Chalvet, Compt. rend. **234**, 2369 (1952).

[1b] O. Chalvet and W. Daudel, J. Chim. Phys. **49**, 629 (1952).

[2] W. Moffitt, Proc. Roy. Soc. (London) **A218**, 486 (1953).

[3] A. Brickstock and J. A. Pople, Trans. Faraday Soc. **50**, 901 (1954).

[4] J. Hirschfelder *et al.*, J. Chem. Phys. **4**, 121, 130 (1936).

[5] $\begin{pmatrix} a & b & c \\ \alpha & \beta & \alpha \end{pmatrix}=\begin{vmatrix} a(1)\alpha(1) & b(1)\beta(1) & c(1)\alpha(1) \\ a(2)\alpha(2) & b(2)\beta(2) & c(2)\alpha(2) \\ a(3)\alpha(3) & b(3)\beta(3) & c(3)\alpha(3) \end{vmatrix}$.

[6] Parr, Craig, and Ross, J. Chem. Phys. **18**, 1561 (1950).

[7] D. P. Craig, Proc. Roy. Soc. (London) **A202**, 499 (1950). See also A. L. Sklar, J. Chem. Phys. **7**, 984 (1939).

$$
{}^2B_1,\ \begin{vmatrix} -24.249 & -0.9313x & -7.556 & -0.2401x & 7.415 & +0.2349x & -0.028 & +0.0076x \\ & & -16.641 & -0.9597x & 0.050 & -0.00x & -6.127 & -0.2401x \\ & & & & -16.050 & -0.9037x & -6.125 & -0.2349x \\ & & & & & & -13.624 & -0.9313x \end{vmatrix} = 0
$$

$$
{}^2A_2,\ \begin{vmatrix} -89.403 & -3.1900x & -25.557 & -0.7788x & -25.029 & -0.7497x & -7.962 & -0.1947x \\ & & -20.029 & -1.0373x & -5.359 & -0.1299x & -7.090 & -0.2596x \\ & & & & -19.401 & -0.9611x & -7.063 & -0.2499x \\ & & & & & & -13.879 & -0.9336x \end{vmatrix} = 0
$$

$$
{}^4A_2,\ \begin{vmatrix} -32.529 & -1.303x \end{vmatrix} = 0
$$

$$x = \mathcal{E} + 3W_{2p}$$

the roots are

-28.963 ($^2A_2$), -26.425 ($^2B_1$), -25.082 ($^4A_2$),
-18.939 ($^2B_1$), -16.678 ($^2A_2$), -15.968 ($^2A_2$),
-14.309 ($^2B_1$), -10.287 ($^2B_1$) and -9.278($^2A_2$).

Moffitt[2] gives a graph which appears in agreement with these figures if the level labeled $^4B_1$, is relabeled $^4A_2$.

The eigenvectors for the ground state ($^2A_2$) of the radical are $C_1=0.862$, $C_2=0.316$, $C_3=0.396$, and $C_4=0.137$. The covalent structures C=C−C+C−C=C alone, described by ψ_1, give an energy only 0.2 ev above that given by the complete treatment.

THE ALLYL ION, C_3^+

For the allyl ion, the base functions are

$$\phi_1 = \begin{pmatrix} a & b \\ \alpha & \beta \end{pmatrix}, \quad \phi_2 = \begin{pmatrix} a & b \\ \beta & \alpha \end{pmatrix}, \quad \phi_3 = \begin{pmatrix} a & c \\ \alpha & \beta \end{pmatrix},$$

$$
{}^1B_1,\ \begin{vmatrix} -67.466 & -2.3480x & -19.610 & -0.5402x & -16.724 & -0.5402x & -17.868 & -0.5200x \\ & & -25.557 & -1.0015x & -3.380 & -0.0777x & -3.086 & -0.0676x \\ & & & & -14.295 & -1.0015x & -2.773 & -0.0676x \\ & & & & & & -11.301 & -0.5000x \end{vmatrix} = 0
$$

$$
{}^3B_1,\ \begin{vmatrix} -44.030 & -1.8076x \end{vmatrix} = 0
$$

$$
{}^3A_2,\ \begin{vmatrix} -50.090 & -1.9222x & -17.530 & -0.4998x \\ & & -25.363 & -0.9985x \end{vmatrix} = 0
$$

$$
{}^1A_2,\ \begin{vmatrix} -48.383 & -1.9222x & -7.322 & -0.2498x \\ & & -14.101 & -0.9985x \end{vmatrix} = 0
$$

$$x = \mathcal{E} + 2W_{2p}$$

the roots are

-30.471 ($^1B_1$), -28.332 ($^3A_2$), -25.450 ($^1A_2$),
-24.358 ($^3B_1$), -22.684 ($^1B_1$), -20.440 ($^3A_2$),
-16.281 ($^1B_1$), -13.438 ($^1A_2$), -10.550 ($^1B_1$).

The eigenvectors for the ground state of the ion ($^1B_1$) are $C_1=0.775$, $C_2=0.627$, $C_9=0.077$, and $C_4=0.576$. Here the high energy structures C−C−C and C−C−C (+ + − +) make an appreciable contribution.

The results agree to within 0.3 ev with the molecular orbital calculations[1a,1b] for all states except the $^1A_1$ state of the ion.

IONIZATION ENERGY OF THE ALLYL RADICAL

The vertical ionization energy of the allyl radical is given by the difference in energy between the ground state of the ion and of the radical:

$$I = \mathcal{E}_{C_3^+} - \mathcal{E}_{C_3} = 2W_{2p} - 30.471 - (3W_{2p} - 28.963) = -W_{2p} - 1.508 \text{ ev.}$$

Mulliken[8,9] has suggested for $-W_{2p}$ the value, 11.28 ev, which makes the ionization energy of the allyl radical 9.77 ev.

Another possible choice for $-W_{2p}$ is the ionization energy, 9.95 ev,[10] of the methyl radical. The radical is usually considered to be planar, leaving the unpaired electron in an unhybridized p-orbital. With it the ionization energy of the allyl radical is 8.44 ev. Finally

$$\phi_4 = \begin{pmatrix} a & c \\ \beta & \alpha \end{pmatrix}, \quad \phi_5 = \begin{pmatrix} b & c \\ \alpha & \beta \end{pmatrix}, \quad \phi_6 = \begin{pmatrix} b & c \\ \beta & \alpha \end{pmatrix},$$

$$\phi_7 = \begin{pmatrix} a & a \\ \alpha & \beta \end{pmatrix}, \quad \phi_8 = \begin{pmatrix} b & b \\ \alpha & \beta \end{pmatrix}, \text{ and } \quad \phi_9 = \begin{pmatrix} c & c \\ \alpha & \beta \end{pmatrix}.$$

The proper combinations are as follows:

$^1B_1$, $\psi_1 = (\phi_1 - \phi_6) - (\phi_2 - \phi_5)$,
$\psi_2 = \phi_3 - \phi_4$, $\psi_3 = \phi_7 + \phi_9$ and $\psi_4 = \phi_8$

$^3B_1$, $\psi_1 = (\phi_1 - \phi_6) + (\phi_2 - \phi_5)$,

$^1A_2$, $\psi_1 = (\phi_1 + \phi_6) - (\phi_2 + \phi_5)$, and $\psi_2 = (\phi_7 - \phi_9)$

$^3A_2$, $\psi_1 = (\phi_1 + \phi_6) + (\phi_2 + \phi_5)$, $\psi_2 = (\phi_3 + \phi_4)$.

which lead to the determinantal equations

[8] R. S. Mulliken, J. Chim. Phys. **46**, 497 (1949).
[9] R. G. Parr and R. S. Mulliken, J. Chem. Phys. **18**, 1338 (1950).
[10] J. L. Franklin and H. E. Lumpkin, J. Chem. Phys. **19**, 1073 (1951).

$-W_{2p}$ may be set equal to the ionization of the propyl radical, 8.69 ev.[11] Here the polarization of three carbon atoms and their environment is included in each W_{2p} which refers to one carbon atom. This choice will make the ionization energy of the allyl free radical equal to 7.48 ev.

The ionization energy of the allyl radical has been determined mass spectrometrically. Evans and Szwarc[12] report 9.05 ev, Franklin and Lumpkin,[10] 8.4 ev, and Lossing, Ingold, and Henderson,[13] 8.16 ev.

Since in mass spectrometry the lowest value is usually the best, the 8.16 ev value is preferred. This is in quite good agreement with calculated value (based on methyl) of 8.44 ev.

When the methyl value for $-W_{2p}$ is used for ethylene, one also obtains good agreement with the experimental ionization energy, 10.6 ev, since $I=-W_{2p}-12.44+13.06$.

On the basis of calculations on ethylene Chalvet and Dandel[11b] suggest $-W_{2p}=9.5$ ev.

RESONANCE ENERGIES

In the calculation of resonance energy there are several choices of the quantum-mechanical reference state.[14,15] The simplest is to neglect the interaction of the carbon atom and the carbon ion with the double bond. The neglect of the interaction will probably lower $R_{C_3^+}$ and raise R_{C_3} so that

$$R_{C_3^+}-R_{C_3}<1.51 \text{ ev.}$$

Following Halpern[10] the resonance energy of the ion can be obtained from appearance potentials

$$A_{R_0^+}-A_{R^+}=R_{R^+},$$

where R_0 is the reference ion. Taking methyl as reference

$$R_{C_3^+}=13.44-10.78=2.66 \text{ ev}$$

the resonance energy of the radical has been found to be close to 1 ev. The vertical resonance energy will be larger than this. Thus

$$R_{C_3^+}-R_{C_3}<1.6.$$

ACKNOWLEDGMENTS

We wish to thank Dr. J. L. Franklin for calling our attention to the problem and Mr. R. E. Tannich for carrying out the calculations on an IBM–CPC calculator.

[11] J. Halpern, J. Chem. Phys. **20**, 744 (1952).
[12] M. G. Evans and M. Szwarc, J. Chem. Phys. **19**, 1322 (1951).
[13] Lossing, Ingold, and Henderson, J. Chem. Phys. **22**, 1489 (1954).
[14] R. S. Mulliken and R. G. Parr, J. Chem. Phys. **19**, 1271 (1951).
[15] In reference 14 there is discussed exchange repulsion between pairs of double bonds in analogy with the exchange repulsion between two helium atoms. A reference state in which there is exchange but atom c carries only spin α and one electron may be constructed from the functions $\begin{pmatrix} a & b & c \\ \alpha & \beta & \alpha \end{pmatrix}$, $\begin{pmatrix} a & b & c \\ \beta & \alpha & \alpha \end{pmatrix}$, $\begin{pmatrix} a & a & c \\ \alpha & \beta & \alpha \end{pmatrix}$, and $\begin{pmatrix} b & b & c \\ \alpha & \beta & \alpha \end{pmatrix}$ has energy $3W_{2p}-27.938$. This gives a vertical resonance energy of $\sim$1 ev very close to the observed thermal resonance energy. It is not clear whether one is including exchange repulsion or neglecting an arbitrary amount of exchange attraction.

THE JOURNAL OF CHEMICAL PHYSICS VOLUME 23, NUMBER 9 SEPTEMBER, 1955

Proton Magnetic Resonance of the CH_3 Group. III. Reorientation Mechanism in Solids*

J. G. POWLES† AND H. S. GUTOWSKY
Noyes Chemical Laboratory, University of Illinois, Urbana, Illinois
(Received December 20, 1954)

The proton magnetic resonance absorption has been reported to change with temperature in a manner suggesting hindered C_3 rotational motions of the CH_3 groups in several solid compounds. In this paper, the reorientation mechanism is considered more closely. The second moments of the absorption lines are calculated as a function of temperature for three types of motion. Similar predictions are obtained for two classical models, a Brownian type rotation by random angles and a random jumping between fixed positions $2\pi/3$ apart. The results are different for the third model, a quantum-mechanical tunnel effect, for which approximate calculations are given.

The experimental data for methyl chloroform, 2,2-dinitropropane, and 2-chloro-2-nitropropane can be fitted either to a classical model or to the tunnel effect by adjusting the potential barrier to the reorientations. However, the activation energies for classical rotation are low, about 2.2 kcal mole^{-1} and the observed frequency factors of 10^7 are unexplained. The tunnel effect gives larger barriers, about 5 kcal, and the predicted frequency factors agree well with experiment. In the case of 2,2-dichloropropane a classical motion is indicated by the large frequency factor of 10^{12}.

I. INTRODUCTION

MOLECULAR motions in solids have been investigated by observing the temperature dependence of nuclear magnetic resonance line shapes. The analysis of the line shape changes often tells one a great deal about the motions; for instance, it tells whether or not there are reorientations about a specific molecular axis. In several molecular solids containing CH_3 groups, there exists a range of temperature in

* Supported in part by the Office of Naval Research.
† Present address: London University, Queen Mary College, London, England.

which the proton absorption line width decreases with increasing temperature because the rate of reorientation of the CH_3 groups about their C_3 symmetry axes increases through a critical value, while the heavy molecular skeleton is fixed in the lattice.[1] These motions appear to be thermally activated hindered reorientations, and one aspect of the problem is to relate the line widths in the transition region to the reorientation frequencies. This gives the rate of reorientation as a function of temperature, from which an activation energy or potential barrier to the reorientations can be inferred.[2]

A second aspect of the problem is more subtle and difficult; it is the detailed manner in which the reorientations occur. The simplest model is the classical one of a particle going over a potential barrier of height E_a. However, only the protons need move and considering their small mass and the low barrier, the reorientations could take place by barrier penetration, i.e., by the tunnel effect. This question has arisen before in connection with proton magnetic resonance experiments.[3,4] The most extensive analysis is that of Sachs[4] who gives a very interesting but inconclusive discussion of quantum-mechanical tunneling of the NH_4^+ ion in the ammonium halides. Recently, the shape and height of the barrier to internal rotation in methyl chloroform were obtained with some precision.[5] And this encouraged us to attempt a comparative analysis of the effects of tunneling and classical rotations upon the proton resonance in the region of changing line width.

II. SECOND-MOMENT VALUES FOR REORIENTING CH_3 GROUPS

The absorption line shape may change as well as the breadth, so the second moment of the absorption is a more satisfactory measure of the temperature effects than some simpler definition of line width.[2] For an isolated trio of protons at the corners of an equilateral triangle of side R, the second moment may be written as[1,6]

$$\Delta H_2^2=(2/3)\alpha^2\sum_{n=1}^{3}(3\cos^2\theta_n-1)^2, \tag{1}$$

where $\alpha=(3/2)\mu/R^3$, μ is the proton magnetic moment, and θ_n is the angle between the nth side of the triangle and the static magnetic field, $\mathbf{H}_0$. Motion of a CH_3 group about its C_3 symmetry axis is expressed conveniently by $\phi(t)$ in the equation

$$(3\cos^2\theta_n-1)=(3/2)\sin^2\psi-1 +(3/2)\sin^2\psi\cos[2\phi_0+(n-1)4\pi/3+2\phi(t)] \tag{2a}$$

$$\equiv A+Bf(t), \tag{2b}$$

where ψ is the angle between the C_3 axis and $\mathbf{H}_0$, and ϕ_0 is the azimuthal position of the CH_3 group at $t=0$. The effect of the motion upon the second moment is obtained by averaging Eqs. (2) over $\phi(t)$ during the appropriate time interval.

If a particular nuclear spin state has a given lifetime during which the line broadening perturbations fluctuate, the resultant broadening is the average over that lifetime. In turn, the mean lifetime δt of a state is related to the spectral line width by the uncertainty principle, $(h\delta\nu)\delta t\cong h/2\pi$. So the appropriate time interval for averaging Eqs. (2) is $1/2\pi\delta\nu$. The frequency width, $\delta\nu$, of a resonance line is here defined as $2\mu\Delta H_2/h$, which is the order of 2×10^4 cps for a fixed CH_3 group. Actually, this time interval is itself an average, as there is a distribution of lifetimes among the nuclear spin states.

Furthermore, the molecular reorientations must be random in character; the reorientation energy must diffuse among the molecules at a rate fast compared to the average reorientation frequency. Otherwise, a small number of "hot" molecules given by the Boltzmann distribution could reorient very rapidly for long periods while the majority stayed in fixed positions. This would reduce the second moment by a few percent at most, but the observed reduction factor of 1/4 at temperatures just above the line-width transition corresponds to *all* CH_3 groups reorienting fast enough to average out the line broadening.

The calculations are simplified considerably if we accept the criterion of Bloombergen *et al.*[7] that a motion reduces the resonance line width when the frequency of motion, ν_c, exceeds the frequency width of the resonance, $\delta\nu$. This procedure is unrealistic in that it gives an all or nothing line broadening effect for a uniform reorientation frequency. However, the assumption of a continuous Fourier spectrum for the reorientations restores continuity to the line width changes, and the over-all results appear satisfactory for the present purpose.

The statistical nature of the motions permits the application of the correlation function method,[8] previously adapted to magnetic resonance.[7] The correlation function of a quantity $F(t)$ is defined as

$$K(\tau)=\langle F(t)F^*(t+\tau)\rangle, \tag{3}$$

where the brackets $\langle\ \rangle$ indicate a time average, over t. The desired $F(t)$ is that given in Eq. (2b), for which

$$K(\tau)=\langle[A+Bf(t)][A+Bf(t+\tau)]\rangle.$$

[1] J. G. Powles and H. S. Gutowsky, J. Chem. Phys. **21**, 1695 (1953).
[2] H. S. Gutowsky and G. E. Pake, J. Chem. Phys. **18**, 162 (1950).
[3] R. Newman, J. Chem. Phys. **18**, 669 (1950).
[4] A. M. Sachs, Ph.D. thesis, Harvard University (1949).
[5] K. S. Pitzer and J. L. Hollenberg, J. Am. Chem. Soc. **75**, 2219 (1953).
[6] J. H. Van Vleck, Phys. Rev. **74**, 1168 (1948).
[7] Bloombergen, Purcell, and Pound, Phys. Rev. **73**, 679 (1948).
[8] M. C. Wang and G. E. Uhlenbeck, Revs. Modern Phys. **17**, 323 (1945).

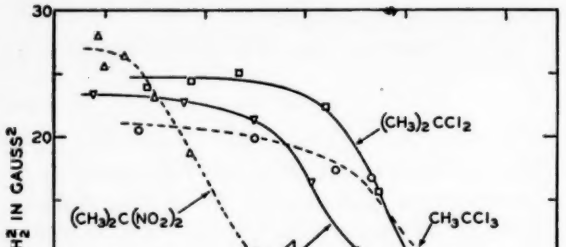

FIG. 1. Experimental second moments of the proton magnetic resonance absorption line as a function of temperature for methyl chloroform, 2,2-dichloropropane, 2-chloro-2-nitropropane, and 2,2-dinitropropane.

but we have $\langle f(t)\rangle=\langle f(t+\tau)\rangle=0$, and therefore

$$K(\tau)=A^2+B^2\langle f(t)f(t+\tau)\rangle. \tag{4}$$

The problem is now reduced to finding $\langle f(t)f(t+\tau)\rangle$, which is itself the correlation function of $f(t)$. The spectral intensity,[8] $J(\nu)$, of this correlation function is

$$J(\nu)=2\int_{-\infty}^{+\infty}\langle f(t)f(t+\tau)\rangle\cos 2\pi\nu\tau d\tau. \tag{5}$$

But frequencies greater than $\delta\nu$ average out the line broadening, so the appropriate averages required for Eq. (1) are of the form[7]

$$\langle(3\cos^2\theta_n-1)^2\rangle_{\delta\nu}=A^2+B^2\int_{-\delta\nu}^{+\delta\nu}J(\nu)d\nu. \tag{6}$$

Substituting Eq. (6) in Eq. (1), and taking a spatial average over ψ since we have a crystal powder, we find

$$\Delta H_2{}^2=(2/5)\alpha^2(1+6I), \tag{7}$$

where

$$I=\int_{-\delta\nu}^{+\delta\nu}J(\nu)d\nu. \tag{8}$$

Now, $J(\nu)$, I, and the corresponding second moment can be evaluated for particular types of motion, $\phi(t)$.

III. BROWNIAN-TYPE ROTATION BY RANDOM ANGLES

If we assume that the CH_3 groups rotate by random angles in a Brownian manner, the correlation function of $f(t)$ has the usual form

$$\langle f(t)f(t+\tau)\rangle=\langle f(t)^2\rangle\exp(-|\tau|/\tau_c), \tag{9}$$

where τ_c is a correlation time related to the reorientation frequency by $\tau_c=1/2\pi\nu_c$. $f(t)$ is given in Eq. (2a) as a simple cosine function; therefore $\langle f(t)^2\rangle$ is 1/2 and we find

$$\langle f(t)f(t+\tau)\rangle=(1/2)\exp(-|\tau|/\tau_c). \tag{10}$$

Substitution of this result in Eq. (5) gives

$$J(\nu)=\frac{\tau_c}{1+(2\pi\nu\tau_c)^2}, \tag{11}$$

which in turn gives from Eq. (8)

$$I=(1/\pi)\tan^{-1}2\pi\delta\nu\tau_c. \tag{12}$$

Therefore, the second moment is obtained as a function of τ_c,

$$\Delta H_2{}^2(\tau_c)=(2/5)\alpha^2[1+(6/\pi)\tan^{-1}2\pi\delta\nu\tau_c]. \tag{13}$$

Equation (13) is similar in form to one used earlier[2] to describe line width changes.

If the motion is a thermally activated process, τ_c may be assumed to depend on temperature through the relation

$$\tau_c=\tau_0\exp(E_a/RT), \tag{14}$$

where E_a is an activation energy and τ_0 is the inverse of a frequency factor. Combining Eqs. (13) and (14) and rearranging gives

$$\ln\left\{\frac{(\Delta H_2)_r}{\Delta H_2}\tan\frac{\pi}{6}\left[\frac{\Delta H_2{}^2}{(\Delta H_2{}^2)_r}-1\right]\right\}=\frac{E_a}{R}\cdot\frac{1}{T}+C, \tag{15}$$

where $C=\ln\tau_0 4\pi\mu(\Delta H_2)_r/h$ and $(\Delta H_2{}^2)_r$ is the second moment for the CH_3 groups in completely effective rotation.

Experimental values of the second moments are plotted against temperature in Fig. 1 for methyl chloroform, 2-chloro-2-nitropropane, and 2,2-dinitropropane, which data were given earlier,[1] and also for 2,2-dichloropropane, not previously reported. The data for methyl chloroform had considerable scatter[1] and several values were re-evaluated. Equation (15) refers to isolated CH_3 groups, and it is not completely proper to use the

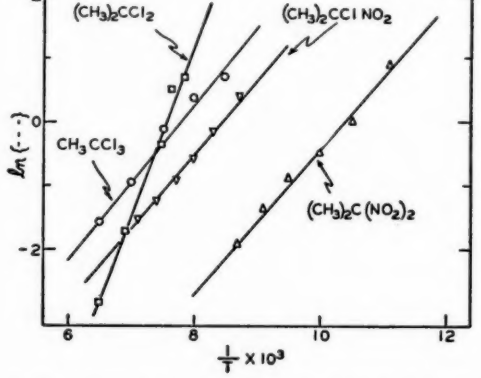

FIG. 2. The term $\ln\{\cdots\}$ in Eq. (15) plotted against $1/T$ for the experimental data given in Fig. 1. Numerical values for the slopes and intercepts of the lines are summarized in Table I.

observed second moments because there are contributions from magnetic interactions between neighboring groups. However, this external broadening is also reduced by the motion and makes a relatively small contribution to the second moments, so little error should be incurred by using the observed values directly in Eq. (15).

Figure 2 represents the fitting of the experimental results to Eq. (15). The term $\ln\{\cdots\}$ is plotted against $1/T$, and the resulting straight lines suggest the validity of the general approach. Activation energies, E_a, were obtained from the slopes of the lines and are listed in Table I with the τ_0 values. The significance of these values is discussed in Sec. VI.

IV. RANDOM MOTION IN A THREE-NODAL POTENTIAL

The potential hindering the internal rotation of the CH_3 groups is three-nodal, and one might well argue that jumps would take place between three discrete orientations rather than over the random angles assumed in the aforementioned. This gives a model in which there are three orientations $2\pi/3$ apart, for which we define probabilities a_1, a_2, and a_3. Assuming that the direction and time of jumping are random, and that the rate per unit time of jumping is $1/\tau_c$, we can write

$$\frac{da_1}{dt}=\frac{1}{\tau_c}\left(-a_1+\frac{a_2}{2}+\frac{a_3}{2}\right). \tag{16}$$

Two similar equations are obtained by cyclic permutation of the suffixes. The solution of these equations, subject to the initial conditions $a_1(0)=1$, $a_2(0)=0$, $a_3(0)=0$, is

$$\begin{aligned} a_1(t)&=(1/3)+(2/3)\exp[-(3/2)t/\tau_c]\\ a_2(t)&=a_3(t)=(1/3)-(1/3)\exp[-(3/2)t/\tau_c]. \end{aligned} \tag{17}$$

Using Eq. (17) for $a(t)$, and defining $\phi_n=2\phi_n+(n-1)\times 4\pi/3$, we have

$$\begin{aligned} &\cos[2\phi_0+(n-1)4\pi/3+2\phi(t)]\\ &\quad=a_1(t)\cos\phi_n+a_2(t)\cos(\phi_n+4\pi/3)\\ &\quad+a_3(t)\cos(\phi_n+8\pi/3)=\cos\phi_n\exp[-(3/2)t/\tau_c]. \end{aligned}$$

And the correlation function for this motion is

$$\begin{aligned} &\langle\cos[\phi_n+2\phi(t)]\cos[\phi_n+2\phi(t+\tau)]\rangle\\ &\quad=\cos^2\phi_n\exp(-|3\tau|/2\tau_c). \end{aligned} \tag{18}$$

When this function is combined with Eqs. (5), (7), and (8), it gives the following relation between the correlation frequency τ_c and the second moment,

$$\nu_c=(4/3)\mu\Delta H_2/\left[h\tan\frac{\pi}{6}\left(\frac{\Delta H_2^2}{(\Delta H_2^2)_r}-1\right)\right]. \tag{19}$$

This is the same as Eq. (13) for rotation by random angles except that here ν_c is smaller by a factor of $2/3$ for a given line width. It has been noted elsewhere[2] that any type of C_3 reorientation gives the same limiting line shape for the CH_3 group when the motion becomes completely effective in narrowing the resonance.

TABLE I. Activation energies and frequency factors for the CH_3 group reorientations. These values come from Fig. 2 in which the experimental second moments are fitted to Eq. (15), based upon a classical model for the reorientations.

Molecule	E_a	τ_0	ν_0	$\Delta S^\ddagger$
CH_3CCl_3	2.2$_2$ kcal	18 $\times10^{-9}$ sec	0.88$\times10^{7}$ cps	-25 eu[a]
$(CH_3)_2CClNO_2$	2.2$_8$	6.2$\times10^{-9}$	2.6 $\times10^{7}$	-23
$(CH_3)_2C(NO_2)_2$	2.2$_1$	0.9$\times10^{-9}$	18 $\times10^{7}$	-19
$(CH_3)_2CCl_2$	5.2	2.5$\times10^{-13}$	6.4 $\times10^{11}$	-2.8

[a] This is an entropy of activation as defined in the theory of absolute reaction rates.

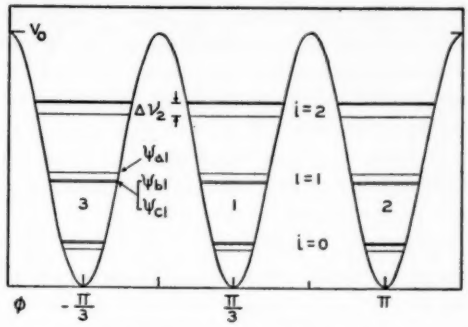

FIG. 3. A schematic representation of the three-fold potential $V=\frac{1}{2}V_0(1+\cos3\phi)$, with torsional oscillation levels E_i, sublevels a,b,c and the splitting $\Delta\nu_i$.

V. REORIENTATIONS via THE TUNNEL EFFECT

The reorientation frequency required to narrow the proton resonance in CH_3 is only about 2×10^4 cps. And, as shown below, this relatively slow rate can be attained by quantum-mechanical tunneling.

The symmetry of the CH_3 group gives three identical potential minima and a set of torsional oscillation levels E_i, each threefold degenerate in the zero approximation.[9] For a finite barrier between the minima, each level E_i is split into two sublevels, one of which is doubly degenerate. The splitting $\Delta\nu_i$ is small compared to the separation between adjacent E_i. Moreover, it can be shown[10] that the frequency of barrier penetration is $\Delta\nu_i$. Also, $\Delta\nu_i$ increases with higher E_i, that is as the area under the barrier decreases. This is given schematically in Fig. 3. E_0 is taken as the zero of energy for E_i.

In this model, molecules in every energy state contribute to the barrier penetration, and the correlation frequency is simply the average tunneling frequency, which is given by the sum

$$\begin{aligned} \nu_c&=(1/Q_t)\sum_i\Delta\nu_i\exp(-E_i/RT)\\ &=\sum_i a_i\Delta\nu_i. \end{aligned} \tag{20}$$

[9] G. Herzberg, *Infrared and Raman Spectra of Polyatomic Molecules* (D. Van Nostrand Company, Inc., New York, 1945), p. 225.

[10] Eyring, Walter, and Kimball, *Quantum Chemistry* (John Wiley and Sons, Inc., New York, 1944), p. 310.

Here Q_t is the partition function for the torsional vibration. And a_i is the probability of the group being in the ith torsional state. The sum in Eq. (20) is not a pure exponential, but over moderate ranges of temperature the deviation is small. If we calculate ν_c as a function of T from Eq. (20) and plot $\ln\nu_c$ *versus* $1/T$, a reasonably straight line is obtained, the slope of which gives an apparent activation energy. This apparent activation energy will be less than the barrier height V_0 by an appreciable amount depending upon the contribution of the lower energy states to the rate of penetration.

In order to apply Eq. (20) and find ν_c it is necessary first to calculate the E_i and $\Delta\nu_i$ values from the barrier shape and height. Koehler and Dennison[11] have given a general analysis of internal rotational energies of a symmetric group. However, exact calculations are tedious for a 3-nodal potential. Instead, we have used a simple, perturbation method to make approximate calculations for a range of barriers. More accurate values of $\Delta\nu_i$ were computed in a few selected cases to establish the error of the perturbation method.

1. Perturbation Calculation of the Splittings $\Delta\nu_i$

The barrier to rotation is assumed to be the form[12] shown in Fig. 3,

$$V(\phi)=(V_0/2)(1+\cos 3\phi). \tag{21}$$

Also, the CH_3 group is considered as attached to a rigid framework. The wave functions for the three noninteracting orientations of the CH_3 group are designated as ψ_{ni}, with $n=1$, 2, and 3, and the zero-order combinations which result from the overlap are‡

$$\begin{aligned}\psi_{ai}&=(1/\sqrt{3})(\psi_{1i}+\psi_{2i}+\psi_{3i})\\ \psi_{bi}&=(1/\sqrt{6})(2\psi_{1i}-\psi_{2i}-\psi_{3i})\\ \psi_{ci}&=(1/\sqrt{2})(\psi_{2i}-\psi_{3i}).\end{aligned} \tag{22}$$

The total Hamiltonian operator for the system may be expressed as

$$\mathcal{H}=-\frac{h\nu}{2}\frac{\partial^2}{\partial y^2}+F(y), \tag{23}$$

where ν is the classical vibration frequancy of infinitesimal amplitude for the group, and the quantity y is given by

$$y=(3/\sqrt{2})(V_0/h\nu)^{\frac{1}{2}}\phi. \tag{24}$$

ν is calculated from the equation $\nu^2=9V_0/8\pi^2 I$, with I the moment of inertia of the CH_3 group.[5]

In Eq. (23) $F(y)$ includes the harmonic oscillator terms as well as the overlap and the anharmonic perturbations. Therefore, to first order, the splittings $\Delta\nu_i$ are obtained as

$$h\Delta\nu_i=(\psi_{bi}^*,\mathcal{H}\psi_{bi})-(\psi_{ai}^*,\mathcal{H}\psi_{ai}). \tag{25}$$

The harmonic oscillator wave functions in terms of y are of the form

$$\psi_{1i}=[1/(2^i i!\sqrt{\pi})^{\frac{1}{2}}]H_i(y-\alpha)\exp[-(y-\alpha)^2/2]. \tag{26}$$

$H_i(y-\alpha)$ is the ith Hermite polynomial, centered at $y=\alpha$. α is defined by the equation

$$\alpha=(\pi/\sqrt{2})(V_0/h\nu)^{\frac{1}{2}}. \tag{27}$$

Substitution in Eq. (25) gives upon simplification

$$\begin{aligned}h\Delta\nu_i=&-\frac{3}{4}h\nu\int(\psi_{3i}^*\psi_{1i}''+\psi_{1i}^*\psi_{3i}'')dy\\ &-\frac{3V_0}{2}\int\left(1+\cos\frac{\pi}{\alpha}y\right)\psi_{1i}^*\psi_{3i}dy.\end{aligned} \tag{28}$$

ψ_{ni}'' is eliminated by the second-order differential equation in H_i. In addition $(1+\cos\pi y/\alpha)$ can be replaced by $(2-\pi^2y^2/2\alpha^2)$; this is a good approximation because the product $\psi_{1i}^*\psi_{3i}$ is significant only near $y=0$, and also $\alpha^2\cong 25$. As a final result we obtain

$$\begin{aligned}h\Delta\nu_i=&3V_0\left\{\frac{\pi^2}{4}-1-\frac{\pi^2 i}{2\alpha^2}\right\}\int\psi_{1i}\psi_{3i}dy\\ &+\frac{3V_0\pi^2}{2\alpha^2}\int y^2\psi_{1i}\psi_{3i}dy.\end{aligned} \tag{29}$$

The overlap integrals in this equation can be integrated by parts to give general expressions in terms of α. In this manner numerical values of $\Delta\nu_0$ and $\Delta\nu_i/\Delta\nu_0$ were computed for several barrier heights with typical results given in Table II.

2. Error Associated with the Perturbation Calculation of $\Delta\nu_i$

The splittings depend on the overlap[11] of the wave functions for the different orientations, as shown in Eq. (29). Unfortunately the harmonic oscillator wave functions used in the perturbation calculation are poorest for the classically forbidden region where the overlap is the largest. A comparison of these functions for the 2-nodal potential well with the exact wave

TABLE II. $\Delta\nu_i$ calculated by the perturbation method, Eq. (29), for several barrier heights, V_0.

V_0	$\Delta\nu_0$	$\Delta\nu_1/\Delta\nu_0$	$\Delta\nu_2/\Delta\nu_0$	$\Delta\nu_3/\Delta\nu_0$	$\Delta\nu_4/\Delta\nu_0$	$\Delta\nu_5/\Delta\nu_0$
2000 cm^{-1}	3.33 cps	56	1.52×10^3	2.57×10^4	3.07×10^5	27.37×10^5
1500	1.81×10^2	48	1.08	1.50	1.46	9.97
1300	1.06×10^3	44	0.91	1.15	0.99	6.15
1017	1.65×10^4	38	0.67	0.70	0.49	2.37
375	4.73×10^7	...	...	...	...	...

[11] J. S. Koehler and D. M. Dennison, Phys. Rev. **57**, 1006 (1940); see also E. B. Wilson, Jr., Chem. Revs. **27**, 17 (1940).

[12] Pitzer and Hollenberg[5] find that a $\cos 6\phi$ term is required to fit the experimental data for methyl chloroform, but the term is small and we shall neglect it.

‡ These wave functions are not strictly normalized since ψ_{1i}, ψ_{2i}, ψ_{3i} are not quite orthogonal. The small correction required has been included in the final result, Eq. (29).

functions, obtainable directly from Tables,[13] shows that the absolute value of the approximate functions is too low in the regions between the wells. Therefore the perturbation calculations with Eq. (29) give splittings which are too small. The extent of the error has been determined by making more accurate calculations in several cases selected for their relative simplicity.

The Schrödinger equation for the system may be written

$$\frac{d^2\psi}{d\phi^2}+(9/2)(V_0/h\nu)^2\left[2\left(\frac{E_i}{V_0}-1\right)-\cos 3\phi\right]\psi=0. \quad (30)$$

For the nondegenerate eigenstates ψ_{ia} this equation is related to that for the 2-nodal case by the simple substitution $3\phi=2x$. So accurate eigenvalues E_{ia} can be obtained from the Tables[13] for values of V_0 up to the tabulation limit of 1200 cm^{-1}. For larger barriers, E_{ia} may be calculated from the continued fractions obtained by solving Eq. (30) in a trigonometric series.[14,15] For even levels

$$1=\cfrac{k^2}{(R_{ia}-3^2)(R_{ia}-6^2)}\Bigg/\cfrac{1-\cfrac{k^2}{(R_{ia}-6^2)(R_{ia}-9^2)}}{1-\cdots\cdot}$$

and for odd levels

$$\tfrac{1}{2}=\cfrac{k^2}{R_{ia}(R_{ia}-3^2)}\Bigg/\cfrac{1-\cfrac{k^2}{(R_{ia}-3^2)(R_{ia}-6^2)}}{1-\cdots\cdot}$$

where $k=(9/4)(V_0/h\nu)^2$ and $E_{ia,\,b}=(V_0/2)+[(h\nu)^2/9V_0]R_{ia,\,b}$.

The degenerate eigenvalues, E_{ib} and E_{ic}, are not simply related to the values for the 2-nodal problem but can be calculated from the continuing fraction

$$1=\cfrac{k^2}{(R_{ib}-1^2)(R_{ib}-4^2)}\Bigg/\cfrac{1-\cfrac{k^2}{(R_{ib}-4^2)(R_{ib}-7^2)}}{1-\cdots\cdot}+\cfrac{k^2}{(R_{ib}-1^2)(R_{ib}-2^2)}\Bigg/\cfrac{1-\cfrac{k^2}{(R_{ib}-2^2)(R_{ib}-5^2)}}{1-\cdots\cdot}.$$

This calculation becomes more complex for larger V_0 and for higher torsional levels.

[13] *Tables Relating to Mathieu Functions* (Columbia University Press, New York, 1951).
[14] See reference 11 with $\sigma=0$.
[15] E. L. Ince, Proc. Roy. Soc. Edinburgh **46**, 20 (1925).

TABLE III. A comparison of "exact" splittings with values given by Eq. (29).

V_0	$\frac{\Delta\nu_0 \text{ exact}}{\Delta\nu_0 \text{ Eq. (29)}}$	$\frac{\Delta\nu_1 \text{ exact}}{\Delta\nu_1 \text{ Eq. (29)}}$	$\frac{\Delta\nu_2 \text{ exact}}{\Delta\nu_2 \text{ Eq. (29)}}$
250 cm^{-1}	7	—	—
500	19	8	33
1017	22	55	—

Values of the splittings $\Delta\nu_i$ have been calculated by these "exact" procedures for several of the lower levels and are compared in Table III with the results from the perturbation method, Eq. (29). The comparison made in Table IV suggests the general accuracy with which Eq. (29) gives the splittings of the excited levels relative to $\Delta\nu_0$. The first row lists values of $\Delta\nu_i/\Delta\nu_0$ obtained from the Tables[13] for the 2-nodal case, multiplied by the factor converting E_{ia} from the 2-nodal to the 3-nodal value. This simple conversion is not appropriate to E_{ib} so the results are not accurate, but they may be expected to have the correct trend. It should be noted that a method analogous to Goldstein's treatment of the 2-nodal problem[16] could be used to calculate accurate values of the splitting for the 3-nodal case.

The comparisons in Tables III and IV show that the perturbation method using Eq. (29) gives splittings which are too small by a factor of 10 to 100. Also, the errors are probably greater for the excited levels than for $\Delta\nu_0$. We have chosen to multiply the perturbation results by a rather arbitrary factor of 30 for comparison with experiment in the following section. This provides a satisfactory preliminary check on the tunneling model without the labor of detailed exact calculations.§ Moreover, at present the shape of the barrier is uncertain in the solid, so any method is necessarily semiquantitative.

3. Comparison of the Tunneling Model with Experiment

The tunneling produces reorientations between positions $2\pi/3$ apart and the process is no doubt random because lattice vibrations can induce rapid exchange of the torsional oscillation energy. Except for the mode of reorientation, this is identical with the classical model discussed in Sec. IV. And in both cases Eq. (19)

TABLE IV. A comparison for higher vibrational levels of relative splittings derived from the 2-nodal case with those from Eq. (29), for a V_0 of 1017 cm^{-1}.

	$\frac{\Delta\nu_1}{\Delta\nu_0}$	$\frac{\Delta\nu_2}{\Delta\nu_0}$	$\frac{\Delta\nu_3}{\Delta\nu_0}$	$\frac{\Delta\nu_4}{\Delta\nu_0}$	$\frac{\Delta\nu_5}{\Delta\nu_0}$
2-nodal value	157	1.8×10^3	2.9×10^4	2.9×10^5	1.5×10^6
By Eq. (29)	38	0.67×10^3	0.70×10^4	0.49×10^5	0.24×10^6

[16] S. Goldstein, Proc. Roy. Soc. Edinburgh **49**, 210 (1929).
§ *Note added in proof.*—Solutions of the Mathieu equations are in progress with the Illiac. E_{ia} and E_{ib} are being computed to sufficient accuracy to give $\Delta\nu_i$ by difference.

TABLE V. Temperature dependence of the tunneling frequency ν_e computed[a] for a V_0 of 1500 cm^{-1}.

i	$a_i(T)\Delta\nu_i/\Delta\nu_0$ 105°K	120°K	135°K	150°K
0	0.97	0.95	0.93	0.91
1	1.40	2.13	2.94	3.77
2	1.10	2.55	4.86	8.10
3	0.62	2.13	5.57	11.91
4	0.28	1.40	4.93	13.41
5	0.10	0.72	3.38	11.57
Σ	4.47	9.88	22.61	49.67
ν_e	24.2 kc	53.7 kc	122.8 kc	269.7 kc

[a] The values obtained via Eqs. (29) and (20) were multiplied by the factor of 30 discussed in Sec. V.2.

gives the dependence of the second moment upon ν_e. The essential difference is that the temperature dependence of ν_e is given for tunneling by the summation in Eq. (20) while the classical model uses the much simpler Eq. (14).

The complex nature of the summation prevents any direct calculation of the barrier height V_0 from the temperature dependence of the experimental ν_e values. Instead a barrier V_0 must be assumed, the $\Delta\nu_i$ and E_i computed, and then ν_e obtained as a function of temperature with Eq. (20) and the probability values a_i. A comparison of these theoretical ν_e values with the experimental values can then be made and the process repeated, if necessary for better agreement. The values of E_i used to calculate a_i were obtained as $(\psi_{1i}{}^*\mathfrak{K}\psi_{1i})$ with the potential function of Eq. (21); any error in this procedure is negligible.

In the terms $a_i\Delta\nu_i$, the value of $\Delta\nu_i$ increases with i while a_i decreases, so the relative changes determine the convergence of the series giving ν_e. Three different situations may occur: (1) $\Delta\nu_0 > \delta\nu$, the line width; (2) $\Delta\nu_0 < \delta\nu$, and the series for ν_e is convergent up to temperatures greater than that at which $\nu_e \cong \delta\nu$; (3) $\Delta\nu_0 < \delta\nu$, but the series for ν_e diverges. In case (1) the tunneling rate is sufficient to narrow the resonance line to the C_3 rotation value even at temperatures approaching 0°K. In case (2) the rigid lattice line is observed up to temperatures at which $\nu_e \cong \delta\nu$, where the line narrows. Case (3) does not arise in regions of present interest. The calculations of ν_e at several temperatures are summarized in Table V for a V_0 of 1500 cm^{-1}. The series begins to exhibit relatively slow convergence at temperatures above 135°K. The terms in the series are calculated only to $i=5$; higher terms are very near the top or above the barrier where classical reorientations could occur as well as "tunneling."

The calculations of the tunneling frequencies for different barriers and temperatures are summarized in Fig. 4 where the results are compared with the ν_e from the line width changes. The solid straight lines represent the fitting of Eq. (19) to the experimental line widths over the temperature range in which the width is changing, for CH_3CCl_3, $(CH_3)_2CClNO_2$, and $(CH_3)_2C(NO_3)_2$. The points and dotted lines are ν_e values computed for V_0 values of 1017, 1500, and 2000 cm^{-1}. The ν_e values computed for the barrier 1017 cm^{-1} in the gaseous CH_3CCl_3 molecule lie far above the observed frequencies. In fact, $\Delta\nu_0$ for this barrier is 5×10^5 cps (Table II) which is fast enough to narrow the resonance line even at very low temperatures, corresponding to case (1). The tunneling frequencies calculated for the 1500 cm^{-1} barrier are still somewhat greater than experiment but those for 2000 cm^{-1} lie along the lowest curve, for CH_3CCl_3.

The ν_e values computed for all three barriers show definite curvature on the low-temperature side; this is because $\nu_e \rightarrow \Delta\nu_0$ as a limiting value at low temperatures. However, when one considers the approximations made in handling of the experimental data, as well as in calculating the tunneling frequencies, the agreement is certainly as good as one could expect. It is particularly encouraging that both the range of ν_e values and the slopes of the curves with respect to $1/T$ are reproduced reasonably well.

The 2,2-dichloropropane is not included in Fig. 4 because the experimental data on it cannot be fitted to our simple tunneling model by any amount of stretching. The line-width observations give a relatively large frequency factor of 6.4×10^{11} cps and an E_a of 5.2 kcal, which cannot be fitted simultaneously. The large difference between this compound and the other three suggests that the CH_3 group reorientations in the 2,2-dichloropropane may be associated in some way with motions of the C_2CCl_2 skeleton.

VI. DISCUSSION

The classical models of Secs. III and IV and the tunneling model of Sec. V explain the characteristics of the line-width transitions equally well, for CH_3CCl_3, $(CH_3)_2CClNO_2$, and $(CH_3)_2C(NO_2)_2$, provided a

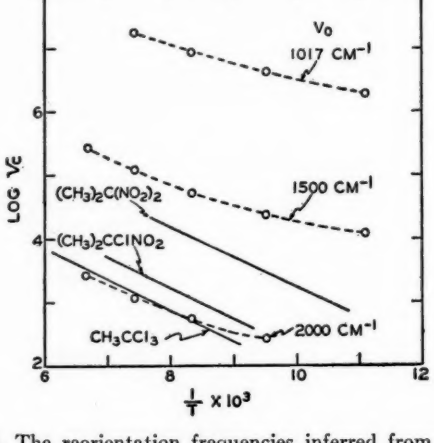

FIG. 4. The reorientation frequencies inferred from the line-width changes compared with the tunneling frequencies calculated for several barriers, V_0. The solid lines fit the experimental data for the three compounds while the plotted points and dotted lines are the theoretical tunneling frequencies.

suitable choice is made for the "activation energy." But a decision between these alternative mechanisms can be based upon the physical reasonableness of the constants required to fit each model to the line-width data.

Consider first the frequency factors, ν_0. The experimental values listed in Table I for the three compounds are between 10^7 and 2×10^8 cps. For a classical rate process, the transition-state theory[17] predicts a frequency factor of 2.7×10^{12} cps. If the difference is ascribed to an entropy of activation $\Delta S\ddagger$, then the values given in Table I, about -22 eu, are required. These are exceptionally large for the relatively simple process of reorientation. On the other hand, low-frequency factors the order of 10^7 arise naturally in the tunneling theory.

The strongest argument for the tunneling mechanism concerns the height of the barriers to rotation. Assume for the moment that the process is classical. Then the barrier height is the experimental E_a of 2.25 kcal plus an allowance of about 0.3 kcal for the zero-point torsional energy, or a total of 2.55 kcal (890 cm^{-1}). However, for a sinusoidal barrier of this magnitude, the tunneling frequency in the ground torsional state is the order of 2.5×10^6 cps. This far exceeds the classical reorientation frequency in the temperature range of interest and in fact would prevent the proton resonance from ever getting broader than the C_3 rotation value. On the other hand, the tunneling model requires barriers between 5 and 6 kcal. And classical reorientation over such barriers, even with a normal frequency factor of 2.7×10^{12}, would be infrequent compared to the tunneling.

There remains the question whether barriers as high as 5 to 6 kcal are reasonable for the solids. These values are nearly double the values found in the gas phase for CH_3CCl_3. No independent estimate is available for the solid. However, as suggested by the results for *t*-butyl chloride,[18] it seems likely that the interactions in the solid would increase the barrier. Of course, it is important that the barrier remain substantially sinusoidal in the solid, if the calculations are to be valid, because the tunneling is sensitive to the barrier shape.

There is some evidence supporting the occurrence of tunneling in other systems. In methanol the internal barrier in the gas phase is[19] only 375 cm^{-1}, and in this case we calculate $\Delta\nu_0$ to be 1.4×10^9 cps (Table II). This is much greater than the rigid lattice line width would be, so the resonance should remain narrow down to very low temperatures provided the barrier to reorientation is mainly the internal barrier. And this agrees with measurements[2,20] down to 85°K, where the line width still corresponds to C_3 reorientation of the CH_3 group. A line width smaller than the rigid lattice value has also been observed[21] in solid methane, and this presumably[22] is due to tunneling similar to that discussed here. Unusually small frequency factors have been found in the study of CH_3 group motions in natural rubber[23] and tunneling may be responsible. More usual ν_0 values were associated with the line-width changes assigned to motions of the chain segments, which is reasonable since such motions would be more nearly classical.

In conclusion, it appears that quantum-mechanical tunneling is an important process governing the motions of protons in some solids. In particular, we believe that the detailed analysis made here favors the tunneling model for the three compounds of Fig. 4. There is insufficient independent evidence for some of the critical parameters in the analysis for it to be conclusive in detail. However, other experiments should provide additional data. Changes in the reorientation frequency are effective in changing the resonance line width only over a comparatively small range of frequencies. Measurements of the spin-lattice relaxation time,[7] which also depends on the motions of the CH_3 group, would give information about the reorientations over a much wider frequency and temperature range. Observation of the proton resonance in partially deuterated compounds, such as CH_2DCCl_3 could be particularly decisive because the isotope effect on tunneling is much greater than on classical motions.

ACKNOWLEDGMENTS

We wish to thank Dr. R. Bersohn and Dr. C. P. Slichter for a number of helpful suggestions and interesting discussions. We are especially grateful to Dr. Bersohn for his critique of the tunneling calculations.

[17] Glasstone, Laidler, and Eyring, *The Theory of Rate Processes* (McGraw-Hill Book Company, Inc., New York, 1941).
[18] J. G. Powles and H. S. Gutowsky, J. Chem. Phys. **21**, 1704 (1953).
[19] E. V. Ivash and D. M. Dennison, J. Chem. Phys. **21**, 1804 (1953).
[20] A. H. Cooke and L. E. Drain, Proc. Phys. Soc. (London) **A65**, 894 (1952).
[21] Thomas, Alpert, and Torrey, J. Chem. Phys. **18**, 1511 (1950).
[22] K. Tomita, Phys. Rev. **89**, 429 (1953).
[23] H. S. Gutowsky and L. H. Meyer, J. Chem. Phys. **21**, 2122 (1953).

Force Constants, Infrared Spectrum, and Thermodynamic Properties of $TiCl_4$†

N. J. HAWKINS AND D. R. CARPENTER
Knolls Atomic Power Laboratory, General Electric Company, Schenectady, New York
(Received December 10, 1954)

The spectrum of gaseous titanium tetrachloride was obtained in the rock salt and potassium bromide regions of the infrared. The thermodynamic functions C_p^0, S^0, and $-(F^0-E_0^0)/T$ were calculated. The orbital valence force field constants were computed, and lead to the conclusion that hybridization changes may be significant in the F_2-vibrations.

INTRODUCTION

THE Raman spectrum of liquid titanium tetrachloride has been the subject of several investigations.[1,2] The original question of whether the molecule was planar or tetrahedral was established by Bhagavantam's measurements on the polarization of the Raman lines.[3] The molecule appeared to be tetrahedral. Heath and Linnett[4,5] have studied the force constants of several tetrahedral molecules of the type XY_4 and found good agreement between the calculated and observed frequencies for all central atoms of group IV *B*-elements but rather poor agreement for the lone group IV *A*-element considered; namely, in $TiCl_4$. It was thought that the infrared spectrum of gaseous $TiCl_4$ might yield some information as to whether the shifts between calculated and observed frequencies were due to the fact that the observed data were obtained from the material in the condensed state, or, whether the shifts were due to something else such as a change in the nature of the bond hybridization of the central atom.[6]

EXPERIMENTAL

Liquid $TiCl_4$ was placed in an all-metal vacuum system and purified. The initial spectra contained a number of bands which disappeared on further purification. The infrared cell construction and the techniques used to obtain the spectra at elevated temperatures have been described.[7] The cell used in this study was of 5 cm length with AgCl windows. The liquid under its own vapor up to 125°C was studied. Spectra were obtained from a Baird double-beam instrument utilizing NaCl and KBr prisms.

DATA

Representative spectra of $TiCl_4(g)$ are shown in Fig. 1. The observed infrared data are summarized in Table I. Two questionable bands in the infrared spectrum at the elevated temperatures are present at 833 and 744 cm^{-1}, which if due to $TiCl_4$, might be assigned as $2\nu_3-\nu_4$ and $\nu_3+2\nu_4$ respectively, but which are probably due to impurities. In general a simple interpretation of the data can be made for the molecule with T_d-symmetry. Values of the fundamental frequency ν_3 and values of ν_1, ν_2, and ν_4 calculated from the observed infrared combination bands are summarized and compared with the Raman data obtained from liquid $TiCl_4$[1] (Table II). The agreement between the data obtained from both methods is good.

THERMODYNAMIC PROPERTIES

The thermodynamic properties C_p^0, S^0, and $-(F^0-E_0^0)/T$ were calculated for one mole of the perfect gas at one atmosphere pressure. In making the calculations the following were used: chemical atomic weights, the rigid rotor-harmonic oscillator approximation using an interatomic distance of 2.18 A, obtained from the electron diffraction study by Lister and Sutton,[8] and the infrared values of the fundamental vibration frequencies in Table II; assumption of a singlet ground electronic ground state; and a symmetry number of twelve. Nuclear spin, anharmonicity, centrifugal distortion, and isotope mixing contributions to the functions were omitted. The results of the calculations are given in Table III.

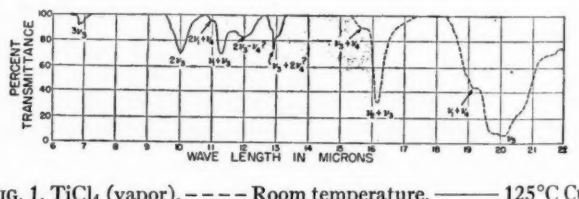

FIG. 1. $TiCl_4$ (vapor), - - - - Room temperature. ——— 125°C Cu cell–5 cm length. AgCl windows.

FORCE CONSTANTS

The force constants were computed using the orbital valence force field (OVFF) approximation discussed

† This work was performed by the Knolls Atomic Power Laboratory, which is operated by the General Electric Company for the U. S. Atomic Energy Commission.

[1] G. Herzberg, *Molecular Spectra and Molecular Structure. II. Infra-red and Raman Spectra of Polyatomic Molecules* (D. Van Nostrand Company, Inc., New York, 1945), pp. 167, 182, 322.

[2] M. L. Delwaulle and F. Francois, J. phys. radium **7**, 15 (1946).

[3] S. Bhagavantam, Indian J. Phys. **7**, 79 (1932).

[4] D. F. Heath and J. W. Linnett, Trans. Faraday Soc. **44**, 561 (1948).

[5] D. F. Heath and J. W. Linnett, Trans. Faraday Soc. **44**, 878 (1948).

[6] J. W. Linnett and P. J. Wheatley, Trans. Faraday Soc. **45**, 33, 39 (1949).

[7] Hawkins, Mattraw, and Carpenter, "Infrared Spectrum of UF_6 at Elevated Temperatures" KAPL Report 1041, February 1, 1954.

[8] M. W. Lister and L. E. Sutton, Trans. Faraday Soc. **37**, 393 (1941).

TABLE I. Infrared bands of $TiCl_4(g)$.

Assignment	(Observed)	(Calc)	Intensity
$3\nu_3$	1447 cm^{-1}	1495 cm^{-1}	weak (125°C)
$2\nu_3$	997	997	medium (125°C)
$2\nu_1+\nu_4$	909	914	weak (125°C)
$\nu_1+\nu_3$	886	886	medium (125°C)
$\nu_3+\nu_4$	637	637	weak (25°C)
$\nu_2+\nu_3$	617	617	strong (25°C)
$\nu_1+\nu_4$	526	526	medium (25°C)
ν_3	498.5		very strong (25°C)

by Heath and Linnett.[5] The equations, using our numbering system, reduce, for $TiCl_4$, to

$$\lambda_1=1.699\times10^{22}(k_1+8A), \quad (1)$$

$$\lambda_2=1.699\times10^{22}\left(k_\alpha'+\frac{28}{13}A\right), \quad (2)$$

$$\lambda_3+\lambda_4=3.376\times10^{22}\left[k_1+\frac{32}{13}A\right]$$

$$+5.053\times10^{22}\left[k_\alpha'+\frac{24}{13}A\right]-3.354\times10^{22}\left[\frac{32}{13}A\right], \quad (3)$$

$$\lambda_3\cdot\lambda_4=(11.436\times10^{44})$$

$$\times\left\{\left(k_1+\frac{32}{13}A\right)\left(k_\alpha'+\frac{24}{13}A\right)-\frac{512}{169}A^2\right\}, \quad (4)$$

where k_1, is the bond stretching constant of the Ti—Cl bond k_α' is the angle bending constant for the angle Cl—Ti—Cl, and A is the constant representing the repulsion between the nonbonded chlorine atoms. Implicit in the equations is the Heath and Linnett assumption that $B/R=2/13\,A$.

The calculation of the force constants k_1, k_α', and A was made by a least squares method developed by W. S. Horton.[9] In performing the calculation the error in the fundamental frequency ν_3 was taken to be ±0.5 cm^{-1} and the error in ν_1, ν_2, and ν_4 was taken as ±2 cm^{-1}. The results of the least squares calculations are summarized in Table IV. The value of B/R was taken as $2/13\,A$ and was not regarded as an independent constant. The values of the fundamental frequencies calculated from the least squares adjusted constants are also summarized in Table IV. The agreement between the calculated and observed frequencies is rather poor (particularly for the bending vibrations ν_2 and ν_4) compared with the results of Heath and Linnett[5] for CCl_4, $SiCl_4$, $GeCl_4$, $SnCl_4$, and all of the corresponding tetrabromides.

TABLE II. Fundamental vibration frequencies of $TiCl_4$.[a]

Frequency	Species	Infrared (this study)	Raman (Herzberg)[b]
ν_1	A_1	388 cm^{-1}	386 cm^{-1}
ν_2	E	119	120
ν_3	F_2	498.5	495
ν_4	F_2	139	141

[a] The F_2-component in the symmetry is required for infrared activity.
[b] See reference 1.

[9] W. S. Horton, J. Chem. Phys. (to be published).

TABLE III. Thermodynamic properties $TiCl_4(g)$ (all in cal/deg/mole).

Temp. °K	$-(F^0-E_0^0)/T$	S^0	C_p^0
100°	51.903	63.281	15.872
150°	56.509	69.850	18.517
200°	60.569	75.525	20.498
250°	64.036	80.203	21.888
273°	65.480	82.149	22.367
298°	66.965	84.134	22.819
350°	69.795	87.849	23.503
400°	72.256	91.027	23.987
500°	76.569	96.448	24.590

Linnett and Wheatley[6] have discussed the possibility that in certain types of bending vibrations, the electronic bond hybridization of the central atom may change "in such a manner as to follow the outer atoms." In T_d-molecules such changes in the hybridization are not possible for Class A_1 and E vibrations, but are possible for F_2 vibrations (i.e., for ν_3 and ν_4 in the present case). In the case of titanium, an element of the IV A group, the inner $3d$-orbitals are available for bonding; inner d-orbitals are not available for bonding in elements in the IV B group. If such a change in bond hybridization takes place, the effect is noted by a smaller effective angle bending constant in the expressions for the force relations of the F_2-vibrations.

Accordingly Eqs. (1), (3), and (4) were solved simultaneously for k_1, A and the angle bending which will now be designated k_β. Even though Eq. (1) is for the class A_1 vibration, for which a central atom hybridization change is forbidden, it is needed to obtain a value of k_1, which will not be particularly sensitive to such a change. The value of A obtained was then used in

TABLE IV. Force constants for $TiCl_4$ (OVFF).[a]

Quantity	Observed	Calculated by Least squares	Calculated by k_β method
$k_1\times10^{-4}$ dyne/cm		22.92	23.21
$k_\alpha'\times10^{-4}$		0.566	1.162
$A\times10^{-4}$		0.792	0.729
$B/R\times10^{-4}$		0.122	0 112
k_β		not used	0.523
ν_1 cm^{-1}	388±2	389	
ν_2	119±2	109	
ν_3	498.5±.5	495.3	
ν_4	139±2	149	

[a] See reference 5 for meaning of symbols.

Eq. (2) to obtain a value for the OVFF bending constant k_α'. The results are tabulated in Table IV. The effective bending constant for the F_2-vibrations was indeed smaller than that calculated for the E-vibration, indicating that a change in hybridization may be taking place. Unfortunately we do not have more equations to check these assumptions.

It is suggested that structures such as $Cl_2Ti{=}Cl^+Cl^-$ are more prominent in the excited vibrational level ν_4, with the bond angle approaching 120°, thus making the observed vibration lower than that calculated for a straightforward sp^3 T_d-molecule. If this particular change in hybridization is due to the relative importance of ionic structures, then it is likely that the effect would be more noticeable in $ZrCl_4$ and TiF_4. Experiments are underway in this laboratory to obtain these infrared spectra for the gases at the appropriate elevated temperatures.

THE JOURNAL OF CHEMICAL PHYSICS VOLUME 23, NUMBER 9 SEPTEMBER, 1955

Thermal Decomposition of Nitric Oxide

FREDERICK KAUFMAN AND JOHN R. KELSO
Ballistic Research Laboratories, Aberdeen Proving Ground, Maryland
(Received November 19, 1954)

The decomposition of pure nitric oxide and of mixtures with nitrogen or helium was studied at T=1170 to 1530°K in quartz vessels. Above about T=1400°K, the reaction is homogeneous and cleanly second order in NO throughout the course of decomposition. A change in the surface to volume ratio leaves the rate unchanged as does the addition of a fourfold excess of nitrogen or helium. Above 1400°K, the activation energy is constant at 63.8±0.6 kcal. The effect of added oxygen was investigated and a mechanism is discussed which reconciles much of the available data.

INTRODUCTION

THOUGH this reaction has been the subject of several investigations, no agreement has been reached concerning its mechanism and temperature dependence. Jellinek[1] used a flow system and found the decomposition approximately second order in NO. Dushman[2] later reinterpreted Jellinek's data in terms of an activation energy which increased from 24 to 71 kcal in the temperature interval (960 to 2025°K). Indirect methods such as the formation of nitric oxide in $H_2-O_2-N_2$ flames led Zeldovich[3] and Frank-Kamenetsky[4] to propose a value of 82±10 kcal for the activation energy of the NO decomposition at high temperatures. Vetter[5] studied the reaction in a flow system between 1200 and 1900°K in the presence of excess oxygen and found a small rate increase due to oxygen. He proposed a chain mechanism involving the reactions

$$O+NO \rightleftharpoons N+O_2 \quad (1) \quad \Delta H_0^0=+32.5 \text{ kcal}$$
$$N+NO \rightleftharpoons O+N_2 \quad (2) \quad \Delta H_0^0=-75.5 \text{ kcal}$$
$$O+NO \rightleftharpoons NO_2 \quad (3) \quad \Delta H_0^0=-71.4 \text{ kcal}$$
$$O+NO_2 \rightleftharpoons NO+O_2 \quad (4) \quad \Delta H_0^0=-45.8 \text{ kcal}$$
$$N+NO_2 \rightleftharpoons 2NO \quad (5) \quad \Delta H_0^0=-78.3 \text{ kcal}$$

and their reverse steps. Wise and Frech[6] studied the reaction in the low temperature range (900 to 1275°K) in the presence of nitrogen and oxygen and reported a strong catalytic effect of oxygen which they explained by a chain process initiated by

$$2NO \rightarrow N_2O+O \quad (6) \quad \Delta H_0^0=+35.9 \text{ kcal}$$

propagated by

$$O+NO \rightarrow N+O_2 \quad (1)$$
$$N+NO \rightarrow O+N_2 \quad (2)$$

and terminated by

$$O+O+M \rightleftharpoons O_2+M \quad (7) \quad \Delta H_0^0=-117.2 \text{ kcal}.$$

Kaufman and Kelso[7] attempted to repeat Wise and Frech's experiments, but were unable to find the strong oxygen catalysis. They also raised objections to the proposed mechanism.

Still more recently, Daniels[8] reported experiments on NO formation and decomposition up to 2120°K in an alundum reactor placed in a molybdenum electric furnace. A flow system was used and the reactor was packed with small alundum spheres. The reaction was found to be homogeneous and second order in NO above 1770°K and a very high activation energy of 116 kcal was reported. This would require the pre-exponential factor to be 10^5 to 10^6 times greater than the binary

[1] K. Jellinek, Z. anorg. u. allgem. Chem. **49**, 229 (1906).
[2] S. Dushman, J. Am. Chem. Soc. **43**, 411 (1921).
[3] Y. B. Zeldovich, Acta Physicochim. U.R.S.S. **21**, 577 (1946).
[4] D. Frank-Kamenetsky, Acta Physicochim. U.R.S.S. **23**, 27 (1947).
[5] K. Vetter, Z. Elektrochem. **53**, 369, 376 (1949).
[6] H. Wise and M. F. Frech, J. Chem. Phys. **20**, 22, 1724 (1952).
[7] F. Kaufman and J. R. Kelso, J. Chem. Phys. **21**, 751 (1953).
[8] Daniels, Slaughter, and Hendrickson, paper presented at the Symposium on The Chemistry of the Oxides of Nitrogen, sponsored by the Office of Ordnance Research, Chicago, Illinois, September 3 and 4, 1953.

collision frequency of NO and would indicate a chain mechanism of considerable length.

Yet, serious objections can be raised to such chain reaction schemes, since they involve highly endothermic steps, particularly where nitrogen atoms are formed. In view of the considerable evidence for the value of 225.2 kcal/mole for the dissociation energy of nitrogen, reaction (1) is endothermic by 32.5 kcal and probably has an activation energy of 40 kcal or more. The reverse steps of (2), (3) and (5) in Vetter's scheme have ΔH's of +75.5, +71.4, and +78.3 kcal, respectively. All four reactions would seem to be ruled out as propagating steps in all but very short chains.

Moreover, some of the older experimental work is open to criticism. Concentration and temperature uniformity may not have been reached in flow systems, particularly when the starting material is NO_2 whose endothermic decomposition to NO and O_2 would increase the temperature lag in the reactor. Reproducibility of reported rates is often uncertain and methods of analysis are of questionable accuracy.

In this work, the emphasis has, therefore, been on accurate control of all variables using a static system up to the highest temperatures attainable. Reaction order, heterogeneity, added gas effect, temperature dependence, and possible induced decomposition of NO were investigated.

EXPERIMENTAL

A schematic drawing of the apparatus is shown in Fig. 1. The furnace was constructed of Babcock and Wilcox Company firebrick K-30 joined with refractory cement and consisted of two halves. A hemisphere of 7 in. diameter was hollowed out of each half of the furnace, a spiral shaped groove was cut around the inner surface into which a coiled chromel wire heating element was inserted. Power was obtained from a 110 volt line regulated by a *2KVA* Sola transformer and a large variac. Surprisingly, the heating elements showed little sign of deterioration after many months of daily operation, 8 to 10 hours at a time, and at temperatures of 1100 to 1260°C. Spherical quartz vessels of 10 and 15 cm diameter served as reaction flasks. Each flask was fitted with a quartz thermocouple well extending to the center. The temperature was measured by a platinum-platinum 10% rhodium thermocouple pushed to the end of the thermocouple well. The pumping system consisted of a forepump and a DPI oil diffusion pump. In addition to standard mercury manometers and McLeod gauges, a Wallace and Tiernan dial pressure gauge Model FA 145 proved extremely useful. Its readings were reproducible and accurate, and equilibrium was reached within $\frac{1}{2}$ sec.

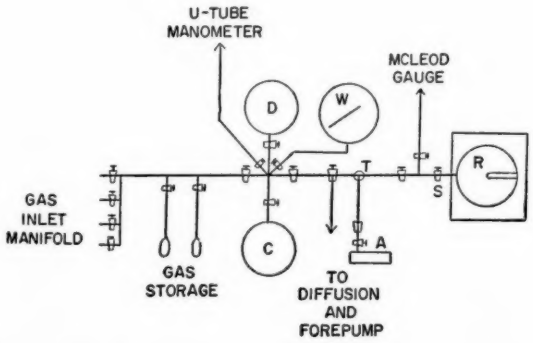

FIG. 1. Apparatus. *C, D*—Mixing and storage flasks. *R*—Quartz reaction flask. *W*—Wallace and Tiernan dial gauge, Model FA 145. *S*—Stopcock. *T*—Three-way stopcock. *A*—Silica or Corex absorption cell.

Tank nitric oxide was passed slowly through an acetone-dry ice trap and an ascarite absorption tube. It was condensed in a liquid nitrogen trap, distilled slowly into another trap and the middle fraction collected. The solid was pale blue, condensible, and contained less than 0.01% of higher oxides of nitrogen. Matheson prepurified nitrogen and helium were used without purification. Analysis of the nitrogen showed it to contain less than 0.01% of oxygen. Tank nitrous oxide was frozen out in a liquid nitrogen trap and pumped on to remove noncondensible gases.

The extent of decomposition was determined by analysis in 2 cm silica or 10 cm Corex absorption cells using a Beckman Spectrophotometer Model DU. In experiments where the % NO decomposed was 30 or higher, excess oxygen to 1 atmos total pressure was added to a known fraction of the reaction mixture in the absorption cell. This converted all of the remaining NO to an $NO_2-N_2O_4$ equilibrium mixture. In experiments where the % NO decomposed was small, excess NO to 1 atmos total pressure was added in the cell. This converted all of the O_2 formed in the decomposition to an equilibrium mixture containing NO_2, N_2O_4 and N_2O_3.

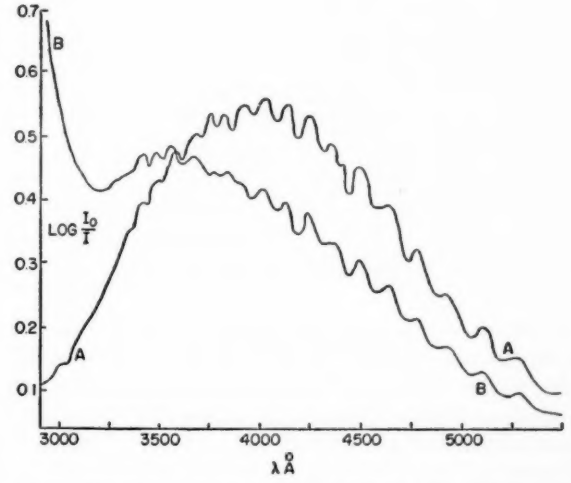

FIG. 2. Absorption spectra of gas mixtures. 10 cm Corex cell. A—7.29 mm NO plus excess O_2 to 1 atmos. B—3.63 mm O_2 plus excess NO to 1 atmos.

TABLE I. Decomposition of NO in the presence of small amounts of N_2O.

	Exp. No.	p_0NO mm	p_0N_2O mm	p_{O_2} found mm	$\frac{1}{2}p_0N_2O+p_{O_2}$ (NO blank)
$T=1223$°K	5A	299	15.94	8.87	8.44
$t=1$ min	9A	298	15.24	8.78	8.11
$T=1323$°K	11A	99.3	4.69	2.86	2.64
$t=1$ min	12A	100.1	4.73	2.83	2.66

Figure 2 shows the absorption spectra of two gas mixtures; one of 7.29 mm of NO with excess oxygen (curve A); the other of 3.63 mm of O_2 with excess NO (curve B). If the N_2O_3 equilibrium pressure were negligible, the two curves would be identical, since equal amounts of NO_2 are formed. Clearly, this is not the case. N_2O_3 is formed to the extent of about 30% in agreement with Verhoek and Daniels' data.[9] Above about 3800 A, NO_2 is the only absorbing species and curve B lies 30% below A. At shorter wavelengths, N_2O_3 apparently absorbs strongly. This emphasizes the need for accurately controlled conditions in the spectrophotometric analysis of NO_2 and may be responsible for some of the discrepancies among prior published results.

Gas mixtures containing excess oxygen were analyzed at 3000 and 3200 A, as Hall and Blacet[10] have shown that in this range the absorption coefficient of N_2O_4 is roughly twice that of NO_2. No account need then be taken of the $NO_2-N_2O_4$ equilibrium. Known mixtures gave excellent agreement with Beer's law. Readings were taken at both wavelengths and their average used.

For mixtures with excess NO, this wavelength region is unsuitable, because it does not measure the variable concentration of N_2O_3. The region where curves A and B cross is best suited for these samples. Agreement with Beer's law was verified separately at 3450, 3500, 3550, and 3600 A, using known mixtures. Unknowns were analyzed at all four wavelengths and the average used.

In kinetic experiments, NO was rapidly admitted to the quartz flask, allowed to react ($t=\frac{1}{2}$ to 40 min) and then expanded into the cell. Care was taken to obtain a representative sample by letting the reacted gas go first to the left of threeway stopcock T, then down into the evacuated cell, and finally letting the pressure equilibrate in the three-way position of T. This procedure took only 2 to 3 sec and prevented the accumulation of unreacted gas from the reactor inlet tube in the absorption cell.

Possible variations in the pressure ratio on expansion of the reacted gas into the cell is another source of error. Such variations would be due to association reactions in the gas cell. In kinetic runs where the extent of decomposition did not exceed a few percent, this error was negligible. In runs with extensive decomposition, the reacted gases were expanded into the cell and into flask D. This lowered the pressure so much that the $NO-O_2$ reaction was negligible during the short time of pressure equilibration as was verified repeatedly by the slow appearance of color due to NO_2 in the cell and flask D.

[9] F. Daniels and F. H. Verhoek, J. Am. Chem. Soc. **53**, 1250 (1931).

[10] T. C. Hall, Jr., and F. E. Blacet, J. Chem. Phys. **20**, 1745 (1952).

RESULTS AND DISCUSSION

The possible importance of a chain scheme at moderate temperatures was tested at the outset of this investigation. The initial step in the thermal decomposition of nitrous oxide is known to yield oxygen atoms. Much new information on this reaction will be presented in a later publication. This decomposition is rapid at about 750°C, where the decomposition of NO is quite slow.

If a small amount of N_2O is added to NO and the gas mixture heated to 950 to 1050°C, all of the N_2O is found by infrared analysis to be decomposed within a few seconds. During this short period, there should be a considerable concentration of oxygen atoms present. In the event of a chain reaction of appreciable chain length, the decomposition of additional NO should be induced when N_2O is present.

A valid objection to this argument is the well-known rate increase in N_2O decomposition when excess NO is present. This is usually attributed to the reaction,

$$N_2O+NO\rightarrow N_2+NO_2$$

in which N_2O is decomposed without the formation of oxygen atoms. Musgrave and Hinshelwood[11] found a greater temperature dependence for the NO catalyzed than for the uncatalyzed decomposition of N_2O, but results in this laboratory did not bear this out. If our results are correct, high temperatures should favor oxygen atom formation.

Experimental data are presented in Table I. Though the amount of oxygen produced is in all cases only slightly greater than the sum of the oxygen derived from N_2O plus that due to the blank decomposition of

TABLE II. Initial order of nitric oxide decomposition.

T, °K	Exp. No.	p_0NO, mm Hg	k, cc mole^{-1} sec^{-1}
	246, 250	100	85.7
1330	247, 249	200	84.4
	248	500	90.0
1413	57, 58	50	312
	52, 53	100	347
	56	200	356
	59, 60	300	350
	61, 62	500	385
1451	114, 115	100	653
	110, 112	200	643

[11] F. F. Musgrave and C. N. Hinshelwood, Proc. Roy. Soc. (London) **A135**, 23 (1932).

NO, this excess roughly corresponds to a doubling of the decomposition rate of NO. These results are less accurate because of the great precision required in making the gas mixtures, because of possible transient temperature peaks due to the rapid decomposition of N_2O, and because of the necessity of calculating a small difference between two large experimental quantities. Nevertheless, a chain reaction of long chain length is incompatible with our results.

THE DECOMPOSITION OF PURE NO

About 100 careful rate experiments were run with pure NO in two quartz flasks. Reproducibility was good, particularly in the high temperature range. Three runs at 1223°K, at about 500 mm Hg initial NO pressure and decomposition of less than one percent gave $k=13.7$, 14.2 and 14.2 cc mole^{-1} sec^{-1}. Seven runs 1423.3±0.7°K at 100 to 150 mm Hg initial NO pressure and decomposition of 2 to 15% gave $k=422$, 406, 397, 423, 412, 407, and 415 cc mole^{-1} sec^{-1}. The latter series has an average of 412.4 and an average deviation of 7.2 cc mole^{-1} sec^{-1} or 1¾% which represents excellent agreement.

The initial order of the reaction was determined repeatedly. Three examples are presented in Table II. It appears that second-order rate constants defined by $-d(\mathrm{NO})/dt=k(\mathrm{NO})^2$ represented the data quite well.

The order during the course of reaction was also determined. As is seen in Table III there is no change in reaction order during the later stages of decomposition at 1424°K. This is evidence against any strong catalytic effect by molecular oxygen such as that reported by Wise and Frech.[6] A very much weaker oxygen effect which becomes observable at or above 1500°K is discussed below.

At lower temperatures, the rate constant does depend slightly on the extent of decomposition. This is not surprising in view of the known heterogeneous nature of the reaction. The results in Table III show the decreasing variation of k with % decomposition as the temperature is increased. It is of interest though, that k always decreases with increasing extent of reaction, since the opposite effect should have been observed if the strong, homogeneous oxygen catalysis reported by Wise and Frech were present.

TABLE III. Dependence of rate constant on % decomposition.

T, °K	Exp. No.	% decomposition	k, cc mole^{-1} sec^{-1}
1123	229, 234, 236	0.5	2.24
	230	1.3	2.19
	231, 235	2.6	1.98
1223	220, 222, 223	0.5	14.1
	221	3.3	12.7
1323	213, 215	1.1	81.0
	214	7.0	75.8
1424	148	2.0	423.0
	143	3.0	422.0
	150	14.0	412.0
	144	17.0	406.0
	156	22.0	414.0
	160, 181	36.0	436.0
	182	54.0	423.0

TABLE IV. Effect of added nitrogen on nitric oxide decomposition. $T=1423.3$°K, $p_0(\mathrm{NO})=100$ mm, $p_0(N_2)=400$ mm Hg.

Exp. No.	% decomposition	k, cc mole^{-1} sec^{-1}
165	2.8	423
170	5.5	417
166	12.3	409
164	23.2	436
168	46.3	419

SURFACE EFFECTS

The relative importance of homogeneous and surface reactions was studied further. There is considerable evidence for the conclusion that the reaction is homogeneous above about 1400°K. This is based on (a) results in two reaction vessels with different surface to volume ratios (b) the reproducibility of high temperature data, (c) the constancy of the rate in the presence or absence of added inert gases, and (d) the constancy of the activation energy at high temperatures.

Of the above evidence, (a) is the most direct. Two quartz vessels were used with surface to volume ratios of 0.65 and 0.42. Four experiments in the large flask at 1414±0.5°K gave an average rate constant of 343 cc mole^{-1} sec^{-1}. Seven experiments in the small flask at 1423.3±0.7°K gave an average of 412.4 cc mole^{-1} sec^{-1} which was corrected to 354 cc mole^{-1} sec^{-1} at 1414°K by its known temperature dependence and is in good agreement with the value of 343 obtained in the large flask. Similarly, five runs in the large flask at 1443.3±0.5°K gave a k of 562. Four runs in the small flask, at 1451.5±0.5°K when corrected for temperature, gave 574, in excellent agreement with the value obtained in the large flask. Thus, the rate constant appears to be independent of the surface to volume ratio, a strong indication that the decomposition is homogeneous in this temperature range.

All other experimental evidence supports this result. The high order of reproducibility reported above is rarely encountered in heterogeneous reactions where the particular conditioning of the surface, rate of admission of gas, or degree of evacuation before a run commonly affect the rate.

INERT GAS EFFECT

The effect of nitrogen and helium on the kinetics was studied for this reason. A homogeneous, bimolecular reaction should not be affected by the addition of inert gas. A surface reaction might be influenced in a number of ways. The inert gas may be adsorbed on the surface and thereby change the surface concentration of reacting

nitric oxide. In case of a chain reaction, the added gas may change the relative importance of initiation or termination reactions at the wall by increasing the average life of chain carriers in the gas phase. Tables IV and V present the results obtained for added nitrogen and helium. The runs with added fourfold excess of nitrogen show no trend with increasing decomposition and are in excellent agreement with blank runs at the same temperature. Their average is 421 cc mole^{-1} sec^{-1} compared with 412.4 obtained as an average of seven blank runs.

The runs with added helium show a slight increase in initial rate, but are in good agreement with blank runs when the extent of decomposition is above 5%. The rate increase in short runs ($t=1$ min) may be due to adiabatic compression of the first part of the gas mixture upon admission to the flask. The high ratio of specific heats in the helium mixture would bring about a higher transient gas temperature and higher decomposition rate for a few seconds. On the whole, the agreement of rates in the presence or absence of a fourfold excess of inert gas is extremely good and serves as additional evidence for the homogeneous nature of the reaction at 1420°K.

TEMPERATURE DEPENDENCE

The temperature dependence of k is shown in Table VI and in Fig. 3. Below 1350°K, the values of k become somewhat questionable in view of the results of Table III. The data in Table VI represent about 80 kinetic runs with the lowest percent decomposition at the respective temperatures. The listed rate constants are average values and in all cases, individual k's differed from the average by 3% or less. They are plotted in Fig. 3 which also includes data from several earlier investigations.[1,5,6]

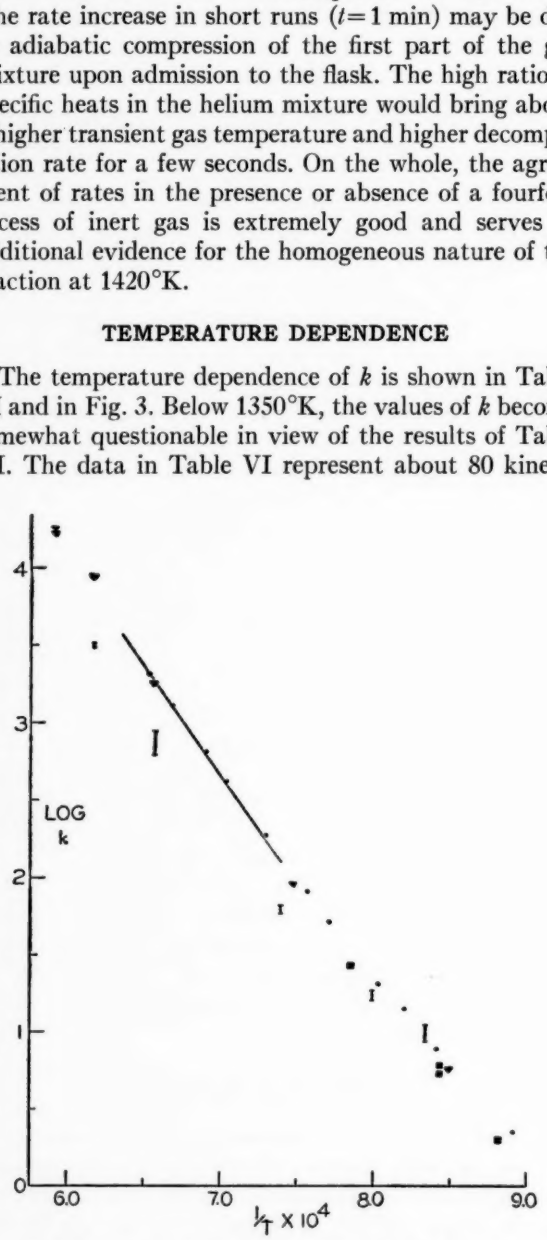

FIG. 3. Temperature dependence. •—This work, ■—Wise and Frech, reference 6, I—Jellinek, reference 1, ▼—Vetter, reference 5.

TABLE V. Effect of added helium on nitric oxide decomposition. $T=1423.8$°K, $p_0(NO)=100$ mm, $p(He)=400$ mm Hg.

Exp. No.	% decomposition	k, cc mole^{-1} sec^{-1}
174, 176	3	469
175, 177	5.5	430
173, 178	22	413
179, 180	36	402

Above 1370°K, the graph is accurately linear up to the highest temperature attained (1535°K) and the activation energy is 63.8±0.6 kcal. In this range, the rate constant is given as $2.6\times10^{12}e^{-63.8/RT}$ cc mole^{-1} sec^{-1}. By comparison, Jellinek's data are generally low and much less reproducible. The points selected from Vetter's[5] data were those with the highest NO/O_2 ratio and they are in excellent agreement with our work. Vetter's results with large excess oxygen at still higher temperatures are not shown, but would lie much above the extension of our linear plot for reasons which will now be discussed.

THE OXYGEN EFFECT

In an attempt to clarify the oxygen effect reported by Vetter, several experiments were carried out at 1423°K and 1473°K with excess O_2 added. Because of the difficulties of premixing NO and O_2 with formation of NO_2 and N_2O_4, O_2 was admitted to the furnace and was followed by a higher pressure of pure NO to give the desired mixture. Mixing in the furnace was very rapid under those conditions as was shown by blank runs in which N_2 was put in the furnace and NO then added. These experiments yielded rate constants identical with those of pure NO alone. Within the somewhat lower accuracy of these runs (±2−4%) it was found that at 1423°K, $p_{NO}=100$ mm Hg, $p_{O_2}=100$ to 200 mm Hg, no rate acceleration was observable. At 1473°K, $p_{NO}=100$ mm Hg, $p_{O_2}=0$ to 400 mm Hg, a small rate increase of about 7% for 100 mm of O_2 was found, in agreement with Vetter's data. This increase was proportional to the square root of the O_2 concentration.

It is now possible to interpret all data within one consistent mechanism. Accepting Vetter's[5] data and representation of the rate by*

$$-d(NO)/dt=k_a(NO)^2+k_b(NO)(O_2)^{\frac{1}{2}} \qquad (8)$$

as was also done by Wise and Frech[6] we can make an improved assignment of k_a and k_b. Vetter observed curvature in the log k_a *vs* $1/T$ plot because he included

* Reference 5, Eq. 10, $b=0$, $c=$const.

data at 1179 and 1338°K where there is considerable heterogeneity. This led him to propose an activation energy of 75 kcal for k_a at the high temperature limit even though his four highest experimental points give a good linear plot with $E=61.7$ kcal. This value compares quite well with our $E=63.8$ kcal.

The activation energy of k_b from Vetter's plot is about 92 kcal. It was redetermined by setting $k_a=2.6\times10^{12}e^{-63.8/RT}$ cc mole^{-1} sec^{-1} as obtained from our work and calculating k_b from all of Vetter's data. These values for k_b are shown in Table VII. Their Arrhenius plot shows improved linearity and yields 101 kcal for the activation energy of k_b. It is now assumed that the oxygen atom concentration is given by the equilibrium expression,

$$(O)=8.5e^{-60.5/RT}\,(O_2)^{\frac{1}{2}},\quad (T=1600-1800°K)$$

and that

$$k_b=2k_1[(O)/(O_2)^{\frac{1}{2}}]$$

because of reactions (1) and (2), neglecting other nitrogen atom reactions. The rate constant, k_1, then turns out to be $8.3\times10^{12}e^{-40.5/RT}$ cc mole^{-1} sec^{-1} which is entirely reasonable in view of its ΔH_0^0 of 32.5 kcal.

The reverse reaction

$$N+O_2\rightarrow NO+O\quad(-1)$$

must, therefore, have a rate constant $k_{-1}=3.8\times10^{13}\times e^{-8.0/RT}$ cc mole^{-1} sec^{-1}. This would indicate that the reaction

$$N+NO\rightarrow N_2+O\qquad(2)$$

at 1600°K could be at most about 50 times faster than (−1) and justifies Vetter's consideration of k_{-1}/k_2 at high oxygen concentrations.

Several questions remain to be answered. The nature of the products of the homogeneous, bimolecular reaction of NO was not determined unequivocally. This simple step may yield N_2O+O as suggested by Wise and Frech followed by fast reactions leading to N_2 and O_2 but without induced decomposition of NO ($N_2O+NO\rightarrow NO_2+N_2$, $O+NO_2\rightarrow NO+O_2$, $O+NO+M\rightarrow NO_2+M$, $2NO_2\rightarrow 2NO+O_2$).

There is some evidence against this scheme. If the reaction

$$2NO\rightarrow N_2O+O\quad(6)\quad \Delta H_0^0=+35.9\text{ kcal}$$

is to be identified with the observed bimolecular decomposition, its activation energy is 63.8 kcal and that of its reverse step,

$$O+N_2O\rightarrow 2NO\quad(-6)$$

would have to be 27.9 kcal. Recent work on the decomposition of N_2O in our laboratories[12] supports a lower value for this reaction. But the reaction seems to have a low pre-exponential factor and is slow despite its low energy of activation. It therefore seems probable that N_2 and O_2 are the immediate products.

The pre-exponential factor of 2.6×10^{12} cc mole^{-1} sec^{-1} is 1/75 of the collision frequency calculated assuming a diameter $\sigma_{NO}=3.7$ A. The presumed rectangular transition state would introduce geometrical restrictions and may have a shorter distance of approach between the NO molecules. Both these corrections would lower the theoretical collision frequency and bring it into agreement with the experimental value.

The source of oxygen atoms for reaction (2) represents another problem. The rate of the reaction

$$O_2+M\rightarrow O+O+M$$

is too small[7] to assure equilibrium oxygen atom concentration. Reactions (4) and (9)

$$O_2+NO\rightleftarrows NO_2+O\quad(4)\quad\Delta H_0^0=+45.9\text{ kcal}$$
$$2NO_2\rightleftarrows 2NO+O_2\quad(9)\quad\Delta H_0^0=+25.6\text{ kcal}$$

appear to be a likely source of oxygen atoms in thermal equilibrium with O_2 at high temperatures.

The thermal decomposition of nitric oxide thus occurs as a surface reaction of low activation energy at low temperatures and becomes a simple, bimolecular reaction around 1400°K. Above about 1600°K, and in the presence of excess O_2, the reaction between atomic oxygen and NO becomes important and, because of its high activation energy, is rate controlling above about 1800 to 1900°K.

The interpretation of the oxygen effect is based in large part on Vetter's experimental measurements. In future work, we will attempt to obtain accurate rate data in a static system up to 1900°K in order to verify this scheme.

TABLE VI. Temperature dependence surface/volume=0.65 cm^{-1}.

T, °K	$1/T\times10^4$	k, cc mole^{-1} sec^{-1}
1123	8.905	2.24
1190	8.403	7.71
1223	8.177	14.1
1247	8.019	20.5
1299	7.699	52.4
1323	7.559	81.0
1373	7.283	188.0
1423	7.026	412.0
1451	6.892	648.0
1499	6.671	1306.0
1533	6.523	2100.0

TABLE VII. Temperature dependence of k_b.

T	k_b, cc$^{\frac{1}{2}}$ mole$^{-\frac{1}{2}}$ sec^{-1}
1525	0.48± 0.01[a]
1690	12.8 ± 1.8
1840	125.0 ±11.0
1912	402.0 ±54.0

[a] This value was obtained by using 1.70×10^3 for k_a instead of 1.94×10^3 cc mole^{-1} sec^{-1}. This choice brings all five runs of Vetter's into excellent agreement and is justified by the small difference between the observed rate and $k_a(NO)^2$.

[12] To be submitted to J. Chem. Phys. shortly.

Magnetic Properties of Uranium Hydride*

DIETER M. GRUEN
Chemistry Division, Argonne National Laboratory, Lemont, Illinois
(Received December 13, 1954)

The magnetic susceptibility of β UH_3 has been measured in the temperature range 191°K to 603°K. From the high-temperature portion of the χ^{-1} *versus* T curve one calculates a magnetic moment of 2.79 Bohr magnetons, with $\Delta = -137$°K. A ferromagnetic transition occurs in the neighborhood of 173°K. Magnetic moment measurements made in the temperature range 63°K to 196°K in fields of 1550 to 8700 oersteds can be extrapolated to yield a saturation magnetic moment of about one Bohr magneton.

INTRODUCTION

A FERROMAGNETIC transition was recently found in UH_3 by Trzebiatowski *et al.*[1] The present study presents more extensive measurements both above and below the Curie point.

PARAMAGNETIC REGION

The Faraday method for measuring magnetic susceptibilities was employed in the region 191°K to 603°K. The apparatus and procedure were similar to those described in detail elsewhere.[2]

The sample of UH_3 was prepared from 23.37 mg of U metal. The metal, prepared by an electrolytic process, was spectroscopically pure and had been electropolished to remove oxide coating. The metal was allowed to react at 250°C with H_2 produced by the decomposition of UH_3. At this temperature one obtains only β UH_3.[3] The sample was sealed off from the line in a 4-mm o.d. thin-walled spherical quartz bulb under 300 mm of H_2 pressure. From the measured uptake of H_2 it was calculated that 96% of the metal had reacted to form hydride. The remaining 4% was assumed to be UO_2. The magnetic measurements of Dawson and Lister[4] on UO_2 were used to correct our measurements on the hydride for this impurity, the correction varying from 1.4% to 3.8% depending on the temperature. The measured forces which varied from 1 mg to 50 mg in the temperature interval studied, were corrected for the diamagnetism of the container. A correction was also applied for the diamagnetic susceptibility of U and H_2. Temperatures above room temperature were obtained by surrounding the sample with a glass tube wound with two glass-fiber covered heating tapes which were supplied with power by means of two variacs. A capacitrol regulating one of the variacs controlled the temperature to within ± 1°. Temperatures below room temperature were obtained by placing the sample in a Dewar filled with freon-12. Pumping on the refrigerant at a controlled rate enabled one to produce any temperature between the boiling point, (242°K) and the triple point (115°K) of this refrigerant.

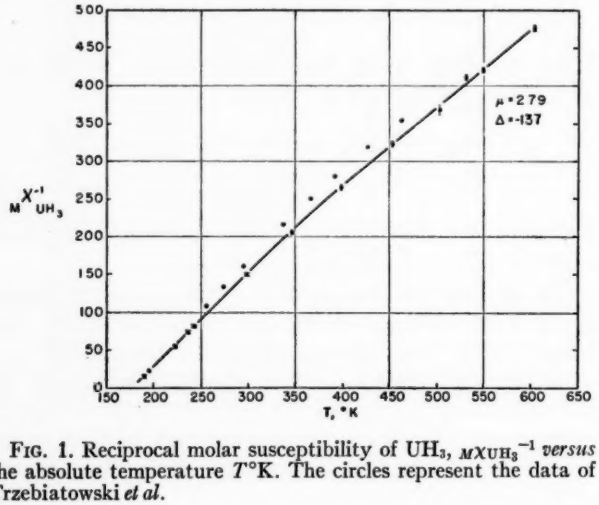

FIG. 1. Reciprocal molar susceptibility of UH_3, $M\chi_{UH_3}^{-1}$ *versus* the absolute temperature T°K. The circles represent the data of Trzebiatowski *et al.*

A total of 48 measurements was made on the compound at the various temperatures and field strengths. No variation in susceptibility with field strength was observed in the range 4000 to 9000 oersteds. The results are summarized in Table I and Fig. 1. Each entry in the table is the arithmetic mean of four measurements at four different field strengths.

The graph was obtained by plotting the tabulated values of $M\chi^{-1}$ as ordinate *versus* T as abscissa. A least-square straight line was drawn through all the points above 390°K. A smooth curve was drawn visually through the remaining points. (The open circles repre-

TABLE I. Molar magnetic susceptibility of UH_3.

T°K	$M\chi \times 10^6$	$M\chi_{UH_3}^{-1}$	T°K	$M\chi \times 10^6$	$M\chi_{UH_3}^{-1}$
603	2101	476	347	4854	206
549	2375	421	298	6711	149
530	2433	411	242	12,048	83
502	2725	367	236	13,513	74
452	3086	324	222	17,857	56
398	3774	265	191	62,500	16

* This work was performed under the auspices of the U. S. Atomic Energy Commission.

[1] Trzebiatowski, Sliwa, and Stalinski, Roczniki Chem. **26**, 110 (1952); **28**, 12 (1954); Chem. Abstracts **46**, 10726 (1952).

[2] D. M. Gruen and C. A. Hutchison, Jr., J. Chem. Phys. **22**, 386 (1954).

[3] Mulford, Ellinger, and Zachariasen, J. Am. Chem. Soc. **76**, 297 (1954).

[4] J. K. Dawson and M. W. Lister, J. Chem. Soc. 2181 (1950).

TABLE II. Magnetic moment per gram of UH_3, $\sigma_{H,T}$.

$H_0 \times 10^{-3}$ Oersted	Temperature, °K													
	63	78	112	124	149	152	160	165	173	181	183	188	191	196
1.55	17.1	16.3	15.1	14.0	11.8	10.9	10.0	7.5						
3.15	18.7	18.0	17.0	16.3	13.6	12.6	11.6	8.7	7.5	4.7	3.4			
4.65	19.2	18.9	18.0	17.0	14.1	13.4	12.1	9.3	8.1	5.5	4.0			
5.80	19.7	19.3	18.1	17.5	14.3	13.6	12.4	9.6	8.3	5.9	4.4	1.9	1.4	0.6
6.60	19.7	19.5	18.4	17.7	14.4	13.8	12.5	9.7	8.4	6.1	4.6	2.4	1.7	0.8
7.15	20.0	19.3	18.3	17.6	14.4	13.6	12.4	9.6	8.3	6.2	4.8	2.2	1.8	0.6
7.65	20.0	19.7	18.6	17.9	14.7	13.9	12.7	9.8	8.8	6.7	5.2	2.6	2.0	0.6
8.02	20.1	19.5	18.7	18.1	14.7	13.8	12.6	9.9	8.8	6.7	5.2	3.0	2.0	0.9
8.35	20.1	19.8	18.7	17.9	14.6	13.9	12.6	9.9	8.9	6.7	5.4	2.8	2.0	1.9
8.70	20.2	20.0	18.8	18.2	14.8	14.1	12.8	10.0	9.0	7.0	5.7	3.1	2.3	1.0

sent the data of Trzebiatowski *et al.*[1]) A value of

$$\mu=[(3k/\beta^2N)S^{-1}]^{\frac{1}{2}}=\left(\frac{7.997}{S}\right)^{\frac{1}{2}} \tag{1}$$

in which S is the slope of χ^{-1} *versus* T above 390°K was calculated and a value of

$$\Delta=\frac{{}_{450}\chi^{-1}}{S}-450 \tag{2}$$

in which ${}_{450}\chi^{-1}$ is the susceptibility at 450°K was calculated. The values found for μ and Δ were

$$\mu=2.79; \quad \Delta=-137°\text{K}.$$

Figure 1 shows that the χ^{-1} *versus* T curve acquires a gentler slope above 350°K. Since our measurements were extended to somewhat higher temperatures than those of Trzebiatowski *et al.*, this decrease in slope is more evident in our data. Consequently, our value for μ is somewhat higher than the value 2.44 reported by the Polish workers.

FERROMAGNETIC REGION

Below 173°K the susceptibility becomes field dependent. The attendant large increase in susceptibility indicates that UH_3 undergoes a ferromagnetic transition near this temperature.

Magnetic moments were determined in the temperature range 63°K to 196°K. The sample, 51.8 mg of UH_3 in a spherical quartz container, was placed in an inhomogeneous field produced by Sucksmith type pole pieces.[5] The sample was held firmly in the center of the field by an arrangement involving two flat phosphor bronze springs.[6] The forces, which ranged from 50 to 500 mg were measured with an Ainsworth Optical Lever microbalance which was used in this case as a null instrument. The sensitivity of the springs was such that a change of one division on the optical scale corresponded to a change in weight of 5 mg. Since changes of half a division were easily measurable, the useful sensitivity of this arrangement was 2.5 mg.

Corrections for oxide content (3% for this sample), diamagnetism of container, U and H_2 were made as before.

The gradient of the field was calibrated using a sample of 99.9% pure nickel in the shape of a rod with length to diameter ratio equal to 5. The measurements of Weiss and Forrer[7] were taken as our standard. The gradient and the magnetic field were measured with two commercially available instruments, a Dyna Lab Gaussmeter and a Rawson rotating coil flux-meter both of which had been calibrated against a Varian Associates proton nuclear resonance meter. The three measurements agreed within ±1.5%. A region of the field was found where the gradient was constant over a length of one inch. The gradient varied from 50 to 400 oersteds per cm in the region 1500 to 8700 oersteds, which was the field region in which the measurements were made.

The desired temperatures were obtained by means of liquified N_2, CH_4, and freon-13. Pumping on these refrigerants enabled one to obtain temperatures between their boiling and triple points.

The magnetizing field was calculated using the expression

$$H=H_0-NI \tag{3}$$

where H=magnetizing field, H_0=applied field, I =magnetization per cm³, and N=demagnetizing constant. For the UH_3 sample, I was obtained from the product of ρ, the bulk density (1.467 g/cm³) and σ, the magnetic moment per gram. The demagnetizing constant was taken to be $4\pi/3$ for the spherical UH_3 sample, and 0.7015 for the Ni rod. Magnetic moments were calculated from the expression

$$F=m\sigma\frac{\partial H}{\partial x} \tag{4}$$

where F=force in x-direction, m=mass of sample, σ=magnetic moment per gram, and $\partial H/\partial x$=magnitude of gradient of magnetic field in x-direction. The measurements are summarized in Table II and Fig. 2. From

[5] W. Sucksmith, Proc. Roy. Soc. (London) **A170**, 551 (1939).
[6] L. F. Bates, *Modern Magnetism* (Cambridge University Press, Cambridge, England, 1951), p. 311.
[7] P. Weiss and R. Forrer, Ann. phys. **10**, 153 (1926).

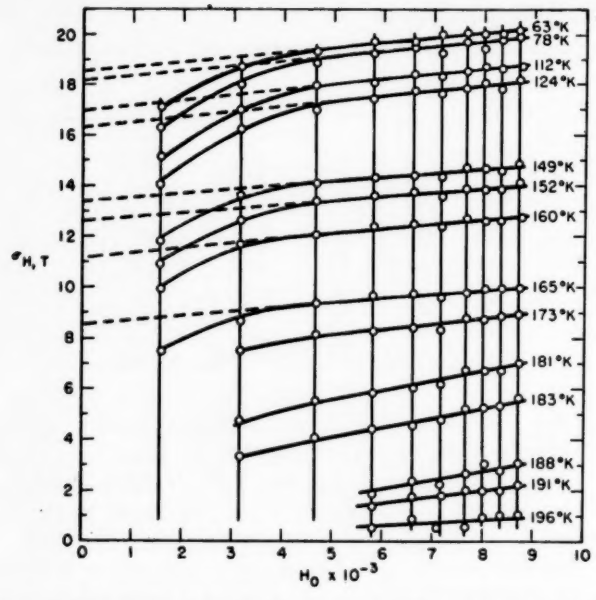

FIG. 2. The magnetic moment per gram UH_3, $\sigma_{H,T}$, at various temperatures as a function of the applied field, H_0.

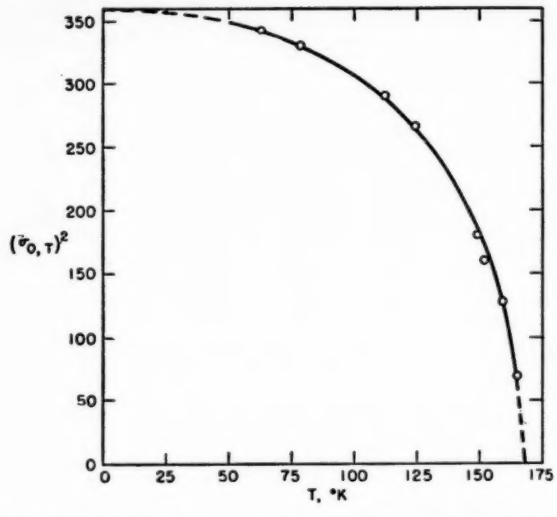

FIG. 3. The square of the spontaneous magnetization per gram of UH_3, $(\sigma_{0,T})^2$, *versus* the absolute temperature T°K.

the figure it can be seen that the susceptibility is already slightly field dependent at 183°K. At 173°K and below, saturation effects are observed beginning at a field strength of approximately 4500 oersteds. The substance appears to be not far from complete saturation at 8700 oersteds, the upper limit of our measurements. Extrapolation of the high-field data for the runs at 165°K and below to zero magnetic field yields values for the spontaneous magnetization. In Fig. 3 are plotted the values of the square of the spontaneous magnetization *versus* the absolute temperature. Extrapolation of this curve to zero spontaneous magnetization gives for the ferromagnetic Curie point 173±2°K.

The data of Table II were also plotted as a function of $1/H_0$ and extrapolated to $1/H_0=0$. The saturation moments obtained in this way were plotted as a function of $T^{\frac{1}{2}}(°K)^{\frac{1}{2}}$. The straight-line portion of this curve was extrapolated to $T=0$ giving the value 23 cgs units for the saturation magnetization per g at 0°K. This saturation moment corresponds to one Bohr magneton where the value for the Bohr magneton is taken as 5587 emu per mole. In view of the extensive extrapolations involved in arriving at this number, it is impossible to set accuracy limits. Preliminary results in very high magnetic fields carried to helium temperatures by Dr. Warren E. Henry of the Naval Research Laboratory indicate that the value given here is somewhat low and that the actual value is closer to 1.2 Bohr magnetons.

Our result for the saturation magnetization at 78°K is 0.9 Bohr magneton. This may be compared with the value 0.65 Bohr magneton at 80°K obtained in an approximate measurement by Trzebiatowski *et al.*[1]

Since our measurements were carried only to N_2 temperatures it is difficult to extrapolate the spontaneous magnetization data to 0°K. The ratio σ_0, $T/\sigma_{0,0}$ was plotted against T and compared with theoretical curves constructed in the usual way from Brouillon functions with $j=\frac{1}{2}$, 1, and ∞. In such a plot, the experimental points lie nearest the theoretical curve with $j=\frac{1}{2}$. This implies that the elementary magnets in UH_3 are electrons whose orbital angular momenta are completely quenched.

ACKNOWLEDGMENTS

It is a pleasure to acknowledge the invaluable aid of H. Flotow in the preparation of the samples, R. Misch and F. Gunzel who electropolished the uranium metal, and J. Pickhardt who constructed the flat springs. Thanks are due W. E. Henry of the Naval Research Laboratory, Washington, D. C. for a number of stimulating discussions.

Study of Chemical Reaction Mechanisms with Molecular Beams. The Reaction of K with HBr*

ELLISON H. TAYLOR AND SHELDON DATZ
Chemistry Division, Oak Ridge National Laboratory, Oak Ridge, Tennessee

(Received December 13, 1954)

The reaction between K and HBr has been studied by a molecular beam technique, using as a detector a surface ionization gauge with a tungsten and a platinum alloy filament, the former sensitive to KBr as well as to K and the latter essentially to K only. The activation energy is 3.4±0.1 kcal/mole and the probability or steric factor is about 0.1. The angular distribution of the KBr suggests that collisions with the H end of the HBr are more often fruitful than other configurations. The total collision cross section for a beam of K at 504°K in HBr at 401°K is 850×10^{-16} cm².

INTRODUCTION

OUR knowledge of the mechanics of reactive molecular collisions comes mainly from measurements of reaction rates in gases as functions of temperature and concentration. Although a great deal has been learned in this way, the finer details of such collisions are obscured by the chaotic nature of the molecular encounters, by the lack of independent control over the energies of the reacting species, and by the somewhat remote connection between the measured rate and the elementary process of interest. It has long been apparent that studies of reactions between molecular beams of species of interest would provide more intimate details about the processes occurring, and suggestions to this end have been occasionally made.[1,2] Some chemical experiments have even been attempted in this way,[3,4] but the results have appeared to be unsatisfactory, either from the published accounts or from the lack of further publication beyond the original mention of work in progress. The primary difficulty has been that of measurement of atoms and molecules of chemical interest in the numbers available from molecular beams. The methods available, the surface ionization gauge for alkali metals and the Pirani gauge for hydrogen and helium, have enabled physicists to prosecute a great deal of work on nuclear moments and on elastic scattering, but the chemist has been unable to study reactive scattering with these elements.

The present work was undertaken in the hope that neutron activation would provide a means of measurement of some further species and thereby enable molecular beam experiments in chemical kinetics to be carried out. The reaction chosen for study was that of K with HBr, with the intention of measuring potassium by the surface ionization gauge and bromine by neutron activation of deposits collected from the scattered products. As described below, neutron activation proved to be unnecessary in this case, and a continuous discrimination can be made between elastic scattering and reaction.

The general arrangement for these experiments is similar to that used by Broadway[5] in elastic scattering in that a well-collimated beam containing the detectable species K is crossed at one point by a slightly collimated beam of the other reactant. In Broadway's case and in some preliminary experiments here the collimated cross-beam was replaced by an uncollimated effusive spray. The detector is pivoted about the scattering point, and measures both K and KBr as a function of angle.

The reactions of alkali metals with halogens and with halides have been studied by Polanyi and co-workers, using the methods of dilute flames and of diffusion flames.[6,7] The specific case of K+HBr was studied by Schay,[8] who found at 600°K a specific rate constant of 1.5×10^{-7} mole/cm³, sec compared with a calculated value of 7×10^{-8} assuming a mean molecular diameter of 3.6 A and reaction on every collision. This apparent excess of reactions over collisions is typical of many of these reactions. Magee has suggested[9] that such reactions occur at abnormally large separations because the potential curves for the ionic and for the homopolar states cross at distances greater than kinetic theory diameters.

APPARATUS

An isometric diagram of the apparatus is shown in Fig. 1. The source of potassium vapor is a nickel oven *A* containing molten potassium. It is heated to 540°K to produce a vapor pressure of approximately 0.1 mm. The vapor passes through a stainless steel, thin-wall tube *B*, into a second nickel oven, *C*, which is maintained at a higher temperature than *A* (540° to 840°K). After a devious passage through *C*, to insure temperature equilibrium, the potassium effuses through oven slits *D*. The effusing *K* is narrowed by fore slits *E* and *E'* and finally

* This paper is based upon work performed under Contract for the Atomic Energy Commission at the Oak Ridge National Laboratory, Oak Ridge, Tennessee.

[1] R. G. J. Fraser, *Molecular Rays* (Cambridge University Press, Cambridge, 1931), p. 191.
[2] W. H. Rodebush, Revs. Modern Phys. **3**, 392 (1931).
[3] M. Kröger, Z. physik. Chem. **117**, 387 (1925).
[4] E. C. Williams in discussion of paper by M. Bodenstein, Trans. Am. Electrochem. Soc. **71**, 353 (1937).
[5] R. G. J. Fraser and L. F. Broadway, Proc. Roy. Soc. (London) **A141**, 626 (1933). L. F. Broadway, *ibid.* **A141**, 634 (1933).
[6] M. Polanyi, *Atomic Reactions* (Williams & Norgate, London, 1932).
[7] C. E. H. Bawn, Chem. Soc. Ann. Repts. **39**, 36 (1943).
[8] G. Schay, Z. physik. Chem. **B11**, 291 (1931).
[9] J. L. Magee, J. Chem. Phys. **8**, 687 (1940).

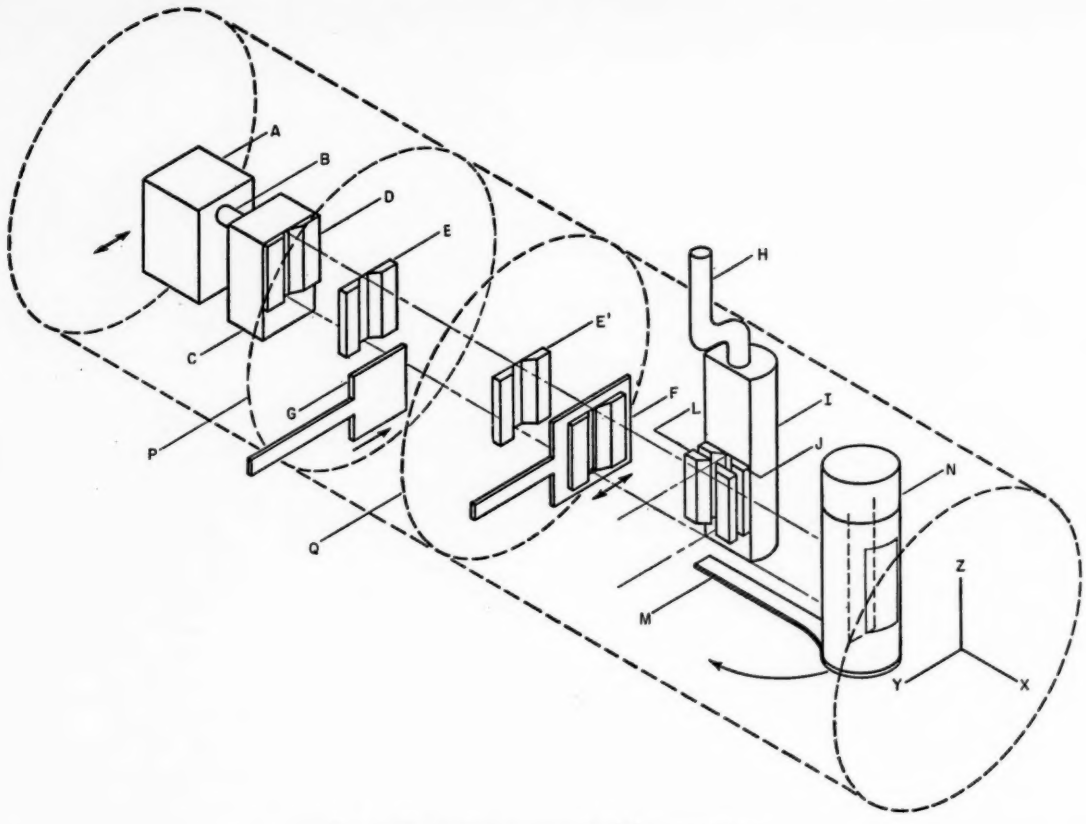

FIG. 1. General arrangement of the apparatus.

collimated by slit F to form a ribbon-shaped beam in the x–z plane. The beam may be interrupted by shutter G.

The purpose of the double oven system is to maintain effusive flow at maximum intensity over the large range of temperatures desired. The requirement for effusive flow, that the mean free path be much greater than the slit width, limits the pressure to a maximum of about 0.1 mm Hg. The vapor in C behaves as a permanent gas, and the intensity of the effusing beam varies only as $T^{-\frac{1}{2}}$ compared with the exponential variation with T if the vapor effused directly from the liquid-containing source.

In the HBr vapor source the gas is frozen in a copper block to produce a vapor pressure of approximately 0.1 mm Hg (125°K). The copper block is in an evacuated glass tube, and is cooled by a small heat leak to a surrounding liquid nitrogen bath. The temperature is controlled by a resistance heater. The gas enters tube H and is brought to the desired temperature in copper oven I (200 to 500°K). It effuses through slits J and L to form a ribbon-shaped beam in the y–z plane.

The path length of the K beam to the scattering center M is 25 cm, while the HBr path length is 1 cm.

The reaction and scattering products are measured by the detector N (described below), which is pivoted at the scattering center M and may be rotated through the first quadrant of the x–y plane. The filaments of the detector are 5.6 cm from the scattering center M.

The entire system, with the exception of the HBr vapor source, is contained in a vacuum envelope consisting of an 8 inch i.d., $\frac{1}{8}$ inch-wall brass tube, 24 inch long, which is divided into three separately-pumped chambers by bulkheads P and Q, containing slits E and E'. The pumps are augmented by liquid nitrogen cooled traps in each chamber.

Detector

The main experimental problem here is to obtain a measurement of the very small amounts of potassium bromide formed in scattering, and to distinguish it from the elastically scattered potassium. Tungsten has been widely used as the filament in the surface ionization gauge for measuring beams of the alkali metals and their halides.[10–13] However, the ionization efficiencies for both potassium and potassium bromide are too nearly equal to permit of their differentiation. In examining the possibility of differential detection by use of a different metal, it was found that while a platinum surface will ionize K quite well it has a very poor efficiency for ionizing KBr. Figures 2 and 3 show the ionization efficiencies for K and for KBr of W and of 92% Pt–8% W,

[10] I. Langmuir and K. H. Kingdon, Proc. Roy. Soc. (London) **A107**, 61 (1925).
[11] J. B. Taylor, Z. Physik **57**, 242 (1929).
[12] W. H. Rodebush and W. F. Henry, Phys. Rev. **39**, 386 (1932).
[13] Hendricks, Phipps, and Copley, J. Chem. Phys. **5**, 868 (1937).

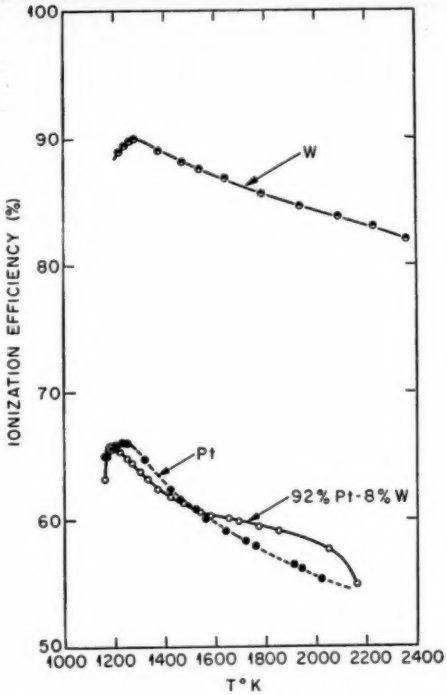

FIG. 2. Ionization efficiencies for K of W, Pt and 92% Pt–8% W.

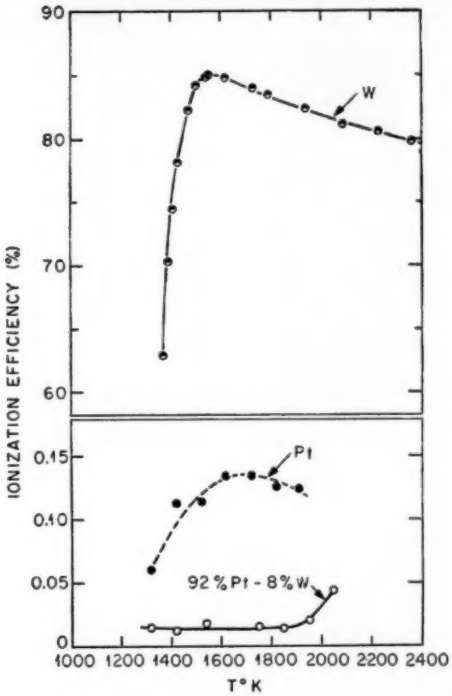

FIG. 3. Ionization efficiencies for KBr of W, Pt and 92% Pt–8% W.

together with those of Pt for comparison. The platinum alloy[14] was used in the actual gauge because of its superior strength. The gauge used in this experiment (Fig. 4) contains a tungsten wire and a Pt alloy wire which may be heated separately. The positive ions are collected at the negative nickel plate, and the current is amplified by a vibrating reed electrometer and recorded on a Brown Electronic potentiometer (10 mv full scale).

Further details of the surface ionization properties of platinum and tungsten for alkali halides will be published separately.

MATERIALS

The K used was from Fischer Scientific Company and from J. T. Baker Chemical Company, each containing about 0.2% Na.

The HBr was anhydrous, 99.1% HBr from Matheson Company, and was further purified by bulb-to-bulb distillations between −80 and −196°C.

PROCEDURE

The system is pumped to a pressure of about 10^{-7} mm Hg, the potassium ovens are heated to operating temperatures and the ovens, collimator, and detector are adjusted to give proper alignment and maximum intensity. The temperatures are controlled to give intensity fluctuations of less than 0.1% over long periods of time.

The intensity profile of the unscattered beam is obtained by a series of measurements at successive angular settings of the gauge. Figure 5 is a typical profile. The intensity I_0 at the peak of the beam corresponds to a flux of about 10^{14} atoms/cm², sec. The area N_0 under this curve is a direct measure of the total number of atoms arriving per second in the beam.

To begin the scattering experiment, HBr is allowed to effuse, forming the cross beam. The scattered peak intensity I is measured and from the attenuation the total number of collisions per second N is obtained, from

$$N=\frac{I_0-I}{I_0}N_0. \tag{1}$$

Next, the ionization efficiency ratio is checked by measuring the peak intensity with each filament. Then the profiles of the scattered beam are obtained by making readings on each filament as a function of angle. The platinum filament readings are multiplied by the ionization efficiency ratio and these numbers subtracted from the tungsten filament readings at the same angle to give the amount of KBr. In Fig. 6 are the results of a typical experiment. The area under the KBr curve is a measure of the number of KBr molecules formed per second, N^*. The flux of KBr at its peak is about 10^{10} molecules/cm², sec.

RESULTS

The general collision theory of chemical reactions provides a satisfactory starting point for the present treatment, particularly since the language is appro-

[14] Alloy No. 479, Sigmund Cohn Corporation, Mount Vernon, New York.

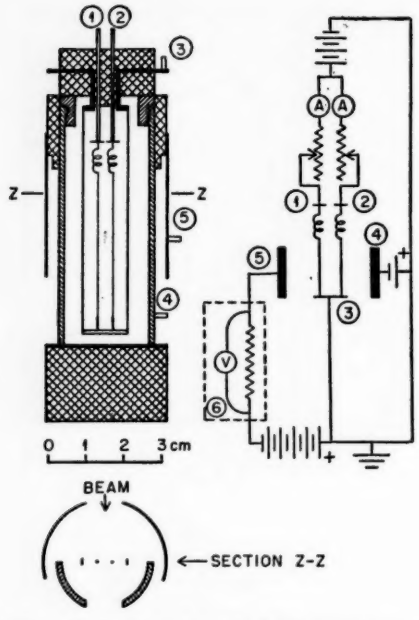

FIG. 4. Two-filament surface ionization gauge and circuit. (1) W filament, 0.002 inch diam. (2) Pt filament, 0.002 inch diam. (3) Common filament lead. (4) Guard ring, Ni. (5) Collector electrode, Ni. (6) Vibrating reed electrometer.

priate to beam experiments. The theory assumes that two potentially reactive molecules will react upon collision if the mutual energy in the collision is above a necessary minimum, E^*, and if any necessary conditions of orientation are fulfilled. With certain simplifications, this gives a form of the Arrhenius equation

$$k=ZPe^{-E^*/RT}, \tag{2}$$

for the specific rate constant k, where Z is the collision rate and P is the probability that necessary orientation conditions are fulfilled in a collision. Both theory and

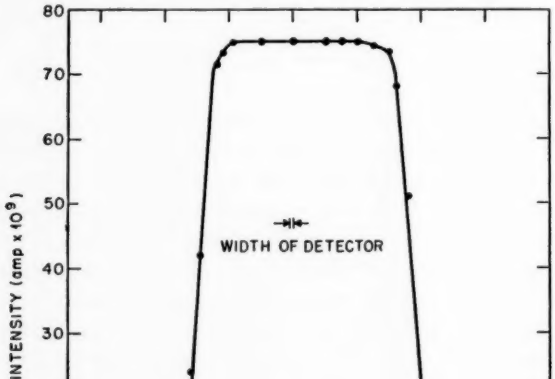

FIG. 5. Typical profile of unscattered beam.

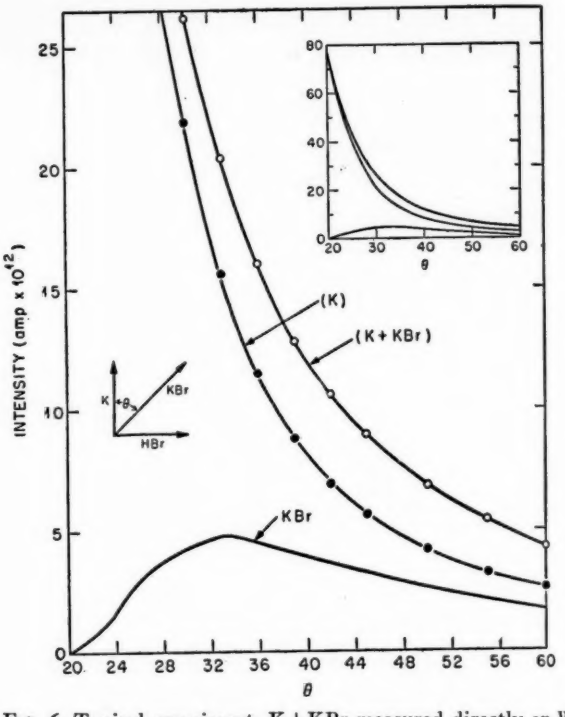

FIG. 6. Typical experiment. K+KBr measured directly on W. K obtained from measurement on Pt and converted to same basis as if on W. KBr by difference.

experiment indicate that the principal effect upon k of temperature is that given by the exponential term.

A more general expression, applicable to the present case, is

$$f=k/Z=C\Phi(T_i,E^*), \tag{3}$$

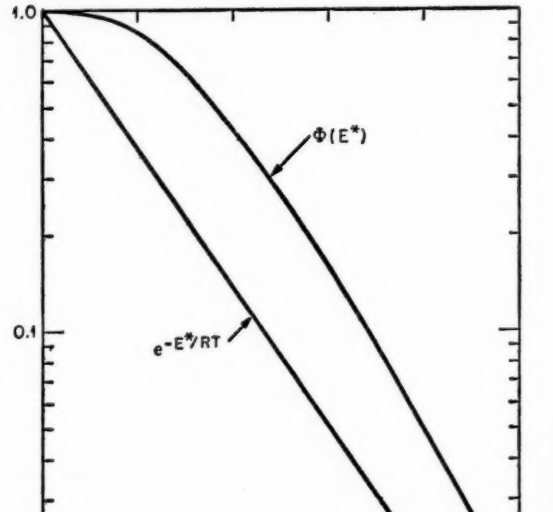

FIG. 7. Comparison of collision energy distribution functions.

where f is the collision yield, C is a term independent of temperature and including orientation factors, and $\Phi(T_i,E^*)$ is the fraction of collisions having sufficient mutual energy. In the ordinary rate experiment this term is the exponential, but in the present case of two beams at different temperatures T_1 and T_2 colliding at right angles it can be shown (Appendix 1) to be

$$\Phi=\frac{\alpha_1^2\alpha_2^2}{(\alpha_1-\alpha_2)^2}\left\{\frac{e^{-\alpha_1V^2}}{\alpha_1}\left[\frac{3\alpha_1-\alpha_2}{\alpha_1(\alpha_1-\alpha_2)}+V^2\right]-\frac{e^{-\alpha_2V^2}}{\alpha_2}\left[\frac{3\alpha_2-\alpha_1}{\alpha_2(\alpha_1-\alpha_2)}-V^2\right]\right\}, \quad (4)$$

where $\alpha_i=M_i/2RT_i$, $V^2=2E^*(M_1+M_2)/M_1M_2$, M_i = molecular weight of reactant i, T_i = temperature of reactant i, R = molar gas constant. For comparison with the collisions in a homogeneous gaseous mixture, values of Φ have been plotted in Fig. 7 for beams of K and HBr at 500°K together with the corresponding distribution in the homogeneous gas. The excess of collisions above any arbitrary energy for the beams case over the other stems from the v^3 term which replaces for a beam the familiar v^2 term of the Maxwell-Boltzmann equation.

TABLE I. Experimental collision yields.

Case	T_K, °K	T_{HBr}, °K	f (collision yield)
A	541	373	1.11×10^{-3}
B	541	460	1.27×10^{-3}
C	700	460	2.55×10^{-3}
D	837	460	3.32×10^{-3}

The Activation Energy

The complexity of Φ precludes a simple graphical or analytical evaluation of the activation energy from the experimental data of collision yield as a function of temperature. The procedure adopted was as follows. First, an empirical collision yield f was calculated for each experiment by dividing the rate of KBr formation N^* by the collision rate N. These are given in Table I. Second, a table of values of Φ was computed for a series of temperatures of each reactant and for a series of values of E^* between 0 and 10 kcal/mole. Figure 8 is a plot of Φ *vs* E^* for the conditions of the four experiments in Table I. Third, all possible pairs of the four experiments were considered in turn, and for the conditions of each pair (i and j) the corresponding ratios Φ_i/Φ_j were taken from the table as a function of E^* and plotted as in Fig. 9. Fourth, the ratios of experimental collision yields f_i/f_j were marked as shown in Fig. 9. The intersection of f_i/f_j with the curve of Φ_i/Φ_j for the same pair of experimental conditions indicates the value of E^* satisfying Eq. (3) for that particular pair. The several values of E_{ij}^* for the several pairs of experiments were weighted for averaging by the slopes of the appropriate Φ_i/Φ_j curves at the points of intersection. It will be noted that in the range of conditions used the collision energy is rather insensitive to the temperature of HBr, as shown by the small slopes of the curves for pairs of experiments differing in that temperature.

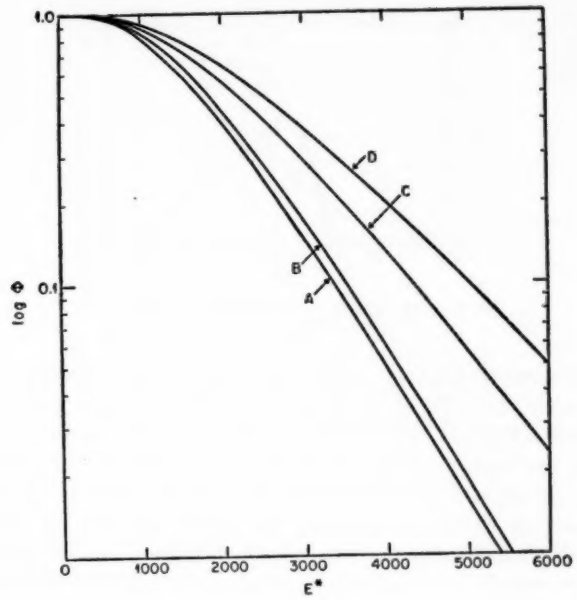

FIG. 8.

The weighted mean of the values for the activation energy is 3.41 kcal/mole with a weighted average deviation from the mean of 0.12 kcal/mole.

The Probability Factor

The remaining factor in Eq. (3) is assumed to be temperature independent, and the present experiments yield an average value of $1.16\times10^{-2}\pm3\%$. This must be corrected for geometrical inefficiency, that is for those

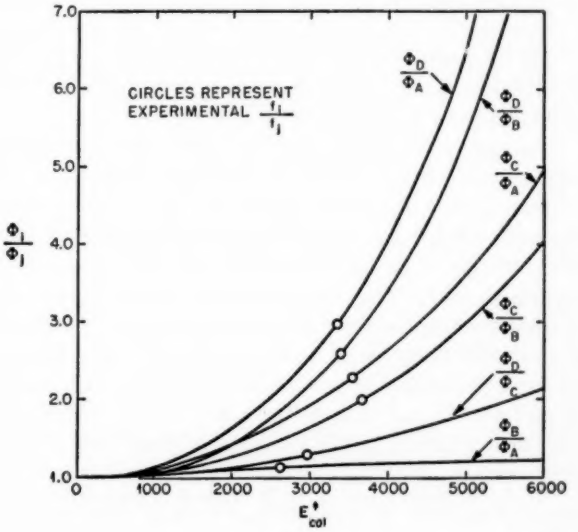

FIG. 9.

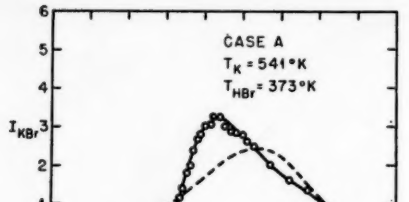

FIG. 10. Angular distribution of KBr.

KBr molecules which pass above or below the ends of the entrance slit of the detector. If the reaction product were KHBr, all of it would lie between the planes defined by the tops and bottoms of the crossed beams (because of conservation of momentum), but the loss of an H atom in the reaction gives the remaining KBr an impulse which may remove it from between those limits. An empirical estimate of 15° for the maximum deviation is suggested by consideration of the angular distribution curves. If the distribution of KBr scattered beyond the limits of the detector is linear with distance above or below the slit, then it is a matter of simple geometry to calculate the efficiency. The detector slit is 1.94 cm high and is 4.53 cm from the scattering center. The beams are each 1.00 cm high. Hence the ratio of KBr subtended by the detector to total KBr is 0.66. The corrected value for the temperature-independent factor then becomes $C=1.75\times10^{-2}$. The true value lies between this and the uncorrected one of 1.16×10^{-2}.

The term C has been defined only as the temperature-independent term in Eq. (3). Its physical significance is the fraction of collisions of adequate energy which lead to reaction, and this suggests a direct equality with the probability factor in the collision theory. However, since the collision cross section measured by the molecular beam method is determined by the limit of the Van der Waals interaction,[15] it is very much larger than that relevant to chemical reaction. Therefore, the constant C should be multiplied by the total cross section Q_T and divided by the gas kinetic value Q_c to give a number comparable to the ordinary probability factor P.

Q_T was determined by measuring the attenuation of a very narrow beam of K by passage through a cell (replacing the cross-beam oven I in Fig. 1) 0.47 cm long containing HBr at measured pressures between 10^{-2} and 10^{-4} mm Hg. The beam entered and left through appropriate slits. The experimental arrangement (including the resolution) and the treatment of the results were similar to those of Rosin and Rabi.[16] The value of Q_T for a potassium temperature of 504°K was found to be 850×10^{-16} cm² with HBr at 401°K, and 890×10^{-16} cm² with HBr at 282°K. Several measurements were made under each set of conditions and the average deviation from the mean was 3% in each case. For the conditions of the reaction experiments, K between 540 and 840°K and HBr between 373 and 460°K, a value of 800×10^{-16} cm² seems reasonable.

For Q_c, a value of 106×10^{-16} cm² is obtained from a K radius of 3.6 A as given by Mais[17] and an HBr radius of 2.2 A from the viscosity data of Harle.[18] Hence, assuming the validity of this estimate of the cross section, P lies between 0.09 and 0.13, the indicated range being determined by the uncertainty as to the geometrical inefficiency of the detector. The correct value is probably nearer the larger one, but a reasonable figure for discussion appears to be 0.1.

DISCUSSION

The values of E^* and of P seem to be reasonable. That for E^* is in qualitative agreement with Schay's results[8] in that E^* is small. Schay did not determine E^* from the temperature coefficient, but from the absolute rate, so that his value is only approximate. E^* can be estimated from the empirical rule[19] that it is less than 5.5% of the dissociation energy plus the zero point energy of the diatomic molecule which, in this case, gives 5.0 kcal/mole.

The value of 0.1 for P is interesting in that it suggests that only a small part of the HBr molecule is sensitive to collisions with K. Since the value depends upon the absolute collision yield which is subject to an uncertain geometrical correction, it is safer to postpone a detailed hypothesis until the angular distribution, which determines the geometrical correction, is understood.

The angular distribution of the KBr is shown in Figs. 10–13. The dotted curves represent the angular distribution $\mathcal{P}(\theta)$ expected if only collisions with energy E greater than 3.4 kcal/mole are fruitful, and if the collision complex KHBr is the product, that is neglecting the impulse given to the KBr by the departing H atom (Appendix 2). There is a striking difference between these curves and the experimental curves, in that in each case the peak of the experimental distribution lies nearer

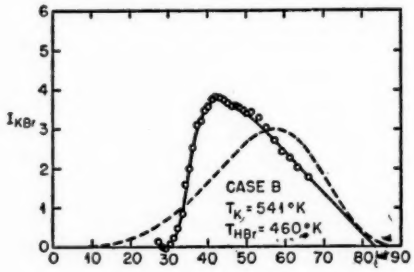

FIG. 11. Angular distribution of KBr.

[15] H. S. W. Massey and E. H. S. Burhop, *Electronic and Ionic Impact Phenomena* (Oxford University Press, London, 1952), p. 396.
[16] S. Rosin and I. I. Rabi, Phys. Rev. **48**, 373 (1935).
[17] W. H. Mais, Phys. Rev. **45**, 773 (1934).
[18] H. Harle, Proc. Roy. Soc. (London) **A100**, 429 (1921).
[19] J. O. Hirschfelder and F. Daniels in Glasstone, Laidler, and Eyring, *Theory of Rate Processes* (McGraw-Hill Book Company, Inc., New York, 1941).

the direction of the K beam than does that of the calculated curve.

The shape of the distribution depends upon several factors not considered in this first approximation. First, the assumption of a single activation energy independent of orientation may be an oversimplification, and a different assumption will alter the calculated shape. Second, the product is not KHBr, and the energy and orientation of the departing H atom will deflect the KBr. The energy of the H atom depends upon the initial kinetic energy of the reactants, upon the value of the heat of reaction, and upon the distribution of the final total energy among the available degrees of freedom. The orientation of the complex upon dissociation will affect the shape of the distribution if the complex dissociates in a time which is short compared with a rotation, as would be expected in this case. If the complex is more easily formed in one configuration than another (i.e. triangular rather than linear) then the geometry of the experimental arrangement will favor a particular orientation of the complex in the laboratory coordinates, and a distortion will be produced in the observed angular distribution. If some more subtle effect is not obscuring the results, then the preference for forward scattering (relative to the K beam) suggests a complex, probably triangular, with the K atom nearer the H end of the HBr molecule.

The present experiments demonstrate the feasibility of studying chemical reactions with molecular beams. The primary requirement, that the reaction products be measurable with adequate sensitivity and reproducibility, is clearly fulfilled, and the possibility of extension to other reactions is obvious.

Some of the potentialities of the method are illustrated by the results already obtained. Thus it is possible to obtain activation energies and steric factors with good precision under conditions where the accuracy is unaffected by uncertainties about wall effects or gas-phase chain reactions. Further, the independent control of the two reactant temperatures allows a wide range of temperatures to be covered without experimental difficulty. Finally, the feasibility of measuring the angular distribution of the products opens up the possibility of direct observation of orientation effects.

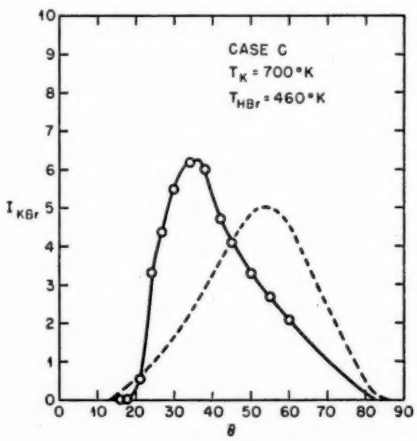

FIG. 12. Angular distribution of KBr.

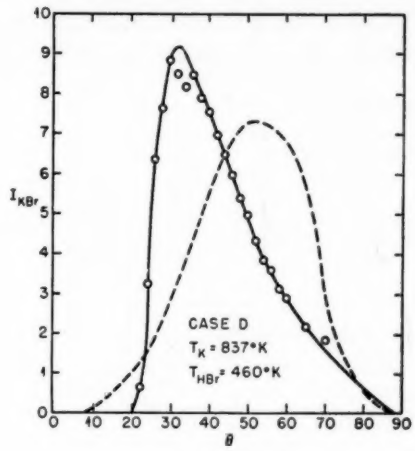

FIG. 13. Angular distribution of KBr.

The authors are grateful to G. T. Trammell for helpful discussions and to E. S. Cantrell, J. K. East, and J. F. Potts for their assistance.

APPENDIX 1. DISTRIBUTION OF COLLISION ENERGIES IN CROSSED BEAMS

The relative energy for two particles whose trajectories are at right angles is

$$E_r = M_1 M_2 v_r^2/2(M_1+M_2),$$

where

$$v_r^2 = v_1^2 + v_2^2.$$

The distribution of velocities in an effusive beam of particles is characterized by

$$\mathcal{P}(v) = (2M/RT)^2 v^3 e^{-Mv^2/2RT} dv \equiv A v^3 e^{-\alpha v^2} dv.$$

Then the distribution of collision energies $\mathcal{P}(v_r)$ is obtained from

$$\mathcal{P}(v_r) = \int \mathcal{P}_1(v_1)\mathcal{P}_2([v_r^2 - v_1^2]^{\frac{1}{2}}) \frac{v_r}{(v_r^2 - v_1^2)^{\frac{1}{2}}} dv_1 dv_2$$

$$= A_1 A_2 v_r e^{-\alpha_2 v_r^2} dv_r \int_0^{v_r} (v_r^2 - v_1^2) v_1^3 e^{-(\alpha_1 - \alpha_2)v_1^2} dv_1.$$

The fraction of collisions with energy greater than E^*, given in Eq. (4) is obtained by integrating $\mathcal{P}(v_r)dv_r$ from V to ∞.

APPENDIX 2. ANGULAR DISTRIBUTION OF CENTER OF MASS VECTORS

In the collision of two particles, the angle θ which the center of mass makes with the trajectory of particle 2 in the laboratory system is given by $\tan\theta = p_1/p_2$. Integra-

tion of the joint distribution $\mathcal{P}_2(p_2)\mathcal{P}_1(p_2\tan\theta)dp_1dp_2$ gives the density of center of mass vectors at each angle

$$\mathcal{P}(\theta)=\frac{16\tan^3\theta\sec^2\theta}{(R^2M_1M_2T_1T_2)^2}d\theta \times\int_0^\infty p_2{}^7\exp\left[-\frac{p_2{}^2}{2RM_1T_1}\left(\frac{M_1T_1}{M_2T_2}+\tan^2\theta\right)\right]dp_2 \equiv B\int_0^\infty p_2{}^7e^{-ap_2{}^2}dp_2.$$

However if only those collisions with relative energy E^* or greater are counted the lower integration limit is changed to P where

$$P=[2E^*M_1M_2(M_1+M_2)/(M_1{}^2+M_2{}^2\tan^2\theta)]^{\frac{1}{2}},$$

from which the distribution is obtained

$$\mathcal{P}(\theta)=\tan^3\theta\sec^2\theta \times[6a^{-4}-e^{-aP^2}(6a^{-4}+6P^2a^{-3}+3P^4a^{-2}+P^6a^{-1})]d\theta.$$

Normalization of this function would be difficult and is not necessary for the present use.

THE JOURNAL OF CHEMICAL PHYSICS VOLUME 23, NUMBER 9 SEPTEMBER, 1955

Vibration-Rotation Band ν_2 of Heavy Water Vapor*

FRED P. DICKEY AND JAMES M. HOFFMAN
Department of Physics, The Ohio State University, Columbus 10, Ohio
(Received December 20, 1954)

The vibration-rotation band ν_2 in the heavy water vapor (D_2O) spectrum has been remeasured. An analysis of the rotational structure has been carried out. From the interpretation of the data the band center, as well as the value of the reciprocals of inertia have been determined. The band center is found to be 1178.45 cm^{-1} and the reciprocals of inertia are $A(V)=16.650$ cm^{-1}, $B(V)=7.345$ cm^{-1}, and $C(V)=4.795$ cm^{-1}.

I. INTRODUCTION

THE far infrared spectrum of heavy water vapor (D_2O) corresponding to transitions between the rotational energy levels only, has been measured by Fuson, Randall, and Dennison[1] and term values have been assigned. The fundamental vibration-rotation band ν_2 has been measured by Barker and Sleator.[2] More recently the band was remeasured and analyzed by Dickey and Nielsen.[3] The molecular constants given in their work have since been modified in papers by Innes, Cross, and Giguere[4] and Benedict, Gailar, and Plyler.[5] It has been found that the high frequency side of the band as previously measured contained numerous H_2O lines. The band has been remeasured using a vacuum spectrometer and considerably higher resolution.

II. EXPERIMENTAL

The fundamental vibration-rotation band ν_2 of D_2O was measured with a prism-grating, automatic recording, vacuum spectrometer. A Perkin-Elmer thermocouple and model 81, thirteen cps amplifier was used to detect the radiation. The grating used was a 6 by 8 in. echelette grating ruled with 4500 lines per in. The grating was ruled by the Bausch and Lomb Optical Company. The sample of D_2O was obtained from the Stuart Oxygen Company and contained at least 99.5% D_2O. The sample was introduced into a cell whose length was approximately 50 cm. The cell windows were of silver chloride.

The band was observed in the region from 1037 cm^{-1} to 1375 cm^{-1}. The effective slit width of the spectrometer varied from 0.13 cm^{-1} to 0.20 cm^{-1}. The wider effective slit width had to be used in the spectral region above 1278 cm^{-1}. The measurements were made with the instrument evacuated so that the water lines appearing on the high frequency side of the band would not be recorded. However, there are still additional lines in the high frequency region caused by the strong fundamental band ν_2 of HDO. These lines could not be eliminated. The frequencies of the lines were determined by superposing higher orders of the 5460.740 A line of mercury on the D_2O spectrum.

A run was made at fast speed and with slightly greater effective slit width (0.25 cm^{-1} to 0.33 cm^{-1}) to show the over-all appearance of the band. This result is shown in Fig. 1. In order to compare this with the spectrum measured, a small portion of the spectrum at higher resolution is shown in Fig. 2. Frequencies in

* This investigation was supported in part through a contract between the Office of Ordnance Research, United States Army, and The Ohio State University Research Foundation.
[1] Fuson, Randall, and Dennison, Phys. Rev. **56**, 982 (1939).
[2] E. F. Barker and W. W. Sleator, J. Chem. Phys. **3**, 660 (1935).
[3] F. P. Dickey and H. H. Nielsen, Phys. Rev. **73**, 1164 (1948).
[4] Innes, Cross, and Giguere, J. Chem. Phys. **19**, 1086 (1951).
[5] Benedict, Gailar, and Plyler, J. Chem. Phys. **21**, 1301 (1953).

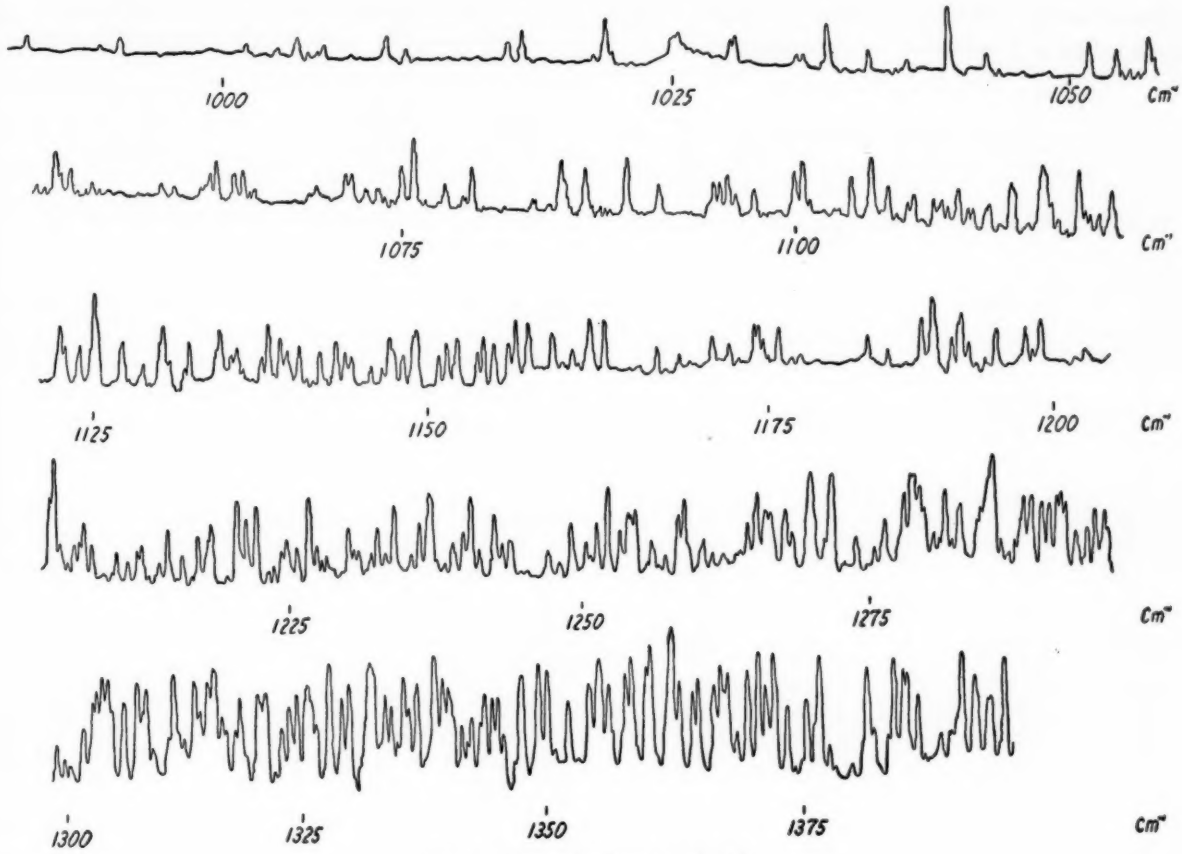

FIG. 1. Absorption band ν_2 of D_2O.

wave numbers, corrected to vacuum, for the measured lines were tabulated.†

III. ANALYSIS OF THE DATA

The identification of the lines measured in the band was made by following the method used by Nielsen[6,7] except that the effect of centrifugal stretching was taken into account using the method of Benedict[8] in his analysis of XY_2 molecules, i.e. by using effective rotational constants A_J', B_J', and C_J' for each value of the quantum number J. These effective rotational constants were obtained using the following method. By trial and error some lines were tentatively identified as caused by transitions involving low values of J. Term values were then determined for these J's using the known term values of the ground state. The effective reciprocals of inertia were determined using the Mecke[9] sum rules for the asymmetric top. These were plotted against $J(J+1)$ which gives essentially a straight line from which one is able to estimate the effective reciprocals of inertia for the next higher J. These estimated A_J''s, B_J''s, and C_J''s were then substituted into the energy formula due to Wang;[10]

$$F(J_\tau)=\tfrac{1}{2}(B+C)J(J+1)+[A-\tfrac{1}{2}(B+C)]W_\tau,$$

to give the tentative energy levels.

As a further aid in identifying the lines of the spectrum, the relative intensities of the lines have been calculated by using the line strengths given by Cross, Hainer, and King.[11] That is,

$$\sum_{XYZ}\sum_{M''}\sum_{M'}|(\phi_{F_g}{}^A)J'',\tau'',M''; J',\tau',M'|^2,$$

where $\phi_{F_g}{}^A$ represents the direction cosine elements of the asymmetric rotator, and XYZ are the space fixed

FIG. 2. Section of band ν_2 with high resolution.

†For detailed paper, extended version, or supplementary material, order Document 4681 from American Documentation Institute, 1719 N Street N.W., Washington 6, D. C., remitting $1.75 for microfilm (images one inch high on standard 35-mm motion picture film readable in microfilm reader or under low-power microscope) or $2.50 for photocopies (6×8 in. readable without optical aid).

[6] H. H. Nielsen, Phys. Rev. **59**, 565 (1941).
[7] H. H. Nielsen, Phys. Rev. **62**, 422 (1942).
[8] W. S. Benedict, Phys. Rev. **75**, 1317 (1949).
[9] R. Mecke, Z. Physik **81**, 313 (1933).
[10] S. C. Wang, Phys. Rev. **34**, 243 (1929).
[11] Cross, Hainer, and King, J. Chem. Phys. **12**, 210 (1944).

Cartesian coordinates. Their values are tabulated for various values of a parameter of asymmetry. That is,

$$K=(2B-A-C)/(A-C).$$

The values used were those tabulated for $K=-0.5$, since the value of K for the state ν_2 is -0.57. The term values used for the ground state were those obtained in a private communication with Benedict.[12]

TABLE I. Vibration-rotation term values for the state ν_2.

J_τ	ν_2, cm^{-1}	J_τ	ν_2, cm^{-1}
0_0	1178.45	6_{-6}	1410.66
1_{-1}	1190.57	6_{-5}	1411.56
1_0	1199.89	6_{-4}	1460.78
1_1	1202.48	6_{-3}	1471.56
2_{-2}	1214.35	6_{-2}	1493.06
2_{-1}	1221.53	6_{-1}	1526.99
2_0	1229.16	6_0	1531.04
2_1	1256.89	6_1	1592.45
2_2	1257.40	6_2	1593.16
3_{-3}	1249.02	6_3	1691.80
3_{-2}	1253.77	6_4	1691.80
3_{-1}	1268.99	6_5	1808.09
3_0	1293.32	6_6	1808.09
3_1	1295.48	7_{-7}	1483.52
3_2	1345.66	7_{-6}	1483.85
3_3	1345.71	7_{-5}	1544.96
4_{-4}	1293.34	7_{-4}	1552.80
4_{-3}	1296.39	7_{-3}	1585.20
4_{-2}	1321.38	7_{-2}	1613.44
4_{-1}	1341.37	7_{-1}	1622.47
4_0	1347.37	7_0	1684.14
4_1	1394.30	7_1	1685.56
4_2	1394.88	7_2	1773.47
4_3	1466.28	8_{-8}	1565.65
4_4	1466.28	8_{-7}	1565.90
5_{-5}	1347.38	8_{-6}	1636.78
5_{-4}	1349.10	8_{-5}	1639.86
5_{-3}	1385.64	8_{-4}	1685.80
5_{-2}	1400.86	9_{-9}	1657.30
5_{-1}	1413.21	9_{-8}	1657.35
5_0	1456.58	10_{-10}	1758.44
5_1	1457.91	10_{-9}	1758.44
5_2	1527.88	11_{-11}	1868.93
5_3	1527.89	11_{-10}	1868.93
5_4	1619.44	12_{-12}	1988.97
5_5	1619.44	12_{-11}	1988.97

TABLE II. Values of $A(V)$, $B(V)$, $C(V)$, and Δ.

	ν_2	ν_2*
$A(V)$	16.650 cm^{-1}	16.58 cm^{-1}
$B(V)$	7.345 cm^{-1}	7.32 cm^{-1}
$C(V)$	4.795 cm^{-1}	4.81 cm^{-1}
Δ_{obs}	0.345×10^{-40} g cm^2	0.307×10^{-40} g cm^2
Δ_{calc}	0.329×10^{-40} g cm^2	0.329×10^{-40} g cm^2

* See reference 5.

After the above method of analysis was completed, the term values were checked using the energy formula due to Ray[13] as corrected by King, Hainer, and Cross;[14]

$$F(J_\tau)=\tfrac{1}{2}(A+C)J(J+1)+\tfrac{1}{2}(A-C)E_\tau^J(K)$$

where K is the asymmetry parameter and $E_\tau^J(K)$ are the eigenvalues of the energy matrix $|E(K)|$. The eigenvalues of the energy matrix were obtained from the Asymmetric Rotor Eigenvalue Table by Turner, Hicks, and Reitwiesner.[15]

Term values determined for the band ν_2 of D_2O are tabulated through $J=6$ in Table I. Some of the levels for higher J's are also given. The identification of the lines have been tabulated together with the observed intensities.†

The values obtained for the reciprocals of inertia are given in Table II. The values are compared with those given by Benedict, Gailar, and Plyler.[5] The value of $\Delta=I_C-I_A-I_B$ is also given in Table II and compared with the calculated value.

[12] W. S. Benedict, Private communication.
[13] B. S. Ray, Z. Physik **78**, 74 (1932).
[14] King, Hainer, and Cross, J. Chem. Phys. **11**, 27 (1943).
[15] Turner, Hicks, and Reitwiesner, Ballistic Research Laboratories Report No. 878.

Letters to the Editor

THIS section will accept reports of new work, provided these are terse and contain few figures, and especially few half-tone cuts. The Editorial Board will not hold itself responsible for opinions expressed by the correspondents. Contributions to this section should not exceed 600 words in length and must reach the office of the Editor not later than the 15th of the second month preceding that of the issue in which the Letter is to appear. No proof will be sent to the authors. The publication charge for Letters is $25 per page, with a minimum of $25 per Letter. If honored, the Institution will be entitled to 100 reprints without covers.

Paramagnetic Resonance of NaCl Crystals Containing Additions of Manganese Impurity

KEICHI OSHIMA, HIDETARO ABE, HIROSHI NAGANO, AND MAHOKO NAGUSA
Institute of Science and Technology, University of Tokyo, Tokyo, Japan
(Received June 8, 1955)

AS part of a study of alkali halide phosphors, paramagnetic resonance line widths of manganese impurities added to the sodium chloride crystal have been measured to determine their state in the crystal and the effects of heat treatment on it.

The samples were prepared by melting and from aqueous solution. The results of the resonance absorption measurements are shown in Figs. 1 and 2 and Table I. All measurements were carried out at room temperature with superheterodyne method at a wavelength of 3 cm. The shape of the curves was Lorentzian and no significant dependence on the concentration of manganese impurity and the orientation of the sample was observed. The samples prepared by melting gave two kinds of resonance curve (1) and (2), depending on their cooling rate. The curve of the crystal from solution resembled that of the quenched sample from melt. The samples gave rise to an orange fluorescence by 2537 A excitation and the quenched samples were brighter than the slowly cooled.

To investigate the effects of heat treatment, the samples from melt were treated in a furnace. No change in the resonance curve was observed by heating the samples below 300°C. On heating over 500°C, a resonance curve of the same dependence on the cooling rate as described in Table I was obtained.

In the middle range of temperature, the curve changed from one type to another with the time of heat treatment. Namely, the sample slowly cooled from melt was heated and maintained at a constant temperature in this range and then cooled rapidly

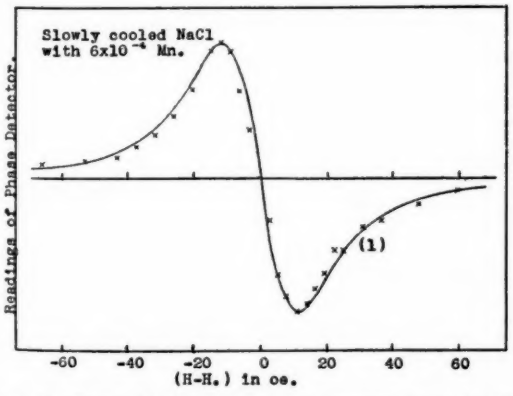

FIG. 1. Derivative of the paramagnetic resonance curve by Mn impurities in a "slowly cooled" NaCl. The full line is a calculated Lorentzian curve having a width of 40 oe.

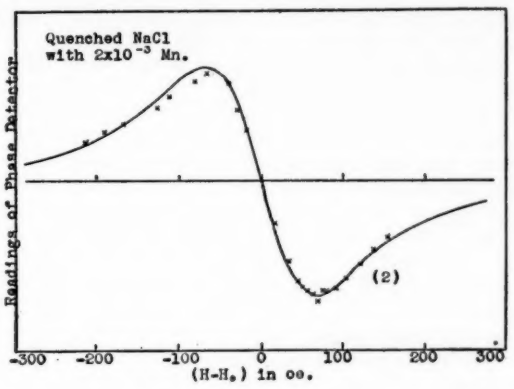

FIG. 2. Derivative of the paramagnetic resonance curve by Mn impurities in a "quenched" NaCl. The full line is a calculated Lorentzian curve having a width of 240 oe.

to room temperature for measurement. By changing the period of this treatment, the curve of the slowly cooled sample (1) first reduced the heights of the peaks, then changed to a superposition of the two curves (1) and (2) as shown in Fig. 3, and, finally, became completely like that of the quenched sample (2).

Assuming that the time t for the curve (1) to become curve (2) is given by $t=t_0\exp(Q/kT)$, 27 kcal/mole was obtained for the

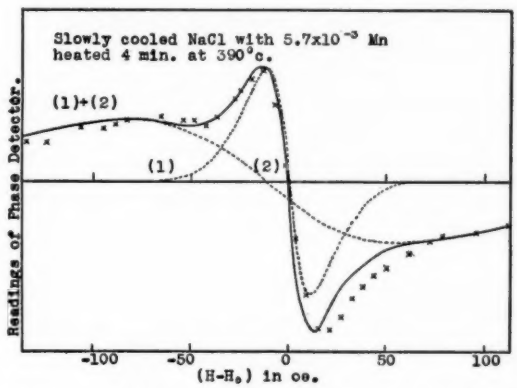

FIG. 3. Derivative of the paramagnetic resonance curve by Mn impurities in "slowly cooled" NaCl treated at 390°C. The full line (1)+(2) indicates the superposition of the derivative curves of nontreated slowly cooled and quenched samples (1) and (2).

activation energy Q from the measurements of the sample treated at 405° and 390°C. The measurement of the specific heat of a slowly cooled sample with 10^{-2} mole manganese gave a broad endothermic peak at 360° to 420°C, corresponding to observations in the resonance curve.

These results indicate that there are two different states of

TABLE I. Paramagnetic resonance absorption of Mn^{++} in NaCl.

Sample	(1) Slowly cooled[a]	(2) Quenched	(3) From aqueous solution[b]
Peak	Single peak	Single peak	Single peak
Line shape	Lorentzian	Lorentzian	Lorentzian
g	2.004 ± 0.002	2.015 ± 0.004	2.018 ± 0.005
Half-width oe	39 ± 5	222 ± 15	220 ± 25
Mn^{++} concentration Mn mole/NaCl mole	$5\times10^{-3}\sim4\times10^{-6}$	$1\times10^{-3}\sim9\times10^{-4}$	4×10^{-4}

[a] 7 hr from 750°C to room temperature.
[b] Paramagnetic resonance of manganese ions in a NaCl crystal was observed first by I. Hayashi with this type of sample.

manganese impurities in NaCl crystal, one stable at temperature above 500°C and the other stable below it. The former occurs in the quenched sample and the latter in the slowly cooled. For luminescence, the former state is much more efficient as a center.

Since both of the resonance curves do not depend upon the concentration of manganese, we may conclude that these states are some local aggregates or clusters of manganese ions and not atomic dispersions. Moreover, from the g-value and the width of the curves, it seems reasonable to suppose that the aggregates for the state in the slowly cooled sample are less dispersed.

The exact nature of these states, however, is not yet possible for us to determine. For example, the half-width of anhydrous manganese chloride is 1250 oe.[1] If the manganese ions are replacing the sodium ions to be arrayed in a (111) plane as a layer with an exchange coupling comparable to that of the anhydrous manganese chloride, the calculated value of the half-width by extreme narrowing[2] is 360 oe. This is larger than that for our quenched sample and much more for the slowly cooled.

The authors are much indebted to Professor S. Makishima and Professor H. Kumagai for many helpful discussions and encouragement in the course of this work.

[1] Kumagai, Ôno and Hayashi, Phys. Rev. **85**, 925 (1952).
[2] P. W. Anderson and P. R. Weiss, Revs. Modern Phys. **25**, 269 (1953).

Mechanism of the Pyrolysis of Ethyl Bromide. A Note on a Paper by Friedman, Bernstein, and Gunning*

ALLAN MACCOLL AND P. J. THOMAS
William Ramsay and Ralph Forster Laboratories, University College, Gower St., London, W.C. 1, England
(Received May 24, 1955)

THREE mechanisms[1] have been discussed in connection with the homogeneous elimination of HBr from ethyl bromide. The first is the direct unimolecular elimination

$$C_2H_5Br \rightarrow C_2H_4+HBr \qquad (1)$$

for which Blades and Murphy,[2] using a flow technique, and Thomas,[3] using a static method have given the rate expressions

$$\log k = 12.86 - 52\,300/2.303RT \qquad (A)$$
$$\log k = 13.42 - 53\,900/2.303RT \qquad (B)$$

respectively. The second is a radical nonchain process

$$C_2H_5Br \rightarrow C_2H_5+Br \qquad (2)$$
$$Br+C_2H_5Br \rightarrow C_2H_4Br+HBr \qquad (3)$$
$$C_2H_5+C_2H_4Br \rightarrow C_2H_4+C_2H_5Br \qquad (4)$$

which may be excluded by the fact that the activation energy would be equal to the C−Br bond energy (∼67 kcal).[4] The third is a radical chain mechanism, involving steps (2) and (3) and

$$C_2H_4Br \rightarrow C_2H_4+Br \qquad (5)$$
$$Br+C_2H_4Br \rightarrow \text{end of chain} \qquad (6)$$

for which the activation energy would be less than the C−Br bond energy.

From their investigation of carbon isotope effects in the pyrolysis of ethyl bromide, Friedman, Bernstein, and Gunning[1] have concluded that the mechanism of elimination of HBr is unimolecular. These authors did not consider the possibility of the decomposition proceeding by a mixed unimolecular and radical chain mechanism, with the latter predominating. It has been shown by Daniels and Veltman that the rate constant of the uninhibited reaction in seasoned vessels is

$$\log k = 14.06 - 53\,200/2.303RT. \qquad (C)$$

This rate is about ten times that given by (A) and (B) and further, the uninhibited reaction differs in two important respects from the inhibited reaction, namely the presence of induction periods and a decrease in rate constant at low pressures. It is most likely that the reaction studied by Daniels and Veltman is predominantly a radical chain reaction. Friedman *et al.* state that their rates were consistently higher than those of Daniels and Veltman, a fact which they attribute to traces of oxygen. There is no reasonable mechanism that can be adduced for oxygen catalysis of the unimolecular mechanism, so it may be concluded that the results of Friedman *et al.* refer neither to the unimolecular nor radical nonchain mechanisms, but to a radical chain mechanism in which oxygen plays a part.

The rate ratio for the radical chain reaction in the case of the pure substituted (k^*) and unsubstituted species (k) is

$$\frac{k}{k^*}=\left(\frac{k_2k_3k_5k_6^*}{k_2^*k_3^*k_5^*k_6}\right)^{\frac{1}{2}}.$$

This expression will not be true for a mixture of substituted and unsubstituted ethyl bromide, since a bromine atom from $C_2^*H_5Br$ will be equally effective in initiating chains in $CH_3C^*H_2Br$, $C^*H_3CH_2Br$ and C_2H_5Br. It can be shown that for the radical chain reaction, Eq. (1) of Friedman *et al.* would become

$$\frac{dx_1}{dx_2}=\frac{k_3a_0}{k_3^*a_0^*+k_3\dagger a_0\dagger}$$

where $a_0=[C_2H_5Br]$, $a_0^*=[CH_3C^*H_2Br]$ and $a_0\dagger=[C^*H_3CH_2Br]$, while k_3, k_3^*, and $k_3\dagger$ are the rate constants for bromine atom attack on the above three isotopic species. If it is now assumed that $k_3\dagger=k_3^*$, which seems reasonable, then from the experimental results at 400°C,

$$(k_3/k_3^*)_{obs}=1.0159$$

on the assumption that the presence of oxygen only affects chain initiation.

* Friedman, Bernstein, and Gunning, J. Chem. Phys. **23**, 109 (1955).
[1] F. Daniels and P. Veltman, J. Chem. Phys. **7**, 756 (1939).
[2] Blades and Murphy, J. Am. Chem. Soc. **74**, 6219 (1952).
[3] Green, Harden, Maccoll, and Thomas, J. Chem. Phys. **21**, 178 (1953).
[4] Lane, Linnett, and Oswin, Proc. Roy. Soc. (London) **216A**, 361 (1953).

Comments on the C^{13} Isotope Effect in the Thermodecomposition of Ethyl Bromide

HENRY L. FRIEDMAN, RICHARD B. BERNSTEIN,* AND HARRY E. GUNNING
Department of Chemistry, Illinois Institute of Technology, Chicago, Illinois
(Received June 27, 1955)

RECENTLY we reported[1] data on the C^{13} isotope effect in the thermodecomposition of ethyl bromide which were thought to support the unimolecular elimination mechanism. Maccoll and Thomas[2] indicate that a radical chain mechanism may be used to explain the results. Preliminary experiments on the photolysis of ethyl bromide in the presence of excess cyclopentane inhibitor gave enrichments in C^{12} similar to those found in the thermodecomposition, and this is probably due to a reaction similar to step (2) of reference 2. Thus the unimolecular model is apparently incorrect.

It is of interest to examine the radical chain mechanism from the viewpoint of the isotope effects. Using the symbols of reference 2, we attempt to evaluate k/k^* and $k/k\dagger$. Step (2) represents C_2H_5-Br dissociation, and one expects k_2 and $k_2\dagger$ to be very similar and both larger than k_2^*. Step (3) is quite complex and the k's probably depend on whether the H abstraction takes place on the α or β carbon and whether C^{12} or C^{13} are involved. To a first approximation all the k_3's may be considered equal. Also, as an approximation, $k_2/k_2^*=k_5/k_5^*$. The termination step (6) may be presumed to occur primarily at the wall; here traces of oxygen could act catalytically by reducing the efficiency of chain-breaking. It is difficult to picture an isotope effect associated with this step. This reasoning leads to the conclusion that k/k^* is approximately equal to k_2/k_2^*, and that $k/k\dagger$ is very close to unity. Since the radical nonchain mechanism leads to the same conclusion,

this work does not seem to differentiate between the two radical mechanisms. Perhaps the use of C^{14} in each of the ethyl bromide positions would show the difference.

Since it was not very clearly stated in the first paper,[1] it should be here noted that S was calculated from the isotopic analyses using the following: [p. 111 after Eq. (6)]

$$\alpha=(C^{13}O_2)/(C^{12}O_2) \text{ from } C_2H_4$$

and

$$a^0=(C^{13}O_2)/(C^{12}O_2) \text{ from } C_2H_5Br.$$

Since each molecule of labeled C_2H_4 and C_2H_5Br yields one molecule each of $C^{12}O_2$ and $C^{13}O_2$,

$$\frac{x_1}{x_2}=\frac{1-\alpha}{2\alpha} \quad \text{and} \quad \frac{a_2^0+a_3^0}{a_1^0}=\frac{2\alpha^0}{1-\alpha^0}.$$

From the definition,

$$S=\frac{\alpha^0(1-\alpha)}{\alpha(1-\alpha^0)}.$$

The structure of the transition state shown on p. 109 is incorrectly drawn. It should be:

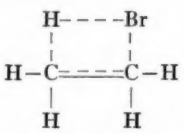

The results of the sample calculation on p. 111 should read:

$$S=1.0068\pm0.0006; \quad \epsilon_0=0.0070\pm0.006$$

$$\frac{2k_1}{k_2+k_3}=1.0070\pm0.0006.$$

The errors range from 0.0004 to 0.0006, so the deviations in the S and S_0 headings in Table I should read $\pm5\times10^{-4}$ and the small subscripts 5's should be deleted.

* Present address: Chemistry Department, University of Michigan, Ann Arbor, Michigan.

[1] Friedman, Bernstein, and Gunning, J. Chem. Phys. **23**, 109 (1955).
[2] A. Maccoll and P. J. Thomas, J. Chem. Phys. **23**, 1722 (1955).

Thermochromism and Photochromism

YEHUDA HIRSHBERG AND ERNST FISCHER
The Daniel Sieff Research Institute, The Weizmann Institute of Science, Rehovoth, Israel
(Received December 23, 1954)

THE phenomenon of reversible formation of colored modifications of compounds related to dianthrone by ultraviolet irradiation at low temperatures was first reported by Y. Hirshberg in 1950[1] and named photochromism.

In subsequent publications from this laboratory details about this phenomenon and its relation to thermochromism were reported both in the dianthrone series[2] and in the spiran series.[3,4]

It was concluded from these investigations that the dyes which were reversibly formed both in thermochromism and in photochromism were identical.

In a recent publication[5] Kortum, Theilacker, and Braun, ignoring the facts mentioned in the beginning of this letter, challenged our above conclusion on the basis that the ultraviolet absorption spectrum of the thermochromic dye B is similar to that of the colorless modification A, whereas the absorption of the photochromic dye C differs from that of A.

These authors thus seem to have disregarded the basic fact elaborated in our above publications that in thermochromism, as distinct from photochromism, only a small and difficultly assessable fraction (generally between 0.1 and 5%) of A is thermally converted into the dye modification. The observed absorption spectrum, therefore, results from the superposition of the spectra of the dye B and a large excess of A, in equilibrium with B. Under such conditions it is practically impossible to estimate with any degree of accuracy the absorption of B in the ultraviolet region, in which A also absorbs. The spectra of B and C can therefore be compared only within the visible region where the excess of A, which accompanies B, does not interfere. Our results clearly show that in this region B and C are indeed identical, apart from changes resulting from the difference in temperatures of measurements (above 100° in thermochromism and below −100° in photochromism).

We wish to point out that Kortum, Theilacker, and Braun's claim in their paper[5] that form C presents absorption bands in the visible region which are not present in form B is based on consideration of a compound which is photochromic and *nonthermochromic*, so that comparison of the spectra of the two forms is obviously impossible. The presumed extra "photochromic" bands appearing in Fig. 3 of the above paper are already recognizable in the curve (same figure) given for irradiation (time not reported) at 20°C, at which temperature form C does not exist. Accentuation of these bands on irradiation (50 minutes) at −115°C may well be due to some photochemical decomposition; no similar bands appear in the case of 1,2,7′,8′-dibenzbianthrone (Fig. 5) (also photochromic only), presumably on account of its greater photochemical stability.

The existence of bianthrone derivatives, which are photochromic and nonthermochromic, may be explained by the following.

Thermochromism represents a thermal equilibrium, the position of which depends on the energy difference between the two modifications A and B. It is, therefore, plausible that for derivatives of dianthrone, which show only photochromism and not thermochromism, this energy difference is so large that no observable shift of the equilibrium towards the colored species occurs within the accessible temperature range.

Note added by Y. Hirshberg:—I infer from Kortum and Theilacker's reply below that they must have been mislead by inadequate knowledge of the French language. In fact, the paper[1] referred to in their reply, and from which a passage is quoted, deals with thermochromism and has nothing to do with photochromism. As to the subsequent arguments of these authors, these are untenable in view of our above Letter to the Editor.

[1] Y. Hirshberg, Compt. rend. **231**, 903 (1950).
[2] Y. Hirshberg and E. Fischer, J. Chem. Soc. 629 (1953).
[3] Y. Hirshberg and E. Fischer, J. Chem. Soc. 4522 (1952); 2184 (1953); 297, 3129 (1954).
[4] Y. Hirshberg and E. Fischer, J. Chem. Phys. **21**, 1619 (1953).
[5] Kortum, Theilacker, and Braun, Z. physik. Chem. N.F. **2**, 179 (1954)

Thermochromism and Photochromism

G. KORTÜM, W. THEILACKER, AND V. BRAUN
Physikalisch-Chemisches Institut der Universität Tübingen, Institut für Organische Chemie der Technischen, Hochschule, Hannover, Germany
(Received January 17, 1955)

THE discovery of the "photochromism" of dehydrodianthrone —as opposed to the "thermochromism" of the same compound—by Bergmann and co-workers[1] has already been quoted by us in a previous paper.[2] Unfortunately a reference to the earlier contribution by Hirshberg[3] was not given in that publication[1] so that we missed it. We are grateful for this having been called to our attention.

The identity of the thermochromic form B and of the photochromic form C of the dehydrodianthrone has been considered as very improbable by Hirshberg himself in the above quoted paper[1] "Il parait probable que la thermochromie à haute et à basse température n'est pas due au même type d'excitation électronique," and reasons for this opinion are discussed. Our measurements also argue against the identity of forms B and C. The possibility of detecting a small contribution of the thermochromic form B in the presence of an excess of the form A of the compound and also in the uv where the absorptions are overlapping, depends firstly on the differences in position and in-

tensity of the bands, secondly on the method in use and the accuracy obtained. We believe that an amount of 4–5% *B* in *A* would not have escaped observation in uv with the method used by us, if, as Hirshberg and Fischer are supposing, the thermochromic form *B* and the photochromic form *C* were identical.

The observation, however, that the absorptions of *B* and *C* are markedly different also in the visible region where *A* does not interfere is especially incompatible with this interpretation. In fact only one band is observed with form *B* but several bands with form *C*. Because of the irreversible changes of dehydrodianthrone by irradiation even at low temperature this difference can only be observed directly with the 1 and 8′ methyl-substituted dehydrodianthrone (Fig. 3 of our paper).[4] These additional bands of the form *C* in the visible region are by no means caused by photochemical decomposition as supposed by Hirshberg and Fischer. The spectrum at 20°C after irradiation, shown in Fig. 3 of our paper, has been obtained in the same solution which previously has been irradiated at −115°C for 50 minutes, then heated to room temperature and rephotographed. The additional bands in the visible region as observed at low temperature have disappeared again, except for a small remainder and therefore prove to be as characteristic for the photochromic form *C* as the long wavelength band at 15 000 cm^{-1}. The interpretation proposed by Hirshberg and Fischer for the observation that there are photochromic but not thermochromic derivatives of dehydrodianthrone has been discussed already in our previous paper.[5] It is, however, obviously not sufficient for the observations mentioned.

Reply to the Note by Y. Hirshberg:—Hirshberg and Fischer[6] state, themselves, that at low temperature a color only develops with dehydrodianthrone if it is irradiated with a wavelength $\lambda < 450$ mμ. This means that the phenomenon names "thermochromie à basse température" does not exist and has only been used as a synonym for "photochromism." The statement of Mr. Hirshberg is therefore completely ununderstandable. Since it does not contribute to the factual discussion, further reply is unnecessary.

[1] E. Bergmann and Mitarb, Bull Soc. chim. France (5) **18**, 88 (1951).
[2] Kortüm, Theilacker, and Zeininger, Chem. Ber. **86**, 298 (1953).
[3] Y. Hirshberg, Compt. rend. **231**, 903 (1950).
[4] Kortüm, Theilacker, and Braun, Z. physik. Chem. N.F. **2**, 179 (1954).
[5] Theilacker, Kortüm and Friedheim, Chem. Ber. **83**, 508 (1950).
[6] Y. Hirshberg and E. Fischer, J. Chem. Soc. 629 (1953).

On the Coincidence of Fusion Points in the Polymorphs of Dibenzoylmethane and of its enol-Ethers

Y. Urushibara, F. Iimura, and K. Ikeda
Department of Chemistry, University of Tokyo, Bunkyo-ku, Tokyo

(Received June 20, 1955)

THE polymorphs and isomers of dibenzoylmethane and its enol-ethers show peculiar coincident melting points.[1–7] The phenomenon may correspond to the coincidence of the crystal structures at least in the instance of fusion, and moreover, the lattice energy can be supposed to depend largely upon the interaction of the groups or structures common to the corresponding species, e.g., benzene nuclei or the skeletal systems (Table I).

Homologous enol-ethers and their polymorphs presented unexpected results: 75° and 78° species of the ethyl and the isopropyl ethers give the uv spectra of the *cis*-ethers.[8,9] Their almost identical x-ray patterns in powder and i.r. spectra in Nujol differ entirely from those of 74° and 78° species of the *trans*-methyl ether. The 75° and 78° species of the ethyl and the isopropyl ethers assumably rearrange to *trans*-forms at about their melting points.[10]

Another 63° species of the *cis*-ethyl ether is obtained and shows the *cis*-form spectrum in solution almost indistinguishable from that of 65° species of the *cis*-methyl ether. We could not isolate the *trans*-forms of ethyl and isopropyl ethers from the equilibrium mixtures obtained on irradiation of the solution of the *cis*-forms though the red-shift of the absorption maxima was the same as the equilibrium mixture of the methyl ether from which the *trans*-form was readily isolated after the less soluble *cis*-form was removed.[11] Thus, the *trans*-forms of the ethyl and the iso-propyl ethers are very unstable in the solid state at the ordinary temperature but as stable as the methyl ether in solution.

TABLE I. Isomers and polymorphs of dibenzoylmethane and its enol-ethers.

	cis-forms				*trans*-forms			1:1 mix
Dibenzoylmethane	71°		78°*		(73°)	78°	(81°)	(66°)
Dibenzoylmethane methyl ether	65°				74°	78°	81°	48°[a]
Dibenzoylmethane ethyl ether	63°	75°	78°	(81°)[b]				(43°)
Dibenzoylmethane isopropyl ether	(50°)[c]	75°	78°					
Dibenzoylmethane *n*-propyl ether	59°							
Dibenzoylmethane *t*-butyl ether	amorphous solid[d]							
Dibenzoylmethane isobutyl ether	(56°)[c]	amorphous solid[d]						
Dibenzoylmethane *n*-butyl ether	liquid at room temperature							

( ) Authors could not obtain.
* Pseudoform of 78° species.
—— Found by authors.
[a] Dr. E. Eistert recently "sinthetisiert" the 45–6° species (probably identical with our 48° species) from 1:1 mixture of 78° and 65° species. Private communication.
[b] Eisenrohr *et al.*[7] reported that 63°, 75°, 78°, and 81° species of ethyl ether gave identical values of dipole moment in solution.
[c] See reference 5.
[d] These species gave no definite patterns in x-ray diffraction measurements.

We must acknowledge that the cooperative phenomenon at the elevated temperature supplies the activation energy for the *cis-trans* isomerization, and that the character of the molecular crystal is predominant at low temperatures while at elevated temperatures the crystal rearranges to the *trans*-form acquiring the energy of intermolecular interaction of ionic or dipole nature. If the rearrangement is very slow, another polymorph or isomer will appear as observed elsewhere. The alternation of configurations and the resonance forms is as follows:

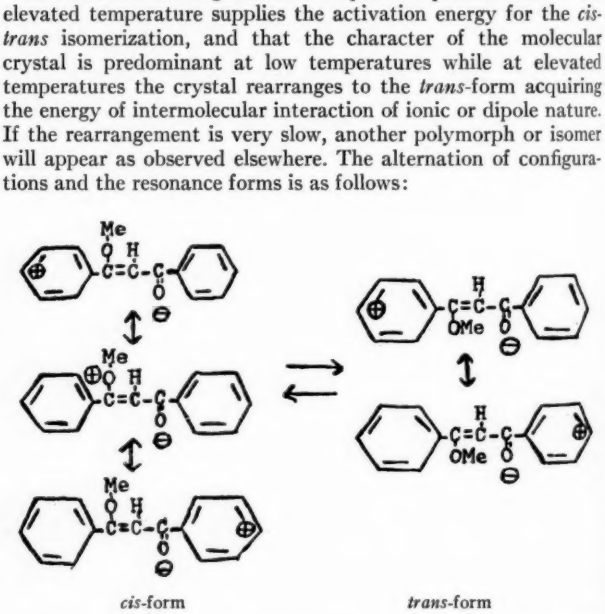

cis-form *trans*-form

The ground of the classification of the polymorphs of dibenzoylmethane is obscure because of their same *trans*-form spectra in solution due to strong tendency for intramolecular hydrogen bonding, and they should be regarded as the *trans*-form. In x-ray patterns, and i.r. spectra, however, 71° species has some reminiscence of 65° methyl, 63° ethyl, and 59° *n*-propyl ethers, the latter three giving very analogous patterns and spectra. The intermolecular hydrogen bonding may give a probable explanation as proposed by Eistert *et al.*[4]

Another problem is the mixed crystals.[12] Their x-ray patterns show almost a superimposition of those of components. But a

crystal melting sharply can be isolated from the solution containing two components of different solubilities, and it always consists of *cis*-and *trans*-isomers in exactly 1:1 ratio in solution.[13]

No distinct differences are observed in x-ray patterns and i.r. spectra in solid between 75° and 78° species of the ethyl and the isopropyl ethers and between 75°, 78°, and 81° species of the methyl ethers. But they are obtained as definite species as shown by many researchers.[1–7]

78° pseudoform of dibenzoylmethane is obtained from 71° species on standing long in the dark. It shows an x-ray pattern and an i.r. spectrum very analogous to those of 71° species, but it melts at 78°. It readily rearranges to intrinsic 78° species on irradiation with x-ray beams or with the sunlight. The prototropy in the double minimum of the intermolecular hydrogen bond or a perfect solid solution of the *trans*-form in the *cis*-form may be a probable explanation.

We must expect many more modes of crystal lattices for the polymorphs characterized by different fusion points.

[1] C. Weygand, Ber. deut. chem. Ges. **59**, 2249 (1926); **60**, 2428 (1927).
[2] C. Weygand, Lieb. Ann. **472**, 143 (1929).
[3] Weygand, Bauer, and Hennig, Ber. deut. chem. Ges. **62**, 562 (1929).
[4] Eistert, Weygand, and Csendes, Ber. deut. chem. Ges. **84**, 745 (1951).
[5] C. Dufraisse and Gérald, Bull. Soc. chim. (4) **31**, 1285 (1922).
[6] C. Dufraisse and Gillet, Ann. Chim. (10) **6**, 291 (1926).
[7] F. Eisenrohr and A. Metzner, Z. physik. Chem. **A178**, 350 (1937).
[8] C. Weygand and W. Lauzendorf, J. prak. Chem. (2) **151**, 227 (1938).
[9] H. Keller and H. v. Halban, Helv. Chem. Acta. **27**, 1253 (1944).
[10] The *trans*-species of the methyl ether spontaneously rearrange to *cis*-form on standing for a long time in the solid state, indicating that the *cis*-form is stable at the ordinary temperature. The *trans*-form is stable at elevated temperature as it can be recrystallized from a hot solution, and, therefore, 74° and 78° species of the methyl ether are considered to retain their *trans*-configurations even in the instance of fusion.
[11] The *cis-trans* equilibrium ratio of the methyl ether is 72:28 (mole %) in *n*-heptane and in alcohol at the room temperature, two weeks being sufficient to effect the equilibrium in the dark.
[12] Two different sorts of molecules generally do not form a stable lattice as is accepted in crystallography, except in special cases, i.e., molecular complex, submicroscopic twin [T. Ito, *X-ray Studies on Polymorphism* (Maruzen Company, 1950)] and clathrate compounds.
[13] A possible explanation for the 1:1 ratio may be given by an analogy to the interpenetration of two independent networks observed in the structure of beta-quinol [see H. M. Powell and P. Riesz, Nature **161**, 52 (1948)].

The "Hump" in the Capacity of the Electrical Double Layer

DAVID C. GRAHAME
Department of Chemistry, Amherst College, Amherst, Massachusetts
(Received July 13, 1955)

WHEN a plot is made of the capacity of the electrical double layer between mercury and most aqueous solutions *versus* polarization potential or surface charge density q,[1] a very characteristic "hump" appears. Recent experiments to be reported in more detail elsewhere,[2,3] show that this "hump" disappears as the temperature is raised, and also that it is absent in methanolic solutions at 0°C and above. (Lower temperatures have not yet been investigated.)

As related a surprising phenomenon is the observation that on the anodic side of the "hump" the capacity of the double layer increases with increasing temperature. These facts are shown in Fig. 1, where the capacity of the diffuse layer has been separated out by a simple method already explained.[1,2] What remains is the capacity C° of the "inner region," that part of the double layer lying between the metallic surface and the plane of closest approach of ions not chemisorbed.

A proposed qualitative explanation for the two characteristics described above is as follows: Let it be supposed that on the anodic side of the "hump" water molecules form a quasi-crystalline layer, not more than a few molecules thick, using hydrogen bonds approximately as in ice. Let it be supposed that this layer has the power to prevent or at least to inhibit the entry of ions of average energy. (Chemisorbed ions can enter, however, because of their energy of adsorption.) Let this layer of water molecules be thought of as a layer of "ice."

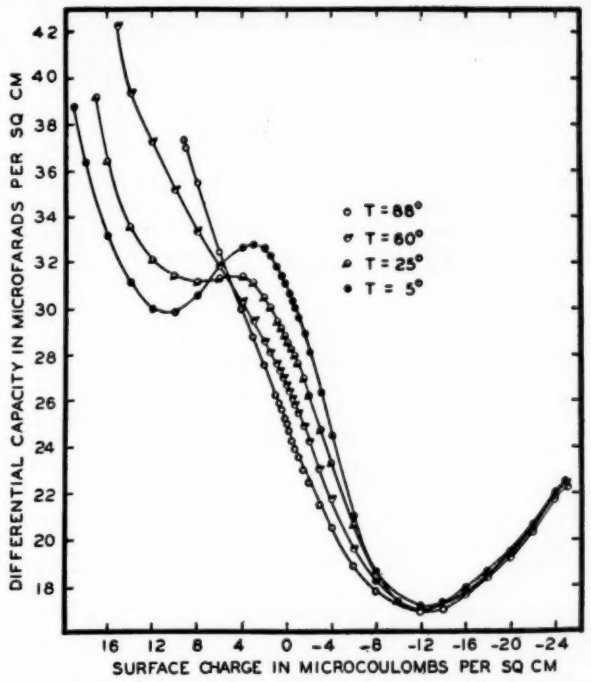

FIG. 1. Differential capacity of the region between a mercury surface and the outer Helmholtz or Gouy plane. C° *vs* q. NaF all concentrations.

Unlike ordinary ice, it does not melt sharply as the temperature is raised at constant surface charge density q. Likewise it does not vanish abruptly with change of q, but gradually diminishes in thickness as the metal is made less anodic or more cathodic (i.e., as q becomes more negative). In ether case the capacity of the double layer increases because the thickness of the inner region decreases. This would account qualitatively for the two major anomalies in double-layer capacity measurements described above.

The "melting" or "thinning" of the quasi-crystalline layer with increasing field strength can be understood in either of two ways, or by a combination of these. (1) The electric field might make the layer more penetrable to cations because of the increasing force of attraction for cations, or (2) it might disrupt the layer by reorienting the water molecules either because of purely electrostatic influences, or possibly also by a more subtle interaction akin to the formation of hydrogen bonds with the metal.

The rapid decrease in the capacity as one approaches the minimum from the left in Fig. 1 has been attributed[2] to dielectric saturation of the inner region. In this connection it must be supposed that there is a strong "natural" field of the metal orienting the water molecules even at an uncharged surface, and that the molecules are there oriented $+-$, the metal being at the left. It is noteworthy that there is no discernible break in the curves in Fig. 1 at $q=0$, showing that this is not a distinctive point for the inner region.

The increase in the capacity to the right of the minimum is attributed to electrostriction, the separation of the poles of the dipole in the intense electric field of the inner region. Temperature has no appreciable effect in this range of potentials because dielectric saturation is complete.

The existence of a hydrogen-bonded interfacial barrier is also suggested by the results of Sinfelt and Drickamer.[4]

The support of this work by the Office of Naval Research is gratefully acknowledged.

[1] D. C. Grahame, Chem. Revs. **41**, 441 (1947).
[2] D. C. Grahame, Z. Elektrochem. (to be published).
[3] D. C. Grahame, Manuscript in preparation.
[4] J. H. Sinfelt and H. G. Drickamer, J. Chem. Phys. **23**, 1095 (1955).

On the Structure of Ethylene*

ALEXANDER VERRIJN STUART
Koninklijke/Shell-Laboratorium, N. V. De Bataafsche Petroleum Maatschappij, Amsterdam, Netherlands
(Received November 5, 1954)

RECENTLY Mueller[1] applied the method of semilocalized orbitals[2] to the case of ethylene, treating the carbon-carbon σ and π bonds independently. A variational parameter, λ, is introduced in the one-electron "semilocalized" orbitals:

$$\psi_{\mathrm{I}}=\varphi_a+\lambda\varphi_b, \quad \text{and} \quad \psi_{\mathrm{II}}=\lambda\varphi_a+\varphi_b.$$

Antisymmetrization gives

$$\psi=(1+\lambda^2)\{\varphi_a(1)\varphi_b(2)+\varphi_b(1)\varphi_a(2)\} +2\lambda\{\varphi_a(1)\varphi_a(2)+\varphi_b(1)\varphi_b(2)\}. \quad (1)$$

Thus the ratio of ionic to covalent terms (referred to as p by Craig[3] in a similar treatment) equals: $p=2\lambda/(1+\lambda^2)$. λ is evaluated by minimizing the energy: $E=\int\psi H\psi d\tau/\int\psi\psi d\tau$, in which the Hamiltonian is chosen as:

$$H=T_1+T_2-\zeta_a/r_{a1}-\zeta_b/r_{b1}-\zeta_a/r_{a2} -\zeta_b/r_{b2}+\zeta_a\zeta_b/r_{ab}+1/r_{12}+C. \quad (2)$$

C stands for the potential due to the electrons outside the σ and π bonds, respectively. The H atoms are disregarded, so that C apparently represents the Coulomb field of the four electrons in carbon sp^2 orbitals involved in the CH bonds, plus that of the π electrons (or σ, respectively) of the CC bond.

ζ is chosen equal to 4, although the exponents of the AO's have the usual Slater value 3.18.

For several reasons the method appears to be a less fortunate one.

In the first place the choice of the parameter λ may easily confuse the calculations. Minimization implies that $\delta E/\delta\lambda=(\delta E/\delta p)(\delta p/\delta\lambda)=0$, but $\delta p/\delta\lambda=2(1-\lambda^2)/(1+\lambda^2)^2$, so that $\delta E/\delta\lambda$ equals zero for the roots of $\delta E/\delta p=0$ (two roots), *and* for $\delta p/\delta\lambda=0$, i.e., for the *trivial* roots $\lambda=\pm1$. According to Mueller's paper λ takes the value 1.00 for the σ bond. This result would seem to represent one of the trivial roots.

Secondly, the formulation of the Hamiltonian (2) seems somewhat unclear. The terms $\zeta_a\zeta_b/r_{ab}$ represents the considerable repulsion of the two carbon nuclei depleted of their valence electrons. Even if the (partially compensating) attraction of the electrons outside the bonds considered is incorporated in the term C, the repulsion will remain in excess of this screening. Hence it would be counted twice, once for the σ bond and once for the π bond.

Furthermore, the replacement of the integral

$$\int\varphi_a(T-\zeta_a/r_a)\varphi_a d\tau$$

by the atomic ionization potential would seem to be unnecessary since all integrals are available from tables.

Finally the separate discussions of the σ and π bonds might be unrealistic. Their interaction depends on the shapes of the orbitals in which the electrons move. Since these orbitals are the objects of the calculations, it seems impossible to introduce them properly.

In view of these aspects the significance of the calculated bond properties is somewhat vague.

It may also be shown that the results greatly depend on the choice of the Slater exponential parameter Z, to which different values are sometimes assigned.[3]

From the table it is seen that the variational procedure causes a lowering of the ground state energies for Hamiltonians similar to (2) for the σ and π bonds ($H\sigma$,$H\pi$) and for Craig's Hamiltonian ($\bar{H}\pi$) but a change of Z causes changes of the same order of magnitude!

Z is chosen in accordance with a best *atomic* wave function by a variational procedure, and its modification thus involves another element of arbitrariness. One must conclude that the parameter p is hardly significant. Thus the idea of mixing ionic terms with the covalent wave functions loses much of its original attraction.

TABLE I.[a] Stabilization energies (in ev).

	$Z=$	Valence bond 3.18	Valence bond 3.432	Variational treatment 3.18		Variational treatment 3.432		Mol. orbital 3.18	Mol. orbital 3.432
H_σ	$-E+2W_s$, (p)	39.44	36.33	39.93	(0.546)	36.97	(0.500)	39.84	36.81
H_π	$-E+2W_p$, (p)	12.28	11.51	12.95	(0.296)	12.02	(0.240)	11.70	10.26
$\bar{H}_\pi$	$-E+2W_p$, (p)	13.14	11.97	14.03	(0.335)	12.61	(0.268)[b]	12.89	10.95

[a] W_s and W_p are the energies of an electron in a $2s$ and a $2p$ carbon orbital, respectively.
[b] Owing to the use of different tables of integrals slightly differing from Craig's values.[3]

* Revised in view of the comments kindly made by Professor Mueller.
[1] C. R. Mueller, J. Chem. Phys. **22**, 120 (1954).
[2] C. R. Mueller and H. Eyring, J. Chem. Phys. **19**, 1495 (1951).
[3] D. P. Craig, Proc. Roy. Soc. (London) **A200**, 272 (1950).

Delocalization and Approximation Methods

C. R. MUELLER
Chemistry Department, Purdue University, West Lafayette, Indiana
(Received November 22, 1954)

IN the preceding Letter to the Editor, A. V. Stuart has discussed some calculations on the ethylene molecule by D. P. Craig[1] and myself.[2] Some of his statements are serious enough to warrant discussion. I shall attempt to deal with them in order of importance.

For homonuclear molecules we[3] have used orbitals, of the form $\varphi a+\lambda\varphi b$, $\lambda\varphi a+\varphi b$, to represent the eigenfunctions of bonding electrons. As has been pointed out this parameter has the extremal values, ±1, restrictions imposed on the orbital method. In the earlier papers on the semilocalized orbital method, we have been primarily concerned with the relationship of atomic and molecular orbital theories, using specific molecules as examples. In previous articles[3,4] we have discussed the orbital form for diatomic molecules. In a later paper[5] we discussed the orbital form for n-center molecules. For this purpose, there is no inconvenience in using a somewhat restricted variational parameter. In the paper on ethylene[2] we develop a secular equation technique utilizing different and unrestricted variational parameters for use in the polarizibility calculations. Since then we have found one molecule O_2, which requires parameters outside the ±1 range.

The use of the parameter λ automatically restricts the results of the variational method to an orbital formulation, but results in some peculiarities outside the normal range. One of these peculiarities is usually that of two maxima at ±1 which Stuart confuses with minima. In the case under consideration there is a real minimum at $\lambda=1$, not a maximum. This means simply that within the orbital range, the molecular orbital formulation of the sigma bond is the best representation.

The second objection made by Mr. Stuart is that the exact value of the variational parameter depends on the eigenfunctions and other calculational approximations. This is indeed true and unavoidable. The result of any approximation is necessarily approximate. If we were to worry unduly over this quirk of fate, we would have made no progress in valency theory. We face here a rather complex mechanical problem and we must proceed, step by step, towards greater certainty. The introduction of variational parameter regulating the ionic character of the bond has improved calculational reliability, and we should not reject this improvement on the grounds that ultimate certainty has not yet been achieved.

Stuart has also objected to the use of the ionization potential for the atomic energies, an approximation suggested by Mulliken.[6]

The reason for this is simply the unreliability of the Slater atomic orbitals. The defense of this approximation is rather involved and, in the main, I refer the reader to the original article by Mulliken. The atomic energies calculated by means of Slater atomic orbitals are usually less than the ionization potential, but should in fact be greater. The actual magnitude of these energies is not important (involving only the magnitude of the energy reference state) but their differences are very important. The orbitals tend to be worse for complex atoms; and introduce systematic errors. The use of ionization potentials may somewhat diminish the source of error. Furthermore the Slater orbitals are extremely poor in calculation of electron affinities and tend to reduce the contribution of the ionic states. Wherever possible it seems advisable to replace some theoretical quantities with empirical quantities until our knowledge is more certain.

Finally the presence of $\zeta a\xi b/\gamma ab$ has no effect on the calculation which we carried out. The separate discussion of σ and π bonds was carried out to parallel previous MO and AO treatments, and Stuart should perhaps direct his criticism elsewhere.

[1] D. P. Craig, Proc. Roy. Soc. (London) **A200**, 272 (1950).
[2] C. R. Mueller, J. Chem. Phys. **22**, 120 (1954).
[3] C. R. Mueller and H. Eyring, J. Chem. Phys. **19**, 1495 (1951).
[4] C. R. Mueller, J. Chem. Phys. **19**, 1498 (1951).
[5] C. R. Mueller, J. Chem. Phys. **20**, 1600 (1952).
[6] R. S. Mulliken, J. chim. phys. **46**, 497 (1949).

Least-Squares Calculation of OVFF Force Constants for XY_4 Tetrahedral Molecules

WILLIAM S. HORTON
Knolls Atomic Power Laboratory, General Electric Company, Schenectady, New York*
(Received January 10, 1955)

WHEN force constants for XY_4 tetrahedral molecules are computed using the orbital valence force field (OVFF) approximation of Heath and Linnett,[1] there arises the problem of determining three theoretical constants from four experimentally determined numbers. In particular, this problem arose in connection with the interpretation of the infrared spectrum of $TiCl_4$ reported by Hawkins and Carpenter.[2]

Ordinarily when the agreement between experiment and theory is reasonably good, one might question the practical value of rigorous attempts to use a least-squares method for determining the constants since only minor variations in the values result when a different permutation of three equations out of the four is chosen for solution. On the other hand when disagreement appears evident, as in the case of $TiCl_4$, one can question the choice of any particular permutation for exact solution. To check the agreement, it is reasonable to use a least-squares method. The problem then is one of indirect observations,[3] and is straightforward except for two aspects. Of these the first, nonlinearity of the constants in Eq. (4) of Hawkins and Carpenter is simply handled by the usual Taylor's expansion in terms of corrections[4] which are successively improved.

The second point involves the assumptions under which least-squares treatments are applied. As long as strict statistical tests for significance or similar procedures are not attempted, these are two in number: (a) the observational errors are not correlated and (b) the errors are of the same magnitude. Requirement (a) is probably not violated here, but the errors, as indicated by the observational quantities in (1) to (4), are obviously of widely differing magnitude. The least-squares treatment, therefore, should be one with weighting factors.[5]

In order to assign weights, extreme limits of error beyond which the probability of error is negligible, may be assigned. As an approximation the distribution may be assumed to be rectangular and continuous, leading to a variance of $\frac{1}{3}l_i^2$ where l_i is the assigned error limit. Furthermore, the variance of functions may be computed by the "propagation of error" technique since the variances are small compared to the variables.

A word of caution must be injected concerning the interpretation of least-squares solutions. The method is based upon the tacit assumption that the forms of the equations are correct. If this is not true, no information which will point out the offenders can be gleaned from the computations. The tendency of the least-squares calculation is to smear out such errors over all the equations.

This has been necessarily a very brief discussion of the least-squares approach to the evaluation of the OVFF approximation. Readers desiring more details, particularly with reference to the data of $TiCl_4$ as reported by Hawkins and Carpenter may obtain them from the writer.

* The Knolls Atomic Power Laboratory is operated by the General Electric Company for the U. S. Atomic Energy Commission. The work reported here was carried out under contract No. W-31 109 Eng-52.
[1] D. F. Heath and J. W. Linnett, Trans. Faraday Soc. **44**, 878 (1948).
[2] N. J. Hawkins and D. R. Carpenter, J. Chem. Phys. **23**, 1700 (1955).
[3] E. Whitaker and G. Robinson: *The Calculus of Observations* (D. Van Nostrand Company, Inc., New York, 1944), fourth edition, p. 223.
[4] A. Hald, *Statistical Theory with Engineering Applications* (John Wiley and Sons, Inc., New York, 1952), p. 641.

Paramagnetic Resonance of X-Irradiated Teflon Effects of Absorbed Oxygen*

WILLIAM B. ARD, HOWARD SHIELDS, AND WALTER GORDY
Department of Physics, Duke University, Durham, North Carolina
(Received June 20, 1955)

WE have examined the paramagnetic resonance of x-irradiated Teflon,[1] $-(CF_2)_n-$, at 9 and 30 kMc. Our results differ significantly from those described by Schneider,[2] who reported the resonance as an unresolved triplet with separations of 19 gauss between peaks. Immediately after irradiation of the sample at room temperature we found the resonance at 9 kMc to have a structure consisting of eight symmetrical components with an additional resonance superimposed near the center of the group which did not fit into the symmetrical pattern of the others. When allowed to age in air after irradiation this superimposed resonance appeared to swallow up its neighbors. After two weeks of aging in air only the central resonance remained.

Soon after we had discovered this strange behavior, one of us (W.G.) mentioned the effect to Dr. D. M. McQueen and Dr. R. M. Joyce, of DuPont. Dr. McQueen suggested that the change of the resonance with aging may be caused by absorption of oxygen from the air. Dr. Joyce stated that the CC bond of the Teflon when broken should pull apart as a result of chain contraction and may thus make it impossible for the bond to reform. This also might leave a hole in which oxygen could get trapped. We put the McQueen suggestion to test by aging one sample in air, one in oxygen, one in nitrogen, and one in a vacuum. The resonances of the samples aged several days in N_2 and in a vacuum were found to have the same structure as they had immediately after irradiation, whereas those aged in air and in oxygen for the same time were found to have only the strong central absorption. There seems to be no question that the central resonance arises from absorbed O_2.

When a Teflon bond is broken to leave

radicals, the odd electron appears to move about over seven F atoms, probably through interaction with the p electron pairs of the F, to form π bonds and thus by interaction with the F^{19} nuclei to give rise to the eight components. To make such a migration possible, the broken chain may coil into a loop of some form. Furthermore, the evidence is that the odd electron spends equal time on each of the seven F's. The components are equally spaced

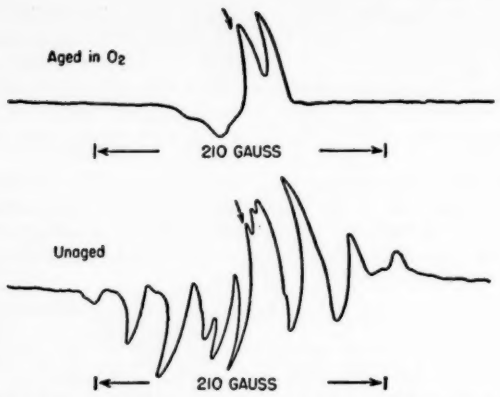

FIG. 1. Electron magnetic resonance of x-irradiated Teflon before and after aging in O_2. Temperature = 25°C, frequency = 23 kMc, x-ray voltage = 50 kv.

and have a Gaussian distribution of intensities. When the O_2 moves in, it must form a bond with a radical and thus put an end to the migration of the odd electron. The bonding of the resulting compound is possibly

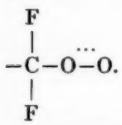

At 23 kMc the F hyperfine structure was found to be similar to that at 9 kMc (bottom curve of Fig. 1). However, the oxygen resonance is here split into a triplet which varies with orientation of the sample in the magnetic field (top curve of Fig. 1). The latter splitting is therefore believed to be crystalline field effect.

The arrow in Fig. 1, near the center of the structural spread, indicates the position for the DPPH resonance, $g = 2.0036$. This differs somewhat from the g-factor, 2.021 reported by Schneider for the central position of the Teflon resonance.

The observations reported above are for room temperature. At 90°K the F^{19} hyperfine structure is not evident. A relatively broad resonance with some evidence of unresolved structure is observed at 90°K.

Resonances have also been found in irradiated Kel-f and polyvinyl fluoride. A more complete report will be given later.

* This work is supported by the Office of Ordnance Research and by the Office of Scientific Research of the Air Research and Development Command.

[1] These results were described by one of us (W.G.) at the Faraday Society Discussion, Cambridge University, England, April, 1955.

[2] E. E. Schneider, J. Chem. Phys. **23**, 978 (1955); also reported at the Faraday Society Discussion, Cambridge University, England, April, 1955.

Potential Energy of a Molecule in a Liquid

L. A. GIRIFALCO
Lewis Flight Propulsion Laboratory, National Advisory Committee for Aeronautics, Cleveland, Ohio

(Received July 13, 1955)

THE cell model as originally proposed by Lennard-Jones and Devonshire[1] has been discussed and modified by a number of authors.[2] One of the problems presented by the cell model is that of finding the potential energy of a molecule moving in its cell. In this letter, a method of finding the potential energy of a molecule in a liquid will be given, that is, independent of the cell model and yet permits factorization of the partition function into N identical terms.

The potential energy of a molecule at a distance r from its mean position can be expressed in terms of the intermolecular potential function and the radial distribution function. Use of the radial distribution function permits the inclusion of all interactions between the central molecule and the rest of the liquid, and makes unnecessary any assumptions concerning the coordination number.

Choose a molecule X in a liquid and construct a spherical shell around its mean position 0 of radius R and thickness dR. At a given instant of time, the molecule X will be at a distance r from the center of the shell. Let x be the distance from the central molecule to some point in the spherical shell.

The number of molecules in the spherical shell at a distance between x and $x+dx$ is easily shown to be

$$\frac{2\pi R}{v}\frac{x}{r}\rho(x)dxdR, \tag{1}$$

where v is the volume per molecule of the liquid, that is V/N, and $\rho(x)$ is the radial distribution function. The energy of interaction between this volume element and the central molecule is simply the product of (1) and the intermolecular potential function. The total potential energy of the molecule at X is obtained by integrating this product first over x to get the energy of interaction between the central molecule and spherical shell, and then over R to get the complete interaction energy between the central molecule and the remainder of the liquid. Thus,

$$\phi(r)=\frac{2\pi}{vr}\int_{R_0}^{\infty}RdR\int_{R-r}^{R+r}x\rho(x)\epsilon(x)dx, \tag{2}$$

where R_0 is the closest distance of approach of two molecules, and $\epsilon(x)$ is the intermolecular potential function.

Equation (2) gives the energy of a molecule as a function of the distance from its mean position. Since $\phi(r)$ has the same form for every molecule, the total potential energy of the liquid can be written as the sum of N terms and the configuration integral can be factored to give

$$Z_\tau=[z_\tau]^N=\left[4\pi\int_0^{\infty}e^{-\phi(r)/kT}r^2dr\right]^N. \tag{3}$$

Therefore, through (2) and (3), the thermodynamic functions of a liquid can be computed if ϵ and ρ are known.

[1] Lennard-Jones and Devonshire, Proc. Roy. Soc. (London) **A163**, 53 (1937); **165**, 1 (1938).

[2] See, for example, Rowlinson and Curtiss. J. Chem. Phys. **19**, 1519 (1951) and Kirkwood, J. Chem. Phys. **18**, 180 (1950).

Note on the X-Band Microwave Spectrum of Heavy Water

D. W. POSENER
Division of Electrotechnology, Commonwealth Scientific and Industrial Research Organization, Sydney, Australia

(Received May 27, 1955)

AN absorption line at 8884.83±0.07 Mc/sec, with an absorption coefficient of about 2×10^{-6} cm^{-1}, has recently been reported by Crawford,[1] and tentatively ascribed to the $5_{32}\rightarrow4_{41}$ transition of D_2O. During a concurrent investigation of heavy water[2] preliminary information on this line was received,[3] but it could not be detected in the region of the then reported frequency, 8870 Mc/sec, with a spectroscope whose sensitivity was at the time of the order of 10^{-7} cm^{-1}.

The spectrum of heavy water in this frequency region has now been re-examined on several occasions, and under varying conditions, with a high-sensitivity Stark spectrometer (to be described elsewhere), again with a negative result. It is expected that a line with an absorption coefficient of 10^{-8} cm^{-1} could have been readily detected; a nearby HDO line at 8837 Mc/sec, with an absorption coefficient of 10^{-7} cm^{-1}, was observed well above noise, as is apparent from the recording of Fig. 1.

The $5_{32}\rightarrow4_{41}$ line of D_2O has been reported elsewhere,[2,4] at 10 947 Mc/sec.

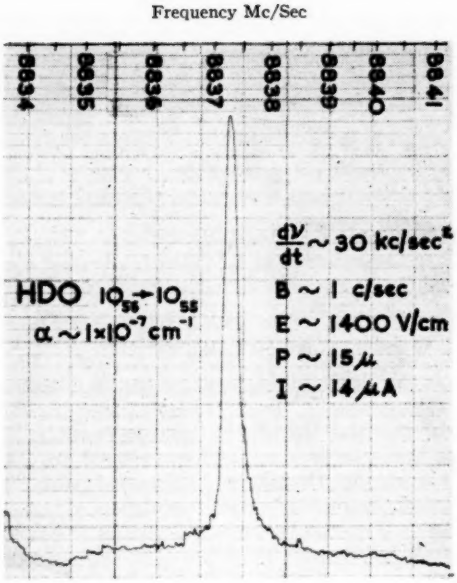

FIG. 1. $10_{56} \rightarrow 10_{55}$ transition of HDO.

Unfortunately, it has not been possible to identify definitely Crawford's line, which appears to be real and not a spurious response such as "guide noise." Examination of the detailed thesis account shows only that deuterated ammonia had been present in the absorption cell; familiarity with the difficulties associated with outgassing ammonia from a cell suggested that this substance should be investigated. A sample of deuterated ammonia was prepared by the simple method of allowing ammonia to mix with heavy water in the cell; the reaction was carried out in the gas phase (at a pressure of about 0.1 mm Hg) and the isotopic exchange occurred apparently instantaneously, as was evident by the appearance of the strong NHD_2 line at 9518 Mc/sec[5,6]; again, no absorption was observed at 8885 Mc/sec.

However, published work shows that a line of formaldehyde occurs at 8884.87 Mc/sec,[7] a value identical with Crawford's frequency within the limits of error; the absorption coefficient of this line has been quoted as 1×10^{-6} cm^{-1}.[8] It may therefore be conjectured that Crawford's line is due to formaldehyde, which could possibly enter the cell from a formaldehyde-resin (such as certain types of glyptal[9]), conceivably used for vacuum-sealing.

[1] H. D. Crawford, J. Chem. Phys. **21**, 2099 (1953); H. D. Crawford, Ph.D. thesis, University of Minnesota, 1953.
[2] D. W. Posener and M. W. P. Strandberg, Phys. Rev. **95**, 374 (1954).
[3] A. van der Ziel, private communication, October, 1952.
[4] C. I. Beard and D. R. Bianco, J. Chem. Phys. **20**, 1488 (1952).
[5] R. L. Kyhl, Massachusetts Institute of Technology Laboratory for Insulation Research Technical Report No. IV, September, 1947.
[6] M. T. Weiss and M. W. P. Strandberg, Phys. Rev. **83**, 567 (1951).
[7] R. B. Lawrance and M. W. P. Strandberg, Phys. Rev. **83**, 363 (1951).
[8] P. Kisliuk and C. H. Townes, "Molecular Microwave Spectra Tables," U. S. National Bureau of Standards Circular 518, June 23, 1952.
[9] L. F. Fieser and M. Fieser, *Organic Chemistry* (D. C. Heath and Company, Boston, 1944), first edition, Chap. 36.

Erratum: On Intermolecular Forces and the Crystal Structures of the Rare Gases

[J. Chem.Phys. **23**, 482 (1955)]

LAURENS JANSEN AND JOHN M. DAWSON
Institute of Molecular Physics, University of Maryland, College Park, Maryland

THE first names of the authors should have read: Laurens Jansen and John M. Dawson.

Transmissivity of Thin Carbon Films

R. J. THORN AND G. H. WINSLOW
Chemistry Division, Argonne National Laboratory, Lemont, Illinois
(Received June 30, 1955)

THE investigation of the rate of vaporization of graphite[1] has necessitated an examination of the optical properties of thin carbon films. This examination has demonstrated the reliability of the transmissivity method of measurement of deposition rates[1,2]; in addition, tentative values of the index of refraction, n, and the extinction coefficient,[3] κ, (where the complex index of refraction is written as $p=n-j\kappa$) have been obtained.

Thin carbon films were formed by allowing the vapor which escaped from the orifice of a graphite Knudsen cell to condense on the water-cooled quartz wall of the apparatus. In Fig. 1 typical data on the optical densities of the vacuum-carbon-quartz system have been plotted *vs* time after the beginning of the deposition. The data, represented by the crosses in Fig. 1, were calculated from the source temperature, the apparent source temperature as viewed through the deposit with an optical pyrometer, the effective pyrometer wavelength (6.61×10^{-5} cm) and from a correction for the low optical density of other media between the deposit and the pyrometer.

By starting with Maxwell's equations, one finds that the transmissivity of this system should be[4]

$$\tau = 16 n_0 (n^2+\kappa^2)/DD^*, \tag{1}$$

where

$$D = (p+n_0)(p+1)\exp(j2\pi px/\lambda) - (p-n_0)(p-1)\exp(-j2\pi px/\lambda). \tag{2}$$

Here n_0 is the index of refraction of the substrate, x is the deposit thickness, $p(=n-j\kappa)$ is its complex index of refraction, and λ is the vacuum wavelength of the light viewed by the (very nearly) monochromatic combination of pyrometer filter and observer eye-sensitivity.

It is considered that Eq. (1) must fail at some small value of x either actually, because the film is not coherent, or effectively, because the optical constants may be changing with thickness. Further, since the present apparatus lacks a shutter, there must

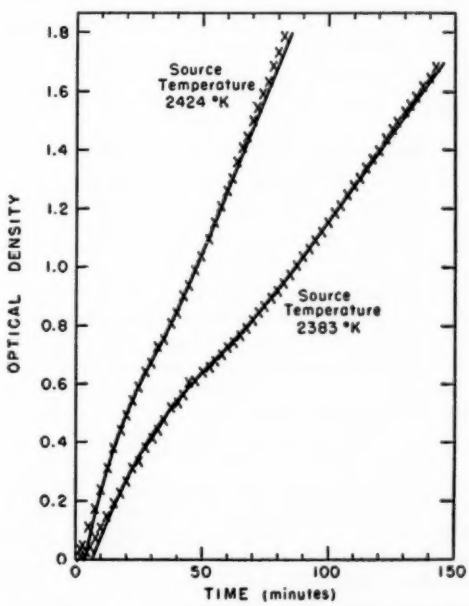

FIG. 1. Variation of optical density with time for deposits formed by condensation of vapor from a graphite Knudsen cell at two temperatures. The crosses are experimental observations. The curves are those expected theoretically for an index of refraction of 2.39 and an extinction coefficient of 1.05 after the rate of deposition and the optical constants become constant.

be some short initial interval when the source temperature is changing. Even if the film were coherent in this interval, its thickness would not be proportional to the time. Adjustment can be made for these effects when the data are analyzed in the light of Eq. (1).

An analysis of the 2383°K data gave $n=2.39$ and $\kappa=1.05$; at the time the theory begins to fit the data (~18 min) the value of the product of absorption coefficient ($4\pi\kappa/\lambda$) and thickness was about sixty percent of what it would have been had conditions after 18 min prevailed from $t=0$. Bulk material having these values of n and κ would have a reflectivity of 0.24, in agreement with values obtained by direct measurements on thick evaporated films[5] and on polished bulk graphite.[6,7] Together with the pyrometer wavelength, these values yield a resistivity of 790 microhm cm at a frequency of 4.5×10^{-6} sec^{-1}; this is slightly less than the steady field value of 813 microhm cm given by Mantell[8] for Acheson graphite electrodes.

The curve through the 2383°K data is the resulting theoretical curve. That through the 2424°K data was derived from the former simply by using an approximately higher rate of deposition.

The departure from the theory at long times has not yet been properly explained, but it is thought likely to result from a slight increase in temperature of the actual source of carbon vapor because of heat reflected back through the orifice from the deposit, or because of a slight change in the optical constants with increasing deposit thickness or temperature. In any case it is believed that the values given here for n and κ are reasonably good. More importantly, the reason for the shape of the curves seems to have been clearly demonstrated, so that one can employ this method with reasonable confidence to measure relative thickness of carbon films.

[1] R. J. Thorn and G. H. Winslow, J. Chem. Phys. **23**, 1729 (1955).
[2] O. C. Simpson and R. J. Thorn, Rev. Sci. Instr. **20**, 504 (1949).
[3] The notation and nomenclature of M. Abraham and R. Becker, *Electricity and Magnetism* (Blackie and Son Limited, London and Glasgow, 1937), p. 189, have been followed here.
[4] For discussion and references on this general problem see K. M. Greenland, Vacuum **2**, 216 (1952) and a symposium report in J. phys. radium **11**, 305 (1950). In particular, Eqs. (1) and (2) can be reproduced from equations given by H. Schopper, Z. Physik **131**, 215 (1952) or D. Malè, Ann. phys. **9**, 10 (1954).
[5] Simpson, Thorn, and Winslow, Argonne National Laboratory Report, ANL-4264, March, 1949, p. 80.
[6] *International Critical Tables* (McGraw-Hill Book Company, Inc., New York, 1926), Vol. V, p. 253.
[7] R. J. Thorn and O. C. Simpson, J. Appl. Phys. **24**, 633 (1953).
[8] C. L. Mantell, *Industrial Carbon* (D. Van Nostrand Company, Inc., New York, 1946), p. 270.

Variation with Vibration of the Fluorine Spin-Rotation Interaction in Li^6F†*

S. O. Kastner, A. M. Russell, and J. W. Trischka
Department of Physics, Syracuse University, Syracuse 10, New York
(Received June 16, 1955)

In the molecule Li^6F, the interaction of the fluorine nuclear magnetic moment with the magnetic field induced by the molecular rotation results in an energy term in the Hamiltonian of the form $c\mathbf{I}\cdot\mathbf{J}$. This letter reports the value of c, as measured by the molecular beam electric resonance method,[1] for each of the three lowest vibrational states.

Spectra due to different vibrational states are separated by the electric resonance method because the Stark splitting of energy levels varies with vibration. The measurements were made on the rotational state $J=2$ where the two quantum transition $m_J=2$ to $m_J=0$ was induced at half the frequency given by the Bohr condition. The line width at this frequency was ~10*kc*.

A strip chart recorder was used which varied the applied frequency continuously while recording the signal. In this way a complete spectrum could be recorded in less than one minute as compared to an hour or more required by the point-by-point method. The chart length was calibrated in terms of frequency and errors due to drifts were minimized.

Table I. Experimental values of c/h for F in Li^6F using the transition $m_J=2\rightarrow m_J=0$ in the $J=1$ rotational state.

Vibrational state	c/h (kc)	Number of measurements	Random error (kc)	Total error (kc)
0	36.28	586	±0.07	±0.16
1	36.11	190	±0.20	±0.27
2	33.89	56	±0.50	±0.54

The values obtained for the spin-rotation coefficient c are given in Table I. The variation of $(\mu^2A)_v$ with vibration was also observed and can be expressed as follows:

$$(\mu^2A)_1-(\mu^2A)_0=(0.0427\pm0.0003)(\mu^2A)_0$$
$$(\mu^2A)_2-(\mu^2A)_1=(0.0438\pm0.0003)(\mu^2A)_0$$

where μ is the electric dipole moment and A is the moment of inertia. The above value of c for the ground vibrational state does not overlap the value 37.3±0.7 kc found by Swartz and Trischka.[2] Although this disagreement casts some doubt on the absolute values it is felt that the relative values are reliable. Further investigation of the absolute values is needed.

The first two interaction constants differ by 0.17±0.31 kc and the second differs from the third by 2.22±0.61 kc. Such a marked nonlinearity in the variation with vibration of a molecular constant is unusual. Wick[3] has shown that the interaction constant may be expressed as the product of an electronic factor and the rotational constant B_v. If B_v is assumed to decrease linearly with an increase in vibrational state, as is the case for other diatomic molecules, the observed nonlinear variation must be due to the electronic factor alone. Thus it appears that the electronic factor increases from $v=0$ to $v=1$ and at a greater rate than from $v=1$ to $v=2$. The latter change may, in fact, be negative.

† Supported in part by the Office of Naval Research. Reproduction in whole or in part is permitted for any purpose of the United States Government.
* Submitted by S. O. Kastner in partial fulfilment of the requirements for the degree of Master of Science in Physics at Syracuse University.
[1] H. K. Hughes, Phys. Rev. **72**, 614 (1947).
[2] J. C. Swartz and J. W. Trischka, Phys. Rev. **88**, 1085 (1952).
[3] G. C. Wick, Phys. Rev. **73**, 51 (1948).

Surface Tension of Ether and Pentane

T. O. Jeffries, M. Derrick, and B. Musgrave
Department of Physics, Birmingham University, England
(Received July 15, 1955)

Measurements of the surface tension of ether and pentane in contact with their own vapor have been made up to temperatures approaching their critical points. The capillary rise method was used, the liquid being vacuum-distilled into a vessel containing a capillary tube and then sealed under vacuum.

Table I. Surface tension of ether and pentane.

Temperature °C	Surface tension of *n*-pentane (dyne cm)	Temperature °C	Surface tension of di-ethyl ether (dyne cm)
21.0	15.86±0.07	126.2	5.19±0.16
35.2	14.11±0.07	130.4	4.83±0.15
42.1	13.33±0.07	131.9	4.71±0.14
52.8	12.14±0.07	136.0	4.34±0.13
65.6	10.81±0.07	139.0	3.94±0.12
74.9	9.93±0.07	140.5	3.94±0.12
86.9	8.84±0.07	144.0	3.56±0.11
97.4	7.89±0.07	148.0	3.29±0.1
105.0	7.16±0.07	148.5	3.28±0.1
121.5	5.73±0.07		
139.1	4.26±0.07		
150.9	3.41±0.07		

Results are given in Table I, the errors quoted being the estimated maximum errors. The necessary values of the density of the liquid and saturated vapor were taken from Timmerman's *Physico-Chemical Constants*.

Paramagnetic Absorption of Potassium Complexes of Aromatic Compounds*

RICARDO C. PASTOR AND JOHN TURKEVICH
Frick Chemical Laboratory, Princeton University, Princeton, New Jersey
(Received July 11, 1955)

ELECTRON paramagnetic absorption in the 3-cm region was observed for the solid product obtained from the reaction between potassium in dioxane and the following substances: naphthalene, anthracene, phenanthrene, pyrene, chrysene, diphenyl, *p*-terphenyl, *p*-quatriphenyl, 1,3,5-triphenylbenzene, and benzophenone. For comparison we have also examined the free radical α,α-diphenyl-β-picrylhydrazyl. All these compounds show a definite paramagnetic absorption band with equipment permitting display of the absorption on an oscilloscope. The intensity of the absorption varies from preparation to preparation and is undoubtedly associated with the extent of the addition reaction.[1] The values for the g factor measured relative to hydrazyl were the same for all compounds (2.002 ± 0.001). Samples cooled in liquid nitrogen showed an increase in intensity expected from the Curie law for paramagnetism. The width of the paramagnetic absorption band did not change with the temperature of the measurement and is characteristic of the product of the interaction of potassium and the aromatic compound. Table I lists both the measured width relative to α,α-diphenyl-β-picrylhydrazyl (powder) of the potassium addition compound and the chemical resonance energy of the aromatic compound[2] before reaction with potassium. The absorption of diphenyl, *p*-terphenyl, and *p*-quatriphenyl was not great enough to permit measurement of the width. Figure 1 shows the linear relationship between the width of the paramagnetic absorption band and the chemical resonance energy. The value for the width for the potassium addition compound of 1,3,5-triphenylbenzene is completely off the curve. Further investigation is in progress to determine the validity and extent of application of this linear relationship between the chemical resonance energy and the width of the paramagnetic absorption band of the solid. If it is valid, it offers an experimental method of determining the chemical resonance energy of a pool of electrons through the investigation of the width of the electron paramagnetic absorption band of the solid compound itself, if it has an odd number of electrons in the pool or of the addition compound with potassium, if the number of electrons in the pool is even and they are paired off. One then uses the empirical relationship, $\Delta E=231-84\Delta H$, where ΔE is the chemical resonance energy in kcal mole^{-1} and ΔH is the width, relative to α,α-diphenyl-β-picrylhydrazyl powder, of the paramagnetic absorption band. The standard used has a full width at half-power of approximately 2.8 gauss. As an illustration of the applicability of this method one would predict from the value of the width of 0.28 gauss for the potassium addition compound of a sample of graphite,[3] the resonance energy for the graphite sample of 223 kcal mole^{-1}.

The following is a tentative explanation for the empirical finding. The potassium transfers its electron to the pool of electrons (π electrons) of the aromatic ring to form a negative radical ion and a positive potassium ion.[4] The number of electrons in the organic molecule is odd and the material is paramagnetic. As the number of electrons in the molecule increases the exchange interaction between them becomes greater, sharpening the energy levels involved in the microwave transition.

TABLE I. Comparison of the width relative to hydrazyl (α,α-diphenyl-β-picrylhydrazyl) with the chemical resonance energy of the aromatic compound before reaction with potassium.

Substance	ΔH	ΔE, kcal mole^{-1}
Naphthalene	1.86	77
Benzophenone	1.43	93
Anthracene	1.34	116
Phenanthrene	1.20	130
Hydrazyl	1.00[a]	...
Pyrene	0.94	152
Chrysene	0.84	163
1,3,5-triphenylbenzene	5.0	200

[a] Standard.

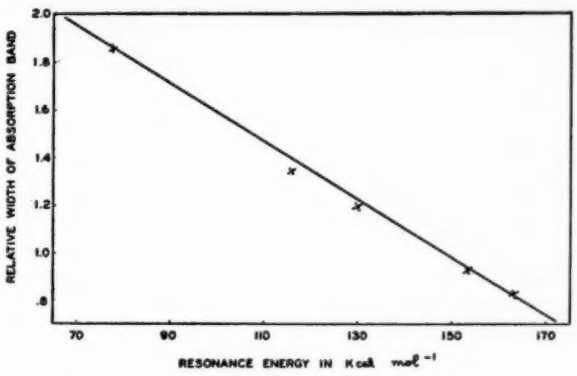

FIG. 1. Chemical resonance energy *versus* the relative width of the paramagnetic absorption band.

We wish to thank Dr. John Weil for help in the experimental measurements.

* This research has been supported by funds of the U. S. Atomic Energy Commission.

[1] N. V. Sidgwick, The Chemical Elements and their Compounds (Oxford University Press, New York, 1951) Vol. 1, pp. 76–77.
[2] G. W. Wheland, *The Theory of Resonance and its Application to Organic Chemistry* (John Wiley and Sons, Inc., New York, 1947), p. 69.
[3] Smaller, Hennig, and Yesaitis, Phys. Rev. **97**, 239 (1955).
[4] Chu, Pake, Townsend, and Weissman, J. Phys. Chem. **57**, 504 (1953)

Heterogeneous Exchange between Chemisorbed Halogen and Methyl Halide

R. COEKELBERGS, A. FRENNET,* P. A. GOSSELAIN,† AND M. J. VAN DER VENNE†
Laboratoire de Chimie Nucléaire, Ecole Royale Militaire, Bruxelles, Belgium
(Received June 9, 1955)

THE high charges resulting from the conversion of the γ rays in Br^{80} (4.5 h) are sufficient to break the C—Br bond in CH_3Br.[1-3] It has been observed[1,3] that, after evacuating a vessel filled with gaseous CH_3Br^{80} (4.5 h), one finds still at the wall an important part of Br^{80} (18 mn).

The phenomenon has been studied in Pyrex bulbs by Coekelbergs, Denaeyer, and Dôme.[4] They measured the ratio Q between the Br^{80} (18 mn) at the wall and the Br^{80} (18 mn) atoms present in the whole system at a given time by removing the CH_3Br^{80} (4.5 h) from the vessel and studying the growth and decay curves of the Br^{80} (18 mn) activity in the gaseous phase. They also calculated this ratio theoretically, postulating first, that the atoms formed in the gaseous phase diffuse to the wall, without any reaction, giving organic retention; secondly, that the subsequent adsorption proceeds irreversibly. Under these conditions, the value of the Q ratio is higher than 0.998 for a vessel with a radius of a few centimeters at pressures lower than 100 mm Hg. At pressures lower than 20 mm Hg, the measured values of Q agree with the calculated ones.

A thorough examination of the problem has shown, however, that the irreversible adsorption hypothesis must be rejected and that a return to the gaseous phase must be considered. This would happen by an elementary heterogeneous exchange process, between a chemisorbed Br atom, and a CH_3Br molecule coming from the gaseous phase. Indeed, when the CH_3Br pressure increases, the experimental values of the Q ratio disagree more and more with the theoretical provisions. Moreover, this deviation from the expected value depends principally on the treatment undergone by the wall: on gold, for instance (coating of about 100 mg ob-

TABLE I.

No.	Wall	T °C	Time mn	[HCl] $\times 10^3$ [a]	[CH_3Cl] $\times 10^3$ [a]	F[b]	R[c]
1	Pyrex	22	150	2.82	2.58	0.00	...
2	Pyrex	307	90	2.82	2.58	0.00	...
3	Au 11.5 mg	262.3	815	3.41	3.35	0.43	0.043
4	W 13.2 mg	262.2	40	3.50	3.65	0.52	6.8
5	W 13.2 mg	262.2	45	0.755	3.54	1.06	15
6	W 13.2 mg	262.2	30	11.89	3.42	0.17	3.5
7	W 13.2 mg	262.2	38	3.58	10.78	0.54	11.4
8	W 13.2 mg	262.2	45	3.52	1.40	0.41	2.4
9	W 13.2 mg	262.2	41	3.61	3.55	0.50	6.3

[a] Concentration in mole liter^{-1}.
[b] F = exchange fraction.
[c] R = rate in mole sec^{-1} mg^{-1} 0.10^{-9}.

tained by evaporation under high vacuum), the Q ratio has a value of about 0.3 for all pressures higher than 20 mm Hg. Finally, all of these deviations increase with temperature. We have furthermore shown that, within experimental errors (sometimes important), practically all the Br^{80} (18 mn) atoms of the gaseous phase were part of organic molecules.

These facts lead us to consider the heterogeneous exchange between systems like CH_3Br/HBr and CH_3Cl/HCl. Such an exchange has been confirmed with HCl/CH_3Cl. Some results are shown in Table I.

They establish that an exchange between inorganic and organic chlorine may take place on a metallic coating. Preliminary measurements show that, on tungsten for instance, the exchange reaction has an apparent activation energy of 20 to 25 kcal.

The absence of exchange reaction in Pyrex bulbs and, at low temperature, on metallic coatings, contrasts with the results obtained in the foregoing with chemisorbed bromine formed by isomeric transition. The strong inhibition by hydrochloric acid, observed for the HCl/CH_3Cl exchange (see 4, 5, 6), may account for it: in isomeric transition, chemisorbed Br^{80}/18 mn is always in extremely low concentration, and only a very small portion of the surface can be covered. Because of these radiochemical quantities, chemisorbed methyl bromide is always in great excess, even when all the inorganic bromine is strongly adsorbed at the wall.

* Boursier de l'Institut Interuniversitaire des Sciences Nucléaires.
† Chercheur agréé de l'Institut Interuniversitaire des Sciences Nucléaires.
[1] D. De Vault and W. Libby, J. Am. Chem. Soc. **63**, 3216 (1941).
[2] J. L. Magee and E. F. Gurvee, J. Chem. Phys. **20**, 834 (1952).
[3] W. H. Hamill and J. A. Young, J. Chem. Phys. **20**, 888 (1952).
[4] Coekelbergs, Denaeyer, and Dôme, Compt. rendu du XXVII Congrès International de Chimie Industrielle, Section 11, Vol. II (to be published).

Surface Recombination of Cadmium Sulfide

S. H. LIEBSON
United States Naval Research Laboratory, Washington, D. C.
(Received June 6, 1955)

A RECENT letter to this journal[1] described measurements of the luminescence of CdS exposed to oxygen and stimulated 3660 A light. Further measurements have been completed which extend these observations to vapors of ammonia, water, and ethyl alcohol, and their effect on the photoconductivity of CdS.

The measurements previously reported were made on large single crystals of CdS which had been crushed under liquid nitrogen to form a powder of new surface area very much larger than that of the original crystals. The powder was placed on the vacuum system while still under liquid nitrogen. This simple procedure was used because nitrogen gas had no detectable effect on either luminescence or photoconductivity. Most of the crystals prepared in this manner showed the behavior depicted in the figure of the earlier letter, although others showed the type of characteristic shown in Fig. 1. For properties dependent on chemisorbed gases the exact form of the pressure dependence is probably strongly related to the nature of impurity and other centers in the surface region.[2] In Fig. 1 is shown the luminescence and photoconductivity for a crystal which had been exposed to air for about a year. The similarity of the pressure dependence for both luminescence and photoconductivity may be interpreted in terms of the theory of Broser and Warminsky,[3] indicating that the surface is a region of nonvisible or nonradiative electron recombination, which decreases the number of electrons in the conduction band available for recombination with luminescent centers.

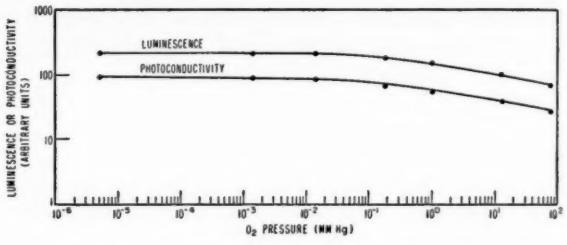

FIG. 1. Luminescence and photoconductivity (ordinates in arbitrary units) as a function of oxygen pressure.

No significant differences were observed in luminescence variations with pressure for crystals of dark resistance between 1 ohm cm and 10^9 ohm cm. Assuming a surface barrier height of the order of 0.5 volt, the barrier thickness for these crystals should vary from less than 10^{-6} to greater than 10^{-4} cm. The absorption coefficient for the light used for stimulation is approximately 2×10^4 cm^{-1}.[4] Most of this light incident on the low resistivity crystals is absorbed beyond the barrier region, making it more likely that electron or hole diffusion rather than surface electric field is of primary importance in recombination. The time for luminescence or photocurrent to return to their vacuum values after exposure to oxygen was greatly facilitated by irradiation with ultraviolet light. This lends weight to the concept of holes diffusing to the surface to combine with chemisorbed oxygen forming free oxygen atoms which desorb as has been reported for zinc oxide.[5]

Figure 2 shows a typical measurement of luminescence as a function of oxygen and ammonia pressure. The results for oxygen are in agreement with the results previously reported. The increase in luminescence at pressures greater than 1 mm for ammonia are also observed with water and alcohol vapor for both luminescence and photoconductivity. This increase may be due to interaction between the adsorbed molecules, resulting in a decreased number of the chemisorbed species.

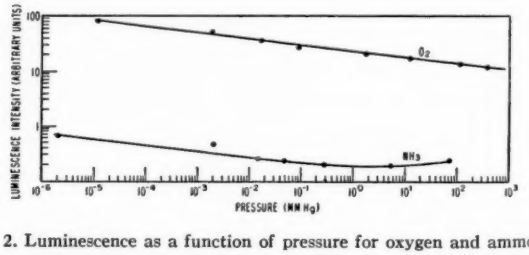

FIG. 2. Luminescence as a function of pressure for oxygen and ammonia.

I would like to express my appreciation to Mr. E. J. West for assistance with measurements.

[1] S. H. Liebson, J. Chem. Phys. (to be published).
[2] P. B. Weisz, J. Chem. Phys. **21**, 1531 (1953).
[3] I. Broser and R. Warminsky, Z. Physik **133**, 340 (1952).
[4] E. Mollwo, Reichsber. Physik **1**, 1 (1944).
[5] D. A. Melnick, University of Pennsylvania, Technical Report No. 9, Contract N6ONR 24914, February 5, 1954.

Effect of Orientational Forces on Second Virial Coefficients

BARBARA J. CASTLE, JOHN M. DAWSON, AND LAURENS JANSEN
Institute of Molecular Physics, University of Maryland, College Park, Maryland
(Received June 9, 1955)

THE second virial coefficients of nonspherical molecules have been evaluated by various authors.[1] A general formulation of the second virial coefficients of axially symmetric molecules was developed by Pople.[2] This author treats the directional intermolecular field as a perturbation on the spherical field and expands the second virial coefficient in the form

$$B(T)=B^{(0)}(T)+B^{(1)}(T)+B^{(2)}(T)+\cdots.$$

For example, the second virial coefficient for an assembly of axially symmetric molecules with a Lennard-Jones (6,12) spherical field, a quadrupole moment Θ, and an anisotropic polarizability (anisotropy factor κ) is given by

$$B(T)=\frac{2\pi N r_0^3}{3}\left\{F(y)-\frac{7}{320}\left(\frac{\Theta^2}{\epsilon r_0^5}\right)^2 H_{10}(y)+0.09\frac{\Theta^2\kappa^2}{\epsilon r_0^5}H_{11}(y)-(0.05\kappa^2+0.095\kappa^4)H_{12}(y)\cdots\right\}, \quad (1)$$

where

$$y=2\left(\frac{\epsilon}{kT}\right)^{\frac{1}{2}}, \quad F(y)=-\frac{y^3}{4}\sum_{p=0}^{\infty}\Gamma\left(\frac{2p-1}{4}\right)\frac{y^p}{p!},$$

$$H_n(y)=y^{(27-n)/6}\sum_{p=0}^{\infty}\Gamma\left(\frac{6p+n-3}{12}\right)\frac{y^p}{p!}. \quad (2)$$

The expressions used for the orientational forces are limiting forms which are not valid at small intermolecular separations. However, in the derivation of the functions $H_n(y)$, the integration is extended into the region of very small separations between the molecular centers. If the directional forces are not extended into the region in which the molecules are separated by distances smaller than r_0, Eq. (1) is modified by the substitution of the functions $H_n{}^{r_0}(y)$ for the functions $H_n(y)$, where

$$H_n{}^{r_0}(y)=y^{(27-n)/6}\sum_{p=0}^{\infty}\Gamma_{y^2}\left(\frac{6p+n-3}{12}\right)\frac{y^p}{p!} \quad (3)$$

and $\Gamma_{y^2}(x)$ is the incomplete Γ function,[3] defined by

$$\Gamma_{y^2}(x)=\int_0^{y^2}e^{-t}t^{x-1}dt. \quad (4)$$

For N_2 at approximately 300°K y^2 is equal to 1.3. $H_6(y)$ occurs in the expression for the second virial coefficient for molecules with permanent dipoles. As can be seen from Table I, the difference between the functions $H_n(y)$ and $H_n{}^{r_0}(y)$ is the greater the shorter the range of the directional forces. Physically it is clear that, for a given n, the relative difference increases with increasing temperature (decreasing y).

Specifically, Buckingham's use[4] of Pople's formulation to determine the molecular parameters (Θ, ϵ, and r_0) of N_2 and CO_2 by combining data on the second virial coefficients with crystal properties is subject to the criticism outlined in the foregoing. In addition, Buckingham included only the first two terms of Eq. (1), while calculations using the experimental values of κ and Θ for N_2 show that at 300°K the anisotropy term is more than twice as large as the contribution due to the quadrupoles and therefore cannot be neglected.

TABLE I. Comparison of the functions $H_n(y)$ and $H_n{}^{r_0}(y)$ for $y^2=1.3$.

n	6	10	11	12
$H_n(y)$	9.424	5.229	4.862	4.593
$H_n{}^{r_0}(y)$	8.091	3.630	3.181	2.828
$\frac{H_n(y)-H_n{}^{r_0}(y)}{H_n(y)}$	0.14	0.31	0.35	0.38

Before the modified expression for the second virial coefficient can be applied to the evaluation of the molecular parameters of nonspherical molecules, it must be supplemented by a term involving the short-range orientational forces, the precise form of which is as yet unknown.

A detailed discussion of this subject will be presented in a forthcoming publication.

The authors are indebted to Miss Dorothy F. Duffy for help with the numerical calculations.

[1] For specific references, see, e. g., Hirschfelder, Curtiss, and Bird, *Molecular Theory of Gases and Liquids* (John Wiley and Sons, Inc., New York, 1954), Chap. 3.
[2] J. A. Pople, Proc. Roy. Soc. (London) **A221**, 508 (1954).
[3] The incomplete Γ function has been tabulated. K. Pearson, *Tables of the Incomplete Γ-Function* (printed by the Cambridge University Press and published by the office of *Biometrika*, 1922, reissued 1951).
[4] A. D. Buckingham, J. Chem. Phys. **23**, 412 (1955).

On the Semiconductivity of Crystalline Aromatic Substances

A. MANY, E. HARNIK, AND D. GERLICH
Department of Physics, The Hebrew University, Jerusalem, Israel
(Received May 23, 1955)

IN recent years a considerable amount of data has been published on the electrical conductivity of crystalline polycyclic aromatic substances.[1-6] All the substances examined showed electronic conductivity which increased exponentially with the reciprocal of absolute temperature. The possibility of impurity conduction being eliminated, it was concluded that these substances were intrinsic semiconductors. An analysis of all the available data revealed a number of interesting points which will be discussed in this communication.

The conductivity of a one-carrier system can be expressed as

$$\sigma=e\mu n \quad (1)$$

where n is the carrier concentration and μ is their mobility, or, assuming the above-mentioned exponential temperature dependence to originate solely from n,

$$\sigma=e\mu N_0\exp(-E/kT), \quad (2)$$

where E is the thermal activation energy and N_0 the effective density of states in the conducting levels of the crystal.

Using the published experimental data, the product μN_0 (which is constant over the limited temperature ranges reported) was calculated for each substance. The figures thus obtained range from 10^9 to 10^{32}. This behavior is most remarkable. In order to clarify its physical significance in terms of the conduction mechanism, an attempt was made to separate the two quantities involved, by assessing the order of magnitude of N_0 at room temperature. The upper limit of the latter can be estimated from a "free molecular model," in which the intermolecular interaction is neglected. In such a model, N_0 should be given by the product of the multiplicity of the first excited electronic levels of each molecule and the concentration of the molecules in the crystal. Taking roughly the multiplicity equal to the number of π electrons in the molecule, the upper limit of N_0- $N_{\max}$- is found to be of the order of 10^{23} in the substances under consideration. The actual value of N_0 in each particular case can be expressed as $\alpha N_{\max}$, where α is a factor smaller than unity, dependent on the amount of interaction between molecules. In crystals with strong binding, such as germanium, α is about 10^{-3}. As the binding in molecular crystals is weak, the lower limit of N_0 can be reasonably taken to be of the order of 10^{20}. Thus it follows that the large

TABLE I. A list of substances examined, their activation energies, and estimated mobilities at room temperature.

Substance	Activation energy (ev)	Estimated mobility (cm^2/volt-sec)
Cynanthrone[3]	0.10	10^{-8}
Indanthrone black[3]	0.28	10^{-11}
Indanthrone[3]	0.32	10^{-12}
Indanthrazine[3]	0.33	10^{-12}
Flavanthrone[3]	0.35	10^{-7}
Isoviolanthrone[2]	0.38	10^{-6}
Violanthrone[2]	0.39	10^{-6}
Isoviolanthrene[2]	0.41	10^{-9}
Violanthrene[2]	0.42	10^{-9}
Pyranthrone[2]	0.53	10^{-9}
Pyranthrene[2]	0.54	10^{-10}
Ovalene[2]	0.56	10^{-8}
m-Naphtodianthrene[2]	0.60	10^{-11}
m-Naphtodianthrone[2]	0.65	10^{-9}
Isodibenzanthrone[1]	0.75	10^{-5}
Anthracene (single crystal)[4]	0.82	10^{-2}
Anthracene (powder)[1]	0.83	10^{-4}
Anthracene (film)[6]	0.96	10^{-4}
Naphtacene (film)[6]	0.82	10^{-3}
Anthanthrene[2]	0.84	10^{-7}
Anthanthrone[2]	0.85	10^{-6}
Pentacene (film)[6]	0.86	10^{-2}
Perylene (film)[6]	0.97	10^{-2}
Coronene[1]	1.15	10^{-3}
Metal free phtalocyanine[1]	1.20	1
Copper phtalocyanine[1]	1.30	10
5,6(*N*)-pyridino-1,9-benzanthrone	1.60	10^2
Hydroviolanthrene[2]	1.70	10^2
Naphtalene (single crystal)[5]	1.85	(10^{11})

variation of μN_0 is mainly due to that of the mobility. The latter was estimated within two orders of magnitude (Table I). N_0 was taken as 10^{21}. It should be pointed out that as far as orders of magnitude are concerned, it is of no importance whether a one- or two-carrier system is assumed.

It is interesting to note that a rough correlation exists between the mobilities and the corresponding activation energies (Table I). The higher mobilities correspond, on the whole, to higher activation energies. This may point to a possible conduction mechanism, involving tunneling of electrons through nontransparent intermolecular barriers. In such a model the mobility should be strongly dependent on the barrier height above the conducting levels, and should hence increase rapidly with activation energy. As the transparency of a barrier is very sensitive to its shape, the large variation in the mobility of the different substances may thus be accounted for, by slight variations in barrier shape.

The enormously high mobility deduced for naphthalene[5] is altogether inconceivable. It can be shown that this implies an unjustifiably high value of $N_0(10^{25})$, even if the drift velocity under unit field is allowed to be as high as the thermal velocity of a free electron at room temperature, which in itself is absurd. This points to the need for a more thorough experimental investigation of naphthalene.

[1] Elley, Parfitt, Perry, and Taysum, Trans. Faraday Soc. **49**, 79 (1953).
[2] H. Inokucki, Bull. Chem. Soc. Japan **24**, 222 (1951).
[3] H. Inokucki, Bull. Chem. Soc. Japan **25**, 28 (1952).
[4] H. Mette and H. Pick, Z. Physik **134**, 566 (1953).
[5] H. Pick and W. Wissman, Z. Physik **138**, 436 (1954).
[6] D. C. Northrop and D. Simpson, Proc. Phys. Soc. (London) **B, 67**, 892 (1954).

Dissociation of Water Vapor in Electric Discharge

E. A. SECCO*
Department of Chemistry, Indiana University, Bloomington, Indiana
(Received June 16, 1955)

IN the low-pressure discharge of water vapor the H_2O molecule is excited by electron impact to the unstable electronic state and may dissociate into radicals, atoms, and ions. Recently, it was reported[1] that, in an apparatus featuring a large pumping capacity and a high-frequency electrodeless discharge (20 Mc/sec), 500 watts (or E=430 kcal) were required to dissociate 15 g of water vapor. If dissociation of this quantity of water yielded normal OH radicals and H atoms, the energy necessary would be *ca* 100 kcal for the rupture of the O−H bond.

However, as it is generally known, an energy value above the theoretical minimum is required to dissociate any molecule with the excess energy being expended in excitation or ionization of the dissociated products. Laidler,[2] in a recent survey of this topic, has suggested a number of processes energetically possible for the dissociation of water. Of all the processes considered, two may be selected as the more probable occurring in the work cited:

$$(1)\ H_2O+e\rightarrow H+OH^++2e,$$
$$(2)\ H_2O+e\rightarrow OH+H^++2e.$$

Each of these processes involves ΔE=430 kcal/mole. If one or both of these processes are operative, 15-g H_2O would require 360 kcal with 70 kcal of the available energy, E, being lost. It seems reasonable to assume the 70 kcal to be dissipated in the power transfer from the coil through the glass tubing. The other possible paths of dissociation in the energy range of 400 kcal/mole are deemed less probable because of the absence of O atoms in the rapid flow system.

It is difficult to evaluate the importance of each process since both are in the same energy range. In any event, the ionic species are so short-lived that any mechanism invoked to explain the formation of H_2O_2 and H_2O at liquid air temperatures would involve basically OH radicals and H atoms.

* Permanent address: St. Francis Xavier University, Antigonish, Nova Scotia, Canada
[1] Giguere, Secco, and Eaton, Discussions Faraday Soc. **14**, 104 (1953).
[2] K. J. Laidler, J. Chem. Phys. **22**, 1741 (1954).

Chlorine Nuclear Quadrupole Resonances in Solid Solutions*

C. DEAN
University of Pittsburgh, Pittsburgh 13, Pennsylvania
(Received June 8, 1955)

THE Cl^{35} nuclear quardupole resonance in p:bromochlorobenzene (p:BrϕCl) has been observed at room temperature in several solid solutions of that substance with p:dibromobenzene (p:$Br_2\phi$). The narrowest resonance was found with 2 mole percent p:BrϕCl, the lowest concentration used. The resonances became progressively broader as the concentration was increased, being too broad for positive identification in pure p:BrϕCl. For comparison the Cl^{35} resonance was studied in a series of solid solutions of p:$Br_2\phi$ with from 1 to 50 mole percent of p:$Cl_2\phi$. The intensity and width of the resonance in each of this second series agreed very closely with that in the p:BrϕCl sample with the same relative abundance of Cl and Br atoms. In a third series of samples ranging from pure p:$Cl_2\phi$ to 50 mole percent p:$Cl_2\phi$ in p:$Br_2\phi$, the Cl^{35} resonance exhibited the same progressive broadening as the concentrations of the two halogens approached equality.

These results support an earlier suggestion[1] that relatively minute local variations in crystal structure can be an important factor in broadening the quadrupole resonances, and hence that in some cases such as pure p:BrϕCl the failure to observe a resonance might be due to excessive broadening by some species of disorder in the solid. X-ray data for p:BrϕCl had shown that its crystal structure is the same as that of p:$Cl_2\phi$, but with a random distribution of Br and Cl atoms occupying the halogen positions; in many respects the resulting crystal is equivalent to the mixed crystal formed by p:$Br_2\phi$ and p:$Cl_2\phi$.[2] Therefore in these crystals we conclude that the excess breadth depends on the probability of finding both Cl and Br atoms at sites near a given Cl atom, so that a narrow resonance occurs only when it is probable that all such sites are occupied either by Br only or by Cl only.

A self-quenched superregenerative spectrometer was used,[1] together with the usual recording techniques. The room-tempera-

ture frequency in some samples was compared with that of a small amount of pure p:$Cl_2\phi$[1,3] placed at one end of the sample vial. The Cl^{35} resonance from 3.4% p:$Cl_2\phi$ in p:$Br_2\phi$ was 12±3 kc higher than that from the pure p:$Cl_2\phi$ reference; the resonance from 7% p:BrϕCl in p:Brϕ was 44±6 kc above the same reference. The line widths obscured any variation of the frequency differences with concentration for these samples. A slight progressive shift with concentration was noticed in the samples with small amounts of p:$Br_2\phi$ in p:$Cl_2\phi$; for 10% p:$Br_2\phi$ the resonance was 6±3 kc higher than in the pure reference.

These frequency shifts are the same order of magnitude as the difference between the Cl^{35} resonance frequencies in the two solid phases of p:$Cl_2\phi$.[1,3] Other evidence[4] had suggested that the corresponding phase change might occur in the solid solutions at or below room temperature. However current quadrupole resonance work in this laboratory indicates that the triclinic structure of the high-temperature phase of pure p:$Cl_2\phi$[5] cannot be formed by p:$Br_2\phi$, and that in fact a few percent of it or of p:BrϕCl in solid solution with p:$Cl_2\phi$ are sufficient to rule out the formation of this phase. Consequently the results that are given here are all for crystals having the monoclinic structure.[6]

* Work done in the Sarah Mellon Scaife Radiation Laboratory and supported by the United States Air Force, through the Office of Scientific Research of the Air Research and Development Command.

[1] C. Dean, thesis, Harvard, 1952 (unpublished).
[2] S. B. Hendricks, Z. Krist. **84**, 85 (1932).
[3] C. Dean, J. Chem. Phys. **20**, 195 (1952).
[4] K. Beck and K. Ebbinghaus, Ber. deut. chem. ges. **39**, 3870 (1906).
[5] G. A. Jeffrey and W. J. McVeagh, J. Chem. Phys. **23**, 1165 (1955).
[6] Croatts, Bezzi, and Bua, Acta Cryst. **5**, 825 (1952).

London Force Contributions to Bond Energies

KENNETH S. PITZER
Department of Chemistry and Chemical Engineering, University of California Berkeley 4, California
(Received June 24, 1955)

IT is well known that the bond energies of the F−F, O−O, N−N single bonds are markedly smaller than those of the corresponding elements in the next row of the periodic table. It has been postulated[1] that at least a substantial portion of this surprising difference arises from the behavior of electrons other than the pair comprising the bond. However, to the writer's knowledge, it has not been recognized that the London (dispersion) attractive forces between these nonbonding electrons may make an important contribution to the bond energy for the elements below the first octet. Born and Mayer[2] did consider the London force terms in lattice energy calculations for ionic crystals and suggested that London forces were probably responsible for the appearance of the CsCl structure for CsCl, CsBr, and CsI. However, the London energy is small in these cases and only affects the structure because of the close balance of other terms.

In cases such as the diatomic halogen molecules, the atoms are brought much closer together. Since the energy has an inverse sixth power dependence, it may now become an appreciable part of the total energy.

We use the London[3] formula

$$-E_L=-\frac{3}{4}\frac{\alpha^2 h\nu}{R^6}$$

where α is the polarizability and $h\nu$ the excitation energy to the principal oscillator frequency, which may be approximated by the ionization potential. Ketelaar's[4] values for the polarizability of the halogen atoms were used in our calculations, together with other parameters from standard sources. Table I gives the dissociation energy, D_0, for the halogens together with the London force contribution E_L and the difference to be attributed to the single electron pair bond as well as other possible effects.

It is evident that inclusion of the London term greatly reduces the anomaly in the series F_2, Cl_2, etc. Since the London formula is only a first approximation and since there are complications from the nonspherical shape of the halogen atoms, the numerical values should not be given undue weight. However, they do justify a qualitative conclusion that the London term is of an important magnitude. We hope to refine these calculations further and to consider other terms appropriate to these molecules.

TABLE I.

	D_0	E_L	D_0-E_L
F_2	39	4	35
Cl_2	57.1	20	37
Br_2	45.4	17	28
I_2	35.6	13	23

[1] K. S. Pitzer, J. Am. Chem. Soc. **70**, 2140 (1948); R. S. Mulliken, *ibid.* **77**, 884 (1955).
[2] M. Born and J. E. Mayer, Z. Physik **75**, 1 (1932).
[3] F. London, Z. physik. Chem. **B11**, 222 (1930).
[4] J. A. A. Ketelaar, *Chemical Constitution* (Elsevier Publishing Company, Amsterdam and Houston, 1953), p. 90.

Molecular Structure of Methylamine from Its Microwave Spectrum

TETSUJI NISHIKAWA, TAKASHI ITOH, AND KOICHI SHIMODA*
Department of Physics, Faculty of Science, University of Tokyo, Tokyo, Japan
(Received June 8, 1955)

THE microwave spectrum of methylamine has been studied in the frequency range between 4 and 40 kMc/sec at the University of Tokyo and Harvard University. Several reports on the spectrum have already appeared[1-4] but the complete analysis has not yet been given. The spectrum consists of more than two hundred lines and is very complicated on account of inversion and hindered internal rotation. The observed lines are divided into two classes corresponding to the transitions $\Delta J=0$ or $\Delta J=\pm 1$.

We have found seven well-defined series of lines which correspond to the transition $\Delta J=0$. These series have been designated by p_1, p_2, q_1, q_2, r_1, r_2, and s_1[1,2] the series with subscript 1 and 2 forming an inversion pair. In the preceding paper[1,2] we have proposed tentative assignments of these series. But the q and r series were incorrectly assigned because of our neglect of the effect of the $K=1\leftrightarrow -1$ interaction on the levels with $K+\tau-1\neq 3m$. Taking account of this effect, we have obtained more reasonable assignments of the series which are listed in Table I. The calculated frequencies of the initial lines of the series and the magnitudes of version doublings using the molecular constants in Table III are also given in Table I.

The lines corresponding to the transitions $\Delta J=\pm 1$, $\Delta K=\mp 1$ are rather irregularly spaced in the observed range. Lide has assigned several lines corresponding to the transitions $J_K=5_1\rightarrow 4_2$

TABLE I. Assignments of series.

Series	Assignment[a] $K\rightarrow K'$	μ, n	Frequency of initial line: Observed (Mc/sec)	Calculated (Mc/sec)	gI[b]	Magnitude of inversion doubling: Observed (Mc/sec)	Calculated (Mc/sec)
p_1	0→1	1, 1	26 734*	26 734	3	6903	6903
p_2	0→1	1, 1	33 637*	33 637	1		
q_1	0→1	−1, 0	···	70 428	1	∼ 5000	8641
q_2	0→1	−1, 0	···	79 069	3		
r_1	0→1	0, 0	···	79 171	3	∼10 000	10 690
r_2	0→1	0, 0	···	89 861	1		
s_1	1→0	0, 1	···	2743	3	>∼30 000	38 064
s_2	1→0	0, 1	···	40 807	1		

[a] μ is defined by $\mu=-(K+\tau-1)$, mod. 3.
[b] The nuclear statistical weight.

TABLE II. Assignments of $\Delta J=\pm1$ lines (1).

$J_K\rightarrow J'_{K'}$	μ, n, γ[a]	Obs freq $g_I=3$	(Mc/sec) $g_I=1$	Calc freq $g_I=3$	(Mc/sec) $g_I=1$
$5_1\rightarrow4_2$	0, 0, 0	23 341*	17 476*	23 341	17 476
	0, 0, 1	36 452*,[b]	30 566*,[b]	36 442	30 576
	1, 0	14 438	10 262	14 301	10 342
	−1, 0	19 777	29 771[b]	20 003	29 795
$5_{-1}\rightarrow4_2$	1, 0	28 534[c]	···	28 440	···
$5_2\rightarrow6_1$	0, 0, 0	23 450*	29 312*,[b]	23 449	29 313
	−1, 0	21 931	12 593	21 709	12 303
$5_2\rightarrow6_{-1}$	1, 0	13 176[c]	···	13 272	···

[a] $\gamma=0$ or $\gamma=1$ according as $J+K_{+1}+K_{-1}$ is even or odd.
[b] These frequencies are taken from reference 4.
[c] These lines are forbidden if we neglect the effect of the $K=1\leftrightarrow-1$ interaction.

and $5_2\rightarrow6_1$,[4] but his assignments of the lines, for which $K+\tau-1\neq3m$, seem to be incorrect. Our assignments, which have been confirmed by the study of the Stark effect and by the theoretical calculations of the frequencies, are listed in Table II.

The inertial constants A, B, C, C_1, C_2, D, the hindering potential constant α, and the constant of inversion doubling Δ_0 in Table III have been obtained from the observed values of the

TABLE III. Molecular constants.[a]

$A=$	37.085×10^{-40} g cm²
$B=$	38.662×10^{-40} g cm²
$C=$	8.136×10^{-40} g cm²
$C_1=$	2.805×10^{-40} g cm²
$C_2=$	5.331×10^{-40} g cm²
$D=-$	0.120×10^{-40} g cm²
$\alpha=$	11.344
$\Delta_0=$	28 604 Mc/sec (for $n=0$)
	29 358 Mc/sec (for $n=1$)

[a] The values given in this table are probably not in error by more than a few tenths of a percent, except for D, in which the maximum possible error is about 0.05×10^{-40} g cm².

frequencies marked by * in Tables I and II and from the Stark coefficients of the lines of p_1 series. The meanings of these constants have been given in reference 2. We have used a slight modification of Burkhard and Dennison's theory,[5] and the interaction of inversion with internal rotation has been treated as described in reference 2. By using the above constants, we have obtained a good agreement between observed and calculated frequencies for all the lines in Tables I and II. The agreement will not be improved further by any additional adjustment of the molecular constants, so long as we use the simplified model which neglects the higher order effects.

TABLE IV. Assignments of $\Delta J=\pm1$ lines (2).

$J_K\rightarrow J'_{K'}$	μ, n, γ	Obs freq $g_I=3$	(Mc/sec) $g_I=1$	Calc freq $g_I=3$	(Mc/sec) $g_I=1$
$9_2\rightarrow8_2$	−1, 0	15 908	6246	16 047	6378
$9_2\rightarrow10_2$	−1, 0	28 515	···	28 378	···
$12_3\rightarrow11_4$	0, 0, 0	23 683	···	23 776	···
	0, 0, 1	23 861	···	23 958	···
$12_4\rightarrow13_3$	0, 0, 0	20 831	12 444	20 800	12 405
	0, 0, 1	20 547	12 162	20 509	12 114
	1, 0	···	11 961	···	11 985
	−1, 0	8412	···	8770	···
$16_4\rightarrow15_5$	0, 0, 0	23 409	12 239	23 754	12 424
	0, 0, 1	23 429	12 259	23 773	12 443
	1, 0	21 713	27 758	21 427	27 637
	−1, 0	···	16 682	···	16 256
$16_5\rightarrow17_4$	0, 0, 0	21 052	···	20 770	···
	0, 0, 1	21 019	···	20 739	···
	1, 0	22 723	16 948	23 091	16 881
$20_5\rightarrow19_6$	0, 0, 0	···	13 415	···	13 775
	0, 0, 1	···	13 417	···	13 777

Frequencies of many other lines can be predicted from the above constants. We have identified about twenty $\Delta J=\pm1$ lines corresponding to $J=8\sim20$ and $n=0$, which are given in Table IV. The agreement between theory and experiment is satisfactory.

The molecular structure of methylamine is determined from the inertial constants in Table III as follows: $d_{CH}=1.093$ A (assumed), $d_{NH}=1.014$ A (assumed), $d_{CN}=1.474\pm0.005$ A, $\angle HCH=109°30'\pm1°$, $\angle HNH=105°50'+1°$, $\angle CNH=112°10'\pm1°$, and the angle between the CN axis and the methyl axis $=3°30'\pm20'$ (The methyl axis passes through the NH_2 triangle.) The CN bond length is in agreement with the electron diffraction data 1.47 A,[6] while the $\angle CNH$ is considerably larger than the $\angle HNH$ in ammonia (106°47'). The large CNH angle may be related to the rather large value of the inversion splitting constant Δ_0, since the large CNH angle will facilitate the inversion motion. The barrier height of internal rotation is calculated to be 691.1 ± 1.0 cm^{-1} from α.

We express our hearty thanks to Dr. D. R. Lide, Jr. for his kind communication of his results. The detailed analysis and discussion will be published in J. Phys. Soc. Japan.

* Now at Columbia University, New York, on leave from the University of Tokyo.
[1] Shimoda, Nishikawa, and Itoh, J. Chem. Phys. **22**, 1456 (1954).
[2] Shimoda, Nishikawa, and Itoh, J. Phys. Soc. Japan **9**, 974 (1954).
[3] D. R. Lide, Jr., J. Chem. Phys. **20**, 1812 (1952); **21**, 571 (1953).
[4] D. R. Lide, Jr., J. Chem. Phys. **22**, 1613 (1954).
[5] D. G. Burkhard and D. M. Dennison, Phys. Rev. **84**, 408 (1951).
[6] P. W. Allen and L. E. Sutton, Acta Cryst. **3**, 46 (1950).

Internal Barrier Height of Methyl Mercaptan*

RALPH W. KILB†
Department of Chemistry, Harvard University, Cambridge, Massachusetts
(Received June 10, 1955)

THE $0_{00}\rightarrow1_{01}$ rotational transition for several isotopic species of methyl mercaptan has been reported[1] and from this data the structure was calculated.[1] The internal barrier, from relative intensities of rotational transitions for molecules in different torsional states, was reported as 1060 ± 120 cal/mole.

The $0_{00}\rightarrow1_{01}$ lines are split by an amount dependent on the barrier height. Lin[2] has extended the theory[3] to CH_3SH type molecules. With this theory and the data in Table I for six isotopes, the barrier was found to be 705 ± 45 cal/mole, which is inside the limits of error for eight of the ten lines used by Solimene and Dailey.[1]

The lowest torsional state is nondegenerate and is governed by a pseudo-rigid asymmetric top Hamiltonian of the form:

$$H=bP_x^2+cP_y^2+aP_z^2.$$

However, b and a are not $1/I_x$ and $1/I_z$ as in a rigid molecule. Because of the symmetry of the molecule, c is equal to $1/I_y$; also b is within a few megacycles of $1/I_x$. Thus the structure analysis of Solimene and Dailey[1] is justified. On the other hand, a is drastically affected (several tens of thousands Mc; compare

TABLE I. $0_{00}\rightarrow1_{01}$ transitions for several isotopic species.

Species	ν_{obs}	ν_N calc	$\Delta\nu_D$ calc	$\Delta\nu_D$ obs.
$C^{12}H_3S^{32}H$	25 291.8 ±0.1 Mc		+1.08 ±0.3 Mc	+1.0 ±0.2 Mc
	25 290.8	25 291.41 ±5 Mc		
$C^{13}H_3S^{32}H$	24 388.0		+0.98	+0.9
	24 387.1	24 381.09		
$C^{12}H_3S^{33}D$	24 387.5	24 386.80		
	24 385.0		−2.46	±2.5
$C^{12}D_3S^{32}H$	20 732.8		+0.57	±0.8
	20 732.0	20 731.24		
$C^{12}H_3S^{34}H$	24 879.8		+0.93	±0.9
	24 878.9	24 881.56		
$C^{12}H_3S^{33}H$	25 079.6		+1.00	±0.9
	25 078.7	25 080.35		

TABLE II. Rotational constants for the nondegenerate torsional state.

	a	b	c
$C^{12}H_3S^{32}H$	170 303 Mc[a]	12 907.36 ±2.5 Mc	12 384.04 ±2.5 Mc
$C^{13}H_3S^{32}H$	170 296	12 433.73	11 947.34
$C^{12}H_3S^{32}D$	91 026	12 659.24	11 727.55
$C^{12}D_3S^{32}H$	120 849	10 541.56	10 189.68
$C^{12}H_3S^{34}H$	170 016	12 694.62	12 186.94
$C^{12}H_3S^{33}H$	170 155	12 797.80	12 282.55

[a] a may be in error by several thousand megacycles because of its sensitivity to the barrier height and certain approximations.

Table II here with Table III of reference 1) and is highly dependent on the barrier. Table II gives a, b, and c for the nondegenerate torsional state. The ν_N of Table I is b plus c.

The second torsional state is degenerate. The rotational spectrum arising from molecules in this state is not that of a pseudo-rigid molecule. The Hamiltonian is

$$H=b'P_z^2+cP_y^2+a'P_z^2+dP_z+fP_x.$$

As d is very large (~100 000 Mc) the spectrum cannot be approximated by a rigid rotor. This explains the observation[1] that the 1→2 lines of $C^{12}H_3S^{32}H$ show no splitting or torsional satellites. Thus the $1_{10}\rightarrow 2_{11}(3b+c)$ and $1_{11}\rightarrow 2_{12}(b+3c)$ lines observed[1] may be unambiguously assigned to the pseudo-rigid rotor spectrum for the nondegenerate torsional state; one-quarter of the sum of these frequencies should be the frequency of the $0_{00}\rightarrow 1_{01}$ line of the nondegenerate torsional state. This is found to be 25 290.9±0.1 Mc, thus confirming the assignment in Table I. The corresponding degenerate torsional state 1→2 lines should be near 50 569.9 and 50 586.2 Mc (~$2b+2c$).

Using the assignment of Table I, we have recalculated the structure. The present data give only four strongly independent equations for the determination of five constants. The difficulty

TABLE III. Structural parameters of methyl mercaptan.

d_{CH}	1.1039 ±0.0020 A	<HCH	110°16′ ±10′
d_{SH}	1.3291 ±0.0040 A	<CSH	100°16′ ±10′
d_{SC}	1.8177 ±0.0002 A		
<CS bond-sym. axis of CH_3		27.5′ ±17′	
V_0	705 ±45 cal. (247 ±15 cm^{-1})		

lies in the fixing of the two parameters of the CH_3 group; this is aggravated to some extent by possible zero point variations for H and D isotopes.[4,5] Table III gives a reasonable set of parameters fitting the data.

Recently Kojima and Nishikawa[6] have reported a barrier of 800±140 cal calculated from a Dennison type[7] analysis on a series of lines originating at 18 000 Mc which they have assigned as Q-branch $K=0\rightarrow 1$ transitions. This series would be extremely barrier dependent. We also find that a barrier of 800 cal would give the origin of the series near 18 000 Mc; but this barrier height would increase the splitting of the $0_{00}\rightarrow 1_{01}$ lines by at least one megacycle. A barrier of 705±45 cal/mole would give the origin of the series at 42 660∓12 000 Mc. We also expect the first few members of the series to be within a 100 Mc spread, which is not the case in the reported series.

For this work we calculated a table of degenerate Mathieu functions and eigenvalues to replace the approximations of reference 3. Copies are available from us.

The author wishes to express his appreciation of the many discussions with Professor E. Bright Wilson, Jr.

* The research reported in this paper was made possible in part by support extended Harvard University by the Office of Naval Research under Office of Naval Research Contract N5ori 76, Task Order V.
† National Science Foundation Predoctoral Fellow.
[1] N. Solimene and B. P. Dailey, J. Chem. Phys. **23**, 124 (1955).
[2] C. C. Lin (to be published).
[3] Wilson, Lin, and Lide, J. Chem. Phys. **23**, 136 (1955).
[4] R. Myers and W. D. Gwinn, J. Chem. Phys. **20**, 1420 (1952).
[5] Miller, Aamodt, Dousmanis, Townes, and Kraitchman, J. Chem. Phys. **20**, 1112 (1952).
[6] T. Kojima and T. Nishikawa, J. Phys. Soc. Japan **10**, 240 (1955).
[7] D. G. Burkhard and D. M. Dennison, Phys. Rev. **84**, 408 (1951).

Surface Tension Temperature Relation

SHASHANKA SHEKHAR MITRA AND NITISH KUMAR SANYAL*
Department of Physics, Allahabad University, Allahabad, India
(Received July 14, 1955)

FROM thermodynamic considerations Pollara[1] has arrived at the following relation between vapor pressure and surface tension of liquids

$$T\log p=-aS\left(\frac{M}{D-d}\right)^{\frac{1}{4}}+b, \tag{1}$$

where p and S are vapor pressure and surface tension, T, M, D, and d are temperature, molecular weight, and densities of the liquid and vapor phases, respectively; a and b are constants.

Now McLeod's[2] well-known relation between surface tension and density is

$$\frac{S}{(D-d)^4}=C \tag{2}$$

C being a constant. Eliminating $(D-d)$ between Eqs. (1) and (2) Mitra and Chakravarty[3] have obtained:

$$T\log p+aS^{5/6}=b \tag{3}$$

a and b being constants for a particular liquid.

The temperature variation of vapor pressure for normal liquids may be approximately expressed by the integrated Clausius-Clapeyron's equation:

$$\log p=C+\frac{d}{T}$$

or

$$T\log p=CT+d. \tag{4}$$

Now by substituting for $T\log p$ in Eq. (3) from Eq. (4) a simple relation for the temperature dependence of surface tension is obtained:

$$S^{5/6}=A-BT. \tag{5}$$

This equation is well applicable to nonassociation pure liquids as is shown in Table I which records the case for benzene. The

TABLE I. Benzene.

T °K	S obs (in cgs units)	S calc (in cgs units)	Constants
273	31.58	31.54	
283	30.22	30.21	
293	28.88	28.88	$A=34.76$
303	27.56	27.60	$B=0.06233$
313	26.26	26.29	
323	24.98	25.02	
333	23.72	23.74	
343	22.48	22.48	
353	21.26	21.21	

maximum percentage error is only 0.23%. For associated liquids the equation is however applicable only in small ranges.

A semitheoretical justification for the well-known Van der Waal-Ferguson[4] empirical relation

$$S=A\left(1-\frac{T}{T_c}\right)^n, \tag{6}$$

T_c representing the critical temperature and n a constant whose value being different for different liquids but being in the neighborhood of 1.21, may be furnished from Eq. (5). In the critical region the surface tension tends to vanish because of the interface between the liquid and the vapor phases disappears. Hence, applying the condition $S=0$ at $T=T_c$ in Eq. (5) one arrives at

$$S=(BT_c)^{6/5}\left(1-\frac{T}{T_c}\right)^{6/5} \tag{7}$$

and since 6/5=1.2 Eq. (7) approaches the empirical relation.[5]

The integrated Clausius-Clapeyron's Eq. (4) is only of an

approximate nature and does not hold good for associated liquids. And since the derivation of Eq. (4) is based on Eq. (4), it could not be expected that Eq. (7) should also explain the temperature variation of surface tension in the case of associated liquids and thus the failure in the applicability of Ferguson's equation to complex and associated liquids becomes clear.

Ferguson's relation can be explained in yet another way. Eötvös[5] has correlated surface tension, molecular weight, density, and temperature of a liquid by the following equation

$$S\left(\frac{M}{D}\right)^{\frac{1}{3}}=K(T_c-T)$$

and because for a particular liquid M is constant, the above equation becomes

$$\frac{S}{D^{\frac{1}{3}}}=K'(T_c-T) \tag{8}$$

K' being a constant. Since the density of vapor is very small as compared to that of the liquid phase McLeod's equation (2) may be simplified to

$$\frac{S}{D^{\frac{1}{3}}}=C. \tag{2'}$$

Eliminating D between Eqs. (8) and (2') one gets

$$S=\left(\frac{K'T_c}{C}\right)^{6/5}\left(1-\frac{T}{T_c}\right)^{6/5} \tag{9}$$

and this equation is similar to Eq. (7).

One of the authors (S.S.M.) wishes to thank the Government of India, Ministry of Education, for providing a senior Research Scholarship.

* Present address is 104 Tagore Town, Allahabad, India.

[1] L. Z. Pollara, J. Phys. Chem. **46**, 1163 (1942).
[2] McLeod, Trans. Faraday Soc. **19**, 38 (1923).
[3] S. S. Mitra and D. N. Chakravarty, J. Indian Chem. Soc. (to be published).
[4] Ferguson, Trans. Faraday Soc. **19**, 408 (1923).
[5] Eötvös, Wied. Ann. **27**, 448 (1886).

Paramagnetic Resonance Absorption in Single Crystals of Diphenylpicrylhydrazyl at Low Temperatures

L. S. SINGER* AND C. KIKUCHI
United States Naval Research Laboratory, Washington, D. C.
(Received May 31, 1955)

PREVIOUS measurements of the paramagnetic resonance absorption of powdered hydrazyl at 10 000 Mc/sec[1] and 25 Mc/sec[2] at various temperatures suggest that the slight decrease in g-factor in going from 77°K to 4.2°K, as well as the discrepancies in the observed line widths, may be related to a temperature dependent anisotropy of the g-factor. The purpose of this note is to present the preliminary results of some measurements of the g-factor anisotropies and of the line widths in the resonance of single crystals of hydrazyl at various temperatures.

The measurements were made at 24 000 Mc/sec in an apparatus similar to that described by Bleaney and Stevens.[3] For each g-factor determination, the relative microwave frequency and magnetic field 5 cm from the hydrazyl sample were measured. The appropriate corrections were then made assuming that the room temperature g-factor of powdered hydrazyl is 2.0036. The two prism-shaped crystals used in the measurements were grown from a CS_2 solution by evaporation and had the dimensions $0.5\times0.03\times0.02$ mm, corresponding roughly to 10^{-9} mole of hydrazyl.

The crystals were rotated about the A axis which is perpendicular to both the broader face and to the long edge of the crystal.[4] The anisotropy results are indicated in Fig. 1. The solid curves are plots of the function $g=a+b[3\cos^2(\theta+\varphi)-1]$, where a, b, and φ have the values given in Table I.

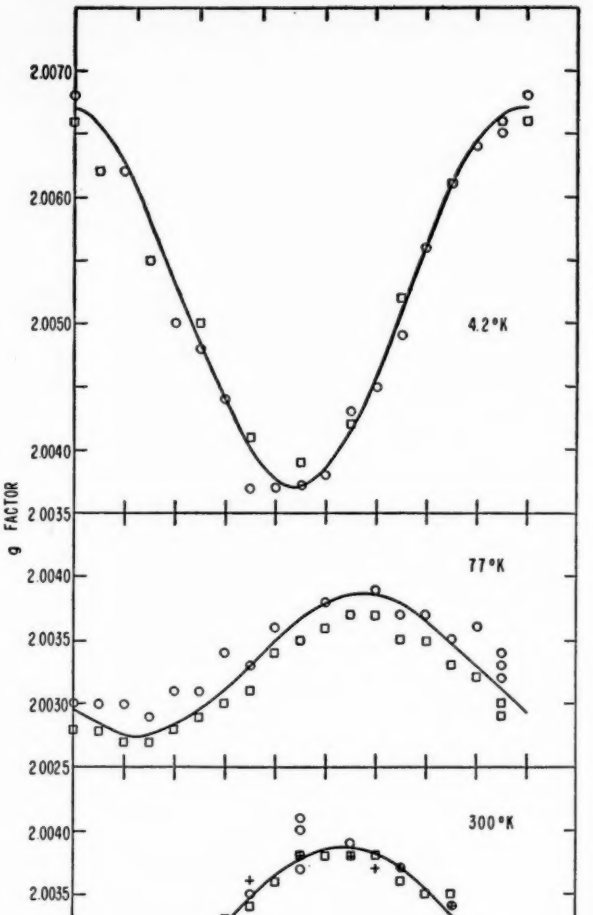

FIG. 1. Anisotropy of the g-factor of diphenyl-picryl hydrazyl at 4.2°, 77°, and 300°K. θ is the angle between the B axis (prism axis) and the magnetic field. The various symbols for the experimental points are for different runs on 2 different crystals.

Two warm-up runs were also made for the orientations $\theta=80$ and 170 degrees. The results were in agreement with those in Fig. 1 and showed that the rapid increase in g factor with decreasing temperature for both orientations began at about 15°K. At 1.6°K the g-factor of a single crystal for the 30, 80, and 170 degree orientations were 2.0102, 2.0050, and 2.0109, respectively. The g-factor for the powder was 2.0036 at 77°K and 2.0032 at 4.2°K. No precise g-factor could be obtained for the powder at 1.6°K because of the large line width. The single crystal line widths were, within the experimental uncertainty of ±20%, independent of orientation. The observed full widths at half-maximum absorption for the single crystals and the powder are given in Table I.

The anisotropy results are in approximate agreement with the earlier room temperature measurements of Kikuchi and Cohen[4] and Berthet.[5] The anisotropy curves in Fig. 1 indicate a shift of the principal magnetic directions as well as a change in magnitude of the principal g-values. The powder g-factors are roughly in agreement with the results of Weidner and Whitmer[1] and Singer and Spencer.[2]

The single crystal line widths also agree approximately with the low frequency powder measurements.[2] This is to be expected since there should be essentially no anisotropy broadening of the

TABLE I.

Temp. °K	a	b	φ (Degrees)	Single crystal line width (gauss)	Powder line width (gauss)
300	2.0031	0.00037	75.0	1.1	2.9
77	2.0031	0.00037	62.5	1.3	3.3
4.2	2.0047	0.00100	2.5	5.0	10
1.6	...	...	...	7.5	>20

powder resonance at 25 Mc/sec. A critical comparison of our line widths with those of Weidner and Whitmer[1] would be difficult, since the temperature dependent anisotropy would undoubtedly contribute to the line width of the powder at 10 000 Mc/sec.

* Present address: National Carbon Research Laboratories, Cleveland, Ohio.

[1] R. T. Weidner and C. A. Whitmer, Phys. Rev. **91**, 1279 (1953).
[2] L. S. Singer and E. G. Spencer, J. Chem. Phys. **21**, 939 (1953).
[3] B. Bleaney and K. W. H. Stevens, Repts. Progr. in Phys. **16**, 108 (1953).
[4] C. Kikuchi and V. W. Cohen, Phys. Rev. **93**, 394 (1954).
[5] G. Berthet, Compt. rend. **240**, 57 (1955).

Anomalous Electron Scattering from Iodine Vapor*

I. L. KARLE
U. S. Naval Research Laboratory, Washington, D. C.
(Received June 27, 1955)

THIS article is a preliminary report on the study of the internuclear distances r and average amplitudes of vibration $\langle l^2\rangle^{\frac{1}{2}}$ of diatomic molecules using the sector microphotometer techniques in electron diffraction. Experimental molecular intensity curves for O_2 and Br_2, extending to s-values of 33, were obtained with 40 kv electrons. These curves reproduced the theoretical intensity function for the molecular portion of the scattering,

$$I_{\text{mole}}=\exp(-l^2s^2/2)\frac{\sin sr}{sr}. \quad (1)$$

The values of r and $\langle l^2\rangle^{\frac{1}{2}}$ for each molecule obtained from both the intensity curves and their Fourier transforms (radial distribution curves) were identical. These values are listed in Table I and compared to spectroscopic values.[1]

The molecular intensity curve for iodine vapor obtained with 40-kv electrons, however, does not reproduce the theoretical function (1). The curve is nearly uniformly shifted to larger s-values and can be approximately represented by a function of the type

$$\frac{\sin(sr-\phi)}{(sr-\phi)} \quad (2)$$

where r is the normal interatomic distance and ϕ is of the order of 0.3. In addition to the phase shift, the damping of the curve is considerably greater than the $\langle l^2\rangle^{\frac{1}{2}}$ computed from spectroscopic data. This experiment was repeated with two different samples of iodine and two different types of nozzles. One nozzle was a continuous-flow type heated to ~90°C. The other nozzle had a solenoid operated plunger pressing against the nozzle aperture next to the electron beam. This type of nozzle has the plunger coordinated with the beam deflector and admits the vapor only during the actual exposure time. The results were identical in each case.

TABLE I.

	Spectroscopic r_e	Spectroscopic $\langle l^2\rangle^{\frac{1}{2}}$	Electron diffraction (40 kv) r_0	Electron diffraction (40 kv) $\langle l^2\rangle^{\frac{1}{2}}$
O_2	1.207	0.037	1.208	0.038
Br_2	2.284	0.045	2.290	0.045

T~300°K

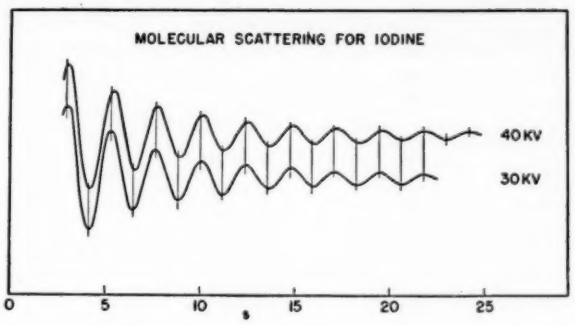

FIG. 1. Molecular scattering curves for I_2 vapor. The vertical lines indicate the theoretical positions for the maxima and minima using values for the equilibrium interatomic distances determined from the separation of the maxima and minima and the separation of the cross-over points on the s-axis. The molecular scattering curve using 30-kv electrons is quite normal whereas that at 40 kv is shifted to larger s-values.

The experiment was then repeated with 30-kv electrons and it was found that the molecular intensity curve was quite normal and reproduced the spectroscopic values. The intensity curves are illustrated in Fig. 1 and the r and apparent $\langle l^2\rangle^{\frac{1}{2}}$ values derived from these curves are listed in Table II.[2]

TABLE II. Iodine (T~360°K).

	Spec.[a]	30 kv	40 kv
r, A	2.666	2.662	2.662
$\langle l^2\rangle^{\frac{1}{2}}$, A	0.0555	0.055	0.063
average shift along s-axis, A^{-1}		0	0.11
λ, A		0.068	0.060

[a] See reference 1.

The kind of phase shift encountered in iodine (shifting of the sine wave along the s-axis) has never before been reported in molecules possessing like or unlike atoms. This experimental observation is important because of its relationship to the analysis of diffraction patterns and because it might add additional factors to the explanation of other phase shift effects (modulation of the sine wave)[3,4] in molecules composed of different kinds of atoms. The phase shift in iodine may be a phenomenon which appears with highly polarizable substances and may be due to a change of the electron distribution about the atoms in the molecule as the molecule vibrates. It is not explained by the known anharmonicity of the vibration in I_2. The phase shift also appears to be a function of the accelerating voltage of the electron beam. Additional experiments with diatomic molecules possessing like and unlike atoms may further elucidate this phenomenon.

* Presented at Meeting of International Union of Crystallography, Paris, July 21–28, 1954.

[1] G. Herzberg, *Spectra of Diatomic Molecules* (D. Van Nostrand Company, Inc., New York, 1951).
[2] C. Finbak and O. Hassel (Arch. Math. Naturvidenskab **45**, No. 3 (1941) obtained an apparently normal scattering curve for I_2 with an r value of 2.674 A using an accelerating voltage of 30 kv.
[3] V. Schomaker and R. Galuber, Nature **170**, 290 (1952).
[4] J. Hoerni and J. Ibers, Phys. Rev. **91**, 1182 (1953).

Structure and Potential Barrier to Hindered Rotation in Methyl Alcohol*

JEROME D. SWALEN†
Chemistry Department, Harvard University, Cambridge 38, Massachusetts
(Received June 13, 1955)

RECENTLY Venkateswarlu, Edwards, and Gordy[1] have measured the frequencies of the $J=0\rightarrow1$ line in six isotopic species of methyl alcohol. All of these lines with the exception of one appear as doublets whose frequency separation is barrier

TABLE I. $0_{00}\rightarrow 1_{01}$ transition frequencies and barrier height in methyl alcohol.

	Observed frequency (in mc)	Calculated frequency (in mc)	Barrier height (in cm^{-1})
$C^{12}H_3OH$	48 377.09		389
	48 372.60	48 379.0	
$C^{13}H_3OH$	47 209.63		376
	47 205.20	47 199.1	
$C^{12}H_3OD$	45 359.43	45 364.9	385
	45 344.30		
$C^{13}H_3OD$	44 241.43	44 236.3	384
	44 228.26		
$C^{12}D_3OH$	39 069.25		385
	39 066.21	39 065.8	
$C^{12}D_3OD$	36 799.01	36 798.3	406
		Average	388 ± 20 cm^{-1}

dependent. Since the barrier height has been determined quite accurately from other lines in the microwave spectrum by Burkhard and Dennison[2] and Ivash and Dennison[3] this analysis was done by a somewhat different treatment following an extension of the method of Wilson, Lin, and Lide[4] as suggested by C. C. Lin[5] in order to confirm the Burkhard, Ivash, Dennison value.

The Hamiltonian for this case of a symmetric top attached to an asymmetric rotor can be written:

$$H_0=\frac{P_x^2}{2I_{xx}}+\frac{I_{zz}-I_\alpha\lambda_z^2}{2d}P_y^2+\frac{I_{yy}-I_\alpha\lambda_y^2}{2d}P_z^2$$
$$\times\frac{I_\alpha\lambda_y\lambda_z}{2d}(P_yP_z+P_zP_y)+\frac{I_{yy}I_{zz}}{2I_\alpha d}p^2+\frac{V_0}{2}(1-\cos 3\alpha)$$
$$H_1=-\frac{(\lambda_yI_{zz}P_y+\lambda_zI_{yy}P_z)}{d}p$$

where $d=I_{yy}I_{zz}-\lambda_y^2I_\alpha I_{zz}-\lambda_z^2I_\alpha I_{yy}$ and H_1 is the perturbation operator. The method now follows similarly to that of reference 4 for the high barrier case except that recently R. W. Kilb has made numerical calculations of the degenerate eigenfunctions and eigenvalues of the torsional part and these were used in the calculations.

The stucture of the molecule was first fitted with the pseudo-rigid rotor lines, i.e., the rigid rotational energy and the non-degenerate state of the ground torsional level. Fortunately these lines are very barrier insensitive so any reasonable barrier could be used; but the doublet separation is mainly dependent on the barrier and the direction cosine between the y principal axis and the top axis, so that these two were determined from the experimental data.

With this value of the barrier, the structure was then fitted to the pseudo-rigid rotor lines; however, the structure cannot be determined completely by least squares since only three parameters are sufficiently independent. The barrier height and one more parameter were determined from the doublet splitting. Finally the last two parameters were varied slightly to obtain a better fit. With this structure, the barrier was redetermined from the splittings. The calculated frequencies and barrier height are given in Table I, and a reasonable structure is given in Table II. In $C^{12}D_3OD$ an accidental degeneracy occurs between the $K=1$ and $K=0$ ground degenerate torsional states; this causes the degenerate line $K=0$ to be split from the pseudo-rigid rotor line possibly as much as 500 Mc, so that only one has been observed. If the splitting were too small to be observed the calculated barrier would be far too high to be consistent.

The barrier calculated could have the possible sources of error: the measured frequencies may be in error by ±0.1 Mc, the treatment itself is only accurate to second order, error in the direction cosine of the top, the barrier and the structure were assumed the same for all species, and zero point variations.

As a result of these errors various barrier heights are obtained. Nevertheless the average barrier height calculated is in agreement with that of Burkhard and Dennison[2] and Ivash and Dennison.[3] The barrier determined by our method is 388 ± 20 cm^{-1} or 1110 ± 60 cal/mole.

Finally the author wishes to express his thanks to Professor E. B. Wilson, Jr. for the many helpful discussions and encouragement on this topic.

* The research reported in this paper was made possible in part by support extended Harvard University by the Office of Naval Research under Office of Naval Research Contract N5ori 76, Task Order V.
† National Science Foundation Predoctoral Fellow.
[1] Venkateswarlu, Edwards, and Gordy, Duke Microwave Laboratory Report No. 8, Department of Physics, Duke University.
[2] D. Burkhard and D. Dennison, Phys. Rev. **84**, 408 (1951).
[3] E. Ivash and D. Dennison, J. Chem. Phys. **21**, 1804 (1953).
[4] Wilson, Lin, and Lide, J. Chem. Phys. **23**, 136 (1955).
[5] C. C. Lin, (to be published).

TABLE II. Methyl alcohol structure.

	Present work	Gordy and Venkateswarlu	Ivash and Dennison
a[a]	0.10634 A	0.08277 A	0.079 A
b	0.79335 A	0.80218 A	0.807 A
c	0.35538 A	0.36114 A	0.306 A
d	1.42410 A	1.4247 A	1.432 A
e	0.37271 A	0.37321 A	0.364 A
f	1.09790 A	1.09610 A	1.093 A
d_{OH}	0.967 A	0.956 A	0.937 A
d_{CO}	1.428 A	1.427 A	1.434 A
d_{CH}	1.098 A	1.096 A	1.093 A
∠HCH	109° 6′	109° 2′	109° 30′
∠COH	107° 16′	108° 52′	105° 56′

[a] See reference 3 for labeling.

Near Ultraviolet Absorption Spectra of *Ortho*-, *Meta*-, and *Para*-Phenylenediamine Vapors

AKIRA SADÔ AND TOSINOBU ANNO
Department of Chemistry, Faculty of Science, Kyushu University, Fukuoka, Japan
(Received June 29, 1955)

THE uv-absorption spectra of three isomeric phenylenediamines in vapor state were photographed with a Hilger E-II medium quartz spectrograph having a linear dispersion of 16 A/mm at 2900 A, using an absorption cell of 40 cm with quartz windows. The results will be briefly described below.

The *ortho*-phenylenediamine molecule has a continuous absorption in the region between 3000 and 2800 A at the saturation pressure of the vapor for 80°C. In the *para*-spectrum 16 bands were observed having equal intervals of about 200 cm^{-1} in the region 3380~3050 A. However, they are very diffuse and have no characteristic structures so that the vibrational analysis seems to be impossible. In the *meta*-spectrum lying in the region 3100 ~2790 A, about 50 bands were observed, a few of which have sharp heads on the violet side. The three isomeric phenylenediamines are found to have absorption maxima in cyclohexane solution: *o*-, $\lambda_{max}=293$ mμ, $\epsilon_{max}=3400$; *m*-, $\lambda_{max}=295$ mμ, $\epsilon_{max}=2300$; *p*-, $\lambda_{max}=319$ mμ, $\epsilon_{max}=1650$. The values of extinction coefficient suggest that the electronic transitions are of the

TABLE I. Fundamental vibration frequencies of *m*-phenylenediamine (in cm^{-1}).

Raman effect[a] $\Delta\nu$	Intensity	Symmetry species in C_{2v}	Present work Ground state	Present work Excited state
			211	
			537	455
757	5	a_1	758	715
993	6	a_1		954
1065	0	a_1		
1172	0	a_1		
1319	4	a_1		1205 or 1318
1593	4	a_1		(1565)
3055	0	a_1		

[a] Landolt-Börnstein, *Zahlenwerte und Funktionen* (Springer-Verlag, Berlin, 1951), sixth edition, Vol. 1, Part 2, p. 314.

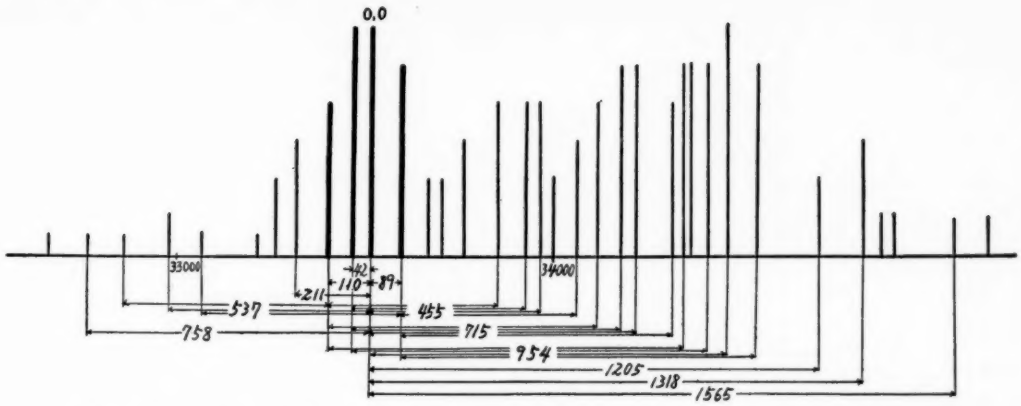

FIG. 1. A schematical diagram showing the main feature of the absorption system of *meta*-phenylenediamine.

"allowed" type, which may be considered to have come from the 2600 A absorption system of the benzene molecule.

The spectrograms for the *m*-compound were taken at the saturation vapor pressures corresponding to the cell temperatures of 70°~150°C. The sharp band at 2983.1 A, which is the strongest on a plate taken at 70°C, is assumed to be the 0,0 band. No progression of bands is seen on the spectrum whose schematical diagram is shown in Fig. 1. Four bands at 33 402=0−110, 33 470=0−42, 33 512=0−0 and at 33 601=0+89 cm^{-1} constitute a band group characteristic in this spectrum. The band at 32 975=0−537 cm^{-1} may give a fundamental frequency in the ground electronic state and 33 967=0+455, 34 227=0+715, and 34 466=0+954-cm^{-1} may give the excited state values. Around each of these absorption bands the above-mentioned characteristic band group is seen to occur. Fundamental frequencies obtained, including less certain ones, are listed in Table I in comparison with those obtained by Raman effect.

The authors express their hearty thanks to Professor S. Imanishi for reading the manuscript and making valuable suggestions.

Mobility of Hydrogen on Tungsten*

R. GOMER AND R. WORTMAN†
Institute for the Study of Metals and Department of Chemistry, University of Chicago, Chicago, Illinois
(Received July 14, 1955)

THE mobility of hydrogen on tungsten is being investigated by a field emission technique similar to that used for studying the mobility of oxygen on tungsten.[1] A sealed-off emission microscope containing a tungsten tip and a small platinum crucible filled with Zr, saturated with hydrogen is immersed in a partially unsilvered liquid helium cryostat. After cleaning of the tip by electric heating to 2000°K the Pt crucible is heated to ~300°K. Hydrogen is released and deposited on the portion of the tip facing the crucible. Contamination of the shadow side of the tip does not occur because the sticking coefficient of hydrogen at 4.2°K is very high and its vapor pressure $<10^{-11}$ mm.

If initial coverages $\gg 1$ are deposited on the exposed portion of the tip, spreading with a sharp moving boundary occurs at extremely low temperatures (<20°K). This is analogous to the low temperature spreading observed with oxygen at 40°K and corresponds to mobility of physically adsorbed hydrogen on top of the chemisorbed layer. Gas may become trapped at the edge of the layer, thus advancing its boundary and permitting further spreading. The temperature of the phenomenon has not been measured accurately as yet but is so low that spreading may be induced by shining a 3-volt flashlight at the tip through the helium bath.

Very low initial coverages give rise to activated diffusion, setting in at approximately 230°K. At this temperature complete equilibration of small amounts of adsorbed hydrogen requires times of the order of 10^4 seconds. Estimates of spreading times at various tip temperatures permit a calculation of activation energies. At very low coverages $E_{act}=16\pm3$ kcal. A semilogarithmic plot of spreading time *vs* $1/T$ is shown in Fig. 1. Full spreading of the initial "dose" of hydrogen raises the average work function by 0.05−0.1 volt, corresponding to coverages of approximately 0.1. The value of the activation energy for the diffusion of hydrogen on tungsten is considerably lower than that of oxygen, 30 kcal.[1] It is interesting that both activation energies may be expressed almost exactly by

$$E_{act}=0.21E \qquad (1)$$

where E is the heat of evaporation of atomic oxygen or hydrogen. The values of E are computed to be 133[2] and 76[3] kcal, respectively from the molar heats of adsorption at low coverage.

Desorption is complete at ~600°K in a few seconds for all coverages. This proves that no oxygen is released by the zirconium source. Low temperature spreading increases the work function of the tip to 5.03 volts, assuming a work function of 4.5 volts for clean tungsten. This is in good agreement with the room temperature value of 4.93 volts reported by Müller.[4] The residual gas left in the tube after hydrogen treatment of the zirconium and sealing-off consists of H_2 at a pressure of about 10^{-6} mm, and traces of O_2. If the tip is contaminated with this gas by evaporat-

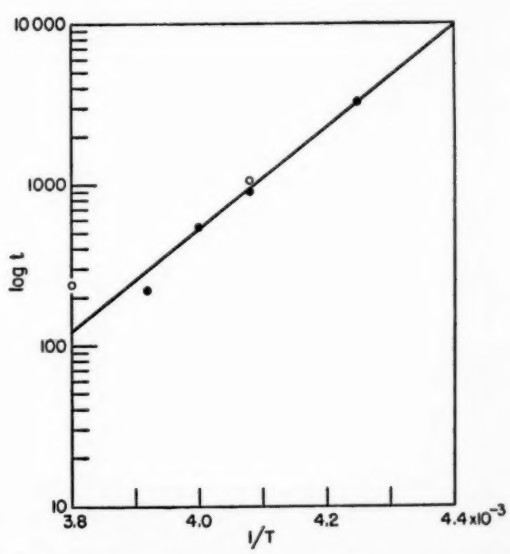

FIG. 1. Plot of logarithm spreading time *vs* $1/T$. t spreading time in seconds, T =temperature in K. Unfilled circles represent dubious points because of uncertainty in the amount of hydrogen dose.

ing the liquid helium and allowing the tube to warm up (in this process H_2 voltilizes before O_2, which has negligible vapor pressure at 20°K[1]) considerable changes in the pattern appear due to adsorption, but the work function is approximately that of clean tungsten. Heating to temperatures near 600°K with the tube at 4.2°K increases the work function. Further heating gives rise to typical oxygen on tungsten patterns in various stages of desorption and oxidation. This suggests that oxygen does not replace hydrogen in the atomically chemisorbed state until the latter begins to evaporate. Recent evidence[1] on the molecular chemisorption of O_2 makes this at least possible.

* Supported in part by the Petroleum Research Fund of the American Chemical Society.
† Standard Oil Company of Indiana Predoctoral Fellow 1954–1955.
[1] R. Gomer and J. K. Hulm, J. Am. Chem. Soc. **75**, 4114 (1953). A somewhat more complete account of the oxygen work is given in R. Gomer, *Advances in Catalysis* (Academic Press, Inc., New York), Vol. VII (to be published).
[2] R. C. L. Bosworth and E. K. Rideal, Physica **4**, 925 (1937).
[3] J. K. Roberts, Proc. Roy. Soc. (London) **A152**, 445 (1935).
[4] E. W. Müller, Ergeb. exakt. Naturwiss. **XXVII**, 355 (1953).

Free Convection between Two Vertical Plates in the Presence of an Inclined Temperature Gradient

STEPHEN PRAGER
Department of Chemistry, University of Minnesota, Minneapolis, Minnesota
(Received July 5, 1955)

IN connection with a study of the Soret effect in liquids, it became necessary recently to establish a temperature gradient without any attendant convection currents. The customary way of accomplishing this is to have the fluid in a vertical column with the temperature gradient directed upward. While this arrangement certainly leads to hydrodynamic equilibrium, even a small deviation of the temperature gradient from the vertical direction will give rise to a steady convection, and it seemed desirable, therefore, to find the velocity distribution in the column under such circumstances.

We consider then a liquid of density ρ, thermal expansion coefficient α, conductivity K, heat capacity C, and viscosity η, confined in the channel between two infinite vertical plates separated by a distance $2a$ from each other. The plates are subjected to a constant temperature gradient of magnitude θ, whose direction makes an angle ϵ with the upward vertical.

Symmetry considerations together with the equation of continuity require that only the vertical component v of the velocity be different from zero; furthermore, v must depend only on the distance y from the plane which bisects the channel. Under these conditions, the Navier-Stokes equation becomes

$$\frac{\partial^3 v}{\partial y^3}=-\frac{\rho g\alpha}{\eta}\frac{\partial T}{\partial y} \tag{1}$$

where T is the temperature and g the gravitational acceleration, while the heat transport equations can be written

$$\frac{\partial^2 T}{\partial y^2}=\frac{\rho C\theta\cos\epsilon}{K}v; \tag{2}$$

it should be noted that T depends on x, the vertical coordinate, as well as on y. Equations (1) and (2) are to be solved subject to the boundary conditions

$$v(a)=v(-a)=0$$
$$\int_{-a}^{a} v\,dy=0 \tag{3}$$
$$T(x,a)-T(x,-a)=2a\sin\epsilon.$$

The solution to Eqs. (1), (2), and (3) takes on two different forms, depending on whether ϵ is less or greater than $\pi/2$. In the former case, which is the one of primary interest here, the velocity distribution is given by

$$v=\frac{\gamma^2 K\tan\epsilon}{a\rho C}\times\left[\frac{\sinh\frac{\gamma}{\sqrt{2}}\left(1+\frac{y}{a}\right)\sin\frac{\gamma}{\sqrt{2}}\left(1-\frac{y}{a}\right)-\sinh\frac{\gamma}{\sqrt{2}}\left(1-\frac{y}{a}\right)\sin\frac{\gamma}{\sqrt{2}}\left(1+\frac{a}{y}\right)}{\cosh\sqrt{2}\gamma-\cos\sqrt{2}\gamma}\right], \tag{4}$$

where

$$\gamma=a\rho^{\frac{1}{2}}\left(\frac{g\alpha C\theta\cos\epsilon}{K\eta}\right)^{\frac{1}{4}}$$

and the temperature by

$$T(x,y)=T(x,0)+a\theta\sin\epsilon\times\left[\frac{\cosh\frac{\gamma}{\sqrt{2}}\left(1+\frac{y}{a}\right)\cos\frac{\gamma}{\sqrt{2}}\left(1-\frac{y}{a}\right)-\cosh\frac{\gamma}{\sqrt{2}}\left(1-\frac{y}{a}\right)\cos\frac{\gamma}{\sqrt{2}}\left(1+\frac{y}{a}\right)}{\cosh\sqrt{2}\gamma-\cos\sqrt{2}\gamma}\right]. \tag{5}$$

For small values of γ the temperature becomes a linear function of y as well as of x, while (4) turns into the familiar expression

$$v=\frac{g\rho\alpha\theta\sin\epsilon}{\epsilon\eta}y(a^2-y^2). \tag{6}$$

If $\gamma\gg 1$, v oscillates rapidly from positive to negative values as y is changed, the wavelength being $\sqrt{2}a/\gamma$; the amplitude of the oscillation will be very small except in the immediate vicinity of the walls of the channel, where it has a value of $\gamma^2 K\tan\epsilon/a\rho C$. The temperature is almost independent of y if γ is large, except for y near $\pm a$, where T changes rapidly. For water in a channel 1 cm wide, with $\theta=10$ deg/cm and ϵ small, γ is about 15, so that (6) is not a useful relation for this case, and (4) should be used instead.

I would like to acknowledge the aid of a grant from the Research Corporation in supporting the work of which this publication is a part.

CONTENTS

Journal of Chemical Physics — Vol. 23, No. 9 — September, 1955

Radical Analysis Followed by Electron Irradiation of Some Esters . . . P. S. Weiss and W. W. Seaquist 1567

Reactions in Ices . . . Herman H. Nechtrieb and George S. Handler 1569

Simple Approximation to the Gaussian Diffusion Integral for the Lennard-Jones 12-6 Model . . . S. C. Saxena and R. N. Srivastava 1571

Diffusion Studies with Radioactive Crystals . . . Donald S. McClure and Otto Schlenz 1575

Infrared Correlations of Organic Vapor Mixtures . . . L. A. Bennett and G. C. Vlases 1587

Emission Spectra of Two-Stage Gold Flame of Diethyl Ether . . . Russell E. Donovan and William G. Agnew 1592

Oxidation States of Technetium-95 Produced by Neutron Irradiation of Potassium Chloride . . . T. A. Carlson and W. S. Koski 1596

Corrections to be Applied to Gas Isotherms Measured in the Presence of Mercury . . . W. B. Jepson and J. S. Rowlinson 1599

Low-Frequency Rotational Spectrum of HDO . Samuel Weissman, Yardley Beers, and Gabriel Farrmann 1601

Kinetics and Mechanism of Intramolecular Reaction in the Decomposition of Ammonium Azide from Hydrazoic Acid . . . David A. Dows, George C. Pimentel, and Eric Whittle 1606

Adsorption of Hydrogen and of Nitrogen on Tungsten . . . George E. Moore and H. W. Allison 1609

Kinetics of the Isotope Exchange Reaction of Fluorine with Hydrogen Fluoride . . . Richard M. Adams, Richard B. Bernstein, and Joseph J. Katz 1622

Absolute Cross Sections of Carbon Dioxide and Carbon Monoxide in the Vacuum Ultraviolet . . . H. Sun and G. L. Weissler 1625

Rate of Convergence of Hadamard Series by the Method of Bertaut . . . David R. Templeton 1629

Some Impurities in Crystals from the Melt . . . G. W. Sears 1630

Absorption of Helium on Thorium Dioxide . . . J. G. Aston, S. V. R. Mastrangelo, and R. J. Tykodi 1633

Vibrational Spectra and Structure of Cyclopropane and Cyclopropane-d_6 . . . A. W. Baker and R. C. Lord 1636

Ionization Potentials of Argon, Krypton, and Xenon . . . E. Whalley and W. G. Schneider 1644

Magnetic Susceptibilities of Some Uranium (IV) Compounds . . . Clyde A. Hutchison, Jr., and Charles M. Hernfeld 1650

Isomeric Shifts in Polynuclear Chains . . . Marshall Fixman 1656

Absorption of the 4260 cm^{-1} Band of HBr . . . Glenn A. Crosby, Edward J. Bair, and Paul C. Cross 1660

Contributions of Displacements and Anisotropy to Dielectric Polarization in Polar Substances . . . Frank R. Harris 1663

Nuclear Magnetic Resonance: Structure of the Amino Group I . . . R. A. Kromhout and W. G. Moulton 1673

Binary Diffusion of Similar or Isotopic Molecules in Three Component Systems . . . William P. Senett, Fred Golleb, and T. I. Taylor 1679

Raman and Infrared Spectra and Structure of 4-Dimagnesiaspiro (3,3) heptane . . . S. C. Sirkar, Fred L. Veelz, and Forrest F. Cleveland 1684

Energy Calculations of Multiple Hydrogen-Atom Systems by VB and MO Methods . . . Richard S. Barker, Richard L. Snow, and Henry Eyring 1695

Complete Self-Consistent Treatment of Allyl Radical and Allyl Ion . . . H. C. Lefkovits, Janice Fain, and F. A. Matsen 1690

Proton Magnetic Resonance of the CH_3 Group. III. Reorientation Mechanism in Solids . . . J. G. Powles and H. S. Gutowsky 1692

Vapor Conductivity, Infrared Spectrum, and Thermodynamic Properties of $TiCl_4$ . . . N. J. Hawkins and D. R. Carpenter 1700

Thermal Decomposition of Nitric Oxide . . . Frederick Kaufman and John R. Kelso 1702

Magnetic Properties of Uranium Hydride . . . Dieter M. Gruen 1706

Study of Chemical Reaction Mechanisms with Molecular Beams. The Reaction of K with HBr . . . Ellison H. Taylor and Sheldon Datz 1711

Absorption Spectrum and ν_2 of Heavy Water Vapor . . . Fred P. Dickey and James M. Hoffman 1718

(Continued on cover three)

LANCASTER PRESS, INC., LANCASTER, PA.